[Cancer Biology & Therapy 3:10, e19-e27, EPUB Ahead of Print, http://www.landesbioscience.com/journals/cbt/abstract.php?ic

EXHIBIT A

Research Paper

Increased Expression of Dystroglycan Inhibits the Growth and Tumorigenicity of Human Mammary Epithelial Cells

Alessandro Sgambato[1,*]
Andrea Camerini[1]
Beatrice Faraglia[1]
Ernesto Pavoni[2]
Micaela Montanari[1]
Daniele Spada[1]
Carmen Losasso[2,†]
Andrea Brancaccio[2]
Achille Cittadini[1]

[1]Centro di Ricerche Oncologiche "Giovanni XXIII"; Istituto di Patologia Generale; Catholic University; Rome, Italy

[2]Istituto di Chimica del Riconoscimento Molecolare—Sezione di Roma (CNR); Istituto di Biochimica e Biochimica Clinica; Catholic University; Rome, Italy

[†]Current address: Department of Biology; University of Padova; via u.Bassi, 58/b; Padova 35121 Italy

*Correspondence to: Alessandro Sgambato; Istituto di Patologia Generale; Centro di Ricerche Oncologiche "Giovanni XXIII"; Università Cattolica del Sacro Cuore; Largo Francesco Vito 1; Rome 00168 Italy; Tel.: +39.06.3016619; Fax: +39.06.3012753; Email: asgambato@rm.unicatt.it

Received 07/12/04; Accepted 08/02/04

This manuscript has been published online, prior to printing, for *Cancer Biology & Therapy* Volume 3, Issue 10. Definitive page numbers have not been assigned. The current citation for this manuscript is: Cancer Biol Ther 2003; 3(10):
http://www.landesbioscience.com/journals/cbt/abstract.php?id=1132
Once the issue is complete and page numbers have been assigned, the citation will change accordingly.

KEY WORDS

breast cancer, adhesion molecule, tumor suppressor gene

ACKNOWLEDGEMENTS

The authors are grateful to Dr. Tamara C. Petrucci (Rome) for helpful advices and critical reading of the manuscript.

This study was supported in part by grants from Università Cattolica (MURST 60%) to A.C. and from Associazione Italiana per la Ricerca sul Cancro (AIRC) to A.S.

ABSTRACT

Dystroglycan (DG) is an adhesion molecule formed by two subunits, α (extracellular) and β (transmembrane) DG, which are codified by a single gene and form a continuous link from the extracellular matrix to the intracellular cytoskeleton. Reduction or loss of expression of DG has been observed in human cancer cell lines and primary tumors and has been suggested to promote tumor development and invasiveness.

In this study, the human breast epithelial non-tumorigenic MCF10F and the breast cancer MCF7 cell lines were engineered to stably express an exogenous DG cDNA and the effects on the phenotype of both cell lines were evaluated. The MCF10F transfected cells displayed an increased expression of both DG subunits which was associated with inhibition of the anchorage-dependent growth, accumulation of cells in the G_0/G_1 phase of the cell cycle and increased adhesion to a substratum. The MCF7 transfected cells were unable to restore α-DG despite an increased expression of the β-DG subunit. Anchorage-dependent and independent growth and the in vivo tumorigenicity were reduced in these derivatives that also displayed a reduced adhesion to a substratum and were shown to release α-DG in the culture medium.

These findings confirm and extend previous evidence that transformation of mammary epithelial cells is associated with loss of their ability to retain α-DG on the cell membrane. Moreover, they indicate that DG is involved in cell functions other than cell adhesion to the extracellular matrix, and that its loss of function might predispose to tumor progression by compromising regulatory controls over cell growth and proliferation.

INTRODUCTION

Interactions with the extracellular matrix (ECM) binding partners represent the critical steps by which cells initiate intracytoplasmic signaling essential for the regulation of their growth, differentiation, attachment and migration, and are important factors in the development and progression of many types of cancer.[1,2] Although studies of cell-ECM interactions have mainly focused on integrins, the role of other non-integrin receptors cannot be excluded and is becoming progressively more important.[1,2] A major non-integrin adhesion molecule is dystroglycan (DG), a pivotal component of the dystrophin-glycoprotein complex, that is expressed in skeletal muscle and in a wide variety of tissues at the interface between the basement membrane and the cell membrane. DG is involved in multiple biological functions, such as skeletal muscle cell stability, maturation of postsynaptic elements in the central and peripheral nervous system and early morphogenesis.[3-5] Moreover, DG has been reported to play a role in cytoskeletal organization, cell polarization and restriction of growth in response to basement membrane proteins in epithelial cells.[6,7]

DG is encoded by a single gene and is formed upon cleavage of a precursor protein into two mature subunits which form a tight non-covalent complex.[6,8] The highly and heterogeneously glycosylated cell surface-associated α-DG binds extracellular matrix molecules, such as laminins and agrin. The transmembrane β-DG anchors α-DG to the cell membrane and is linked to the actin cytoskeleton via dystrophin or its paralogue utrophin.[3,6,9]

We and others recently demonstrated that DG expression, and mainly α-DG, is reduced or lost in a variety of human cancer cell lines[7,10,11] and in primary breast, colon and prostate cancers.[11,12] It has been also observed that a reduction in the expression levels of DG is most pronounced in high-grade diseases[11,12] and has a prognostic significance in breast cancer patients.[11] Although the exact molecular mechanisms have not been identified, yet regulation of DG expression appears to occur at a post-transcriptional level both in primary tumors and cancer cell lines.[7,10,11,13] However, the exact role of DG in the regulation of mammary epithelial cell growth and tumorigenesis remains largely unknown.

To address the effects of DG expression levels on the phenotype of breast normal and cancer cells, in this study we obtained derivatives of the MCF7 human breast cancer and of the MCF10F non-tumorigenic mammary epithelial cell line that stably express an exogenous DG cDNA. We found that DG overexpression inhibits the growth of both cell lines. The anchorage-independent growth and tumorigenicity of the MCF7 cells were also inhibited. The implications of these findings are discussed.

MATERIALS AND METHODS

Cells and Cell Culture. The spontaneously immortalized human mammary epithelial cell line MCF10F14 was routinely cultured in a 1:1 (vol:vol) mixture of DMEM and Ham's F12 medium supplemented with 0.5 µg/ml hydrocortisone, 0.1 µg/ml cholera toxin, 10 µg/ml insulin, 20 ng/ml Epidermal Growth Factor (all from Sigma, St. Louis, MO) and 5% horse serum (Gibco, Merelbeke, Belgium). The HC11 mouse mammary epithelial cell line was clonally derived from a spontaneously immortalized mammary epithelial cell culture originally established from a midterm pregnant BALB/c mouse[15] and was grown and maintained in RPMI-1640 medium (RPMI) (Gibco) supplemented with 10% heat inactivated Fetal Bovine Serum (FBS). The MCF7 cells were obtained from the American Type Culture Collection and cultured according with the instructions of the supplier.

Cloning of DG cDNA, Construction of Expression Vectors and Transfection Procedure. The full-length mouse DG cDNA (2,7 Kb), including its signal peptide, was obtained from the HC11 cell line using standard reverse transcriptase polymerase chain reaction (RT-PCR) protocols, as previously described.[16] Total RNA was extracted from exponentially growing HC11 cells using the RNeasy Mini kit (Qiagen, Hilden, Germany), in accordance with the manufacturer's instructions. First strand cDNA was then synthesized using the Enhanced Avian RT-PCR kit (Sigma) and used as a template for PCR. The sequences of the PCR primers were: M-start (forward) 5'-CCC GAA TTC ATG TCT GTG GAC AAC TGG CTA CTG -3' and M-stop (reverse) 5'-CCC GAA TTC TTA AGG GGG AAC ATA CGG AGG GGG- 3'. *EcoRI* target sequences are reported in bold. PCR reactions (50 µl volume) were performed in a GeneAmp PCR System 2400 temperature cycler (Perkin Elmer) using 10 ng of cDNA as template, and 2.5 U of AccuTaq DNA polymerase (Sigma). After an initial denaturation at 95°C for 15 min, 30 cycles of PCR amplification were performed, each consisting of a denaturing step of 96°C for 45 sec, annealing at 60°C for 45 sec and extension at 72°C for 210 sec, followed by a final step at 72°C for 10 min. The amplified fragments were detected by 1% (W/v) agarose gel electrophoresis and staining with 0.3 mg/ml ethidium bromide (Sigma, St. Louis, MO). Upon purification, the 2,7 Kb DNA fragment corresponding to full length mouse DG cDNA was subcloned into the EcoRI site of the eukaryotic expression vector pcDNA3 in the sense orientation and its correct sequence was verified by complete sequence analysis. The resulting pcDNA-DG plasmid, or the control vector pcDNA3, were transfected into the MCF7 or the MCF10F cells using GeneJammer (Stratagene, La Jolla, CA). The transfected cells were selected by growth in 700 µg/ml of G418 (Boehringer Mannheim Corporation, Indianapolis, IN) for 15 days. G418 resistant colonies were then pooled, expanded and analyzed for α-DG expression. The pools showing a significant increase in DG expressions were used for these studies.

Preparation of Purified α-DG. Native α-DG was been isolated from chicken skeletal muscles,as previously described.[17] Briefly, 10 g of freshly frozen muscle was homogeneized in 40 ml of lysis buffer (0.2 M NaCl, 50 mM Tris, 2.5 mM N-ethylmaleimide, 1 mM phenylmethanesulfonyl fluoride, 1 µg/ml leupeptine and benzamidine). After centrifugation (15000 rpm) the supernatant was filtered using a Whatman filter paper and loaded on a DEAE-Sepharose Fast Flow (Pharmacia) column (2x10cm) equilibrated with lysis buffer, at 4°C. After extensive washing, the protein was eluted with two column volumes of the same buffer containing 0.5 M NaCl. The eluted solution was applied directly to a 10 ml wheat-germ lectin (WGL) affinity column (Sepharose 6MB, Pharmacia), equilibrated with the 0.5 M containing NaCl buffer. WGL is a well-known glycoprotein binding agent which was shown to have a high affinity towards α-DG.[17] After washing (with approximately ten column volumes) elution was carried out with two volumes of the same buffer containing 0.25 M N-acetyl-glucosamine. After extensive dialysis against H_2O, the α-DG solution was lyophilized and then quantitated using a spectrophotometrical assay kit (Protein Assay, Bio-Rad).

Growth Studies. The exponential doubling times and saturation densities were determined essentially as previously described.[18,19] Briefly, cells were plated at a density of 1 x 10^4 cells per 35 mm diam. well in triplicate. Every two days the cultures were refed with fresh medium and the number of cells per well was determined every day using a Coulter counter. The doubling times were calculated from the initial exponential phase of the growth curves and the saturation densities from the plateau of the growth curves. Plating efficiency assays were performed by seeding 1000 cells per 10 cm dish in complete medium. Cells were refed with fresh medium every three-four days for about three weeks. The cells were then fixed and stained with Giemsa and the number of grossly visible colonies was counted. All assays were performed in triplicate and all experiments were repeated several times and gave similar results.

Flow Cytometric Analysis. Exponentially growing cells were collected, washed with PBS and fixed in 5 ml of 70% ethanol and stored at 4°C.[18,19] For the analysis, cells were collected by centrifugation and the pellets were resuspended in 0.2 mg/ml of propidium iodide in Hank's balanced salt solution containing 0.6% NP-40 and RNase (1 mg/ml). The cell suspension was then filtered and analyzed for DNA content on a Coulter EPICS 753 flow cytometer. The percent of cells in different phases of the cell cycle was determined using a ModFit 5.2 computer program. Assays were repeated at least three times and gave similar results. The data reported are the results of a typical experiment.

Cell Attachment Assay. Cells were plated at 60,000 cells/well in six-well tissue culture plates pretreated with 10 mg/ml Matrigel (Becton Dickinson) for 1 hr at 37°C, followed by blocking with 1% BSA for 1 hr. Cells were allowed to adhere and at different time points (from 30 min to 6 hours after plating) non-attached cells were washed away with PBS and shaking and the remaining attached cells were counted using a Coulter counter. Cell adhesion was determined for each derivative compared with parental and vector control cells. The assay was performed in complete medium in triplicate. Conditioned media (72 hours) were collected from subconfluent cultures and concentrated 10 times by liophylization. To deplete them of DG, 50 ml of conditioned media were first dialyzed against H_2O and then incubated with 5 ml of WGL-resin (Pharmacia), equilibrated in PBS buffer, overnight at 4°C. Upon a mild centrifugation step (2000 rpm), the supernatant was collected and liophilysed. For the assay shown in Figures 7 and 8, conditioned media were added at the indicated percent to regular medium and the number of attached cells was evaluated after six hours.

Soft Agar and Tumorigenicity Assays. Anchorage independent growth was determined by soft agar analysis, as previously described.[19,20] Briefly, 1 ml of 0.5% agar in complete medium was placed in each 35 mm well of 6 well plates. Then 2 ml of 0.3% agar in complete medium containing 1 x 10^5 cells were layered on top of the solidified layer of bottom agar. Colony formation was monitored up to 3 weeks and the final numbers of colonies larger than 0.05 mm diam. were determined.

Tumorigenicity assay was performed as described previously.[19] Briefly, cells (5 x 10^6) were injected subcutaneously into multiple sites in athymic (nude) mice. Each vector control and DG overexpressing derivative was injected in twenty independent sites (4 sites/mouse). The animals were monitored for tumor formation every week and sacrificed 2 months later. Tumor length (L) and width (W) were measured at the end of the experiment and tumor volume was calculated by the formula (L x W^2)/2.

Total Protein Extraction and Western Blot Analysis. Exponentially growing cultures of each cell lines were collected by cell scraping and cell pellets were added to 3-5 volumes of sonication buffer containing proteases and phosphatase inhibitors (20 mM Tris-HCl pH 7.4, 2 mM EGTA, 6 mM

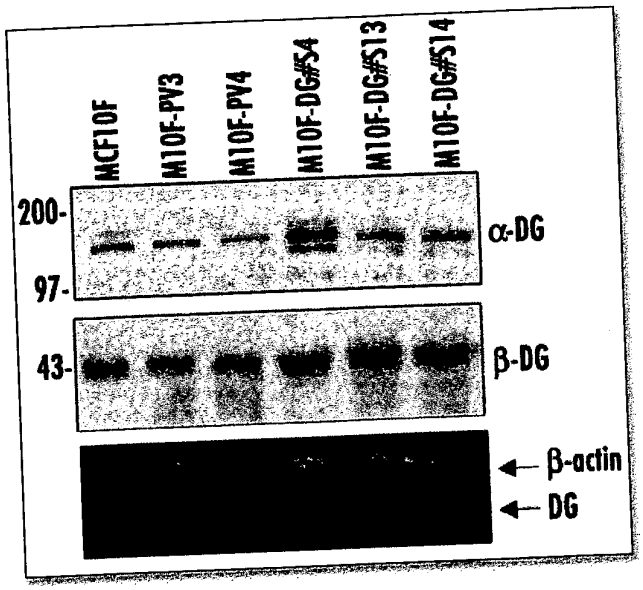

Figure 1. Constitutive overexpression of DG in the MCF10F human non-tumorigenic mammary epithelial cell line. Western blot analysis of α- (top panel) and β- (middle panel) DG expression in the MCF10F cells, vector controls (M10F-PV3 and M10F-PV4) and DG-overexpressing derivatives (M10F-DG#S4, S13 and S14). The polyclonal anti-α-DG antibody recognizing the N-terminal region of the protein was used to detect α-DG. Bottom panel, Reverse transcriptase polymerase chain reaction (RT-PCR) analysis of DG gene expression in the same cell lines, amplifying β-actin (as internal control) with DG. The sizes of the specific RT-PCR products were 550 bp for β-actin and 485 bp for DG.

Table 1 **Cell Cycle Distribution, Saturation Density and Plating Efficiency of DG-Overexpressing Derivatives (DG#S4, S13, S14) Compared to Vector Control (PV1 and 2) and Parental MCF10F Human Non-Tumorigenic Mammary Epithelial Cells**

			Cell Cycle distribution*				
Cell lines	D.T. (h)[a]	S.D. (x10 ^{6})#	G_0/G_1	S	G_2	P.E. (%)	A.I.G. (%)
MCF10F	29.2 ± 3	2.7 ± 0.2	52.6	31.9	15.5	6.7 ± 1	0
M10F-PV3	28.5 ± 2	3.3 ± 0.2	50.4	33.9	15.7	6.5 ± 1	0
M10F-PV4	28.4 ± 3	2.8 ± 0.3	52.6	34.9	12.5	5.3 ± 1	0
M10F-DG#S4	33.2 ± 3	2.2 ± 0.1	62.4	25.6	12.0	9.5 ± 2	0
M10F-DG#S13	34.6 ± 4	1.5 ± 0.1	70.2	20.2	9.6	9.8 ± 2	0
M10F-DG#S14	33.8 ± 5	1.7 ± 0.05	67.6	23.4	9.1	10.7 ± 3	0

[a]D.T. = Doubling time, corresponds to the initial exponential phase of cell growth; S.D. = Saturation density, represents the total number of cells per 35-mm well when the cultures reached a plateau; P. E. = Plating efficiency; A.I.G. = Anchorage independent growth, expressed as colony forming efficiency in soft agar; Values for D.T., S.D., P.E. and A.I.G. indicate the mean ± SD (n = 6). *Exponentially growing cultures of the indicated cell lines were analyzed by flow cytometry. The values represent the percentage of the total cell population in each phase of the cell cycle.

β-mercaptoethanol, 1% NP40, 0.1% SDS, 50 mM NaF, 15 μg/ml benzamidine, 10 μg/ml aprotinin, 10 μg/ml leupeptin and 1 mM phenylmethylsulfonyl fluoride) and sonicated at 4°C, as previously described.[11,19,21] Homogenates were incubated in ice for 30 minutes and then centrifuged at 14000 rpm for 15 min at 4°C. The supernatants were assayed for protein content and 50 μg of protein from each sample were separated by SDS-PAGE and transferred to immobilon-P membranes (Millipore, Bedford, MA) at 100 volts for 1 hour at 4°C. Immunodetection was performed using the enhanced chemiluminescence kit for western blotting detection (Amersham Pharmacia Biotech, Freiburg, Germany) and multiple film exposure for different lengths of time were made to establish a linear range. Bands were analysed on the image analysis system Gel Doc 200 System (Biorad Laboratories S.r.l., Milan, Italy) and quantitated using the Quantity One Quantitaton Software (Biorad).

Immunoreagents. The monoclonal antibodies to α-DG (clone VIA4-1) and to β-DG (clone 43DAG/8D5) were obtained from Upstate Biotechnology (Lake Placid, NY) and from Novocastra (Newcastle, UK), respectively and were used as previously described.[11] The polyclonal antibody to α-DG was raised in rabbits immunised with a recombinant fragment spanning the N-terminal region of mouse α-DG (30-315)[22] and was previously shown to be able to detect α-DG protein in western blot analysis.[23]

Semiquantitative Reverse Transcriptase Polymerase Chain Reaction (RT-PCR) Analysis. Total RNA was extracted from exponentially growing cultures of each cell line using the RNeasy Mini kit (Qiagen, Hilden, Germany), in accordance with the manufacturer's instructions and the RNA samples were reverse transcribed using the One-step RT-PCR kit (Qiagen).

PCR was performed using the Gene Amp PCR Systems 9600 (Perkin-Elmer Corp., Norwalk, CT, USA). The following DG-specific primers, which amplify both human and mouse DG cDNA, were used: DAGMH (forward) 5'-GGAGAACCCAACCAGCGCCCAGAGC-3' and DAGAH (reverse) 5'-CGGGTGATATTCTGCAGGGTGATGG-3' which amplify a 485-bp region covering the C-terminal region of α-DG and the N-terminal region of β-DG. A second primer pair: forward 5'-TCACCCACACTGTGCCCATCT-3' and reverse 5'-ACGGAGTACTTGCGCTCAGG-3' were used to amplify a 550-bp region of the β-actin transcript. After an initial denaturation at 95°C for 15 min, 20 cycles of PCR amplification were performed, each consisting of a denaturing step of 94°C for 45 sec, annealing at 55°C for 30 sec and extension at 72°C for 1 min, followed by a final step at 72°C for 10 min. The number of twenty cycles was selected because in preliminary experiments we verified that with this number of cycles the reaction was still in a linear range for both genes (data not shown). The amplified fragments were detected by 3% (W/v) agarose gel electrophoresis and staining with 0.3 mg/ml ethidium bromide (Sigma, St. Louis, MO).

Statistical Analysis. Mean values were compared using the Student t-test and the two-tailed P value was reported. The Mann-Whitney test was used to determine the statistical significance between the median tumor volumes of the vector control and DG-overexpressing pools. Calculations were performed using the STATA 6.0 statistical software package (Stata Corporation, College Station, Texas) and the results were considered statistically significant when the p value was ≤ 0.05.

RESULTS

Transfection and Expression of an Exogenous DG cDNA in the MCF10F Cells. The MCF10F human non-tumorigenic mammary epithelial cell line was transfected with the pcDNA3 mammalian expression vector or its derivative pcDNA-DG containing a full length DG cDNA sequence in the sense orientation. Following G418 selection, pools of thousands of resistant colonies were obtained both from the cultures transfected with the pcDNA-DG construct and those transfected with the pcDNA3 vector (vector control cells) and analyzed for the expression of α- and β-DG by western blot analysis.

We choose two vector control pools (M10F-PV3 and M10F-PV4) and three DG-overexpressing derivatives (M10F-DG#S4, S13 and S14) for further studies. Densitometric analysis of western blots indicated that expression of both α- and β-DG was increased more than three fold in the DG-overexpressing derivatives compared to the vector control pools (Fig. 1). To further confirm the expression of the exogenous DG cDNA in the

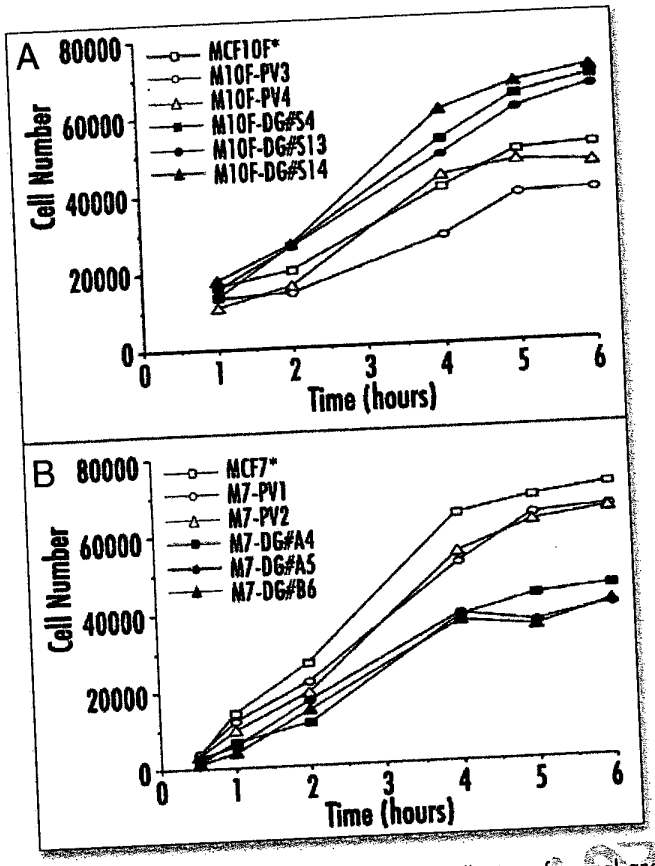

Figure 2. Effects of DG-overexpression on cell adhesion of normal and cancer mammary epithelial cells. Vector control and DG-overexpressing derivatives of the MCF10F (A) and MCF7 (B) cell lines were seeded in well plates precoated with Matrigel and allowed to attach for the indicated times when the number of adherent cells was assessed by cell counting. The assay was repeated four times in triplicate and standard deviation was lower than 20% at all time points. *Mean values were significantly different ($p < 0.01$) between DG overexpressing and vector control cells at all time points for both cell lines.

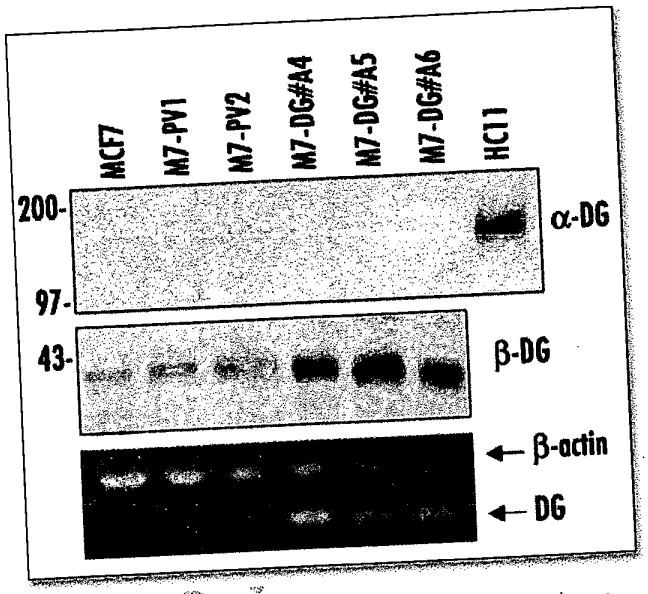

Figure 3. Constitutive overexpression of DG in the MCF7 human breast cancer cell line. Western blot analysis of α- (top panel) and β- (middle panel) DG expression in the MCF7 cells, vector controls (M7-PV1 and M7-PV2) and DG-overexpressing cells (M7-DG#A4, A5 and B6) were performed as described in Figure 1 legend. The HC11 mouse mammary epithelial cells that express high levels of α-DG were also included as a positive control for the anti-α-DG antibody. *Bottom panel*, RT-PCR analysis of DG gene expression in the same cell lines, as in Figure 1.

DG-overexpressing derivatives, DG mRNA expression level was evaluated in the same cell lines by semi-quantitative RT-PCR analysis, as previously described.[11] Briefly, primers which amplify a sequence encompassing both α-and β-DG were used for PCR amplification of cDNA prepared from exponentially growing cultures of vector control and DG-overexpressing derivatives. The results of the RT-PCR analysis confirmed the correct size of the overexpressed DG mRNA whose expression level was significantly increased in the DG-overexpressing derivatives (Fig. 1, bottom panel).

Overexpression of DG Inhibits Cell Growth and Increases Adhesion of the MCF10F Normal Mammary Epithelial Cells. Overexpression of DG did not alter the morphology of the MCF10F cells (data not shown). Cell cycle parameters were examined in exponentially growing cultures of the MCF10F control and DG-overexpressing cells by FACS (fluorescence-activated cell sorting) analysis. The DG-overexpressing pools displayed an increase in the percentage of cells in the G_0/G_1 phase of the cell cycle (range 62–70 vs 50–53%) associated with a reduction in the percentage of cells in the S phase (range 20–26 vs 32–35%) when compared with the vector control cells (Table 1). It is noteworthy that we also observed the presence of a subdiploid peak (about 10%), indicative of apoptosis, in the DG-overexpressing derivatives of the MCF10F cells (data not shown). The DG-overexpressing derivatives also displayed a lengthening of the doubling time (about 34 vs 29 h) associated with a reduction of the saturation density (about 1.8 vs 2.9 x 10^6 cells) compared to vector control cells (Table 1). On the other hand, the plating efficiency was increased in the same derivatives (about 10 vs 6%) (Table 1). The differences for each of these parameters were highly reproducible and were significant when each of the vector control cell line was compared with any of the DG-overexpressing derivatives ($p < 0.05$).

DG forms a physical link between the extracellular matrix (ECM) and intracellular cytoskeleton and mediates adhesion of cells to ECM components.[24] Thus, it was of interest to verify whether overexpression of an exogenous DG cDNA could affect adhesion of normal mammary epithelial cells to ECM.

Asynchronous adherent cultures of vector control and DG-overexpressing derivatives of the MCF10F cells were trypsinized and replated in matrigel-precoated plates. Matrigel is a solubilized basement membrane preparation extracted from the Engelbreth-Holm-Swarm mouse sarcoma, a tumor rich in ECM proteins, whose major component is laminin.[25] Cells were allowed to adhere and the number of attached cells was determined at various times thereafter. As shown in Figure 2A, DG-overexpressing cells displayed an increase of cell adhesion, evaluated as resistance of cells to detachment, which was already evident (about 16%) 1 hour after plating and improved thereafter (about 50% after six hours) (Fig. 2A) being always significantly different compared to vector control cells at all time points ($p<0.01$). Confirmatory results were obtained evaluating the number of attached cells by the MTT test (data not shown).

Transfection and Expression of an Exogenous DG cDNA in the MCF7 Cells. The MCF7 breast cancer cell line, that displays a reduced expression of β-DG with loss of expression of the α-DG subunit,[7,10,11] was transfected with the pcDNA3 vector or its derivative pcDNA-DG, as previously described, and pools of thousands of resistant colonies, both from the cultures transfected with the pcDNA-DG construct and the cultures transfected with the pcDNA3 vector (vector control cells), were analyzed for the expression of α- and β-DG by western blot analysis.

Interestingly, while an increase in β-DG expression level was easily detected in the MCF7 cells transfected with the pcDNA-DG construct, we were not able to detect the expression of α-DG in any of the DG-transfected

Table 2 **Cell Cycle Distribution, Daturation Density and Plating Efficiency of DG-overexpressing Derivatives (DG#A4, A5, B6) Compared to Vector Control (PV1 and 2) and Parental MCF7 Breast Cancer Cells**

Cell lines	D.T. (h)[a]	S.D. (x10^6)	Cell Cycle distribution* G_0/G_1	S	G2	P.E. (%)	A.I.G. (%)
MCF7	27.5 ± 2	4.2 ± 0.6	49.8	38.1	12.1	27 ± 4	17.2 ± 3
M7-PV1	28.3 ± 2	4.6 ± 0.5	50.0	34.5	14.5	27 ± 3	18.4 ± 4
M7-PV2	27.9 ± 3	4.2 ± 0.4	51.6	32.8	15.6	25 ± 5	22.5 ± 5
M7-DG#A4	37.2 ± 6	1.5 ± 0.3	62.2	24.6	13.2	14 ± 2	11.5 ± 3
M7-DG#A5	35.3 ± 3	1.7 ± 0.2	62.0	26.1	11.9	5 ± 1	10.2 ± 2
M7-DG#B6	33.7 ± 4	1.7 ± 0.4	54.5	29.4	16.1	18 ± 3	10.5 ± 3

[a]D.T. = Doubling time, corresponds to the initial exponential phase of cell growth; S.D. = Saturation density, represents the total number of cells per 35-mm well when the cultures reached a plateau; P. E. = Plating efficiency; A.I.G. = Anchorage independent growth, expressed as colony forming efficiency in soft agar. Values for D.T., S.D., P.E. and A.I.G. indicate the mean ± SD (n = 6). * Exponentially growing cultures of the indicated cell lines were analyzed by flow cytometry. The values represent the percentage of the total cell population in each phase of the cell cycle.

pools. It is noteworthy that α-DG was not detectable in the MCF7-transfected cells using either the monoclonal anti α-DG antibody which recognizes carbohydratic epitopes on the α-DG molecule and the polyclonal anti-α-DG antibody which specifically recognizes and binds the N-terminal region of the α-DG aminoacidic chain (Fig. 3 and data not shown). We selected two vector control pools (M7-PV1 and 2) and three DG-overexpressing pools (M7-DG#A4, #A5 and #B6) of the MCF7 for the studies described below. As for the MCF10F cells, densitometric analysis of western blots indicated that β-DG expression was increased more than three fold in the DG-overexpressing derivatives of the MCF7 cells compared to the vector control pools (Fig. 3).

The RT-PCR analysis confirmed the correct size of the overexpressed DG mRNA whose expression level was significantly increased in the DG-overexpressing derivatives (Fig. 3, bottom panel).

Overexpression of DG Inhibits Cell Growth and Adhesion of the MCF7 Breast Cancer Cells. Overexpression of DG did not alter the morphology of the MCF7 cells (data not shown). Analysis of cell cycle parameters by FACS in exponentially growing cultures of the MCF7 control and DG-overexpressing cells demonstrated an increase in the percentage of cells in the G_0/G_1 phase of the cell cycle (about 60 vs 50%) and a decrease in the percentage of cells in the S phase (about 27 vs 35%) in the DG-overexpressing derivatives of the MCF7 cells compared with the corresponding vector control cells (Table 2). No subdiploid peak was observed in the DG-overexpressing derivatives of the MCF7 cells (data not shown). The same derivatives also displayed a longer doubling time (about 35 vs 28 h) and a reduced saturation density (about 1.6 vs 4.3 x 10^6 cells). However, unlike the MCF10F derivatives, the DG-overexpressing MCF7 cells displayed a reduction of the plating efficiency when compared with the corresponding vector control cells (about 11 vs 19%) (Table 2). Although not dramatic, the differences for each of these parameters were highly reproducible and were significant when each of the vector control cell line was compared with any of the DG-overexpressing derivatives ($p<0.05$).

When analyzed in the cell adhesion assay on matrigel-coated dishes, the DG-overexpressing derivatives of the MCF7 cells displayed a decrease of their strength to adhere to the substratum, as indicated by the decrease in their resistance to detachment, which was already significantly lower (about 48%) at 30' after plating and remained significantly lower than vector control cells at all the time points ($p<0.01$) (Fig. 2B). Similar results were obtained evaluating the number of attached cells by the MTT test (data not shown).

Overexpression of DG Reduces Anchorage-independent Growth and Tumorigenicity in the MCF7 Breast Cancer Cells. As shown in Table 2, when grown in suspension in 0.3% agar in complete medium, the MCF7 and the vector control M7-PV cells formed large colonies with a colony-forming efficiency of about 19%. We found that expression of an exogenous DG cDNA significantly decreased the anchorage-independent growth of the MCF7 cells: in fact, colony-forming efficiency in soft agar of the three DG-overexpressing pools was about 11% and the average colony size was smaller than that seen with the vector control cells (Table 2 and Fig. 4A).

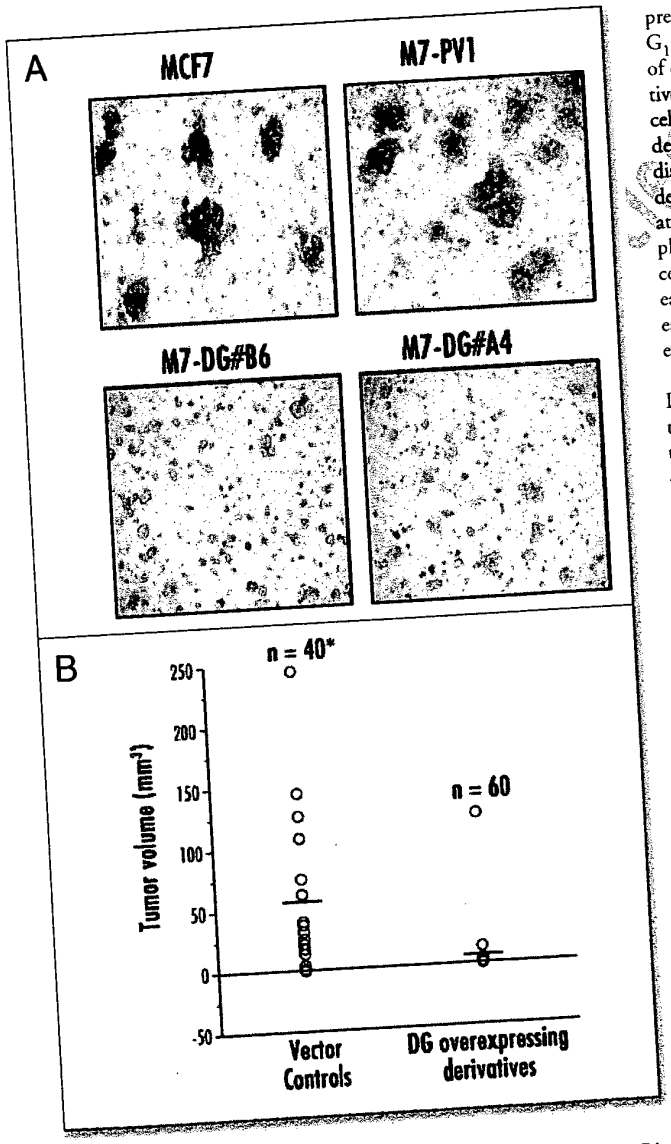

Figure 4. (A) Effects of stable DG-overexpression on the anchorage-independent growth of the MCF7 breast cancer cell line. Representative examples of the growth in soft agar of the DG-overexpressing derivatives (M7-DG#A4 and M7-DG#B6) compared with a vector control (M7-PV1) and parental MCF7 cells. (B) Effects of stable overexpression of DG on the in vivo tumorigenicity of the MCF7 breast cancer cells in nude mice. Cells (5 x 10^6) from exponentially dividing cultures of each vector and DG-overexpressing pools were injected s.c. into multiple sites in athymic (nude) mice. The animals were monitored for tumor formation up to 2 months when they were sacrificed and tumor volumes were calculated. *Mean values for each group, shown by horizontal lines, were significantly different ($p < 0.001$).

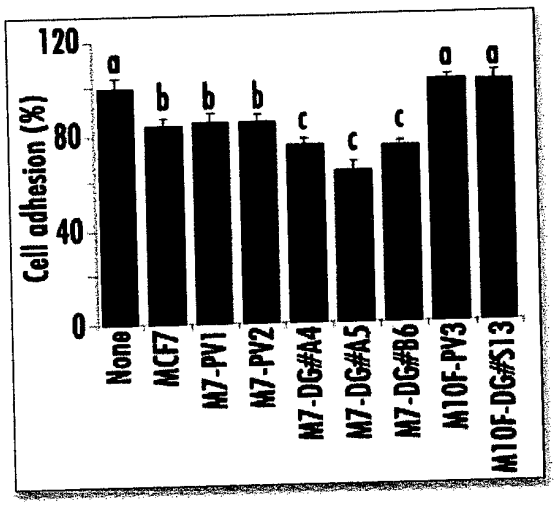

Figure 5. Effects of conditioned media from MCF7 and DG-overexpressing derivatives on epithelial cell adhesion. The HC11 non-tumorigenic immortalized mouse mammary epithelial cells, that express high levels of α-DG, were plated on tissue culture plates coated with Matrigel and were allowed to adhere. Cells were resuspended in media containing 5% of the concentrated conditioned medium from the indicated cell line. After 6 hours non-attached cells were washed away with PBS and shaking and the remaining attached cells were counted. The results are expressed relative to the values obtained in the absence of conditioned medium (None). Shown are the mean ± S.D. of six determinations, each performed in triplicate. Values corresponding to columns not sharing the same letter were significantly different ($p < 0.05$).

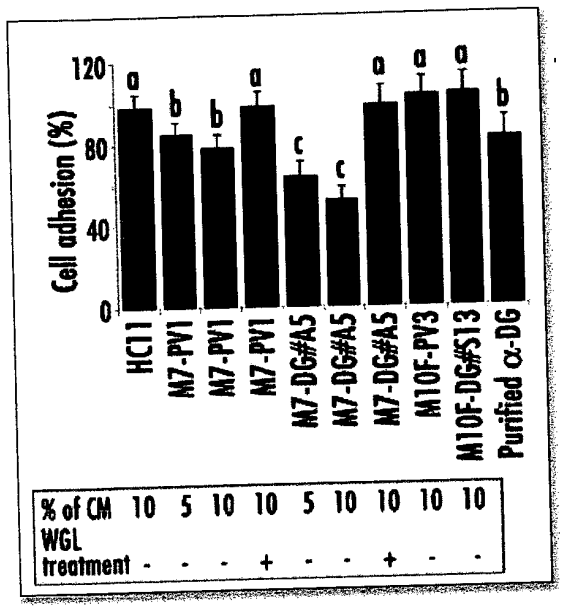

Figure 6. Depletion of DG prevents inhibition of cell adhesion due to conditioned medium of MCF7 vector and DG-overexpressing derivatives. The HC11 non-tumorigenic immortalized mouse mammary epithelial cells, that express high levels of α-DG, were plated on tissue culture plates coated with Matrigel and were allowed to adhere. Cells were resuspended in media containing the indicated percent of the concentrated conditioned medium from the indicated cell line. Passage through a WGL column was used in some cases (+) to deplete conditioned media of α-DG. After 6 hours non-attached cells were washed away with PBS and shaking and the remaining attached cells were counted. The results are expressed relative to the values obtained in the absence of conditioned medium. Purified α-DG was used at a concentration of 1ng/μl in this experiment. Shown are the mean ± S.D. of six determinations, each performed in triplicate. Values corresponding to columns not sharing the same letter were significantly different ($p < 0.05$).

Since anchorage-independent growth is the in vitro assay that best correlates with the in vivo tumorigenicity, these results suggested that increased expression of the DG protein might reduce tumorigenicity of the MCF7 cells. To verify this hypothesis, tumorigenicity of the DG-overexpressing derivatives was assayed in nude mice, compared with vector control cells, by s.c. injection of 5×10^6 cells/injection site. As expected, the M7-PV cells produced tumors in all of the injection sites (n = 40) with a volume ranging between 4 and 245 mm^3 (mean: 54.3; median: 39). The DG-overexpressing cells displayed a dramatically reduced tumorigenicity: in fact, tumors developed only in 19 of the 60 injection sites and were significantly smaller than in the corresponding vector control cells (range 1 to 126 mm^3; mean: 4.6; median: 0) ($p < 0.001$) (Fig. 4B).

α-DG is Secreted in the Culture Medium of Cancer but not Normal Mammary Epithelial Cells. The reduced tumorigenicity of DG-overexpressing derivatives of the MCF7 cells could be explained by the reduced proliferation rate, plating efficiency and anchorage-independent growth. However, it was not apparent why, despite the fact that these cells constitutively expressed high levels of the DG mRNA and β-DG protein, they did not display an increased expression of α-DG and an increased cell adhesion. As mentioned above, this was likely not due to our inability to detect α-DG since we used two different antibodies, one directed against carbohydratic epitopes of the protein and the other directed against the aminoacidic chain. Thus, another possibility was that cancer cells secrete α-DG rather than retain it on the membrane. We were unable to detect the presence of a clear band corresponding to the correct size of the α-DG protein in the medium of the MCF7 cell line and its DG-overexpressing derivatives (data not shown). This might be due to the presence of several unrelated serum proteins in the medium which mask the α-DG-specific signal although it cannot be excluded that the secreted α-DG is degraded and thus present in form of smaller fragments in the extracellular medium. To test this hypothesis, we evaluated the ability of conditioned medium from MCF7 cells to inhibit the adhesion to matrigel-coated dishes of the HC11 mouse mammary epithelial cells that express high levels of α-DG.[11] In fact, several evidence suggest that DG plays an important role in modulating attachment of cells to matrigel.[24,26] We found that the conditioned medium from the MCF7, but not from the MCF10F cells, caused a significant inhibition of cell adhesion to matrigel-coated dishes (Fig. 5). We then tested the conditioned media from the DG-overexpressing derivatives of the MCF7 cells and found that they exerted a significantly higher inhibition of cell adhesion thus suggesting that part or all of the overexpressed α-DG is likely released in the medium, although other unknown mechanism could not be excluded (Fig. 5). No inhibition was observed with conditioned media from the DG-overexpressing derivatives of the MCF10F cells (Figs. 5 and 6 and data not shown). To further verify that the effect of conditioned media to inhibit cell adhesion was due to α-DG, conditioned media from MCF7 vector control and DG-overexpressing derivatives were depleted of DG using WGL, which specifically binds and retains the α-DG protein.[17] Depletion of α-DG was able to abolish the conditioned media-induced inhibition of cell adhesion of both MCF7 vector and DG-overexpressing derivatives (Fig. 6). The likely involvement of α-DG released in the medium in mediating the inhibition of cell adhesion is further supported by the observation that addiction of purified α-DG protein to cell culture inhibited adhesion of the HC11 cells to matrigel-coated dishes in a dose-dependent fashion (Fig. 6 and data not shown).

DISCUSSION

Cell adhesion to extracellular matrix (ECM) binding partners is a requirement for cell growth and survival for a wide variety of cell types. Moreover, interaction between cancer cells and the ECM is known to influence tumor outcome and its disruption might provide a mechanism by which certain tumor types are prone to invade surrounding tissues and metastasize.[27] Dystroglycan (DG), a ubiquitously

expressed integral membrane glycoprotein, links the ECM to the actin cytoskeleton, thus providing structural integrity and perhaps transducing signal, in a manner similar to integrins.[6,28-32] It has been hypothesized that loss of DG expression might play an important role in tumor development by altering the interactions between cells and the surrounding matrix.[7,10-12] From this point of view, DG might act as a tumor suppressor gene and its loss of function could influence the formation of strong contacts between basement membranes and the cytoskeleton of cells, thus favoring tumor development and invasiveness. The exact role of DG in the process of tumor development and in the maintenance of the malignant phenotype, however, remains to be defined.

This study demonstrates that increasing the expression of DG markedly inhibited the anchorage-dependent growth and proliferation of the MCF10F human non-tumorigenic mammary epithelial cells (Table 1). Similarly, overexpression of an exogenous DG cDNA in the MCF7 human breast cancer cell line was associated with inhibition of cell growth and proliferation and with a marked reduction of the anchorage-independent growth and of the in vivo tumorigenicity (Table 2 and Fig. 4).

The MCF10F cell line, established from the mammary gland tissue, has retained important characteristics of normal mammary epithelium and has proven to be an invaluable in vitro model for characterizing molecular events involved in proliferation, differentiation and transformation of mammary epithelial cells.[14,19] The MCF7 breast cancer cell line is one of the most well characterized human breast cancer cell line, is widely used as an in vitro model of breast cancer and was selected because, as the majority of human breast cancer cell lines, it does not express α-DG and displays a reduced expression of the β-DG subunit.[7,10,11] Thus, we believe that the results presented in this study are representative of both normal and transformed mammary epithelial cells and are valuable for a better understanding of the role played by DG in the regulation of growth in both normal and transformed cells.

To our knowledge, this is the first report analyzing the effects of DG overexpression on the phenotype of non-transformed mammary epithelial cells. Inhibition of cell growth observed in the DG-overexpressing derivatives of the MCF10F cell line was associated with an accumulation of cells in the G_0/G_1 phase of the cell cycle and a reduction of cells in the S phase (Table 1). This finding is consistent with previous data demonstrating that overexpression of DG caused a decreased growth rate in vascular endothelial cells.[33] It is also consistent with recent data demonstrating that DG is a suppressor of integrin-mediated extracellular signal-regulated kinase (ERK) activation[34] and with the observation that α-DG-dependent signal transduction pathway can stimulate differentiation, thus inhibiting proliferation of both muscle[26] and epithelial[7,35] cells. Cell adhesion to matrigel-coated dishes, as well as plating efficiency, was also increased in the DG-overexpressing derivatives of the MCF10F cells, as compared to control cells (Table 1 and Fig. 2A). Matrigel is a solubilized basement membrane preparation rich in laminin.[25] Thus, this finding is an agreement with the well known role of α-DG in mediating cell interaction with ECM mainly through binding to laminin.[24]

In this study, for the first time the effects of DG overexpression were evaluated in parallele and in detail on the phenotype of both transformed and non-transformed mammary epithelial cells. An interesting finding was that overexpression of an exogenous DG cDNA was not able to restore α-DG expression in the MCF7 breast cancer cell line. The mechanisms responsible for the loss of α-DG in breast cancer cells remain unknown. We believe it is due to a post-transcriptional event and is likely a consequence of the lack of membrane targeting of α-DG in these cells. Indeed, we were unable to restore expression of the α-DG protein in the DG-overexpressing derivatives of the MCF7 cells, despite the fact that they expressed increased levels of the DG mRNA and of the β-DG protein (Fig. 3). The failure to detect α-DG in the DG-overexpressing derivatives of the MCF7 cells cannot simply be a consequence of an altered glycosylation of the α-DG subunit since it was also undetectable using a polyclonal antibody which specifically recognizes and binds the N-terminal region of the α-DG core protein.[23] We previously demonstrated that reduction or loss of α-DG expression in most breast cancer cell lines is associated with accumulation of a low molecular weight form of the β-DG subunit[10] which has been shown to be a product of a proteolytic processing of the extracellular domain of β-DG likely due to a membrane-associated matrix metalloproteinase (MMP) activity.[10,13] The MCF7 cells have been reported to express the MMP15 and MMP16 enzymes[36] which might play a role in the loss of α-DG expression. However, we did not observe any change in the low molecular weight form of the β-DG in the DG-overexpressing derivatives of the MCF7 cells compared to vector control cells (data not shown) and, in preliminary studies, we did not observe changes (i.e., restoration) of α-DG expression in the MCF7 cells and their derivatives by treatment with a broad MMPs inhibitor (unpublished data). Studies are ongoing to definitively identify the mechanism(s) responsible for loss of α-DG expression in breast cancer cells.

Our findings suggest that breast cancer cells have lost their ability to retain α-DG on cell membrane and that overexpression of an exogenous DG cDNA is not able to override this inability. Release of α-DG from cell surface has been previously reported in other cell models, including bovine aortic endothelial cells[24] and rat schwannoma cells.[37] It is of interest that overexpression of an exogenous DG cDNA was previously reported to be not able to restore α-DG expression in a series of breast cancer cell lines.[7] We hypothesize that, since DG subunits are encoded by a single gene and are formed upon cleavage of a precursor protein,[6,8] breast cancer cells have developed a specific post-transcriptional mechanism responsible for the lack of expression of α-DG. Overexpression of an exogenous α-DG, however, was previously reported in the T4-2 breast cancer cell line.[7] It is of interest that this cell line lacks expression of both α and β-DG subunits. Thus, unlike most of the other breast cancer cell lines, a genetic or transcriptional alteration might be responsible for the loss of the entire endogenous DG complex in the T4-2 cell line. This observation suggests that multiple mechanisms might be responsible for the lack of α-DG expression in different cancer cell lines and primary tumors but this hypothesis remains to be verified.

Despite the lack of expression of α-DG, the DG-transfected MCF7 cells displayed a growth inhibition associated with an accumulation of cells in the G_0/G_1 phase of the cell cycle and a reduction of cells in the S phase (Table 2). The DG-overexpressing derivatives of the MCF7 cells also displayed inhibition of the anchorage-independent growth (Fig. 4A) and a reduced tumorigenicity in vivo (Fig. 4B). A reduction of the tumorigenic potential was previously observed in the DG-transfected T4-2 breast cancer cells.[7] However, it is noteworthy that in the latter study the DG-transfected T4-2 cells displayed an increased expression of both α- and β-DG. Our results demonstrate, for the first time, that increasing β-DG is *per se* able to reduce the growth and tumorigenicity of breast cancer cells

independently of an increase in the α-DG-associated signaling transduction pathway.

A surprising result of this study was that, unlike the MCF10F cells, overexpression of DG in the breast cancer-derived MCF7 cells was associated with a reduction in their ability to adhere to a substratum, including matrigel-coated dishes, compared with vector control cells (Table 2 and Fig. 2B). We believe this finding is also a consequence of the lack of membrane targeting of the exogenous α-DG. In fact, although we were unable to detect the presence of a band corresponding to the correct size of the α-DG protein in the conditioned media by western blot analysis (data not shown) we demonstrated that the MCF7 and its derivatives likely release α-DG, or other related molecules (i.e., degradation products), in the culture medium (Figs. 5 and 6). Thus, conditioned media of the MCF7 cells and their derivatives inhibited adhesion to laminin of DG-expressing cells (Fig. 5) and this inhibition was prevented by depleting the conditioned media of α-DG using WGL17 (Fig. 6). We hypothesize that breast cancer cells have lost their ability to retain α-DG on cell membrane an that an increase in the amount of secreted α-DG, or other related products, in the DG-overexpressing derivatives of the MCF7 cancer cells might interact with and saturate the binding domains of ECM components thus causing a reduction, rather than an increase, of cell attachment to a substratum. Another possibility is that accumulation of an isolated β-DG can by itself inhibit cell adhesion by activating inhibitory signals or interfering with a signal transduction pathway.

The observed reduced adhesion of the DG-overexpressing derivatives of the MCF7 cells is important for our understanding of the growth inhibitory effects associated with increased expression of DG. In fact, overexpression of adhesion molecules, such as integrin and cadherin has been reported to suppress cell proliferation.[38-40] Thus, a decreased rate of proliferation was expected by overexpression of DG and it is not surprising for the MCF10F derivatives that also displayed an increased adhesion to a substratum (Table 1 and Fig. 2A). More surprising is the observation of a reduced proliferation rate in the MCF7 derivatives that, on the contrary, displayed a reduced adhesion (Table 2 and Fig. 2B). These results suggest that the DG complex might negatively regulate cell growth independently by the interaction with ECM components, at least in the MCF7 cells. In preliminary studies, we observed differential effects on the cell cycle regulatory proteins cyclin D1 and $p27^{Kip1}$ in the DG-overexpressing derivatives of the MCF10F and MCF7 cells (unpublished results) which might further support the hypothesis that different mechanisms mediate the cell growth inhibition observed in the two cell lines analyzed. Indeed, βDG can bind Grb2,[29,41] the growth factor receptor bound adapter protein involved in the activation of several signaling pathways, including the recruitment to plasma membrane and subsequent activation of the Ras oncogene.[42] Thus, an excess of βDG might inhibit proliferation not only by a direct effect (i.e., activating inhibitory signals) but also by an indirect effect blocking or interfering with stimulatory signals (i.e., sequestering Grb2 and inhibiting activation of Grb2-dependent signaling pathways). Future studies looking at downstream molecules that mediate DG-dependent intracellular signaling pathways will be necessary to definitively assess the role(s) of DG complex on the regulation of cell growth and proliferation.

Although the underlying molecular mechanisms remain unknown, the results of the present study confirm that DG and related proteins might play an important role in the regulation of mammary epithelial cell growth and tumorigenesis. The altered adhesion of cancer cells to extracellular matrix is undoubtedly a critical factor in the metastatic cascade; however, the biology of tumor cells invasion and metastasis is still not well understood. DG expression may influence the ability of cancer cells to interact with the endothelium of lymphovascular channels and/or to migrate through the extracellular matrix at primary as well as secondary sites and reduced or loss of expression of this protein might induce an increased ability of cancer cells to detach from the primary site in the metastatic process. As for integrins, in fact, it may result in less sticky tumour cells able to move unhindered in the extracellular matrix, thus predisposed to metastasize.[43] The results of the present study, however, confirm previous evidence that DG is involved in multiple and complex cell functions, other than cell adhesion to ECM, and can regulate still unknown intracellular signaling pathways. Thus, the cellular functions regulated by DG expression in the process of tumor development might not be simply related to cell-matrix adhesion. Loss of DG expression may predispose to tumor progression by compromising regulatory control(s) over growth and differentiation as suggested by our finding that overexpression of an exogenous DG cDNA inhibits the ability of breast cancer cells to growth and establish tumors in nude mice (Table 1 and Fig. 4B). Cancer cells with decreased DG expression may thus display an increased growth other than invasive potential.

These findings are of great interest in view of a potential exploitment of DG as a prognostic factor of risk of recurrence and metastasis and/or as a target for the development of novel therapies to halt tumor cell growth and metastasis. Indeed, restoration of DG expression and function has been suggested as a new potential therapeutic strategy to inhibit tumor cell growth and spreading.[7,10,11] Our results, however, suggest caution since they demonstrate that attempts to restore DG expression through a gene-therapy approach, as the one used in this study, while suitable for cancer treatment since it can inhibit cancer cell growth and tumorigenicity, might ultimately promote tumor cells spreading and metastasis by reducing cell attachment to ECM.

In conclusion, further studies on the role played by DG in the regulation of epithelial cell growth and transformation and on its possible role as tumor suppressor gene are warranted and we believe that they might not only provide useful insights into the significance of decreased DG expression for human tumor pathogenesis but also contribute to the development of novel strategies to inhibit tumor cell growth and invasiveness.

References

1. Lin CQ, Bissell MJ. Multi-faceted regulation of cell differentiation by extracellular matrix. FASEB J 1993; 7:737-43.
2. Kadar A, Tokes AM, Kulka J, Robert L. Extracellular matrix components in breast carcinomas. Semin Cancer Biol 2002; 12:243-57.
3. Ibraghimov-Beskrovnaya O, Ervasti JM, Leveille CJ, Slaughter CA, Sernett SW, Campbell KP. Primary structure of dystrophin-associated glycoproteins linking dystrophin to the extracellular matrix. Nature 1992; 355:696-702.
4. Durbeej M, Henry MD, Ferletta M, Campbell KP, Ekblom P. Distribution of dystroglycan in normal adult mouse tissues. J Histochem Cytochem 1998; 46:449-57.
5. Michele D, Campbell K. Dystrophin-glycoprotein complex: Post-translational processing and dystroglycan function. J Biol Chem 2003; 278:15457-60.
6. Winder SJ. The complexities of dystroglycan. TIBS 2001; 26:118-24.
7. Muschler J, Levy D, Boudreau R, Henry M, Campbell K, Bissell MJ. A role for dystroglycan in epithelial polarization: loss of function in breast tumor cells. Cancer Res 2002; 62:7102-9.
8. Holt KH, Crosbie RH, Venzke DP, Campbell KP. Biosynthesis of dystroglycan: Processing of a precursor peptide. FEBS Lett 2000; 468:79-83.
9. Ibraghimov-Beskrovnaya O, Mialtovich A, Ozcelik T, Yang B, Koepnick K, Francke U, et al. Human dystroglycan: Skeletal muscle cDNA, genomic structure, origin of tissue specific isoforms and chromosomal localization. Hum Mol Gen 1993; 2:1651-7.

10. Losasso C, Di Tommaso F, Sgambato A, Ardito R, Cittadini A, Giardina B, et al. Anomalous dystroglycan in carcinoma cell lines. FEBS Letters 2000; 484:194-8.
11. Sgambato A, Migaldi M, Montanari M, Camerini A, Brancaccio A, Rossi G, et al. Dystroglycan expression is frequently reduced in human breast and colon cancers and is associated with tumor progression. Am J Pathol 2003; 162:849-60.
12. Henry MD, Cohen MB, Campbell KP. Reduced expression of dystroglycan in breast and prostate cancer. Hum Pathol 2001; 32:791-5.
13. Yamada H, Saito F, Fukuta-Ohi H, Zhong D, Hase A, Arai K, et al. Processing of β-dystroglycan by matrix metalloproteinase disrupts the link between the extracellular matrix and cell membrane via the dystroglycan complex. Hum Mol Genetics 2001; 10:1563-9.
14. Soule Hd, Maloney TM, Wolman SR, WD Peterson J, Brenz R, McGrath CM, et al. Isolation and characterization of a spontaneously immortalized human breast epithelial cell line, MCF-10. Cancer Research 1990; 50:6075-86.
15. Ball RK, Friis RR, Schoenenberger CA, Doppler W, Groner B. Prolactin regulation of β-casein gene expression and of a cytosolic 120-kd protein in a cloned mouse mammary epithelial cell line. The EMBO Journal 1988; 7:2089-95.
16. Brancaccio A, Ruegg MA, Engel J. Cloning and sequencing of mouse skeletal α-dystroglycan. Matrix Biol 1995; 14:681-5.
17. Brancaccio A, Schulthess T, Gesemann M, Engel J. Electron microscopic evidence for a mucin-like region in chick muscle alpha-dystroglycan. FEBS Lett 1995; 368:139-42.
18. Sgambato A, Han EK-H, Zhou P, Schieren I, Weinstein IB. Overexpression of cyclin E in the HC11 mouse mammary cell line is associated with growth inhibition and increased expression of p27Kip1. Cancer Res 1996; 56:1389-99.
19. Sgambato A, Zhang Y-J, Ciaparrone M, Soh J-W, Cittadini A, Santella RM, et al. Overexpression of p27kip1 inhibits the growth of both normal and transformed human mammary epithelial cells. Cancer Res 1998; 58:3448-54.
20. Han EK, Sgambato A, Jiang W, Zhang Y, Santella RM, Doki Y, et al. Stable overexpression of cyclin D1 in a human mammary epithelial cell line prolongs the S-phase and inhibits growth. Oncogene 1995; 10:953-62.
21. Sgambato A, Ratto G, Faraglia B, Merico M, Ardito R, Schinzari G, et al. Reduced expression and altered subcellular localization of the CDK inhibitor $p27^{Kip1}$ in human colon cancer. Mol Carcinogenesis 1999; 26:172-9.
22. Brancaccio A, Schulthess T, Gesemann M, Engel J. The N-terminal region of α-dystroglycan is an autonomous globular domain. Matrix Biol 1997; 246:166-77.
23. Zaccaria ML, Di Tommaso F, Brancaccio A, Paggi P, Petrucci TC. Dystroglycan distribution in adult mouse brain: A light and electron microscopic study. Neuroscience 2001; 104:311-24.
24. Shimizu H, Hosokawa H, Ninomiya H, Mineres JH, Masaki T. Adhesion of cultured bovine aortic endothelial cells to laminin-1 mediated by dystroglycan. J Biol Chem 1999; 274:11995-2000.
25. Kleinman HK, McGarvey ML, Lotta LA, Robey PG, Tryggvason K, Martin GR. Isolation and characterization of type IV procollagen, laminin, and heparan sulfate proteoglycan from the EHS sarcoma. Biochemistry 1982; 21:6188-93.
26. Montanaro F, Lindenbaum M, Carbonetto S. α-dystroglycan is a laminin receptor involved in extracellular matrix assembly on myotubes and muscle cell viability. J Cell Biol 1999; 145:1325-40.
27. Ruoslahti E. Control of cell motility and tumour invasion by extracellular matrix interactions. Br J Cancer 1992; 66:239-42.
28. Ervasti JM, Campbell KP. Dystroglycan: An extracellular matrix receptor linked to the cytoskeleton. Curr Opin Cell Biol 1996; 8:625-631.
29. Russo K, Di Stasio E, Macchia G, Rosa G, Brancaccio A, Petrucci TC. Characterization of the beta-dystroglycan-growth factor receptor 2 (Grb2) interaction. Biochem Biophys Res Commun 2000; 274:93-8.
30. Cavaldesi M, Macchia G, Barca S, Defilippi P, Tarone G, Petrucci TC. Association of the dystroglycan complex isolated from bovine brain synaptosomes with proteins involved in signal transduction. J Neurochem 1999; 72:1648-55.
31. Chockalingam PS, Cholera R, Oak SA, Zheng Y, Jarrett HW, Thomason DB. Dystrophin-glycoprotein complex and Ras and Rho GTPase signaling are altered in muscle atrophy. Am J Physiol Cell Physiol 2002; 283:500-11.
32. Langenbach KJ, Rando TA. Inhibition of dystroglycan binding to laminin disrupts the PI3K/AKT pathway and survival signaling in muscle cells. Muscle Nerve 2002; 26:644-53.
33. Hosokawa H, Ninomiya H, Kitamura Y, Fujiwara K, Masaki T. Vascular endothelial cells that express dystroglycan are involved in angiogenesis. J Cell Sci 2001; 115:1487-96.
34. Ferletta M, Kikkawa Y, Yu H, Talts JF, Durbeej M, Sonnenberg A, et al. Opposing roles of integrin α6Aβ1 and dystroglycan in laminin-mediated extracellular signal-regulated kinase activation. Mol Biol Cell 2003; 14:2088-103.
35. Jiang F, Georges-Labouesse E, Harrison LC. Regulation of laminin-1 induced pancreatic β-cell differentiation by α 6 integrin and β-dystroglycan. Mol Medicine 2001; 7:107-14.
36. Giambernardi TA, Grant GM, Taylor GP, Hay RJ, Maher VM, Mccormick JJ, et al. Overview of matrix metalloproteinase expression in cultured human cells. Matrix Biol 1998; 16:483-96.
37. Matsumura K, Chiba A, Yamada H, Fukuta-Ohi H, Fujita S, Endo T, et al. A role of dystroglycan in schwannoma cell adhesion to laminin. J Biol Chem 1997; 272:13904-10.
38. Giancotti FG, Ruoshlati E. Elevated levels of the fibronectin receptor suppress the transformed phenotype of Chinese hamster ovary cells. Cell 1990; 60:849-59.
39. Watabe M, Nagafuchi A, Tsukita S, Takeichi M. Induction of polarized cell-cell association and retardation of growth by activation of the E-cadherin-catenin adhesion system in a dispersed carcinoma line. J Cell Biol 1994; 127:247-56.
40. Vizirianakis I, Yao C, Chen Y, Ziober B, Tsiftsoglou A, Kramer R. Transfection of MCF-7 carcinoma cells with human integrin alpha7 cDNA promotes adhesion to laminin. Arch Biochem Biophys 2001; 385:108-16.
41. Yang B, Jung D, Motto D, Meyeer J, Koretzky G, Campbell KP. SH3 domain mediated interaction of dystroglycan and Grb2. J Biol Chem 1995; 270:11711-4.
42. Chardin P, Cussac D, Maignan S, Ducruix A. The Grb2 adaptor. FEBS Lett 1995; 369:47-51.
43. Gui GPH, Puddefoot JR, Vinson GP, Wells CA, Carpenter R. Altered cell-matrix contact: A prerequisite for breast cancer metastasis? Br J Cancer 1997; 75:623-33.

ELSEVIER

European Journal of Cancer 40 (2004) 2143–2151

European Journal of Cancer

www.ejconline.com

Aberrant expression, processing and degradation of dystroglycan in squamous cell carcinomas

Jie Jing [a,b], Chun Fu Lien [a], Sanjay Sharma [b], Jill Rice [a], Peter A. Brennan [a,b], Dariusz C. Górecki [a,b,*]

[a] *School of Pharmacy and Biomedical Sciences, Institute of Biomedical and Biomolecular Sciences, Molecular Medicine Group, University of Portsmouth, St. Michael's Building, White Swan Road, Portsmouth PO1 2DT, UK*

[b] *Maxillofacial Unit, Queen Alexandra Hospital, Cosham, UK*

Received 11 May 2004; accepted 17 May 2004
Available online 3 July 2004

Abstract

The α- and β- dystroglycan (DG) proteins are involved in epithelial cell development, formation of the basement membrane and maintenance of tissue integrity. Recently, specific changes in the expression patterns of DGs have been described in some cancers. We studied the expression and localisation of α- and β-DG using Western blotting, immunohistochemistry and reverse transcriptase–polymerase chain reaction analyses in samples of normal oral mucosa, oral squamous cell carcinoma (SCC) and cancer cell lines. The α- and β-DG were localised in the basal layers of normal oral mucosa.However, β-DG expression in cancer tissues showed evidence of aberrant expression, processing and degradation. α-DG was altered in all oral cancer samples and cell lines, despite the persistent presence of DG mRNA in cancer cells. Using matrix metalloproteinase (MMP) inhibitors, we determined that β-DG degradation in carcinoma cell lines can be mediated by MMPs but this process is highly variable, even in cells from the same cancer type. Considering the multifaceted role of DG in epithelial development, it appears that the role of DG degradation in cancer growth and spread, although currently poorly understood, may be important.

Keywords: Squamous cell carcinoma; α- and β-Dystroglycan; Matrix metalloproteinases

1. Introduction

Oral squamous cell carcinoma (SCC) is the sixth most common malignancy worldwide. The tongue and the floor of mouth are the most common sites of origin in the Western world. Furthermore, the incidence of oral cancer has increased over the same time period in both the United Kingdom (UK) and United States of America (USA), particularly in the under 50-year old age group [3,16]. In UK alone, there are ≈3500 new cases of oral cancer diagnosed per year, and 1600 deaths. Both the disease and its treatment are associated with a high rate of morbidity, and despite improvements in the diagnosis and management of oral SCC, the crude 5-year mortality rate of ≈45% has changed little in the last 30 years. Moreover, metastasis to the cervical lymph nodes reduces the chance of cure by 50% [33]. A greater understanding of the disease processes is needed in order to improve patients outcome and develop novel treatment modalities.

The cell–cell and cell-extracellular matrix (ECM) interactions have a pivotal function in the development and maintenance of the cytoarchitecture in normal tissues and play an important role in the development and progression of many types of cancer. In fact, abnormalities in the interactions between tumour cells and ECM proteins are often implicated in the aberrant behaviour of carcinoma cells and defects in the structure and function of basement membranes are hallmarks of metastatic disease [19].

The roles of the different adhesion molecules and their binding ligands are not fully understood. It is clear

* Corresponding author. Tel.: +44-2392-843566; fax: +44-2392-843565.
E-mail address: darek.gorecki@port.ac.uk (D.C. Górecki).

0959-8049/$ - see front matter © 2004 Elsevier Ltd. All rights reserved.
doi:10.1016/j.ejca.2004.05.018

that these proteins are multi-functional – they not only connect cells to the basal lamina, but also contribute to the exchange of information with the extracellular environment, connect and organise the cytoskeleton, and participate in signal transduction processes [19]. As such, adhesion molecules are critically important for proper tissue growth, differentiation and maintenance of cytoarchitecture. Until recently, studies on cell adhesion molecules involved in cancer have mainly concentrated on the integrin family [4,19]. However, there is a growing body of evidence that other adhesion molecules may play an equally important role.

We have focused our attention on the function of the dystroglycan (DG) complex. DG is a cellular receptor expressed in a variety of tissues and it interacts with extracellular proteins like laminin, perlecan and agrin [41] and also membrane proteins – e.g., neurexins [36].

The biosynthesis and structure of DG are complex [41]. DG is a product of a single gene, but the primary peptide is post-translationally cleaved, resulting in two protein subunits (α and β), which interact to form a functional non-covalent complex [18]. The β-DG is a 43 kDa transmembrane protein. The predicted 72 kDa α-DG peptide undergoes further post-translational modifications resulting in a heavily glycosylated extracellular protein. Its molecular mass can vary in different tissues (120–180 kDa), depending on the degree of glycosylation.

In muscle tissue, α/β-DG functions as part of a large dystrophin-associated protein (DAP) complex, which is an array of transmembrane, cytoplasmic and extracellular proteins that are crucial for proper muscle function. Mutations disrupting this complex result in muscular dystrophy. However, DG also has a role in non-muscle tissues. The DG gene knockout in mice results in embryonic death *in utero*. This early lethality is caused by disruption of the Reichert's membrane – an early basement membrane [39]. Later in foetal development, this protein has been shown to have a crucial role in kidney and salivary gland epithelial morphogenesis [8]. Moreover, in the adult mouse, DG is present in epithelial cells in several other non-muscle organs (including squamous epithelia) [7]. It is particularly enriched at the basal interfaces of cells directly apposing basement membranes [14]. Finally, disruption of brain DG results in neuronal migration errors in the developing brain [27,28]. This evidence points to DG having a role in epithelial cell development and the formation of the basement membrane and indicates its importance in the formation and maintenance of tissue integrity.

Recently, specific changes in DG expression in human breast, colon and prostate cancers have been described [15,25,32].

Herein, we analysed DG expression in samples of normal human oral epithelia, primary and metastatic SCCs and a range of tumorigenic SCC lines to study its involvement in oral cancer.

2. Materials and methods

2.1. Primary antibodies

Mouse monoclonal anti-β-DG NCL-b-DG (Novocastra, UK) recognising 15 amino acids at the extreme C-terminus of human DG; mouse monoclonal (clone 56, BD Biosciences, UK) generated against an epitope encompassing amino acids 655–767 in the middle of human β-DG and two mouse monoclonal antibodies anti-α-DG: VIA4-1 (Upstate Lab, USA) and anti-α-DG (IgM, US Biological, USA), both generated using rabbit skeletal muscle membrane preparation as an immunogen were used. Only VIA4-1 is suitable for immunolocalisation.

2.2. Cell lines

SCC-4, SCC-9, SCC-15 and SCC-25 (human tongue SCCs) and HT-29 (human colon adenocarcinoma grade II) were obtained from the American Tissue Culture Collection (LGC Promochem, Middlesex, UK). Cells were grown in Dulbecco's modified Eagle's medium supplemented with nutrient mixture F-12 Ham's (containing 15 mM HEPES, NaHCO, pyridoxine and L-glutamine), 10% foetal bovine serum, penicillin, streptomycin and 400 ng/ml hydrocortisone (Sigma–Aldrich, Poole, UK). Cultures were maintained at 37 °C in a humidified atmosphere with 5% CO_2.

For the matrix metalloproteinase (MMP) inhibition studies, cells were grown to confluence as described above, and the growth media substituted with a fresh one of the same composition but containing 25 μM of the GM6001 inhibitor (Ilomastat) or 2–20 μM of MMP2/MMP9 inhibitor IV (SB-3CT). Both inhibitors were obtained from Chemicon International and used according to the manufacturer's instruction. The inhibitor stocks were prepared in dimethyl sulfoxide (DMSO). Ilomastat was added directly to the culture medium, while SB-3CT was diluted in buffer R (50 mM HEPES [pH 7.5], 150 mM NaCl, 5 mM $CaCl_2$, 0.01% Brij-35 and 50% DMSO) prior to addition.

After incubation for 48 h in the presence of either inhibitor, cells were washed three times with phosphate buffered saline (PBS) and used for protein extraction as described below.

2.3. Tumour samples

Surgically resected primary tumours, metastatic lymph nodes and control samples of squamous epithelia were obtained and used in accordance with the institutional guidelines and the ethical permissions granted. All studies were performed using fresh-frozen specimens.

2.4. Immunolocalisation

Cryosections (10 μm) were cut, mounted on poly-L-lysine-coated glass slides and fixed with 4% (w/v) paraformaldehyde in PBS for 15 min on ice. Following blocking of endogenous peroxidases, the sections were pre-incubated for 30 min in PBS containing 10% (v/v) normal horse serum, and further treated with Vector Blocking kit (Vector Laboratories, UK) to block endogenous biotin activity. After blocking, the sections were incubated overnight at 4 °C in PBS containing 10% (v/v) normal horse serum and mouse monoclonal β-DG antibody NCL-b-DG at a 1:100 dilution. Following incubation with the primary antibody, the sections were washed, incubated for 30 min with horse anti-mouse biotinylated secondary antibody (1:200, Vector Laboratories, UK) diluted in PBS with 2% normal horse serum and the signal was visualised with Vectastain ABC reagent and Vector VIP substrate kit. The sections were counter-stained with methyl green (Vector Laboratories, UK).

For the immunolocalisation of α-DG with the mouse monoclonal antibody VIA4-1 the protocol was as described above, but with the following modifications. Blocking was in PBS with 8% bovine albumin and the primary antibody was diluted 1:500 in PBS with 1% bovine albumin.

2.5. Western blotting

2.5.1. Protein extraction

Tissues (tumour and control human muscle samples) were homogenised in ice-cold buffer containing 10 mM 2-[4-(2-Hydroxyethyl)-1-piperazine]ethane Sulfonic acid (pH 7.5), 0.5% Triton X-100, 5 mM EGTA, 5 mM ethylene (oxyethylene nitrilo)tetraacetic acid (EDTA), 2 mM sodium *ortho*vanadate, 50 mM sodium fluoride, 100 mM sodium chloride and protease inhibitors (Complete™, Roche) using polytron. After incubation on ice for 25 min on a shaking platform, the samples were centrifuged at 200*g* for 5 min at 4 °C and the supernatants were centrifuged again at 16 000*g* for 25 min at 4 °C. For immunoblotting, the pellets were solubilised for 4 min at 100 °C in solubilisation buffer (50 mM Tris–HCl; pH 7.5, 2% (w/v) sodium dodecyl sulphate (SDS), and 1% (w/v) dithiothreitol).

Proteins from the tumour cell lines were extracted as described above or using a simplified protocol: in this case, cells were scraped off the dish in PBS, pelleted and solubilised in the Triton lysis buffer (1% Triton X-100, 150 mM NaCl, 10 mM Tris pH 7.4, 1 mM EDTA, 1 mM EGTA, 0.5% Tergitol NP-40 with Complete™ protease inhibitors, Roche). Following 20 min incubation on ice with shaking and brief centrifugation, the supernatant containing the total protein extract was used for the SDS–polyacrylamide gel electrophoresis (PAGE) analysis. Both methods were run concurrently and produced equivalent results.

2.5.2. SDS–PAGE

Solubilised proteins (30–50 μg) were mixed with Laemmli sample buffer (Bio RAD, UK) and 0.05% mercaptoethanol, heated to 95 °C for 4 min, separated on 6–10% SDS–polyacrylamide gels and electroblotted onto Hybond ECL membranes (Amersham Pharmacia Biotech, Bucks, UK). The blots were incubated overnight with a blocking solution containing 5% non-fat milk powder in PBST (PBS/0.05% Tween 20) at 4 °C and then incubated with NCL-b-DG, clone 56, VIA4-1 or US Bio antibodies at 1:50, 1:500, 1:100 and 1:1000 dilutions, respectively, in the same blocking solution for 2 h at room temperature. Following three washes with PBST, membranes were incubated with horseradish peroxidase-conjugated secondary anti-mouse IgG (1:10 000, Amersham Pharmacia, Biotech UK) or, in the case of US Bio, anti-mouse IgM (Vector Laboratories, UK), at room temperature for 30 min and the signal was then visualised on films using the enhanced chemiluminescence (ECL) plus kit (Amersham Pharmacia Biotech, UK). As a negative control, the primary antibody was omitted from the incubation mixture and the rest of the protocol was performed as described above. Rat brain and human skeletal muscle were used as positive controls (detecting specific bands of 130 and 156 kDa, respectively).

2.6. Reverse transcriptase–polymerase chain reaction analysis

Total cellular RNA was extracted from SCC cells using the total RNA isolation system (Promega, Southampton UK) according to the manufacturer's instructions. RNA samples (3 μg) were digested with 3 U of amplification grade deoxyribonuclease I (Life Technologies, Paisley, UK) for 20 min at room temperature to eliminate the contaminating DNA. Half of the resulting RNA sample was reverse-transcribed at 42 °C using 200 ng of random primers, 400 U of Superscript II reverse transcriptase (Life Technologies, Paisley, UK) and 40 U of RNasin (Promega, Southampton UK) in a final volume of 50 μl. The remaining RNA was used to prepare a control sample in which the reverse transcriptase was omitted. One to two microlitre aliquots of each sample were used for reverse transcriptase–polymerase chain reaction (RT–PCR) analysis in a 50 μl reaction volume containing 200–500 nM primers, 3 mM $MgCl_2$, 200 μM of each deoxynucleoside triphosphate (dNTP) and 2.5 U of *Taq* polymerase (Qiagen, Crawley, UK or Life Technologies, Paisley, UK).

Two primer sets were designed and used as described before [12].

Set 1: Gly–1Rv: 5′-CGCGGGTGATGTTCTG-CAGGGTGA-3′ and Gly–2Fvd: 5′-ACCCA ACCAG-CGCCCAGAGCTCAAG-3′.

Set 2: Gly–1Rv: as above and Gly–3Fvd: 5′-AT-GGCTCCTCCAGTCAGGGATCCTG-3′.

Cycling conditions were: 94 °C for 4 min, followed by 35 cycles of 94 °C for 60 s, 55 °C for 60 s, 72 °C for 60 s with a final extension step of 72 °C for 7 min.

PCR products were resolved by electrophoresis in 1–2% agarose gels and visualised by ethidium bromide staining.

3. Results

We initially analysed the localisation of α- and β-DG in normal human squamous epithelium (tongue). Both α- and β-DG were found to co-localise in the basal cell layers of the squamous epithelium (Figs. 2(a) and 1(a), respectively). Staining with β-DG was concentrated almost exclusively on the basolateral surfaces of the basal cell layer, while weak staining with α-DG was also present in the upper layers. The specificity of staining with both antibodies was confirmed by an internal tissue

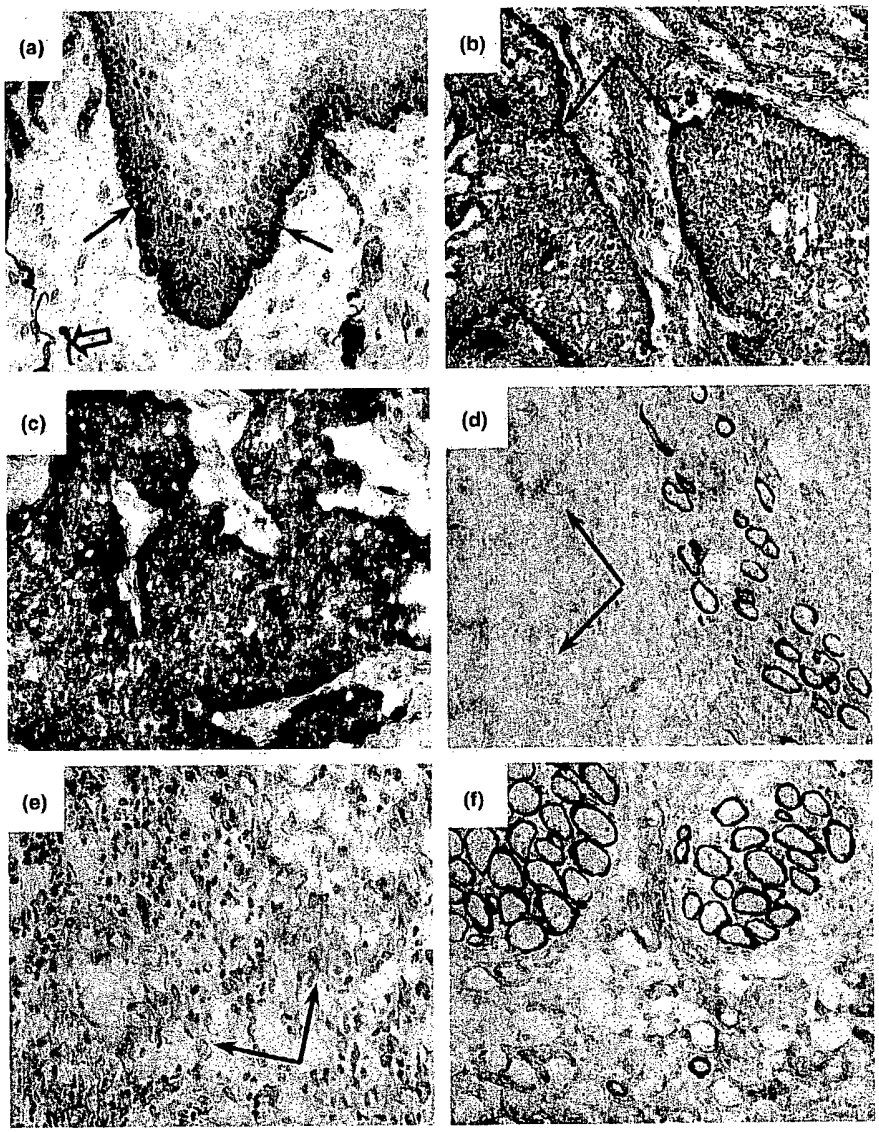

Fig. 1. Immunolocalisation of β-dystroglycan (β-DG) in normal oral epithelium and oral cancer. Mouse monoclonal anti-β-DG antibody: NCL-b-DG (Novocastra) was used in this study. (a) Normal oral epithelium. Note the strong staining in the basal cell layer (arrows) and in blood vessels in the stroma (open arrow). (b)–(f) Oral cancers (b). Soft palate squamous cell carcinoma (SCC), moderately/poorly differentiated. Strong expression in cancer cells in areas directly in contact with the stroma (arrows). (c) Soft palate SCC, moderately differentiated. Note the strong expression in cancer cell membranes in the entire tumour mass. (d) and (f) Tongue SCC, poorly differentiated. Note the complete lack of β-DG expression in the tumour mass (arrows) with strong expression in the muscle fibre membranes (e). SCC metastasis in a neck lymph node (arrows). The primary tumour from which this metastasis developed is shown in (b). Magnifications: (a), (e) and (f) 400×; (b) 100×; (c) and (d) 200×.

control as there was strong expression in the sarcolemma of the adjacent skeletal muscle fibres (Figs. 1(d) and (f) and 2(a)). There was also clear staining with β-DG antibody present in the blood vessels within the tissue (Fig. 1(a)).

In contrast, this pattern of expression was completely altered in the samples from 11 cases of primary oral SCCs (tongue, 8; soft palate/pharyngeal, 3). Unlike the specific expression pattern in normal epithelium, the β-DG staining in cancer tissue was highly variable. In three cases, the cancer cell membranes in areas directly in contact with the stroma showed strong staining, resulting in clearly delineated clusters of cancer cells (Fig. 1(b)). This resembled the pattern of staining found in the normal epithelium where the basal cell layer in contact with basal lamina was strongly positive. In two other oral cancer samples, the β-DG staining was significantly increased. The expression was no longer localised to the margin of the tumour mass, but most cancer cells were immunopositive, with both membrane and cytoplasmic staining being clearly noticeable (Fig. 1(c)). Finally, in three other cases the expression of β-DG was completely absent from the cancer cells (Fig. 1(d) and (f)). In the same samples, the membranes of skeletal muscle found between the infiltrating cancer cells were strongly positive (Fig. 1(d)). Apart from the blood vessels, all the stromal cells were negative for β-DG.

In contrast to β-DG, the α-DG staining was entirely absent from all the oral SCC samples (Fig. 2(b)–(d)). The skeletal muscle membranes between the infiltrating cancer cells were strongly positive (Fig. 2(b)), confirming staining specificity.

The same β- and α-DG antibodies failed to detect any staining in metastatic cancer in lymph nodes of the neck (Fig. 1(e)). These nodes were dissected from the two cases from which the primary carcinomas were analysed and found to be positive for β-DG.

To confirm these immunolocalisation findings, we analysed protein extracts from rat skin and primary SCC samples, which were used in the immunohistochemical studies (Fig. 3(a)). In skin and skeletal muscle samples used as positive controls, we found one band of the expected size (43 kDa). In all tumour samples, there were different proportions of two bands (43 kDa and a weaker ≈30 kDa band), the higher molecular mass band corresponded to the expected size for β-DG. In one sample (oral carcinoma), we found a band of ≈80 kDa, with little or no bands of 43 and ≈30 kDa. This large band was detected with two β-DG antibodies (against

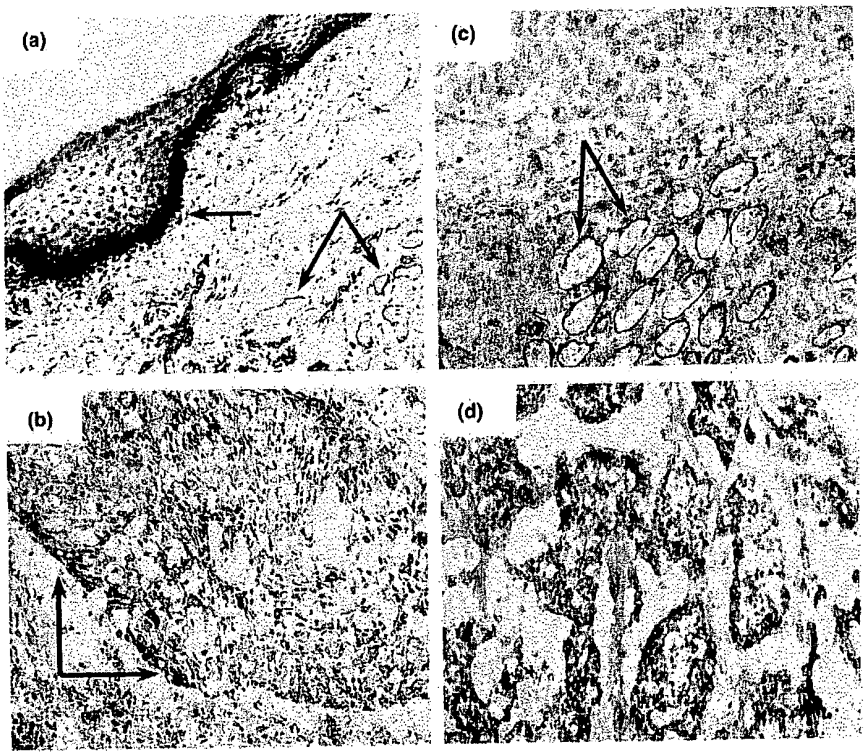

Fig. 2. Immunolocalisation of α-dystroglycan (α-DG) in normal oral epithelium and in oral cancer. (a) Normal oral epithelium. The strong staining located in the basal cell layer (arrow), in muscle sarcolemma and blood vessels in the stroma (arrows). (b)–(d) Oral cancer; note a total lack of α-DG staining in the tumour mass, while the skeletal muscle membranes are clearly stained. (b) Tongue squamous cell carcinoma (SCC), poorly differentiated. (c) Neck lymph node metastasis originating from a soft palate tumour. (d) Soft palate SCC, moderately differentiated. Magnifications: (a) 100×; (b) 400×; (c) and (d) 200×.

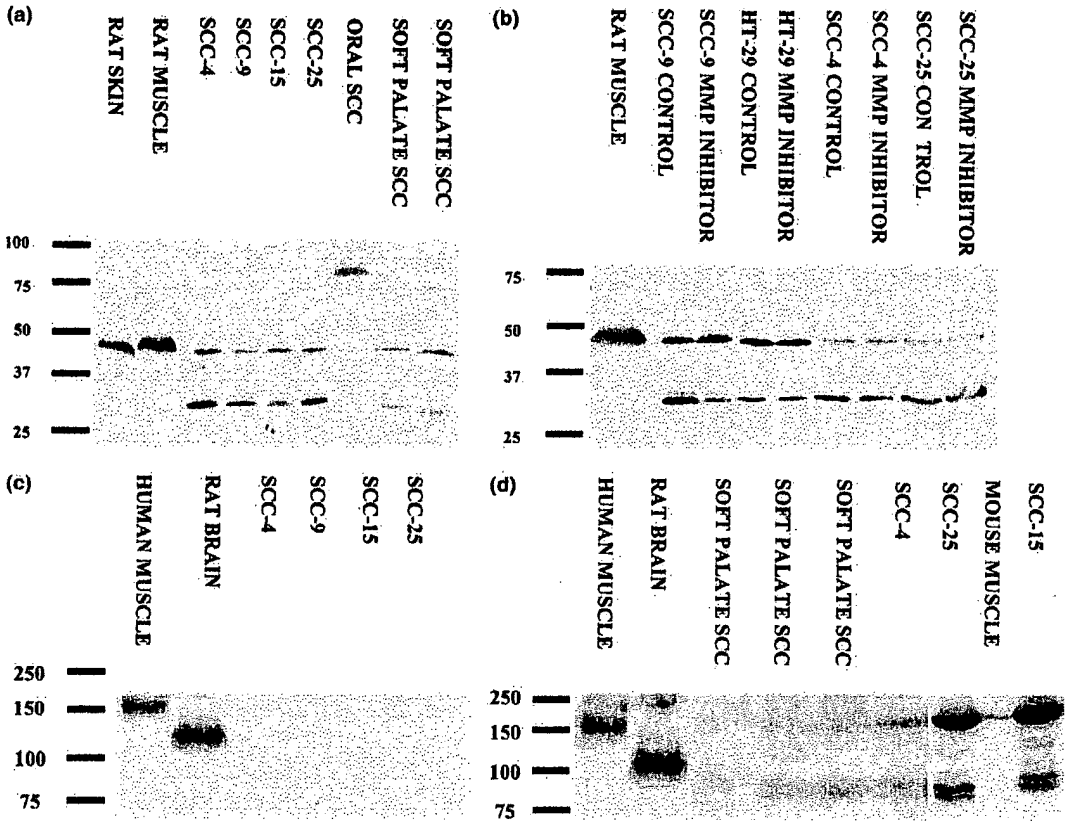

Fig. 3. Western blotting analysis of α- and β-dystroglycan (α- and β-DG) in oral cancer. (a) Protein samples from oral cancers and squamous cell carcinoma (SCC) lines (SCC-4, 9, 15 and 25) were processed for Western blotting and probed with β-DG antibody. (b) Effects of matrix metalloproteinase (MMP) inhibition on β-DG degradation. (c) Immunoblotting analysis of α-DG with VIA4-1 antibody. (d) Immunoblotting analysis of α-DG with US Bio antibody.

the N- and C-terminal epitopes), and corresponds to an improperly processed DG protein.

The same blots probed with the α-DG antibody used in the immunolocalisation analysis (VIA4-1) were negative in all tumour samples (data not shown). Different protein extraction procedures, use of varying sets of protease inhibitors and different amounts of protein all gave identical results. However, when another α-DG antibody was used (US Bio), two weak bands were detected, one corresponded to the expected size of α-DG and a smaller one. This smaller band was fuzzy and sometimes appeared as a doublet (Fig. 3(d)). In the control muscle samples, only a single, expected size band was observed.

Western blotting was carried out to analyse proteins extracted from several human SCC cell lines. In all of the cell lines, the same β-DG antibody detected a common 43 kDa band, identical to that in control skeletal muscle extracts and corresponding to the expected size for β-DG. In addition to this band, there was again a band of reduced molecular mass (about 30 kDa) in all of the cell lines (Fig. 3(a)). In three cell lines (SCC-25, SSC-4 and SSC-9), this band was more abundant than the 43 kDa band. When we used an antibody (BD Bioscience) recognising an epitope located in the middle of the β-DG molecule (as opposed to the C-terminal epitope targeted by the first antibody), only the 43 kDa band was detected (data not shown).

In some normal tissues [42] and cancer cell lines [25,32], β-DG can be degraded by the MMPs. To study whether the ≈30 kDa protein was identical with this product of β-DG proteolysis, we studied the effects of inhibition of MMP activity on the β-DG protein in SCC lines. We found that in SCC-9 cells cultured in the presence of the pan-MMP inhibitor GM6001 (Ilomastat), there was a drastic decrease in the level of the lower molecular size band and a concomitant increase in the intensity of the normal β-DG protein (Fig. 3(b)). At the concentration used (25 μM), GM6001 inhibits a range of MMPs including 1, 2, 3, 8, 9, 12 and 14. However, the same treatment of SCC-25, SCC-4 and HT-29 cells (colorectal cancer cell line used as a positive control for β-DG degradation) showed no significant effects (Fig. 3(b)). Moreover, use of the specific MMP2/MMP9 inhibitor IV had no effect in any cell line studied (data not shown).

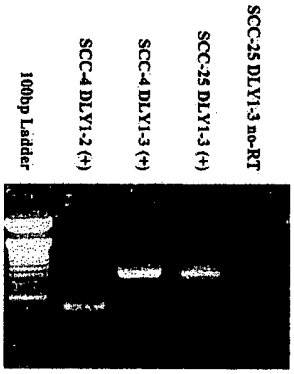

Fig. 4. Reverse transcriptase–polymerase chain reaction (RT–PCR) analysis of dystroglycan (DG) mRNA expression in squamous cell carcinoma (SCC) cells. The figure shows representative examples of agarose gel analysis of amplification products obtained with two specific primer sets. Lane 1: 100 bp ladder (Gibco-BRL). No-RT – negative control used to exclude genomic DNA contamination.

Interestingly, as in the primary tumour samples, in all SCC lines the α-DG antibody (VIA4-1) used for Western blotting gave negative results (Fig. 3(c)). However, another α-DG antibody (US Bio.) produced two bands, one of the expected size and another, smaller one (Fig. 3(d)). The smaller band often appeared as a doublet and in SCC cells further weak bands of variable size were often visible.

To analyse whether the lack of α-DG expression and aberrant β-DG expression could be the result of mRNA processing and to confirm the specificity of results obtained, we used two DG-specific primer sets in a RT–PCR analysis to amplify the pan-DG transcript. In all of the cell lines, the α/β-DG mRNA was clearly detectable and no major rearrangements within the region tested were found (Fig. 4), thus confirming the presence of DGs in SCC cells.

4. Discussion

DG α/β is a transmembrane/extracellular protein linking the extracellular basement membrane, cell membrane and intracellular cytoskeleton, providing structural integrity and interacting with a complex of proteins with putative signalling roles. To our knowledge, this is the first study demonstrating aberrant expression, processing and degradation of DG in oral SCCs.

We found that β-DG expression varies substantially among oral SCCs. In general, reduced expression of this subunit was more frequently associated with poorly differentiated tumours and increased expression was found in moderately/well-differentiated cancers. Moreover, the pattern of tumour staining was distinctive. In well-differentiated samples, the β-DG localised primarily on the tumor margin, resembling the staining pattern found in normal squamous epithelium. Moreover, we found a loss of β-DG expression in lymph nodes metastases, despite the presence of β-DG in the corresponding primary tumours. Unlike Hosokawa and colleagues [20], who found increased expression of β-DG in vascular endothelial cells within malignant tumours, we did not observe such an increase in oral cancer metastases. Our data is consistent with the recent results by Sgambato and colleagues [32]. This large series of breast and colon cancers showed a heterogeneous DG expression and low expression correlated with a higher tumour stage, high proliferation index and lower overall survival.

In addition to the variability in β-DG expression, we found no evidence of α-DG expression in the cancer tissues and SCC lines we investigated in this study with the VIA4-1 antibody. However, when another α-DG antibody was used, several immunoreactive bands were detected. Unfortunately, this antibody is not suitable for immunolocalisation. Nevertheless, this result indicates that the difficulty in detecting α-DG using the first antibody might be due to an altered post-translational processing, especially glycosylation of this protein in oral cancer. This would be in agreement with the detection of normal DG transcripts in our RT–PCR analyses. Abnormal glycosylation of DG has been found to be responsible for a number of human diseases [29] and abnormalities in glycosylation may play a role in cancer [24].

The significance of such a reduction/aberrance in DG expression in oral SCCs is currently unclear. DG is known to be involved in epithelial differentiation [6,8,21,30], epithelial cell migration/repair after injury [38] and interactions with basement membrane components [41]. Invasive growth of cancer cells is a complex process involving specific interactions between tumour cells and the orderly, integrated complexes of the ECM. Maintained integrity or disruption of the basement membranes has been proposed to play a critical role in regulating cancer invasion and metastasis. Components of the basement membrane and its overall structure are altered during tumour invasion [40].

We have shown here that the reduced expression of β-DG in oral cancer tissues and SCC lines *in vitro* was accompanied by increased levels of a ≈30 kDa product. This band was only detected by an antibody recognising the C-terminal epitope. This indicated that this smaller band was a N-terminally truncated form of β-DG. This observation is consistent with other data where this truncated form has been observed in other cancers [25,32].

An important group of proteolytic enzymes that are capable of degrading the basement membrane, as well as certain cell membrane proteins, are the MMPs [22]. We found (in one cell line) that the proteolysis of the β-DG subunit may be inhibited by a pan-matrix MMP

inhibitor. This agrees with observations made by Yamada and coworkers [42] in some normal tissues. However, we also found that the mechanism of β-DG degradation can vary dramatically in specific SCC, despite their common origin (all SCC lines used in this study were derived from tongue cancers). In three out of four cell lines, MMP inhibitors were ineffective. At the concentrations used in this study, GM6001 should inhibit MMP 1, 2, 3, 8, 9, 12 and 14, while SB3-CT should block MMP 2 and 9 function. We are currently analysing the proteinases expressed in SCC cell lines. There is evidence linking the activity of MMPs with both tumour invasion and metastasis in many tumours, including oral SCC [9,23,37,44] and the high activity of proteinases in oral carcinomas appears to be responsible for the highly invasive nature of these tumours [1,9,23].

Importantly, the data described here shows that, in addition to basement membrane proteins, β-DG may be yet another target for proteolytic degradation. Yamada and colleagues [42] showed that such processing disintegrates the DG complex and disrupts the link between the cells and the ECM.

Adhesion molecules, including DG, have multiple functions: they are critically important for proper tissue growth, differentiation and maintenance of cytoarchitecture. DG regulates the distribution of caveolin-3, which, in turn, affects α-integrin 7 receptor expression [5,35]. Therefore, dysregulation of DG may directly alter its binding to the ECM and indirectly affect adhesion *via* integrin pathways.

Moreover, degradation of β-DG may also affect cell signalling. β-DG itself is implicated in intracellular signal transduction *via* its interactions with Grb-2, an adaptor protein involved in several signalling pathways [31,34,43]. Furthermore, DG is part of the larger complex of dystrophin/utrophin-associated proteins (DAP) anchoring specific signalling molecules e.g., nitric oxide synthase [2], protein kinases [13,17,26] and specific ion channels [11]. Finally, hAG-2 and hAG-3, two unique secreted proteins involved in differentiation, interact with α-DG in a subset of breast cancers [10].

It is therefore, clear that the disruption of the DG complex may have far-reaching consequences other than just a loss of attachment to the basal lamina.

It has been shown that a lack of or altered glycosylation of brain DG in mouse knockouts results in disruption of the whole DAP complex [27,28]. It is conceivable that in cancer cells degradation of β-DG and aberrant processing/glycosylation of α-DG may have the same effect on DAP and result in changes in the properties of this complex.

In conclusion, our study indicates that abnormalities in DG expression may be a common feature in carcinogenesis and that the role of DG in cancer development and spread, although currently unclear, may be important. Considering the multifaceted role of DG in epithelial development, further studies into the clinical implications of these processes and into abnormal DG expression and processing in oral SCCs and in cancers in general are warranted.

Conflict of Interest Statement

The authors declare they have no conflict of interest.

Acknowledgements

This work was supported by a grant from The Royal College of Surgeons of England.

The China Scholarship Council, PR of China sponsored Mr. Jie Jing. The authors thank Mr. M. Ethunandan for his helpful suggestions.

References

1. Aznavoorian S, Moore BA, Alexander-Lister LD, Hallit SL, Windsor LJ, Engler JA. Membrane type I-matrix metalloproteinase-mediated degradation of type I collagen by oral squamous cell carcinoma cells. *Cancer Res* 2001, **61**, 6264–6275.
2. Brenman JE, Chao DS, Gee SH, *et al.* Interaction of nitric oxide synthase with the postsynaptic density protein PSD-95 and α1-syntrophin mediated by PDZ domains. *Cell* 1996, **84**, 757–767.
3. Chen JK, Eisenberg E, Krutchkoff DJ, Katz RV. Changing trends in oral cancer in the United States, 1935 to 1985: a Connecticut study. *J Oral Maxillofac Surg* 1991, **49**, 1152–1158.
4. Christofori G. Changing neighbours, changing behaviour: cell adhesion molecule-mediated signalling during tumour progression. *EMBO J* 2003, **22**, 2318–2323.
5. Cote PD, Moukhles H, Carbonetto S. Dystroglycan is not required for localization of dystrophin, syntrophin, and neuronal nitric-oxide synthase at the sarcolemma but regulates integrin α 7B expression and caveolin-3 distribution. *J Biol Chem* 2002, **277**, 4672–4679.
6. Durbeej M, Larsson E, Ibraghimov-Beskrovnaya O, Roberds SL, Campbell KP, Ekblom P. Non-muscle α-dystroglycan is involved in epithelial development. *J Cell Biol* 1995, **130**, 79–91.
7. Durbeej M, Henry MD, Ferletta M, Campbell KP, Ekblom P. Distribution of dystroglycan in normal adult mouse tissues. *J Histochem Cytochem* 1998, **46**, 449–457.
8. Durbeej M, Larsson E, Ibraghimov-Beskrovnaya O, *et al.* Dystroglycan binding to laminin α1LG4 module influences epithelial morphogenesis of salivary gland and lung *in vitro*. *Differentiation* 2001, **69**, 121–134.
9. Fidler IJ, Ellis LM. The implications of angiogenesis for the biology and therapy of cancer metastasis. *Cell* 1994, **79**, 185–188.
10. Fletcher GC, Patel S, Tyson K, *et al.* hAG-2 and hAG-3, human homologues of genes involved in differentiation, are associated with oestrogen receptor-positive breast tumours and interact with metastasis gene C4.4a and dystroglycan. *Brit J Cancer* 2003, **88**, 579–585.
11. Gee SH, Madhavan R, Levinson SR, Caldwell JH, Sealock R, Froehner SC. Interaction of muscle and brain sodium channels with multiple members of the syntrophin family of dystrophin-associated proteins. *J Neurosci* 1998, **18**, 128–137.
12. Górecki DC, Derry JMJ, Barnard E. Dystroglycan: brain localisation and chromosome mapping in the mouse. *Hum Molec Genet* 1994, **3**, 1589–1597.

13. Hasegawa M, Cuenda A, Spillantini MG, *et al.* Stress-activated protein kinase-3 interacts with the PDZ domain of α1-syntrophin. A mechanism for specific substrate recognition. *J Biol Chem* 1999, **274**, 12626–12631.
14. Henry MD, Campbell KP. A role for dystroglycan in basement membrane assembly. *Cell* 1998, **95**, 859–870.
15. Henry MD, Cohen MB, Campbell KP. Reduced expression of dystroglycan in breast and prostate cancer. *Hum Pathol* 2001, **32**, 791–795.
16. Hindle I, Nally F. Incidence of oral cancer. *Brit Dent J* 1991, **170**, 432.
17. Hogan A, Shepherd L, Chabot J, *et al.* Interaction of γ 1-syntrophin with diacylglycerol kinase-ζ. Regulation of nuclear localization by PDZ interactions. *J Biol Chem* 2001, **276**, 26526–26533.
18. Holt KH, Crosbie RH, Venzke DP, Campbell KP. Biosynthesis of dystroglycan: processing of a precursor propeptide. *FEBS Lett* 2000, **468**, 79–83.
19. Hood JD, Cheresh DA. Role of integrins in cell invasion and migration. *Nat Rev Cancer* 2002, **2**, 91–100.
20. Hosokawa H, Ninomiya H, Kitamura Y, Fujiwara K, Masaki T. Vascular endothelial cells that express dystroglycan are involved in angiogenesis. *J Cell Sci* 2002, **115**, 1487–1496.
21. Jiang FX, Georges-Labouesse E, Harrison LC. Regulation of laminin 1-induced pancreatic β-cell differentiation by α6 integrin and α-dystroglycan. *Mol Med* 2001, **7**, 107–114.
22. Jiang Y, Goldberg ID, Shi YE. Complex roles of tissue inhibitors of metalloproteinases in cancer. *Oncogene* 2002, **21**, 2245–2252.
23. Kawamata H, Uchida D, Hamano H, *et al.* Active-MMP2 in cancer cell nests of oral cancer patients: correlation with lymph node metastasis. *Int J Oncol* 1998, **13**, 699–704.
24. Kellokumpu S, Sormunen R, Kellokumpu I. Abnormal glycosylation and altered Golgi structure in colorectal cancer: dependence on intra-Golgi pH. *FEBS Lett* 2002, **516**, 217–224.
25. Losasso C, Di Tommaso F, Sgambato A, *et al.* Anomalous dystroglycan in carcinoma cell lines. *FEBS Lett*. 2000, **484**, 194–198.
26. Lumeng C, Phelps S, Crawford GE, Walden PD, Barald K, Chamberlain JS. Interactions between β 2-syntrophin and a family of microtubule-associated serine/threonine kinases. *Nat Neurosci* 1999, **2**, 611–617.
27. Michele DE, Barresi R, Kanagawa M, *et al.* Post-translational disruption of dystroglycan-ligand interactions in congenital muscular dystrophies. *Nature* 2002, **418**, 417–422.
28. Moore SA, Saito F, Chen J, *et al.* Deletion of brain dystroglycan recapitulates aspects of congenital muscular dystrophy. *Nature* 2002, **25**(418), 422–425.
29. Muntoni F, Brockington M, Blake DJ, Torelli S, Brown SC. Defective glycosylation in muscular dystrophy. *Lancet* 2002, **360**, 1419–1421.
30. Muschler J, Levy D, Boudreau R, Henry M, Campbell K, Bissell MJ. A role for dystroglycan in epithelial polarization: loss of function in breast tumor cells. *Cancer Res* 2002, **62**, 7102–7109.
31. Russo K, Di Stasio E, Macchia G, Rosa G, Brancaccio A, Petrucci TC. Characterization of the β-dystroglycan–growth factor receptor 2 (Grb2) interaction. *Biochem Biophys Res Commun* 2000, **274**, 93–98.
32. Sgambato A, Migaldi M, Montanari M, *et al.* Dystroglycan expression is frequently reduced in human breast and colon cancers and is associated with tumor progression. *Am J Pathol* 2003, **162**, 849–860.
33. Shah JP, Lydiatt W. Treatment of cancer of the head and neck. *CA Cancer J Clin* 1995, **45**, 352–368.
34. Sotgia F, Lee H, Bedford MT, Petrucci T, Sudol M, Lisanti MP. Tyrosine phosphorylation of β-dystroglycan at its WW domain binding motif, PPxY, recruits SH2 domain containing proteins. *Biochemistry* 2001, **40**, 14585–14592.
35. Sotgia F, Lee JK, Das K, *et al.* Caveolin-3 directly interacts with the C-terminal tail of β-dystroglycan. Identification of a central WW-like domain within caveolin family members. *J Biol Chem* 2000, **275**, 38048–38058.
36. Sugita S, Saito F, Tang J, Satz J, Campbell K, Sudhof TC. A stoichiometric complex of neurexins and dystroglycan in brain. *J Cell Biol* 2001, **154**, 435–445.
37. Werner JA, Rathcke IO, Mandic R. The role of matrix metalloproteinases in squamous cell carcinomas of the head and neck. *Clin Exp Metastasis* 2002, **19**, 275–282.
38. White SR, Wojcik KR, Gruenert D, Sun S, Dorscheid DR. Airway epithelial cell wound repair mediated by α-dystroglycan. *Am J Respir Cell Mol Biol* 2001, **24**, 179–186.
39. Williamson RA, Henry MD, Daniels KJ, *et al.* Dystroglycan is essential for early embryonic development: disruption of Reichert's membrane in Dag1-null mice. *Hum Mol Genet* 1997, **6**, 831–841.
40. Wilson DF, Jiang DJ, Pierce AM, Wiebkin OW. Oral cancer: role of the basement membrane in invasion. *Aust Dent J* 1999, **44**, 93–97.
41. Winder SJ. The complexities of dystroglycan. *Trends Biochem Sci* 2001, **26**, 118–124.
42. Yamada H, Saito F, Fukuta-Ohi H, *et al.* Processing of β-dystroglycan by matrix metalloproteinase disrupts the link between the extracellular matrix and cell membrane via the dystroglycan complex. *Hum Mol Genet* 2001, **10**, 1563–1569.
43. Yang B, Jung D, Motto D, Meyer J, Koretzky G, Campbell KP. SH3 domain-mediated interaction of dystroglycan and Grb2. *J Biol Chem* 1995, **270**, 11711–11714.
44. Yorioka CW, Coletta RD, Alves F, Nishimoto IN, Kowalski LP, Graner E. Matrix metalloproteinase-2 and -9 activities correlate with the disease-free survival of oral squamous cell carcinoma patients. *Int J Oncol* 2002, **20**, 189–194.

EXHIBIT C

EJSO (2004) 30, 589-592

Available online at www.sciencedirect.com

SCIENCE DIRECT

EJSO
the Journal of Cancer Surgery

www.ejso.com

REVIEW

Dystroglycan complex in cancer

P.A. Brennan[a,*], J. Jing[b], M. Ethunandan[a], D. Górecki[b]

[a]*Maxillofacial Unit, Department of Head and Neck Surgery, Queen Alexandra Hospital, Portsmouth PO6 3LY, UK*
[b]*Molecular Medicine Group, School of Pharmacy and Biomedical Sciences, Institute of Biomedical and Biomolecular Sciences, St Michael's Building, White Swan Road, Portsmouth, UK*

Accepted for publication 20 March 2004

Available online 19 May 2004

KEYWORDS
Dystroglycan; Cancer; Adhesion; Metastasis; Review

Summary Abnormalities in the interactions between tumour cells, adhesion molecules and extracellular matrix proteins are often implicated in the behaviour of carcinoma cells. The α- and β-dystroglycan (DG) proteins form part of the large dystrophin-associated protein (DAP) complex. They are involved in epithelial cell development, formation of the basement membrane and maintenance of tissue integrity. Specific changes and reduction or loss of DG expression have been reported in human breast, colon, head and neck, and prostate cancers, implicating it in tumour invasion and dissemination. Degradation of β-DG by matrix metalloproteinase (MMP) enzymes may assist tumour dissemination. We report the present knowledge of the DG interactions in solid tumour biology.

Introduction

Cell-cell and cell-extracellular matrix interactions are essential in the development and maintenance of normal tissue cytoarchitecture and play an important role in the development and progression of many types of cancer. Abnormalities in the interactions between tumour cells and extracellular matrix proteins are often implicated in the aberrant behavior of carcinoma cells and defects in the structure and function of basement membranes often occur in metastatic disease.[1]

The roles of different adhesion molecules and their binding ligands are not fully understood. It is clear that these proteins have multiple functions. They connect epithelial cells to the basal lamina and contribute to exchange of information with the extracellular environment, connect and organize the cytoskeleton, and participate in signal transduction processes.[1] As such, adhesion molecules are critically important for proper tissue growth, differentiation and maintenance of cyto-architecture. Until recently, studies on the cell adhesion molecules in cancer concentrated mainly on the integrin protein family.[1,2] However, there is a growing body of evidence that other adhesion proteins may play an equally important role. There has been considerable interest in recent years in the role that dystroglycan (DG) and related proteins play in cancer.

Dystroglycan receptor

Dystroglycan (DG) is a cellular receptor expressed by a variety of tissues, interacting with extracellular proteins including laminin, perlecan and agrin,[3]

*Corresponding author. Tel.: +44-2392-286064; fax: +44-2393-286089.
E-mail address: peter.brennan@porthosp.nhs.uk

0748-7983/$ - see front matter © 2004 Elsevier Ltd. All rights reserved.
doi:10.1016/j.ejso.2004.03.014

and membrane proteins such as the neurexins.[4] The biosynthesis and the structure of DG are complex.[3] DG is a product of a single gene but the primary peptide is post-translationally cleaved, resulting in two protein subunits (α and β), which interact to form a functional non-covalent complex. β-dystroglycan (β-DG) is a 43 kDa transmembrane protein, while the predicted 72 kDa α-dystroglycan (α-DG) peptide undergoes further post-translational modifications resulting in a heavily glycosylated extracellular protein. Its molecular mass can vary in different tissues (120-180 kDa), depending on the degree of glycosylation. Dystroglycan exists in a tight association with either dystrophin or its autosomal homologue—utrophin and plays a significant part in a complex of proteins assembled around them.

Functions of dystroglycan

In muscle, where its role has been characterized most extensively, α and β DG functions as a part of a large dystrophin-associated protein (DAP) complex. This contains an array of transmembrane, cytoplasmic and extracellular proteins crucial for proper muscle function. Dystrophin and utrophin bind actin filaments of the cytoskeleton. Therefore, α/β DG is a transmembrane/extracellular protein complex linking the extracellular basement membrane (e.g. laminin), cell membrane and the intracellular cytoskeleton, and provides structural integrity. It also interacts with a complex of proteins with different properties, including putative signaling roles (Fig. 1). Mutations disrupting this complex result in muscular dystrophy. However, DG has an increasingly recognized important role in non-muscle tissues. Knockout of the DG gene in mice results in embryonic death in utero. This early lethality is caused by disruption of the Reichert's membrane—an early basement membrane.[5] Later in foetal development this protein has a crucial role in kidney and salivary gland epithelial morphogenesis.[6] DG is expressed by squamous epithelium[7] at the basal interfaces of the cells directly apposing basement membranes. DG disruption results in neuronal migration errors in the developing brain.[8] All these studies point to DG having a role in epithelial and neuronal cell development, formation of the basement membrane and maintenance of tissue integrity.[9] Dystroglycan expression and its interactions with other proteins such as laminin may be a prerequisite for the deposition of other basement membrane proteins.[9]

DG regulates the distribution of caveolin-3 in epithelial tissue and the subsequent expression of the alpha-integrin 7 receptor.[10,11] Therefore, dysregulation of DG probably also affects cellular adhesion via integrin pathways. Abnormal expression of DG not only results in the disruption of the structural link between the extracellular matrix, the cell membrane and the intracellular cytoskeleton, but also leads to changes in cell shape and loss of adhesion. It may also affect signaling pathways. Dystroglycan itself is implicated in intracellular signal transduction via its interactions with Grb-2, an adaptor protein involved in several signaling pathways.[12] Being part of the larger complex of dystrophin/utrophin associated proteins (DAP), dystrogylcan and related protein subclasses (such as the syntrophins) are responsible for anchoring specific protein kinases.[11,13] hAG-2 and hAG-3, two unique secreted proteins involved in cellular differentiation, interact with α-DG in a subset of breast cancers.[14] It is, therefore, clear that disruption of the DG complex may have far more reaching consequences than just a loss of attachment to basal lamina.

Dystroglycan and solid tumours

Specific changes in DG expression have been described in human breast, colon and prostate cancers.[15-17] A large series of breast and colon cancers showed heterogeneity of β-DG expression and low or absent α-DG expression when compared to normal epithelial tissue.[17] Low or absent α-DG correlated with a higher tumour stage, high proliferation index and lower overall survival in these cancers. Reduced α-DG has been demonstrated in prostate cancer, which was also associated with tumour progression.[16] We have recently found similar results in oral squamous cell carcinomas[18] and in skin cancers. We demonstrated that loss of both β-DG and α-DG was a consistent finding in lymph node metastasis from patients with a primary oro-pharyngeal tumour.[18] These studies indicate that abnormalities in DG expression can be a common feature in carcinogenesis and may play a role in tumour spread and metastasis. DG proteins may have a far wider role than just an epithelial cell-basal lamina interaction. β-DG appears to have a role to play in angiogenesis since its immunohistochemical expression is increased in vascular endothelium within malignant tumours, although it is not expressed in normal endothelium.[19] It also appears to be involved with cellular differentiation, since it interacts with a number of proteins involved in this process in breast cancer.[14] Loss of DG also results in loss of polarization of breast cancer cells.[20] Taken together, these processes suggest that DG has many other functions both in normal

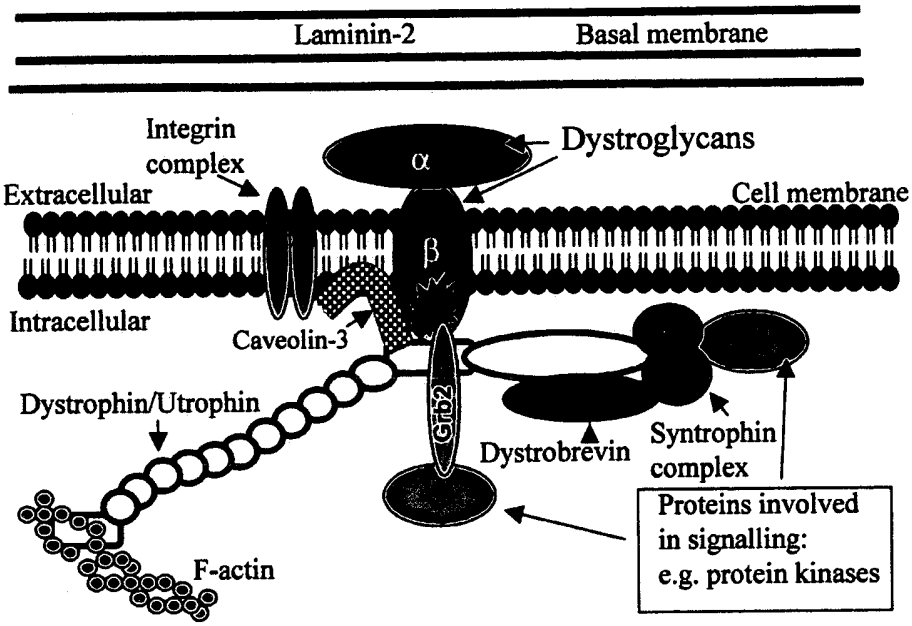

Figure 1 The complex relationship of the dystrophin associated protein complex and related proteins to the cell membrane and basal lamina.

epithelium and cancer, which warrant further evaluation.

Degradation of dystroglycan by matrix metalloproteinases

Disruption of the basement membranes occurs in cancer invasion and metastasis. An important group of proteins involved in metastasis are the matrix metalloproteinases (MMPs). These highly homologous proteolytic enzymes are involved in the degradation of basement membrane and other extracellular components as well as certain cell membrane proteins. The overall effect of MMP depends on the interaction and an alteration in balance with their natural inhibitors, tissue inhibitors of metallo-proteinases (TIMP).[21,22] MMP-2 and MMP-9 activity correlates with both tumour invasion and metastasis in many tumours, and expression of these enzymes may also correlate with poor outcome.[23-25] DG is another target of the MMP family. Yamada et al.[26] showed that β-DG degradation by MMP disintegrates the DG complex and disrupts the link between epithelial cells and the extracellular matrix via the dystroglycan complex. It was concluded that this mechanism could have profound effects on cell viability, and that dystroglycan may play a crucial role in the molecular pathogenesis various muscular dystrophies.[26] The results of this study can be extrapolated such that MMP-dependent disruption of the DG complex might play an important role in human tumour development and progression. In our own studies, we found that β-DG degradation in cancer cell lines was inhibited with the pan-MMP inhibitor drug Ilomastat in head and neck cancer.[18] However, since this proteolysis may be executed by a broad spectrum of MMPs, attempts to use specific MMP inhibitor drugs to control such degradation may be difficult.

The data suggests that, in addition to basement membrane proteins, β-DG is yet another target for MMP activity in cancers. However, while MMPs are certainly involved in the DG proteolysis in specific SCC cells, such degradation is not necessarily dependent on one particular type of MMP but rather can be executed by a range of proteinases. Different cancer cells producing specific subsets of MMPs would still be able to degrade β-DG. Therefore, MMP-dependent disruption of the DG complex might play an important role in human tumour development and progression.

Conclusions

Adhesion molecules, including DG, have multiple functions. Not only do they connect epithelial cells to the basal lamina, but they also contribute to exchange of information with the extracellular environment, connect and organize the cytoskeleton, and participate in signal transduction

processes. They are critically important for proper tissue growth, differentiation and maintenance of cytoarchitecture. When considering the multifaceted role of DG in normal epithelial cell development, further studies into the clinical implications of these processes and into abnormalities of DG expression and processing in all the common cancers and in carcinogenesis in general are warranted. It appears that the role of DG both in cancer development and spread, although currently not understood, may be significant.

References

1. Hood JD, Cheresh DA. Role of integrins in cell invasion and migration. *Nat Rev Cancer* 2002;**2**:91–100.
2. Christofori G. Changing neighbours, changing behaviour: cell adhesion molecule-mediated signalling during tumour progression. *EMBO J* 2003;**22**:2318–23.
3. Winder SJ. The complexities of dystroglycan. *Trends Biochem Sci* 2001;**26**:118–24.
4. Sugita S, Saito F, Tang J, Satz J, Campbell K, Sudhof TC. A stoichiometric complex of neurexins and dystroglycan in brain. *J Cell Biol* 2001;**154**:435–45.
5. Williamson RA, Henry MD, Daniels KJ, Hrstka RF, Lee JC, Sunada Y, Ibraghimov-Beskrovnaya O, Campbell KP. Dystroglycan is essential for early embryonic development: disruption of Reichert's membrane in Dag1-null mice. *Hum Mol Genet* 1997;**6**:831–41.
6. Durbeej M, Larsson E, Ibraghimov-Beskrovnaya O, Roberds SL, Campbell KP, Ekblom P, Durbeej M, Talts JF, Henry MD, Yurchenco PD, Campbell KP, Ekblom P. Dystroglycan binding to laminin alpha1LG4 module influences epithelial morphogenesis of salivary gland and lung in vitro. *Differentiation* 2001;**69**:121–34.
7. Durbeej M, Henry MD, Ferletta M, Campbell KP, Ekblom P. Distribution of dystroglycan in normal adult mouse tissues. *J Histochem Cytochem* 1998;**46**:449–57.
8. Moore SA, Saito F, Chen J, Michele DE, Henry MD, Messing A, Cohn RD, Ross-Barta SE, Westra S, Williamson RA, Hoshi T, Campbell KP. Deletion of brain dystroglycan recapitulates aspects of congenital muscular dystrophy. *Nature* 2002;**418**: 422–5.
9. Henry MD, Campbell KP. A role for dystroglycan in basement membrane assembly. *Cell* 1998;**95**:859–70.
10. Sotgia F, Lee JK, Das K, Bedford M, Petrucci TC, Macioce P, Sargiacomo M, Bricarelli FD, Minetti C, Sudol M, Lisanti MP. Caveolin-3 directly interacts with the C-terminal tail of beta-dystroglycan. Identification of a central WW-like domain within caveolin family members. *J Biol Chem* 2000;**275**: 38048–58.
11. Cote PD, Moukhles H, Carbonetto S. Dystroglycan is not required for localization of dystrophin, syntrophin, and neuronal nitric-oxide synthase at the sarcolemma but regulates integrin alpha 7B expression and caveolin-3 distribution. *J Biol Chem* 2002;**277**:4672–9.
12. Russo K, Di Stasio E, Macchia G, Rosa G, Brancaccio A, Petrucci TC. Characterization of the beta-dystroglycan-growth factor receptor 2 (Grb2) interaction. *Biochem Biophys Res Commun* 2000;**274**:93–8.
13. Yang B, Jung D, Motto D, Meyer J, Koretzky G, Campbell KP. SH3 domain-mediated interaction of dystroglycan and Grb2. *J Biol Chem* 1995;**270**:11711–4.
14. Fletcher GC, Patel S, Tyson K, Adam PJ, Schenker M, Loader JA, Daviet L, Legrain P, Parekh R, Harris AL, Terrett JA. hAG-2 and hAG-3, human homologues of genes involved in differentiation, are associated with oestrogen receptor-positive breast tumours and interact with metastasis gene C4.4a and dystroglycan. *Br J Cancer* 2003;**88**:579–85.
15. Losasso C, Di Tommaso F, Sgambato A, Ardito R, Cittadini A, Giardina B, Petrucci TC, Brancaccio A. Anomalous dystroglycan in carcinoma cell lines. *FEBS Lett* 2000;**484**:194–8.
16. Henry MD, Cohen MB, Campbell KP. Reduced expression of dystroglycan in breast and prostate cancer. *Hum Pathol* 2001;**32**:791–5.
17. Sgambato A, Migaldi M, Montanari M, Camerini A, Brancaccio A, Rossi G, Cangiano R, Losasso C, Capelli G, Trentini GP, Cittadini A. Dystroglycan expression is frequently reduced in human breast and colon cancers and is associated with tumor progression. *Am J Pathol* 2003;**162**:849–60.
18. Jing J, Lien CF, Sharma S, Brennan PA, Gorecki DG. Aberrent expression, processing and degradation of dystroglycans in oral squamous cell carcinoma (unpublished data).
19. Hosokawa H, Ninomiya H, Kitamura Y, Fujiwara K, Masaki T. Vascular endothelial cells that express dystroglycan are involved in angiogenesis. *J Cell Sci* 2002;**115**:1487–96.
20. Muschler J, Levy D, Boudreau R, Henry M, Campbell K, Bissell MJ. A role for dystroglycan in epithelial polarization: loss of function in breast tumor cells. *Cancer Res* 2002;**62**:7102–9.
21. Jiang Y, Goldberg ID, Shi YE. Complex roles of tissue inhibitors of metalloproteinases in cancer. *Oncogene* 2002; **21**:2245–52.
22. Werner JA, Rathcke IO, Mandic R. The role of matrix metalloproteinases in squamous cell carcinomas of the head and neck. *Clin Exp Metastasis* 2002;**19**:275–82.
23. O-Charoenrat P, Rhys-Evans P, Modjtahedi H, Court W, Box G, Eccles S. Overexpression of epidermal growth factor receptor in human head and neck squamous carcinoma cell lines correlates with matrix metalloproteinase-9 expression and in vitro invasion. *Int J Cancer* 2000;**86**:307–17.
24. Cho NH, Shim HS, Rha SY, Kang SH, Hong SH, Choi YD, Hong SJ, Cho SH. Increased expression of matrix metalloproteinase 9 correlates with poor prognostic variables in renal cell carcinoma. *Eur Urol* 2003;**44**:560–6.
25. Azenshtein E, Luboshits G, Shina S, Neumark E, Shahbazian D, Weil M, Wigler N, Keydar I, Ben-Baruch A. The CC chemokine RANTES in breast carcinoma progression: regulation of expression and potential mechanisms of promalignant activity. *Cancer Res* 2002;**62**:1093–102.
26. Yamada H, Saito F, Fukuta-Ohi H, Zhong D, Hase A, Arai K, Okuyama A, Maekawa R, Shimizu T, Matsumura K. Processing of beta-dystroglycan by matrix metalloproteinase disrupts the link between the extracellular matrix and cell membrane via the dystroglycan complex. *Hum Mol Genet* 2001;**10**: 1563–9.

Journal of Mammary Gland Biology and Neoplasia, Vol. 8, No. 4, October 2003 (© 2004)

EXHIBIT D

Dystroglycan: Emerging Roles in Mammary Gland Function

M. Lynn Weir[1] and John Muschler[1,2]

Dystroglycan (DG) is a single receptor that binds to multiple basement membrane proteins and forms a transmembrane link to the actin cytoskeleton. It was first isolated as a component of the dystrophin–glycoprotein complex, which plays a role in the maintenance of muscle cell integrity and is defective in many muscular dystrophies. Although studied most extensively in muscle tissues, DG is present at most cell–basement membrane interfaces, and only recently has investigation of DG functions in nonmuscle cells gained momentum. Information emerging from recent studies in epithelial cells is implicating DG in a wide range of critical cell responses to the basement membrane, ranging from organization of tissue architecture to cell survival. Moreover, DG functions appear to be frequently absent in carcinoma cells, implicating its loss in cancer progression. Although many questions remain as to its precise role in mammary tissue, DG is emerging as a potentially important player in mammary gland function.

KEY WORDS: dystroglycan; laminin; epithelial; carcinoma; mammary; breast.

INTRODUCTION

It has been well established that receptors for basement membrane (BM) proteins are essential regulators of mammary epithelial architecture and function, with particular importance given to receptors for laminins. BM receptors expressed in mammary epithelial cells are known to mediate signals for growth inhibition, cell shape and cytoskeletal changes, survival, polarization, and tissue-specific gene expression (1–4). It is also well established that the response of cells to the BM is altered in breast carcinoma cells, and that such alterations are critical steps in cancer progression (5). Revealing the distinct and cooperative functions of BM receptors in mammary epithelial cells is required to understand the regulation of normal mammary development and the signaling alterations leading to the progression of breast cancer. However, dissection of the exact roles played by BM receptors operating in mammary development and differentiation has proceeded slowly. Among these receptors, the greatest attention has been given to the well-characterized integrin family. But, attention is increasingly turning to other, nonintegrin BM receptors, which are proving to have important roles in the mammary gland distinct from those of integrins (e.g. (6,7)).

One of the latest BM receptors to be implicated in mammary epithelial function is dystroglycan (DG). DG is a single receptor that binds to multiple BM proteins, including laminins and perlecan (8–14). DG was discovered in the study of muscle cells, where loss of DG function has been implicated in the pathology of some muscular dystrophies (15,16). Consequently, intense investigation has focused on DG's roles in muscle biology and, although DG was identified more than a decade ago, its characterization in epithelial cell function has lagged. So few studies have directly addressed DG's role in mammary epithelial cells (or even in epithelial cells) that this subject could be argued not to justify a review. Yet, the information that exists, pooled from

[1] Cancer Research Department, California Pacific Medical Center Research Institute, San Francisco, California.
[2] To whom correspondence should be addressed at California Pacific Medical Center Research Institute, 2330 Clay St., San Francisco, California 94115; e-mail: muschler@cooper.cpmc.org.

Abbreviations used: BM, basement membrane; DG, dystroglycan; ECM, extracellular matrix; ES, embryonic stem; LG, laminin G-like; T4-2, HMT-3522-T4-2.

1083-3021/03/1000-0409/0

work in a variety of cell types, strongly suggests important roles for DG in normal mammary epithelial development and homeostasis, including growth control, cell polarization, cell survival, tissue morphogenesis, BM assembly, cytoskeletal organization and tissue-specific gene expression (see below). Coupled with this information is the observation that DG function is clearly compromised in many carcinoma cells, and such a loss likely contributes to cancer progression (see below). Therefore, the roles of DG in mammary gland function and breast cancer appear to comprise important and neglected avenues of research.

It is the purpose of this review to introduce DG to the field of mammary gland biology and to summarize what is known of its functions as they relate to the mammary gland and its pathology. This information will be pooled from work in a variety of cell types and from the few intriguing studies in epithelial cells.

DG DISCOVERY

What we currently know (and don't know) about DG is the consequence of its initial discovery in skeletal muscle cells and its high relevance to muscular dystrophies. DG was first isolated in 1990 during the search for membrane molecules associated with dystrophin, the cytoskeletal protein that is defective in Duchenne's muscular dystrophy (17). These efforts resulted in the discovery of a novel complex of glycoproteins, labeled as the "dystrophin–glycoprotein complex" (18). Subsequent cloning of these molecules revealed the complex to consist of multiple transmembrane molecules (15). The dystrophin–glycoprotein complex from skeletal muscle cells is illustrated in Fig. 1. DG forms the core of the complex and is composed of two subunits, α and β. The β-DG subunit spans the membrane, while the α-DG subunit is held to the cell surface by noncovalent

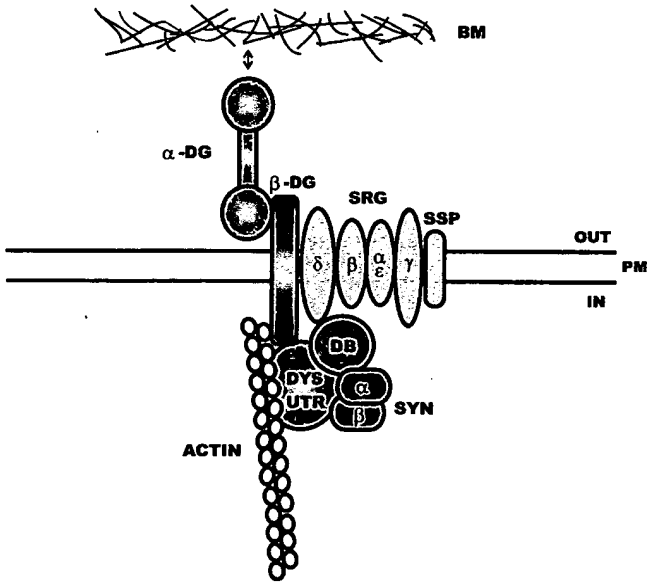

Fig. 1. *Structure of the dystrophin–glycoprotein complex in skeletal muscle cells.* The α- and β-subunits of dystroglycan (DG), sarcoglycans (SRG), and sarcospan (SSP) comprise the main proteins of the complex. Cytoplasmic binding partners include dystrophin/utrophin (DYS/UTR), dystrobrevin (DB), and syntrophins (SYN). The complex serves as a transmembrane link between basement membrane (BM) proteins and the actin cytoskeleton. (PM = plasma membrane.)

interactions with β-DG. Other members of the dystrophin–glycoprotein complex include the transmembrane proteins, sarcoglycans, and sarcospan. This complex, in turn, interacts with multiple cytoplasmic proteins, including dystrobrevin, syntrophin, utrophin, and dystrophin, the latter two linking to actin.

Almost immediately following the isolation of DG, it was recognized that the α-subunit binds to laminin-1 with high affinity, revealing α- and β-DG to be two components of a transmembrane link between the extracellular matrix and the actin cytoskeleton (19). In retrospect, it was revealed that α-DG had been identified at least twice previously through its high affinity interactions with laminin; α-DG was reported in 1987 as a laminin-binding protein, then named "cranin," which was present in many cultured cell types, from fibroblasts to neural cells (20), and was identified again in 1988, as a laminin-interacting receptor in chick neural tissue (21).

Following characterization of the dystrophin–glycoprotein complex in muscle cells, it was recognized that DG expression is widespread, being evident in muscle, neural tissue, and in epithelia, including those of the mammary gland (19,22,23). In epithelia, DG is primarily polarized to the basal domain, as expected of a BM receptor. Some pericellular immunostaining of DG was also observed in mammary epithelial cells in vivo, and DG has been reported at cell–cell contacts in MCF-10 breast epithelial cells (22,24). The localization of DG at the basal side of mammary epithelial cells was the first indication that it might play an important role in these cells' function.

Extensive information has been assembled about the molecular characteristics of DG and about DG-associated molecules, although few of these data come from investigations in epithelial cells. Even the composition of the dystrophin–glycoprotein complex in epithelial cells is uncertain. Observations in kidney and lung epithelia indicate that most sarcoglycans and sarcospan are not expressed (25). In muscle cells, some sarcoglycans are necessary to stabilize α-DG at the cell surface (26–28); therefore, presumably some DG-associated molecules are present in epithelial cells to carry out similar functions. Syntrophin and dystrobrevin are found in kidney epithelial cells (29,30), as are dystrophin isoforms and utrophin (25,29,31). But, the presence of dystrophin–glycoprotein complex components in mammary epithelial cells has not been directly tested.

MOLECULAR CHARACTERISTICS OF DG

In mammals, DG is encoded by a single gene, *DAG1*, consisting of two exons and one intron, with no evidence of alternate spliced exons (19,32,33). In humans, the DG gene is located on chromosome 3 band 21 (32) and in mice, on chromosome 9 (34). Protein sequence comparisons reveal that DG is a structurally distinct molecule and is not a member of a receptor family. It lacks strong homology with other proteins, although some homology has been noted with immunoglobulin and cadherin-like domains (35,36). This lack of significant homology with other molecules is remarkable, considering that DG is an ancient protein, as are other dystrophin–glycoprotein complex components, with homologs identified in *Drosophila* and *C. elegans* (16). The DG protein sequence is highly conserved within mammalian species (32).

Posttranslational cleavage of DG early in processing separates the precursor translation product into the two polypeptides, α- and β-DG. The α-DG subunit possesses two globular regions separated by a mucin-like domain (37). The protein molecular mass of α-DG is only 72 kDa, while it migrates on polyacrylamide gels between 120 and 200 kDa, reflecting extensive glycosylation. The globular domains include potential sites for N-glycosylation, and the mucin-like region includes multiple consensus sites for O-linked glycosylation. Most extracellular matrix (ECM) binding sites within α-DG appear to involve a carbohydrate with an uncommon O-mannosyl linkage, presumably within the mucin-like region (38).

The β-DG subunit, consisting of 241 amino acids, contains a potential N-linked glycosylation site at its extracellular N-terminal and a single membrane-spanning region located in the center of the sequence (19). Within its cytoplasmic domain, there are numerous proline-rich (PXXPX) motifs and Y(Ph)XXh (Ph = phosphorylation potential; h = hydrophobic) sequences, which are recognized by SH3 and SH2 domain proteins, respectively (19,39). The PPPY sequence at position 889–892 of β-DG is known to be tyrosine phosphorylated in cultured cells and tissues in vivo (40–42) and overlaps with one SH3 and two SH2 domain protein recognition motifs (19,39). This region is of particular importance for associations with intracellular binding partners (see below). The N-terminal extracellular region of β-DG interacts noncovalently with the C-terminal portion of α-DG between amino acids 550–585 (43).

EXTRACELLULAR LIGANDS

DG binds via its α-subunit to many known ligands, including: laminin-1 (9), laminin-2 (8,14), laminin-10/11 (44), perlecan (8,13), agrin (11), neurexin (10), and biglycan (12) (Fig. 2(A)). Those ligands for DG that are prevalent in the mammary gland are the laminins and perlecan. Expression of biglycan has been detected in this tissue, but is not widespread (45). Agrin too has been reported in epithelial BM (46), but its presence in the mammary gland has not yet been described. However, the National Center for Biotechnology Information (NCBI) nucleotide database does contain agrin cDNAs derived from this tissue, suggesting that it is expressed.

Glycosylation of α-DG, presumably within the mucin-like domain, allows binding to most ligands in a calcium-dependent manner through their "laminin G-like" (LG) modules, a protein motif present in many ECM proteins (47). So far, the one exception is biglycan, which interacts somewhere within the C-terminal globular domain of α-DG (amino acids 494–653), independent of glycosylation (12). Whether this site overlaps with the binding region for β-DG (amino acids 550–585) (43) has yet to be determined. In perlecan, binding to DG has been mapped to the C-terminal domain V, which contains the LG modules (8). In laminin-1, laminin-2, and laminin-10/11, the association with α-DG has been mapped within the LG4, LG1-3 plus LG4-5, and LG4-5 regions of their α-chains, respectively (Fig. 2(B)) (8,44). The C-terminal LG motifs are distinct among different laminin α-subunits, and the characteristics of DG binding to each is distinct (8,48). The LG4-5 region of laminin α2 chain has been crystallized, detailing the structural basis for α-DG interaction with this domain (49). The binding site of α-DG on laminin-1 is significant because the LG4-5 region comprises the "E3 fragment" (Fig. 2(B)). This fragment is one of several derived from elastase digests of laminin-1 and has been used extensively to assign biological functions to receptors that interact with this domain. The E3 fragment has been applied as a competitive inhibitor of receptor–laminin binding in studies of epithelial morphogenesis and function, and exhibits clear effects on cell behavior (see below). Although actions of the E3 fragment include DG inhibition, they cannot be attributed to it alone with certainty; in addition to DG, the E3 fragment of laminin associates with heparin, heparan sulfates, sulfatides, some BM molecules, and BM receptors (8,50).

CYTOPLASMIC INTERACTIONS

Data obtained using immunoprecipitations, ligand affinity columns and in vitro binding assays suggest that DG may interact with a large variety of intracellular proteins via the C-terminus of its β-subunit, although the in vivo significance of such associations is unknown (Fig. 2(A)). Many of these molecules are ubiquitously expressed and, while they have not been directly assessed in mammary cells, may associate with β-DG in mammary tissue as well. The extreme C-terminus of β-DG is a hotbed of binding activity, containing three known sites for protein interaction, recognized by SH3, WW, and SH2 domain proteins (Fig. 2(A)). Since these motifs are in close proximity, there is competition among molecules for association with DG. Additional sequences recognized by SH2 and SH3 domain proteins exist within other regions of the β-DG cytoplasmic domain, but have yet to be implicated in DG binding.

One site of interest for β-DG interactions consists of the proline-rich motif PYVPP at position 891–895, a consensus sequence recognized by SH3 domain proteins (39). Immunoprecipitations and ligand affinity columns using skeletal muscle and brain extracts show that Grb-2 (growth factor receptor-bound protein-2) associates with the C-terminus of β-DG (51,52), and in vitro binding assays reveal interactions between the Grb2-SH3 domains and the last 20 amino acids of β-DG, which encompass the PYVPP motif (53).

A second site of importance for β-DG binding partners is the PPPY sequence at position 889–892. Both dystrophin and utrophin associate with this motif in part via a WW domain at their C-termini (54). WW motifs, comprising 35 amino acids of which two tryptophan (W) residues are essential, recognize proline-rich sequences in binding partners (54). In vitro binding assays have demonstrated that dystrophin inhibits the interaction of β-DG with Grb2 (53), presumably due to the overlap of recognition sites on β-DG. Interestingly, immunoprecipitations and in vitro binding assays have shown that phosphorylation of DG's tyrosine 892 disrupts DG association with dystrophin/utrophin recombinant domains (40,41). Such phosphorylation is cell adhesion-dependent (41), induced by cell attachment to ECM proteins (42), enhanced by Src (55) and correlates with the intracellular localization of β-DG in cultured cells and skeletal muscle tissue in vivo (42). In vitro binding assays have revealed that the interaction of DG with dystrophin and utrophin recombinant

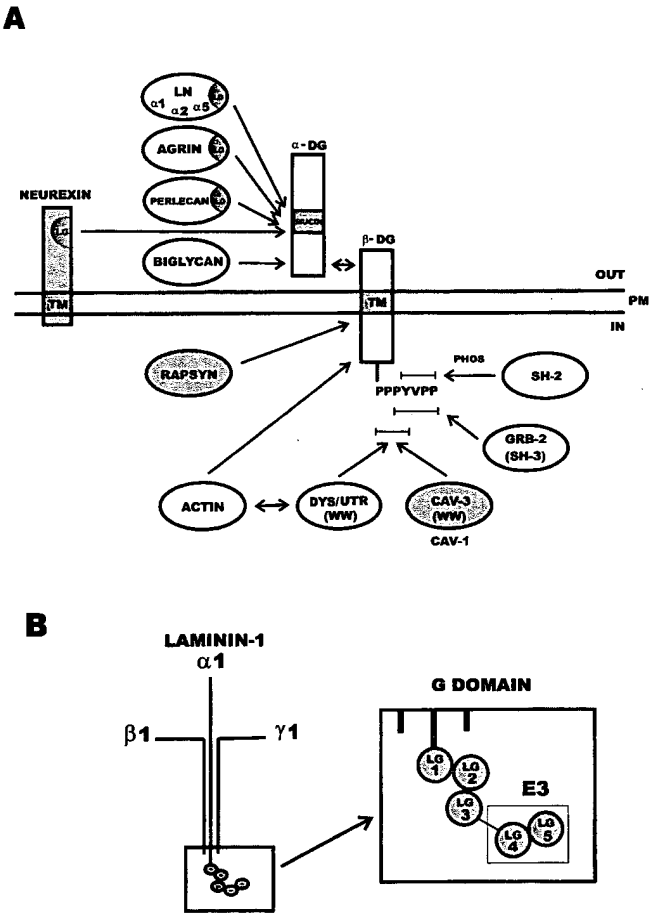

Fig. 2. *Extracellular and intracellular binding partners of dystroglycan.* (A) The α-dystroglycan subunit (α-DG) interacts with basement membrane proteins, such as laminin (LN), agrin, perlecan, and biglycan, as well as the transmembrane (TM) protein, neurexin. All but one of these molecules associate with glycosylated α-DG, presumably within the mucin-like region, via their laminin G-like (LG) domains. The β-dystroglycan subunit (β-DG) may interact with many cytoplasmic proteins, including rapsyn, actin, dystrophin/utrophin (DYS/UTR), caveolin-1 and -3 (CAV-1; CAV-3), Grb-2 and SH2 domain proteins. Binding sites within amino acids 889–895 from the C-terminus of β-DG are shown by lines over and under the sequence. Proteins not found in mammary gland are shaded grey. Arrows show protein associations. (PHOS = phosphorylation of tyrosine 892; PM = plasma membrane.) (B) Structure of the G domain in laminin-1. The C-terminal of the α1 chain contains five laminin G-like modules (LG1-5), of which LG4-5 comprises the E3 fragment, generated by elastase digestion of laminin-1.

domains is also inhibited by calmodulin, which binds to dystrophin and utrophin (56,57). Like dystrophin, caveolin-3, a muscle-specific component of caveolae, also uses its WW domains to associate with the PPPY motif in β-DG (58). Ligand affinity columns and immunoprecipitations have shown that caveolin-3 can compete with dystrophin recombinant domains for binding to DG, but this interaction is not influenced by phosphorylation of DG's tyrosine 892, unlike dystrophin (58). Like mutation of dystrophin–glycoprotein complex components, mutation of the caveolin-3 gene in humans can cause muscular dystrophy (16). Caveolin-1 also interacts with β-DG, but there are conflicting reports as to whether phosphorylation of DG's tyrosine 892 affects binding (55,58). Caveolin-1, but not −3, is present in the mammary gland (59), but interactions with β-DG have yet to be investigated in this tissue.

A third site for molecular associations with β-DG is the YVPP sequence at position 892–895 which, when phosphorylated, becomes a consensus sequence recognized by SH2 domain proteins (39). This motif overlaps with the regions at which WW and SH3 domain proteins bind to DG. When DG's tyrosine 892 is phosphorylated, dystrophin/utrophin can no longer associate with the PPPY site (40,41) and is replaced by SH2 domain proteins, such as c-Src, Csk, SHC, Fyn, and NCK (55). Such phosphorylation may act as a regulatory switch to inhibit binding of certain WW domain proteins (dystrophin/utrophin) and allow recruitment of other WW domain proteins (caveolin) and SH2 domain proteins.

Additional binding partners for DG may include actin, which has been shown to interact directly with the cytoplasmic domain of β-DG by yeast 2-hybrid and in vitro binding assays (60). Rapsyn is important in neuromuscular junction formation and interacts with an intracellular site near the transmembrane domain of β-DG (61). Although rapsyn is also expressed in nonmuscle cells, there have been no reports of a mammary gland presence (62). FAK (focal adhesion kinase, p125) has also been found in the Grb2/DG complex from brain, but may bind Grb2, rather than DG (52).

DG FUNCTIONS IN EPITHELIA

The earliest indications of DG function were from muscular dystrophies, where alterations in the dystrophin–glycoprotein complex are evident in humans and in mouse models of the disease (16). However, these diseases do not involve direct mutation of the DG molecule, leaving its precise role undefined. Knockout of the DG gene in transgenic mice results in lethality at embryonic day 6.5, which is attributed to disrupted formation of Reichert's membrane, suggesting defects in early BM formation (63). Since that study, conditional knockout of DG has been achieved in adult skeletal muscle and the central nervous system of transgenic mice (64–66). These knockouts mimic effects observed in human diseases, producing mild muscle dystrophy with hypertrophy, brain malformations, and defects in neural migration. However, the exact functions of DG remain obscure, and these studies have not shed light on the role of DG in epithelial cells.

To date, only a few publications have addressed the role of DG in mammary epithelial cells, with some additional studies in other epithelial systems. In retrospect, the first manipulations of DG function in mammary epithelial cells were through use of the laminin-1 E3 fragment, which competes with laminin-1 for DG binding and inhibits DG's actions. Cultured mammary epithelial cells exposed to laminin exhibit multiple responses, including growth inhibition, cell shape changes, and the induction of tissue-specific gene expression (β-casein) (3,4). Intriguingly, the E3 fragment has been shown to block all of these signals (3,4). β1 and α6 integrin-blocking antibodies also inhibit β-casein expression, but do not mimic the other effects of the E3 fragment (4). From these observations, it was concluded that a nonintegrin receptor for the laminin E3 fragment initiates signals for growth inhibition and morphogenic changes in mammary epithelial cells, and possibly signals for tissue-specific gene expression. The effects of the E3 fragment are mimicked by heparin, which also blocks the laminin-DG interaction (4), but neither the E3 fragment nor heparin is a specific inhibitor for this receptor-ligand association. Thus the data at hand suggest that DG is involved in basement membrane interactions, but firm evidence is lacking. The most direct experiments in which DG was manipulated in mammary epithelial cells employed overexpression of the DG cDNA in breast tumor cells lacking normal responses to BM proteins. In the breast tumor cell line, HMT-3522-T4-2 (T4-2), overexpression of the DG cDNA elevated α-DG from low levels (6). Correspondingly, T4-2 cells expressing increased amounts of α- and β-DG exhibited an enhanced response to BM proteins, including cell shape changes, cytoskeletal alterations and restricted growth (6). Importantly, corresponding with the restoration of cell shape changes, the DG

overexpressing cells regained the ability to polarize and restrict growth in 3D cultures of BM proteins, indicating that DG can mediate polarity signals known to originate from interactions with the BM (6). A role for DG in epithelial polarization was subsequently supported by genetic manipulations in *Drosophila*, where deletion of the DG gene in chimeric organisms causes a loss of polarity in the follicle epithelial cells (67). In the *Drosophila* study, cells lacking DG (DG−/−) ultimately disappeared from the adult organism, suggesting that DG function is also required for cell survival. The role of DG in signals for survival and β-casein expression in mammary epithelial cells has not yet been directly tested. Another open question is whether DG is expressed in the myoepithelial cells of the mammary gland and, if so, what its role might be.

In addition to signals for polarity, DG has also been implicated in branching morphogenesis in some epithelial tissues (23,68), although this role has not yet been addressed in the mammary gland. In kidney epithelial cells the E3 fragment of laminin-1 perturbed branching morphogenesis in an integrin-independent manner (69). Subsequently, antibodies against DG or laminin thought to interfere with the DG-laminin interaction were demonstrated to disrupt branching morphogenesis in kidney, lung, and salivary gland (23,68).

The epithelial cell system where DG function has been assessed most thoroughly is in the epiblast layer of embryoid bodies. Embryoid bodies are formed by culturing of aggregated embryonic stem (ES) cells in suspension, where they can recapitulate some events of early development. The result is the formation of cavitated, multilayered structures consisting of a polarized epiblast cell layer surrounded by a BM and an outside endodermal cell layer (70). Using this system, it has been demonstrated that cell contact with laminin-1 induces BM formation, epiblast polarization, tissue-specific gene expression, and cell survival (70). Embryoid bodies have been generated using genetically engineered ES cells lacking the DG gene (DG−/−) with contradictory results that in some cases suggest an essential role for DG in BM assembly (71), and in others do not (72). In the latter study, DG was found not to be essential for BM assembly or epithelial polarization, although subtle alterations in BM and epithelial architecture were observed. All the same, defects in BM formation have been seen in vivo in tissues lacking DG function (38,66,67). The most dramatic effect of DG deletion in embryoid bodies was on survival of epithelial cells contacting the BM, where DG appeared to be essential, consistent with observations in *Drosophila* (67,72).

The studies listed above suggest that DG may be involved in many cellular functions in epithelial cells, but results differ between tissues and cell systems. Tissue-specific actions of DG may explain some of these discrepancies. In addition, the competing and complementary roles of other BM receptors are certain to influence DG function. For example, it appears that DG and other BM receptors may compensate for each other in signaling BM formation and cell polarity: studies of embryoid bodies lacking β1 integrins revealed that these receptors are also not essential for these functions when exogenous laminin-1 is added, and there is evidence for the existence of other BM receptors (neither DG nor integrin) that bind to the LG4-5 domain of laminin and facilitate BM assembly (72). Finally, DG and integrins appear to cooperate in the polymerization of laminin at the surface of cultured muscle and ES cells (73,74). In contrast, the actions of DG and β1 integrin appeared to be opposed in a study of breast epithelial cell polarization: in T4-2 cells, elevation of DG levels restored cell polarity in response to BM proteins (6), while in this same system, elevated expression of β1 integrins caused loss of polarity (75). Cross-modulation among BM receptors and cell signaling pathways also complicates the dissection of signals from BM receptors. DG has been suggested to suppress the activation of MAPK by α6 integrins in epithelial cells (76). Loss of DG in skeletal muscle cells causes upregulation of the α7 integrin (64). Deletion of β1 integrins from ES cells results in DG overexpression (72).

DG DEFECTS IN CANCER PROGRESSION

One of the most consistent observations about DG in epithelial cells is that loss of DG function accompanies epithelial cancer progression. When DG was examined in breast and prostate tumors by immunohistochemistry, loss of DG detection correlated with tumor progression (77,78). Examination of DG proteins in carcinoma cell lines revealed similar trends: α-DG is reduced or not detected in the majority of them, and its absence is most common in those that are invasive (6,33,78). Yet, β-DG is present in all cell lines, demonstrating continued expression of the DG gene (6,33,78). Transfection and expression of the wild-type DG cDNA failed to restore detectable α-DG in most cell lines lacking this subunit, indicating that loss of α-DG does not result from mutations

in the DG gene (6). All of this information points to posttranslational modifications playing a role in the loss of α-DG detection and its corresponding laminin binding function in tumor cells.

Shedding of α-DG from the cell surface has been detected in normal and tumorigenic cells (79,80), and may be a normal method for DG regulation that becomes excessive in cancer cells. Modifications of β-DG by metalloprotease-mediated cleavage of this subunit have been observed (33,81), possibly leading to shedding of α-DG from the cell surface. However, cleavage of β-DG is not always evident in cells lacking detectable α-DG (6), and treatment with protease inhibitors, including ones for metalloproteases, did not restore functional α-DG to the surface of invasive breast carcinoma cells (Singh, Itahana, and Muschler, unpublished results). Another possibility is that altered glycosylation of α-DG causes loss of this subunit's detection and function in carcinoma cells. The monoclonal antibodies used to detect α-DG, clones IIH6 and VIA4, both depend on carbohydrate moieties for epitope binding (9). Therefore, altered glycosylation of the α-DG molecule could explain loss of detection by these antibodies. Supporting this suggestion, immunoprecipitation of the dystrophin–glycoprotein complex from surface labeled cells revealed a smaller (~100 kDa) form of α-DG in invasive breast carcinoma cells (e.g. MDA-MB-231 and MDA-MB-468), suggesting altered glycosylation (Singh, Itahana, and Muschler, unpublished results).

Several glycosyltransferases have been implicated in processing the carbohydrates required for DG binding to BM proteins, and mutations in some of these genes have been demonstrated to cause loss of DG function in muscular dystrophies (15). Interestingly, it now appears that similar defects in DG may arise in cancer progression.

A loss of DG function in breast cancer cells could have profound effects on progression of the disease since suggested roles of DG include growth inhibition, tissue-specific gene expression, cell polarity, tissue architecture, and BM formation. Defects in each of these functions are hallmarks of cancer progression, and in carcinoma cells the loss of these attributes correlates strongly with loss of DG (6). Overexpression of DG in T4-2 cells not only restored polarity and growth control, but also reduced the tumorigenic potential of these cells when injected into mice (6). Therefore, at least in this one cell system, DG apparently can function as a tumor suppressor. Although loss of DG has not yet been directly implicated in invasion and metastasis, it is evident that DG function is distinctly absent in many invasive carcinoma cells, suggesting a possible connection (6) (Itahana, Singh, and Muschler, unpublished observation).

CONCLUSION

The study of DG signaling and function in mammary epithelial cells is at a very early stage. Although DG has been implicated in growth control, cell survival, cytoskeletal organization, BM assembly, branching morphogenesis, polarity, and tumor suppression in epithelial cells, many questions remain about the degree to which DG participates in each of these roles. Discrepancies exist in the assessment of DG's functions from one cell system to another, including roles in signaling polarity and BM assembly. Some of these disparities may be explained by differences in tissue-specific functions and/or by the complement of other BM receptors present that may overlap with DG in their effects. Identification of DG binding partners has proceeded quickly, but their significance as mediators of DG functions is also unclear. A great deal of work remains to place these associated molecules within pathways for specific signals emanating from DG.

The challenge now is to integrate this molecule into the existing knowledge of other adhesion receptors in mammary epithelial cells and to determine how they work together to direct epithelial architecture and function in the mammary gland. A thorough understanding of DG's roles in this tissue will not only be important for dissecting the mechanisms regulating normal mammary gland development, but will also be critical to discovering the signaling imbalances that result from the frequent loss of this BM receptor in breast cancer progression.

ACKNOWLEDGMENTS

We thank Selena Knight-Krajewski for helpful discussion. This work was supported by Department of Defense Breast Cancer Research Program Grant DAMD17-01-1-0292 and by California Breast Cancer Research Program Grant 7KB-0017A.

REFERENCES

1. M. L. Li, J. Aggeler, D. A. Farson, C. Hatier, J. Hassell, and M. J. Bissell. (1987). Influence of a reconstituted basement membrane and its components on casein gene expression and secretion in mouse mammary epithelial cells. *Proc. Natl. Acad. Sci. U.S.A.* **84**:136–140.

2. M. H. Barcellos-Hoff, J. Aggeler, T. G. Ram, and M. J. Bissell (1989). Functional differentiation and alveolar morphogenesis of primary mammary cultures on reconstituted basement membrane. *Development* **105:**223–235.
3. C. H. Streuli, C. Schmidhauser, N. Bailey, P. Yurchenco, A. P. Skubitz, C. Roskelley, *et al.* (1995). Laminin mediates tissue-specific gene expression in mammary epithelia. *J. Cell Biol.* **129:**591–603.
4. J. Muschler, A. Lochter, C. D. Roskelley, P. Yurchenco, and M. J. Bissell (1999). Division of labor among the alpha6beta4 integrin, beta1 integrins, and an E3 laminin receptor to signal morphogenesis and beta-casein expression in mammary epithelial cells. *Mol. Biol. Cell* **10:**2817–2828.
5. M. J. Bissell, D. C. Radisky, A. Rizki, V. M. Weaver, and O. W. Petersen (2002). The organizing principle: Microenvironmental influences in the normal and malignant breast. *Differentiation* **70:**537–546.
6. J. Muschler, D. Levy, R. Boudreau, M. Henry, K. Campbell, and M. J. Bissell (2002). A role for dystroglycan in epithelial polarization: Loss of function in breast tumor cells. *Cancer Res.* **62:**7102–7109.
7. W. F. Vogel, A. Aszodi, F. Alves, and T. Pawson (2001). Discoidin domain receptor 1 tyrosine kinase has an essential role in mammary gland development. *Mol. Cell Biol.* **21:**2906–2917.
8. J. F. Talts, Z. Andac, W. Gohring, A. Brancaccio, and R. Timpl (1999). Binding of the G domains of laminin alpha1 and alpha2 chains and perlecan to heparin, sulfatides, alpha-dystroglycan and several extracellular matrix proteins. *EMBO J.* **18:**863–870.
9. J. M. Ervasti and K. P. Campbell (1993). A role for the dystrophin–glycoprotein complex as a transmembrane linker between laminin and actin. *J. Cell Biol.* **122:**809–823.
10. S. Sugita, F. Saito, J. Tang, J. Satz, K. Campbell, and T. C. Sudhof (2001). A stoichiometric complex of neurexins and dystroglycan in brain. *J. Cell Biol.* **154:**435–445.
11. S. H. Gee, F. Montanaro, M. H. Lindenbaum, and S. Carbonetto (1994). Dystroglycan-alpha, a dystrophin-associated glycoprotein, is a functional agrin receptor. *Cell* **77:**675–686.
12. M. A. Bowe, D. B. Mendis, and J. R. Fallon (2000). The small leucine-rich repeat proteoglycan biglycan binds to alpha-dystroglycan and is upregulated in dystrophic muscle. *J. Cell Biol.* **148:**801–810.
13. H. B. Peng, A. A. Ali, D. F. Daggett, H. Rauvala, J. R. Hassell, and N. R. Smalheiser (1998). The relationship between perlecan and dystroglycan and its implication in the formation of the neuromuscular junction. *Cell Adhes. Commun.* **5:**475–489.
14. Y. Sunada, S. M. Bernier, C. A. Kozak, Y. Yamada, and K. P. Campbell (1994). Deficiency of merosin in dystrophic dy mice and genetic linkage of laminin M chain gene to dy locus. *J. Biol. Chem.* **269:**13729–13732.
15. D. E. Michele and K. P. Campbell (2003). Dystrophin-glycoprotein complex: Posttranslational processing and dystroglycan function. *J. Biol. Chem.* **278:**15457–15460.
16. M. Durbeej and K. P. Campbell (2002). Muscular dystrophies involving the dystrophin–glycoprotein complex: An overview of current mouse models. *Curr. Opin. Genet. Dev.* **12:**349–361.
17. J. M. Ervasti, K. Ohlendieck, S. D. Kahl, M. G. Gaver, and K. P. Campbell (1990). Deficiency of a glycoprotein component of the dystrophin complex in dystrophic muscle. *Nature* **345:**315–319.
18. J. M. Ervasti and K. P. Campbell (1991). Membrane organization of the dystrophin–glycoprotein complex. *Cell* **66:**1121–1131.
19. O. Ibraghimov-Beskrovnaya, J. M. Ervasti, C. J. Leveille, C. A. Slaughter, S. W. Sernett, and K. P. Campbell (1992). Primary structure of dystrophin-associated glycoproteins linking dystrophin to the extracellular matrix. *Nature* **355:**696–702.
20. N. R. Smalheiser and E. Kim (1995). Purification of cranin, a laminin binding membrane protein. Identity with dystroglycan and reassessment of its carbohydrate moieties. *J. Biol. Chem.* **270:**15425–15433.
21. S. H. Gee, R. W. Blacher, P. J. Douville, P. R. Provost, P. D. Yurchenco, and S. Carbonetto (1993). Laminin-binding protein 120 from brain is closely related to the dystrophin-associated glycoprotein, dystroglycan, and binds with high affinity to the major heparin binding domain of laminin. *J. Biol. Chem.* **268:**14972–14980.
22. M. Durbeej, M. D. Henry, M. Ferletta, K. P. Campbell, and P. Ekblom (1998). Distribution of dystroglycan in normal adult mouse tissues. *J. Histochem. Cytochem.* **46:**449–457.
23. M. Durbeej, E. Larsson, B. O. Ibraghimov, S. L. Roberds, K. P. Campbell, and P. Ekblom (1995). Non-muscle alpha-dystroglycan is involved in epithelial development. *J. Cell Biol.* **130:**79–91.
24. A. M. Belkin and N. R. Smalheiser (1996). Localization of cranin (dystroglycan) at sites of cell–matrix and cell–cell contact: Recruitment to focal adhesions is dependent upon extracellular ligands. *Cell Adhes. Commun.* **4:**281–296.
25. M. Durbeej and K. P. Campbell (1999). Biochemical characterization of the epithelial dystroglycan complex. *J. Biol. Chem.* **274:**26609–26616.
26. F. Duclos, V. Straub, S. A. Moore, D. P. Venzke, R. F. Hrstka, R. H. Crosbie, *et al.* (1998). Progressive muscular dystrophy in alpha-sarcoglycan-deficient mice. *J. Cell Biol.* **142:**1461–1471. A1
27. M. Durbeej, R. D. Cohn, R. F. Hrstka, S. A. Moore, V. Allamand, B. L. Davidson, *et al.* (2000). Disruption of the beta-sarcoglycan gene reveals pathogenetic complexity of limb-girdle muscular dystrophy type 2E. *Mol. Cell* **5:**141–151.
28. K. H. Holt, L. E. Lim, V. Straub, D. P. Venzke, F. Duclos, R. D. Anderson, *et al.* (1998). Functional rescue of the sarcoglycan complex in the BIO 14.6 hamster using delta-sarcoglycan gene transfer. *Mol. Cell* **1:**841–848.
29. A. M. Kachinsky, S. C. Froehner, and S. L. Milgram (1999). A PDZ-containing scaffold related to the dystrophin complex at the basolateral membrane of epithelial cells. *J. Cell. Biol.* **145:**391–402.
30. N. Y. Loh, S. E. Newey, K. E. Davies, and D. J. Blake (2000). Assembly of multiple dystrobrevin-containing complexes in the kidney. *J. Cell Sci.* **113**(Pt. 15):2715–2724.
31. M. Durbeej, D. Jung, T. Hjalt, K. P. Campbell, and P. Ekblom (1997). Transient expression of Dp140, a product of the Duchenne muscular dystrophy locus, during kidney tubulogenesis. *Dev. Biol.* **181:**156–167.
32. O. Ibraghimov-Beskrovnaya, A. Milatovich, T. Ozcelik, B. Yang, K. Koepnick, U. Francke, *et al.* (1993). Human dystroglycan: Skeletal muscle cDNA, genomic structure, origin of tissue specific isoforms and chromosomal localization. *Hum. Mol. Genet.* **2:**1651–1657.
33. C. Losasso, F. Di Tommaso, A. Sgambato, R. Ardito, A. Cittadini, B. Giardina, *et al.* (2000). Anomalous dystroglycan in carcinoma cell lines. *FEBS Lett.* **484:**194–198.
34. S. Yotsumoto, H. Fujiwara, J. H. Horton, T. A. Mosby, X. Wang, Y. Cui, *et al.* (1996). Cloning and expression analyses of mouse dystroglycan gene: Specific expression in maternal decidua at the peri-implantation stage. *Hum. Mol. Genet.* **5:**1259–1267.

35. N. J. Dickens, S. Beatson, and C. P. Ponting (2002). Cadherin-like domains in alpha-dystroglycan, alpha/epsilon-sarcoglycan and yeast and bacterial proteins. *Curr. Biol.* **12**:R197–R199.
36. D. Bozic, J. Engel, and A. Brancaccio (1998). Sequence analysis suggests the presence of an IG-like domain in the N-terminal region of alpha-dystroglycan which was crystallized after mutation of a protease susceptible site (Arg168–>His). *Matrix Biol.* **17**:495–500.
37. A. Brancaccio, T. Schulthess, M. Gesemann, and J. Engel (1995). Electron microscopic evidence for a mucin-like region in chick muscle alpha-dystroglycan. *FEBS Lett.* **368**:139–142.
38. D. E. Michele, R. Barresi, M. Kanagawa, F. Saito, R. D. Cohn, J. S. Satz, *et al.* (2002). Posttranslational disruption of dystroglycan-ligand interactions in congenital muscular dystrophies. *Nature* **418**:417–422.
39. T. Pawson and J. D. Scott (1997). Signaling through scaffold, anchoring, and adaptor proteins. *Science* **278**:2075–2080.
40. J. L. Ilsley, M. Sudol, and S. J. Winder (2001). The interaction of dystrophin with beta-dystroglycan is regulated by tyrosine phosphorylation. *Cell. Signal.* **13**:625–632.
41. M. James, A. Nuttall, J. L. Ilsley, K. Ottersbach, J. M. Tinsley, M. Sudol, *et al.* (2000). Adhesion-dependent tyrosine phosphorylation of (beta)-dystroglycan regulates its interaction with utrophin. *J. Cell Sci.* **113**(Pt. 10):1717–1726.
42. F. Sotgia, G. Bonuccelli, M. Bedford, A. Brancaccio, U. Mayer, M. T. Wilson, *et al.* (2003). Localization of phospho-beta-dystroglycan (pY892) to an intracellular vesicular compartment in cultured cells and skeletal muscle fibers in vivo. *Biochemistry* **42**:7110–7123.
43. M. Bozzi, G. Veglia, M. Paci, F. Sciandra, B. Giardina, and A. Brancaccio (2001). A synthetic peptide corresponding to the 550–585 region of alpha-dystroglycan binds beta-dystroglycan as revealed by NMR spectroscopy. *FEBS Lett.* **499**:210–214.
44. H. Yu and J. F. Talts (2003). beta1 Integrin and alpha-dystroglycan binding sites are localized to different laminin-G-domain-like (LG) modules within the laminin alpha5 chain G domain. *Biochem. J.* **371**:289–299.
45. E. Leygue, L. Snell, H. Dotzlaw, S. Troup, T. Hiller-Hitchcock, L. C. Murphy, *et al.* (2000). Lumican and decorin are differentially expressed in human breast carcinoma. *J. Pathol.* **192**:313–320.
46. C. J. Raats, J. van den Born, M. A. Bakker, B. Oppers-Walgreen, B. J. Pisa, H. B. Dijkman, *et al.* (2000). Expression of agrin, dystroglycan, and utrophin in normal renal tissue and in experimental glomerulopathies. *Am. J. Pathol.* **156**:1749–1765.
47. R. Timpl, D. Tisi, J. F. Talts, Z. Andac, T. Sasaki, and E. Hohenester (2000). Structure and function of laminin LG modules. *Matrix Biol.* **19**:309–317.
48. E. A. Pall, K. M. Bolton, and J. M. Ervasti (1996). Differential heparin inhibition of skeletal muscle alpha-dystroglycan binding to laminins. *J. Biol. Chem.* **271**:3817–3821.
49. D. Tisi, J. F. Talts, R. Timpl, and E. Hohenester (2000). Structure of the C-terminal laminin G-like domain pair of the laminin alpha2 chain harbouring binding sites for alpha-dystroglycan and heparin. *EMBO J.* **19**:1432–1440.
50. N. Suzuki, H. Nakatsuka, M. Mochizuki, N. Nishi, Y. Kadoya, A. Utani, *et al.* (2003). Biological activities of homologous loop regions in the laminin alpha chain G domains. *J. Biol. Chem.*
51. B. Yang, D. Jung, D. Motto, J. Meyer, G. Koretzky, and K. P. Campbell (1995). SH3 domain-mediated interaction of dystroglycan and Grb2. *J. Biol. Chem.* **270**:11711–11714.
52. M. Cavaldesi, G. Macchia, S. Barca, P. Defilippi, G. Tarone, and T. C. Petrucci (1999). Association of the dystroglycan complex isolated from bovine brain synaptosomes with proteins involved in signal transduction. *J. Neurochem.* **72**:1648–1655.
53. K. Russo, E. Di Stasio, G. Macchia, G. Rosa, A. Brancaccio, and T. C. Petrucci (2000). Characterization of the beta-dystroglycan-growth factor receptor 2 (Grb2) interaction. *Biochem. Biophys. Res. Commun.* **274**:93–98.
54. J. L. Ilsley, M. Sudol, and S. J. Winder (2002). The WW domain: Linking cell signalling to the membrane cytoskeleton. *Cell. Signal.* **14**:183–189.
55. F. Sotgia, H. Lee, M. T. Bedford, T. Petrucci, M. Sudol, and M. P. Lisanti (2001). Tyrosine phosphorylation of beta-dystroglycan at its WW domain binding motif, PPxY, recruits SH2 domain containing proteins. *Biochemistry* **40**:14585–14592.
56. J. T. Anderson, R. P. Rogers, and H. W. Jarrett (1996). Ca2+-calmodulin binds to the carboxyl-terminal domain of dystrophin. *J. Biol. Chem.* **271**:6605–6610.
57. A. Tommasi di Vignano, G. Di Zenzo, M. Sudol, G. Cesareni, and L. Dente (2000). Contribution of the different modules in the utrophin carboxy-terminal region to the formation and regulation of the DAP complex. *FEBS Lett.* **471**:229–234.
58. F. Sotgia, J. K. Lee, K. Das, M. Bedford, T. C. Petrucci, P. Macioce, *et al.* (2000). Caveolin-3 directly interacts with the C-terminal tail of beta -dystroglycan. Identification of a central WW-like domain within caveolin family members. *J. Biol. Chem.* **275**:38048–38058.
59. D. S. Park, H. Lee, C. Riedel, J. Hulit, P. E. Scherer, R. G. Pestell, *et al.* (2001). Prolactin negatively regulates caveolin-1 gene expression in the mammary gland during lactation, via a Ras-dependent mechanism. *J. Biol. Chem.* **276**:48389–48397.
60. Y. J. Chen, H. J. Spence, J. M. Cameron, T. Jess, J. L. Ilsley, and S. J. Winder (2003). Direct interaction of beta-dystroglycan with F-actin. *Biochem. J.*
61. A. Cartaud, S. Coutant, T. C. Petrucci, and J. Cartaud (1998). Evidence for in situ and in vitro association between beta-dystroglycan and the subsynaptic 43K rapsyn protein. Consequence for acetylcholine receptor clustering at the synapse. *J. Biol. Chem.* **273**:11321–11326.
62. L. S. Musil, D. E. Frail, and J. P. Merlie (1989). The mammalian 43-kD acetylcholine receptor-associated protein (RAPsyn) is expressed in some nonmuscle cells. *J. Cell Biol.* **108**:1833–1840.
63. R. A. Williamson, M. D. Henry, K. J. Daniels, R. F. Hrstka, J. C. Lee, Y. Sunada, *et al.* (1997). Dystroglycan is essential for early embryonic development: Disruption of Reichert's membrane in Dag1-null mice. *Hum. Mol. Genet.* **6**:831–841.
64. P. D. Cote, H. Moukhles, M. Lindenbaum, and S. Carbonetto (1999). Chimaeric mice deficient in dystroglycans develop muscular dystrophy and have disrupted myoneural synapses. *Nat. Genet.* **23**:338–342.
65. R. D. Cohn, M. D. Henry, D. E. Michele, R. Barresi, F. Saito, S. A. Moore, *et al.* (2002). Disruption of DAG1 in differentiated skeletal muscle reveals a role for dystroglycan in muscle regeneration. *Cell* **110**:639–648.
66. S. A. Moore, F. Saito, J. Chen, D. E. Michele, M. D. Henry, A. Messing, *et al.* (2002). Deletion of brain dystroglycan recapitulates aspects of congenital muscular dystrophy. *Nature* **418**:422–425.
67. W. M. Deng, M. Schneider, R. Frock, C. Castillejo-Lopez, E. A. Gaman, S. Baumgartner, *et al.* (2003). Dystroglycan is required for polarizing the epithelial cells and the oocyte in Drosophila. *Development* **130**:173–184.

68. M. Durbeej, J. F. Talts, M. D. Henry, P. D. Yurchenco, K. P. Campbell, and P. Ekblom (2001). Dystroglycan binding to laminin alpha1LG4 module influences epithelial morphogenesis of salivary gland and lung in vitro. *Differentiation* **69:**121–134.
69. Y. Kadoya, K. Kadoya, M. Durbeej, K. Holmvall, L. Sorokin, and P. Ekblom (1995). Antibodies against domain E3 of laminin-1 and integrin alpha 6 subunit perturb branching epithelial morphogenesis of submandibular gland, but by different modes. *J. Cell Biol.* **129:**521–534.
70. S. Li, D. Edgar, R. Fassler, W. Wadsworth, and P. D. Yurchenco (2003). The role of laminin in embryonic cell polarization and tissue organization. *Dev. Cell* **4:**613–624.
71. M. D. Henry and K. P. Campbell (1998). A role for dystroglycan in basement membrane assembly. *Cell* **95:**859–870.
72. S. Li, D. Harrison, S. Carbonetto, R. Fassler, N. Smyth, D. Edgar, *et al.* (2002). Matrix assembly, regulation, and survival functions of laminin and its receptors in embryonic stem cell differentiation. *J. Cell Biol.* **157:**1279–1290.
73. H. Colognato, D. A. Winkelmann, and P. D. Yurchenco (1999). Laminin polymerization induces a receptor-cytoskeleton network. *J. Cell Biol.* **145:**619–631.
74. M. D. Henry, J. S. Satz, C. Brakebusch, M. Costell, E. Gustafsson, R. Fassler, *et al.* (2001). Distinct roles for dystroglycan, (&bgr;)1 integrin and perlecan in cell surface laminin organization. *J. Cell Sci.* **114:**1137–1144.
75. V. M. Weaver, O. W. Petersen, F. Wang, C. A. Larabell, P. Briand, C. Damsky, *et al.* (1997). Reversion of the malignant phenotype of human breast cells in three-dimensional culture and in vivo by integrin blocking antibodies. *J. Cell Biol.* **137:**231–245.
76. M. Ferletta, Y. Kikkawa, H. Yu, J. F. Talts, M. Durbeej, A. Sonnenberg, *et al.* (2003). Opposing roles of integrin alpha6Abeta1 and dystroglycan in laminin-mediated extracellular signal-regulated kinase activation. *Mol. Biol. Cell* **14:**2088–2103.
77. M. D. Henry, M. B. Cohen, and K. P. Campbell (2001). Reduced expression of dystroglycan in breast and prostate cancer. *Hum. Pathol.* **32:**791–795.
78. A. Sgambato, M. Migaldi, M. Montanari, A. Camerini, A. Brancaccio, G. Rossi, *et al.* (2003). Dystroglycan expression is frequently reduced in human breast and colon cancers and is associated with tumor progression. *Am. J. Pathol.* **162:**849–860.
79. K. Matsumura, A. Chiba, H. Yamada, H. Fukuta-Ohi, S. Fujita, T. Endo, *et al.* (1997). A role of dystroglycan in schwannoma cell adhesion to laminin. *J. Biol. Chem.* **272:**13904–13910.
80. H. Shimizu, H. Hosokawa, H. Ninomiya, J. H. Miner, and T. Masaki (1999). Adhesion of cultured bovine aortic endothelial cells to laminin-1 mediated by dystroglycan. *J. Biol. Chem.* **274:**11995–12000.
81. H. Yamada, F. Saito, H. Fukuta-Ohi, D. Zhong, A. Hase, K. Arai, *et al.* (2001). Processing of beta-dystroglycan by matrix metalloproteinase disrupts the link between the extracellular matrix and cell membrane via the dystroglycan complex. *Hum. Mol. Genet.* **10:**1563–1569.

Queries to Author:

A1. Au: Kindly provide the names of all authors in place of *et al.* for the following ref. nos.: 26–28, 32–34, 38, 41, 42, 45, 46, 50, 58, 59, 63, 65–67, 72, 74–76, 78, 79, 81 (if possible).
A2. Au: Kindly update these refs. Ref. nos.: 50 and 60.

EXHIBIT E

American Journal of Pathology, Vol. 162, No. 3, March 2003

Dystroglycan Expression Is Frequently Reduced in Human Breast and Colon Cancers and Is Associated with Tumor Progression

Alessandro Sgambato,* Mario Migaldi,† Micaela Montanari,* Andrea Camerini,* Andrea Brancaccio,‡ Giulio Rossi,† Rodolfo Cangiano,* Carmen Losasso,‡ Giovanni Capelli,§ Gian Paolo Trentini,† and Achille Cittadini*

From the Centro di Ricerche Oncologiche "Giovanni XXIII," Istituto di Patologia Generale, the Istituto di Chimica del Riconoscimento Molecolare,‡ Sezione di Roma (Consiglio Nazionale Ricerche) c/o Istituto di Biochimica e Biochimica Clinica, and the Istituto di Igiene,§ Catholic University, Rome; and the Dipartimento Misto di Anatomia Patologica e di Medicina Legale,† Sezione di Anatomia Patologica, University of Modena and Reggio Emilia, Modena, Italy*

Dystroglycan (DG) is an adhesion molecule responsible for crucial interactions between extracellular matrix and cytoplasmic compartment. It is formed by two subunits, α-DG (extracellular) and β-DG (transmembrane), that bind to laminin in the matrix and dystrophin in the cytoskeleton, respectively. In this study we evaluated by Western blot analysis the expression of DG in a series of human cancer cell lines of various histogenetic origin and in a series of human primary colon and breast cancers. Decreased expression of DG was observed in most of the cell lines and in both types of tumors and correlated with higher tumor grade and stage. Analysis of the mRNA levels suggested that expression of DG protein is likely regulated at a posttranscriptional level. Evaluation of α-DG expression by immunostaining in a series of archival cases of primary breast carcinomas confirmed that α-DG expression is lost in a significant fraction of tumors (66%). Loss of DG staining correlated with higher tumor stage ($P = 0.022$), positivity for p53 ($P = 0.033$), and high proliferation index ($P = 0.045$). A significant correlation was also observed between loss of α-DG and overall survival ($P = 0.013$ by log-rank test) in an univariate analysis. These data indicate that DG expression is frequently lost in human malignancies and suggest that this glycoprotein might play an important role in human tumor development and progression. ***(Am J Pathol 2003, 162:849–860)***

Cellular interactions with the extracellular matrix are important factors in the development and progression of many types of cancer. Originally characterized as a member of the so-called dystrophin-glycoprotein complex in muscle sarcolemma, dystroglycan (DG) is a transmembrane glycoprotein expressed in a wide variety of tissues at the interface between the basement membrane and cell membrane linking the extracellular matrix to the intracellular cytoskeleton.[1,2] DG is encoded by a single gene and is formed on cleavage of a precursor protein into two mature proteins that form a tight noncovalent complex.[2,3] The cell surface-associated (extracellular) α-DG binds extracellular matrix molecules, such as laminins and agrin, whereas the transmembrane β-DG anchors α-DG to the cell membrane and is linked to the cytoskeleton actin via dystrophin or its paralogue utrophin.[2,4,5] Thus, it has been proposed that DG forms a continuous link from the extracellular matrix to the actin cytoskeleton, providing structural integrity and perhaps transducing signal, in a manner similar to integrins.[2,6,7] DG knockout mice undergo premature death early in embryogenesis and genetic defects of DG have not been reported as causes of hereditary diseases in humans.[8] Disruption of the DG-dystrophin interaction, however, has been described in several forms of hereditary neuromuscular disease such as Duchenne muscular dystrophy.[9,10]

The highly and heterogeneously glycosylated cell surface-associated α-DG has a size that ranges from 120 to 180 kd, depending on different amounts of glycosylation. β-DG has been identified as a 43-kd band, sometimes accompanied by a 31-kd band that likely originates from proteolytic fragmentation.[11,12] We recently demonstrated that the 31-kd band is expressed at an increased level in a series of human breast cancer cell lines compared with normal mammary epithelial cells.[11] Increased expression of the 31-kd band was usually associated with a reduced expression of the 43-kd band. Interestingly, expression of

Supported in part by grants from Cofinanziamento Ministero Istruzione, Università e Ricerca (MIUR) 2001 (to A.C. and G.P.T.), the Università Cattolica and MIUR (Programma Oncologia L 444/99) (to A.C.), and the Compagnia di San Paolo (to A.S.).

Accepted for publication November 21, 2002.

Address reprint requests to Alessandro Sgambato, M.D., Istituto di Patologia Generale, Centro di Ricerche Oncologiche "Giovanni XXIII," Università Cattolica del Sacro Cuore, Largo Francesco Vito 1, 00168 Rome, Italy. E-mail: asgambato@rm.unicatt.it.

α-DG was reduced or absent in most of the cell lines in which β-DG was found as a 31-kd band. Indeed, we demonstrated that both the 43-kd and 31-kd α-DG bands harbor their transmembrane segment.[11] Thus, the cleavage likely occurs within the extracellular domain of β-DG and disrupts the integrity of the DG complex that is strictly dependent on noncovalent interactions between the extracellular domain of β-DG and the C-terminal domain of α-DG.[13] The accumulation of the 31-kd band was interpreted as the consequence of posttranscriptional events as demonstrated by reverse transcriptase-polymerase chain reaction (RT-PCR) experiments that allowed to exclude other phenomena, such as mRNA alternative splicing.[11] We hypothesized that an aberrant processing of DG might play an important role in tumor development by altering the interactions between cells and the surrounding matrix. Thus, a reduction of DG function could influence the formation of strong contacts between basement membranes and the cytoskeleton of cells; thus eventually favoring tumor development and invasiveness. Indeed, Henry and colleagues[14] recently reported a reduction in the expression levels of DG in human primary prostate and breast cancers that was most pronounced in high-grade disease. Yamada and co-workers[12] also recently confirmed that the 31-kd form of β-DG is the product of a proteolytic processing of the extracellular domain of β-DG and reported evidence that this processing is because of the membrane-associated matrix metalloproteinase (MMP) activity and disintegrates the DG complex. Taken together these data suggest that reduced expression of DG may lead to abnormal cell-extracellular matrix interactions and thus contribute to progression to metastatic disease and justify the needs for further studies on the regulation of DG in epithelial cells and its alterations in tumor cells.

In this study we analyzed the expression of DG by Western blot analysis in a series of human cancer cell lines and primary breast and colon cancers. We also investigated the expression of α-DG in a series of breast carcinomas and evaluated its relation with other tumor characteristics and with the clinical outcome of the patients. The results obtained suggest that loss of DG is a frequent event in human tumors with potential prognostic significance and warrant further studies on the involvement of this protein in tumor development.

Materials and Methods

Cell Culture

The 184B5 human immortalized mammary epithelial cells were grown in complete serum-free mammary epithelial cell growth medium (MEGM) medium supplemented with growth factors (Clonetics-BioWhittaker, East Rutherford, NJ), as previously described.[15] All of the other cell lines used for this study were obtained from the American Type Culture Collection (Rockville, MD) and cultured according with the instructions of the supplier.

Patient Characteristics and Tissue Samples

Samples were from patients who underwent surgery in our institution. No patient received preoperative chemotherapy or radiotherapy. Surgical specimens were snap-frozen in liquid nitrogen immediately after surgery and stored at −80°C until use. For colon normal mucosa samples, biopsies were taken where the mucosa appeared free from cancer at a distance of at least 5 cm to resection site. For tumor samples, only fragments containing at least 80% tumor cells, as assessed by hematoxylin and eosin staining, were used for subsequent analyses. Histological tumor grading and staging were assessed according to standard criteria. Other clinicopathological parameters, such as age and gender, were also recorded. The samples were coded and the names of the patients were not revealed.

For immunohistochemical studies, samples were obtained from a series of consecutive, unselected patients who underwent routine surgery for breast cancer at the Division of Surgery, County Hospital, Modena, Italy, from June 1989 to April 1991 and for whom clinicopathological data were available. After excluding cases with previous personal and/or familiar tumor history and patients with evidence of distant metastatic disease at diagnosis or who received any treatment before surgery or lost to follow-up, a cohort of 102 patients was selected for this study with a mean age at diagnosis of 59 years (range, 28 to 83 years) and a mean follow-up of 72 months (range, 2 to 135 months). Treatment remained reasonably consistent during the study period. Briefly, all patients had either a mastectomy or a segmental resection followed by radiation therapy. Axillary dissection with histopathological examination was performed in all patients and if metastases were detected adjuvant therapy was given in the form of tamoxifen to postmenopausal and chemotherapy treatment to premenopausal patients. No further treatment was given to node-negative patients and no patients received any therapy before surgery. The selection did not require approval by an Institutional Review Board because the samples were coded and the names of the patients were not revealed. Our series included 96 ductal and 6 lobular carcinomas. Histological grading and staging were assessed according to standard criteria.[16,17] Tumor stage was pT1 in 38, pT2 in 44, pT3 in 4, and pT4 in 16. Five (5.2%) cases were classified as well (G1), 59 (61.5%) as moderately (G2), and 32 (33.3%) as poorly (G3) differentiated tumors.

Total Protein Extraction

Frozen tissues were washed twice with ice-cold phosphate-buffered saline (PBS) containing 1 mmol/L of $MgCl_2$, finely diced on ice with a surgical blade, and spun down in a microcentrifuge at 4°C to recover pellets. After removing the supernatants, pellets were resuspended in 3 to 5 volumes of sonication buffer containing proteases and phosphatase inhibitors (20 mmol/L Tris-HCl, pH 7.4, 2 mmol/L EGTA, 6 mmol/L β-mercaptoethanol, 1% Nonidet P-40, 0.1% sodium dodecyl sulfate, 50 mmol/L NaF,

15 μg/ml benzamidine, 10 μg/ml aprotinin, 10 μg/ml leupeptin, and 1 mmol/L phenylmethyl sulfonyl fluoride) and sonicated at 4°C with a Sonifier Cell Disruptor (Ultrasonic Instruments International, Inc., Farmingdale, NY). Homogenates were incubated on ice for 30 minutes and then centrifuged at 14,000 rpm in a microcentrifuge for 15 minutes at 4°C. The supernatants were assayed for protein content by the BioRad protein assay method (BioRad Laboratories GmbH, München, Germany) and stored at −80°C. For cell lines, exponentially growing cultures of each cell lines were washed with cold PBS, collected by cell scraping and cell pellets were added to 3 to 5 volumes of sonication buffer and processed as for tumor pellets.

Western Blot Analysis

For Western blotting, 50 μg of protein from each sample were separated by sodium dodecyl sulfate-polyacrylamide gel electrophoresis and then transferred to Immobilon-P membranes (Millipore, Bedford, MA) at 100 V for 1 hour at 4°C. Total cell lysate from SW620 cells was always included and was used as an internal positive control for standardization of the different blots. Immunodetection was performed using the enhanced chemiluminescence kit for Western blotting detection (Amersham Pharmacia Biotech, Freiburg, Germany) and multiple film exposure for different lengths of time were made to establish a linear range. Bands were analyzed on the image analysis system Gel Doc 200 System (BioRad) and quantitated using the Quantity One Quantitation Software (BioRad). The monoclonal antibody to α-DG (clone VIA4-1) was obtained from Upstate Biotechnology (Lake Placid, NY) and was used diluted at 1:2000. The monoclonal antibody to β-DG (clone 43DAG/8D5) was from Novocastra (Newcastle, UK) and was used diluted at 1:50. Experimental validation of anti-DG antibody reactivity was done using a cell line engineered to overexpress an exogenous DG cDNA (data not shown). Protein extraction was independently performed two times for each sample. Similar results were obtained when the two protein extracts from each sample were independently tested. The densitometric data shown are the mean values of the results obtained in four separate experiments (two runs for each protein extract) after correction for the internal control and are expressed as the ratios of DG to β-actin bands. Two values were arbitrarily considered identical when the difference between them was less than 10%.

Semiquantitative RT-PCR Analysis

Total RNA was extracted from exponentially growing cultures of each cell line using the RNeasy Mini kit (Qiagen, Hilden, Germany), in accordance with the manufacturer's instructions. For reverse transcriptase reaction, the RNA samples were reverse transcribed using the One-Step RT-PCR kit (Qiagen).

PCR was performed using the Gene Amp PCR Systems 9600 (Perkin-Elmer Corp., Norwalk, CT). The following DG-specific primers for the human DG sequence were used: DAGMH (forward) 5′-GGAGAACCCAACCAGCGCCCAGAGC-3′ and DAGAH (reverse) 5′-CGGGTGATATTCTGCAGGGTGATGG-3′ that amplify a 485-bp region encompassing both α-DG and β-DG. A second primer pair: forward 5′-TCACCCACACTGTGCCCATCT-3′ and reverse 5′-ACGGAGTACTTGCGCTCAGG-3′ were used to amplify a 550-bp region of the β-actin transcript. After an initial denaturation at 95°C for 15 minutes, 20 cycles of PCR amplification were performed, each consisting of a denaturing step of 94°C for 45 seconds, annealing at 55°C for 30 seconds, and extension at 72°C for 1 minute, followed by a final step at 72°C for 10 minutes. The number of 20 cycles was selected because in preliminary experiments we verified that with this number of cycles the reaction was still in a linear range for both genes (data not shown). The amplified fragments were detected by 3% (w/v) agarose gel electrophoresis and staining with 0.3 mg/ml of ethidium bromide (Sigma, St. Louis, MO). Each band was quantitated and the specific gene expression level was determined semiquantitatively by calculating the ratio of densitometric value from the DG band in relation to the internal standard represented by β-actin. The densitometric data shown are the mean values of the results obtained in three independent experiments.

Immunohistochemistry

All immunohistochemical analyses were performed on routinely processed, formalin-fixed, paraffin-embedded tissues using an avidin-biotin complex immunoperoxidase technique (Vectastain ABC kit; Vector Laboratories, Burlingame, CA), as previously described.[18–20] Briefly, successive 5-μm tissue sections were cut from blocks selected for the presence of representative tumor tissue. Sections were dewaxed, rehydrated, and then microwave pretreated (10 minutes at 800 W in 1 mmol/L of ethylenediaminetetraacetic acid buffer, pH 8.0), followed by incubation with 0.3% hydrogen peroxide in methanol for 30 minutes to block endogenous peroxidase. After blocking with horse serum for 1 hour at room temperature, the primary antibodies were applied overnight at 4°C in a high-humidity chamber. Binding was visualized using the Vectastain diaminobenzidine kit (Vector Laboratories) and counterstaining was performed with 1% modified Harris hematoxylin, as described.[18–20] The following antibodies were used diluted in PBS: monoclonal anti-α-DG antibody (clone VIA4-1) (Upstate Biotechnology) diluted 1:100; monoclonal anti-Ki67 antibody (clone MIB-1; DAKO, Glostrup, Denmark) diluted 1:100; and monoclonal anti-p53 DO7 antibody (DAKO, Milan, Italy) diluted 1:750. Detection of estrogen and progesterone receptor status (ER, PR) was also performed by immunohistochemistry and has been previously reported.[21] Controls for specificity of staining were performed by immunostaining duplicate sections in the absence of the primary antibody. A breast carcinoma with known positive immunostaining served as a positive control for each antibody. Positive and negative control slides were included within each batch of slides. For the anti-α-DG antibody only a clear staining of the cell membrane was

regarded as positive. For p53 and Ki67 immunostaining nuclei were considered positive when they showed a distinct brown color in the absence of cytoplasmic and background staining. The fraction of positive cells was scored by examining at least 10 random high-power fields (×400) for each sample and the percentage of cells with positive reaction was calculated semiautomatically by means of a computer-assisted cellular image analyzer (Image-Pro Plus; Media Cybernetics, Silver Spring, MD) on a total of at least 1000 tumor cells per case. All scoring and interpretations of the results were made by two of the authors independently (AS and MM) without knowledge of clinical outcome or other clinicopathological variables. To assess interobserver variation, the results of the two measurements were compared by paired *t*-test and no statistical differences were found (data not shown). The few cases with discrepant scoring were re-evaluated jointly on a second occasion, and agreement was reached. The cutoff values for ER and PR (20% positive cells) and for Ki67 (15% positive cells) are routinely used for therapeutic and prognostic evaluation of breast cancer patients and were selected following the indications of the Italian Multicentric Study of Breast Cancer.[21] The figure 20% was used as the cutoff for p53 positivity because it has been mostly used in previous publications regarding primary breast cancers.[22,23]

Analysis of DNA Content

DNA analysis was performed on tumor samples as previously reported.[24,25] Briefly, 50-μm tissue sections were cut from paraffin blocks, dewaxed, rehydrated, and digested in a solution of 0.5% pepsin (Sigma). After washings cell pellets were resuspended in a hypotonic citrate-propidium iodide solution (0.05 mg/ml) containing Nonidet P-40 (50 μg/ml) and RNase (50 μg/ml) and were incubated at 4°C in the dark overnight. The cell suspension was then filtered and analyzed for DNA content on a FACScan flow cytometer (Becton Dickinson, San Jose, CA). Normal human peripheral white blood cells were stained with propidium iodide under the same conditions and were used as the internal reference. Tumor ploidy was determined by the ratio of the mean peak values for the sample and the internal reference, according to international conventions.[26] Four cases were not used for this study because of the scarcity of the material or because the coefficient of variation was not acceptable in repeated analyses.

Statistical Analysis

The association between DG expression and other molecular and clinicopathological parameters were calculated using contingency table methods and tested for significance using the Pearson's chi-square test. Median values were compared using the Mann-Whitney test. Survival curves were calculated using the Kaplan-Meier method and the log-rank test was used for the analysis. Univariate and multivariate relative risks were calculated using Cox proportional hazards regression. Two patients who died accidentally for causes unrelated to tumor disease were not included in the survival analyses. For grade and stage the G1 grade and the pT1 stage were used as baseline, respectively. The proportional hazard assumption was tested following the generalization by Grambsch and Therneau.[27] All calculations were performed using the STATA 6.0 statistical software package (Stata Corporation, College Station, TX) and the results were considered statistically significant when the *P* value was ≤0.05.

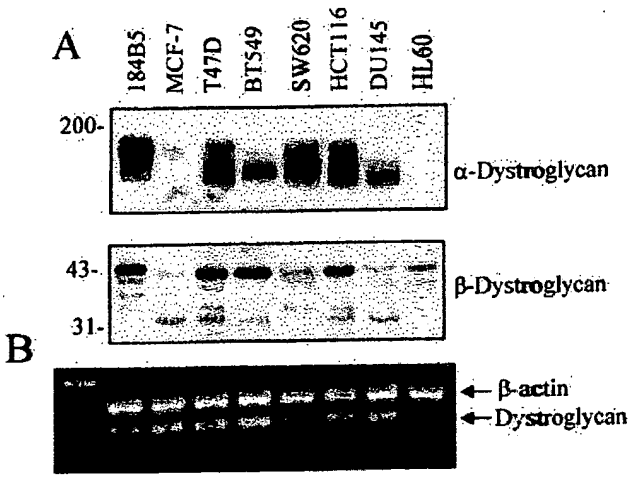

Figure 1. A: Levels of expression of α- and β-DG in a series of human normal and cancer cell lines as assessed by Western blot analysis. **B:** RT-PCR analysis of DG gene expression in the same cell lines amplifying β-actin (as internal control) with DG. In **lane 1** the DNA molecular marker standard is shown. The sizes of the specific RT-PCR products were 550 bp for β-actin and 485 bp for DG.

Results

DG Is Differentially Expressed in a Series of Cancer Cell Lines

We previously reported the accumulation of an aberrant β-DG-related band of ~31 kd in tumor cell lines and tissues compared with normal counterparts.[11] The presence of the 31-kd band was frequently associated with a reduction in the expression level of the expected 43-kd β-DG band and with a reduced or absent expression of the α-DG (see Introduction). A reduction or loss of α-DG expression was also observed in some cell lines expressing normal levels of the 43-kd β-DG band (data not shown).[11] We hypothesized that loss of DG, and mainly α-DG, might be related with cell transformation and might play an important role in the process of tumor development.

To test this hypothesis we analyzed the expression of both α-DG and β-DG in a series of human cancer cell lines of various histogenetic origin. As shown in Figure 1, α-DG was expressed at a high level in the T47D but its expression was reduced in the MCF-7 and BT549 breast cancer cell lines compared with the 184B5 nontumorigenic immortalized human mammary cell line. A reduced expression of α-DG was also observed in the DU145 prostate cancer cells and in the HL60 promyelocytic

Table 1. Expression of Dystroglycan mRNA and Protein in Human Normal and Cancer Cell Lines*

Cell line	mRNA	α-Dystroglycan	β-Dystroglycan
184B5	0.21 ± 0.014	8.67 ± 0.776	2.60 ± 0.248
MCF-7	0.33 ± 0.092	0.01 ± 0.002	0.50 ± 0.025
T-47D	0.38 ± 0.120	10.64 ± 1.224	3.40 ± 0.214
BT-549	0.41 ± 0.134	3.03 ± 0.114	2.26 ± 0.255
SW-620	0.22 ± 0.014	6.27 ± 0.856	0.46 ± 0.055
HCT116	0.25 ± 0.042	12.46 ± 1.280	2.79 ± 0.187
DU145	0.25 ± 0.028	2.93 ± 0.086	0.27 ± 0.023
HL60	0.06 ± 0.013	0.05 ± 0.007	1.07 ± 0.059

*Values are ratios of dystroglycan to β-actin (mean ± SD). Cell lines include the 184B5 normal mammary epithelium; the MCF-7, T-47D, and BT-549 breast; the SW-620 and HCT116 colon; the DU145 prostate adenocarcinomas; and the HL60 promyelocytic leukemia cells.

leukemic cells (it is noteworthy that α-DG was also not detectable in cell extracts of human peripheral white blood cells, data not shown). α-DG was expressed in the SW620 and HCT116 colon cancer cell lines but its loss was previously observed in the HT29 colon cancer cell line.[11] A reduced expression of the 43-kd β-DG band was observed in the MCF-7, SW620, DU145, and HL60 cell lines whereas the β-DG related 31-kd band was clearly visible in the MCF-7, T47D, HCT116, and DU145 cell lines (Figure 1). To evaluate whether variations in the expression of the DG protein were related to changes in the levels of DG mRNA, primers were designed that amplify a sequence of 485 bp corresponding to the C-terminal region of α-DG, next to the posttranslational proteolytic site, and the N-terminal region of β-DG. These primers were used for PCR amplification of cDNA prepared from total RNA isolated from the same cell lines. Assessment of DG mRNA expression by RT-PCR was determined semiquantitatively by calculating the ratio of densitometric values from the DG band in relation to the internal standard represented by β-actin (Figure 1). As shown in Table 1, the expression of DG mRNA was not related to the expression of the corresponding protein thus suggesting that variations in the expression of DG protein in different cell lines are likely because of post-transcriptional events.

DG Expression Is Frequently Reduced in Human Colon Cancers

The results obtained with the cell lines suggested that DG is differentially expressed in tumor cell lines. To evaluate whether this reduction also occurs in primary tumors and how it relates with tumor features, the expression levels of α-DG and β-DG were analyzed by Western blot analyses in a series of 43 human primary colon cancers and paired adjacent normal colonic mucosa samples and the results obtained were quantitated by densitometry (Figure 2). According to Duke's criteria tumors were classified as 3 stage A, 19 stage B, 13 stage C, and 8 stage D. We observed a variable expression of both subunits in normal and tumor samples. However, expression of α-DG was considered reduced, unchanged, or increased in 30 (70%), 6 (14%), and 7 (16%) of 43 tumors, respectively, compared with normal adjacent mucosa. This reduction was less frequent in well (G1) (5 of 9, 55%) than in moderately (14 of 20, 70%) and poorly (11 of 14, 79%) differentiated tumors but the difference was not significant. The reduced expression of α-DG was observed in all 3 Duke's A (100%), in 9 of 19 (47%) Duke's B, 11 of 13 (85%) Duke's C, and in 7 of 8 (87%) Duke's D tumors. These differences were not significant.

The expression level of the 43-kd β-DG band was also reduced in 17 (39%) tumors whereas it was considered unchanged or increased in 8 (19%) and 18 (42%) tumors, respectively, compared with normal adjacent mucosa samples. Tumors with reduced expression of β-DG included three G1 (33%), eight G2 (40%), and six G3 (43%) tumors and, in terms of tumor stage, one Duke's A (33%), eight Duke's B (42%), six Duke's C (46%), and two Duke's D (25%) tumors. These differences were not significant. The truncated 31-kd β-DG band was clearly detectable in 22 of the 43 paired samples (51%) and it was increased in 13 (59%) of them which included 3 of 7 G1 (43%), 3 of 8 G2 (37%), and 7 of 7 G3 (100%) tumors. In terms of disease stage, increased expression of the 31-kd band of DG was observed in two of two (100%) Duke's A, two of eight Duke's B (25%), seven of eight (87%) Duke's C, and all (100%) Duke's D tumors.

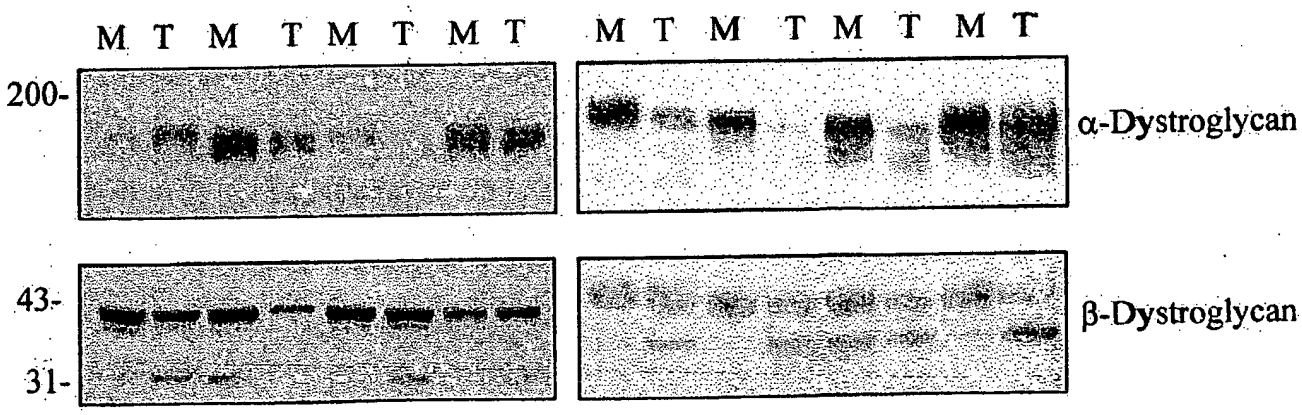

Figure 2. Levels of expression of α- and β-DG in representative cases of primary colon carcinomas (T) and paired normal adjacent mucosa (M) as assessed by Western blot analysis.

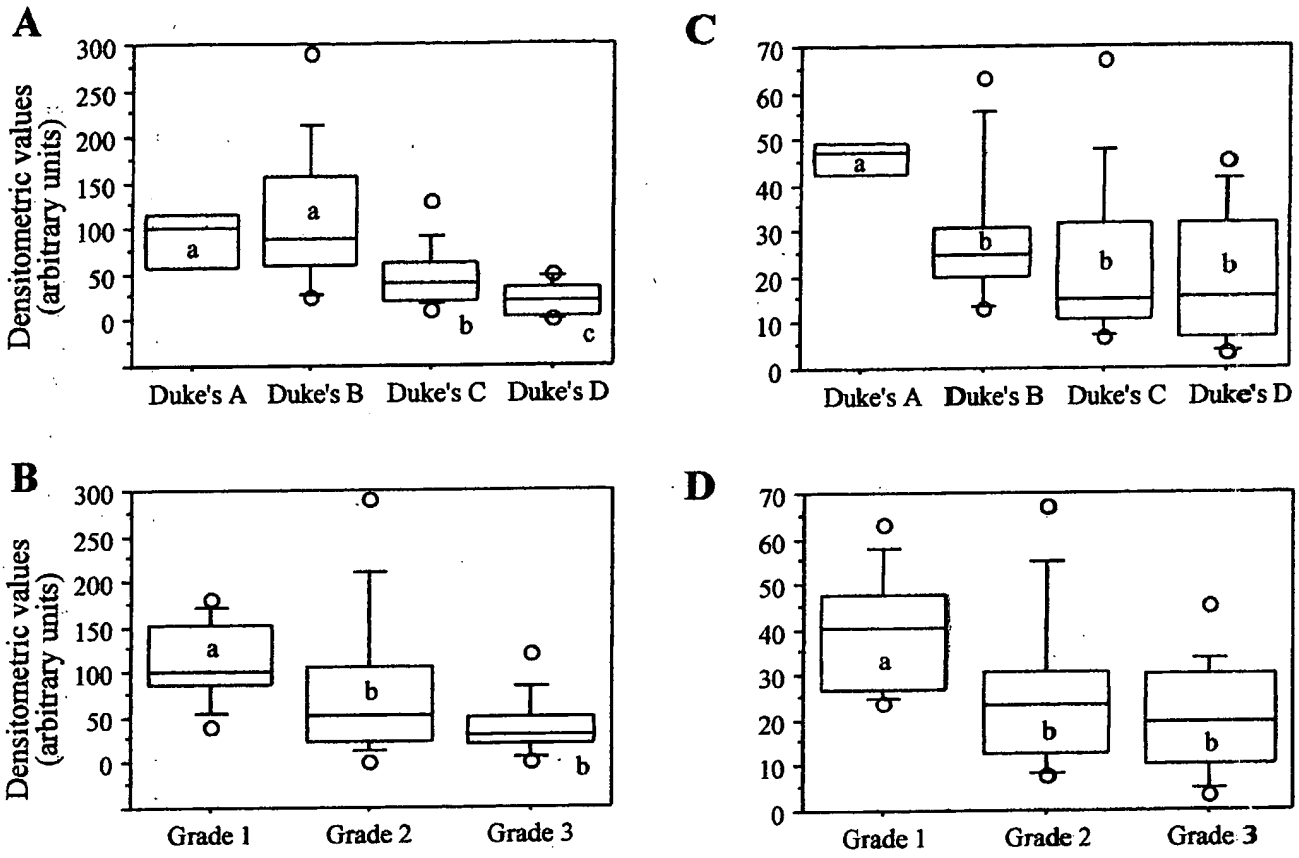

Figure 3. Box-plot of relative density values of α-DG (**A** and **B**) and β-DG (**C** and **D**) expression in primary colon carcinomas stratified according with tumor stage (**A** and **C**) and grade (**B** and **D**). The values shown represent the average of four experiments as shown in Figure 2. The intensities of each of the bands on the Western blots were quantitated and adjusted according with the value of the internal positive control represented by total cell extract of the SW620 cells (not shown). For each group, the **bottom** and **top** edges of the box are the 25th and 75th percentiles, respectively. Median values are shown by the **lines** within the boxes. The **circles** indicate the minimum and maximum values, respectively. Whiskers are obtained by not including the data points in the extreme 20% of the observed values. Within each set (**A–D**) groups of values not sharing the same letter were significantly different ($P < 0.05$).

We then analyzed the absolute values of the expression of α-DG and β-DG in the same tumors. The mean densitometric values for α-DG and β-DG expression in the tumor samples were 73.1 (range, 1.0 to 290.0) and 26.6 (range, 3.5 to 67.0), respectively. According to Duke's stages, the mean densitometric values for α-DG were 87.0 (range, 41.0 to 120.0), 110.5 (range, 25.0 to 290.0), 47.2 (range, 10.0 to 130.0), and 21.4 (range, 1.0 to 50.0) for stages A, B, C, and D, respectively. According to tumor grade, the mean densitometric values for α-DG were 112.4 (range, 41.0 to 180.0), 76.8 (range, 2.0 to 290.0), and 40.2 (range, 1.0 to 120.0) for G1, G2, and G3 tumors, respectively (Figure 3, A and B).

Similarly, the mean densitometric values for the 43-kd band β-DG were 45.7 (range, 40.5 to 49.6), 28.8 (range, 12.0 to 67.0), 23.5 (range, 7.0 to 67.0), and 19.6 (range, 3.5 to 45.0) for stages A, B, C, and D, respectively. According to tumor grade, the mean densitometric values for β-DG were 39.8 (range, 24.0 to 63.0), 25.4 (range, 7.0 to 67.0), and 20.0 (range, 3.5 to 45.0) for G1, G2, and G3 tumors, respectively (Figure 3, C and D). Thus, we observed a significant progressive reduction of α-DG and β-DG expression with increased tumor grade and stage.

Assessment of DG mRNA expression in a series of selected colon cancer samples by RT-PCR demonstrated that, as previously reported for cell lines, the expression of DG mRNA is not related to the expression of the corresponding protein thus suggesting that variations in the expression of DG protein in colon carcinomas are also likely because of posttranscriptional events (Figure 4).

DG Expression in Human Primary Breast Cancers

The expression levels of DG were analyzed by Western blot analyses in a series of primary breast cancers. Total cell extracts were prepared from 10 breast ductal carcinomas including three G1, four G2, and three G3 tumors. As shown in Table 2, these tumors expressed variable levels of both α-DG (range, 1.96 to 10.48) and β-DG (range, 0.11 to 1.21) protein. The mean densitometric values for α-DG were 8.47 (range, 5.76 to 10.48), 5.18 (range, 3.21 to 7.98), and 2.96 (range, 1.96 to 4.18) for grade G1, G2, and G3 cancers, respectively. The corresponding values for β-DG were 0.72 (range, 0.6 to 0.85),

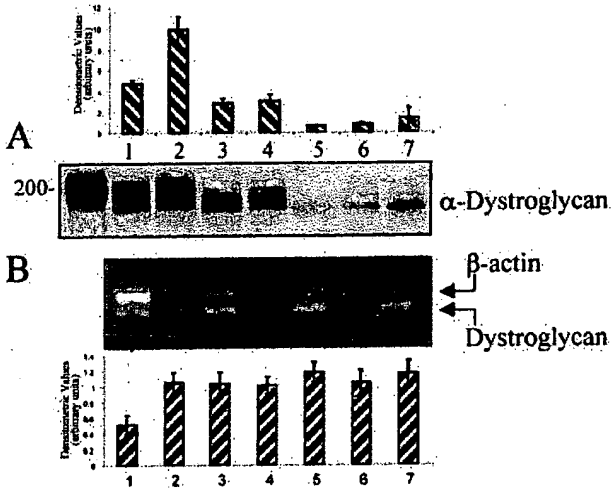

Figure 4. A: α-DG expression was assayed by Western blot analysis in a series (1 to 7) of selected primary colon cancer samples. Cell lysate from the SW620 cell line was also included for comparison (first lane). **B:** Expression of DG mRNA was evaluated in the same tumors by RT-PCR (see Figure 1). Values of ratios of DG to β-actin are shown in the associated graphs.

0.71 (range, 0.25 to 1.21), and 0.40 (range, 0.11 to 0.89), respectively. Thus, as for colon cancers we observed a progressive reduction of α-DG and β-DG expression with increased tumor grade in this limited series of cases. We also evaluated the expression of DG in three samples of normal breast epithelium obtained during reduction mammoplasty. The median values of α-DG and β-DG were 9.9 ± 4.2 and 1.1 ± 0.36 (mean ± SD), respectively, thus confirming that expression of DG tends, indeed, to be reduced in breast cancers compared with normal mammary tissue.

To further investigate the significance of DG in human breast cancer, the expression of α-DG was evaluated by immunostaining in a series of 102 primary human breast carcinomas. We decided to analyze the expression of α-DG because the available anti-β-DG antibody recognizes the cytoplasmic tail of β-DG that is common to both the 43-kd and the 31-kd β-DG-related bands.[11] Thus, the staining attainable using this antibody would have been confused by the simultaneous assessment of both bands being not possible to determine the contribution of each of them. Only cells with a clear membranous staining were regarded as positive. In normal glands a strong staining of mammary epithelial cells was always observed (Figure 5). In tumor cells immunostaining was frequently heterogeneous within one specimen, both in terms of percentage of positive cells and staining intensity with few cases displaying well-differentiated areas with clear positive staining and poorly differentiated areas showing decrease or loss of α-DG expression (data not shown). The percentage of positive cells ranged from 0 to 85% with a median value of 0 (mean, 13.6; SD, 24.9).

Expression of α-DG was not detectable in tumor cells in 67 (66%) specimens despite the fact that adjacent

Table 2. Expression of Dystroglycan Protein in Human Primary Breast Cancers*

No.	Grade	α-DG	43-kd β-DG	31-kd β-DG
1	G1	10.48 ± 2.36	0.718 ± 0.03	0.60 ± 0.06
2	G1	5.76 ± 1.67	0.60 ± 0.03	ND
3	G1	9.18 ± 3.12	0.85 ± 0.71	0.12 ± 0.03
4	G2	7.98 ± 1.21	0.25 ± 0.01	ND
5	G2	4.20 ± 0.95	1.21 ± 0.06	0.18 ± 0.01
6	G2	5.35 ± 1.31	0.67 ± 0.21	ND
7	G2	3.21 ± 1.01	0.70 ± 0.06	ND
8	G3	4.18 ± 1.01	0.19 ± 0.01	0.13 ± 0.06
9	G3	2.75 ± 0.61	0.89 ± 1.03	0.31 ± 0.08
10	G3	1.96 ± 0.231	0.11 ± 0.01	0.10 ± 0.01

*Values are ratios of dystroglycan to β-actin (mean ± SD). ND, not detectable.

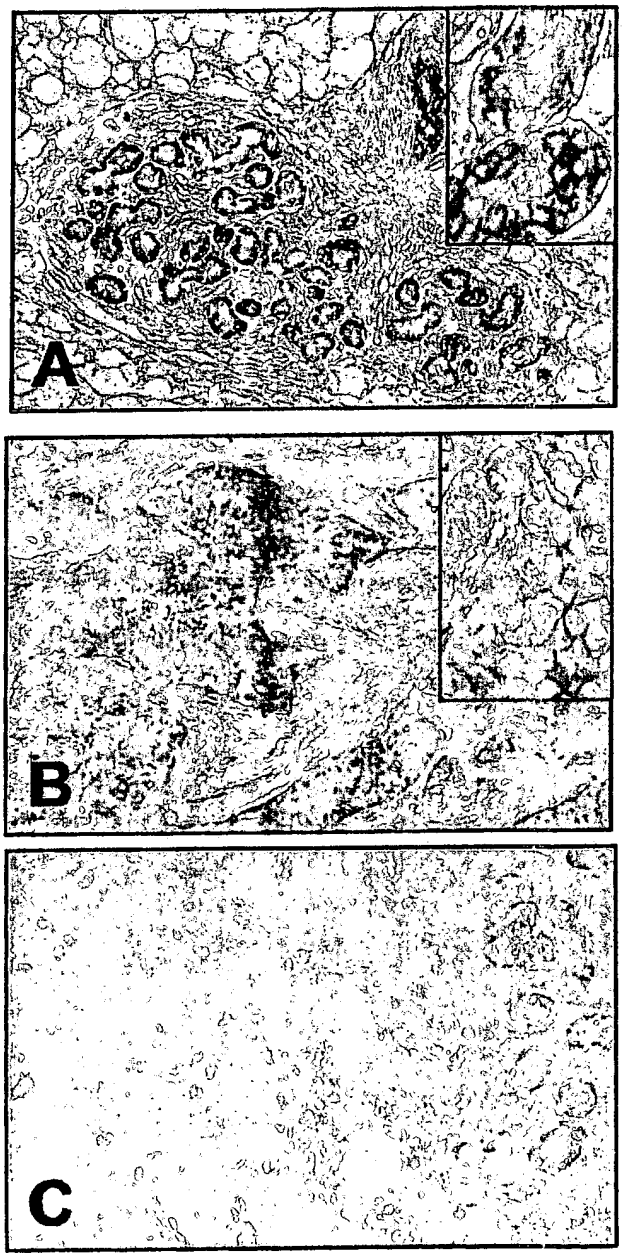

Figure 5. Immunohistochemical staining of α-DG in representative cases of breast carcinomas. **A:** Immunostaining shows a clear membranous staining in normal ductal epithelial cells. **B:** Representative case of ductal carcinoma with positive membranous staining. **C:** Loss of α-DG expression in high-grade ductal carcinoma (**left**). Normal lobules (**right**) display a pagetoide invasion with positive staining in the residual normal ducts but not in the infiltrating neoplastic cells. Original magnifications: ×100 (**A** and **B**); ×200 (**C**); ×800 (**insets** in **A** and **B**).

Table 3. α-Dystroglycan Expression and Clinicopathological Parameters in Human Primary Breast Cancers

	Total	α-Dystroglycan expression		P value
		Positive (%)	Negative (%)	
Age (yr)				
≥60	50	14 (28%)	36 (72%)	
≤60	52	21 (40%)	31 (60%)	0.19
Tumor grade†				
G1/G2 (5/59)	64	24 (38%)	40 (62%)	
G3	32	10 (31%)	22 (69%)	0.65
Tumor stage				
pT1	38	19 (50%)	19 (50%)	
pT2	44	12 (27%)	32 (73%)	
pT3/T4 (4/16)	20	3 (15%)	17 (85%)	0.014
Nodal status				
Negative	32	15 (47%)	17 (53%)	0.114
Positive	70	20 (29%)	50 (71%)	
p53 expression*				
Positive (≥20%)	20	3 (15%)	17 (85%)	
Negative (<20%)	79	32 (41%)	47 (59%)	0.033
Ki67 expression*				
High (≥15%)	28	5 (18%)	23 (82%)	
Low (<15%)	72	28 (39%)	44 (61%)	0.045
DNA ploidy*				
Diploid	67	27 (40%)	40 (60%)	
Aneuploid	31	7 (23%)	24 (77%)	0.09
ER expression*				
High (>20)	46	30 (65%)	16 (35%)	
Low (≤20)	52	37 (71%)	15 (29%)	0.53
PR expression*				
High (>20)	45	16 (36%)	29 (64%)	
Low (≤20)	54	18 (33%)	36 (67%)	0.82

Statistical analyses were performed by the Pearson chi-square test. $P < 0.05$ was considered significant.
*Not all parameters were available for all cases.
†Six lobular carcinomas were not graded.

normal glands were stained positively (Figure 5C). No correlation was observed with age ($P = 0.19$), tumor grade ($P = 0.65$), tumor invasion ($P = 0.14$), lymph node status ($P = 0.08$), progesterone ($P = 0.8$) and estrogen ($P = 0.5$) receptor status, and DNA ploidy ($P = 0.09$). On the other hand, a significant association was observed with tumor stage. In fact, negative staining for α-DG was observed in 19 of 38 (50%) pT1, 32 of 44 (73%) pT2, 3 of 4 (75%) pT3, and 14 of 16 (87%) pT4 tumors ($P = 0.014$) (Table 3). A weak association was also observed with Ki67 staining and p53 expression. In fact, loss of expression was observed in 44 of 72 (61%) tumors with a low Ki67 index and in 23 of 28 (82%) tumors with a high Ki67 index ($P = 0.045$) (Table 3). Negative staining for α-DG was found in 47 of 79 (59.5%) tumors negative for p53 protein expression and in 17 of 20 (85%) p53-overexpressing tumors ($P = 0.033$) (Table 3).

Prognostic Significance of α-DG Expression in Primary Breast Cancers

Twelve of 34 tumors (35%) positive for α-DG and 28 of 66 (42%) negative cases recurred in our series of breast cancers during the period of follow-up. This difference was not significant ($P = 0.49$). On the other hand, 8 of 34 tumors (23%) positive for α-DG and 32 of 66 (48%) negative cases died of disease during the period of follow-up. This difference was significant ($P = 0.016$). Thus, death for disease occurred more frequently in patients of our series whose cancer did not express α-DG compared with positive tumors.

The Kaplan-Meier curves of overall survival within patients with negative *versus* positive cancers showed a significant separation ($P = 0.013$ by log-rank test) which, as expected, was not significant in terms of disease-free survival ($P = 0.35$ by log-rank test) (Figure 6).

In an univariate analysis high tumor stage ($P = 0.0002$ by log-rank test), lymph node involvement ($p = 0.0006$), high tumor grade ($P = 0.0008$), high Ki67 index ($P = 0.001$), low progesterone receptor expression ($P = 0.002$), DNA ploidy ($P = 0.03$) but not age, estrogen receptor, and p53 expression were significantly associated with a shorter overall survival in our series of patients.[28–30]

Multivariate analysis of the variables was performed using two different models. Lymph node involvement ($P = 0.006$; relative risk, 3.790), loss of α-DG expression ($P = 0.044$; relative risk, 2.286), and high tumor grade ($P = 0.001$; relative risk, 3.099) confirmed to be independent predictors of overall survival when a Cox proportional hazards model was constructed that only included these three parameters. However, when a second model was built by adding age of patients at the diagnosis and all of the other parameters that were significant at the univariate analyses, only lymph node involvement ($P = 0.008$; relative risk, 3.766), high tumor grade ($P = 0.008$; relative risk, 2.872), and low progesterone receptor expression ($P = 0.026$; relative risk, 2.464) appeared to be independent predictors of overall survival (Table 4). Loss of α-DG expression was not an independent predictor of survival although it remained not far from significance with a relative risk of 1.842. Similar results were also obtained when DNA ploidy was included in the model or when age and/or Ki67 index were not included in the analysis (data not shown). Tumor stage was not included in the model because it was significantly correlated with lymph node status and models with both variables were heavily affected by collinearity.

In an univariate analysis lymph node involvement ($P = 0.003$), high tumor stage ($P = 0.005$ by log-rank test), high tumor grade ($P = 0.02$), high Ki67 index ($P = 0.013$), low progesterone receptor expression ($P = 0.007$) but not age, estrogen receptor, DNA ploidy and, finally, α-DG expression were significantly associated with a shorter disease-free survival in our series of patients.

When a Cox proportional hazards model was constructed that included age of patients at the diagnosis, lymph node involvement, tumor grade, Ki67 index, DG, and progesterone receptor expressions, only lymph node involvement ($P = 0.006$; relative risk, 3.497) and progesterone receptor expression ($P = 0.015$; relative risk, 2.435) confirmed to be independent predictors of disease-free survival (Table 5). Similar results were also obtained when age and/or α-DG expression were not included in the analysis (data not shown). Tumor stage was not included in the model because of the high collinearity with lymph node involvement.

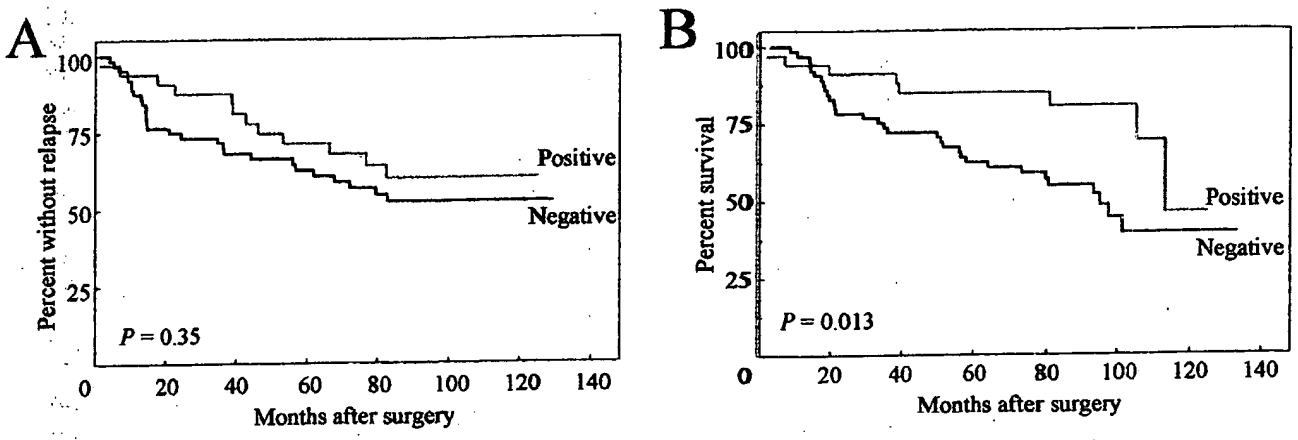

DG expression		Events observed	expected
Positive	34	12	14.83
Negative	66	28	25.17
Total	100	40	40

DG expression		Events observed	expected
Positive	34	8	15.61
Negative	66	32	24.39
Total	100	40	40

Figure 6. Kaplan-Meier curves for disease-free (**A**) and overall (**B**) survival in 100 patients who underwent surgery for breast carcinoma stratified according to α-DG expression.

Discussion

DG is a transmembrane glycoprotein expressed in a wide variety of tissues at the interface between the basement membrane and cell membrane linking the extracellular matrix to the actin cytoskeleton, providing structural integrity and perhaps transducing signal, in a manner similar to integrins.[1,2,7] This is the first study that demonstrates that DG expression is frequently lost in human cancer cells and might have prognostic significance in breast cancer patients.

We previously reported the accumulation of an aberrant form of the β-subunit of DG in a series of human cancer cell lines and in rat mammary tumors. We observed that the presence of this aberrant band was associated with the reduction or loss of expression of α-DG. However, α-DG was also lost in some cell lines despite the presence of a normal β-DG band.[11] We hypothesized that loss of DG might be associated with cell transformation and might play a role in cancer development. In this study the expression of α- and β-DG were analyzed by Western blot analyses in a series of human cancer cell lines of various histogenetic origin. We found that DG is differentially expressed in various cell lines and demonstrated that expression of DG protein is not related with the level of the corresponding mRNA thus suggesting that regulation of DG expression mainly occurs at a post-transcriptional level (Figure 1 and Table 1). The series also included one breast normal (184B5) and three breast cancer (MCF-7, BT549, and T47-D) cell lines and it is of interest that DG expression was reduced in two of the three breast cancer cell lines compared with the normal counterpart (Figure 1).

We also determined by Western blot analyses the expression of DG in a series of human primary colon and

Table 4. Contribution of Various Potential Prognostic Factors to Overall Survival by Cox Regression Analysis in Breast Cancers

Variable	Risk ratio	95% Confidence Interval	*P* value
Age	1.440	0.692–2.995	0.329
Grade	2.872	1.323–6.236	0.008
Nodal status*	3.766	1.417–10.008	0.008
Dystroglycan†	1.842	0.762–4.454	0.175
Ki67‡	1.257	0.564–2.807	0.576
Progesterone†	2.464	1.115–5.445	0.026

*The risk ratio is given as node-positive *versus* node-negative patients.
†The risk ratio is given as negative *versus* positive tumors.
‡The risk ratio is given as high (>15% positive cells) *versus* low proliferation index.

Table 5. Contribution of Various Potential Prognostic Factors to Disease-Free Survival by Cox Regression Analysis in Breast Cancers

Variable	Risk ratio	95% Confidence Interval	*P* value
Age	1.174	0.593–2.322	0.645
Grade	1.812	0.915–3.588	0.088
Nodal status*	3.497	1.443–8.475	0.006
Dystroglycan†	1.058	0.508–2.204	0.880
Ki67‡	1.634	0.806–3.310	0.173
Progesterone†	2.435	1.188–4.994	0.015

*The risk ratio is given as node-positive *versus* node-negative patients.
†The risk ratio is given as negative *versus* positive tumors.
‡The risk ratio is given as high (>15% positive cells) *versus* low proliferation index.

breast cancers and found that its expression varies significantly among tumors. Expression of α- and β-DG were considered reduced in 70% and 39% of colon cancers, respectively, compared with normal adjacent mucosa. Reduced expression of DG was more frequent in less differentiated (G3) and in more advanced cases compared with well-differentiated and earlier lesions (Figure 3). These findings are in agreement with a previous report demonstrating that a reduction in the expression levels of DG is a frequent event in human primary prostate and breast cancers and is most pronounced in high-grade disease.[14] We also demonstrated that the reduced expression of DG is not associated with a reduced level of the corresponding mRNA thus suggesting that, as previously demonstrated for cell lines, regulation of DG expression in colon cancers mainly occur at a posttranscriptional level (Figure 4). The truncated 31-kd β-DG band was clearly detectable in 22 of 43 (51%) colon cancer and in 6 of 10 (60%) breast cancer samples. We could not perform a statistical analysis because of the small number of cases. These results suggest, however, that an altered processing of β-DG might play an important role in the observed reduced expression of both α-DG and β-DG because, as previously mentioned, the 31-kd band lacks the extracellular domain of β-DG essential for the interaction with α-DG.[13]

Western blot analysis demonstrated that DG expression is also reduced in human breast cancers and that its loss is associated with higher tumor grade (Table 2). To extend this analysis, we determined by immunostaining the expression of α-DG in a series of archival human primary breast cancers and found that expression of α-DG is lost in 66% of tumors. Loss of α-DG expression was significantly associated with high tumor stage ($P = 0.01$), high Ki67 index ($P = 0.045$), and p53 overexpression ($P = 0.033$) but not with other clinicopathological features (Table 3). The association with p53 and Ki67 might depend on the association with stage because both high Ki67 index and positivity for p53 were associated with higher tumor stage (data not shown).

Survival analyses by Kaplan-Meier demonstrated that in an univariate analysis loss of α-DG was associated with an increased risk of death for disease ($P = 0.013$ by log-rank test) but not with a shorter disease-free survival (Figure 6). Loss of α-DG expression confirmed to be an independent predictor of overall survival ($P = 0.044$; relative risk, 2.286) when a Cox proportional hazards model was constructed that only included α-DG expression, lymph node involvement, and tumor grade. When a second model was built by including all of the parameters that were significant at the univariate analyses, loss of α-DG expression was no longer an independent predictor of survival but it remained not far from significance with a relative risk of 1.842 (Table 4).

Our series of patients included both node-negative and node-positive patients. It is well known, as also demonstrated by this study, that lymph node involvement is one of the strongest prognostic markers for breast cancer patients. Adjuvant therapy is the standard of care for women with axillary node involvement. Efficacy of adjuvant therapy in node-negative patients is still uncertain and the decision is currently based on risk factors such as tumor stage, estrogen receptor status, and proliferation index. However, in most cases there are no clear indications for treatment choice and there is a great need for useful prognostic markers able to identify node-negative patients with high risk of recurrence and death. Thus, it will be of interest to evaluate the prognostic significance of α-DG expression in the subgroup of node-negative patients. We could not perform this analysis because the small number of eligible cases in our series did not allow a reliable statistical analysis.

To our knowledge this is the first study investigating the expression of DG protein in a series of human cancer cell lines and primary tumors. We provide evidence that the expression of both DG subunits is frequently reduced in human cancer cell lines and in primary colon and breast cancers, being associated with higher grade, higher stage diseases. Henry and colleagues[14] previously evaluated the immunohistochemical expression of DG in breast and prostate cancer and found that reduced expression of DG is a consistent feature of both types of tumors. They, however, evaluated only the expression of β-DG and their series was too limited to perform any statistical analysis. In this study, the expression of α-DG was evaluated by immunostaining in a large series of primary breast carcinomas. We found that α-DG expression is frequently lost in breast cancer cells and observed a progressive loss of its expression with advancing tumor stage. It is noteworthy that although most of the tumors display a negative staining it is likely that, as suggested by the Western blot analysis (Table 2), they still express α-DG although at a level that is undetectable by the immunohistochemical technique. Our data, however, suggest that loss of α-DG expression may be an early event in the multistep process of breast carcinogenesis because it was already detected in ~50% of pT1 tumors and was also observed in some cases of *in situ* carcinoma (Table 3 and data not shown). It has been demonstrated that the 31-kd form of β-DG is the product of a proteolytic processing of the extracellular domain of β-DG.[11,12] This processing is because of the membrane-associated MMP activity and disintegrates the DG complex with loss of α-DG.[12] We could, indeed, demonstrate that α-DG is released in the medium of the MCF-7 breast cancer cell line (unpublished data), although the underlying molecular mechanisms are still unknown. Compelling evidence has demonstrated that MMP activity can enhance tumor growth, invasion, and metastasis. Indeed MMPs are invariably up-regulated in the stromal compartment of invasive epithelial cancers.[31] Further *in vitro* and *in vivo* studies are required to elucidate whether MMP activity is also responsible for the reduced expression of α-DG observed in breast carcinomas. It is of interest, however, that inhibitors of such activity have proved effective for the treatment of human cancers[32] and it cannot be excluded, on the basis of our results, that some of their beneficial effects might be in part because of the reduced processing of DG after their treatment that could contribute to halt tumor cell growth and spreading.

The exact significance of reduced expression of DG in human tumors remains unknown. We are convinced,

however, that our results warrant further studies on the role of this glycoprotein in human tumor development and on its potential prognostic significance in breast and in other cancers. Our preliminary data suggest that its evaluation could have prognostic value, possibly adding information to that obtained from conventional prognostic parameters. In fact, an unexpected finding of the present study was that loss of expression of DG in tumor cells is associated with shorter overall survival. It is tempting to hypothesize that tumors with reduced expression of DG have an enhanced metastatic potential that would be responsible for the poor outcome of the patients. Thus, further investigation on the significance of DG expression level in a more homogeneous group of patients (ie, young node-negative cases) could provide greater insights into the prognostic significance of DG expression.

Intracellular signal transduction pathways activated by the adhesion of cells to other cells or to the extracellular matrix play crucial roles in cellular differentiation, migration, and proliferation and their alterations might play an important role in the process of tumor development. Indeed, defects in extracellular matrix organization with perturbations of the basement membrane separating the epithelial and stromal compartments have long been considered a hallmark of malignant tumors, particularly adenocarcinomas.[33,34] Moreover, transformed cells have altered relationship with the extracellular matrix, showing decreased association of fibronectin and laminin with their surfaces compared with their normal counterparts.[35,36] Taken together our data demonstrate the presence of a large variations in the expression of DG among tumors and suggest that reduced expression of DG is a frequent event in human tumorigenesis and might contribute to tumor progression. Our hypothesis is that an aberrant expression of DG might play a role in tumor development by altering the interactions between cells and the surrounding matrix. A reduction of DG function, in fact, may lead to abnormal cell-extracellular matrix interactions and thus contribute to tumor progression and metastasis rather than merely being a consequence of neoplastic transformation. It has been also proposed that DG might be involved in signal transduction pathways, in a manner similar to integrins. Indeed, β-DG can bind Grb2,[7,37] the growth factor receptor bound adapter protein involved in the activation of several signaling pathways, including the recruitment to plasma membrane and subsequent activation of the Ras oncogene.[38]

In conclusion, further studies on the role played by DG in the regulation of epithelial cell growth and transformation and on its possible role as a tumor suppressor gene are warranted and we believe that they might provide insights into the mechanisms of human tumor pathogenesis and contribute to our understanding of tumor cell growth and invasiveness.

References

1. Durbeej M, Henry MD, Ferletta M, Campbell KP, Ekblom P: Distribution of dystroglycan in normal adult mouse tissues. J Histochem Cytochem 1998, 46:449–457
2. Winder SJ: The complexities of dystroglycan. Trends Biochem Sci 2001, 26:118–124
3. Holt KH, Crosbie RH, Venzke DP, Campbell KP: Biosynthesis of dystroglycan: processing of a precursor peptide. FEBS Lett 2000, 468:79–83
4. Ibraghimov-Beskrovnaya O, Ervasti JM, Leveille CJ, Slaughter CA, Sernett SW, Campbell KP: Primary structure of dystrophin-associated glycoproteins linking dystrophin to the extracellular matrix. Nature 1992, 355:696–702
5. Ibraghimov-Beskrovnaya O, Mialtovich A, Ozcelik T, Yang B, Koepnick K, Francke U, Campbell KP: Human dystroglycan: skeletal muscle cDNA, genomic structure, origin of tissue specific isoforms and chromosomal localization. Hum Mol Genet 1993, 2:1651–1657
6. Ervasti JM, Campbell KP: Dystroglycan: an extracellular matrix receptor linked to the cytoskeleton. Curr Opin Cell Biol 1996, 8:625–631
7. Russo K, Di Stasio E, Macchia G, Rosa G, Brancaccio A, Petrucci TC: Characterization of the beta-dystroglycan-growth factor receptor 2 (Grb2) interaction. Biochem Biophys Res Commun 2000, 274:93–98
8. Williamson RA, Henry MD, Daniels KJ, Hrstka RF, Lee JC, Sunada Y, Ibraghimov-Beskrovnaya O, Campbell KP: Dystroglycan is essential for early embryonic development: disruption of Reichert's membrane in Dag1-null mice. Hum Mol Genet 1997, 6:831–841
9. Ervasti JM, Ohlendieck K, Kahl SD, Gaver MG, Campbell KP: Deficiency of a glycoprotein component of the dystrophin complex in dystrophic muscle. Nature 1990, 345:315–319
10. Ohlendieck K, Matsumura K, Ionasescu VV, Towbin JA, Bosch EP, Weinstein SL, Sernett SW, Campbell KP: Duchenne muscular dystrophy: deficiency of dystrophin-associated proteins in the sarcolemma. Neurology 1993, 43:795–800
11. Losasso C, Di Tommaso F, Sgambato A, Ardito R, Cittadini A, Giardina B, Petrucci TC, Brancaccio A: Anomalous dystroglycan in carcinoma cell lines. FEBS Lett 2000, 484:194–198
12. Yamada H, Saito F, Fukuta-Ohi H, Zhong D, Hase A, Arai K, Okuyama A, Maekawa R, Shimizu T, Matsumura K: Processing of β-dystroglycan by matrix metalloproteinase disrupts the link between the extracellular matrix and cell membrane via the dystroglycan complex. Hum Mol Genetics 2001, 10:1563–1569
13. Sciandra F, Schneider M, Giardina B, Baumgartner S, Petrucci TC, Brancaccio A: Identification of the β-dystroglycan binding epitope within the C-terminal region of α-dystroglycan. Eur J Biochem 2001, 268:4590–4597
14. Henry MD, Cohen MB, Campbell KP: Reduced expression of dystroglycan in breast and prostate cancer. Hum Pathol 2001, 32:791–795
15. Sgambato A, Doki Y, Schieren I, Weinstein IB: Effects of cyclin E overexpression on cell growth and response to TGF-β depend on cell context and $p27^{Kip1}$ expression. Cell Growth Differ 1997, 8:393–405
16. Bearhs OH, Henson DE, Hutter RVP, Kennedy BJ: Manual for Staging of Cancer. Philadelphia, J. B. Lippincott, 1992
17. Elston CW, Ellis IO: Pathological prognostic factors in breast cancer. The value of histological grade in breast cancer: experience from a large study with long-term follow-up. Histopathology 1991, 19:403–410
18. Sgambato A, Ratto G, Faraglia B, Merico M, Ardito R, Schinzari G, Romano G, Cittadini A: Reduced expression and altered subcellular localization of the CDK inhibitor $p27^{Kip1}$ in human colon cancer. Mol Carcinog 1999, 26:172–179
19. Sgambato A, Zhang Y-J, Arber N, Hibshoosh H, Doki Y, Ciaparrone M, Santella RM, Cittadini A, Weinstein IB: Deregulated expression of $p27^{Kip1}$ in human breast cancers. Clin Cancer Res 1997, 3:1879–1887
20. Sgambato A, Migaldi M, Faraglia B, Garagnani L, Romano G, De Gaetani C, Ferrari P, Capelli G, Trentini GP, Cittadini A: Loss of $p27^{Kip1}$ expression correlates with tumor grade and with reduced disease-free survival in primary superficial bladder cancers. Cancer Res 1999, 13:3245–3250
21. Zunarelli E, Nicoll JA, Migaldi M, Trentini GP: Apolipoprotein E polymorphism and breast carcinoma: correlation with cell proliferation indices and clinical outcome. Breast Cancer Res Treat 2000, 63:193–198
22. Railo M, Lundin J, Haglund C, von Smitten K, von Boguslawsky K, Nordling S: Ki67, p53, ER receptors, ploidy and S-phase as prognostic factors in T1 node negative breast cancer. Acta Oncol 1997, 36:369–374
23. Mirza AN, Mirza NQ, Vlastos G, Singletary SE: Prognostic factors in node-negative breast cancer. Ann Surg 2002, 235:10–26
24. Hedley DW, Friedlander ML, Taylor IW, Rugg CA, Musgrove EA:

Method for analysis of cellular DNA content of paraffin-embedded pathological material using flow cytometry. J Histochem Cytochem 1983, 31:1933–1935
25. Sgambato A, Migaldi M, Faraglia B, De Aloysio G, Ferrari P, Ardito R, De Gaetani C, Capelli G, Cittadini A, Trentini GP: Cyclin D1 expression in papillary superficial bladder cancer: its association with other cell cycle-associated proteins, cell proliferation and clinical outcome. Int J Cancer 2002, 97:671–678
26. Hiddemann W, Schumann J, Andreeff M, Barlogie B, Herman CJ, Leif RC, Mayall BH, Murphy RF, Sandberg AA: Convention on nomenclature for DNA cytometry. Cytometry 1984, 5:445–446
27. Grambsch PM, Therneau TM: Proportional hazards tests and diagnostics based on weighted residuals. Biometrika 1994, 81:515–526
28. Clark GM: Interpreting and integrating risk factors for patients with primary breast cancer. J Natl Cancer Inst Monogr 2001, 30:17–21
29. Costa SD, Lange S, Klinga K, Merkle E, Kaufmann M: Factors influencing the prognostic role of oestrogen and progesterone receptor levels in breast cancer—results of the analysis of 670 patients with 11 years of follow-up. Eur J Cancer 2002, 38:1329–1334
30. Schnitt SJ: Traditional and newer pathologic factors. J Natl Cancer Inst Monogr 2001, 30:22–26
31. Hanahan D, Weinberg RA: The hallmark of cancer. Cell 2000, 100: 57–70
32. Maekawa R, Maki H, Yoshida H, Hojo K, Tanaka H, Wada T, Uchida N, Takeda Y, Kasai H, Okamoto H, Tsuzuki H, Kambayashi Y, Watanabe F, Kawada K, Toda K, Ohtani M, Sugita K, Yoshioka T: Correlation of antiangiogenic and antitumor efficacy of N-biphenylo sulfonyl-phenylalanine hydroxiamic acid (BPHA), an orally-active, selective matrix metalloproteinase inhibitor. Cancer Res 1999, 59:1231–1235
33. Bonkhoff H, Wernert M, Dhom G, Remberger K: Distribution of basement membranes in primary and metastatic carcinomas of the prostate. Hum Pathol 1992, 23:408–421
34. Ozzello L: The behavior of basement membranes in intraductal carcinoma of the breast. Am J Pathol 1959, 35:887–900
35. Hayman EG, Engvall E, Ruoslahti E: Concomitant loss of cell surface fibronectin and laminin from transformed rat kidney cells. J Cell Biol 1981, 88:352–357
36. Hynes RO, Wyke JA: Alterations in surface proteins in chicken cells transformed by temperature-sensitive mutants of Rous sarcoma virus. Virology 1975, 64:492–504
37. Yang B, Jung D, Motto D, Meyeer J, Koretzky G, Campbell KP: SH3 domain mediated interaction of dystroglycan and Grb2. J Biol Chem 1995, 270:11711–11714
38. Chardin P, Cussac D, Maignan S, Ducruix A: The Grb2 adaptor. FEBS Lett 1995, 369:47–51

EXHIBIT F

Modeling tissue-specific signaling and organ function in three dimensions

Karen L. Schmeichel and Mina J. Bissell

Lawrence Berkeley National Laboratory, 1 Cyclotron Road, MS 83-101, Berkeley, CA 94720, USA

Correspondence (emails: mjbissell@lbl.gov; klschmeichel@lbl.gov)

Journal of Cell Science 116, 2377-2388 © 2003 The Company of Biologists Ltd
doi:10.1242/jcs.00503

Summary

In order to translate the findings from basic cellular research into clinical applications, cell-based models need to recapitulate both the 3D organization and multicellular complexity of an organ but at the same time accommodate systematic experimental intervention. Here we describe a hierarchy of tractable 3D models that range in complexity from organotypic 3D cultures (both monotypic and multicellular) to animal-based recombinations in vivo. Implementation of these physiologically relevant models, illustrated here in the context of human epithelial tissues, has enabled the study of intrinsic cell regulation pathways and also has provided compelling evidence for the role of the stromal compartment in directing epithelial cell function and dysfunction. Furthermore the experimental accessibility afforded by these tissue-specific 3D models has implications for the design and development of cancer therapies.

Key words: Human epithelial cells, Three dimensional, Organotypic models, Tissue-specific signaling

Introduction

Qualitative evaluation of the cellular complexity and structural integrity of organ biopsies has been used by pathologists for decades to gain insight into human diseases. The well-accepted correlation between tissue structure and health or disease conveys important lessons for the development of experimental models for the study of normal human biology and associated disease progression. Optimally, model design should recapitulate both the 3D organization and the differentiated function of any given organ but at the same time allow experimental intervention. By doing so, cell-based models facilitate systematic analyses that address, at the molecular level, how normal organ structure and function are maintained or how the balance is lost in cancer.

Because of the ethical, technical and financial constraints inherent in research on human cells and tissues, the demand for models that faithfully parallel human form and function considerably outweighs the supply. We and others asserted more than two decades ago that development of physiologically relevant models of both rodent and human origin should recognize that organs and tissues function in a 3D environment (Elsdale and Bard, 1972; Hay and Dodson, 1973; Emerman and Pitelka, 1977; Bissell, 1981; Ingber and Folkman, 1989). Further, that in the final analysis, the organ itself is the unit of function (Bissell and Hall, 1987). We now know that exposure of cells to the spatial constraints imposed by a 3D milieu determines how cells perceive and interpret biochemical cues from the surrounding microenvironment [e.g. the extracellular matrix, growth factors and neighboring cells (for reviews, see Roskelley et al., 1995; Bissell et al., 2002; Cunha et al., 2002; Ingber, 2002; Radisky et al., 2002)]. Furthermore, it is in this biophysical and biochemical context that cells display bona fide tissue and organ specificity.

Here, we describe studies of epithelial-cell-based systems that demonstrate the importance of developing and utilizing 3D human organotypic models to understand the molecular and cellular signaling events underlying human organ biology (Fig. 1). In their most simplistic form, these models comprise homogeneous epithelial cell populations that are cultured within 3D basement-membrane-like matrices. These relatively simple 'monotypic' cell models have progressively evolved into 3D co-culture models containing multiple cell types, which approximate organ structure and function in vitro and enable systematic analyses of the molecular contributions of multiple cell types. Finally, we go on to explore how human 3D culture models are being coupled to existing technologies in the mouse to generate models in vivo that could elucidate the fundamental influence of stromal-epithelial interactions in normal organ function as well as those that perturb organ homeostasis and lead to disease. As a result of these advancements, we are equipped with a hierarchy of related models that appreciate the importance of 3D environments but vary with respect to cellular complexity. By using this collection of experimental models interchangeably, we can test molecular markers and targets in models of defined at the molecular level with increasing physiological relevance (culminating in vivo); conversely, results in vivo can be translated into less complex models that are more suitable for diagnostic and therapeutic development.

Monotypic 3D cell culture assays

For several decades, we and others have taken a relatively simple approach of developing monotypic 3D culture models that are composed of single cell types but nonetheless recapitulate the minimum unit of the differentiated tissue (Bissell and Radisky, 2001; Cukierman et al., 2002). In addition to cell source, the composition of two basic

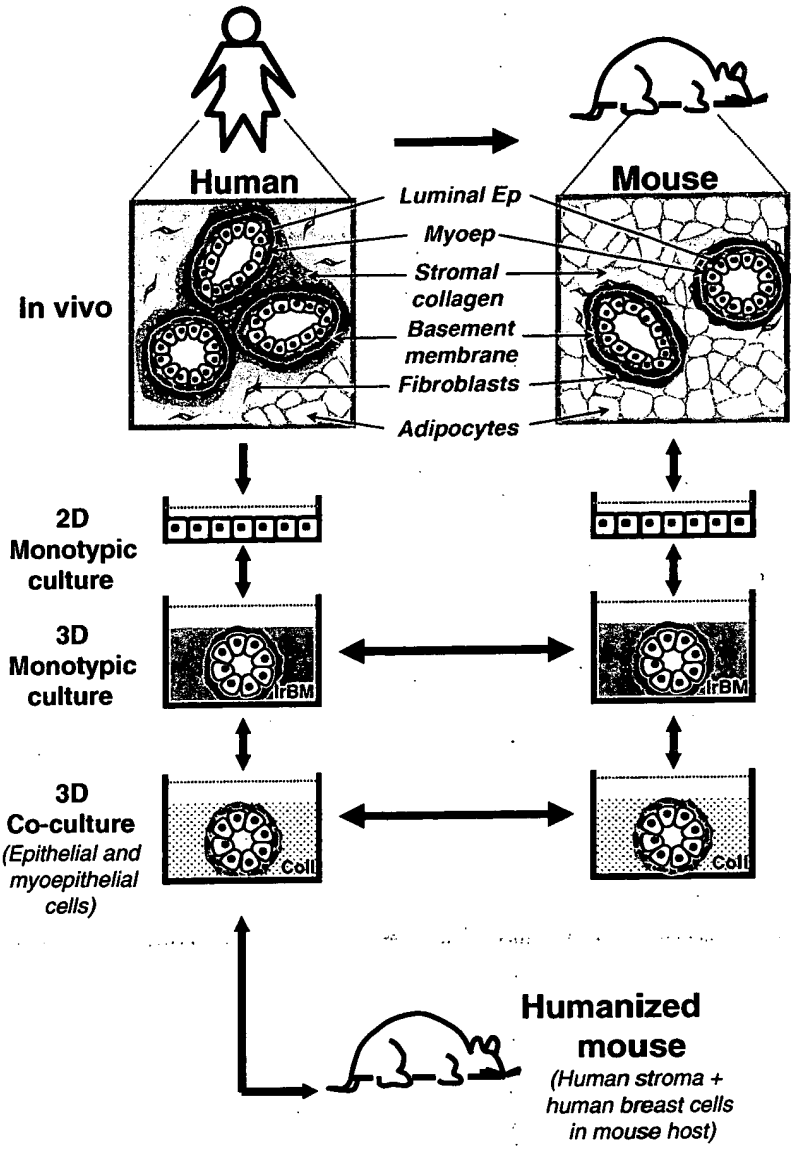

Fig. 1. Hierarchical modeling of human breast function. Similarities between the organization of human and mouse mammary glands have enabled observations in one tissue to be transferred to the other. This dynamic exchange of information has led to the gradual development of mammary gland models that now represent a continuum of organotypic systems ranging in complexity from monotypic 3D cultures to multicellular co-cultures to in vivo xenograft models. Each of the 3D models depicted here represents a physiologically relevant assay in its own right. However, when engineered with common cellular components and used in series, these models become invaluable tools for the identification and verification of disease-related molecules as well as for the design and translation of effective drug therapies. Future in vivo models that are more faithful to the human mammary microenvironment may be achieved in a 'humanized' mouse model in which mammary glands are entirely repopulated by breast cell types of human origin. Ep, epithelial cell; Myoep, myoepithelial cell. Adapted from previous publications (Ronnov-Jessen et al., 1996; Schmeichel et al., 1998).

components must be considered when one establishes physiologically relevant 3D culture models: the extracellular matrix (ECM) and the medium. Cell sources, both primary or immortalized, are most useful when they are capable of supporting tissue-specific differentiated function(s) in response to appropriate stimuli. Likewise, both the composition and delivery of the ECM and its molecules should reflect the physiology of the tissue in question. For example, laminin-rich Matrigel (Kleinman et al., 1986) is a reasonable substratum for use in 3D cultures of epithelia since epithelial cells are embedded in laminin-rich basement membrane (lrBM) in vivo. (In the discussion below, Matrigel will be generally referred to as lrBM. It should be noted, however, that whereas Matrigel is currently a cost-effective and biochemically reasonable substitute for BM, it is in fact a rather crude and ill-defined mixture of extracellular matrix proteins derived from a mouse tumor.) ECM presentation is also a critical parameter since cells cultured in (or on) thick and malleable matrices become differentiated, whereas cells grown on ECM delivered as a thin, planar coating on plastic do not (Roskelley et al., 1994; Cukierman et al., 2002). Finally, unlike chemically defined growth media, media containing serum or other complex supplements often interfere with differentiation.

A number of cell models have been coupled with appropriate 3D matrices and show fruitful results in recapitulating tissue functions in 3D. Extensive studies have been reported for liver, salivary gland, vasculature, bone, lung, skin, intestine, kidney and mammary and thyroid glands (see Table 1 and references therein). Other cells, such as MDCK (O'Brien et al., 2001; Troxell et al., 2001) and fibroblasts (Harkin and Hay, 1996; Cukierman et al., 2001), have also been monitored in 3D contexts and have provided valuable insight into the basic molecular mechanisms of polarity, branching morphogenesis, adhesion and cell migration (reviewed in Cukierman et al., 2002; O'Brien et al., 2002; Walpita and Hay, 2002).

In some cases, however, the relationship between these models in culture and a counterpart in vivo is unclear. We contend that, in order to be useful as a translational tool for the study of human disease progression, 3D organotypic models must be developed that are true to human form and function. In the following sections, we will describe the development of 3D culture models in human breast (and, briefly, in skin) that demonstrate how appropriate choice of cell source and ECM substrata can enable the establishment of physiologically relevant assay systems. By virtue of their resemblance to organ structure and function in vivo, these models facilitate meaningful dissection of the molecular mechanisms involved in the regulation of tissue specificity.

Table 1. Examples of 3D environments used in monotypic 3D cultures

Matrix	Cell type	Reference
Collagen I	Liver	Michalopoulos and Pitot, 1975; Bader et al., 1996
	Mammary gland	Emerman et al., 1977; Emerman and Pitelka, 1977; Howlett et al., 1995; Gudjonsson et al., 2002a
	Skin	Asselineau et al., 1985; Kopan et al., 1987
Amniotic basement membrane	Pancreas	Ingber et al., 1986
	Lung	Sakamoto et al., 2001
Reconstituted basement membrane	Liver	Bissell, D. M. et al., 1987; Ben-Ze'ev et al., 1988
	Mammary gland	Li et al., 1987; Barcellos-Hoff et al., 1989
	Pancreas	Oliver et al., 1987; Gittes et al., 1996
	Endothelia	Kubota et al., 1988; Grant et al., 1989
	Prostate	Bello-DeOcampo et al., 2001
	Lung	Schuger et al., 1990
	Salivary gland	Hoffman et al., 1996
	Thyroid gland	Mauchamp et al., 1998
	Kidney	Sakurai et al., 1997
	Intestine	Sanderson et al., 1996
	Bone	Vukicevic et al., 1990
Rotary cultures	Mammary gland	Runswick et al., 2001
	Prostate	Clejan et al., 2001

Monotypic 3D cultures for modeling mammary gland and epithelial signaling

A large body of work performed in mammary epithelial cells from mice demonstrates the central importance of 3D cell-microenvironment interactions in promoting a differentiated cellular response (Lin and Bissell, 1993; Roskelley et al., 1995; Boudreau and Bissell, 1998). Mammary cells embedded in lrBM adopt a spherical, polarized structure that resembles the normal mammary alveolus (or acinus) and that is capable of mammary-gland-specific function (e.g., producing milk in response to lactogenic hormones) (Barcellos-Hoff et al., 1989) (reviewed in Stoker et al., 1990). Human luminal epithelial cells, both primary and immortalized, respond to ECM in much the same way as their mouse counterparts by forming acini in 3D (Fig. 2) (Petersen et al., 1992; Howlett et al., 1995; Weaver et al., 1997). [The same cells grown in an interstitial ECM, such as collagen I, show altered integrins and abnormal polarity and organization (Howlett et al., 1995; Gudjonsson et al., 2002a; Weaver et al., 2002), thereby underscoring the importance of matching cell types with appropriate substrata.] Human breast tumor cells fail to show a differentiated phenotype in 3D lrBM, but instead form cellular masses that are disorganized and apolar (Petersen et al., 1992). Collectively, these studies demonstrate that human mammary epithelia respond to structural and biochemical cues provided by the ECM and that these cell-ECM interactions are sufficient to reveal innate cellular phenotypes.

3D organotypic cultures are amenable to a variety of experimental manipulations and have been effectively used to re-examine molecular pathways previously characterized by conventional culture methodologies as well as to elucidate novel signaling pathways. Recent examples are described below and are summarized in Fig. 2.

Coupled signaling mechanisms and reversion

When used in conjunction with well-defined human mammary cell cultures, monotypic 3D assays have proven useful for understanding how altered cell-ECM communication regulates breast tumor progression. One such cell source is the HMT-3522 human breast tumor progression series, which comprises a continuum of cell populations that arise from a common precursor but range in phenotype from non-malignant (S1) to tumorigenic (T4-2) (Briand et al., 1987; Nielsen et al., 1994; Briand et al., 1996). Dissection of the molecular differences between these cells revealed that surface expression of the ECM receptor β1 integrin is dramatically upregulated in T4-2 tumor cells in comparison with their non-malignant counterparts. When treated in 3D cultures with antibodies that block β1 integrin function, T4-2 cells dramatically reorganize: cell colonies become phenotypically reverted, assuming a polarized and growth-arrested status comparable to that observed of non-malignant S1 cells (Fig. 2) (Weaver et al., 1997). Reduced β1 integrin signaling results in downregulation of endogenous β1 integrins as well as in reduced signaling and levels of the epidermal growth factor receptor (EGFR) (Wang et al., 1998). In a reciprocal fashion, neutralizing the activity of EGFR effectively normalizes β1 integrin signaling and levels (Fig. 2). Such β1 integrin and EGFR reciprocal cross-modulation is apparently dependent upon a 3D context as neutralizing antibodies do not elicit reciprocal cross-modulation in cells cultured as 2D monolayers (Wang et al., 1998).

To determine the extent to which adhesion and growth factor receptor signaling is coupled in more aggressive tumors, Wang et al. recently assayed a series of metastatic human breast cancer cell lines for sensitivity to β1 integrin and EGFR cross-talk inhibitors in 3D lrBM cultures (Wang et al., 2002). Unlike results from the tumorigenic, but non-metastatic, T4-2 cells, single inhibitors induce only partial phenotypic reversion in aggressive carcinoma cells (Fig. 2). Instead, specific pairs of inhibitors, applied in tandem, are required to revert the malignant phenotype or cause apoptosis. Therefore, as signaling pathways become increasingly disconnected, they require intervention at multiple sites to elicit reversion and/or apoptosis.

Collectively, these studies show that recapitulation of phenotypically normal tissue in 3D lrBM assays correlates with

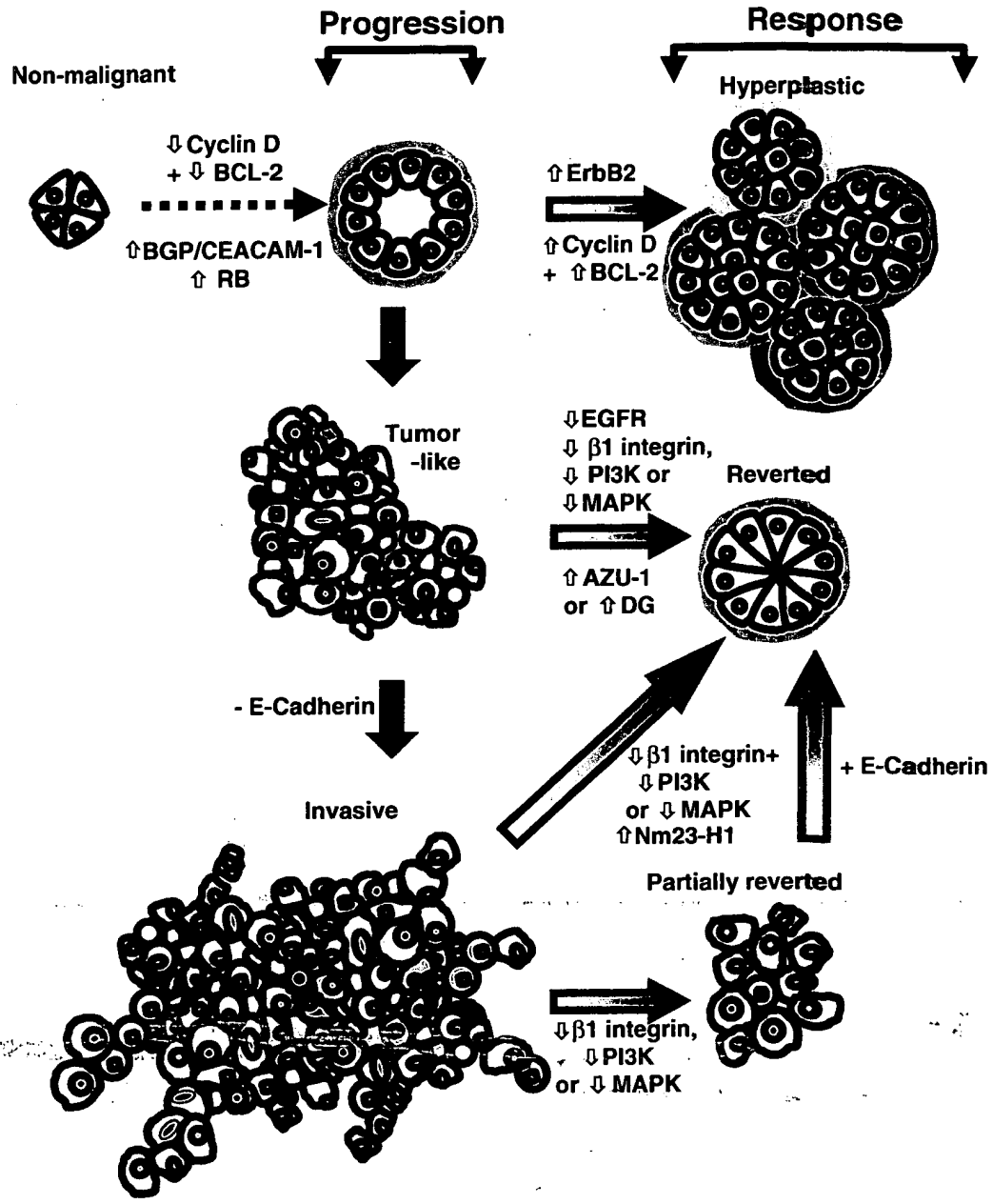

Fig. 2. Signaling mechanisms studied in monotypic 3D cultures of human mammary epithelial cell lines. The phenotypes of human mammary epithelial cells can be readily distinguished in the context of 3D lrBM assays. After 10 days in culture, non-malignant cells form growth-arrested, polarized acini with central lumens, whereas malignant cells form apolar colonies of continually growing cells that vary in size and shape depending on the degree of tumorigenicity. A number of studies, some of which are depicted here, have utilized this assay to explore the molecular regulation of normal breast (e.g., lumen formation) as well as aberrant signaling during tumor progression and/or reversion. Individual studies are referenced in the text.

the ability of adhesion and growth factor receptor signaling pathways to engage in reciprocal cross-modulation. Moreover, the intracellular signaling pathways directing cell polarity and proliferation in human mammary epithelial tissues are orchestrated in profoundly different ways, depending on whether cells are cultured in a 2D or 3D context. These studies also constitute proof that 3D assays of phenotypic reversion can be exploited further to characterize potential modulators of the malignant phenotype in breast.

Tumor suppressors and oncogenes

3D lrBM assays can be used to search for oncogenes and tumor suppressors as well as to understand their mechanisms of action. For example, Howlett et al. examined the extent to which restoration of Nm23-H1, a metastasis-suppressor gene (Leone et al., 1993), could restore 'normal' cell morphology (Howlett et al., 1994). They transfected a metastatic breast carcinoma cell line MDA-MB-435 with an Nm23-H1 transgene and assayed the resulting transgenic cells 3D lrBM cultures. They found that cells overexpressing Nm23-H1 formed organized acinus-like spheres with appropriately polarized basal and apical surfaces (Fig. 2) and thus provided evidence that suppressive effects of Nm23-H1 might be due to its role in growth inhibition and differentiation in response to cues from the ECM. Spancake et al. examined the effects of downmodulating the retinoblastoma (RB) tumor-suppressor pathway in human mammary epithelial cells. Whereas loss of

RB function did not affect polarity of these epithelial cells in 3D (Spancake et al., 1999), the 3D acini were not growth arrested and failed to display several markers of differentiation found in primary cells, thereby demonstrating that RB function plays a role in mammary cell differentiation.

AZU-1 is a gene product that was isolated by comparative gene expression analysis of premalignant and malignant cells of the HMT-3522 series (Chen et al., 2000). *AZU-1* [also called *TACC2* (Still et al., 1999)] mRNA is significantly downregulated in a variety of human breast tumor cells, which is consistent with it having a tumor suppressor role in breast tissue. Normalizing the expression of AZU-1 in T4-2 tumor cells causes phenotypic reversion of the cells, as revealed in 3D lrBM assays. These findings, in combination with in vivo tumorigenicity assays, provides experimental evidence that AZU-1 is a novel breast tumor suppressor. Interestingly, AZU-1 levels, which are very low in T4-2 cells, become normalized in tumor cells reverted by EGFR or β1 integrin inhibition, which suggests that AZU-1 expression is also sensitive to cues from the microenvironment (Chen et al., 2000).

More recently, the non-integrin cell surface ECM receptor dystroglycan (DG) was also shown to display a tumor-suppressive function in T4-2 cells (Muschler et al., 2002). Re-expression of DG in tumor cells lacking α-DG expression but expressing E-cadherin produced profound repolarization of cells in the 3D lrBM assay. This finding suggests that, at the cell surface, normal cellular function might be a result of a competitive balance that is achieved by signaling through integrins, growth factors and dystroglycan.

Novel aspects of the function of the oncogene ErbB2 in tumor progression have been revealed in 3D human mammary epithelial cell cultures as well. ErbB2 is particularly interesting as a potential oncogene in the breast because its overexpression correlates with a poor clinical prognosis (reviewed in Eccles, 2001; Yarden, 2001). Human MCF10A mammary epithelial cells were recently engineered to express conditionally activated ErbB2 and analyzed in monotypic 3D cultures (Fig. 2) (Muthuswamy et al., 2001). When ErbB2 receptor, but not ErbB1, is activated in mature 3D acini, the MCF10A cells lose their polarized organization and develop structures consisting of multiple acinar-like units with filled lumina. These structures do not display any invasive properties and thus represent a reasonable model for ductal carcinoma in situ (DCIS). This finding also raised the possibility that excessive signaling through ErbB2 in 3D cultures is sufficient to induce growth and to protect cells from apoptosis within the luminal space (Huang et al., 1999; Muthuswamy et al., 2001) (see also discussion below).

Sensitivity and resistance to cell death

More than two decades ago, Hall et al. showed that, when murine mammary cells are sandwiched between two layers of ECM, they form a lumen (Hall et al., 1982). Since then, 3D monotypic cultures have been used to explore the basic developmental pathways of the mammary gland, including lumen formation. The work of Frisch and colleagues indicated that adhesion to any ECM molecule is a survival cue and that loss of adhesion hastens a cell's demise (anoikis) (Frisch and Francis, 1994). Boudreau et al. showed that adhesion to an inappropriate ECM ligand, at least in the case of epithelial cells, only delays cell death temporarily (Boudreau et al., 1995) and that adhesion to relevant substrata, such as lrBM or laminin, is necessary to maintain long-term survival. Once the cells lose contact with BM, caspases are induced and the cells apoptose. Coucouvanis and Martin showed subsequently in developing mouse embryos that, whereas contact with BM protects the outer cell layer, the inner cell mass cavity is carved by apoptosis of cells that had no contact with BM (Coucouvanis and Martin, 1995). Others have since shown that cavitation of the lumen of the mammary gland is also mediated by induction of apoptosis (Blatchford et al., 1999) (see also below).

Several recent reports using 3D human mammary epithelial cell models have provided important insights into the molecules and pathways involved in the apoptotic events leading to lumen formation. For example, Huang et al. showed that biliary glycoprotein (BGP, also known as CEACAM1 or CD66a), a transmembrane protein expressed on the luminal surface of mammary epithelia, is required for lumen formation in MCF10A-derived acini cultured in 3D lrBM (Huang et al., 1999). Re-expression of a short isoform of BGP in MCF7 breast carcinoma cells (that is, cells that lack BGP and fail to form lumena in 3D lrBM assays) results in cells that form morphologically normal mammary acini with properly formed central lumena in 3D cultures (Kirshner et al., 2003). This model revealed that BGP adopts an apical localization during morphogenesis and influences lumen formation by initiation of apoptotic pathways.

Two recent studies by Muthuswamy et al. and Debnath and colleagues show that lumen formation in the MCF10A model is not mediated solely by the action of pro-apoptotic signals (Muthuswamy et al., 2001; Debnath et al., 2002). Rather growth control signals and increased apoptotic signaling cooperate to direct lumen formation in this 3D monotypic model. Because chronic activation of ErbB2 is sufficient to cause accumulation of colonies with cell-filled lumina, ErbB2 oncogenic signaling probably exerts multiple biological effects, coordinating signals that affect both proliferation and apoptosis during cavitation (Debnath et al., 2002). These studies provide a compelling example of how the study of developmental processes (such as lumen formation) can benefit from the experimental accessibility of these simple tissue-specific models to yield physiologically relevant information at the molecular level.

The HMT-3522 culture model was recently employed to address mechanisms of resistance to chemotherapeutic-agent-induced apoptosis in vivo (Weaver et al., 2002; see also Yamada and Clark, 2002). Formation of 3D polarized structures confers protection against apoptosis in both non-malignant and malignant mammary epithelial cells. Destabilizing the polarity of these structures by disrupting β4 integrin ligation, and thus perturbing hemidesmosome organization, allows induction of apoptosis. Loss of β4 integrin results in the inactivation of NFκB, a known positive modulator of expression and stability of apoptosis regulators. This topic is of critical relevance to considerations of apoptotic drug resistance and tumor dormancy. Metastasized tumor cells, either as single cells or clusters, may resist death induced by chemotherapeutic agents when the microenvironment and spatial information at the secondary site is conducive to the establishment of cell polarity and survival.

The functional significance of nuclear structure

The status of nuclear organization is an important indicator of tissue homeostasis and differentiation in vivo (Lelievre et al., 2000; Nickerson, 2001). In 3D cultures, the nuclear structure of HMT-3522-S1 cells differs radically from that of the same cells cultured in a monolayer (Lelievre et al., 1998). Furthermore, a series of structural changes are evident within the nucleus throughout acinar morphogenesis in 3D. The observed structural modifications are apparently coupled to S1 cell function, as targeted disruption of the nuclear structure in fully differentiated S1 cells causes upregulation of matrix metalloproteinase activity, an event that ultimately alters the quality of the underlying basement membrane (Lelievre et al., 1998). Collectively these studies point to a dynamic and reciprocal functional connection between nuclear structure and cell function that is dependent upon the presence of an appropriate 3D context. Much remains to be understood about how communication between the BM, the 3D structure and the nucleus is established. However, the idea that understanding these connections requires 3D models is now being more widely championed. Commenting on recent papers by Debnath et al. and Weaver et al., Jacks and Weinberg conclude: "Suddenly, the study of cancer cells in two dimensions seems quaint, if not archaic" (Debnath et al., 2002; Weaver et al., 2002; Jacks and Weinberg, 2002).

Modeling organs in vitro: organotypic co-cultures

Whereas the monotypic 3D culture models described above effectively approximate the biochemical and spatial contributions required for tissue-specific function, organs comprise numerous cell types, matrices and other environmental factors. By reproducing a total organ environment in culture models, the significance of autocrine and paracrine interactions, long appreciated for their roles in organ biogenesis and development (for a review, see Cunha, 1994), can be examined in molecular and cellular terms. This is particularly important given the growing interest in the broader role of the stroma (loosely defined as other cell types plus the ECM) in regulating normal epithelial cell function (see Bissell and Radisky, 2001; Liotta and Kohn, 2001; Silberstein, 2001; Tlsty and Hein, 2001; Cunha et al., 2002; Fuchs and Raghavan, 2002; Mueller and Fusenig, 2002). Studies in human skin provide extensive examples of how 3D co-culture methodologies can be used to recapitulate organ function and allow systematic analysis of underlying molecular pathways.

The co-culture paradigm: human skin

3D organotypic co-culturing methodologies have been particularly successful in epidermal biology. A cultured version of a 'skin equivalent' has been achieved through culturing of keratinocytes either on de-epidermized dermis (Regnier et al., 1981; Watt, 1988; Fartasch and Ponec, 1994) or on collagen gels embedded with dermal fibroblasts (Bell et al., 1981; Regnier et al., 1981; Asselineau and Prunieras, 1984; Asselineau et al., 1985; McCance et al., 1988; Watt, 1988; Coulomb et al., 1989; Fartasch and Ponec, 1994). Such co-cultures give rise to stratified epithelium that displays many of the morphological and functional features of an epidermis in vivo (Bell et al., 1981; Kopan et al., 1987; Watt, 1988; Kopan and Fuchs, 1989; Hertle et al., 1991; Parenteau et al., 1991; Fusenig, 1994; Smola et al., 1998).

Differentiated human skin equivalents are produced in co-cultures containing fibroblasts of either human or mouse origin (Choi and Fuchs, 1990; Turksen et al., 1991; Kaur and Carter, 1992). Given this inherent compatibility, which probably reflects a similarity in the synthesis of paracrine factors between species, one can supplement skin co-cultures with fibroblasts derived from genetically engineered mice. An elegant example of such a substituted culture allowed examination of the role of AP-1 transcription factor subunits c-jun and junB in skin homeostasis (Fig. 3) (Szabowski et al., 2000; Angel and Szabowski, 2002). Unlike wild-type murine fibroblasts, the presence of c-jun-deficient or junB-deficient fibroblasts had dramatic and distinct effects on keratinocyte proliferation and differentiation when included in skin co-cultures. These studies elucidated a double paracrine mechanism in which keratinocytes produce Il-1, which, in turn, induces the expression of keratinocyte growth factor (KGF) and granulocyte macrophage colony stimulating factor (GM-CSF) in dermal fibroblasts through AP-1 activation (Maas-Szabowski et al., 2000; Szabowski et al., 2000; Maas-Szabowski et al., 2001).

When used in combination with skin tumor progression models, 3D co-cultures also effectively distinguish between non-malignant and malignant phenotypes. Such strategies were used to show that MMP1, a matrix metalloproteinase implicated in tumor induction and progression, is upregulated not only in more aggressive tumor types but also in the co-cultured fibroblasts themselves (Fusenig and Boukamp, 1998). Other studies have established that embryonic stem (ES) cells from normal animals can produce well-differentiated epidermis in 3D co-cultures (Bagutti et al., 1996). Taking advantage of this compatibility, Bagutti et al. recently demonstrated that β1-integrin-null stem cells respond and differentiate in epidermal skin cultures only in the presence of excess stromal factors and that loss of β1 integrin decreases the sensitivity of ES cells to soluble factors that induce differentiation (Bagutti et al., 2001).

Given the development of these tractable models of human skin that display an unquestionable resemblance to skin in vivo, it is not surprising that these models are being productively utilized in pharmacotoxicological studies (Gay et al., 1992) and in skin grafting procedures (Boyce and Warden, 2002). Furthermore, they provide critical guidance for modeling the complexities of other human organ systems, such as the breast, in culture.

Modeling breast complexity in culture

The unit morphology of a mammary duct is a double-layered structure in which a continuous sheet of polarized epithelium is surrounded by a layer of myoepithelial cells. Because of their contractile nature, myoepithelial cells have generally been recognized for their function in the extrusion of secreted milk from mammary gland during lactation. However, accumulating evidence indicates that myoepithelial-luminal epithelial cell interactions contribute to homeostasis within the mammary gland and that disruption of this interaction might be an

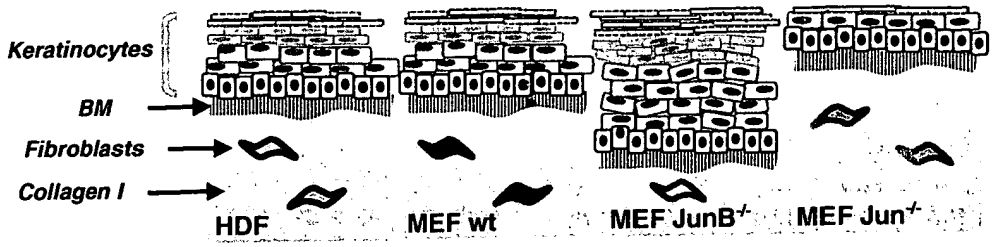

Fig. 3. Using genetically engineered fibroblasts to elucidate stromal-epithelial interactions in organotypic skin co-cultures. Primary human keratinocytes maintain their stratified and differentiated morphology in 3D organotypic co-cultures regardless of whether dermal fibroblasts included are of human (HDF, A) or mouse (MEF, mouse embryonic fibroblasts, B) origin. Substitution of wild-type mouse fibroblasts with genetically engineered fibroblasts from transgenic animals allows for a detailed analysis of the molecular underpinnings of epithelial stromal interactions. Here, c-jun$^{-/-}$ (C) and junB$^{-/-}$ (D) fibroblasts are shown to have hypo- or hyperproliferative effects, respectively, on the morphology of human skin. This study demonstrates the utility of 3D co-culture methodologies in dissecting the molecular determinants of paracrine signaling networks. This figure is summarized from a previously published figure (Szabowski et al., 2000).

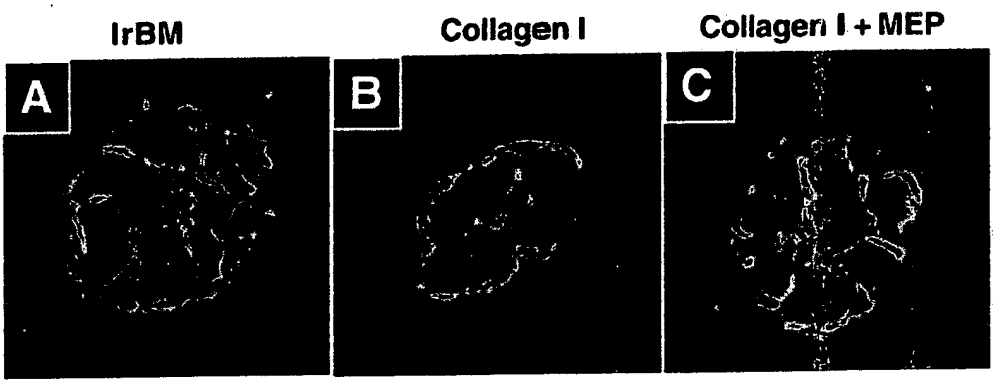

Fig. 4. Modeling mammary acinar structure in 3D organotypic co-cultures. Purified primary human luminal epithelial cells were embedded and cultured in lrBM (A) or collagen I gels (B,C) in the absence (A,B) or presence (C) of purified myoepithelial cells (MEP). Cultures were double stained for the lumenal marker, sialomucin (red) and the basolateral marker, epithelial-specific antigen (ESA; green). Luminal epithelial cells form polarized organotypic spheres in lrBM but adopt inverse polarity in collagen I gels. Addition of purified myoepithelial cells to luminal epithelial cells in collagen I corrects acinar polarity (C) and results in formation of a bilayered organotypic structure. Reproduced with permission from Gudjonsson et al. (Gudjonsson et al., 2002a).

important step in tumor progression (Zou et al., 1994; Sternlicht et al., 1997; Man, 2002).

Recently, several studies performed in 3D organotypic co-culture models have examined the role of myoepithelia in organizing and maintaining normal gland structure and function. Runswick and colleagues mixed purified human luminal epithelial cells and myoepithelial cells and incubated them in a 3D rotary culture environment (Runswick et al., 2001). Under these conditions, double-layered structures formed, containing a central core of polarized luminal epithelial cells surrounded by a layer of myoepithelial cells. Perturbation of myoepithelium-specific desmosomal cadherins disrupted basal positioning of myoepithelial cells (Runswick et al., 2001), thereby demonstrating that physical associations between myoepithelial and luminal epithelial cells are important for the establishment of higher-order organ structure in the mammary gland.

The interdependence of luminal and myoepithelial cells has also been analyzed in 3D ECM cultures in which purified primary luminal epithelial cells were combined within 3D collagen I gels in the presence or absence of purified myoepithelial cells (Gudjonsson et al., 2002a). As expected from previous studies of human mammary epithelial cells in 3D collagen I cultures (Howlett et al., 1995; Lelievre et al., 1998), the primary luminal epithelial cells alone fail to show appropriate polarity in 3D collagen I. However, collagen-based co-cultures containing both luminal epithelial and myoepithelial cells show polarized, bilayered organization (Fig. 4). Normal myoepithelial cells direct luminal epithelial cell polarity by synthesizing laminin 1; tumor-derived myoepithelial cells, expressing no or low levels of laminin 1, fail to yield double-layered organotypic structures in 3D collagen co-cultures (Gudjonsson et al., 2002a). Thus, the basal positioning of myoepithelial cells is not only well-suited for contractile events that occur during lactation (a known function of myoepithelial cells) but also provides important spatially restricted biochemical cues that drive cell polarity and normal function in the breast (see Bissell and Bilder, 2003).

Indeed, it is now conceivable that the human breast could be reasonably recapitulated in vitro by systematic pairing of different cell types in 3D culture. In a recent report, Hass and Kratz reported the results of co-culturing primary human mammary epithelial cells and adipocytes derived from the same patient (Huss and Kratz, 2001). In these cultures, differentiated epithelial structures are embedded in clusters of adipocytes in patterns reminiscent of the human breast in vivo. Whether these structures reflect the ability of adipocytes to contribute to a BM and whether there are other functions provided by the fat cells remain to be determined. Additional modeling work, perhaps incorporating stem cell populations as described above for skin or immortalized progenitor cells of the breast (Gudjonsson et al., 2002b), will be required if we

are to achieve the full complement of mammary gland components in 3D culture.

Stromal-epithelial interactions in 3D in vivo

Mouse xenograft models

The question of stromal control of organ function has been effectively addressed in whole animal studies in which human epithelial cells are transplanted as 3D xenografts along with normal or aberrant stroma and monitored over time. Overall, the findings parallel observations made in 3D organotypic cultures and indicate that progression of the epithelial cell tumor is not cell autonomous. Rather, the chromosomal instability that eventually leads to cancer is promoted, and probably sometimes induced, by the anomalies in the surrounding stroma and microenvironment (Moinfar et al., 2000; reviewed in Petersen et al., 2001).

One compelling demonstration of the stromal control of epithelial behavior comes from Olumi and colleagues, who developed a model in which non-malignant prostatic epithelial cells (normal or SV40-immortalized) were mixed in collagen gels with prostate-derived fibroblasts from normal epithelial organoids or cultures of carcinoma-associated cells. These 3D cultures were then transplanted beneath the renal capsule of athymic mice, and epithelial outgrowth was monitored (Olumi et al., 1999). Neither epithelial cells nor fibroblasts, alone, promoted tumor formation on their own. However, xenografts that included carcinoma-associated fibroblasts (CAFs) along with SV-40-immortalized epithelial cells shows a dramatic tumorigenic response. These findings demonstrate in an in vivo setting that the altered signaling capacity of the CAFs is sufficient to catalyze tumor progression in a cell type that displays a mildly altered genotype.

Parmar et al. have recently used a similar renal grafting approach to address the role of mammary stromal fibroblasts in mammary gland function and development (Parmar et al., 2002). They mixed normal human mammary epithelial cells, prepared as organoids, with mammary fibroblasts and grafted them into renal capsules of nude mice. These transplants show a robust elaboration of a mammary structure, which does not occur in the absence of mammary stroma and appears to be responsive to hormonal stimulation from estrogen and progesterone (e.g., they can be induced to produce milk when analyzed in pregnant animals) (Parmar et al., 2002).

Human xenograft and tissue transplant models are thus powerful tools for analyzing the complexities of organ function, especially when results can be reciprocally tested and scrutinized in simpler 3D culture models. However, opinions differ with respect to the optimum site of tissue transplantation within the animal and its preparation. Does the outgrowth of human mammary epithelium in the kidney, for example, truly represent normal mammary events or does the mouse fat pad provide a more relevant environment for outgrowth? Indeed, it has long been known that mouse mammary epithelial cells display differential developmental responses depending upon their site of delivery (see Miller et al., 1981; Neville et al., 1998). A recent study revealed that human mammary epithelial cells harboring three cancer-predisposing genetic alterations have differential tumorigenic responses in nude mice, the most extreme response being associated with transplantation into cleared mammary fat pad (Elenbaas et al., 2001). Considering the range of responses from both 'normal' and tumorigenic cells within a given animal, perhaps we should also ask whether the rodent fat pad is of sufficient relevance to reconstitute a human cell behavior that is true to the human form or whether we should be striving to humanized mouse mammary models?

Developing a 'humanized' mammary gland in the mouse fat pad

In very general terms, the mouse and human mammary glands share a reasonable level of similarity but also some differences (Fig. 1) (Ronnov-Jessen et al., 1996). Because the mouse mammary gland has high levels of adipose stroma, it is reasonable to suggest that the environment of the mouse mammary fat pad in mice is not entirely equivalent to human breast (Neville et al., 1998). Cleared fat pads, commonly used in transplant studies, also include several other cell types, such as fibroblasts, endothelial cells and cells of the immune system, all of which could influence mammogenesis. Moreover, techniques routinely used to prepare orthotopic sites, such as irradiation, may in fact induce profound and lasting stromal effects by themselves (Barcellos-Hoff and Ravani, 2000; Barcellos-Hoff, 2001). Furthermore, human mammary epithelial cells injected into cleared fat pads do not elaborate ductal structures (Sheffield, 1988), which emphasizes the apparent incompatibility between human and mouse mammary organs.

To study breast homeostasis with ultimate physiological relevance, we must model not just tissues but entire organs in vivo (Bissell and Hall, 1987; Bissell and Radisky, 2001). One future goal would be to develop 'humanized' mammary glands in rodents by replacing mouse mammary gland components with their human counterparts and reconstructing an organ that is comparable to the human gland in its architecture and organization (Fig. 1). As daunting as this task seems, progress is currently being made to craft such a 'humanized' mammary gland model in mouse. Human stromal fibroblasts grafted into the fat pads of nude mice support elaboration of transplanted human mammary epithelial cells into an infiltrating ductal tree that is highly differentiated and responsive to lactogenic cues (C. Kuperwasser and R. A. Weinberg, personal communication). Establishment of such a 'humanized' animal paves the way for the systematic inclusion of genetically modified epithelial or stromal cells and thereby provides a model for controlled analysis of specific molecules and pathways in an in vivo context. Furthermore, the 'humanized' mouse could also be important in the development of strategies for reconstructing human breast after surgical intervention (Huss and Kratz, 2001).

Future versions of 'humanized' mice could incorporate human mammary progenitor cells in this type of transplant model. The existence of mammary epithelial stem cells has been the subject of much debate, but recent evidence demonstrates the existence of precursor cells within the luminal epithelial pool (Smith, 1996; Stingl et al., 1998; Smalley et al., 1999). Recently, Gudjonnson et al. have isolated and immortalized a human mammary progenitor cell that gives rise to structures that resemble terminal ductal lobular units (TDLU) when implanted either in Matrigel or orthotopically into nude mice (Gudjonsson et al., 2002b). Thus it seems

plausible that introduction of human progenitor cells in the mouse mammary gland may be a useful strategy for generating chimeric animals with extensively humanized mammary organs.

Concluding remarks

We have described a series of experimental models that range in complexity from monotypic 3D cultures to multicellular 'humanized' organs in vivo. Because of the physiologically relevant structural and functional features they display, each model is a powerful tool in and of itself. However, when these models are linked together in progressive fashion, their potential for defining the molecular determinants of normal organ function and for elucidating pathways compromised during disease progression is amplified. Already, by using a combination of 3D culture and animal xenograft strategies, researchers have demonstrated a role for the stroma as an important regulator of epithelial function and carcinoma progression. Streamlining our approaches to utilize the same cell type at each incremental step will clarify the underlying molecular details of these phenomena. Moreover, effective utilization of a hierarchy of 3D models has an enormous potential for improving disease target identification and drug design. If the behavior of candidate regulators can be verified in models of increasing physiological relevance, this would provide a more convincing rationale for the design of clinical trials in human subjects. Moreover, implementation of high-throughput screening in the context of simpler 3D organotypic cultures will probably waste less time during drug development and have the potential to yield molecules that will sustain efficacy in clinical trials (Balis, 2002; Bhadriraju and Chen, 2002; Weaver et al., 2002). The progress made thus far towards these goals is already reason for excitement.

The work from the authors' laboratory was supported by the United States Department of Energy, Office of Biological and Environmental Research (DE-AC03 SF0098 to M.J.B.). Additional funding was contributed by the Department of Defense Breast Cancer Research Program (#DAMD 17-01-1-0294 to K.L.S. and an Innovator Award to M.J.B.) and the National Cancer Institute (CA64786-02 to M.J.B., and CA57621 to Zena Werb and M.J.B.). The authors would like to thank Derek Radisky and Erica Werner for their editorial comments of the manuscript.

References

Angel, P. and Szabowski, A. (2002). Function of AP-1 target genes in mesenchymal-epithelial cross-talk in skin. *Biochem. Pharmacol.* **64**, 949-956.

Asselineau, D. and Prunieras, M. (1984). Reconstruction of 'simplified' skin: control of fabrication. *Br. J. Dermatol.* **111 Suppl. 27**, 219-222.

Asselineau, D., Bernhard, B., Bailly, C. and Darmon, M. (1985). Epidermal morphogenesis and induction of the 67 kD keratin polypeptide by culture of human keratinocytes at the liquid-air interface. *Exp. Cell Res.* **159**, 536-539.

Bader, A., Knop, E., Kern, A., Boker, K., Fruhauf, N., Crome, O., Esselmann, H., Pape, C., Kempka, G. and Sewing, K. F. (1996). 3-D coculture of hepatic sinusoidal cells with primary hepatocytes-design of an organotypical model. *Exp. Cell Res.* **226**, 223-233.

Bagutti, C., Hutter, C., Chiquet-Ehrismann, R., Fassler, R. and Watt, F. M. (2001). Dermal fibroblast-derived growth factors restore the ability of beta(1) integrin-deficient embryonal stem cells to differentiate into keratinocytes. *Dev. Biol.* **231**, 321-333.

Bagutti, C., Wobus, A. M., Fassler, R. and Watt, F. M. (1996). Differentiation of embryonal stem cells into keratinocytes: comparison of wild-type and beta 1 integrin-deficient cells. *Dev. Biol.* **179**, 184-196.

Balis, F. M. (2002). Evolution of anticancer drug discovery and the role of cell-based screening. *J. Natl. Cancer Inst.* **94**, 78-79.

Barcellos-Hoff, M. H. (2001). Three down and counting: the transformation of human mammary cells from normal to malignant in three steps. *Trends Mol. Med.* **7**, 142-143.

Barcellos-Hoff, M. H. and Ravani, S. A. (2000). Irradiated mammary gland stroma promotes the expression of tumorigenic potential by unirradiated epithelial cells. *Cancer Res.* **60**, 1254-1260.

Barcellos-Hoff, M. H., Aggeler, J., Ram, T. G. and Bissell, M. J. (1989). Functional differentiation and alveolar morphogenesis of primary mammary cultures on reconstituted basement membrane. *Development* **105**, 223-235.

Bell, E., Ehrlich, H. P., Buttle, D. J. and Nakatsuji, T. (1981). Living tissue formed in vitro and accepted as skin-equivalent tissue of full thickness. *Science* **211**, 1052-1054.

Bello-DeOcampo, D., Kleinman, H. K., Deocampo, N. D. and Webber, M. M. (2001). Laminin-1 and alpha6beta1 integrin regulate acinar morphogenesis of normal and malignant human prostate epithelial cells. *Prostate* **46**, 142-153.

Ben-Ze'ev, A., Robinson, G. S., Bucher, N. L. and Farmer, S. R. (1988). Cell-cell and cell-matrix interactions differentially regulate the expression of hepatic and cytoskeletal genes in primary cultures of rat hepatocytes. *Proc. Natl. Acad. Sci. USA* **85**, 2161-2165.

Bhadriraju, K. and Chen, C. S. (2002). Engineering cellular microenvironments to improve cell-based drug testing. *Drug Discov. Today* **7**, 612-620.

Bissell, D. M., Arenson, D. M., Maher, J. J. and Roll, F. J. (1987). Support of cultured hepatocytes by a laminin-rich gel. Evidence for a functionally significant subendothelial matrix in normal rat liver. *J. Clin. Invest.* **79**, 801-812.

Bissell, M. J. (1981). The differentiated state of normal and malignant cells or how to define a "normal" cell in culture. *Int. Rev. Cytol.* **70**, 27-100.

Bissell, M. and Bilder, D. (2003). Polarity determination in breast tissue: desmosomal adhesion, myoepithelial cells, and laminin. *Breast Cancer J.* **2**, 117-119.

Bissell, M. J. and Hall, H. G. (1987). Form and function in the mammary gland: the role of extracellular matrix. In *The Mammary Gland* (eds M. C. Neville and C. W. Daniel), pp. 97-146. New York: Plenum Press.

Bissell, M. J. and Radisky, D. (2001). Putting tumours in context. *Nat. Rev. Cancer* **1**, 46-54.

Bissell, M. J., Radisky, D. C., Rizki, A., Weaver, V. M. and Petersen, O. W. (2002). The organizing principle: microenvironmental influences in the normal and malignant breast. *Differentiation* **70**, 537-546.

Blatchford, D. R., Quarrie, L. H., Tonner, E., McCarthy, C., Flint, D. J. and Wilde, C. J. (1999). Influence of microenvironment on mammary epithelial cell survival in primary culture. *J. Cell Physiol.* **181**, 304-311.

Boudreau, N. and Bissell, M. J. (1998). Extracellular matrix signaling: integration of form and function in normal and malignant cells. *Curr. Opin. Cell Biol.* **10**, 640-646.

Boudreau, N., Sympson, C. J., Werb, Z. and Bissell, M. J. (1995). Suppression of ICE and apoptosis in mammary epithelial cells by extracellular matrix. *Science* **267**, 891-893.

Boyce, S. T. and Warden, G. D. (2002). Principles and practices for treatment of cutaneous wounds with cultured skin substitutes. *Am. J. Surg.* **183**, 445-456.

Briand, P., Nielsen, K. V., Madsen, M. W. and Petersen, O. W. (1996). Trisomy 7p and malignant transformation of human breast epithelial cells following epidermal growth factor withdrawal. *Cancer Res.* **56**, 2039-2044.

Briand, P., Petersen, O. W. and van Deurs, B. (1987). A new diploid nontumorigenic human breast epithelial cell line isolated and propagated in chemically defined medium. *In Vitro Cell Dev. Biol.* **23**, 181-188.

Chen, H. M., Schmeichel, K. L., Mian, I. S., Lelievre, S., Petersen, O. W. and Bissell, M. J. (2000). AZU-1: a candidate breast tumor suppressor and biomarker for tumor progression. *Mol. Biol. Cell* **11**, 1357-1367.

Choi, Y. and Fuchs, E. (1990). TGF-beta and retinoic acid: regulators of growth and modifiers of differentiation in human epidermal cells. *Cell Regul.* **1**, 791-809.

Clejan, S., O'Connor, K. and Rosensweig, N. (2001). Tri-dimensional prostate cell cultures in simulated microgravity and induced changes in lipid second messengers and signal transduction. *J. Cell Mol. Med.* **5**, 60-73.

Coucouvanis, E. and Martin, G. R. (1995). Signals for death and survival: a two-step mechanism for cavitation in the vertebrate embryo. *Cell* **83**, 279-287.

Coulomb, B., Lebreton, C. and Dubertret, L. (1989). Influence of human dermal fibroblasts on epidermalization. *J. Invest. Dermatol.* **92**, 122-125.

Cukierman, E., Pankov, R., Stevens, D. R. and Yamada, K. M. (2001). Taking cell-matrix adhesions to the third dimension. *Science* **294**, 1708-1712.

Cukierman, E., Pankov, R. and Yamada, K. (2002). Cell interactions with three-dimensional matrices. *Curr. Opin. Cell Biol.* **14**, 633-639.

Cunha, G. R. (1994). Role of mesenchymal-epithelial interactions in normal and abnormal development of the mammary gland and prostate. *Cancer* **74**, 1030-1044.

Cunha, G. R., Hayward, S. W. and Wang, Y. Z. (2002). Role of stroma in carcinogenesis of the prostate. *Differentiation* **70**, 473-485.

Debnath, J., Mills, K., Collins, N., Reginato, M., Muthuswamy, S. and Brugge, J. (2002). The role of apoptosis in creating and maintaining luminal space within normal and oncogene-expressing mammary acini. *Cell* **111**, 29-40.

Eccles, S. A. (2001). The role of c-erbB-2/HER2/neu in breast cancer progression and metastasis. *J. Mammary Gland Biol. Neoplasia* **6**, 393-406.

Elenbaas, B., Spirio, L., Koerner, F., Fleming, M. D., Zimonjic, D. B., Donaher, J. L., Popescu, N. C., Hahn, W. C. and Weinberg, R. A. (2001). Human breast cancer cells generated by oncogenic transformation of primary mammary epithelial cells. *Genes Dev.* **15**, 50-65.

Elsdale, T. and Bard, J. (1972). Collagen substrata for studies on cell behavior. *J. Cell Biol.* **54**, 626-637.

Emerman, J. T. and Pitelka, D. R. (1977). Maintenance and induction of morphological differentiation in dissociated mammary epithelium on floating collagen membranes. *In Vitro* **13**, 316-328.

Emerman, J. T., Enami, J., Pitelka, D. R. and Nandi, S. (1977). Hormonal effects on intracellular and secreted casein in cultures of mouse mammary epithelial cells on floating collagen membranes. *Proc. Natl. Acad. Sci. USA* **74**, 4466-4470.

Fartasch, M. and Ponec, M. (1994). Improved barrier structure formation in air-exposed human keratinocyte culture systems. *J. Invest. Dermatol.* **102**, 366-374.

Frisch, S. M. and Francis, H. (1994). Disruption of epithelial cell-matrix interactions induces apoptosis. *J. Cell Biol.* **124**, 619-626.

Fuchs, E. and Raghavan, S. (2002). Getting under the skin of epidermal morphogenesis. *Nat. Rev. Genet.* **3**, 199-209.

Fusenig, N. E. (1994). Epithelial-mesenchymal interactions regulate keratinocyte growth and differentiation in vitro. In *The Keratinocyte Handbook* (eds I. Leigh B. Lane and F. Watt), pp. 71-94. Cambridge: Cambridge University Press.

Fusenig, N. E. and Boukamp, P. (1998). Multiple stages and genetic alterations in immortalization, malignant transformation, and tumor progression of human skin keratinocytes. *Mol. Carcinog.* **23**, 144-158.

Gay, R., Swiderek, M., Nelson, D. and Ernesti, A. (1992). The living skin equivalent as a model in vitro for ranking the toxic potential of dermal irritants. *Toxic In Vitro* **6**.

Gittes, G. K., Galante, P. E., Hanahan, D., Rutter, W. J. and Debase, H. T. (1996). Lineage-specific morphogenesis in the developing pancreas: role of mesenchymal factors. *Development* **122**, 439-447.

Grant, D. S., Tashiro, K., Segui-Real, B., Yamada, Y., Martin, G. R. and Kleinman, H. K. (1989). Two different laminin domains mediate the differentiation of human endothelial cells into capillary-like structures in vitro. *Cell* **58**, 933-943.

Gudjonsson, T., Ronnov-Jessen, L., Villadsen, R., Rank, F., Bissell, M. J. and Petersen, O. W. (2002a). Normal and tumor-derived myoepithelial cells differ in their ability to interact with luminal breast epithelial cells for polarity and basement membrane deposition. *J. Cell Sci.* **115**, 39-50.

Gudjonsson, T., Villadsen, R., Nielsen, H. L., Ronnov-Jessen, L., Bissell, M. J. and Petersen, O. W. (2002b). Isolation, immortalization, and characterization of a human breast epithelial cell line with stem cell properties. *Genes Dev.* **16**, 693-706.

Hall, H. G., Farson, D. A. and Bissell, M. J. (1982). Lumen formation by epithelial cell lines in response to collagen overlay: a morphogenetic model in culture. *Proc. Natl. Acad. Sci. USA* **79**, 4672-4676.

Harkin, D. G. and Hay, E. D. (1996). Effects of electroporation on the tubulin cytoskeleton and directed migration of corneal fibroblasts cultured within collagen matrices. *Cell Motil. Cytoskeleton* **35**, 345-357.

Hay, E. D. and Dodson, J. W. (1973). Secretion of collagen by corneal epithelium. I. Morphology of the collagenous products produced by isolated epithelia grown on frozen-killed lens. *J. Cell Biol.* **57**, 190-213.

Hertle, M. D., Adams, J. C. and Watt, F. M. (1991). Integrin expression during human epidermal development in vivo and in vitro. *Development* **112**, 193-206.

Hoffman, M. P., Kibbey, M. C., Letterio, J. J. and Kleinman, H. K. (1996). Role of laminin-1 and TGF-beta 3 in acinar differentiation of a human submandibular gland cell line (HSG). *J. Cell Sci.* **109**, 2013-2021.

Howlett, A. R., Bailey, N., Damsky, C., Petersen, O. W. and Bissell, M. J. (1995). Cellular growth and survival are mediated by beta 1 integrins in normal human breast epithelium but not in breast carcinoma. *J. Cell Sci.* **108**, 1945-1957.

Howlett, A. R., Petersen, O. W., Steeg, P. S. and Bissell, M. J. (1994). A novel function for the nm23-H1 gene: overexpression in human breast carcinoma cells leads to the formation of basement membrane and growth arrest. *J. Natl. Cancer Inst.* **86**, 1838-1844.

Huang, J., Hardy, J. D., Sun, Y. and Shively, J. E. (1999). Essential role of biliary glycoprotein (CD66a) in morphogenesis of the human mammary epithelial cell line MCF10F. *J. Cell Sci.* **112**, 4193-4205.

Huss, F. R. and Kratz, G. (2001). Mammary epithelial cell and adipocyte co-culture in a 3-D matrix: the first step towards tissue-engineered human breast tissue. *Cells Tissues Organs* **169**, 361-367.

Ingber, D. E. (2002). Cancer as a disease of epithelial-mesenchymal interactions and extracellular matrix regulation. *Differentiation* **70**, 547-560.

Ingber, D. E. and Folkman, J. (1989). How does extracellular matrix control capillary morphogenesis? *Cell* **58**, 803-805.

Ingber, D. E., Madri, J. A. and Jamieson, J. D. (1986). Basement membrane as a spatial organizer of polarized epithelia. Exogenous basement membrane reorients pancreatic epithelial tumor cells in vitro. *Am. J. Pathol.* **122**, 129-139.

Jacks, T. and Weinberg, R. A. (2002). Taking the study of cancer cell survival to a new dimension. *Cell* **111**, 923-925.

Kaur, P. and Carter, W. G. (1992). Integrin expression and differentiation in transformed human epidermal cells is regulated by fibroblasts. *J. Cell Sci.* **103**, 755-763.

Kirshner, J., Chen, C. J., Liu, P., Huang, J. and Shively, J. E. (2003). CEACAM1-4S, a cell-cell adhesion molecule, mediates apoptosis and reverts mammary carcinoma cells to a normal morphogenic phenotype in a 3D culture. *Proc. Natl. Acad. Sci. USA* **100**, 521-526.

Kleinman, H. K., McGarvey, M. L., Hassel, J. R., Star, V. L., Cannon, F. B., Laurie, G. W. and Martin, G. R. (1986). Basement membrane complexes with biological activity. *Biochemistry* **25**, 312-318.

Kopan, R. and Fuchs, E. (1989). A new look into an old problem: keratins as tools to investigate determination, morphogenesis, and differentiation in skin. *Genes Dev.* **3**, 1-15.

Kopan, R., Traska, G. and Fuchs, E. (1987). Retinoids as important regulators of terminal differentiation: examining keratin expression in individual epidermal cells at various stages of keratinization. *J. Cell Biol.* **105**, 427-440.

Kubota, Y., Kleinman, H. K., Martin, G. R. and Lawley, T. J. (1988). Role of laminin and basement membrane in the morphological differentiation of human endothelial cells into capillary-like structures. *J. Cell Biol.* **107**, 1589-1598.

Lelievre, S. A., Bissell, M. J. and Pujuguet, P. (2000). Cell nucleus in context. *Crit. Rev. Eukaryot. Gene Expr.* **10**, 13-20.

Lelievre, S. A., Weaver, V. M., Nickerson, J. A., Larabell, C. A., Bhaumik, A., Petersen, O. W. and Bissell, M. J. (1998). Tissue phenotype depends on reciprocal interactions between the extracellular matrix and the structural organization of the nucleus. *Proc. Natl. Acad. Sci. USA* **95**, 14711-14716.

Leone, A., Flatow, U., VanHoutte, K. and Steeg, P. S. (1993). Transfection of human nm23-H1 into the human MDA-MB-435 breast carcinoma cell line: effects on tumor metastatic potential, colonization and enzymatic activity. *Oncogene* **8**, 2325-2333.

Li, M. L., Aggeler, J., Farson, D. A., Hatier, C., Hassell, J. and Bissell, M. J. (1987). Influence of a reconstituted basement membrane and its components on casein gene expression and secretion in mouse mammary epithelial cells. *Proc. Natl. Acad. Sci. USA* **84**, 136-140.

Lin, C. Q. and Bissell, M. J. (1993). Multi-faceted regulation of cell differentiation by extracellular matrix. *FASEB J.* **7**, 737-743.

Liotta, L. A. and Kohn, E. C. (2001). The microenvironment of the tumour-host interface. *Nature* **411**, 375-379.

Maas-Szabowski, N., Stark, H. J. and Fusenig, N. E. (2000). Keratinocyte growth regulation in defined organotypic cultures through IL-1-induced keratinocyte growth factor expression in resting fibroblasts. *J. Invest. Dermatol.* **114**, 1075-1084.

Maas-Szabowski, N., Szabowski, A., Stark, H. J., Andrecht, S., Kolbus, A., Schorpp-Kistner, M., Angel, P. and Fusenig, N. E. (2001). Organotypic

cocultures with genetically modified mouse fibroblasts as a tool to dissect molecular mechanisms regulating keratinocyte growth and differentiation. *J. Invest. Dermatol.* **116**, 816-820.

Man, Y. G., Shekitka, K. M, Bratthauer, G. L. and Tavassoli, F A. (2002). Immunohistochemical and genetic alterations in mammary epithelial cells immediately overlying focally disrupted myoepithelial cell layers. *Breast Cancer Research Treatment* **76 (Supplement 1)**, S143.

Mauchamp, J., Mirrione, A., Alquier, C. and Andre, F. (1998). Follicle-like structure and polarized monolayer: role of the extracellular matrix on thyroid cell organization in primary culture. *Biol. Cell* **90**, 369-380.

McCance, D. J., Kopan, R., Fuchs, E. and Laimins, L. A. (1988). Human papillomavirus type 16 alters human epithelial cell differentiation in vitro. *Proc. Natl. Acad. Sci. USA* **85**, 7169-7173.

Michalopoulos, G. and Pitot, H. C. (1975). Primary culture of parenchymal liver cells on collagen membranes. Morphological and biochemical observations. *Exp. Cell Res.* **94**, 70-78.

Miller, F. R., Medina, D. and Heppner, G. H. (1981). Preferential growth of mammary tumors in intact mammary fatpads. *Cancer Res.* **41**, 3863-3867.

Moinfar, F., Man, Y. G., Arnould, L., Bratthauer, G. L., Ratschek, M. and Tavassoli, F. A. (2000). Concurrent and independent genetic alterations in the stromal and epithelial cells of mammary carcinoma: implications for tumorigenesis. *Cancer Res.* **60**, 2562-2566.

Mueller, M. M. and Fusenig, N. E. (2002). Tumor-stroma interactions directing phenotype and progression of epithelial skin tumor cells. *Differentiation* **70**, 486-497.

Muschler, J., Levy, D., Boudreau, R., Henry, M., Campbell, K. and Bissell, M. J. (2002). A Role for dystroglycan in epithelial polarization: loss of function in breast tumor cells. *Cancer Res.* **62**, 7102-7109.

Muthuswamy, S. K., Li, D., Lelievre, S., Bissell, M. J. and Brugge, J. S. (2001). ErbB2, but not ErbB1, reinitiates proliferation and induces luminal repopulation in epithelial acini. *Nat. Cell Biol.* **3**, 785-792.

Neville, M. C., Medina, D., Monks, J. and Hovey, R. C. (1998). The mammary fat pad. *J. Mammary Gland Biol. Neoplasia* **3**, 109-116.

Nickerson, J. (2001). Experimental observations of a nuclear matrix. *J. Cell Sci.* **114**, 463-474.

Nielsen, K. V., Madsen, M. W. and Briand, P. (1994). In vitro karyotype evolution and cytogenetic instability in the non-tumorigenic human breast epithelial cell line HMT-3522. *Cancer Genet. Cytogenet.* **78**, 189-199.

O'Brien, L. E., Jou, T. S., Pollack, A. L., Zhang, Q., Hansen, S. H., Yurchenco, P. and Mostov, K. E. (2001). Rac1 orientates epithelial apical polarity through effects on basolateral laminin assembly. *Nat. Cell Biol.* **3**, 831-838.

O'Brien, L. E., Zegers, M. M. and Mostov, K. E. (2002). Opinion: Building epithelial architecture: insights from three-dimensional culture models. *Nat. Rev. Mol. Cell Biol.* **3**, 531-537.

Oliver, C., Waters, J. F., Tolbert, C. L. and Kleinman, H. K. (1987). Growth of exocrine acinar cells on a reconstituted basement membrane gel. *In Vitro Cell Dev. Biol.* **23**, 465-473.

Olumi, A. F., Grossfeld, G. D., Hayward, S. W., Carroll, P. R., Tlsty, T. D. and Cunha, G. R. (1999). Carcinoma-associated fibroblasts direct tumor progression of initiated human prostatic epithelium. *Cancer Res.* **59**, 5002-5011.

Parenteau, N., Nolte, C., Bilbo, P., Rosenberg, M., Wilkins, L., Johnson, E., Watson, S., Mason, V. and Bell, E. (1991). Epidermis generated in vitro: practical considerations and applications. *J Cell Biochem.* **45**, 245-251.

Parmar, H., Young, P., Emerman, J. T., Neve, R. M., Dairkee, S. and Cunha, G. R. (2002). A novel method for growing human breast epithelium in vivo using mouse and human mammary fibroblasts. *Endocrinology* **143**, 4886-4896.

Petersen, O. W., Ronnov-Jessen, L., Howlett, A. R. and Bissell, M. J. (1992). Interaction with basement membrane serves to rapidly distinguish growth and differentiation pattern of normal and malignant human breast epithelial cells. *Proc. Natl. Acad. Sci. USA* **89**, 9064-9068.

Petersen, O. W., Lind Nielsen, H., Gudjonsson, T., Villadsen, R., Ronnov-Jessen, L. and Bissell, M. J. (2001). The plasticity of human breast carcinoma cells is more than epithelial to mesenchymal conversion. *Breast Cancer Res.* **3**, 213-217.

Radisky, D., Muschler, J. and Bissell, M. J. (2002). Order and disorder: the role of extracellular matrix in epithelial cancer. *Cancer Invest.* **20**, 139-153.

Regnier, M., Prunieras, M. and Woodley, D. (1981). Growth and differentiation of adult human epidermal cells on dermal substrates. *Frontiers Matrix Biol.* **9**, 4-35.

Ronnov-Jessen, L., Petersen, O. W. and Bissell, M. J. (1996). Cellular changes involved in conversion of normal to malignant breast: importance of the stromal reaction. *Physiol. Rev.* **76**, 69-125.

Roskelley, C. D., Desprez, P. Y. and Bissell, M. J. (1994). Extracellular matrix-dependent tissue-specific gene expression in mammary epithelial cells requires both physical and biochemical signal transduction. *Proc. Natl. Acad. Sci. USA* **91**, 12378-12382.

Roskelley, C. D., Srebrow, A. and Bissell, M. J. (1995). A hierarchy of ECM-mediated signalling regulates tissue-specific gene expression. *Curr. Opin. Cell Biol.* **7**, 736-747.

Runswick, S. K., O'Hare, M. J., Jones, L., Streuli, C. H. and Garrod, D. R. (2001). Desmosomal adhesion regulates epithelial morphogenesis and cell positioning. *Nat. Cell Biol.* **3**, 823-830.

Sakamoto, T., Hirano, K., Morishima, Y., Masuyama, K., Ishii, Y., Nomura, A., Uchida, Y., Ohtsuka, M. and Sekizawa, K. (2001). Maintenance of the differentiated type II cell characteristics by culture on an acellular human amnion membrane. *In Vitro Cell Dev. Biol. Anim.* **37**, 471-479.

Sakurai, H., Barros, E. J., Tsukamoto, T., Barasch, J. and Nigam, S. K. (1997). An in vitro tubulogenesis system using cell lines derived from the embryonic kidney shows dependence on multiple soluble growth factors. *Proc. Natl. Acad. Sci. USA* **94**, 6279-6284.

Sanderson, I. R., Ezzell, R. M., Kedinger, M., Erlanger, M., Xu, Z. X., Pringault, E., Leon-Robine, S., Louvard, D. and Walker, W. A. (1996). Human fetal enterocytes in vitro: modulation of the phenotype by extracellular matrix. *Proc. Natl. Acad. Sci. USA* **93**, 7717-7722.

Schmeichel, K. L., Weaver, V. M. and Bissell, M. J. (1998). Structural cues from the tissue microenvironment are essential determinants of the human mammary epithelial cell phenotype. *J. Mammary Gland Biol. Neoplasia* **3**, 201-213.

Schuger, L., O'Shea, K. S., Nelson, B. B. and Varani, J. (1990). Organotypic arrangement of mouse embryonic lung cells on a basement membrane extract: involvement of laminin. *Development* **110**, 1091-1099.

Sheffield, L. G. (1988). Organization and growth of mammary epithelia in the mammary gland fat pad. *J. Dairy Sci.* **71**, 2855-2874.

Silberstein, G. B. (2001). Tumour-stromal interactions. Role of the stroma in mammary development. *Breast Cancer Res.* **3**, 218-223.

Smalley, M. J., Titley, J., Paterson, H., Perusinghe, N., Clarke, C. and O'Hare, M. J. (1999). Differentiation of separated mouse mammary luminal epithelial and myoepithelial cells cultured on EHS matrix analyzed by indirect immunofluorescence of cytoskeletal antigens. *J. Histochem. Cytochem.* **47**, 1513-1524.

Smith, G. H. (1996). Experimental mammary epithelial morphogenesis in an in vivo model: evidence for distinct cellular progenitors of the ductal and lobular phenotype. *Breast Cancer Res. Treat.* **39**, 21-31.

Smola, H., Stark, H. J., Thiekotter, G., Mirancea, N., Krieg, T. and Fusenig, N. E. (1998). Dynamics of basement membrane formation by keratinocyte-fibroblast interactions in organotypic skin culture. *Exp. Cell Res.* **239**, 399-410.

Spancake, K. M., Anderson, C. B., Weaver, V. M., Matsunami, N., Bissell, M. J. and White, R. L. (1999). E7-transduced human breast epithelial cells show partial differentiation in three-dimensional culture. *Cancer Res.* **59**, 6042-6045.

Sternlicht, M. D., Kedeshian, P., Shao, Z. M., Safarians, S. and Barsky, S. H. (1997). The human myoepithelial cell is a natural tumor suppressor. *Clin. Cancer Res.* **3**, 1949-1958.

Still, I. H., Hamilton, M., Vince, P., Wolfman, A. and Cowell, J. K. (1999). Cloning of TACC1, an embryonically expressed, potentially transforming coiled coil containing gene, from the 8p11 breast cancer amplicon. *Oncogene* **18**, 4032-4038.

Stingl, J., Eaves, C. J., Kuusk, U. and Emerman, J. T. (1998). Phenotypic and functional characterization in vitro of a multipotent epithelial cell present in the normal adult human breast. *Differentiation* **63**, 201-213.

Stoker, A. W., Streuli, C. H., Martins-Green, M. and Bissell, M. J. (1990). Designer microenvironments for the analysis of cell and tissue function. *Curr. Opin. Cell Biol.* **2**, 864-874.

Szabowski, A., Maas-Szabowski, N., Andrecht, S., Kolbus, A., Schorpp-Kistner, M., Fusenig, N. E. and Angel, P. (2000). c-Jun and JunB antagonistically control cytokine-regulated mesenchymal-epidermal interaction in skin. *Cell* **103**, 745-755.

Tlsty, T. D. and Hein, P. W. (2001). Know thy neighbor: stromal cells can contribute oncogenic signals. *Curr. Opin. Genet. Dev.* **11**, 54-59.

Troxell, M. L., Loftus, D. J., Nelson, W. J. and Marrs, J. A. (2001). Mutant cadherin affects epithelial morphogenesis and invasion, but not transformation. *J. Cell Sci.* **114**, 1237-1246.

EXHIBIT G

Vol. 9, 4227–4239, September 15, 2003

Clinical Predictive Value of the *in Vitro* Cell Line, Human Xenograft, and Mouse Allograft Preclinical Cancer Models[1]

Theodora Voskoglou-Nomikos,[2] Joseph L. Pater, and Lesley Seymour

National Cancer Institute of Canada Clinical Trials Group, Cancer Clinical Trials Division, Cancer Research Institute, Queen's University, Kingston, Ontario, K7L 3N6 Canada

ABSTRACT

Purpose: **We looked at the value of three preclinical cancer models, the *in vitro* human cell line, the human xenograft, and the murine allograft, to examine whether they are reliable in predicting clinical utility.**

Experimental Design: **Thirty-one cytotoxic cancer drugs were selected. Literature was searched for drug activity in Phase II trials, human xenograft, and mouse allografts in breast, non-small cell lung, ovary, and colon cancers. Data from the National Cancer Institute Human Tumor Cell Line Screen were used to calculate drug *in vitro* preclinical activity for each cancer type. Phase II activity *versus* preclinical activity scatter plot and correlation analysis was conducted for each model, by tumor type (disease-oriented approach), using one tumor type as a predictor of overall activity in the other three tumor types combined (compound-oriented approach) and for all four tumor types together.**

Results: **The *in vitro* cell line model was predictive for non-small cell lung cancer under the disease-oriented approach, for breast and ovarian cancers under the compound-oriented approach, and for all four tumor types together. The mouse allograft model was not predictive. The human xenograft model was not predictive for breast or colon cancers, but was predictive for non-small cell lung and ovarian cancers when panels of xenografts were used.**

Conclusions: **These results suggest that under the right framework and when panels are used, the *in vitro* cell line and human xenograft models may be useful in predicting the Phase II clinical trial performance of cancer drugs. Murine allograft models, as used in this analysis, appear of limited utility.**

INTRODUCTION

Both basic science studies and clinical trials are essential components of the cancer drug discovery process. Potential therapeutics found to be significantly better than no treatment or standard therapies (*i.e.*, active) in preclinical laboratory cancer models or compounds with novel chemotypes and equivalent effectiveness to standard treatments are advanced to confirmatory testing in early (Phase I and II) clinical trials. Considering that RR[3] is a reasonable surrogate end point for survival (required but not sufficient), a favorable RR in Phase II trials advances a drug into additional clinical testing and is considered a prerequisite of drug success in the clinic.

Advancing of a candidate drug from preclinical testing in the laboratory to testing in Phase II clinical trials is based on the assumption that drug activity in cancer models translates into at least some efficacy in human patients, *i.e.*, that cancer laboratory models are clinically predictive. In addition, the relevance of tumor type-specific preclinical results for the corresponding human cancers in the clinic can be viewed through two different approaches: compound-oriented, where a drug is assumed to have potential activity against all human tumor types if it is effective against a single test tumor type, and disease-oriented, where a drug with preclinical activity in a single tumor type would only be expected to be effective in the same tumor type in patients.

Although widely adopted, the above-mentioned assumption and approaches have not been confirmed by studies to date. In addition, all studies aimed to examine the clinical predictive value of laboratory cancer models inevitably suffer from inherent bias because compounds with no activity in preclinical models are generally not advanced to clinical trials.

This work was undertaken to examine the clinical predictive value of three preclinical cancer models that have found wide use: the human *in vitro* cell line; the mouse allograft; and the human xenograft. In these models, tumor volume or life span (*in vivo* mouse models) or cell growth (*in vitro* cell lines) is compared between the treatment group receiving the new drug and a control group (active or inactive control).

The use of preclinical cancer models for selection of potential cancer therapeutics was pioneered by the NCI in the United States in the mid-1950s. The screening strategies used until 1990 were essentially compound oriented and involved a

Received 3/26/03; revised 6/3/03; accepted 6/4/03.

The costs of publication of this article were defrayed in part by the payment of page charges. This article must therefore be hereby marked *advertisement* in accordance with 18 U.S.C. Section 1734 solely to indicate this fact.

[1] Supported in part by the National Cancer Institute of Canada, Clinical Trials Group. Presented in part at the 2002 Annual Meeting of the American Society of Clinical Oncology (Abstract 360).

[2] To whom requests for reprints should be addressed, at National Cancer Institute of Canada Clinical Trials Group, Cancer Clinical Trials Division, Cancer Research Institute, Queen's University, 10 Stuart Street, Kingston, Ontario, K7L 3N6 Canada. Phone: (613) 533-6430; Fax: (613) 533-2941; E-mail: dnomikos@ctg.queensu.ca.

[3] The abbreviations used are: RR, response rate; NCI, National Cancer Institute; NSCLC, non-small cell lung cancer; NSC, National Service Center; T/C%, treated over control tumor volume ratio.

small number of predominantly murine allograft tumors, with emphasis on leukemia (1–7). Several studies from the NCI and others demonstrated that this approach had low clinical predictive value for activity in Phase II trials (5–9) and yielded compounds with selective activity toward human leukemias and lymphomas (10–12). Thus, in 1990, the NCI introduced a disease-oriented *in vitro* Human Tumor Cell Line Screen comprised of 60 cell lines from the most common adult tumors (13–17). The screen was designed so that each tumor type was represented by a panel of cell lines, selected on the basis of different subhistological features, and common drug resistance profiles. It was hoped that this screen would help identify drug leads with high potency and/or selective activity against particular tumor types.

Recently, the NCI examined the correlation between drug activity in Phase II clinical trials and preclinical activity in cancer models (18). Important findings were: (*a*) with the exception of NSCLC, preclinical activity in human xenografts of a particular tumor type did not correlate significantly with Phase II activity in the same type of tumor, (*b*) with the exception of breast and colon histologies, human xenografts did not significantly predict Phase II clinical activity in other cancers types; and (*c*) compounds that were active in at least one-third of all tested human xenografts were likely to have at least some activity in Phase II clinical trials.

Studies examining the clinical predictive value of preclinical cancer models outside the scope of the NCI screening programs have focused on the human xenograft model and have looked predominately into same-tumor correlations (disease-oriented approach). These studies have produced both positive (the model was found clinically predictive) and negative (the model was found to have no clinical predictive value) results in various tumor types (19–27).

Two major criticisms can be made on the overall body of literature concerning the clinical predictive value of preclinical cancer models. First, the vast majority of studies to date, both within and outside the NCI, have based their conclusions on the observation of trends rather than the use of statistical methods. Second, all studies conducted previously have used dichotomous definitions of preclinical and/or clinical activity based on largely invalidated cutoff values of measures of activity: a 20% RR in Phase II clinical trials and (most commonly) a 42% T/C% in human xenografts and mouse allografts.

In addition, two important questions have not been addressed at all by previous studies: the clinical predictive value of the *in vitro* cell line model and the relative clinical usefulness of the different preclinical cancer models in use today (*i.e.*, how different models compare with each other in terms of their ability to identify clinically effective drugs).

Thus, we conducted a study comparing the clinical (Phase II) predictive value of three widely used preclinical laboratory cancer models, the *in vitro* human cell line, the mouse allograft, and the human xenograft. We used quantitative measures of both clinical and preclinical activity and statistical methods. We considered three relevant questions: (*a*) the clinical predictive value of the three models within the same tumor type (disease-oriented approach); (*b*) the clinical predictive value of the three models when one preclinical tumor type is used as a predictor of overall clinical activity in all other tumor types (compound-oriented approach); and (*c*) the clinical predictive value of the three models when overall preclinical and clinical activity in all tumor types combined is considered.

MATERIALS AND METHODS

Study Design

A retrospective, literature-based study was conducted. Data were retrieved from studies published between 1985 and 2000. This period was chosen as one when all three preclinical cancer models of interest to this study were in use and because it was long enough and close enough to the present as to afford data on a relatively large number of recently developed drugs.

The data search was restricted to four of the most common and commonly studied solid tumor types, breast, colorectal, ovarian, and non-small cell lung cancers, to ensure that sufficient data would be available.

The Medline and CancerLit databases were used for the collection of published data. In an attempt to minimize publication bias, both paper publications (peer reviewed) and meeting abstracts (nonpeer reviewed) were used as sources of information. If published data were not available for identified drugs, manufacturers were contacted for unpublished data.

Selection of Drugs

Drugs were identified by searching the Medline and CancerLit databases for compounds that had undergone single agent Phase I clinical trial testing either in 1991 or 1992. Agents with novel targets such as signal transduction or angiogenesis modulators were not included.

This Phase I-based approach to agent identification was used to ensure selection of agents developed within the study time frame of 1985–2000: agents with a published Phase I clinical trial in 1991 or 1992 were expected to have been through preclinical testing between 1985 and 1990 and to have undergone Phase II clinical evaluation by the year 2000. In addition, this approach was adopted to minimize publication bias: publication of Phase I trials is generally less dependent on the observation of favorable tumor responses than publication of Phase II trials or of preclinical cancer model experiments.

Data Collection and Drug Activity

Phase II Clinical Trials. Phase II clinical trials for each drug were identified by searching the Medline and CancerLit databases for scientific papers, reviews, or meeting abstracts. Duplicate publications were discarded. For trials with only abstract information, an additional search by author and/or institution name was conducted in Medline or CancerLit. Scientific papers were used in preference to abstracts, where possible.

Two restrictions were applied. The first was a geographic restriction: to ensure uniform methodology in trial conduct and RR assessment, only Phase II trials conducted in the Americas, Western Europe and Australia were included in the analysis. The second restriction referred to the treatment population and aimed to ensure that uniformly responsive populations of patients would be considered. For breast and ovarian cancer, only Phase II trials that included patients who had received prior chemotherapy for metastatic disease were used, whereas for

NSCLC and colon cancers, the Phase II trials selected included patients who had received no prior chemotherapy.

For each individual Phase II trial the following information was collected: disease site; previous chemotherapy; disease stage; number of patients entered; eligible; evaluable and evaluable for response; number of complete and partial responses; and criteria used for response (standard WHO *versus* other). Trials had to have enrolled a minimum of 14 patients, at least 12 of whom must have been evaluable for response. Completed Phase II trials for which >20% of entered patients were listed as inevaluable for response were considered methodologically unacceptable and were not used. For trials in progress at the time of reporting (meeting abstract format only), the available data were used even if they represented <80% of the enrolled patients, provided that they met the 14-patient criterion. If a trial publication did not specify the previous chemotherapy treatment status of patients, it was not used. Information from Phase I-II trials was used only when the Phase I and II components of the trial were separately conducted and reported. Phase II information was collected regardless of drug dose and route of administration.

For a given drug, in a given cancer type, the activity in a single Phase II clinical trial was recorded as the RR: the number of partial and complete tumor responses over the total number of patients evaluable for response. The number of evaluable rather than eligible patients was used to accommodate information from trials for which final results were not available. In the very few cases where the number of patients evaluable for response was not provided, the number of evaluable patients, the number of eligible patients, or the number of patients entered in the trial (whichever was provided by the investigators) in that priority order was used.

To obtain a drug's overall clinical activity in multiple Phase II trials of patients with the same tumor type, all responses and the collective number of patients evaluable for response were pooled from individual trials to calculate an overall RR. Finally, to get the Phase II activity for any three or four cancer types combined, the individual tumor RRs were averaged.

Human Xenografts and Mouse Allografts. The search strategy for mouse cancer model data were similar to the Phase II process. The only exclusion in this case were results obtained with mouse tumors that were engineered to have special characteristics such as, for example, overexpression of proteins conferring drug resistance.

For each murine allograft or human xenograft, numerical value(s) of activity for drugs of interest was retrieved only if expressed as the treated over control tumor volume ratio (T/C%) or the tumor volume growth inhibition ratio (GI%; and T/C% = 100% − GI%) in the literature sources. In addition, only T/C% values calculated by the formula T/C% = [(RVtreated)/(RV-control)] × 100% were collected (where RV = relative volume), whereas T/C% values defined for regressions [T/C% = [(RVtreated (0) − RVtreated(t))/RVtreated (0)] × 100%] were excluded to ensure uniform calculation methods. If the T/C% was not provided but a relative tumor growth curve was given as a figure in a publication, the numerical values for the treatment and control groups provided in this graph were used to calculate the T/C%. Activity reported as all mice cured or 100% complete responses was considered equivalent to and recorded as a T/C% = 0. If no exact T/C% value was given but an interval of values was provided instead (*i.e.*, T/C% >42), a T/C% equal to the interval midpoint value (*i.e.*, a T/C% = 71) was assigned. Finally, where preclinical activity was reported as GI%, it was converted to T/C% by the formula T/C% = 100% − GI%. The activity value for the most effective, nontoxic dose in each schedule was recorded.

Single tumor type preclinical activity of each drug in the murine allograft or human xenograft models was defined as the mean T/C% value from all tested allografts/xenografts of that tumor type. Where the same laboratory had tested a single xenograft/allograft with multiple schedules of the same drug and/or where the same xenograft/allograft had been tested with the same drug by more than one laboratories, T/C% values for a single tumor were obtained by first averaging the same laboratory T/C% values and then the same xenograft T/C% values.

Overall preclinical activity in xenografts/allografts for all four tumor types together was expressed as the average of single tumor mean T/C% values.

***In Vitro* Human Tumor Cell Lines.** The publicly available data from the NCI's Human Tumor Cell Line Screen was used as the information source for the *in vitro* tumor cell line model. Information from the NCI *in vitro* Human Tumor Cell Line Screen was favored because it was a readily available, well-defined, comprehensive, validated, and extensive single source of data. Another important reason was that as an exploratory literature search showed, there was such a wide variation between different investigators in the types of assays used and the nature of cell lines tested that it would have been impossible to comprehensively combine published data from various laboratories.

Acquisition of NCI Human Tumor Cell Line Screen data were done through the internet.[4] Information for each drug was obtained through its NCI code number or NSC number. Such numbers, where available, were identified either from the literature or from a cross-reference of compound names and NSC numbers in the NCI database (also available on the NCI web site).[4]

Testing of compounds in the NCI *in vitro* Human Tumor Cell Line Screen has been described previously (17). Briefly, growth inhibition in cell lines is measured by the GI_{50}, defined as the drug concentration that causes a 50% reduction in cell number in test plates relative to control plates. For every drug entering the screen, a concentration range comprised of five, 10-fold dilutions is tested in each of a group of 60–80 cell lines. The optical densities between treated and control plates, as resulting from the sulforhodamine B assay, are used to construct a dose-response curve for each cell line in the screen, leading to the calculation of a GI_{50} in every case by interpolation. In the case of compounds with low (*i.e.*, the highest concentration tested causes <50% growth inhibition) or high (*i.e.*, the lowest concentration tested causes >50% growth inhibition) potency where interpolation is not possible, the highest and lowest concentrations, respectively, in the tested drug concentration

[4] Internet address: http://www.dtp.nci.nih.gov/docs/cancer/searches/cancer_open_compounds.html.

range are recorded as the approximated GI_{50}s. GI_{50}s are then converted to their Log_{10} values and the overall mean $Log_{10}GI_{50}$ across all cell lines in the screen is calculated. Finally, the results are displayed by a bar graph called the mean graph (28). This graph lists all of the cell lines and their corresponding $Log_{10}GI_{50}$s and relates the magnitude of every individual cell line $Log_{10}GI_{50}$ to the mean $Log_{10}GI_{50}$ across all of the cell lines by a bar to the right (more sensitive than average) or to the left (less sensitive than average) of a vertical line. The experiment is repeated several times for each concentration range. In cases where mean graphs are based on mostly approximated GI_{50}s, other higher or lower concentration ranges of the drug (again made of five, 10-fold dilutions) are also tested. Thus, for each compound tested in the NCI *in vitro* Human Tumor Cell Line Screen, multiple GI_{50} mean graphs (one for each concentration range tested) based on multiple experiments each and with a different content of approximated *versus* calculated (by interpolation) GI_{50}s may exist in the NCI database.

We obtained all of the available GI_{50} mean graph information from the NCI web site for all drugs in our list of compounds with known NSC numbers.[4] For every drug, we recorded the number of concentration ranges tested in the NCI *in vitro* Human Tumor Cell Line Screen, the number of experimental repetitions conducted for each concentration range, and, finally, the number of approximated $Log_{10}GI_{50}$s in each mean graph.

The drug concentration range that produced the mean graph with the smallest number of approximated $Log_{10}GI_{50}$s was used for scoring a drug's activity in the NCI *in vitro* Human Tumor Cell Line Screen, unless a different concentration range existed, with a number of approximated $Log_{10}GI_{50}$s varying $<10\%$ from the first but for which more experiments were done.

Preclinical activity in the NCI *in vitro* Human Tumor Cell Line Screen was scored in two different ways: by the mean $Log_{10}GI_{50}$ and by what was termed the activity fraction. For a given drug, in a given tumor type, the mean $Log_{10}GI_{50}$ was computed by averaging the $Log_{10}GI_{50}$s from all of the cell lines of that tumor type in the mean graph corresponding to the most appropriate concentration range. The activity fraction was arbitrarily defined as the number of cell lines of a given tumor type in which the individual $Log_{10}GI_{50}$s were more sensitive to the drug than the average $Log_{10}GI_{50}$ (for all cell lines of all cell types) in the mean graph over the total number of cell lines tested from that tumor type. The activity fraction was also calculated from the mean graph corresponding to the most appropriate concentration range. Overall mean $Log_{10}GI_{50}$s or activity fractions for all four cancer types combined were calculated by averaging the single tumor values.

Table 1 Drugs selected for data collection. NSC numbers are shown, where available

Drug	NSC number
Taxotere	628503
Paclitaxel	125973
Topotecan	609699
Irinotecan	
Rhizoxin	332598
Gemcitabine	
Fazarabine	281272
Teniposide	122819
Menogaril	269148
Fosquidone	D611615
Elsamitrucin	369327
Amonafide	308847
Didemnin B	325319
Suramin	
Raltitrexed	639186
Flavone acetic acid	347512
Epirubicin	256942
CI-921	343499
Trimetrexate	352122
Multitargeted antifol	
Vinorelbine	
Piritrexim	351521
Fotemustine	
CI-980	
Chloroquinoxaline sulfonamide	339004
Ilmofosine	
CI-941	
Tiazofurin	286193
Pyrazine diazohydroxide	361456
Tallimustine	
Crisnatol	

Statistical Analysis

For each preclinical cancer model, 9 Phase II *versus* preclinical activity relationships were examined for a total of 27: relationships by tumor type (disease-oriented approach, 4 relationships/model), predictive ability of one tumor type for the other three tumor types combined (compound-oriented approach, 4 relationships/model), and general predictive ability for all four tumor types combined (1 relationship/model).

Relationships were first examined descriptively with the construction of various Phase II overall activity *versus* preclinical activity scatter plots (Microsoft Excel software). Each point on these scatter plots represented data from one drug for which both Phase II and preclinical activity values had been calculated from literature sources, as described above.

After descriptive evaluation of the data, Spearman rank correlation coefficients were obtained using the SAS software, UNIX version 6.12. A significance test of every correlation coefficient was performed, and the corresponding *P*s were calculated. Spearman rank (nonparametric) correlation coefficients were used because the distributions of the x (preclinical activity) and y (clinical activity) variables were not normal (29).

When multiple comparisons are made within a group of data such as in this work, there is increased possibility that some correlations will come up as statistically significant solely because of chance (false positives). To avoid this, multiple comparison correction methods (*e.g.*, Bonferroni approach) are often used to adjust the significance level to a lower P than conventionally used. However, relying on corrected probabilities increases the possibility that meaningful correlations will be missed (false negatives), making the nature of the scientific work key to the decision to use multiple comparison adjustment methods or not. Because this was an exploratory study, we were willing to accept a higher probability of false positives to ensure that potentially meaningful associations would not be discarded. We therefore did not correct for multiple comparisons and chose a level of significance of 0.05.

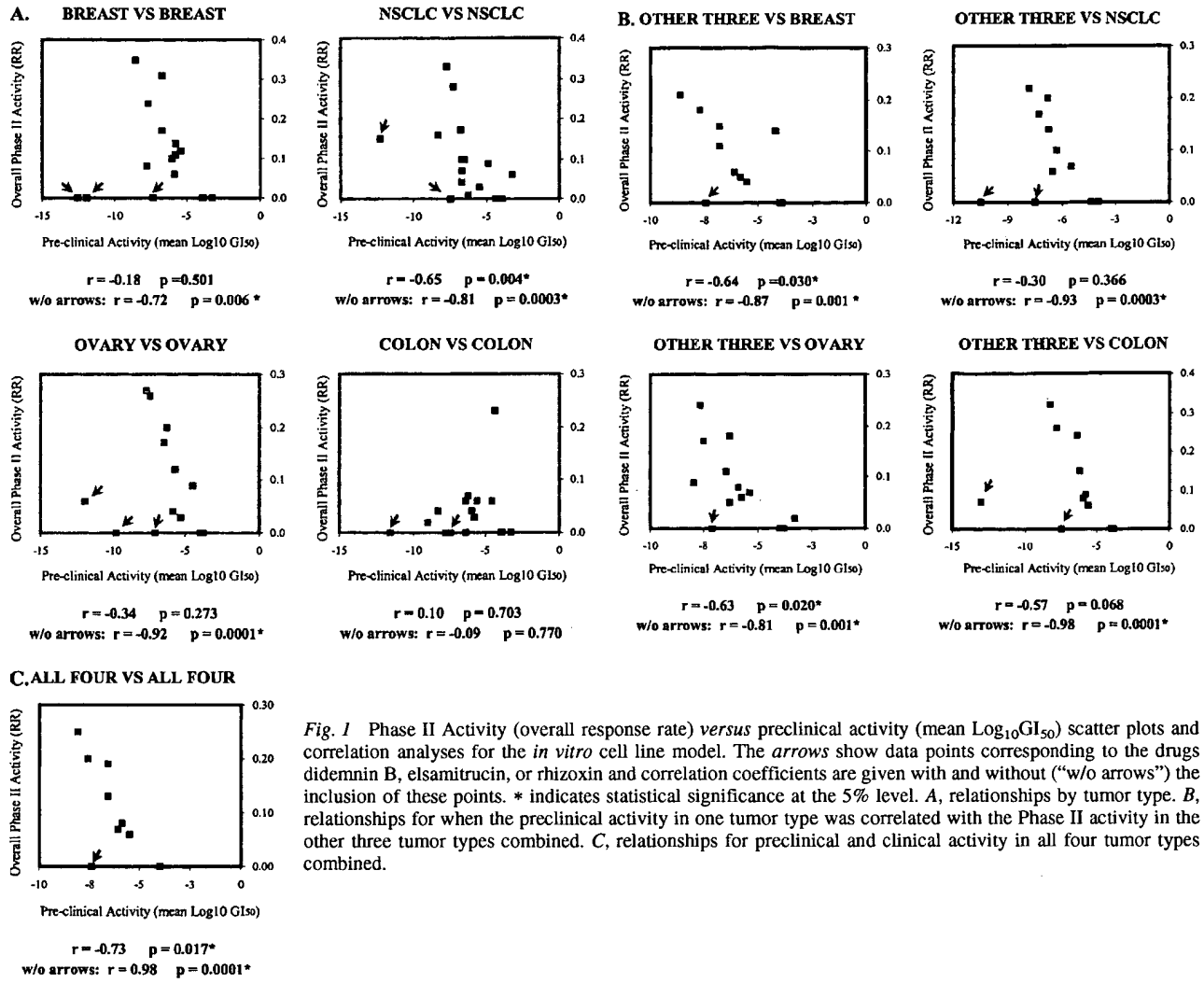

Fig. 1 Phase II Activity (overall response rate) *versus* preclinical activity (mean $Log_{10}GI_{50}$) scatter plots and correlation analyses for the *in vitro* cell line model. The *arrows* show data points corresponding to the drugs didemnin B, elsamitrucin, or rhizoxin and correlation coefficients are given with and without ("w/o arrows") the inclusion of these points. * indicates statistical significance at the 5% level. *A*, relationships by tumor type. *B*, relationships for when the preclinical activity in one tumor type was correlated with the Phase II activity in the other three tumor types combined. *C*, relationships for preclinical and clinical activity in all four tumor types combined.

RESULTS

The Medline and CancerLit databases were searched for cancer drugs (excluding agents with novel targets such as signal transduction or angiogenesis modulators) that had undergone single agent Phase I clinical trial testing either in 1991 or 1992. This search led to 97 drug names. After excluding drugs that were eliminated from additional clinical testing for practical reasons (for example difficulties with the drug formulation), drugs that were specifically developed for a certain type of cancer (as for example hormone-regulating compounds for breast cancer) and drugs that were still the subject of published Phase I studies in 1991 and 1992 despite already being licensed for human use before 1985, a list of 31 agents was obtained (Table 1). After applying the restrictions and criteria mentioned under "Materials and Methods," we extracted from the literature preclinical and Phase II activity information for those agents on four common cancer types, breast, NSCLC, ovary, and colon. Overall, 100 preclinical and 307 Phase II clinical literature references were used spanning the period between 1985 and 2000.

No preclinical data were found for 5 of the 31 drugs researched. Of the 26 drugs remaining, availability of preclinical and Phase II data varied, depending on which preclinical and clinical tumor(s) had been tested and published in each case. Thus, each of the relationships examined had a different number of data points as different subsets of drugs were included. The most data points for any relationship were 17. For six relationships, five or fewer data points were available (relationships with fewer than five data points were not included in the results presented below).

***In Vitro* Cell Line Model.** Fig. 1 shows the Phase II activity *versus* preclinical activity scatter plots and correlation analysis for the *in vitro* cell line model when the mean $Log_{10}GI_{50}$ was used as the measure of preclinical activity. Because the lower the mean $Log_{10}GI_{50}$, the higher the potency of a drug, a negative correlation between mean $Log_{10}GI_{50}$ and Phase II overall RR was expected if the model had a good clinical predictive value. Significant negative correlations were found for NSCLC (Fig. 1*A*), for breast or ovarian cell lines *versus* overall Phase II activity in the other three tumor types

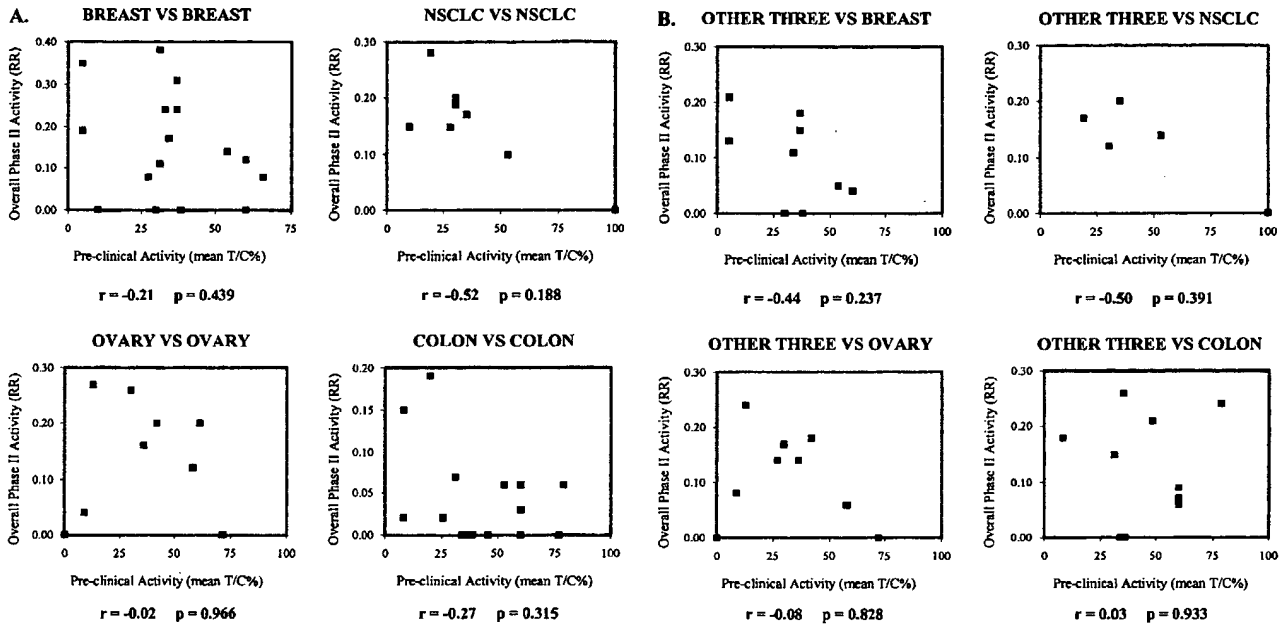

Fig. 2 Phase II activity (overall response rate) *versus* preclinical activity (mean T/C%) scatter plots and correlation analyses for the human xenograft model. *A*, relationships by tumor type. *B*, relationships for when the preclinical activity in one tumor type was correlated with the Phase II activity in the other three tumor types combined.

(Fig. 1*B*), and for preclinical activity *versus* Phase II activity in all four tumor types (Fig. 1*C*).

Although the trends observed with the activity fraction were similar to ones seen for the mean $Log_{10}GI_{50}$ measure, no correlations were statistically significant in this case (data not shown).

Human Xenograft Model. A negative correlation between Phase II RRs and mean T/C% values was expected to be indicative of a good clinical predictive value for the human xenograft model. As shown in Fig. 2, no significant correlations between preclinical and clinical activity were observed for this model in our analysis.

For some of the drugs, preclinical activity calculations were based on multiple human xenografts of the same tumor type (*i.e.*, panels) while for others on only a single xenograft. The relationships in Fig. 2 were reanalyzed, including only the drugs for which preclinical information on more than one human xenograft was available (Fig. 3). The results did not change for breast or colon tumors (compare Fig. 3*A* with Fig. 2*A*). However, the relationship for NSCLC became statistically significant and a highly significant correlation was seen for ovarian cancer (Fig. 3*A*). A near significant correlation was obtained when ovarian human xenograft panels were used to predict clinical activity in the other three tumor types combined (Fig. 3*B*).

Murine Allografts. No significant correlations between preclinical and clinical activity were observed for any of the relationships examined in this study for the murine allograft model (data not shown).

Additional Analyses. The scatter plots in Fig. 1 revealed an interesting observation: in every relationship except for colon cancer under the disease oriented approach, an obvious trend toward a negative correlation was evident except for one to three outlier data points (Fig. 1, *arrows*). Interestingly, in all cases, these outlier data points corresponded to the same three drugs, namely elsamitrucin, didemnin B, and rhizoxin.

In an attempt to provide a possible explanation for this observation, we considered the mechanism of action of all drugs that were included in the correlations in Fig. 1. From a total of 18 drugs (Table 2), 5, namely, elsamitrucin, didemnin B, rhizoxin, flavone acetic acid, and fosquidone, were distinct in that they seemed to act through mostly unknown pathways that were not the typical DNA-based mechanisms of action of cytotoxic cancer agents. Thus, although flavone acetic acid and fosquidone fitted the rest of the data, there seemed to be a plausible mechanistic basis for the outlier behavior of the data points for elsamitrucin, didemnin B, and rhizoxin. In fact, exclusion of these three drugs led to highly significant correlations in all cases except for the same tumor relationship in colon cancer (Fig. 1, correlation coefficients and *P*s for "w/o arrows"). It should be noted that none of the relationships examined for the human xenograft models (Figs. 2 and 3) included elsamitrucin, didemnin B, or rhizoxin as data points.

Because of the intriguing results obtained with the human NSCLC and ovarian xenograft panels in Fig. 3*A*, a more detailed examination of these panels was pertained. As seen in Figs. 4*A* and 5*A*, the 6 ovarian and 7 NSCLC xenograft panels differed both in the numbers (minimum of 6 and maximum of 13 for ovary and minimum of 2 and maximum of 8 for NSCLC) and the identity of the xenografts that they contained. Analysis by grade/histology was hindered by lack of complete information on all xenografts. However, some patterns appeared distinguish-

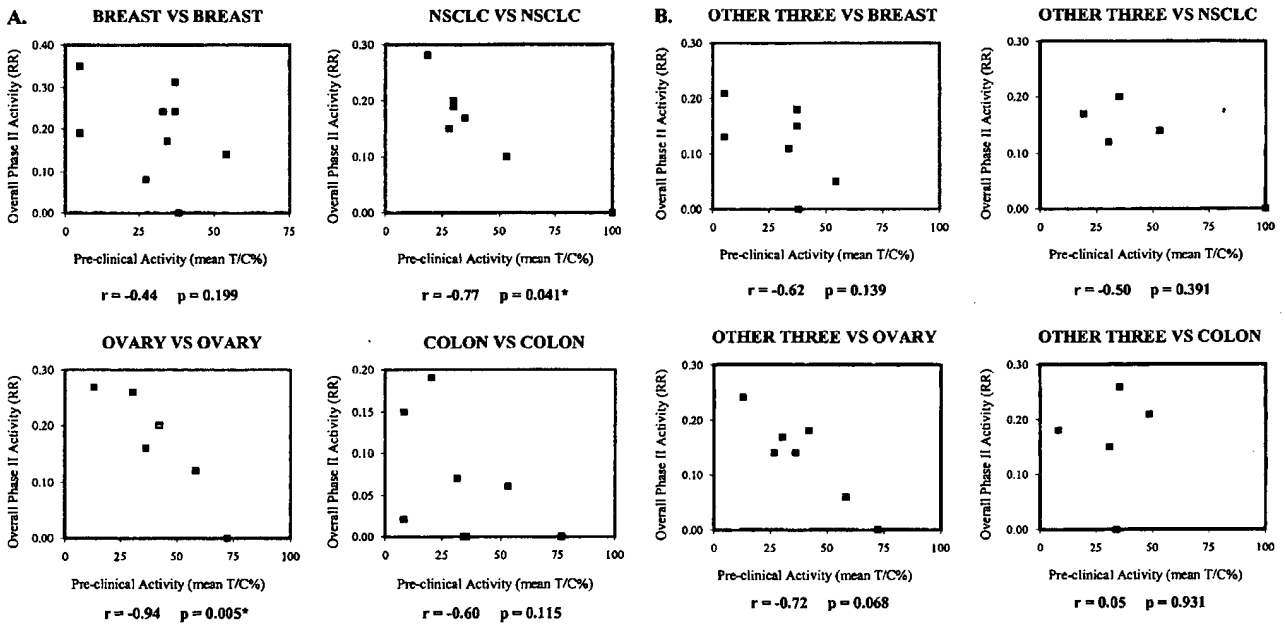

Fig. 3 Phase II activity (overall response rate) *versus* preclinical activity (mean T/C%) scatter plots and correlation analyses for the human xenograft model. Only data points for which two or more human xenografts were used to generate the preclinical activity values are shown. * indicates statistical significance at the 5% level. *A*, relationships by tumor type. *B*, relationships for when the preclinical activity in one tumor type was correlated with the Phase II activity in the other three tumor types combined.

Table 2 Mechanisms of action of drugs used in clinical vs. pre-clinical correlations for the *in vitro* cell line model (Fig. 1)
Atypical cytotoxics are shown in bold.

Drug	Mechanism of action
Amonafide	DNA intercalator
CI-921	Acts on topoisomerase II
Didemnin B	Not understood. Believed to act on protein synthesis
Elsamitrucin	Not understood. It has been observed to inhibit topoisomerase I and II in *in vitro* experiments (relevance to *in vivo* uncertain). In cells in culture it has been observed to cause a cytostatic effect.
Epirubicin	Attaches to DNA at G bases
Fazarabine	Probably inhibits DNA synthesis by incorporation into DNA.
Flavone acetic acid	Has antivascular action in mice (probably not applicable to humans). Also believed to induce cell cycle arrest by generating reactive oxygen species that act on DNA.
Menogaril	Causes cleavage of double-stranded DNA by inhibiting topoisomerase II
Piritrexim	Inhibits dihydrofolate reductase
Rhizoxin	Not fully understood. May interact with tubulin (different binding site than taxoids) and lead to cell cycle arrest. Also observed to act as an angiogenesis inhibitor.
Taxol	Microtubule destabilizing agent that causes apoptosis
Taxotere	Microtubule destabilizing agent that causes apoptosis
Teniposide	DNA synthesis inhibition by stabilization of cleavable DNA complexes
Topotecan	Topoisomerase I inhibitor
Trimetrexate	Antifolate
Fosquidone	Unknown. Not a DNA binder or a topoisomerase inhibitor
Tomudex	Thymidylate synthase inhibitor
Tiazofurin	Inhibits 5′-phosphodehydrogenase, the rate-limiting enzyme for guanine ribonucleotide synthesis

able. All ovarian panels contained 10–20% undifferentiated tumors and also included both poorly differentiated and moderately differentiated subtypes (Fig. 4*B*). For NSCLC, all panels included adenocarcinoma xenografts with a frequency of >30% (Fig. 5*B*). These observations suggested that the frequency of histological/grade subtypes within a xenograft panel may be an important determinant of clinical predictivity rather than the number or the nature of the xenografts.

In an attempt to explore this hypothesis and to further examine the validity of the results obtained for ovarian cancer and NSCLC in Fig. 3*A*, the literature was reviewed for additional data. Six more agents with known overall Phase II RRs in

A.

NAME	HISTOLOGY / GRADE	DATA POINTS (DRUGS)					
		EPIRUBICIN	FOSQUIDONE	GEMCITABINE	MENOGARIL	TAXOTERE	PACLITAXEL
MRI-H-207	undifferentiated	+	+		+	+	
A2780	undifferentiated	+		+	+		+
Ov.He	mod. diff., mucinous	+	+	+	+		
Ov.Me	carcinosarcoma	+	+		+		
OvRiC	mod. diff., serous	+	+	+	+		
Fma	poorly diff., mucinous	+	+		+	+	
Ov.Pe	mod. diff., mucinous	+	+	+	+	+	
Fco	clear cell sarcoma	+	+		+		
T17	cystoadenocarcinoma	+					
T385	adenocarcinoma	+					
OvGR	mod. diff., mucinous		+				
Fko	mod. diff., serous		+	+		+	
OvG1	poorly diff., serous		+				
OVCAR-3	adenocarcinoma			+		+	+
A121a	?					+	+
HOC18	poorly diff., serous					+	+
HOC22	poorly diff., serous					+	+
A2780/DDP	undifferentiated						+
A2780/DX	undifferentiated						+
SKOV-3	adenocarcinoma						+
1° ovary 1	cystoadenocarcinoma						+
1° ovary 2	dediff. serous adenoc.						+
IGROV 1	moderately diff.						+
OVCAR-8	poorly diff. adenoc.						+
OVCAR-5	adenocarcinoma						+
OvSh	poorly diff., serous					+	
HOC22-S	poorly diff., serous					+	
TOTAL NO.		10	10	6	8	10	13

B.

HISTOLOGY/GRADE FREQUENCIES IN HUMAN OVARIAN XENOGRAFT PANELS						
HISTOLOGY / GRADE	EPIRUBICIN NO. (%)	FOSQUIDONE NO. (%)	GEMCITABINE NO. (%)	MENOGARIL NO. (%)	TAXOTERE NO. (%)	PACLITAXEL NO. (%)
undifferentiated	2 (20)	1 (10)	1 (17)	2 (25)	1 (10)	3 (23)
mod. diff., mucinous	2 (20)	3 (30)	2 (33)	2 (25)	1 (10)	0 (0)
mod. diff., serous	1 (10)	2 (20)	2 (33)	1 (12.5)	1 (10)	0 (0)
poorly diff., mucinous	1 (10)	1 (10)	0 (0)	1 (12.5)	1 (10)	0 (0)
poorly diff., serous	0 (0)	1 (10)	0 (0)	0 (0)	4 (40)	2 (15)
unspecified	4 (40)	2 (20)	1 (17)	2 (25)	2 (20)	8 (62)
TOTAL	10 (100)	10 (100)	6 (100)	8 (100)	10 (100)	13 (100)

Fig. 4 Human ovarian xenograft panels for the six data points (drugs) used in the "Ovary *versus* Ovary" relationship in Fig. 3*A*. *A*, names and histology/grade (? = unknown, mod. diff. = moderately differentiated, poorly diff. = poorly differentiated, dediff. = dedifferentiated, adncrc = adenocarcinoma) of all of the xenografts tested. Inclusion of a particular xenograft in one of the panels is shown by a "+" sign in the corresponding row and under the appropriate drug column. *B*, histology/grade subtypes in the human ovarian xenograft panels by number and percentage.

previously treated patients with ovarian cancer were found. Five and one of these compounds had been tested in a panel of 15 and 6 human ovarian xenografts, respectively (26, 30), which fitted the histology/grade patterns identified in Fig. 4*B*. Fig. 6*A* lists the names and Phase II RRs (31–56) of these additional drugs together with the six compounds that were included in the analysis in Fig. 3*A*. Fig. 6, *A* and *B*, also shows mean T/C% values scatter plots and statistical analyses for two cases: first, for when all of the available xenograft information was used, and second, for when mean T/C% calculations were based, where possible, on the arithmetically smallest panel, namely the one used for gemcitabine in Fig. 4. Highly significant correlations were obtained in both cases (Fig. 6*B*).

For NSCLC information on two additional agents was found: amsacrine [mean T/C% of 62 (26) and Phase II RR equal to 0.06 (31)] and doxorubicin [mean T/C% of 47 (26) and Phase II RR equal to 0.12 (32)]. Both had been tested in NSCLC human xenograft panels that included all three histological subtypes and had adenocarcinoma contents of 29 and 33%, respectively. As for ovarian cancer, those two additional data points (Fig. 5*C*, *arrows*) enhanced the statistical significance of the relationship observed in Fig. 3*A*.

DISCUSSION

A literature-based, retrospective study was conducted to examine the clinical predictive value of three widely used preclinical cancer models, namely, the *in vitro* human tumor cell line, the human xenograft, and the murine allograft models. Four solid tumor types were selected, breast, NSCLC, ovary and colon, and data on a set of 31 anticancer agents (excluding agents with novel targets such as signal transduction or angiogenesis modulators) were collected. Preclinical activity in each model was correlated with RRs in Phase II clinical trials by tumor type (disease-oriented approach) in the case when one preclinical tumor type was used as a predictor of overall clinical activity in the other three tumor types combined (compound-oriented approach) and for all four tumor types together.

A.

XEN. NAME	XENOGRAFT HISTOLOGY	DRUGS						
		EPI	FAZ	GEM	IRINO	PACLIT	TOPO	VINRLB
T222	squamous cell	+						
T291	adenocarcinoma	+						
UCLA-P3	adenocarcinoma		+					
ACCOLU-78	squamouse cell		+					
NCI-H460	large cell			+	+	+	+	+
A549	adenocarcinoma			+	+	+	+	+
CaLu-6	adenocarcinoma			+				
H-74	?			+				
LC-376	?			+				
QG-56	squamous cell				+			+
NCI-H23	adenocarcinoma				+	+		
NCI-H226	squamous cell				+	+	+	
MV-522	adenocarcinoma					+		
CaLu-3	adenocarcinoma					+		
1° NSCLC	adenocarcinoma					+		
L2987	adenocarcinoma					+		
L-27	adenocarcinoma							+
LC-06	large cell							+
LU-65	large cell							+
PC-12	adenocarcinoma							+
LU-99	large cell							+
TOTAL NO.		2	2	5	5	8	3	8

B.

HISTOLOGY FREQUENCY IN HUMAN NSCLC XENOGRAFT PANELS							
HISTOLOGY	EPI NO. (%)	FAZ NO. (%)	GEM NO. (%)	IRINO NO. (%)	PACLIT NO. (%)	TOPO NO. (%)	VINORLB NO. (%)
adenocarcinoma	1 (50)	1 (50)	2 (40)	2 (40)	6 (75)	1 (33.3)	3 (37.5)
large cell	0 (0)	0 (0)	1 (20)	1 (20)	1 (12.5)	1 (33.3)	4 (50)
squamous cell	1 (50)	1 (50)	0 (0)	2 (40)	1 (12.5)	1 (33.3)	1 (12.5)
unknown			2 (40)				
TOTAL	2 (100)	2 (100)	5 (100)	5 (100)	8 (100)	3 (100)	8 (100)

C. NSCLC VS NSCLC (ADDITIONAL DATA)

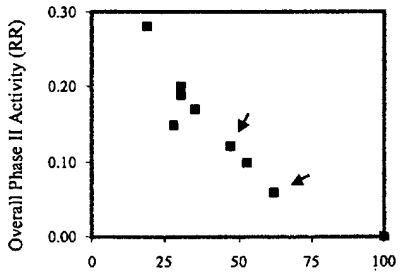

r = -0.90 p = 0.001*

Fig. 5 Human NSCLC xenograft panels for the seven data points (drugs) used in the NSCLC *versus* NSCLC relationship in Fig. 3*A*. *A*, drug names (EPI = epirubicin, FAZ = fazarabine, GEM = gemcitabine, IRINO = irinotecan, PACLIT = paclitaxel, TOPO = topotecan, VINRLB = vinorelbine) and histological subtypes (? = unknown) of all of the xenografts tested. Inclusion of a particular xenograft in one of the panels is shown by a "+" sign in the corresponding row and under the appropriate drug column. *B*, histological subtypes in the human NSCLC xenograft panels by number and percentage. *C*, scatter plot and correlation analysis for the same tumor clinical *versus* preclinical activity relationship in NSCLC, including the seven drugs in Fig. 6*A* as well as two additional agents, doxorubicin and amsacrine (data points shown with *arrows*), with known NSCLC Phase II and human xenograft activities.

Colon cancer was the only site for which a disproportional amount of clinically active *versus* inactive agents were identified: only 3 drugs with Phase II RRs > 0.15 and 8 with ≤0.10 (Figs. 1–3). However, this was likely a reflection of the lack of clinically effective drugs for this tumor type rather than the result of selection and publication bias.

When the mean $Log_{10}GI_{50}$ measure of preclinical activity was used, the *in vitro* cell line model was found to be predictive of Phase II clinical performance for NSCLC under the disease-oriented approach in breast and ovarian cancers under the compound-oriented approach and in the case of all four tumor types together. Highly significant correlations were observed in all cases, except colon cancer, when three consistent outlier data points corresponding to the mechanistically nontypical cytotoxic agents didemnin B, elsamitrucin, and rhizoxin were excluded in exploratory analysis. Thus, the *in vitro* cell line model

A.

	DRUG	PHASE II RESPONSE RATE	HUMAN OVARIAN XENOGRAFT MEAN T/C %	
			ALL TESTED	GEMCITABINE PANEL
STUDY DRUGS	EPIRUBICIN	0.20	42	-
	FOSQUIDONE	0.00	72	-
	GEMCITABINE	0.16	36	36
	MENOGARIL	0.12	58	-
	PACLITAXEL	0.26	30	-
	TAXOTERE	0.27	13	-
ADDITIONAL DRUGS	DOXORUBICIN	0.19[23,26]	47[30]	47[30]
	AMSACRINE	0.05[31]	75[26]	-
	CISPLATIN	0.25[37,38]	41[30]	46[30]
	HEXAMETHYL-MELAMINE	0.19[39,44]	28[30]	31[30]
	METHOTREXATE	0.09[45,46]	76[30]	84[30]
	5-FU	0.10[47,66]	71[30]	71[30]

B.

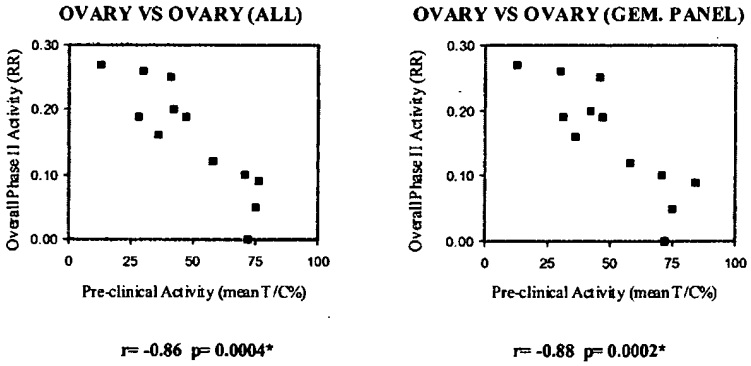

Fig. 6 *A*, preclinical and Phase II clinical activity data for ovarian cancer, including the six drugs in Fig. 3*A* ("Study Drugs") as well as an additional six drugs ("Additional Drugs") with known ovarian Phase II and human xenograft activities. Literature references are shown in superscript font. *B*, scatter plots and correlation analysis for the same tumor clinical *versus* preclinical activity relationship in ovarian cancer based on the data in Fig. 5*A*. Analysis was done for (*a*) when all of the xenografts were included in preclinical activity calculations ("All") and (*b*) when only the six xenografts in the gemcitabine panel were used for preclinical activity calculations, where possible ("Gem. Panel"). Stars indicate statistical significance at the 5% level.

might be predictive in the case of typical cytotoxic cancer agents but might fail to provide reliable information for at least some of the noncytotoxic cancer drugs. Additional studies are needed to explore this observation.

The fact that drug potency (mean $Log_{10}GI_{50}$), a pharmacological measure, was found to be predictive of Phase II performance was somewhat surprising but has been noted previously: a recent study by Johnson *et al.* (18) demonstrated a highly significant correlation between potency in the NCI human tumor cell line screen and activity in the hollow fiber assay. Pharmacological considerations (pharmacological differences between the species) might provide a possible explanation why some anticancer agents appear effective in *in vivo* mouse models but fail to show efficacy in Phase II trials. Experience with some agents (57) has shown that the maximum-tolerated dose in mouse can be higher than in humans, presumably because of an intrinsic ability of mouse cells to tolerate higher drug doses and/or more efficient elimination in the mouse.

In contrast to the *in vitro* cell line, our results suggest that the murine allograft model, as used in this analysis, is not predictive of clinical Phase II performance. This is in agreement with the conclusions from a large body of information originating from the NCI screening programs in use from 1975 to·1990 (5–8, 10–12).

The human xenograft model showed good tumor-specific predictive value for NSCLC and ovarian cancers when panels of xenografts were used. However, it failed to adequately predict clinical performance both in the disease and compound-oriented settings for breast and colon tumors. The results with breast cancer were in agreement with a recent study (18) but were contradictory to the work reported by Bailey *et al.* (20), Inoue *et al.* (21), and Mattern *et al.* (24). However, given that the latter studies did not use formal statistical methods, our conclusions may be more robust. The results for ovarian cancer were in agreement with studies by Taetle *et al.* (23) and Mattern *et al.* (24) but contradicted the conclusions of the recent NCI United States study by Johnson *et al.* (18). Our results for NSCLC were consistent with the observations from all previous studies that examined same tumor correlations in this cancer type (18, 24).

For NSCLC and ovarian cancer patients, a panel of xenografts was more predictive than single xenografts confirming preliminary observations by Bellet *et al.* (19).

In an effort to identify the properties that may render an ovarian or NSCLC human xenograft panel predictive of Phase II drug performance, common characteristics were sought. There was no similarity in number and only limited overlap in identity of xenografts between same tumor type panels. However, certain patterns in histology/grade content were found. These ob-

servations suggest that the relative histology/grade content rather than the number or identity of xenografts within a panel may be the important determinant of clinical predictivity. To our knowledge, no other study has attempted to identify ovarian or NSCLC human xenograft panel features that might lead to accurate predictions of a drug's Phase II performance.

This is the only study that has examined the clinical predictive value of three preclinical cancer models together and thus allows for direct comparisons between them. The results suggest that the human xenograft model is more predictive than its murine allograft counterpart and that the *in vitro* cell line model is of, at least, equivalent usefulness to the human xenograft model.

The NCI work with cancer drug screening programs from 1955 to 1990 (Refs. 5–8, 10–12; leukemia-based preclinical, compound-oriented screens preferentially yielding compounds active against hematological malignancies) in combination with our work and recent conclusions by Johnson *et al.* (Ref. 18; statistically significant results under the compound-oriented approach for some solid tumors) suggest that the compound-oriented strategy may be successful when used only within solid tumors or only within hematological malignancies but not when the two disease groups are considered together.

In general, our results suggest that the *in vitro* human tumor cell line and the human xenograft models might have good clinical predictive value in some solid tumors (such as ovary and NSCLC) under both the disease and compound-oriented strategies, as long as an appropriate panel of tumors is used in preclinical testing.

In conclusion, given the results in this study and those of others (6, 7, 10–12), continued use of the murine allograft model in drug development may not be justified. The work presented here argues for emphasis to be placed on *in vitro* cell lines (in the context of the NCI Human Tumor Cell Line Screen) and appropriate panels of the human xenograft model.

Recent years have seen an explosion in the molecular understanding of cancer, which has led to the development of not only more effective cytotoxic cancer drugs but of potentially cytostatic or antimetastatic agents as well. The future preclinical and clinical development of traditional cytotoxic compounds will likely follow similar procedures with those practiced today, and in that sense, the present findings could contribute to the more efficient discovery of such agents. However, the existing cancer models and parameters of activity in both the preclinical and clinical settings may have to be redesigned to fit the mode of action of the novel cytostatic, antimetastatic, antiangiogenesis, or immune response-modulating agents (58). In the preclinical cancer model front, the case is being made for the use of the orthotopic mouse xenograft and transgenic models (59–61) because those are thought to more accurately simulate human disease, especially in terms of growth characteristics and metastatic behavior. New end points of preclinical activity are contemplated such as the demonstration that a new molecule truly hits the intended molecular target (58). In Phase II clinical trials, there is a growing effort toward validating new surrogate endpoints of drug efficacy (58). The next decade will probably answer many of the questions regarding the effectiveness of these novel agents and will likely define a new role for traditional cytotoxic therapies, but it will also bring new challenges in terms of preclinical predictors of activity.

REFERENCES

1. Curt, G. A. The use of animal models in cancer drug discovery and development. Stem Cells, *12:* 23–29, 1994.

2. Goldin, A., Serpick, A. A., and Mantel, N. Experimental screening procedures and clinical predictability value. Cancer Chemother. Rep., *50:* 173–218, 1966.

3. Venditti, J. M. Drug evaluation branch program: report to screening contractors. Cancer Chemother. Rep., *5:* 1–4, 1975.

4. Venditti, J. M. Preclinical drug development: rationale and methods. Semin. Oncol., *8:* 349–353, 1981.

5. Venditti, J. M., Wesley, R. A., and Plowman, J. Current NCI preclinical antitumor screening *in vivo*: results of tumor panel screening, 1976–1982 and future directions. Adv. Pharmacol. Chemother., *20:* 1–19, 1984.

6. Venditti, J. M. The National Cancer Institute antitumor drug discovery program, current and future perspectives: a commentary. Cancer Treat. Rep., *67:* 767–772, 1983.

7. Staquet, M. J., Byar, D. P., Green, S. B., and Rozencweig, M. Clinical predictivity of transplantable tumor systems in the selection of new drugs for solid tumors: rationale for a three-stage strategy. Cancer Treat. Rep., *67:* 753–765, 1983.

8. Goldin, A., Venditti, J. M., MacDonald, J. S., Muggia, F. M., Henney, J. E., and De Vita V. T. Current results of the screening program at the division of cancer treatment, National Cancer Institute. Eur. J. Cancer, *17:* 129–142, 1981.

9. Marsoni, S., and Wittes, R. Clinical development of anticancer agents: A National Cancer Institute perspective. Cancer Treat. Rep., *68:* 77–85, 1983.

10. De Vita, V. T., and Schein, P. S. The use of drugs in combination for the treatment of cancer N. Engl. J. Med., *288:* 998–1006, 1973.

11. Zubrod, C. G. Chemical control of cancer. Proc. Natl. Acad. Sci. USA, *69:* 1042–1047, 1972.

12. Marsoni, S., Hoth, D., Simon, R., Leyland-Jones, B., De Rosa, M., and Wittes, R. E. Clinical drug development: an analysis of Phase II trials, 1970–1985. Cancer Treat. Rep., *71:* 71–80, 1987.

13. Shoemaker, R. H., Monks, A., Alley, M. C., Scudiero, D. A., Fine, D. L., McLemore, T. L., Abbott, B. J., Paull, K. D., Mayo, J. G., and Boyd, M. R. Development of human tumor cell line panels for use in disease-oriented drug screening. Prog. Clin. Biol. Res., *276:* 265–286, 1988.

14. Skehan, P., Storeng, R., Scudiero, D., Monks A., McMahon, J., Vistica, D., Warren, J. T., Bokesch, H., Kenney, S., and Boyd, M. R. New colorimetric cytotoxicity assay for anticancer drug screening. J. Natl. Cancer Inst. (Bethesda), *82:* 1107–1112, 1990.

15. Rubinstein, L. V., Shoemaker, R. H., Paull, K. D., Simon, R. M., Tosini, S., Skehan, P., Scudiero, D., Monks, A., and Boyd, M. R. Comparison of *in vitro* anticancer drug screening data generated with a tetrazolium assay *versus* a protein assay against a diverse panel of human tumor cell lines. J. Natl. Cancer Inst. (Bethesda), *82:* 1113–1118, 1990.

16. Alley, M. C., Scudiero, D., Monks, A., Hursey, M. L., Czerwinski, M. J., Fine, D. L., Abbott, B. J., Mayo, J. G., Shoemaker, R. H., and Boyd, M. R. Feasibility of drug screening with panels of human tumor Cell lines using a microculture tetrazolium assay. Cancer Res., *48:* 589–601, 1988.

17. Monks, A., Scudiero, D., Skehan, P., Shoemaker, R. H., Paull, K. D., Vistica, D., Hose, C., Langley, J., Cronise, P., Vaigro-Wolff, A., Gray-Goodrich, M., Campbell, H., Mayo, J., and Boyd, M. R. Feasibility of a high-flux anticancer drug screen using a diverse panel of cultured human tumor cell lines. J. Natl. Cancer Inst. (Bethesda), *83:* 757–766, 1990.

18. Johnson, J. I., Decker, S., Zaharevitz, D., Rubinstein, L. V., Venditti, J. M., Schepartz, S., Kalyandrug, S., Christin, M., Arbuck, S., Hollingshead, M., and Sausville, E. A. Relationships between drug

activity in NCI preclinical *in vitro* and *in vivo* models and early clinical trials. Br. J. Cancer, *84:* 1424–1431, 2001.

19. Bellet, R. E., Danna, V., Mastrangelo, M. J., and Berd, D. Evaluation of a "nude" mouse-human tumor panel as a predictive secondary screen for cancer chemotherapy agents. J. Natl. Cancer Inst. (Bethesda), *63:* 1185–1187, 1979.

20. Bailey, M. J., Gazet, J-C., Smith, I. E., and Steel, G. G. Chemotherapy of human breast-carcinoma xenografts. Br. J. Cancer, *42:* 530–536, 1980.

21. Inoue, K., Fujimote, S., and Ogawa, M. Antitumor efficacy of seventeen anticancer drugs in human breast cancer xenograft (MX-1) transplanted in nude mice. Cancer Chemother. Pharmacol., *10:* 182–186, 1983.

22. Steel, G. G., Courtenay, V. D., and Peckhan M. J. The response to chemotherapy of a variety of human tumor xenografts. Br. J. Cancer, *47:* 1–13, 1983.

23. Taetle, R., Rosen, F., Abramson, I., Venditti, J., and Howell, S. Use of nude mouse xenografts as preclinical drug screens: *in vivo* activity of established chemotherapeutic agents against melanoma and ovarian carcinoma xenografts. Cancer Treat. Rep., *71:* 297–304, 1987.

24. Mattern, J., Bak, M., Hahn, E. W., and Volm, M. Human tumor xenografts as models for drug testing. Cancer Metastasis Rev., *7:* 263–284, 1988.

25. Boven, E., Winograd, B., Fodstad, O., Lobbezzoo, M. W., and Pinedo, H. M. Preclinical Phase II studies in human tumor lines: a European multicenter study. Eur. J. Cancer, *24:* 567–573, 1988.

26. Boven, E., Winograd, B., Berger, D. P., Dumant, M. P., Braakhuis, B. J. M., Fodstad, O., Langdon, S., and Fiebig, H. H. Phase II preclinical drug screening in human tumor xenografts: a first European multicenter collaborative study. Cancer Res., *52:* 5940–5947, 1992.

27. Langdon, S., Hendriks, H. R., Braakhuis, B. J. M., Pratesi, G., Berger, D. P., Fodstad, O., Fiebig, H., and Boven, E. Preclinical Phase II studies in human tumor xenografts: a European multicenter follow-up study. Ann. Oncol., *5:* 415–422, 1994.

28. Paull, K. D., Shoemaker, R. H., Hodes, L., Monks, A., Scudiero, D., Rubinstein, L. V., Plowman, J., and Boyd, M. R. Display and analysis of patterns of differential activities of drugs against human tumor cell lines: development of mean graph and COMPARE algorithm. J. Natl. Cancer Inst. (Bethesda), *81:* 1088–1092, 1989.

29. Rosner, B. Non-parametric Methods. *In:* Fundamentals of Biostatistics, 4th ed., p. 575. Belmont, CA: Duxbury Press, Wadsworth Publishing Company, 1994.

30. Kolfscoten, G. M., Pinedo, H. M., Scheffer, P. G., Schluper, H. M. M., Erkelens, C. A. M., and Boven, E. Development of a panel of 15 human ovarian cancer xenografts for drug screening and determination of the role of the glutathione detoxification system. Gynecol. Oncol., *76:* 362–368, 2000.

31. Louie, A. C., and Issell, B. F. Amsacrine (AMSA): a clinical review. J. Clin. Oncol., *3:* 562–592, 1985.

32. Minna, J. D., Pass, H., Glatsein, E., and Inde, D. Cancer of the lung. *In:* V. T. DeVita, S. Hellman, and S. A. Rosenberg (eds.), Cancer Principles and Practice of Oncology, pp. 660 (Table 22–48). Philadelphia: J. B. Lippincott, 1989.

33. Gordon, A. N., Granai, C. O., Rose, P. G., Hainsworth, J., Lopez, A., Weissman, C., Rosales, R., and Sharpington, T. Phase II study of liposomal doxorubicin in platinum- and paclitaxel-refractory epithelial ovarian cancer. Clin. Oncol., *18:* 3093–3100, 2000.

34. Israel, V. P., Garcia, A. A., Roman, L., Muderspach, L., Burnett, A., Jeffers, S., and Muggia, F. M. Phase II study of liposomal doxorubicin in advanced gynecologic cancers. Gynecol. Oncol., *78:* 143–147, 2000.

35. Muggia, F. M., Hainsworth, J. D., Jeffers, S., Miller, P., Groshen, S., Tan, M., Roman, L., Uziely, B., Muderspach, L., Garcia, A., Burnett, A., Greco, F. A., Morrow, C. P., Paradiso, L. J., and Liang, L. J. Phase II study of liposomal doxorubicin in refractory ovarian cancer: antitumor activity and toxicity modification by liposomal encapsulation. J. Clin. Oncol., *15:* 987–993, 1997.

36. Blum, R. H., and Carter, S. K. Adriamycin: a new anticancer drug with significant clinical activity. Ann. Intern. Med., *80:* 249–259, 1974.

37. Thigpen, J. T., Lagasse, L., Homesley, H., and Blessing, J. A. *Cis*-platinum in the treatment of advanced or recurrent adenocarcinoma of the ovary. A Phase II study of the Gynecology Oncology. Group. Am. J. Clin. Oncol., *6:* 431–435, 1983.

38. Wiltshaw, E., and Kroner, T. Phase II study of *cis*-dichlorodiammineplatinum(II) (NSC-119875) in advanced adenocarcinoma of the ovary. Cancer Treat. Rep., *60:* 55–60, 1976.

39. Bonomi, P. D., Mladineo, J., Morrin, B., Wilbanks, G., Jr., and Slayton, R. E. Phase II trial of hexamethylmelamine in ovarian carcinoma resistant to alkylating agents. Cancer Treat. Rep., *63:* 137–138, 1979.

40. Johnson, B. L., Fisher, R. I., Bender, R. A., DeVita, V. T., Jr., Chabner, B. A., and Young, R. C. Hexamethylmelamine in alkylating agent-resistant ovarian carcinoma. Cancer (Phila.), *42:* 2157–2161, 1978.

41. Omura, G. A., Blessing, J. A., Morrow, C. P., Buchsbaum, H. J., and Homesley, H. D. Follow-up on a randomized trial of melphalan (M) *vs.* melphalan plus hexamethylamine (M+H) *versus* Adriamycin plus cyclophosphamide (A+C) in advanced ovarian carcinoma. Proc. Am. Assoc. Cancer Res., *22:* 470, 1981.

42. Bolis, G., D'Incalci, M., Belloni, C., and Mangioni, C. Hexamethylmelamine in ovarian cancer resistant to cyclophosphamide and Adriamycin. Cancer Treat. Rep., *63:* 1375–1377, 1979.

43. Manetta, A., MacNeill, C., Lyter, J. A., Scheffler, B., Podczaski, E. S., Larson, J. E., and Schein, P. Hexamethylmelamine as a single second-line agent in ovarian cancer. Gynecol. Oncol., *36:* 93–96, 1990.

44. Rosen, G. F., Lurain, J. R., and Newton, M. Hexamethylmelamine in ovarian cancer after failure of cisplatin-based multiple-agent chemotherapy. Gynecol. Oncol., *27:* 173–179, 1987.

45. Parker, L. M., Griffiths, C. T., Yankee, R. A., Knapp, R. C., and Canellos, G. P. High-dose methotrexate with leucovorin rescue in ovarian cancer: a Phase II study. Cancer Treat. Rep., *63:* 275–279, 1979.

46. Barlow, J. J., and Piver, M. S. Methotrexate (NSC-740) with citrovorum factor (NSC-3590) rescue, alone and in combination with cyclophosphamide (NSC-26271), in ovarian cancer. Cancer Treat. Rep., *60:* 527–533, 1976.

47. Morgan, R. J., Jr., Speyer, J., Doroshow, J. H., Margolin, K., Raschko, J., Sorich, J., Akman, S., Leong, L., Somlo, G., and Vasilev, S. Modulation of 5-fluorouracil with high-dose leucovorin calcium: activity in ovarian cancer and correlation with CA-125 levels. Gynecol. Oncol., *58:* 79–85, 1995.

48. Markman, M., Reichman, B., Hakes, T., Hoskins, W., Rubin, S., Jones, W., and Lewis, J. L., Jr. Intraperitoneal chemotherapy as treatment for ovarian carcinoma and gastrointestinal malignancies: the Memorial Sloan-Kettering Cancer Center experience). Acta Med. Austriaca, *16:* 65–67, 1989.

49. Prefontaine, M., Donovan, J. T., Powell, J. L., and Buley, L. Treatment of refractory ovarian cancer with 5-fluorouracil and leucovorin. Gynecol. Oncol., *61:* 249–252, 1996.

50. Kamphuis, J. T., Huider, M. C., Ras, G. J., Verhagen, C. A., Kateman, I., Vreeswijk, J. H., and Burghouts, J. T. High-dose 5-fluorouracil and leucovorin as second-line chemotherapy in patients with platinum-resistant epithelial ovarian cancer. Cancer Chemother. Pharmacol., *37:* 190–192, 1995.

51. Burnett, A. F., Barter, J. F., Potkul, R. K., Jarvis, T., and Barnes, W. A. Ineffectiveness of continuous 5-fluorouracil as salvage therapy for ovarian cancer. Am. J. Clin. Oncol., *17:* 490–493, 1994.

52. Reed, E., Jacob, J., Ozols, R. F., Young, R. C., and Allegra, C. 5-Fluorouracil (5-FU) and leucovorin in platinum-refractory advanced stage ovarian carcinoma. Gynecol. Oncol., *46:* 326–329, 1992.

53. Ozols, R. F., Speyer, J. L., Jenkins, J., and Myers, C. E. Phase II trial of 5-FU administered Ip to patients with refractory ovarian cancer. Cancer Treat. Rep., *68:* 1229–1232, 1984.

54. Long, H. J., III, Nelimark, R. A., Su, J. Q., Garneau, S. C., Levitt, R., Goldberg, R. M., Poon, M. A., and Kugler, J. W. Phase II evaluation of 5-fluorouracil and low-dose leucovorin in cisplatin-refractory advanced ovarian carcinoma. Gynecol. Oncol., *54:* 180–183, 1994.

55. Look, K. Y., Muss, H. B., Blessing, J. A., and Morris, M. A. Phase II trial of 5-fluorouracil and high-dose leucovorin in recurrent epithelial ovarian carcinoma. A Gynecology Oncology Group Study. Am. J. Clin. Oncol., *18:* 19–22, 1995.

56. De Graeff, A., van Hoef, M. E., Tjia, P., Heintz, A. P., and Neijt, J. P. Continuous infusion of 5-fluorouracil in ovarian cancer patients refractory to cisplatin and carboplatin. Ann. Oncol., *2:* 691–692, 1991.

57. Volpe, D. A., Tomaszewski, J. E., Parchment, R. E., Garg, A., Flora, K. P., Murphy, M. J., and Grieshaber, C. K. Myelotoxic effects of the bifunctional alkylating agent bizelesin in human, canine and murine myeloid progenitor cells. Cancer Chemother. Pharmacol., *39:* 143, 1996.

58. Gelmon, K. A., Eisenhauer, E. A., Harris, A. L., Ratain, M. J., and Workman, P. Anticancer agents targeting signaling molecules and cancer cell environment: challenges for drug development? J. Natl. Cancer Inst. (Bethesda), *91:* 1281–1287, 1999.

59. Killion, J. J., Radinsky, R., and Fidler, I. J. Orthotopic models are necessary to predict therapy of transplantable tumors in mice. Cancer Metastasis Rev., *17:* 279–284, 1999.

60. Kerbel, R. S. What is the optimal rodent model for anti-tumor drug testing? Cancer Metastasis Rev., *17:* 301–304, 1999.

61. Rosenberg, M. P., and Bortner, D. Why transgenic and knockout animal models should be used (for drug efficacy studies in cancer). Cancer Metastasis Rev., *17:* 295–299, 1999.

EXHIBIT H

1: J Natl Cancer Inst. 1979 Nov;63(5):1185-8.

Related Articles, Links

Evaluation of a "nude" mouse-human tumor panel as a predictive secondary screen for cancer chemotherapeutic agents.

Bellet RE, Danna V, Mastrangelo MJ, Berd D.

Nine established human melanoma tissue-cultured cell lines heterotransplanted in C57BL/6 "nude" mice were exposed to each of 4 chemotherapeutic agents of known clinical activity against human melanoma. Two of the therapeutic agents, 1,3-bis(2-chloroethyl)-1-nitrosourea (BCNU) and 5-(3,3-dimethyl-1-triazino) imidazole-4-carboxamide (DTIC), are known to be active against human melanoma; the other two, adriamycin and 5-azacytidine, are known to be inactive. Sterile saline served as a control agent. In 2 cell line heterotransplants, the control tumor spontaneously regressed. Of the 7 cell lines that remained for evaluation, 4 were sensitive to DTIC, 1 was sensitive to BCNU, and none was sensitive to adriamycin or 5-azacytidine. These data indicate that the nude mouse-human tumor model may be a predictive secondary screen for cancer chemotherapeutic agents.

PMID: 91697 [PubMed - indexed for MEDLINE]

Display Abstract Show: 20 Sort Send to Text

1: Br J Cancer. 1980 Oct;42(4):530-6.

Chemotherapy of human breast-carcinoma xenografts.

Bailey MJ, Gazet JC, Smith IE, Steel GG.

Five lines of human breast-carcinoma xenografts have been tested for sensitivity to cyclophosphamide, methotrexate, 5-fluorouracil, adriamycin, vincristine and melphalan, alone and in combination, using tumour growth delay as an end-point. The xenograft lines were established and passaged in mice immune-suppressed by thymectomy and whole-body irradiation. There was a considerable range of sensitivity of the different lines to the agents studied, and within this variation there was evidence that the most effective single agent or combination differed for each tumour. Combination chemotherapy was more effective than single agents in 3 of the lines, but melphalan was more effective than either combination in the other 2. It is suggested that a panel of human breast tumours grown in immune-suppressed mice may prove useful in testing new cytotoxic agents for activity against breast cancer before their use in clinical trials, and that more effective combinations of existing drugs might be designed with the aid of this system.

PMID: 6254553 [PubMed - indexed for MEDLINE]

1: Cancer Chemother Pharmacol. 1983;10(3):182-6.

Related Articles, Links

Antitumor efficacy of seventeen anticancer drugs in human breast cancer xenograft (MX-1) transplanted in nude mice.

Inoue K, Fujimoto S, Ogawa M.

To validate the usefulness of a human tumor-nude mice xenograft system as a potential model in the secondary screening of anticancer agents, the antitumor activity of 17 anticancer drugs has been studied in the treatment of a human breast cancer tumor (MX-1) transplanted to nude mice. For evaluation of the antitumor activity of the drugs we employed the LD10 predetermined in BDF1 mice as a standard therapeutic dose. Drugs were administered IV, IP, or PO, and antitumor activity was assessed by drug-induced growth inhibition measured by caliper. Among the 17 anticancer drugs, the most active compounds (maximum inhibition rate of tumor growth: greater than or equal to 90%) are mitomycin C, chromomycin A3, vincristine, vinblastine, vindesine, and hexamethylmelamine. Another group of compounds showed moderate activity (maximum inhibition rate of tumor growth: 89%-50%), these being adriamycin, daunomycin, mitoxantrone, bleomycin, 5-FU, 6-TG, and ftorafur. The remaining four drugs (peplomycin, cytosine arabinoside, 6-MP, and methotrexate) were inactive against the MX-1 tumor. These results suggested that in the nude mouse-human tumor xenograft system of the MX-1 tumor there was a good correlation between the antitumor activity of various anticancer drugs and their clinical efficacy; this system is therefore expected to be a useful model for the secondary screening system.

PMID: 6305523 [PubMed - indexed for MEDLINE]

Display Abstract Show: 20 Sort Send to Text

1: Br J Cancer. 1983 Jan;47(1):1-13. Related Articles, Links

The response to chemotherapy of a variety of human tumour xenografts.

Steel GG, Courtenay VD, Peckham MJ.

The results of a series of projects on the cytotoxic drug response of human tumour xenografts are compared. All were performed in one laboratory, using conventional CBA mice that were usually immunosuppressed by thymectomy, cytosine arabinoside treatment, and whole-body irradiation. Results on human tumours arising in 9 anatomical sites are included, with the main emphasis on colo-rectal, pancreas, breast, lung and testis carcinomas, also melanomas. Growth acceleration during successive passage of most of these tumour types was observed. When therapeutic response was measured by a growth-delay method there were wide differences in response to chemotherapy. Testicular teratomas and small-cell lung tumours responded well; breast tumours showed modest response; melanomas, colo-rectal tumours and non-small-cell lung tumours responded poorly. Studies of clonogenic cell survival were made in 11 xenografted tumour lines. They confirmed the range of responsiveness and tendency towards individuality of the growth delay data. Cell survival in most cases was exponentially related to drug dose. This compilation of a large amount of experimental data supports the belief that human tumour xenografts broadly maintain the level of chemotherapeutic responsiveness of the source tumours in man.

Publication Types:
- Review

PMID: 6336942 [PubMed - indexed for MEDLINE]

1: Cancer Treat Rep. 1987 Mar;71(3):297-304. Related Articles, Links

Use of nude mouse xenografts as preclinical drug screens: in vivo activity of established chemotherapeutic agents against melanoma and ovarian carcinoma xenografts.

Taetle R, Rosen F, Abramson I, Venditti J, Howell S.

To evaluate the utility of nude mouse xenografts as preclinical drug screens, the activity of ten established chemotherapeutic agents was evaluated against seven melanoma and three ovarian carcinoma xenografts. Xenografts were established using primary explants from patients who had not received chemotherapy and serially passaged as sc tumors in nude mice. In vivo drug activities for dactinomycin, carmustine, vinblastine, melphalan, amsacrine, cisplatin, bleomycin, mitomycin, doxorubicin, and etoposide were evaluated by 4 weekly ip injections of 10% less than LD10 doses. Plots of relative tumor growth versus time were nearly log-linear. Analysis of in vivo activity was performed using percent control growth (treated/control tumor volume) and by calculation of a novel growth delay index obtained by fitting growth curves to a quadratic regression model. Both modes of data analysis identified alkylating agents (melphalan, carmustine, and mitomycin) as the most active drugs against human melanomas. Melphalan, mitomycin, and cisplatin showed the greatest activity against ovarian xenografts. However, complete tumor regressions were noted only with melphalan, mitomycin, and cisplatin against a single ovarian tumor xenograft. Correlation analysis suggested xenograft tumor growth rate was an important determinant of drug response. These results suggest that preclinical, new-drug screening with melanoma xenografts would identify drugs such as alkylating agents as active, and may not provide an advantage over murine leukemia screens. However, screening with ovarian xenografts may more closely reflect clinical drug activity. Criteria for detecting active drugs in such systems are discussed.

PMID: 3815395 [PubMed - indexed for MEDLINE]

1: Cancer Metastasis Rev. 1988 Nov;7(3):263-84.

Human tumor xenografts as model for drug testing.

Mattern J, Bak M, Hahn EW, Volm M.

Department of Experimental Pathology, German Cancer Research Center, Heidelberg, FRG.

This paper reviews the history of xenografts, the endpoints commonly used to evaluate response and chemotherapeutic results obtained with serially maintained human tumor xenografts from different laboratories, and discusses the potential clinical relevance of the heterotransplant model for cancer chemotherapy. Specifically, an attempt is made to correlate the published xenograft data with the clinical data. Drug testing with different types of xenotransplanted tumors has shown that the response of xenografts obtained in immune-deficient animals is comparable to that in clinical practice. In addition, xenografts of a particular tumor type are able to identify agents of known clinical activity against that disease.

Publication Types:
- Review
- Review, Tutorial

PMID: 3067903 [PubMed - indexed for MEDLINE]

Display Abstract Show: 20 Sort Send to Text

1: Eur J Cancer Clin Oncol. 1988 Mar;24(3):567-73.

Preclinical phase II studies in human tumor lines: a European multicenter study.

Boven E, Winograd B, Fodstad O, Lobbezoo MW, Pinedo HM.

Department of Oncology, Free University Hospital, Amsterdam, The Netherlands.

In an attempt to increase the predictability and to extend the differential capacity of the anticancer drug development program the American National Cancer Institute has recently proposed the introduction of a screening system consisting of human tumor cell lines to select drugs in a disease-oriented fashion rather than by the previously applied drug-oriented strategy. Although this new approach offers great advantages, assay limitations can be identified in testing unknown compounds for antitumor activity in vitro. Human tumor xenografts grown in nude mice may play an additional role in the prediction of clinical activity and the assessment of the spectrum of activity of potential anticancer drugs, because they have a better relationship with the clinical situation of cancer treatment. In a European multicenter collaboration it has been proposed to use panels of human tumor lines from solid tumor types to study: the antitumor activity of three different drugs per tumor type; the reliability of 'preclinical' phase II studies by comparison of the obtained data with results of phase II clinical trials; the feasibility of this joint project, such as the methodology, the reproducibility of experimental data and the introduction of uniform activity criteria. If preclinical phase II studies in human tumor lines generate reliable results, this in vivo screening system will create a unique possibility to better identify promising clinical candidate compounds or analogs of conventional cytostatic agents as well as those tumor types likely to respond to the selected investigational drugs.

PMID: 3383962 [PubMed - indexed for MEDLINE]

Display Abstract Show: 20 Sort Send to Text

Cancer Research, Vol 52, Issue 21 5940-5947, Copyright © 1992 by American Association for Cancer Research

ARTICLES

Phase II preclinical drug screening in human tumor xenografts: a first European multicenter collaborative study

E Boven, B Winograd, DP Berger, MP Dumont, BJ Braakhuis, O Fodstad, S Langdon and HH Fiebig
Department of Medical Oncology, Free University Hospital, Amsterdam, The Netherlands.

In a European joint project carried out in 6 laboratories a disease-oriented program was set up consisting of a panel of 7 tumor types, each represented by 4 to 8 different human tumor lines, for secondary screening of promising anticancer drugs. Human tumor lines were selected on the basis of differences in histology, growth rate, and sensitivity to conventional cytostatic agents. Xenografts were grown s.c. in nude mice, and treatment was started when tumors reached a mean diameter of 6 mm in groups of mice where at least 6 tumors were evaluable. Drugs were given at the maximum tolerated dose. For evaluation of drug efficacy, median tumor growth curves were drawn, and specific growth delay and treated/control x 100% were calculated. Doxorubicin (8 mg/kg i.v. days 1 and 8) was effective (treated/control < 50%, and specific growth delay > 1.0) in 0 of 2 breast cancers, 1 of 3 colorectal cancers, 2 of 5 head and neck cancers, 3 of 6 non-small cell lung cancers, 4 of 6 small cell lung cancers, 0 of 3 melanomas, and 3 of 6 ovarian cancer lines. Amsacrine (8 mg/kg i.v. days 1 and 8) was not effective, while datelliptium (35 mg/kg i.p. days 1 and 8) was active against 2 of 6 small cell lung cancer lines. Brequinar sodium (50 mg/kg i.p. days 1-5) showed efficacy in 4 of 5 head and neck cancers, 5 of 8 non-small cell lung cancers, and 4 of 5 small cell lung cancer lines. The project has been shown to be a feasible approach. Clinical activity for doxorubicin and inactivity for amsacrine against solid tumor types was confirmed in the human tumor xenograft panel. Additional anticancer drugs will be studied in the European joint project to further define the reliability of this novel, promising screening approach.

This article has been cited by other articles:

Annals of Oncology

Annals of Oncology, Vol 5, Issue 5 415-422, Copyright © 1994 by European Society for Medical Oncology

ARTICLES

Preclinical phase II studies in human tumor xenografts: a European multicenter follow-up study

S. P. Langdon, H. R. Hendriks, B. J. Braakhuis, G. Pratesi, D. P. Berger, O. Fodstad, H. H. Fiebig and E. Boven
ICRF Medical Oncology Unit, Western General Hospital, Edinburgh, UK.

BACKGROUND: The EORTC New Drug Development Office has initiated a multicenter collaborative program to evaluate the use of human tumor xenografts to predict phase II clinical activity. A first study confirmed the efficacy of doxorubicin and inactivity of amsacrine against human tumor xenografts (Boven et al., Cancer Res: 52, 5940, 1992). In the follow-up study reported here, the activities of cisplatin, AZQ (diaziquone), pazelliptine and retelliptine have been evaluated against a panel of 40 established tumor lines grown subcutaneously in nude mice. DESIGN: The xenografts used represent carcinomas of the breast, colon, head+neck, ovary, small cell lung cancer (SCLC), non-small cell lung cancer (NSCLC) and melanoma. Drugs were administered intravenously on days 0 and 7. Doses were for cisplatin 5 mg/kg, AZQ 3-7 mg/kg, pazelliptine 20-80 mg/kg and retelliptine 6-12.5 mg/kg and were selected to give a median loss of about 10%-15% body weight. RESULTS: When activity was defined as a specific growth delay > 1 and a tumor growth inhibition > 50%, then cisplatin demonstrated activity in 15 of 40 xenografts tested (3 of 5 breast, 1 of 6 colon, 0 of 5 head+neck, 2 of 6 NSCLC, 4 of 7 SCLC, 1 of 5 melanoma and 4 of 6 ovarian cancers); AZQ was active in 23 of 38 xenografts (2 of 3 breast, 2 of 7 colon, 4 of 5 head+neck, 3 of 6 NSCLC, 6 of 6 SCLC, 2 of 5 melanoma, 4 of 6 ovarian cancers); pazelliptine was active in 2 of 38 xenografts (1 of 5 breast cancers, 1 of 5 melanoma) while retelliptine was active in 1 of 39 xenografts (a breast cancer xenograft) tested. CONCLUSIONS: These results are reasonably consistent with the clinical activity of cisplatin, but overpredict the clinical efficacy of AZQ. Since pazelliptine and retelliptine are investigational compounds, the clinical phase II studies will provide a prospective test for this model. The results of the present study and the previous one indicate that the human tumor xenograft model could be suitable for predicting the activity of novel compounds to be developed for treatment of cancer patients.

This article has been cited by other articles:

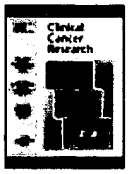

EXHIBIT I

Mini-Review

The Use of 3-D Cultures for High-Throughput Screening: The Multicellular Spheroid Model

LEONI A. KUNZ-SCHUGHART,[1] JAMES P. FREYER,[2] FERDINAND HOFSTAEDTER,[1] and REINHARD EBNER[3]

Over the past few years, establishment and adaptation of cell-based assays for drug development and testing has become an important topic in high-throughput screening (HTS). Most new assays are designed to rapidly detect specific cellular effects reflecting action at various targets. However, although more complex than cell-free biochemical test systems, HTS assays using monolayer or suspension cultures still reflect a highly artificial cellular environment and may thus have limited predictive value for the clinical efficacy of a compound. Today's strategies for drug discovery and development, be they hypothesis free or mechanism based, require facile, HTS-amenable test systems that mimic the human tissue environment with increasing accuracy in order to optimize preclinical and preanimal selection of the most active molecules from a large pool of potential effectors, for example, against solid tumors. Indeed, it is recognized that 3-dimensional cell culture systems better reflect the in vivo behavior of most cell types. However, these 3-D test systems have not yet been incorporated into mainstream drug development operations. This article addresses the relevance and potential of 3-D in vitro systems for drug development, with a focus on screening for novel antitumor drugs. Examples of 3-D cell models used in cancer research are given, and the advantages and limitations of these systems of intermediate complexity are discussed in comparison with both 2-D culture and in vivo models. The most commonly used 3-D cell culture systems, multicellular spheroids, are emphasized due to their advantages and potential for rapid development as HTS systems. Thus, multicellular tumor spheroids are an ideal basis for the next step in creating HTS assays, which are predictive of in vivo antitumor efficacy. (*Journal of Biomolecular Screening* 2004:273-285)

Key words: cell-based assay, 3-D culture, spheroid, co-culture, anti-tumor drug testing

INTRODUCTION

ADVANCES IN GENOMICS AND PROTEOMICS have revolutionized drug discovery and target validation and have already started to provide researchers and the pharmaceutical industry with a rapidly increasing number of molecular targets for therapeutic intervention. Successful development and selection of the most active drug leads for a particular disease, such as cancer, requires reliable and robust test systems. Today, most pharmaceutical companies use a set of specific high-throughput screening (HTS) assays as the initial step in drug lead discovery (see Figure 1). Numerous HTS assays have been established over the past 5 to 10 years, incorporating a broad range of technological and instrument advances. This promising process is still ongoing, but the value of any individual HTS assay to predict in vivo efficacy has not been firmly established. One field of research and development for HTS focuses on automation and miniaturization issues to provide ultra–high-throughput approaches.[1,2] Another field concentrates instead on the design and adaptation of novel, more complex test systems to gain deeper insight into the effects and functions of molecules in a cellular context, that is, within the complex milieu of an intact cell. Currently available cell-based assays can be divided into 3 major categories: (a) generic cellular responses to external stimuli (eg, proliferation, viability, cytotoxicity); (b) assays to monitor signal transduction pathways (eg, ion channels, second messengers, kinase activation); and (c) cellular responses at the transcriptional/translational level (eg, reporter gene or protein,

[1]Institute of Pathology, University of Regensburg, 93042 Regensburg, Germany.

[2]Bioscience Division, Los Alamos National Laboratory, Los Alamos, NM, USA.

[3]Avalon Pharmaceuticals Inc., Germantown, MD, USA.

Received Feb 2, 2004, and in revised form Feb 20, 2004. Accepted for publication Mar 1, 2004.

Journal of Biomolecular Screening 9(4); 2004
DOI: 10.1177/1087057104265040

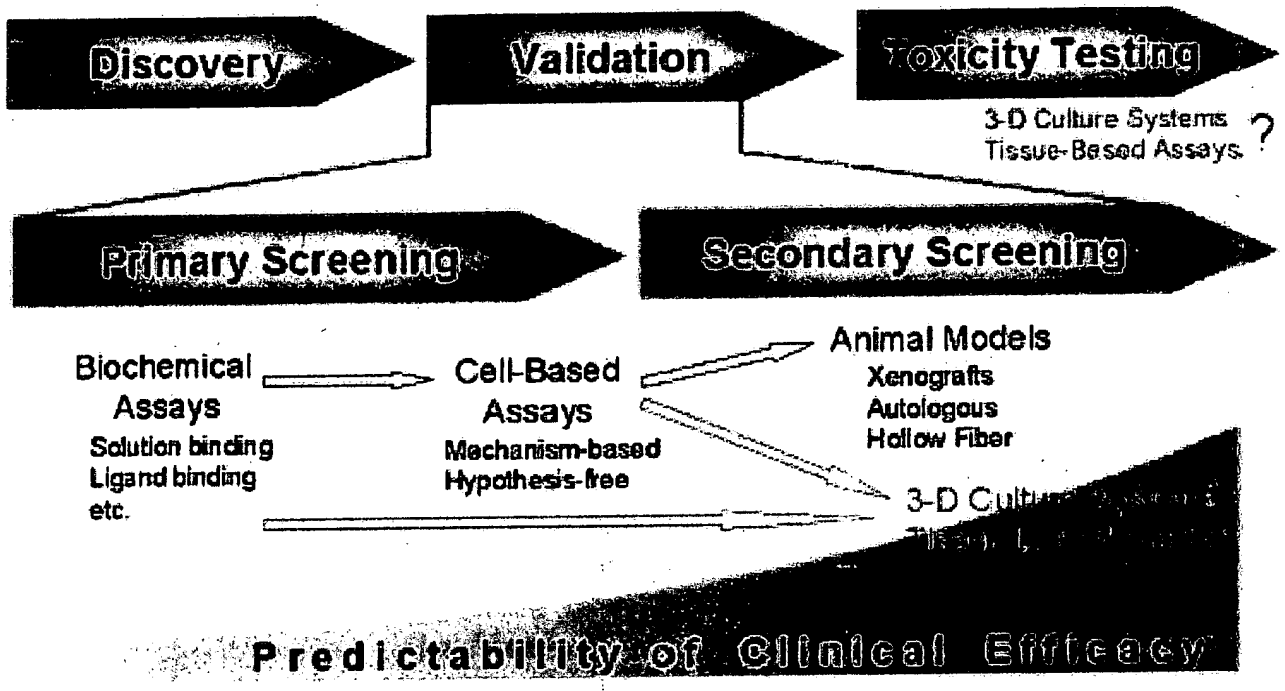

FIG. 1. Overview of the drug discovery process focusing on current strategies for the preclinical validation of antitumor candidate therapeutics via primary and secondary screening tools. Although utilization of 3-D culture assays in routine toxicity testing of candidate therapeutics is still speculative, incorporation of 3-D culture systems and tissue-based assays such as the multicellular tumor spheroid model as a secondary screening tool in drug discovery and development operations has the potential to allow increased predictability of clinical efficacy from in vitro validation and to help minimize or replace whole animal test models, thereby contributing savings in both development cost and time. This is relevant for a broad variety of drug candidates including those that affect cellular phenotype/differentiation, proliferative activity, signaling pathways, transcriptional activity, or physiological and metabolic behavior.

transcription factor activation). The latter 2 are functional, cell-based assay technologies that reflect a recent shift in the anticancer drug discovery and screening strategy from empirical to mechanistic approaches.[3-7]

Today, the common approach used by many pharmaceutical companies to screen small-molecule libraries in biochemical-based or ligand-binding assays, and to build new classes of lead compounds, is frequently complemented by a series of in vitro toxicity and functional HTS assays. However, although cell-based screening is established in the drug discovery process, particularly in the many well-described cell line models for cancer,[3] its value in predicting clinical response to new agents is limited. This lack of predictability of commonly employed 2-dimensional (2-D) cellular assays is attributable to the fact that such systems do not mimic the response of cells in the 3-D microenvironment present in a tissue, or tumor, in vivo. The focus of this review is on HTS for anticancer therapy, although the basic concepts discussed should be applicable to other disease states. We will discuss the role of 3-D in vitro culture systems in improving the ability of cell-based HTS to predict clinical effectiveness and also their potential to replace some animal models, as illustrated in Figure 1.

IN VIVO VERSUS CELL-BASED ASSAYS FOR ANTI-TUMOR DRUG TESTING

It is generally recognized that rodent test systems will remain necessary for pharmacokinetic (dosage, formulation, administration, half-life) and toxicological (systemic and organ specific) evaluation of candidate therapeutic compounds for at least decades to come. However, the number of animal models used in the initial discovery of lead compounds has already begun to gradually decline, and the same is expected in target validation. This tendency is driven not only by ethical and economic concerns but also by the fact that xenograft activity is often not predictive of clinical efficacy, particularly for a specific histological tumor type. Thus, pharmaceutical corporations often maintain 30-35 xenograft models simultaneously to identify the few that are active for a particular compound, thereby increasing the predictive value of their in vivo testing. Another strategy is reflected by the shift in the screening policy of the U.S. National Cancer Institute Developmental Therapeutic Program implemented in the late 1980s involving replacement of the P388 in vivo tumor model by an in vitro anticancer drug screen. Today, the 60-cell line screen is preceded by a 3-cell

Table 1. Summary of Three-Dimensional Cell Culture Systems Currently Employed in Tumor and Normal Cell Research

System	*Description*	*Uses*
Multicellular spheroid	Spherical aggregate of cells in static or stirred suspension culture	Tumor cell biology, therapy resistance, cell-cell interactions, invasion, drug penetration, modeling, tumor markers, nutrient gradients, tumor cell metabolism[14-16]
Cellular multilayer	Layers of cells cultured on top of a porous membrane	Drug transport and binding, therapy resistance, invasion[17,18]
Matrix-embedded culture	Single cells or aggregates embedded in a porous extracellular matrix	Tumor cell biology, cell-cell interactions, cell migration and invasion, artificial organs[19,20]
Hollow-fiber bioreactor	Cells cultured within a network of perfused artificial capillaries	Tumor cell metabolism, therapy resistance, artificial organs[21-23]
Ex vivo culture	Piece of tissue or tumor excised and cultured in vitro	Therapy resistance, cell-cell interactions, tumor markers[24,25]

The list of uses and literature citations is not intended to be exhaustive but rather to reflect the most common types of studies published.

line, 1-dose prescreen, and followed by in vivo application in a hollow fiber assay.[8] Recent reviews on the NCI-DTP experience revealed both the hollow fiber model and the in vitro human cancer cell line assay to be useful predictors of xenograft activity, with the NCI 60-cell line in vitro cancer drug screen yielding slightly higher confidence values than the hollow fiber assay.[3,8,9] However, no significant correspondence was observed between any single in vitro or in vivo preclinical model and actual clinical results. Only for compounds with activity in a large proportion of tested xenograft models was there any correlation with ultimate activity in at least some phase II trials. At first glance, this would imply that in vitro assays with monolayer cultures can already be as predictive of clinical efficacy at this stage of the drug development process as the currently used common animal test systems. Although controversy continues in this arena, several reports have emphasized the limited predictive value of routinely applied in vitro and in vivo drug screening models for clinical efficacy.[4,5,10-12] The shortcomings of these models lend further strong support to the development of complex, 3-D culture systems that better reflect the in vivo pathophysiological situation in human tumor tissues to soon replace some animal test strategies.

Indeed, cell-based models that are able to predict in vivo, clinical behavior offer obvious advantages in savings of time and money. However, as is the case with the xenograft model, many of the current in vitro systems for cell-based screening and target validation remain unreliable and nonpredictive for clinical efficacy.[4,5,10] We therefore entirely agree with Bhadriraju and Chen[13] who proposed in a recent review article that "a principle component of this failure results from our lack of understanding of, and inattention to, how to culture cells specifically so that they phenotypically represent their in vivo counterparts." It is beyond dispute that cells can behave differently depending on their environment and the culture conditions. For example, the choice of medium and medium supplements (eg, serum, growth factors, pH, oxygen), cell density, and the composition of the culture surface have a critical impact on cell proliferation, differentiation, migration, and death by affecting intracellular signal transduction. This interferes with both random and target-specific screening approaches, leading to results with high variability and questionable relevance. A better understanding of how the cellular microenvironment modulates the cellular phenotype is necessary to design more appropriate physiologic and pathophysiologic in vitro models.

Currently available cell-based assays for HTS, although retaining more cellular architectural features than cell-free biochemical test systems, still reflect a highly artificial cellular environment. For economic and ethical reasons, test systems that mimic the human tissue environment with increasing accuracy will soon need to be considered to optimize preclinical and preanimal selection of the most active molecules from the large and growing pool of drug candidates. Efforts to establish and optimize new tools for advanced cell-based in vitro screening are necessary and should be encouraged. As an example, the recent use of microfabrication technologies to control cell adhesion, cell shape, intercellular contact, and heterologous cell interactions is a promising new attempt to design better and more economic in vitro models.[13] However, it is as important to recognize the power of established sophisticated in vitro model systems that have been applied by the academic community for nonscreening purposes to better mimic the in vivo situation. Three-dimensional culture systems, either cell line or tissue based, are known to reflect the in vivo behavior of many cell types and are promising approaches for advanced drug screening. The most common 3-D cell culture systems employed in basic and applied tumor biology are described in Table 1.[14-25] A major reason that these and other 3-D culture systems have not entered the drug screening process to date is the lack of simple, controlled techniques and protocols for rapid, standardized assay of cellular responses in situ. In addition, the emphasis in improvements for in vitro drug screening has been on increasing the throughput of simple culture systems (eg, 384-well plates, microfabrication of miniaturized culture chambers, single-cell analysis methods) with little regard for whether the basic culture system being used is predictive of in vivo activity. However, as discussed in detail below, there are possibilities to adapt certain HTS methods originally

developed for monolayers to culture systems with higher complexity. This may well improve the in vivo predictability of the screening system while maintaining a high-throughput format.

RATIONALE FOR USING COMPLEX CELL SYSTEMS IN ANTITUMOR DRUG TESTING

It is well known that many cells of normal and malignant origin lose some of their phenotypic properties when grown in vitro as monolayer or suspension cultures. Current attempts to obtain, and maintain, functional differentiation of human cells similar to that seen in vivo can be divided into 3 different approaches and combinations of these: (a) culturing of primary tissues or isolated early passage primary cells, (b) application of established cell lines on specially manufactured growth surfaces and/or in controlled heterologous monolayer systems, and (c) propagation of established cell lines in 3-D culture systems.

The use of primary cells in vitro is preferable in several respects but is hampered by limited availability and high variability, as well as by ethical restrictions, at least with respect to human tissue. However, there are attempts to use such material in drug testing. Notable is the effort to establish patient-specific therapeutic test systems for specific tumor entities, such as the ex vivo ATP-based chemosensitivity assay (ATP-TCA), which is based on the 2-D culturing of tumor cells isolated from primary tissue biopsies.[26-29] Also, in parallel to improvements in the tissue engineering field, diverse culture approaches have been developed that may allow reproducible maintenance of viability and differentiation in isolated primary tissue material of different origin in a 3-D format, such as the NASA bioreactor,[30-33] various perfusion-type or gradient container systems,[34-41] or the tumor fragment spheroid model.[42-44] Some of the above-mentioned systems are still under refinement to better match specific properties of differentiated tissues.[41]

Because the availability of primary material will always be the limiting step for HTS, there is increasing demand in the pharmaceutical industry for advanced in vitro test systems based on established human cell lines. This requires restoration of morphological and functional features of the corresponding tissue in vivo. However, the formation of tissue structures is highly inhibited in monolayer culture due to the strong affinity of cells to most artificial substrates and the restriction to a 2-D space, severely limiting intercellular contacts and interaction. It is beyond the scope of this article to detail progress in engineering 2-D or pseudo-3-D microenvironments that mimic the in vivo situation,[13] but the recent advances in heterologous co-culture systems to reassemble some in vivo features of cells and tissues should be noted.[45-48] Three-dimensional heterotypic collagen assays that were primarily applied in the past few years to resemble breast epithelial morphogenesis and neoplasia are a promising approach that could also be useful for antitumor drug screening.[47,49] In the anticancer drug development arena, multiple in vitro assays are commercially available to monitor particular steps in the angiogenic cascade and the effect of antiangiogenic compounds. Most of these assays utilize multiwell plates with surfaces coated with natural or artificial ECM components and established endothelial cell lines. A promising new type of assay consisting of endothelial cells and fibroblasts in co-culture was recently shown to more closely resemble the in vivo capillary bed when compared to the commonly used Standard and Growth Factor Reduced Matrigel™ assays.[50,51] Tubule formation by endothelial cells reflects to some extent a switch from a 2-D to a pseudo-3-D structure (The term *pseudo-3-D* is used because long-term co-culturing results in a multilayered structure, but the multilayering is restricted to areas showing formation of vessel-like structures and does not exceed 3-4 cell layers). This interesting co-culture assay has the disadvantage of requiring 10-14 days of culture. Also, the system has not been made amenable to high-throughput usage so far. However, this holds true for most complex culture systems, even for some that are well established and have been used by cell biologists for decades.

Three-dimensional cultures have been utilized in biomedical research since the first half of the 20th century to gain deeper insight into the mechanisms of organogenesis and expression of malignancy. Today, it is well known that in contrast to conventional monolayer or suspension cultures, 3-D cultures can restore specific biochemical and morphological features similar to the corresponding tissue in vivo. The relevance of this observation for mechanistic studies and advanced drug testing has long been ignored by both academic researchers and the pharmaceutical industry. The National Cancer Institute program Signatures of the Cancer Cell and Its Microenvironment is a new $40 million per year effort designed to investigate the impact of the microenvironment on tumor cell behavior. This initiative will emphasize 3-D culture technologies and will clearly foster the acceptance of such approaches. Also, Alison Abbott's report "Biology's New Dimension"[52] and the corresponding commentary of the editor, "Goodbye Flat Biology," were overdue and more than welcome by scientists working in the field. In this news feature, experts in cell biology emphasize the basic necessity for 3-D culture systems before turning to whole-animal studies, for therapeutics development as well as basic research in tumor biology. Also in this article is a prediction by the chief scientific officer of a large pharmaceutical company, which has attracted major attention: "In 10 years, anyone trying to use 2-D analyses to get relevant and novel biological information will find it difficult to get funded." With respect to the utilization of relevant biological information from 3-D culture analyses for HTS approaches in drug discovery and development, there is a strong need for intercollaborations between the pharmaceutical industry and academic institutions both to provide proof of predictive value and to rapidly reach practical feasibility of such 3-D systems for sophisticated drug screening. Indeed, advances in tissue engineering, including the development of diverse bioreactor systems such as those mentioned above and of 3-D scaffolds (eg, bioactive, biodegradable, or nondegradable polymers), have improved the variety, fidelity, and quantity of models that can be utilized in cancer research. However, only a small number of 3-D model systems are sufficiently well characterized to simulate the

pathophysiological cellular microenvironment in a tumor, reconstitute a tissue-like cytoarchitecture with cell-to-cell and cell-to-matrix interactions, and present growth, differentiation, and therapy response similar to that seen in tumors in vivo.

The classical and best described 3-D tumor model system, which fulfills all of the characteristics just described, was not mentioned in the cited news feature: the multicellular tumor spheroid model (MCTS). This system was adapted for cancer research in the early 1970s by Sutherland and associates[53,54] and is in use in many laboratories throughout the world today. The spheroid culture model has not only considerably contributed to our knowledge of cellular response to a variety of treatment modalities but also has been critical in more basic studies investigating the microenvironmental regulation of tumor cell physiology.[15,16,55-58] In contrast to the other 3-D in vitro models described in Table 1, MCTS have considerable potential for application as HTS systems in anticancer drug development. This potential as well as the limitations of this unique 3-D culture system shall thus be highlighted.

MULTICELLULAR TUMOR SPHEROIDS

Over the past 30 years, the (patho)physiological behavior of diverse tumor cell types of animal and human origin has been studied in MCTS culture in detail. Today, it is well accepted in the academic community that MCTS provide an important supplement to the use of monolayer cultures and animal in vivo systems due to their intermediate complexity,[45,56] as illustrated in Figure 2. Accordingly, MCTS have served as a model for a variety of experimental therapy studies using radiotherapy, chemotherapy, radioimmunotherapy, cell- and antibody-based immunotherapy, hyperthermia, gene therapy, and photodynamic treatment.[55-71] MCTS have also been used extensively in basic studies of the microenvironmental regulation of proliferation, viability, energy metabolism, nutrient metabolism, invasion, cell-cell interactions, and extracellular matrix composition. Based on their long-term experience, experts in the field agree with Mueller-Klieser's final conclusion in a 2000 review article: "Keeping in mind the fundamental differences between monolayers and spheroids with regard to cellular sensitivity to various treatment modalities, tumor spheroids should be mandatory models in applied cancer research, for example in major programs for drug screening and development."[15] This article is just one out of a review series published in the November 2000 issue of *Critical Reviews in Oncology/Hematology*, which was devoted to 3-D spheroid cultures and is recommended reading for both spheroid specialists and laymen. A general survey of previous research with the spheroid model, including technical descriptions of a variety of spheroid methods, is given in 2 rather dated but still very informative books.[72,73] More recent book chapters[46,74] and several review articles published within the past 5 years focusing on different applications of spheroids[16,45,57,75,76] provide further information to define the rationale for developing MCTS technology for HTS of chemotherapeutic

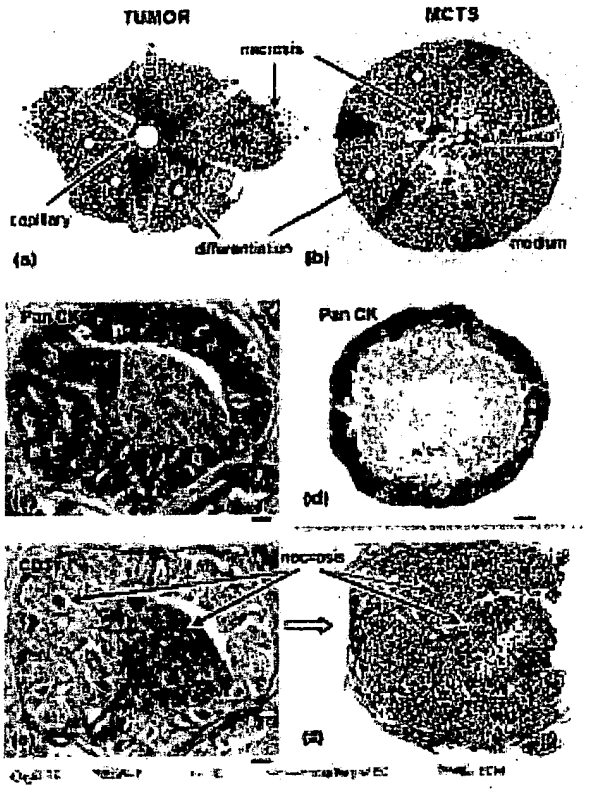

FIG. 2. Schematic illustration of the analogy between (*a*) tumor microregion and (*b*) multicellular tumor spheroid (MCTS) demonstrating the pathophysiological inside-out situation in MCTS (modified from Kunz-Schughart, 1999). (*c/d*) Labeling of tumor cells in 5 µm sections of paraffin-embedded material using a monoclonal Pan-cytokeratin (Pan-CK) antibody (clone KL1, Beckman Coulter, Fullerton, California), 2-step routine immunohistochemical staining with DAB (3'3'diaminobenzidine) as chromogen, and hematoxylin counterstain: (*c*) microregion of a colon carcinoma (G3), and (*d*) HT29 colon tumor spheroid. (*e*) Parallel section of colon carcinoma shown in (*c*) stained with the endothelial cell marker CD31 (monoclonal mouse–anti human IgG1, DakoCytomation, Hamburg, Germany) to visualize capillaries primarily located in the stromal tumor areas. (*f*) Schematic illustration of the G3 colon carcinoma shown in (*c/e*) to visualize the distribution of different cell types in this tumor microregion with TC, tumor cells; F, fibroblasts/fibroblastoid cells; EC, endothelial cells; IC, immune cells, for example, tumor-associated macrophages; ECM, extracellular matrix. Bar, 100 µm.

drug candidates. This rationale is based on the following 4 important features of MCTS.

First, MCTS reestablish morphological, functional, and mass transport features of the corresponding tissue in vivo. In particular, tumor cells in MCTS restore a differentiation pattern similar to that observed in vivo, which is maintained for several weeks of culture.[16,55,56,77-79] These features are initiated and maintained by the tumor cell–derived extracellular matrix (ECM) assembly and a

complex 3-D network of cell-to-cell and cell-to-matrix interactions, which are largely absent from monolayer cultures. In addition, the 3-D spheroid structure is relevant for both the modeling of distribution and function of (patho)physiologically occurring factors in tissues, as well as the penetration, binding, and bioactivity of drugs.

Second, MCTS approximate many characteristics of avascular tumor nodules, micrometastases, or intervascular regions of large solid tumors with regard to both tumor growth kinetics and pathophysiological micromilieu (Figure 2). Analogous to solid tumors and metastases in vivo, spheroid growth can be mathematically modeled by the Gompertz equation as well as by several more biologically based mathematical models that have been applied to tumors.[67,80-85] A proliferation gradient is observed in spheroids, with proliferating tumor cells at the periphery, cell-cycle-arrested cells at larger distances from the surface, and a necrotic core in most spheroids larger than 400-500 μm. In parallel, inward oxygen and nutrient gradients as well as outward catabolite gradients are present, analogous (again) to the situation in poorly vascularized regions of solid tumors. These variations in cellular physiology and tumor micromilieu are associated with alterations in sensitivity to a wide variety of anticancer therapies in both tumors and spheroids.

Third, the well-defined, spherically symmetric geometry of MCTS allows direct comparison of structure to function, that is, the microenvironmental gradients that determine spheroid morphology are spatially correlated with the changes in cellular physiology. This has several advantages for the use of spheroids as in vitro tumor models. A primary advantage is that assays of cellular physiology and drug response can be directly related to location in the microenvironment, either by a variety of in situ histologic assays[16,86-89] or on cell subpopulations isolated from different spheroid regions.[16,90-94] A second advantage is that the spherical symmetry enables relatively simple theoretical analyses, for example, to predict radiation response,[95,96] drug penetration, and binding/activity[97-99] or to interpret the regulation of cellular physiology, proliferation, and viability.[67,80-82,84,100] A third advantage of the spheroid geometry is that aggregates cultured from the same cell type under the same external conditions are essentially identical in structure, morphology, microenvironment, and cellular physiology. This allows the efficient generation of a few up to literally thousands of individual, identical cultures for assay.

Finally, spheroids are amenable to the co-culture of different cell types, in particular, tumor cells and normal cells, such as stromal fibroblasts, endothelial cells, or cells of the hematopoietic/immune system.[16,45,101-106] These co-cultures retain some, if not all, of the advantages mentioned above for homologous cultures, notably the intimate and complex cell-cell and cell-matrix interactions that are present in tumors in vivo. Heterologous spheroid co-cultures have not been as extensively utilized, or even characterized, as those of pure tumor cell spheroids. However, improvements in techniques and development of more rapid assay systems promise to expand the spheroid co-culture into a very unique and multifunctional in vitro drug-testing system, as discussed in more detail below.

Due to these characteristics, MCTS have become a powerful tool to study therapeutic problems associated with metabolic and proliferative gradients, for example, the treatment sensitivity of tumor cells chronically deprived of nutrients. Thus, MCTS serve as a well-controlled, 3-D experimental, and theoretical model to better estimate in vivo antitumor effective dose ranges and treatment modalities. MCTS come into particular focus with the expectation that some lead candidates designed via modern drug discovery processes to precisely target tumor cells not only should attack the primary tumor and local relapse but also be effective against metastatic disease. As a model of avascular micrometastases (eg, diameter < 1 mm), spheroids can uniquely contribute to the understanding of, and screening for, drug penetration and the local pattern of cellular uptake and effectiveness.

EXTENSIONS TO THE USE OF THE MCTS MODEL

The reflection of additional aspects of the in vivo situation may be desired not only for cancer research but also for drug screening purposes. Thus, application of different therapy-responsive tumor cells in mixed or mosaic spheroids[61,61,107-111] or tumor and stromal host cells in spheroid co-culture[16,45,101-106] is a promising approach to further mimic the heterologous cellular environment in a solid tumor or at sites of metastasis. Indeed, in addition to the application of mixed cell populations on nonadherent surfaces, there is a wide range of strategies to co-culture different normal and tumor cell types using spheroids, each with particular advantages and disadvantages, and for specific fields of application. MCTS can, for example, be grown on monolayer cultures of fibroblasts and endothelial cells to investigate specific host-tumor cell interactions. Culturing MCTS on confluent endothelial cells with an underlying ECM is adequate to investigate aspects of tumor cell evasion and to evaluate endothelial cell injury by tumor cells. Confrontation cultures of MCTS with endothelial cell aggregates in a collagen gel or with embryonic stem cells (embryoid bodies) have been established to study endothelial cell differentiation and sprouting phenomena in vitro.[102,112-114] The application of fibroblast spheroids allows investigation of some tumor cell invasion/migration phenomena by adding tumor cell suspensions, and also enables one to study those tumor cells that do not form MCTS by themselves. Incubation of tumor or stromal spheroid cultures of defined sizes with immune cell suspensions is an interesting approach to mimic local immune responses, including migration and differentiation/activation processes.[42,101,103,105,115,116] The latter spheroid co-culture systems have been primarily used to gain deeper insight into the reciprocal interactions between tumor cells and their cellular environment, rather than for drug testing. However, it is expected that adjacent host cells can affect tumor cell drug sensitivity, and therefore spheroid co-culture systems could be utilized both for advanced in vitro

drug testing and to screen agents that affect the host-tumor interaction.

Although the attempt to routinely initiate spheroid growth directly from patient tumors for patient-specific predictive drug testing has had relatively little success, MCTS still serve as an excellent in vitro screening system in mechanistic studies of drug penetration, binding, and action (ie, with respect to new, innovative therapeutic strategies such as combination therapy, administration of drugs under defined environmental conditions, or treatment with toxin-conjugated antibodies). Bearing in mind, for example, that the heterogeneity in the binding of monoclonal antibodies depends on both cell and antibody type, as well as on cell cycle and metabolic status of the cells,[88,98,117-120] spheroid mono- and cocultures should be considered as a screening tool for local penetration, distribution, and efficacy of new drug candidates.

A final area of potential for MCTS in drug testing involves the additional culture of spheroids from normal, untransformed cells. The current literature indicates that normal cell spheroids can, with limitations, be applied to study some developmental and functional aspects of normal cells and tissues such as hepatocytes/liver,[121-125] chondrocytes/cartilage,[126-128] retinal cells forming so-called retinospheroids,[129-132] trabecular cells showing a network tissue structure in spheroid culture,[133] and pancreatic epithelial cells producing hollow spheres.[134,135] The patterns of morphological, biological, and functional development seen in these cultures are, in many respects, consistent with the differentiation seen in vivo. To date, nonhuman cell types are most frequently applied in normal spheroid culture systems; adaptation to cells of human origin would be preferable but will in most cases be limited due to availability and ethical restrictions. However, provided the limitations of the spheroid model for normal cells are recognized and respected (eg, pure normal tissue-type spheroids should not show necrosis), normal cell spheroids represent a potentially powerful tool for application in initial toxicity assays or in confrontation/mixed cultures of tumor and normal cell types[16,45] for the evaluation of drug selectivity and specificity.

DEVELOPMENT OF SPHEROIDS FOR HTS

Application of 3-D culture systems for drug screening, including homotypic MCTS, is hampered by lack of standardized, rapid analytical tools. The only systematic study using various methods for assaying cytotoxic effects in spheroids is now somewhat dated and involved only small spheroids without central necrosis,[136,137] thus limiting its relevance for evaluating drug effects on hypoxic and cell-cycle arrested tumor cell populations in nonperipheral, viable regions present in most spheroid types with a diameter of ≥ 500 μm (see Figure 2). Fortunately, one of the most widely used spheroid production techniques involves culture of a single spheroid in each well of an agar-coated multiwell plate.[16,46,72] Thus, there are several screening techniques currently applied to monolayer cultures in a multiwell plate format that should be easily adapted to spheroids, such as various assays for cytotoxicity, proliferation, drug binding, apoptosis, and ATP level. Simple measurement of the growth or shrinkage of spheroids can be accomplished by standard phase-contrast microscopy and computer image analysis, something that is very difficult to do accurately with monolayer or multilayer cell cultures. Commercial automated microscopy systems could be easily configured to provide a rapid method for screening drugs for effects on spheroid growth. A recent approach for toxicological and biomedical testing with some potential for adaptation to HTS with spheroid cultures is a so-called biohybrid sensor system, which is a new type of bioelectrical microarray for 3-D in vitro tissues on the basis of electrode/spheroid surface impedance measurements.[138-140] Although these HTS methods would be useful as an initial screen for drug activity in spheroids, the response would be an average from all the cells in the aggregate. Even though such a screening system would still incorporate the advantages of the 3-D in vitro model discussed above, any information on differential response of cells at different locations in the spheroid would be lost.

There are other possibilities to develop new screening methods that would take better advantage of the symmetrical morphology, microenvironment, and cellular physiology present in spheroids, as discussed above. As an example, work is under way in our laboratories to develop confocal microscopy methods for rapidly measuring drug penetration into individual spheroids, which could potentially be automated into a high-throughput approach. Here, the advantage of the MTCS culture system is the fact that drug candidates must penetrate a tumor-like tissue to be effective. The effectiveness of 3-D model systems for studying drug penetration effects has been established both in MCTS and in cell multilayers.[18,58,97,141-150] Cell multilayers are not easily adapted to an HTS approach; however, the use of spheroids opens up a whole new area of in vitro screening for the penetration and binding of drugs in a 3-D tissue-like structure. Analogous to the case with cellular assays, simple assays of total drug binding in individual tumor and host stromal spheroids in a multiwell format represent an easy system for screening drugs with different binding properties. Following drug uptake as a function of time in individual spheroids would allow kinetic analysis and perhaps even the extraction of effective diffusion coefficients, as has been demonstrated for bulk cultures of spheroids.[151-153] In addition, it should be possible to develop simple staining methods for measuring the extent of necrosis in intact, individual spheroids, which would then provide an assay for drug effects on the viability of the inner-region spheroid cells. There are certainly other staining techniques available that could be applied to an imaging-based screening system for MCTS, such as measuring apoptosis, proliferation, and various metabolism markers. Development of HTS techniques that measure the response of specific subpopulations in spheroids (eg, hypoxic cells, nonproliferating cells) would considerably enhance the usefulness of MCTS as a drug-screening tool, particularly in light of efforts under way to design drugs targeted against specific microenvironmental adaptations.

Another area that holds promise for HTS using spheroids is the use of microfabrication and other miniaturization techniques for cell cultures. Because most of these techniques are directed toward very small numbers of cells, or even single cells, they should be relatively easy to adapt to larger sized spheroid aggregates. One could envision a microfluidic device that contained large numbers of individual spheroids in separate culture chambers equipped with perfusive nutrient supply. Such a device could be combined with a computer-controlled imaging system to measure spheroid growth or drug penetration as discussed above. One could also potentially use the microfluidic system to introduce test compounds and measure the kinetics of spheroid response.[139,140]

One limitation to the use of spheroids for HTS is the fact that it takes a relatively longer time for the aggregates to grow as compared to monolayer cultures, especially if one wants to use spheroids of sufficient size to contain gradients in proliferation and a central necrotic core. The length of time for a typical tumor spheroid to grow from a few-cell aggregate to a large structure with proliferative and viability gradients ranges from 2 to 4 weeks. One could "jump-start" this process by forcing the aggregation of large numbers of cells into a single spheroid in a culture well, but it would still take a few days, at a minimum, for the microenvironmental and pathophysiological gradients to develop. However, for most HTS applications, only the time required to set up the assays is extended: the actual screening of drugs could be done as rapidly as with traditional monolayers once the MCTS are established. Considered in the overall context of an HTS method, the advantages of using MCTS for anticancer drug screening would appear to outweigh this time limitation.

As discussed above, the use of spheroid co-cultures of tumor and normal cells is a potentially very powerful system for advanced drug screening. Currently lacking to make this co-culture system most useful are techniques for obtaining a large population of uniformly sized spheroids with a reproducible cellular composition. One approach to improve the analysis of co-cultured spheroids would be the application of cell types expressing fluorescent markers, such as GFP or GFP analogues. One could then create large numbers of spheroid co-cultures and sort them according to size and fluorescence intensity using a modified flow sorter,[154] thereby obtaining a population with a uniform composition and size. With some developmental work in this area, it should be possible to generate a set of standard tumor:normal co-cultured spheroids that are well characterized and reproducible to serve as an HTS platform that incorporates tumor-normal cell interactions. Confocal fluorescence microscopy is an additional or alternative technical tool that could be improved to be applied for the analysis of such co-cultures.[155-157]

A final limitation to spheroids that should be mentioned is that the MCTS in vitro model will never be developed to the point that it will entirely replace the use of animals in the drug-testing process. Although the use of tumor/normal, or even purely normal cell spheroid co-cultures, is an exciting and powerful extension that will allow for a better evaluation of local bioactivity and penetration of new drug candidates, this model obviously lacks the complexity required for standard absorption, distribution, metabolism, elimination, toxicity (ADMET) screening. Considering the rapidly continuing improvements in reproducibility, throughput, and sophistication of other 3-D culture systems for nontumorous cells, for example, in tissue engineering, an increasing number of valuable complex culture models may be available in the near future for basic compound safety testing. However, as depicted in Figure 1, utilization of 3-D culture assays for routine toxicity testing of candidate therapeutics is speculative, and also pharmacokinetics still requires animal models, as there is currently no way to extrapolate these parameters from in vitro systems.

Although it is clear that some technology development work is required to bring the MCTS system into the arena of HTS, the significant advantages of this in vitro tumor model argue persuasively in favor of such an approach. Methods for simply screening, for example, cytotoxicity or growth arrest, could be quickly developed into high-throughput methods with spheroids. Techniques that would allow the rapid screening for effectiveness in tumor spheroids would be largely applicable to testing in mixed-cell spheroids and spheroids composed only of normal cells. Other limitations to HTS discussed above may preclude rapid assays for some endpoints, but it is important to recognize that these "limitations" could actually be advantages for more advanced screening techniques. For example, candidates identified by a rapid screen to be effective in killing or growth-arresting MCTS could be further screened for drug penetration, host-tumor interactions, and effects on nutrient-stressed subpopulations using the same basic in vitro model from which they were initially selected.

CONCLUSION

The fact that no preclinical study can yet replace phase II clinical trials is not disputed. However, not scientific reasoning but regulatory and legal requirements, and strong clinical tradition, remain the most important incentives for rodent model studies. The main reason and justification for routinely maintaining a large number of animal model systems for drug screening is that the predictive power for clinical efficacy is statistically poor for any single in vivo tumor model. Because the cost of drug development increases drastically at the stage of rodent tumor models, the guiding principle in the cancer drug industry has been to identify poor candidates earlier rather than later. It has therefore been proposed that increased reliance on cell-based validation early in the drug development process will prove economically advantageous. In the pathway from a simple solution-binding assay to in vivo testing, cell-based screening has proven to be a valuable stepping stone to quickly weed out toxic and nonfunctional compounds. The low cost and high speed of screening compounds in cell culture, and the obvious advantage of using intact cells as the most expedient representation of the living patient, have made cell-based screening a key component of drug discovery programs.[158] This article has reviewed the unique features of tumor spheroids as an in vitro

model system, and has also highlighted the options of heterologous tumor/stromal cell co-cultures to mimic aspects of in vivo tumor heterogeneity. The application of heterologous spheroid co-cultures in cancer research allows cellular analysis in a controlled and reproducible format. Although the complexity and limitations of these 3-D co-culture systems have to be recognized, MCTS methodology provides an important supplement to the use of animal in vivo systems, in particular, for research with human cells. Further technical developments should allow the future application of spheroids, with all of their in vivo characteristics, in HTS for anticancer drugs as well as potentially for other drug discovery and development efforts.

ACKNOWLEDGMENT

We thank Dr. Juergen Seidl for his assistance in manuscript and image preparation.

REFERENCES

1. Hertzberg RP, Pope AJ: High-throughput screening: new technology for the 21st century. *Curr Opin Chem Biol* 2000;4:445-451.
2. Sundberg SA: High-throughput and ultra-high-throughput screening: solution- and cell-based approaches. *Curr Opin Biotechnol* 2000;11:47-53.
3. Johnson JI, Decker S, Zaharevitz D, Rubinstein LV, Venditti JM, Schepartz S, et al: Relationships between drug activity in NCI preclinical in vitro and in vivo models and early clinical trials. *Br J Cancer* 2001;84:1424-1431.
4. Sausville EA: Overview. Cancer drug discovery: pathway promise or covalent certainty for drug effect—quo vadis? *Curr Opin Invest Drugs* 2000;1:511-513.
5. Balis FM: Evolution of anticancer drug discovery and the role of cell-based screening. *J Natl Cancer Inst* 2002;94:78-79.
6. Umezawa Y: Assay and screening methods for bioactive substances based on cellular signaling pathways. *J Biotechnol* 2002;82:357-370.
7. Hauptschein RS, Eustace BK, Jay DG: Global high-throughput screens for cellular function. *Exp Hematol* 2002;30:381-387.
8. Monga M, Sausville EA: Developmental therapeutics program at the NCI: molecular target and drug discovery process. *Leukemia* 2002;16:520-526.
9. Newell DR: Flasks, fibres and flanks—pre-clinical tumour models for predicting clinical antitumour activity. *Br J Cancer* 2001;84:1289-1290.
10. Pelkonen O, Boobis AR, Gundert-Remy U: In vitro prediction of gastrointestinal absorption and bioavailability: an experts' meeting report. *Eur J Clin Pharmacol* 2001;57:621-629.
11. Kerbel RS: Human tumor xenografts as predictive preclinical models for anticancer drug activity in humans: better than commonly perceived—but they can be improved. *Cancer Biol Ther* 2003;2:S134-S139.
12. Voskoglou-Nomikos T, Pater JL, Seymour L: Clinical predictive value of the in vitro cell line, human xenograft, and mouse allograft preclinical cancer models. *Clin Cancer Res* 2003;9:4227-4239.
13. Bhadriraju K, Chen CS: Engineering cellular microenvironments to improve cell-based drug testing. *Drug Discov Today* 2002;7:612-620.
14. Sutherland RM: Cell and environment interactions in tumor microregions: the multicell spheroid model. *Science* 1988;240:177-184.
15. Mueller-Klieser W: Tumor biology and experimental therapeutics. *Crit Rev Oncol Hematol* 2000;36:123-139.
16. Kunz-Schughart LA, Kreutz M, Knuechel R: Multicellular spheroids: a three-dimensional in vitro culture system to study tumour biology. *Int J Exp Pathol* 1998;79:1-23.
17. Hicks KO, Ohms SJ, van Zijl PL, Denny WA, Hunter PJ, Wilson WR: An experimental and mathematical model for the extravascular transport of a DNA intercalator in tumours. *Br J Cancer* 1997;76:894-903.
18. Padron JM, van der Wilt CL, Smid K, Smitskamp-Wilms E, Backus HH, Pizao PE, et al: The multilayered postconfluent cell culture as a model for drug screening. *Crit Rev Oncol Hematol* 2000;36:141-157.
19. Casciari JJ, Hollingshead MG, Alley MC, Mayo JG, Malspeis L, Miyauchi S, et al: Growth and chemotherapeutic response of cells in a hollow-fiber in vitro solid tumor model. *J Natl Cancer Inst* 1994;86:1846-1852.
20. Muralidhar RV, Jayachandran G, Singh P: Development of high-density cultivation systems by bioencapsulation. *Curr Sci* 2001;81:263-269.
21. Legallais C, David B, Dore E: Bioartificial livers (BAL): current technological aspects and future developments. *J Membrane Sci* 2001;81:81-95.
22. Dulong JL, Legallais C, Darmy S, Reach G: A novel model of solute transport in a hollow-fiber bioartificial pancreas based on a finite element method. *Biotechnol Bioeng* 2002;78:575-582.
23. Gillies RJ, Galons JP, McGovern KA, Schaer PG, Lien YH, Job C, et al: Design and application of NMR-compatible bioreactor circuits for extended perfusion of high-density mammalian cell cultures. *NMR Biomed* 1993;6:95-104.
24. Ochs RL, Fensterer J, Ohori NP, Wells A, Gabrin M, George LD, et al: Evidence for the isolation, growth, and characterization of malignant cells in primary cultures of human tumors. *In Vitro Cell Dev Biol Anim* 2003;39:63-70.
25. Berglund A, Glimelius B, Bergh J, Brodin O, Fjallskog ML, Hagberg H, et al: Selection of chemotherapy by ex vivo assessment of tumor sensitivity to cytotoxic drugs: results of a clinical trial. *Med Oncol* 2002;19:151-159.
26. Andreotti PE, Cree IA, Kurbacher CM, Hartmann DM, Linder D, Harel G, et al: Chemosensitivity testing of human tumors using a microplate adenosine triphosphate luminescence assay: clinical correlation for cisplatin resistance of ovarian carcinoma. *Cancer Res* 1995;55:5276-5282.
27. Cree IA, Kurbacher CM, Untch M, Sutherland LA, Hunter EM, Salvadi AM, et al: Correlation of the clinical response to chemotherapy in breast cancer with *ex vivo* chemosensitivity. *Anticancer Drugs* 1996;7:630-635.
28. Kurbacher CM, Cree IA, Bruckner HW, Brune U, Kurbacher JA, Muller K, et al: Use of an ex vivo ATP luminescence assay to direct chemotherapy for recurrent ovarian cancer. *Anticancer Drugs* 1998;9:51-57.
29. Kurbacher CM, Grecu OM, Stier U, Gilster TJ, Janat MM, Untch M, et al: ATP chemosensitivity testing in ovarian and breast cancer: early clinical trials. *Recent Results Cancer Res* 2003;161:221-230.
30. Duray PH, Hatfill SJ, Pellis NR: Tissue culture in microgravity. *Sci Med (Phila)* 1997;4:46-55.
31. Hammond TG, Hammond JM: Optimized suspension culture: the rotating-wall vessel. *Am J Physiol Renal Physiol* 2001;281:F12-F25.
32. Lappa M: Organic tissues in rotating bioreactors: fluid-mechanical aspects, dynamic growth models, and morphological evolution. *Biotechnol Bioeng* 2003;84:518-532.
33. Unsworth BR, Lelkes PI: Growing tissues in microgravity. *Nat Med* 1998;4:901-907.
34. Kloth S, Kobuch K, Domokos J, Wanke C, Monzer J: Polar application of test substances in an organotypic environment and under continuous medium flow: a new tissue-based test concept for a broad range of applications in pharmacotoxicology. *Toxicol In Vitro* 2000;14:265-274.
35. Minuth WW, Schumacher K, Strehl R, Kloth S: Physiological and cell biological aspects of perfusion culture technique employed to generate differenti-

ated tissues for long term biomaterial testing and tissue engineering. *J Biomater Sci Polym Ed* 2000;11:495-522.

36. Minuth WW, Steiner P, Strehl R, Schumacher K, de Vries U, Kloth S: Modulation of cell differentiation in perfusion culture. *Exp Nephrol* 1999;7:394-406.
37. Schumacher K, Strehl R, de VU, Minuth WW: Advanced technique for long term culture of epithelia in a continuous luminal-basal medium gradient. *Biomaterials* 2002;23:805-815.
38. Weibezahn KF, Knedlitschek G, Bier W, Schaller T: Mechanically processed microstructures used to establish an in vitro tissue model. In Reichl H, Heuberger A (eds): *Micro System Technologies '94, 4th International Conference on Micro Electro, Opto, Mechanical Systems and Components*. Berlin: vde-verlag gmbh, 1994:873.
39. Knedlitschek G, Schneider F, Gottwald E, Schaller T, Eschbach E, Weibezahn KF: A tissue-like culture system using microstructures: influence of extracellular matrix material on cell adhesion and aggregation. *J Biomech Eng* 1999;121:35-39.
40. Giselbrecht S, Gottwald E, Knedlitschek G, Weibezahn KF, Welle A, Guber AE, et al: Further development of microstructured culture systems and their use in tissue engineering. *Biomed Tech (Berl)* 2002;47(Suppl 1 Pt 1):373-376.
41. Gottwald E: Gewebezüchtung. Hilfsarbeiter für die Leber. *Spektrum der Wissenschaft* 2002;1:44-51.
42. Olsnes C, Heimdal JH, Kross K, Olofsson J, Aarstad HJ: Mechanisms for monocyte activation in co-culture with autologous tumor spheroids. *Cell Immunol* 2002;219:11-21.
43. Tonn JC, Ott MM, Bouterfa H, Kerkau S, Kapp M, Muller-Hermelink HK, et al: Inverse correlation of cell proliferation and expression of progesterone receptors in tumor spheroids and monolayer cultures of human meningiomas. *Neurosurgery* 1997;41:1152-1159.
44. Fjellbirkeland L, Bjerkvig R, Laerum OD: Tumour fragment spheroids from human non-small-cell lung cancer maintained in organ culture. *Virchows Arch* 1995;426:169-178.
45. Kunz-Schughart LA: Multicellular tumor spheroids: intermediates between monolayer culture and in vivo tumor. *Cell Biol Int* 1999;23:157-161.
46. Kunz-Schughart LA, Mueller-Klieser W: Three-dimensional culture. In Masters JRW (ed): *Animal Cell Culture*. Oxford, UK: Oxford University Press, 2000:Chap 5.
47. Gudjonsson T, Ronnov-Jessen L, Villadsen R, Bissell MJ, Petersen OW: To create the correct microenvironment: three-dimensional heterotypic collagen assays for human breast epithelial morphogenesis and neoplasia. *Methods* 2003;30:247-255.
48. Olumi AF, Dazin P, Tlsty TD: A novel coculture technique demonstrates that normal human prostatic fibroblasts contribute to tumor formation of LNCaP cells by retarding cell death. *Cancer Res* 1998;58:4525-4530.
49. Bissell MJ, Radisky DC, Rizki A, Weaver VM, Petersen OW: The organizing principle: microenvironmental influences in the normal and malignant breast. *Differentiation* 2002;70:537-546.
50. Bishop ET, Bell GT, Bloor S, Broom IJ, Hendry NF, Wheatley DN: An in vitro model of angiogenesis: basic features. *Angiogenesis* 1999;3:335-344.
51. Donovan D, Brown NJ, Bishop ET, Lewis CE: Comparison of three in vitro human 'angiogenesis' assays with capillaries formed in vivo. *Angiogenesis* 2001;4:113-121.
52. Abbott A: Cell culture: biology's new dimension. *Nature* 2003;424:870-872.
53. Inch WR, McCredie JA, Sutherland RM: Growth of nodular carcinomas in rodents compared with multi-cell spheroids in tissue culture. *Growth* 1970;34:271-282.
54. Sutherland RM, McCredie JA, Inch WR: Growth of multicell spheroids in tissue culture as a model of nodular carcinomas. *J Natl Cancer Inst* 1971;46:113-120.
55. Mueller-Klieser W: Multicellular spheroids. A review on cellular aggregates in cancer research. *J Cancer Res Clin Oncol* 1987;113:101-122.
56. Mueller-Klieser W: Three-dimensional cell cultures: from molecular mechanisms to clinical applications. *Am J Physiol* 1997;273:C1109-C1123.
57. Santini MT, Rainaldi G: Three-dimensional spheroid model in tumor biology. *Pathobiology* 1999;67:148-157.
58. Desoize B, Jardillier J: Multicellular resistance: a paradigm for clinical resistance? *Crit Rev Oncol Hematol* 2000;36:193-207.
59. Ballangrud AM, Yang WH, Charlton DE, McDevitt MR, Hamacher KA, Panageas KS, et al: Response of LNCaP spheroids after treatment with an alpha-particle emitter (213Bi)-labeled anti-prostate-specific membrane antigen antibody (J591). *Cancer Res* 2001;61:2008-2014.
60. Boyd M, Mairs RJ, Cunningham SH, Mairs SC, McCluskey A, Livingstone A, et al: A gene therapy/targeted radiotherapy strategy for radiation cell kill by [^{131}I]meta-iodobenzylguanidine (MIBG). *J Gene Med* 2001;3:165-172.
61. Boyd M, Mairs SC, Stevenson K, Livingstone A, Clark AM, Ross SC, Mairs RJ: Transfectant mosaic spheroids: a new model for evaluation of tumour cell killing in targeted radiotherapy and experimental gene therapy. *J Gene Med* 2002;4:567-576.
62. Carlin S, Cunningham SH, Boyd M, McCluskey AG, Mairs RJ: Experimental targeted radioiodide therapy following transfection of the sodium iodide symporter gene: effect on clonogenicity in both two- and three-dimensional models. *Cancer Gene Ther* 2000;7:1529-1536.
63. Dubessy C, Merlin JM, Marchal C, Guillemin F: Spheroids in radiobiology and photodynamic therapy. *Crit Rev Oncol Hematol* 2000;36:179-192.
64. Durand RE, Olive PL: Resistance of tumor cells to chemo- and radiotherapy modulated by the three-dimensional architecture of solid tumors and spheroids. *Methods Cell Biol* 2001;64:211-233.
65. Essand M, Gronvik C, Hartman T, Carlsson J: Radioimmunotherapy of prostatic adenocarcinomas: effects of 131I-labelled E4 antibodies on cells at different depth in DU 145 spheroids. *Int J Cancer* 1995;63:387-394.
66. Filippovich IV, Sorokina N, Robillard N, Faivre-Chauvet A, Bardies M, Chatal JF: Cell death induced by a 131I-labeled monoclonal antibody in ovarian cancer multicell spheroids. *Nucl Med Biol* 1996;23:623-626.
67. Marusic M, Bajzer Z, Freyer JP, Vuk-Pavlovic S: Analysis of growth of multicellular tumour spheroids by mathematical models. *Cell Prolif* 1994;27:73-94.
68. Kamuhabwa AA, Huygens A, De Witte PA: Photodynamic therapy of transitional cell carcinoma multicellular tumor spheroids with hypericin. *Int J Oncol* 2003;23:1445-1450.
69. Madsen SJ, Sun CH, Tromberg BJ, Hirschberg H: Repetitive 5-aminolevulinic acid-mediated photodynamic therapy on human glioma spheroids. *J Neurooncol* 2003;62:243-250.
70. Olive PL, Durand RE: Drug and radiation resistance in spheroids: cell contact and kinetics. *Cancer Metastasis Rev* 1994;13:121-138.
71. Fracasso G, Colombatti M: Effect of therapeutic macromolecules in spheroids. *Crit Rev Oncol Hematol* 2000;36:159-178.
72. Acker H, Carlsson J, Durand R, Sutherland RM (eds): *Spheroids in Cancer Research*. Berlin: Springer-Verlag, 1984.
73. Bjerkvig R (ed): *Spheroid Culture in Cancer Research*. Boca Raton, FL: CRC, 1992.
74. Durand R, Olive PL: Resistance of tumor cells to chemo- and radiotherapy modulated by three-dimensional architecture of solid tumors and spheroids.

In Darzynkiewics Z, Crissman HA, Robinson JP (eds): *Methods in Cell Biology: Cytometry.* San Diego: Academic Press, 2000:Chap 41.

75. Santini MT, Rainaldi G, Indovina PL: Multicellular tumour spheroids in radiation biology. *Int J Radiat Biol* 1999;75:787-799.
76. O'Connor KC: Three-dimensional cultures of prostatic cells: tissue models for the development of novel anti-cancer therapies. *Pharm Res* 1999;16:486-493.
77. Clejan S, O'Connor K, Rosensweig N: Tri-dimensional prostate cell cultures in simulated microgravity and induced changes in lipid second messengers and signal transduction. *J Cell Mol Med* 2001;5:60-73.
78. Mayer B, Klement G, Kaneko M, Man S, Jothy S, Rak J, et al: Multicellular gastric cancer spheroids recapitulate growth pattern and differentiation phenotype of human gastric carcinomas. *Gastroenterology* 2001;121:839-852.
79. Hedlund TE, Duke RC, Miller GJ: Three-dimensional spheroid cultures of human prostate cancer cell lines. *Prostate* 1999;41:154-165.
80. Chignola R, Schenetti A, Andrighetto G, Chiesa E, Foroni R, Sartoris S, et al: Forecasting the growth of multicell tumour spheroids: implications for the dynamic growth of solid tumours. *Cell Prolif* 2000;33:219-229.
81. Ward JP, King JR: Mathematical modelling of avascular-tumour growth. *IMA J Math Appl Med Biol* 1997;14:39-69.
82. Adam JA: Mathematical models of prevascular spheroid development and catastrophe-theoretic description of rapid metastatic growth/tumor remission. *Invasion Metastasis* 1996;16:247-267.
83. Sherratt JA, Chaplain MA: A new mathematical model for avascular tumour growth. *J Math Biol* 2001;43:291-312.
84. Dormann S, Deutsch A: Modeling of self-organized avascular tumor growth with a hybrid cellular automaton. *In Silico Biol* 2002;2:393-406.
85. Pjesivac-Grbovic J, Freyer JP, Cantrell C, Jiang Y: Multiscale model of avascular tumor growth. *J Math Biol*, submitted.
86. Walenta S, Doetsch J, Mueller-Klieser W, Kunz-Schughart LA: Metabolic imaging in multicellular spheroids of oncogene-transfected fibroblasts. *J Histochem Cytochem* 2000;48:509-522.
87. Oloumi A, MacPhail SH, Johnston PJ, Banath JP, Olive PL: Changes in subcellular distribution of topoisomerase IIalpha correlate with etoposide resistance in multicell spheroids and xenograft tumors. *Cancer Res* 2000;60:5747-5753.
88. Pervez S, Kirkland SC, Epenetos AA, Mooi WJ, Evans DJ, Krausz T: Effect of polarity and differentiation on antibody localization in multicellular tumour spheroid and xenograft models and its potential importance for in vivo immunotargeting. *Int J Cancer* 1989;44:940-947.
89. Hemmerlein B, Kugler A, Ozisik R, Ringert RH, Radzun HJ, Thelen P: Vascular endothelial growth factor expression, angiogenesis, and necrosis in renal cell carcinomas. *Virchows Arch* 2001;439:645-652.
90. Freyer JP, Sutherland RM: Selective dissociation and characterization of cells from different regions of multicell tumor spheroids. *Cancer Res* 1980;40:3956-3965.
91. Kwok TT, Twentyman PR: The relationship between tumour geometry and the response of tumour cells to cytotoxic drugs—an in vitro study using EMT6 multicellular spheroids. *Int J Cancer* 1985;35:675-682.
92. Freyer JP, Schor PL: Automated selective dissociation of cells from different regions of multicellular spheroids. *In Vitro Cell Dev Biol* 1989;25:9-19.
93. Freyer JP, Schor PL: Regrowth kinetics of cells from different regions of multicellular spheroids of four cell lines. *J Cell Physiol* 1989;138:384-392.
94. Kunz-Schughart LA, Habbersett RC, Freyer JP: Mitochondrial function in oncogene-transfected rat fibroblasts isolated from multicellular spheroids. *Am J Physiol* 1997:273:C1487-C1495.
95. Ginsberg T, Ulmer W, Düchting W: Computer simulation of fractionated radiotherapy: further results and their relevance to percutaneous irradiation and brachytherapy. *Strahlenther Onkol* 1993;169:304-310.
96. Düchting W, Ginsberg T, Ulmer W: Modeling of radiogenic responses induced by fractionated irradiation in malignant and normal tissue. *Stem Cells* 1995:13(Suppl 1):301-306.
97. Wenning LA, Murphy RM: Coupled cellular trafficking and diffusional limitations in delivery of immunotoxins to multicell tumor spheroids. *Biotechnol Bioeng* 1999;62:562-575.
98. Graff CP, Wittrup KD: Theoretical analysis of antibody targeting of tumor spheroids: importance of dosage for penetration, and affinity for retention. *Cancer Res* 2003;63:1288-1296.
99. Ward JP, King JR: Mathematical modelling of drug transport in tumour multicell spheroids and monolayer cultures. *Math Biosci* 2003;181:177-207.
100. Roose T, Netti PA, Munn LL, Boucher Y, Jain RK: Solid stress generated by spheroid growth estimated using a linear poroelasticity model small star, filled. *Microvasc Res* 2003;66:204-212.
101. Silzle T, Kreutz M, Dobler MA, Brockhoff G, Knuechel R, Kunz-Schughart LA: Tumor-associated fibroblasts recruit blood monocytes into tumor tissue. *Eur J Immunol* 2003;33:1311-1320.
102. Oudar O: Spheroids: relation between tumour and endothelial cells. *Crit Rev Oncol Hematol* 2000;36:99-106.
103. Furbert-Harris PM, Laniyan I, Harris D, Dunston GM, Vaughn T, Abdelnaby A, et al: Activated eosinophils infiltrate MCF-7 breast multicellular tumor spheroids. *Anticancer Res* 2003;23:71-78.
104. Heimdal JH, Aarstad HJ, Olsnes C, Olofsson J: Human autologous monocytes and monocyte-derived macrophages in co-culture with carcinoma F-spheroids secrete IL-6 by a non-CD14-dependent pathway. *Scand J Immunol* 2001;53:162-170.
105. Konur A, Kreutz M, Knuchel R, Krause SW, Andreesen R: Cytokine repertoire during maturation of monocytes to macrophages within spheroids of malignant and non-malignant urothelial cell lines. *Int J Cancer* 1998;78:648-653.
106. de Ridder L, Cornelissen M, de Ridder D: Autologous spheroid culture: a screening tool for human brain tumour invasion. *Crit Rev Oncol Hematol* 2000;36:107-122.
107. Frenzel KR, Saller RM, Kummermehr J, Schultz-Hector S: Quantitative distinction of cisplatin-sensitive and -resistant mouse fibrosarcoma cells grown in multicell tumor spheroids. *Cancer Res* 1995;55:386-391.
108. Thomsen LL, Baguley BC, Wilson WR: Nitric oxide: its production in host-cell-infiltrated EMT6 spheroids and its role in tumour cell killing by flavone-8-acetic acid and 5,6-dimethylxanthenone-4-acetic acid. *Cancer Chemother Pharmacol* 1992;31:151-155.
109. Tofilon PJ, Arundel CM, Deen DF: Response to BCNU of spheroids grown from mixtures of drug-sensitive and drug-resistant cells. *Cancer Chemother Pharmacol* 1987;20:89-95.
110. Kunz-Schughart LA, Heyder P, Schroeder J, Knuechel R: A heterologous 3-D coculture model of breast tumor cells and fibroblasts to study tumor-associated fibroblast differentiation. *Exp Cell Res* 2001;266:74-86.
111. Nakamura K, Hanibuchi M, Yano S, Tanaka Y, Fujino I, Inoue M, et al: Apoptosis induction of human lung cancer cell line in multicellular heterospheroids with humanized antiganglioside GM2 monoclonal antibody. *Cancer Res* 1999;59:5323-5330.
112. Offner FA, Schiefer J, Wirtz HC, Bigalke I, Pavelka M, Hollweg G, et al: Tumour-cell-endothelial interactions: free radicals are mediators of melanoma-induced endothelial cell damage. *Virchows Arch* 1996;428:99-106.

113. Lichtenbeld HH, Muller AD, van Dam-Mieras MC, Blijham GH: Tumor spheroid-induced vesicle formation on endothelial cells is associated with procoagulant properties. *J Cell Sci* 1993;106(Pt 2):657-662.
114. Wartenberg M, Donmez F, Ling FC, Acker H, Hescheler J, Sauer H: Tumor-induced angiogenesis studied in confrontation cultures of multicellular tumor spheroids and embryoid bodies grown from pluripotent embryonic stem cells. *FASEB J* 2001;15:995-1005.
115. Jääskeläinen J, Kalliomaki P, Paetau A, Timonen T: Effect of LAK cells against three-dimensional tumor tissue. In vitro study using multi-cellular human glioma spheroids as targets. *J Immunol* 1989;142:1036-1045.
116. Gottfried E, Faust S, Fritsche J, Kunz-Schughart LA, Andreesen R, Miyake K, et al: Identification of genes expressed in tumor-associated macrophages. *Immunobiology* 2003;207:351-359.
117. Cheng FM, Hansen EB, Taylor CR, Epstein AL: Diffusion and binding of monoclonal antibody TNT-1 in multicellular tumor spheroids. *J Natl Cancer Inst* 1991;83:200-204.
118. Carlsson J: Tumor spheroids in studies of immunotherapy. In Bjerkvig R (ed): *Spheroid Culture in Cancer Research*. Boca Raton, FL: CRC, 1992:277.
119. Wartenberg M, Frey C, Diedershagen H, Ritgen J, Hescheler J, Sauer H: Development of an intrinsic P-glycoprotein-mediated doxorubicin resistance in quiescent cell layers of large, multicellular prostate tumor spheroids. *Int J Cancer* 1998;75:855-863.
120. McFadden R, Kwok CS: Mathematical model of simultaneous diffusion and binding of antitumor antibodies in multicellular human tumor spheroids. *Cancer Res* 1988;48:4032-4037.
121. Abu-Absi SF, Friend JR, Hansen LK, Hu WS: Structural polarity and functional bile canaliculi in rat hepatocyte spheroids. *Exp Cell Res* 2002;274: 56-67.
122. Depreter M, Walker T, De Smet K, Beken S, Kerckaert I, Rogiers V, et al: Hepatocyte polarity and the peroxisomal compartment: a comparative study. *Histochem J* 2002;34:139-151.
123. Hamamoto R, Yamada K, Kamihira M, Iijima S: Differentiation and proliferation of primary rat hepatocytes cultured as spheroids. *J Biochem (Tokyo)* 1998;124:972-979.
124. Roberts RA, Soames AR: Hepatocyte spheroids: prolonged hepatocyte viability for in vitro modeling of nongenotoxic carcinogenesis. *Fund Appl Toxicol* 1993;21:149-158.
125. Tong JZ, Sarrazin S, Cassio D, Gauthier F, Alvarez F: Application of spheroid culture to human hepatocytes and maintenance of their differentiation. *Biol Cell* 1994;81:77-81.
126. Denker AE, Nicoll SB, Tuan RS: Formation of cartilage-like spheroids by micromass cultures of murine C3H10T1/2 cells upon treatment with transforming growth factor-beta 1. *Differentiation* 1995;59:25-34.
127. Rixen H, Dyckhoff G, Kauhl W, Kirkpatrick CJ, Mittermayer C: Comparative studies on collagen expression of chondrocytes in monolayer and spheroid culture. *Verh Dtsch Ges Pathol* 1990;74:365-367.
128. Anderer U, Libera J: In vitro engineering of human autogenous cartilage. *J Bone Miner Res* 2002;17:1420-1429.
129. Layer PG, Rothermel A, Hering H, Wolf B, deGrip WJ, Hicks D, et al: Pigmented epithelium sustains cell proliferation and decreases expression of opsins and acetylcholinesterase in reaggregated chicken retinospheroids. *Eur J Neurosci* 1997;9:1795-1803.
130. Layer PG, Rothermel A, Willbold E: Inductive effects of the retinal pigmented epithelium (RPE) on histogenesis of the avian retina as revealed by retinospheroid technology. *Semin Cell Dev Biol* 1998;9:257-262.
131. Stelck S, Robitzki A, Willbold E, Layer PG: Fucose in alpha(1-6)-linkage regulates proliferation and histogenesis in reaggregated retinal spheroids of the chick embryo. *Glycobiology* 1999;9:1171-1179.
132. Willbold E, Reinicke M, Lance-Jones C, Lagenaur C, Lemmon V, Layer PG: Muller glia stabilizes cell columns during retinal development: lateral cell migration but not neuropil growth is inhibited in mixed chick-quail retinospheroids. *Eur J Neurosci* 1995;7:2277-2284.
133. Matsuo T, Matsuo N: Reconstruction of trabecular tissue from human trabecular cells as a multicellular spheroid. *Acta Med Okayama* 1997;51:213-218.
134. Lehnert L, Trost H, Schmiegel W, Roder C, Kalthoff H: Hollow-spheres: a new model for analyses of differentiation of pancreatic duct epithelial cells. *Ann N Y Acad Sci* 1999;880:83-93.
135. Lehnert L, Lerch MM, Hirai Y, Kruse ML, Schmiegel W, Kalthoff H: Autocrine stimulation of human pancreatic duct-like development by soluble isoforms of epimorphin in vitro. *J Cell Biol* 2001;152:911-922.
136. Kosaka T, Fukaya K, Tsuboi S, Pu H, Ohno T, Tsuji T, et al: Comparison of various methods of assaying the cytotoxic effects of ethanol on human hepatoblastoma cells (HUH-6 line). *Acta Med Okayama* 1996;50:151-156.
137. Kosaka T, Tsuboi S, Fukaya K, Pu H, Ohno T, Tsuji T, et al: Spheroid cultures of human hepatoblastoma cells (HuH-6 line) and their application for cytotoxicity assay of alcohols. *Acta Med Okayama* 1996;50:61-66.
138. Reininger-Mack A, Thielecke H, Robitzki AA: 3D-biohybrid systems: applications in drug screening. *Trends Biotechnol* 2002;20:56-61.
139. Thielecke H, Mack A, Robitzki A: A multicellular spheroid-based sensor for anti-cancer therapeutics. *Biosens Bioelectron* 2001;16:261-269.
140. Thielecke H, Mack A, Robitzki A: Biohybrid microarrays—impedimetric biosensors with 3D in vitro tissues for toxicological and biomedical screening. *Fresenius J Anal Chem* 2001;369:23-29.
141. Martin C, Walker J, Rothnie A, Callaghan R: The expression of P-glycoprotein does influence the distribution of novel fluorescent compounds in solid tumour models. *Br J Cancer* 2003;89:1581-1589.
142. Frankel A, Man S, Elliott P, Adams J, Kerbel RS: Lack of multicellular drug resistance observed in human ovarian and prostate carcinoma treated with the proteasome inhibitor PS-341. *Clin Cancer Res* 2000;6:3719-3728.
143. Bigelow CE, Mitra S, Knuechel R, Foster TH: ALA- and ALA-hexylester-induced protoporphyrin IX fluorescence and distribution in multicell tumour spheroids. *Br J Cancer* 2001;85:727-734.
144. Mairs RJ, Angerson WJ, Babich JW, Murray T: Differential penetration of targeting agents into multicellular spheroids derived from human neuroblastoma. *Prog Clin Biol Res* 1991;366:495-501.
145. Durand RE: Slow penetration of anthracyclines into spheroids and tumors: a therapeutic advantage? *Cancer Chemother Pharmacol* 1990;26:198-204.
146. Wilson WR, Pullen SM, Hogg A, Helsby NA, Hicks KO, Denny WA: Quantitation of bystander effects in nitroreductase suicide gene therapy using three-dimensional cell cultures. *Cancer Res* 2002;62:1425-1432.
147. Myrdal S, Foster M: Time-resolved confocal analysis of antibody penetration into living, solid tumor spheroids. *Scanning* 1994;16:155-167.
148. Erlanson M, Daniel-Szolgay E, Carlsson J: Relations between the penetration, binding and average concentration of cytostatic drugs in human tumour spheroids. *Cancer Chemother Pharmacol* 1992;29:343-353.
149. Civiale C, Paladino G, Marino C, Trombetta F, Pulvirenti T, Enea V: Multilayer primary epithelial cell culture from bovine conjunctiva as a model for in vitro toxicity tests. *Ophthalmic Res* 2003;35:126-136.
150. Hicks KO, Pruijn FB, Sturman JR, Denny WA, Wilson WR: Multicellular resistance to tirapazamine is due to restricted extravascular transport: a

pharmacokinetic/pharmacodynamic study in HT29 multicellular layer cultures. *Cancer Res* 2003;63:5970-5977.

151. Groebe K, Erz S, Mueller-Klieser W: Glucose diffusion coefficients determined from concentration profiles in EMT6 tumor spheroids incubated in radioactively labeled L-glucose. *Adv Exp Med Biol* 1994;361:619-625.
152. Casciari JJ, Sotirchos SV, Sutherland RM: Glucose diffusivity in multicellular tumor spheroids. *Cancer Res* 1988;48:3905-3909.
153. Freyer JP, Sutherland RM: Determination of diffusion constants for metabolites in multicell tumor spheroids. *Adv Exp Med Biol* 1983;159:463-475.
154. Freyer JP, Wilder ME, Jett JH: Viable sorting of intact multicellular spheroids by flow cytometry. *Cytometry* 1987;8:427-436.
155. Yoshida D, Watanabe K, Noha M, Takahashi H, Teramoto A, Sugisaki Y: Anti-invasive effect of an anti-matrix metalloproteinase agent in a murine brain slice model using the serial monitoring of green fluorescent protein-labeled glioma cells. *Neurosurgery* 2003;52:187-196.
156. Yoshida D, Watanabe K, Noha M, Takahashi H, Teramoto A, Sugisaki Y: Tracking cell invasion of human glioma cells and suppression by anti-matrix metalloproteinase agent in rodent brain-slice model. *Brain Tumor Pathol* 2002;19:69-76.
157. Chatterjee S, Matsumura A, Schradermeier J, Gillespie GY: Human malignant glioma therapy using anti-alpha(v)beta3 integrin agents. *J Neurooncol* 2000;46:135-144.
158. Giese K, Kaufmann J, Pronk GJ, Klippel A: Unravelling novel intracellular pathways in cell-based assays. *Drug Discov Today* 2002;7:179-186.

Address reprint requests to:
Dr. Leoni A. Kunz-Schughart
Institute of Pathology
University of Regensburg
Franz-Josef-Strauss-Allee 11
D-93053 Regensburg
Germany

E-mail: *leoni.kunz-schughart@klinik.uni-regensburg.de*

EXHIBIT J

ELSEVIER

European Journal of Cancer 40 (2004) 785–793

European Journal of Cancer

www.ejconline.com

Update on NCI *in vitro* drug screen utilities

S.L. Holbeck*

National Cancer Institute, Developmental Therapeutics Program, Information Technology Branch, Rockville, MD, USA

Received 1 October 2003; received in revised form 20 October 2003; accepted 17 November 2003

Abstract

Development of new anti-cancer drugs is a costly and risky proposition. The Developmental Therapeutics Program (DTP) of the National Cancer Institutes of the United States (U.S.) facilitates the drug development process by providing access to preclinical screening services. Since the early 1990's, DTP has screened tens of thousands of compounds against a panel of 60 human tumour cell lines representing nine tissue sites. At the same time, DTP began to accumulate information on the expression of molecular entities in the same 60 cell line panel. Many of these data are freely available to the public at http://dtp.nci.nih.gov. More recently, additional, more focused screens have entered the picture, with data also available through the web site. These include screening of roughly 100 000 compounds against a panel of yeast mutants, and screening of the NCI Diversity Set in assays designed to detect effects on Molecular Targets of interest.
Published by Elsevier Ltd.

Keywords: Neoplasms; Antineoplastic agents; Computational biology; Molecular biology; Proteomics; Genomics; Pharmacogenetics; Human Genome Project; Genetic Research; (Therapies, Investigational); *Saccharomyces cerevisiae*

1. Introduction

The development of anti-cancer drugs is an expensive and time-consuming process. The Developmental Therapeutics Program (DTP) of the United States (U.S.) National Cancer Institute (NCI) reduces the risks in this process by providing *in vitro* and *in vivo* screening services, as well as access to pharmacological and formulation resources. Just as valuable is the publicly available information on the data derived from these screens. This review will focus on the data and information analysis tools that DTP provides for the *in vitro* screens. Other articles in this issue will focus on *in vivo* testing and late preclinical resources provided by DTP.

Compound screening at DTP has focused on the response of a panel of 60 human tumour cell lines, with data on tens of thousands of compounds. An ongoing programme characterises expression of molecular targets within this panel. Nearly 100 000 compounds were analysed in a collaboration with the Fred Hutchinson Cancer Research Center for their ability to inhibit the growth of a panel of yeast strains with alterations in cancer-relevant genes. Screening campaigns were conducted for compounds affecting several molecular targets of interest. All of these data are freely available through a web site maintained by the NCI-DTP at http://dtp.nci.nih.gov/.

2. Compounds submitted to NCI-DTP

The acquisition of compounds for screening by the NCI began in 1955, and continues to this day, with over 500 000 compounds currently registered. This collection contains compounds from a large number of suppliers, including scientists in academia or government laboratories, as well as small biotechnology companies and large pharmaceutical companies. Researchers from over 100 countries have submitted compounds to the NCI screening programmes. Roughly half of the compounds were submitted under NCI's discreet screening agreement, which precludes NCI from disseminating data on these compounds. For the remainder, the data is publicly available through the DTP web site (http://dtp.nci.

* National Cancer Institute, Developmental Therapeutics Program, Information Technology Branch, 6130 Executive Blvd. Room 8014, Bethesda, MD 20892-7444, USA. Tel.: 301-435-9178; fax: 301-480-4808.

E-mail address: holbecks@mail.nih.gov (S.L. Holbeck).

0959-8049/$ - see front matter Published by Elsevier Ltd.
doi:10.1016/j.ejca.2003.11.022

Basic Chemical Data

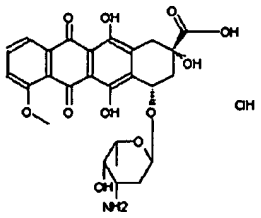

NSC 123127 **CAS 25316-40-9**

Molecular Formula: C27H29NO11.ClH **Molecular Weight:** 580

Chemical Names

- ADR
- FI 106
- DOX HCl
- FI 6804
- Adriacin
- Adriblastin
- Doxorubicin
- Adriblastina
- ADM hydrochloride
- Adriamycin hydrochloride

Fig. 1. The results of a search at http://dtp.nci.nih.gov/docs/dtp_search.html for chemical information on doxorubicin (Adriamycin). The web page displays a two-dimensional structure, NSC number, CAS number, Molecular Formula, Molecular Weight, and chemical names by which a compound is known.

nih.gov/), including compound structures, data from the NCI 60 human tumour cell line screen, the NCI acquired immunodeficiency syndrome (AIDS) screen and the NCI Yeast Anticancer Drug Screen. Those interested in submitting compounds for testing may do so using DTP's on-line submission form (http://dtp.nci.nih.gov/docs/misc/common_files/submit_compounds.html).

While the DTP compound collection contains many compounds with an identified mechanism of action, for the vast majority the target remains to be identified. Many were designed as chemically interesting structures, or are purified natural products. Some compounds were designed to interact with particular cellular targets. Many others are structural analogues of compounds with a known mechanism. The resulting collection is diverse, with a broad range of chemotypes and biological activities represented. Several plated sets have been developed to allow researchers to exploit this diversity in novel drug screens. The Diversity Set is a group of 1990 compounds selected to represent a broad range of chemotypes. The utility of this set is demonstrated by the success of several novel targeted screens [4,35,8,23]. The Mechanistic Diversity Set is comprised of 879 compounds chosen based on diversity of activity in the 60 cell line screen. Recently, a plated set of 235 purified natural products was developed. A large plated set contains 140 000 compounds. Before investing significant resources in lead development, researchers may wish to verify the structure, as DTP does not routinely perform chemical analyses on compounds, and some samples may degrade during storage.

The DTP web site provides basic chemical data on over 250 000 compounds. This includes (if available) two-dimensional and three-dimensional structures, CAS number, molecular formula, molecular weight and chemical names. Researchers may search for compound data using the NSC number (the NCI's identification number for a compound), by CAS number, by chemical name or by chemical structure at http://dtp.nci.nih.gov/docs/dtp_search.html. Fig. 1 displays the results of a search for doxorubicin (Adriamycin) (NSC 123127).

3. NCI 60 Human tumour cell line panel

In 1989, the NCI-DTP initiated an *in vitro* screen for potential anti-cancer drugs utilising a panel of 60

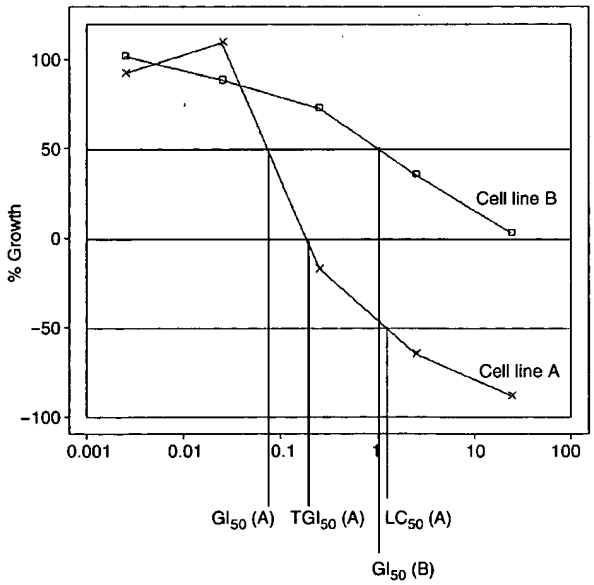

Fig. 2. Three endpoints (negative $\log_{10}$ of the concentration inhibiting the growth of 50% of the cells (GI_{50}), total growth inhibition (TGI) and negative $\log_{10}$ concentration need to kill 50% of the cells (LC_{50}) are calculated from 5-log dose response curves for compounds tested in the National Cancer Institute (NCI) 60 human tumour cell line screen. In this example, cell line A is much more sensitive than cell line B, with a GI_{50} value roughly 10-fold lower. Cell line B never reaches the TGI and LC_{50} endpoints in this concentration range. For the purposes of COMPARE, these endpoints are assigned the maximum concentration tested.

human tumour cell lines derived from various tissue types [27]. Compounds are tested over a 5-log concentration range against each of the 60 cell lines for their ability to inhibit the growth of, or to kill, the cells in a 2-day assay. Fig. 2 displays a simplified dose-response curve showing the response of two cell lines to doxorubicin. To facilitate analysis of the data, three endpoints are calculated for each cell line. The GI_{50} value is the negative $\log_{10}$ of the concentration required to inhibit the growth of that cell line by 50% (relative to untreated cells). TGI is the negative $\log_{10}$ minimum concentration that causes total growth inhibition, and LC_{50} reflects the negative $\log_{10}$ concentration needed to kill 50% of the cells. Paull and colleagues [34] developed the Mean Graph as a way of easily visualising the results from all 60 cell lines at once. A sample is shown in Fig. 3. To generate these graphs, the mean of each of the endpoints across all 60 cell lines is calculated. For each cell line, the difference between the GI_{50} for that cell line and the mean GI_{50} across all cell lines is calculated. When these differences are graphed, it becomes apparent at a glance which cell lines are more sensitive (those with bars deflecting to the right of the mean), and which cell lines are less sensitive (bars deflecting to the left). This screening service is available free of charge. To date, roughly 85 000 compounds have been screened. 60 cell line data for 43 000 compounds are currently available to the public through the DTP web site.

4. COMPARE

Compounds with similar mechanisms of actions tend to have similar patterns of growth inhibition in the 60 cell line screen, i.e. the same set of cell lines will tend to be more sensitive to both compounds, with a different subset being less sensitive to both. This can be visualised as compounds having similar Mean Graphs. To capitalise on this, Paull and colleagues [34] developed the COMPARE algorithm, which can be thought of as quantitating the similarity of Mean Graphs from different compounds. This algorithm takes the pattern for a "seed" compound and calculates Pearson correlation coefficients (PCCs) for it against each of the thousands of other compounds in the database, then returns a list of the highest correlations. Thus, one can start with a compound of unknown mechanism and determine whether it behaves similarly to compounds of defined mechanism that have been through the screen previously. This approach has been utilised to identify

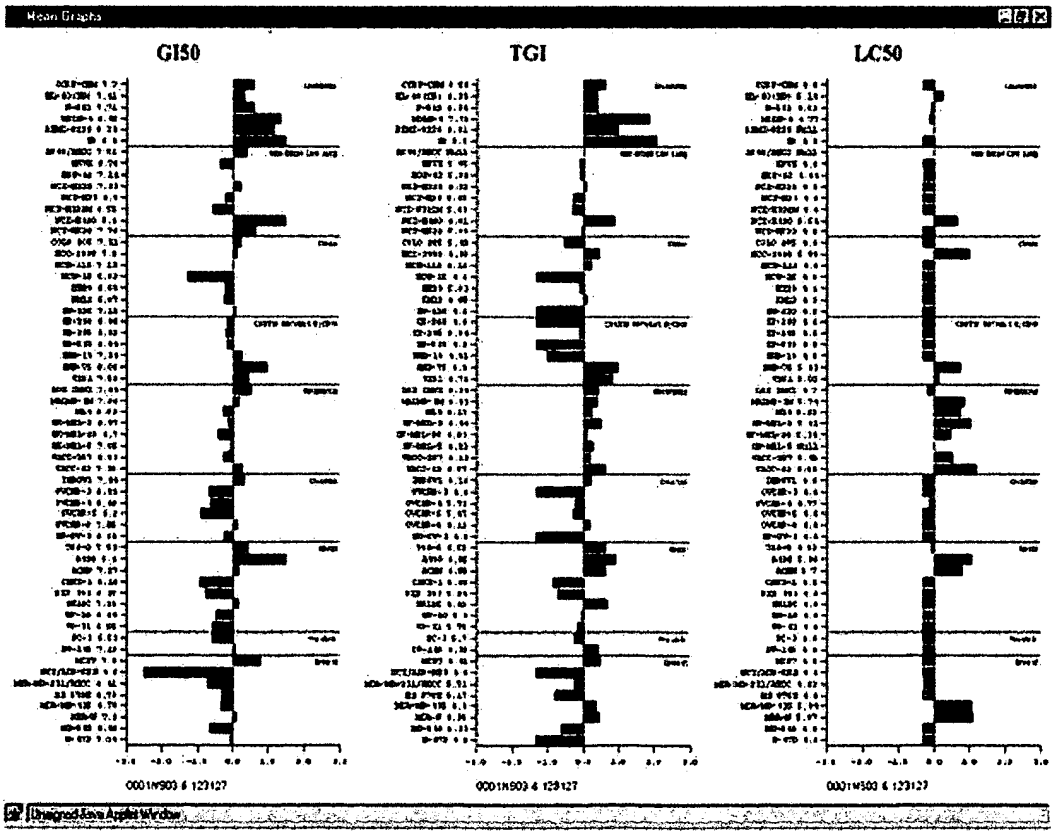

Fig. 3. A mean graph for doxorubicin is shown. The midline of each portion of the graph represents the mean for that endpoint, calculated across all 60 cell lines. This mean value is then subtracted from the value for each individual cell line and plotted. Cell lines more sensitive to doxorubicin are visualised as bars deflecting to the right, while more resistant cell lines have bars extending to the left of the mean.

novel tubulin-interacting compounds, topoisomerase poisons, vacuolar-type (H+)-adenosine triphosphatase (ATPase), and dihydroorotate dehydrogenase inhibitors [6,54,10,25,40]. Results may be unexpected, as with a series of Lavendustin A analogues submitted to the screen as having kinase inhibition activity, but were suggested by COMPARE to be possible tubulin inhibitors, a result that was experimentally verified [29]. Alternatively, one may wish to identify new chemotypes with a mechanism similar to that of a pharmaceutically intractable compound, in the hopes of identifying agents that might lack the undesirable features. In this case, one uses the compound of known mechanism as a seed, and COMPARE will return a list of compounds with the best correlations—these become candidates for testing to determine whether they do indeed share a common mechanism with the seed. Such an approach was used to identify a novel class of cyclin-dependent kinase (CDK) inhibitors, the paullones, starting with flavopiridol as a seed [57].

COMPARE can be accessed through the DTP web site. Currently, the old COMPARE interface is still operational, although no longer supported. The new COMPARE interface may be found at http://itbwork.nci.nih.gov/PublicServer/servlet/CompareServer, and allows users to utilise either compound or Molecular Target data (described in detail in the next section) as a seed for running COMPARE against either compound or Molecular Target databases. In addition, users can create their own seed data. Since all 60 cell line screening data, even on compounds not covered by a confidentiality agreement, is kept confidential for 2 years, the ability to create one's own seed data allows suppliers access to COMPARE for recently screened compounds. In addition, as data for compounds that are covered by a confidentiality agreement is not available through the public web site, this allows suppliers to create a seed to access COMPARE for their own confidential compounds. One might also create a seed to create composite patterns, such as co-expression of several molecular targets.

5. Molecular Targets in the 60 cell line panel

The sensitivity of a cell line to a compound is necessarily determined by the cellular environment—which genes are being expressed, which signalling pathways are turned on or off, whether various repair pathways are operational, etc. For some compounds, a single component may be a major determinant of sensitivity, while for others many components contribute to the response. In order to address this, DTP has an ongoing programme to characterise "Molecular Targets" within the 60 cell line panel. Molecular Targets in this context are used to denote measurable entities in the cell lines. The inclusion of a particular Target is driven by interest from the cancer research community, with most of the data provided by researchers outside of DTP. Researchers apply to measure a target (or targets) of interest. If approved, DTP provides them with 60 cell line materials at no cost, with the proviso that data may be posted on the DTP web site once the researcher has had an opportunity to publish the results. Interested parties can find more information on this programme at http://dtp.nci.nih.gov/mtargets/mt_index.html.

Data currently available include mutation status of genes important in cancer (including *p53* and the *Ras* genes), as well as quantitation of proteins within the cells (e.g. cyclins and CDKs), RNA levels (e.g. for many tyrosine kinases and phosphatases), and enzyme activity (e.g. DT-diaphorase and multidrug resistant (MDR) activities). Table 1 summarises the Molecular Targets for which data are currently available to the public. Microarray data, measuring the baseline expression of thousands of genes, is also available from two separate experiments. The first utilised a cDNA array to analyse baseline expression of 9706 entities in each of the 60 cell lines, relative to expression in a pool of 12 of these cell lines [36,38]. A second microarray experiment performed at Millennium Pharmaceuticals analysed baseline expression of 5365 features in each of the 60 cell lines utilising oligonucleotide arrays.

The COMPARE algorithm, in additional to identifying compounds with similar growth inhibitory patterns, can be used with Molecular Target data. Target data can be visualised in a Mean Graph, just as for a compound. COMPARE can be used to identify positive correlations, where cell lines with higher levels of a Target tend to be more sensitive to a compound. While negative correlations are not generally used when comparing compounds with other compounds, it can make sense in comparing compounds to Targets. This would identify cases where cell lines with lower levels of the Target tend to be more sensitive to the compound, or, stated differently, where cell lines with higher levels of the Target tend to be resistant to the compound. COMPARE can also be used to identify Targets that are co-expressed (positively correlated) with other Targets, as well as those that tend not to be expressed simultaneously (negative correlations).

The value of using COMPARE to identify compound mechanisms has been validated by several success stories. Kubo and colleagues [22] analysed p16 status in the 60 cell lines and tested compounds that COMPARE determined to have the highest correlations. They demonstrated that one of those compounds had activity against CDK4, an enzyme that is regulated by p16. Wosikowski and colleagues [52] measured RNA levels for several genes in the epidermal growth factor receptor (EGFR) and ErbB2 pathways. By screening a small number of compounds suggested by COMPARE, they

identified 14 compounds with demonstrable activity against these pathways. Sensitivity of cells to an inhibitor of brain glycogen phosphorylase correlates with expression of this target [39]. Cluster analysis with homoharringtonine against the microarray database suggested a correlation with EGFR expression, which was verified experimentally [13].

In most cases, the correlations between compound and target data is more modest than between two compounds. This may be because few Molecular Targets are

Table 1
Molecular targets measured in the NCI 60 cell line panel

88 KINASES, INCLUDING	CELL CYCLE CONTROL	REDOX
ABL	Cdc2	ALDH1 & ALDH3
AXL	Cdc25A, Cdc25B, Cdc25C	aldose reductase
CSF1R	cdc7	Cytochrome b5 reductase
CSK	Cdks 2, 4, 5, 6	Cytochrome P450 activity
EGFR	Chk1	Cytochrome P450 reductase
EphA1-8	Cyclins A, B, D1, D2, D3, E	Dihydrodiol dehydrogenase
EphB1-5	MDM2	DT-diaphorase
ErbB2-4	p16	GGCS
FGFR1-4	p19	GGT
FGR	p53	Glutathione
FLT1	Rb	GSTs A1, M1a, M1b, M2, M3,-mu,-pi
FLT4	Waf-1	HSI reductase
FYN		Thioredoxin
IGF1R		Thioredoxin reductase
INSR		
JAK1-2	**APOPTOSIS**	**SIGNAL TRANSDUCTION**
KDR		
KIT	AIF	FGF2
LCK	Bad	K-Ras, K-Ras, N-Ras
LYN	Bag1	TGF-alpha
MET	Bax	
PDGFRa	Bcl2	
PDGFRb	Bcl-xl	
RET	Bid	
SRC	c-IAP	
TRKA-C	FAP-1	
YES	Survivin	
ZAP70	x-IAP	
35 PHOSPHATASES, INCLUDING	**DNA REPAIR**	**OTHERS**
BAS	ERCCs 1, 2, 3	Actins beta & gamma
BDP1	Gadd45	BCRP
CD45	MGMT	Carcinoembryonic antigen
DEP-1	Mlh1	c-myc
ESP	Msh2	Desmin
GLEPP1	PCNA	Dihydropyrimidine dehydrogenase
IA2	Topo II alpha & beta	F1ATPase
IAR	XPA	Glycogen phosphorylase
MEG		HSC70
Meg2	**TRANSPORT**	HSP60
PCP-2		HSP90
PEST	ABC2	Laminin B
PTP	ABCAs 5, 6,12, 13	nm23
PTP-1B	ABCG5	Protein disulphide isomerase
SAP	ABCG8	Thymidine Kinase
SHP1	LRP	Thymidylate Synthase
SHP2	MDR activity	TRAG-3
STEP	MDR1	Tubulin beta
TC-PTP	MRP	Vimentin
ZPEP	RFC1	

PCNA, proliferating cell nuclear antigen; MDR1, multidrug resistance protein 1, TGF-alpha, transforming growth factor-alpha. This table summarises the results of Molecular Target measured in the NCI 60 human tumor cell line panel, not including data from microarray experiments. Targets are grouped according to function. Much of the data for kinase [7,9,52], cell cycle [3,22,32], apoptosis [3,19,21,26,43–45], DNA repair [3,31,46,55], transport [1,2,18,24,28,37,48,53], redox [12,41,47,51,56], signal transduction [9,20] and other targets [11,15,17,31,39,42] have been published. For all Targets, experimental details may be found by searching http://dtp.nci.nih.gov/mtargets/mt_index.html.

the single major influence on sensitivity. An exception to this is seen for Targets that influence the amount of active compound within the cell. For example, compounds that are substrates for the P-glycoprotein (Pgp) efflux pump show very strong negative correlations with Pgp activity, i.e. cells with high levels of Pgp activity are resistant to these drugs [1,2,53]. Thus, cellular components that influence the uptake or efflux of compounds may be found by a COMPARE analysis. A second category of Targets with a major influence on the amount of active compound within a cell are enzymes that can alter a compound, either activating a pro-drug, or destroying an active compound. An example of this is the positive correlations found between activity of the quinone-metabolising enzyme DT-diaphorase [14] and the sensitivity of the 60 cell line panel to EO9 and related compounds that are activated by this enzyme.

For cases where multiple cellular components influence drug sensitivity, COMPARE can still be of use. COMPARE with Diethyldithiocarbamate (NSC 4857), a reported inhibitor of nuclear factor (NF)-kappa B [30], as a seed yields modest correlations (0.35 to 0.51) with multiple genes involved in interleukin-1 (IL-1) signalling, including the IL-1 receptor and phospholipase C. Activation of the IL-1 pathway leads to the nuclear translocation of NF-kappa B.

Occasionally, the actual Molecular Target of a compound will be found by COMPARE. Sensitivity to an ErbB2 immunotoxin is dependent on expression of the gene, and yields a fairly high PCC of 0.54. Pasquale and colleagues [33] recently determined the ability of the 60 cell line panel to be infected by adeno-associated virus 5 (AAV5), and used those data as a seed to run COMPARE against the microarray dataset. One of the genes whose expression correlated with infectivity was the platelet-derived growth factor alpha, which they demonstrated to be the cellular receptor for the AAV5 virus.

6. NCI yeast anticancer drug screen

In the mid-1990's, a novel anti-cancer drug screen was initiated by Leland Hartwell and Stephen Friend at the Fred Hutchinson Cancer Research Center in Seattle, utilising a panel of *Saccharomyces cerevisiae* strains altered in DNA damage repair or cell cycle control genes. This project was begun as an NCI field station, and later converted into a contract managed by NCI-DTP. A more detailed review of this screen will be published elsewhere in Ref. [16]. Nearly 100 000 compounds were subjected to the initial stage (Stage 0) of this screen, against six strains at a single dose. Compounds meeting activity criteria were selected for further testing at two doses (Stage 1). The most promising compounds were selected for testing at five doses against 13 yeast strains (Stage 2). The data from all stages of the yeast screen are available at http://dtp.nci.nih.gov/yacds/index.html. One can search for data by NSC number, or browse Stage 0 and Stage 1 data by patterns of activity. Stage 2 data can be searched by NSC number, or one may browse through summaries of compounds with selective activity against a particular yeast strain. For example, compounds highly selective for strains with mutations in *rad50* and *rad52*, genes needed for repair of double-stranded DNA breaks, include known topoisomerase poisons such as 9-amino camptothecin (NSC 603071), which inhibits only these two strains over the ~2 log range of concentrations tested. In addition to compounds expected to introduce DNA breaks, several novel structures showed selectivity for these two strains. Two such compounds were demonstrated to interact with topoisomerase I [12]. Many of the Stage 2-tested compounds showed selectivity for the mitotic spindle checkpoint mutant *bub3*. While the DTP repository has a large number of tubulin-interactive compounds, which would be expected to trigger the spindle checkpoint, many compounds that interact with mammalian tubulin fail to bind yeast tubulin [5]. Thus, many of the *bub3*-selective hits are candidates for interfering with other components of the mitotic apparatus.

7. Downloadable datasets

For those interested in finding information on one or a few compounds, the DTP web site provides tools to retrieve and analyse data, as described in the preceding sections. Other researchers are interested in mining the large datasets. Most of the data on the DTP web site is available as downloadable datasets, and are in comma-delimited format that users can import into relational databases or spreadsheets and manipulate as desired. Thus, users can download 60 cell line data for approximately 43 000 compounds. This is organised into three files, each comprised of data for a single endpoint (GI_{50}, TGI or LC_{50}). Three additional files contain the data for just the Diversity Set. Two-dimensional structures for the 60 cell line tested compounds are available in MDL's SDFile format. In order to utilise the structural data, users will need to obtain a chemical software package. These datasets may be downloaded from http://dtp.nci.nih.gov/docs/cancer/cancer_data.html.

The Molecular Target data for the 60 cell line panel may be downloaded at http://dtp.nci.nih.gov/mtargets/download.html. There are currently three datasets available. There are two files with microarray data. The first presents data from a cDNA microarray experiment [36,38], analysing baseline mRNA expression in each of the 60 cell lines, relative to that in a pool of 12 of these cell lines. This dataset contains 9706 individual measurements for each of the cell lines. The second microarray

dataset contains data provided by Millennium Pharmaceuticals using Affymetrix oligonucleotide microarrays. This dataset consists of 5365 feature sets for which baseline mRNA expression was assayed in each of the 60 cell lines. For both of these microarray datasets, the gene assignments associated with each measurement are updated periodically utilising data from the human UniGene database of the National Center for Biotechnology Information. For the cDNA array data, the assignments are derived using the GenBank accession number for the sequence derived from the 3′ end of the cDNA. For the oligonucleotide array data, gene assignments are made using the GenBank accession number of the sequence used to design the oligonucleotides. A third dataset contains data determined from individual experiments (non-microarray data) and currently includes data from 255 measurements, including DNA mutation status, RNA expression, protein data and enzyme activity measurements.

Files containing structural information on several hundred thousand compounds may be downloaded at http://dtp.nci.nih.gov/docs/3d_database/structural_information/structural_data.html. Three-dimensional coordinates and Simplified Molecular Input Line Entry Specification (SMILES) strings are provided for several hundred thousand compounds. For those that are interested in particular subsets of compounds, separate files are available with structural data for compounds in the Diversity Set, the Mechanistic Set, the complete set of 140 000 plated compounds, as well as for compounds that were tested in the 60 cell line screen or in the AIDS screen. Chemical software is needed to utilise the information contained in these files.

Yeast screen data is provided in comma-delimited files for each of the 3 stages of the screen (http://dtp.nci.nih.gov/yacds/download.html). These files contain data for 87 264 compounds tested in the initial Stage 0 phase of the screen, 14 837 compounds that underwent further testing in Stage 1, and 2189 compounds that were selected for multi-dose testing in Stage 2. AIDS Antiviral Screen data for 43 905 compounds tested for ability to protect human CEM cells from infection by human immunodeficiency viris-1 (HIV-1) is available for download at http://dtp.nci.nih.gov/docs/aids/aids_screen.html [50].

Recently, DTP has begun to assemble these diverse datasets into a unified data warehouse. In this model, all assay results and chemical data are being merged into a single set of relational database tables. These tables are in a public Oracle instance, with a library of Java classes to facilitate data retrieval. Researchers will be able to write their own code to access the DTP data, and to seamlessly integrate it with their own data. Currently, the data warehouse contains GI_{50}, TGI and LC_{50} data from the 60 cell line screen (both the standard 2 day screen, as well as a non-routine 6 day assay), yeast screen data, data from the molecularly-targeted screens, chemical data, AIDS screen data and data from NCI's historical *in vivo* drug screen. The presentation of these data on the DTP web site is currently utilising the data warehouse architecture and the library of Java classes. Researchers interested in querying the data warehouse directly can find information at http://dtp.nci.nih.gov/dw/dw_main.html.

8. Conclusions

The DTP databases represent a tremendous resource available to the public, particularly to those interested in the drug discovery process. Suppliers submit their compounds to the 60 cell line screen for a variety of reasons. Some submit a series of compounds and utilise the resulting data to aid in selection of a lead compound for further development. Others with an interest in a particular type of cancer wish to determine whether a particular class of molecules has activity against human tumour cell lines derived from that tissue type. Some researchers have already done *in vitro* testing and seek to use the 60 cell line data for a COMPARE analysis, to help develop hypotheses about how the compound might function.

It is important to emphasise that while COMPARE has proven valuable in the generation of hypotheses, that any correlations need to be verified experimentally. There are some issues that arise frequently in doing a COMPARE analysis. Many of the compounds tested in the 60 cell line screen showed minimal activity, and were not tested further. The data for singly tested compounds should be scrutinised before investing resources in following up on such a correlation. Often compounds tested just once show little variability in the response of the cell lines. Other times, the pattern might appear to be dominated by one or a few cell lines, yielding correlation coefficients that may be quite high. While such results may be real, if the compound was only tested once, one does not know whether these results would be reproducible.

When running COMPARE with Molecular Target data, it is important to consider how a particular gene is regulated. This is particularly true in interpreting data from microarray experiments. RNA levels are not always well correlated with expression data for the protein it encodes [49]. Even with protein measurements, the relevant measure for interaction with a particular compound might be a modified form of the protein (i.e. phosphorylated, acetylated, acylated, etc.). A protein might localise to different locations within the cell, or might need to associate with other cellular components. These caveats make it particularly important to experimentally verify any correlations between compounds and Molecular Targets.

Since different researchers have differing goals for utilising the DTP databases, the web site provides multiple ways of accessing the datasets. Users may explore the data using the tools that DTP provides to retrieve and analyse particular pieces of data. For those who wish to develop their own analysis tools and techniques, the datasets can be downloaded and subjected to these protocols.

Acknowledgements

The author wishes to credit those who have performed the screening and developed many of the analysis tools described in this article. 60 cell line screening was performed in DTP's Screening Technology Branch, directed by Robert Shoemaker and Dominic Scudiero. Richard Klausner, Leland Hartwell, Stephen Friend, Julian Simon, Michele Cronk, Heather Dunstan, David Evans, John Lamb, and Philippe Szankasi contributed to the Yeast screen, which was performed at the Fred Hutchinson Cancer Research Center in Seattle. Data analysis tools and the DTP web site are developed by members of DTP's Information Technology Branch, including Daniel Zaharevitz, David Segal, Marie Hose, Mark Kunkel, Timothy Myers, Ken Paull and Penny Svetlik. Molecular Target data in the 60 cell line panel was generated by numerous researchers. Credit for each of these measurements is indicated on the DTP web site.

References

1. Alvarez M, Paull K, Monks A, *et al.* Generation of a drug resistance profile by quantitation of mdr-1/P-glycoprotein in the cell lines of the National Cancer Institute Anticancer Drug Screen. *J Clin Invest* 1995, **95**, 2205–2214 PMID: 7738186.
2. Alvarez M, Robey R, Sandor V, *et al.* Using the national cancer institute anticancer drug screen to assess the effect of MRP expression on drug sensitivity profiles. *Mol Pharmacol* 1998, **54**, 802–814.
3. Amundson SA, Myers TG, Scudiero D, Kitada S, Reed JC, Fornace Jr AJ. An informatics approach identifying markers of chemosensitivity in human cancer cell lines. *Cancer Res* 2000, **60**, 6101–6110 PMID: 11085534.
4. Blaskovich MA, Sun J, Cantor A, Turkson J, Jove R, Sebti SM. Discovery of JSI-124 (cucurbitacin I), a selective Janus kinase/signal transducer and activator of transcription 3 signaling pathway inhibitor with potent antitumor activity against human and murine cancer cells in mice. *Cancer Res* 2003, **62**, 1270–1279 PMID: 12649187.
5. Bode CJ, Gupta ML, Reiff EA, Suprenant KA, Georg GI, Himes RH. Epothilone and paclitaxel: unexpected differences in promoting the assembly and stabilization of yeast microtubules. *Biochemistry* 2002, **41**, 3870–3874.
6. Boyd MR, Farina C, Belfiore P, *et al.* Discovery of a novel antitumor benzolactone enamide class that selectively inhibits mammalian vacuolar-type (H+) ATPases. *J Pharmacol Exp Ther* 2001, **297**, 114–120 PMID: 11259534.
7. Budde RJ, Ke S, Levin VA. Activity of pp60c-src in 60 different cell lines derived from human tumors. *Cancer Biochem Biophys* 1994, **14**, 171–175 PMID: 7537173.
8. Bykov VJ, Issaeva N, Shilov A, *et al.* Restoration of the tumor suppressor function to mutant p53 by a low-molecular-weight compound. *Nat Med* 2002, **8**, 282–288 PMID: 11875500.
9. Chandler LA, Sosnowski BA, Greenlees L, Aukerman SL, Baird A, Pierce GF. Prevalent expression of fibroblast growth factor (FGF) receptors and FGF2 in human tumor cell lines. *Int J Cancer* 1999, **81**, 451–458 PMID: 10209961.
10. Cleaveland ES, Monks A, Vaigro-Wolff A, *et al.* Site of action of two novel pyrimidine biosynthesis inhibitors accurately predicted by the compare program. *Biochem Pharmacol* 1995, **49**, 947–954 PMID: 7741767.
11. Duan Z, Feller AJ, Toh HC, Makastorsis T, Seiden MV. TRAG-3, a novel gene, isolated from a taxol-resistant ovarian carcinoma cell line. *Gene* 1999, **229**, 75–81 PMID: 10095106.
12. Dunstan HM, Ludlow C, Goehle S, *et al.* Cell-based assays for identification of novel double-strand break-inducing agents. *J Natl Cancer Inst* 2002, **94**, 88–94 PMID: 11792746.
13. Efferth T, Sauerbrey A, Halatsch ME, Ross DD, Gebhart E. Molecular modes of action of cephalotaxine and homoharringtonine from the coniferous tree Cephalotaxus hainanensis in human tumor cell lines. *Naunyn Schmiedebergs Arch Pharmacol* 2003, **367**, 56–67 PMID: 12616342.
14. Fitzsimmons SA, Workman P, Grever M, Paull K, Camalier R, Lewis AD. Reductase enzyme expression across the National Cancer Institute Tumor cell line panel: correlation with sensitivity to mitomycin C and EO9. *J Natl Cancer Inst* 1996, **88**, 259–269.
15. Grem JL, Danenberg KD, Behan K, *et al.* Thymidine kinase, thymidylate synthase, and dihydropyrimidine dehydrogenase profiles of cell lines of the National Cancer Institute's Anticancer Drug Screen. *Clin Cancer Res* 2001, **7**, 999–1009 PMID: 11309351.
16. Holbeck SL, Simon J. The FHCRC/NCI yeast anticancer drug screen. In Nitiss JL, Heitman J, eds. *Yeast as a Tool in Cancer Research*, in press.
17. Imai Y, Nakane M, Kage K, *et al.* C421A polymorphism in the human breast cancer resistance protein gene is associated with low expression of Q141K protein and low-level drug resistance. *Mol Cancer Ther* 2002, **1**, 611–616 PMID: 12479221.
18. Izquierdo MA, Shoemaker RH, Flens MJ, *et al.* Overlapping phenotypes of multidrug resistance among panels of human cancer-cell lines. *Int J Cancer* 1996, **65**, 230–237 PMID: 8567122.
19. Kitada S, Krajewska M, Zhang X, *et al.* Expression and location of pro-apoptotic Bcl-2 family protein BAD in normal human tissues and tumor cell lines. *Am J Pathol* 1998, **152**, 51–61 PMID: 9422523.
20. Koo HM, Monks A, Mikheev A, *et al.* Enhanced sensitivity to 1-beta-D-arabinofuranosylcytosine and topoisomerase II inhibitors in tumor cell lines harboring activated ras oncogenes. *Cancer Res* 1996, **56**, 5211–5216 PMID: 8912859.
21. Krajewska M, Zapata JM, Meinhold-Heerlein I, *et al.* Expression of Bcl-2 family member Bid in normal and malignant tissues. *Neoplasia* 2002, **4**, 129–140 PMID: 11896568.
22. Kubo A, Nakagawa K, Varma RK, *et al.* The p16 status of tumor cell lines identifies small molecule inhibitors specific for cyclin-dependent kinase 4. *Clin Cancer Res* 1999, **5**, 4279–4286.
23. Lazo JS, Aslan DC, Southwick EC, *et al.* Discovery and biological evaluation of a new family of potent inhibitors of the dual specificity protein phosphatase Cdc25. *J Med Chem* 2001, **44**, 4042–4049 PMID: 11708908.
24. Lee JS, Paull K, Alvarez M, *et al.* Rhodamine efflux patterns predict P-glycoprotein substrates in the National Cancer Institute drug screen. *Mol Pharmacol* 1994, **46**, 627–638.
25. Leteurtre F, Sackett DL, Madalengoitia J, *et al.* Azatoxin derivatives with potent and selective action on topoisomerase II. *Biochem Pharmacol* 1995, **49**, 1283–1290 PMID: 7763310.
26. Meinhold-Heerlein I, Stenner-Liewen F, Liewen H, *et al.* Expression and potential role of Fas-associated phosphatase-1 in ovarian cancer. *Am J Pathol* 2001, **158**, 1335–1344 PMID: 11290551.

27. Monks A, Scudiero D, Skehan P, *et al.* Feasibility of a high-flux anticancer drug screen using a diverse panel of cultured human tumor cell lines. *J Natl Cancer Inst* 1991, **83**, 757–766.
28. Moscow JA, Connolly T, Myers TG, Cheng CC, Paull K, Cowan KH. Reduced folate carrier gene (RFC1) expression and antifolate resistance in transfected and non-selected cell lines. *Int J Cancer* 1997, **72**, 184–190 PMID: 9212241.
29. Mu F, Coffing SL, Riese 2nd DJ, *et al.* Design, synthesis, and biological evaluation of a series of lavendustin A analogues that inhibit EGFR and Syk tyrosine kinases, as well as tubulin polymerisation. *J Med Chem* 2001, **44**, 441–452 PMID: 11462983.
30. Mulsch A, Schray-Utz B, Mordvintcev PI, Hauschildt S, Busse R. Diethyldithiocarbamate inhibits induction of macrophage NO synthase. *FEBS Lett* 1993, **321**, 215–218.
31. Myers TG, Anderson NL, Waltham M, *et al.* A protein expression database for the molecular pharmacology of cancer. *Electrophoresis* 1997, **18**, 647–653 PMID: 9150955.
32. O'Connor PM, Jackman J, Bae I, *et al.* Characterization of the p53 tumor suppressor pathway in cell lines of the National Cancer Institute anticancer drug screen and correlations with the growth-inhibitory potency of 123 anticancer agents. *Cancer Res* 1997, **57**, 4285–4300 PMID: 9331090.
33. Pasquale GD, Davidson BL, Stein CS, *et al.* Identification of PDGFR as a receptor for AAV-5 transduction. *Nat Med* in press. PMID: 14502277.
34. Paull KD, Shoemaker RH, Hodes L, *et al.* Display and analysis of patterns of differential activity of drugs against human tumor cell lines: development of mean graph and COMPARE algorithm. *J Natl Cancer Inst* 1989, **81**, 1088–1092.
35. Rapisarda A, Uranchimeg B, Scudiero DA, *et al.* Identification of small molecule inhibitors of hypoxia-inducible factor 1 transcriptional activation pathway. *Cancer Res* 2002, **62**, 4316–4324 PMID: 12154035.
36. Ross DT, Scherf U, Eisen MB, *et al.* Systematic variation in gene expression patterns in human cancer cell lines. *Nat Genet* 2000, **24**, 227–235.
37. Scheffer GL, de Jong MC, Monks A, *et al.* Increased expression of beta 2-microglobulin in multidrug-resistant tumour cells. *Br J Cancer* 2002, **86**, 1943–1950 PMID: 12085191.
38. Scherf U, Ross DT, Waltham M, *et al.* A gene expression database for the molecular pharmacology of cancer. *Nat Genet* 2000, **24**, 236–244.
39. Schnier JB, Nishi K, Monks A, Gorin FA, Bradbury EM. Inhibition of glycogen phosphorylase (GP) by CP-91,149 induces growth inhibition correlating with brain GP expression. *Biochem Biophys Res Commun* 2003, **309**, 126–134 PMID: 12943673.
40. Solary E, Leteurtre F, Paull KD, Scudiero D, Hamel E, Pommier Y. Dual inhibition of topoisomerase II and tubulin polymerization by azatoxin, a novel cytotoxic agent. *Biochem Pharmacol* 1993, **45**, 2449–2456 PMID: 8392342.
41. Sreerama L, Sladek NE. Class 1 and class 3 aldehyde dehydrogenase levels in the human tumor cell lines currently used by the National Cancer Institute to screen for potentially useful antitumor agents. *Adv Exp Med Biol* 1997, **414**, 81–94 PMID: 9059610.
42. Stinson SF, Alley MC, Kopp WC, *et al.* Morphological and immunocytochemical characteristics of human tumor cell lines for use in a disease-oriented anticancer drug screen. *Anticancer Res* 1992, **12**, 1035–1053 PMID: 1503399.
43. Takayama S, Krajewski S, Krajewska M, *et al.* Expression and location of Hsp70/Hsc-binding anti-apoptotic protein BAG-1 and its variants in normal tissues and tumor cell lines. *Cancer Res* 1998, **58**, 3116–3131 PMID: 9679980.
44. Tamm I, Kornblau SM, Segall H, *et al.* Expression and prognostic significance of IAP-family genes in human cancers and myeloid leukemias. *Clin Cancer Res* 2000, **6**, 1796–1803 PMID: 10815900.
45. Tamm I, Wang Y, Sausville E, Scudiero DA, Vigna N, Oltersdorf T, Reed JC. IAP-family protein survivin inhibits caspase activity and apoptosis induced by Fas (CD95), Bax, caspases, and anticancer drugs. *Cancer Res* 1998, **58**, 5315–5320 PMID: 9850056.
46. Taverna P, Liu L, Hanson AJ, Monks A, Gerson SL. Characterization of MLH1 and MSH2 DNA mismatch repair proteins in cell lines of the NCI anticancer drug screen. *Cancer Chemother Pharmacol* 2000, **46**, 507–516 PMID: 11138465.
47. Tew KD, Monks A, Barone L, *et al.* Glutathione-associated enzymes in the human cell lines of the National Cancer Institute Drug Screening Program. *Mol Pharmacol* 1996, **50**, 149–159 PMID: 8700107.
48. Vulevic B, Chen Z, Boyd JT, *et al.* Cloning and characterization of human adenosine 5′-triphosphate-binding cassette, sub-family A, transporter 2 (ABCA2). *Cancer Res* 2001, **61**, 3339–3347 PMID: 11309290.
49. Washburn MP, Koller A, Oshiro G, *et al.* Protein pathway and complex clustering of correlated mRNA and protein expression analyses in Saccharomyces cerevisiae. *Proc Natl Acad Sci USA* 2003, **100**, 3107–3112.
50. Weislow OS, Kiser R, Fine DL, Bader J, Shoemaker RH, Boyd MR. New soluble-formazan assay for HIV-1 cytopathic effects: application to high-flux screening of synthetic and natural products for AIDS-antiviral activity. *J Natl Cancer Inst* 1989, **81**, 577–586.
51. Woo ES, Monks A, Watkins SC, Wang AS, Lazo JS. Diversity of metallothionein content and subcellular localization in the National Cancer Institute tumor panel. *Cancer Chemother Pharmacol* 1997, **41**, 61–68 PMID: 9443615.
52. Wosikowski K, Schuurhuis D, Johnson K, *et al.* Identification of epidermal growth factor receptor and c-erbB2 pathway inhibitors by correlation with gene expression patterns. *J Natl Cancer Inst* 1997, **89**, 1505–1515.
53. Wu L, Smythe AM, Stinson SF, *et al.* Multidrug-resistant phenotype of disease-oriented panels of human tumor cell lines used for anticancer drug screening. *Cancer Res* 1992, **52**, 3029–3034 PMID: 1350507.
54. Xia Y, Yang ZY, Xia P, *et al.* Antitumor Agents. 211. Fluorinated 2-phenyl-4-quinolone derivatives as antimitotic antitumor agents. *J Med Chem* 2001, **44**, 3932–3936 PMID: 11689079.
55. Xu Z, Chen ZP, Malapetsa A, *et al.* DNA repair protein levels vis-a-vis anticancer drug resistance in the human tumor cell lines of the National Cancer Institute drug screening program. *Anticancer Drugs* 2002, **13**, 511–519 PMID: 12045463.
56. Yu LJ, Matias J, Scudiero DA, *et al.* P450 enzyme expression patterns in the NCI human tumor cell line panel. *Drug Metab Dispos* 2001, **29**, 304–312 PMID: 11181500.
57. Zaharevitz DW, Gussio R, Leost M, *et al.* Discovery and initial characterization of the paullones, a novel class of small-molecule inhibitors of cyclin-dependent kinases. *Cancer Res* 1999, **59**, 2566–2569.

EXHIBIT K

Int J Gynecol Cancer 2003, 13(suppl 2), 133–139

Proteomic analysis for early detection of ovarian cancer: A realistic approach?

E. V. STEVENS, L. A. LIOTTA & E. C. KOHN
Laboratory of Pathology, National Cancer Institute, Center for Cancer Research, Bethesda, MD

Abstract. Stevens EV, Liotta LA, Kohn EC. Proteomic analysis for early detection of ovarian cancer: A realistic approach? *Int J Gynecol Cancer* 2003;13(suppl 2):133–139.

Ovarian cancer is a multifaceted disease wherein most women are diagnosed with advanced stage disease. One of the most imperative issues in ovarian cancer is early detection. Biomarkers that allow cancer detection at stage I, a time when the disease is amenable to surgical and chemotherapeutic cure in over 90% of patients, can dramatically alter the horizon for women with this disease. Recent developments in mass spectroscopy and protein chip technology coupled with bioinformatics have been applied to biomarker discovery. The complexity of the proteome is a rich resource from which the patterns can be gleaned; the pattern rather than its component parts is the diagnostic. Serum is a key source of putative protein biomarkers, and, by its nature, can reflect organ-confined events. Pioneering use of mass spectroscopy coupled with bioinformatics has been demonstrated as being capable of distinguishing serum protein pattern signatures of ovarian cancer in patients with early- and late-stage disease. This is a sensitive, precise, and promising tool for which further validation is needed to confirm that ovarian cancer serum protein signature patterns can be a robust biomarker approach for ovarian cancer diagnosis, yielding improved patient outcome and reducing the death and suffering from ovarian cancer.

KEYWORDS: biomarker, mass spectroscopy, ovarian cancer, proteomic.

The leading cause of death from gynecologic malignancies in the US is epithelial ovarian cancer[1]. It is forecast that 25,400 new cases of ovarian cancer will be diagnosed in the US in 2003, and 14,300 ovarian cancer patients will succumb to disease. Although 212,600 women will be diagnosed with breast cancer during that same time, the mortality rate is approximately 19%, compared to 56% in ovarian cancer. This dramatic increase in risk of death for women with ovarian cancer is because breast cancer is most commonly diagnosed at an early stage either by self-examination or by noninvasive imaging[2]. The lack of a diagnostic symptom profile or simple noninvasive diagnostic physical examination techniques makes ovarian cancer almost impossible to diagnose early clinically. Most women are diagnosed with ovarian cancer after it has spread beyond the ovary into the peritoneal cavity. The chance of patients living 5 years after diagnosis in this advanced stage is between 20 and 25%[3]. The mortality rate could greatly decrease with a presymptomatic screening test that has adequate sensitivity and specificity to detect ovarian cancer when it is organ-confined and can be resected with increased probability for cure. New screening techniques using proteomic approaches are being developed with higher preliminary success rates than conventional methods.

Address correspondence and reprint requests to: Dr Elise C. Kohn, MD, 10 Center Drive MSC 1500, Building 10, Room B1B51, Bethesda, MD 20892-1500. Email: kohne@mail.nih.gov

Limitations in diagnostic screening

Reliable, accurate, sensitive, and specific biomarkers for early detection and prognostication of ovarian cancer remain a critical need[4–8]. Ovarian cancer is considered a relatively rare disease with approximately one in 2500 postmenopausal women in the general population affected and a much lower incidence in premenopausal women. The burden of proof for any biomarker becomes more difficult as the disease is less common. A specificity of 99.6% on a background of 100% sensitivity has been identified as the minimum requirement of a biomarker for the detection of ovarian cancer at a positive predictive value of the biomarker of 10%[8]. This means that very stringent conditions are needed to find the one ovarian cancer in 10 women presenting for cause. After a patient's screening results are positive, the next step is a diagnostic exploratory laparotomy or laparoscopy to confirm the diagnosis pathologically and debulk disease.

Detection and surgical removal of early-stage ovarian cancer, when the cancer is still confined to the ovaries, results in cure in over 90% of patients[9]. Thus, the first task in tackling ovarian cancer is to develop a reliable screening system to identify patients when the disease is organ confined or minimally spread, stage I/II disease, and triage them to appropriate gynecologic oncologic care. CA125, the only biomarker available for ovarian cancer monitoring, has been approved only for use in monitoring ovarian cancer patients for recurrence of disease[4–8,10], but not for screening, even in the genetically high-risk patients. Nonetheless, it is used commonly in that high-risk group, alone or in concert with ultrasound imaging[10]. The combination has not been successful in selective identification of early-stage disease patients, although it has yielded an overall improved survival rate[11]. CA125 is elevated in approximately 80–85% of women with advanced stage ovarian cancer at diagnosis[4–8,10]. However, it is only abnormal in 50–60% of patients with early-stage disease and in all stages is most likely to be elevated in serous cancers[12]. Newer approaches, such as the Risk of Ovarian Cancer Algorithm[13,14], discussed elsewhere in this meeting report, may make the predictive reliability of CA125 better. Unfortunately, there are many sources of false positively elevated CA125 that need be considered including benign gynecologic disease, benign and malignant breast and colon disease, and other irritants of the peritoneal cavity[15,16].

New technologies and bioinformatic approaches are under development to be applied to the question of biomarkers for early detection of ovarian cancer. Few cancers are characterized by a single reliable biomarker. Thus, the challenge in identification of an ovarian cancer screening tool is how and what information to combine to engineer the most sensitive, specific, and reliable discriminate of disease. Current directions, which are discussed by Dr Jacobs elsewhere in this issue, combine clinical history, CA125, and, where indicated, color Doppler flow ultrasound with the Risk of Ovarian Cancer Algorithm[10,11]. Whether the combination of this approach with new biomarker panels or technologies will further advance its progress is an important question.

Application of mass spectroscopy proteomic approaches

The field of proteomics has brought new technology with which to approach ovarian cancer detection and offers a series of new directions that may bear fruit. Our group hypothesized that circulating blood is exposed to disease even when organ confined and therefore could harbor occult information regarding that disease[17]. This is not a novel hypothesis, in that we know that prostate-specific antigen (PSA) can be elevated in organ-limited prostate cancer, and elevated human chorionic gonadotrophin (β-HCG) is a marker of pregnancy, also an organ-confined process. The twist on the hypothesis is that the proteins in the circulating blood may be iterated into patterns that provide diagnostic information in the absence of specific identification. Proteins, the 'effector organs' of genomics and transcriptomics, are often secreted or released into the local microenvironment where they may end up in the circulating blood. Application of micromass spectroscopy coupled with complex bioinformatic techniques to samples of blood from affected and unaffected patients has shown promise for the identification of discriminating protein signature patterns in the blood of organ-confined disease for ovarian cancer and other solid tumors[17].

SELDI (surface-enhanced laser desorption and ionization) or MALDI (matrix-assisted laser desorption and ionization) with time of flight (TOF) detection are mass spectroscopy approaches that allow us to 'see' selected components of the low-molecular-weight proteome, a heretofore untapped information reserve[18–21]. Low-molecular-weight proteins, indistinguishable by conventional techniques, could reflect the pathological state of organs and aid in the new discovery of proteomic patterns unique to early stages of ovarian cancer[17]. Serum samples of less than 10 μl obtained from a routine venipuncture have been used in the SELDI–TOF system.

The serum samples are applied to protein chips of different protein-binding specificities. This provides a preselection of proteins in the sample through binding to the treated chip surface, such that only a subset of proteins within the serum sample are bound to the matrix and therefore detected as shown in Figure 1. The use of multiple capture chip matrices provides different views of the proteome.

The serum protein-bound chips are introduced into a mass spectroscopy machine. Data output reflect the different species of serum proteins captured on the chip. Separation and detection of proteins results from ionization of proteins with laser energy and their 'flight' off the chip down the vacuum tube to the detector. This occurs in direct proportion to the size and net electrical charge of the protein (m/z) and is not a quantitative reflection of the presence of the species in the sample. Depending upon the resolution of the mass spectroscopy unit, the datastream can contain 15,000–350,000 datapoints in the region below 20,000 Da/charge ratio[19]. This portion of the proteome is frequently mono-charged, thereby reflecting the molecular weight of the protein in most but not all cases. The mass spectroscopy pattern is shown as a chromatographic pattern wherein the peak amplitude is represented on the y-axis at a given mass/charge assignment (x-axis). These x,y coordinate datapoints in the datastream are applied via ASCII file to the bioinformatic program for analysis[17].

Application of advanced bioinformatic algorithms to the mass spectroscopy datastreams mines the data for diagnostic patterns of information. The algorithm approach we have used teaches the bioinformatic program what it should be looking for by presenting datastreams from a teaching set of defined populations. We 'educated' the bioinformatic program with known mass spectroscopy datastreams from serum from women unaffected with ovarian cancer and from a cohort of women with varied stages of disease from whom blood was ascertained prior to surgical and chemotherapeutic intervention. The program was charged with defining an algorithm that fully segregates the unaffected from affected sera (Fig. 2). It begins by randomly selecting a set of five features (the x,y coordinates) and asking whether they discriminate the two known cohorts. It continues iterating until it identifies a set of features, beginning with 5 and going up as required, which successfully meets the criteria, in this case 100% segregation of unaffected from affected. This is the optimized diagnostic pattern. This pattern is then used to classify diagnostically unknown samples from which to test its true discriminative ability. A diagnostic signature pattern for ovarian cancer has been developed from at least three different chip selection matrix backgrounds, and in each case has consisted of five key discriminant features. Use of the weak cation exchange chip (WCXII) has consistently resulted in signature patterns that are 99–100% sensitive and 99–100% specific when queried with blinded unknown samples (Table 1).

These results coupled with preliminary application of this technology by other several groups have shown it to be promising as a new biomarker tool. Our demonstration of a sensitivity and specificity, both 99–100%, indicates that this approach may have the power to detect ovarian cancer signatures in the range required for a realistic biomarker. Large-scale

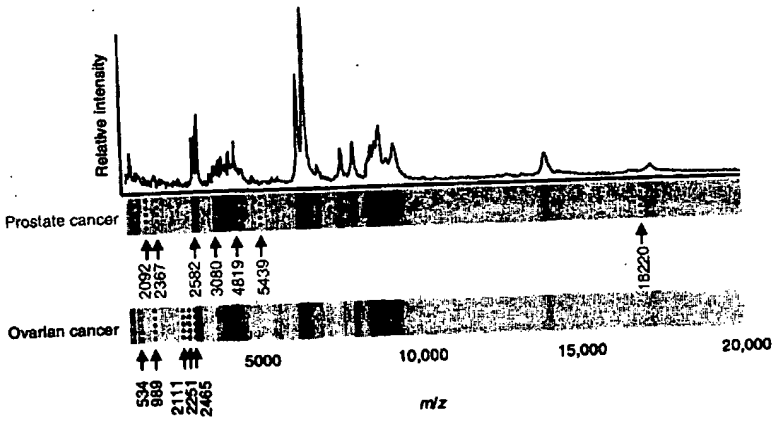

Fig. 1. Mass chromatograms of ovarian and prostate cancer patients' serum. Ovarian and prostate cancer patient serum samples are bound to the C18 reverse-phase hydrophobic chip surfaces. The ovarian cancer mass spectroscopy band patterns from the C18 chip are translated into a peak intensity spectra with mass/charge values on the x-axis and a relative amplitude on the y-axis. A gel view of the chromatogram is shown for both the prostate (upper) and the ovarian (lower) cancer samples below. The prostate cancer and ovarian cancer share common visible band patterns. However, the key feature diagnostic subset is different for the two cancers and requires seven features to segregate prostate cancer and five key features to identify ovarian cancer (noted below gel view by arrows and m/z size)[34]. The signature differences could not be attributed to simple gender differences[17].

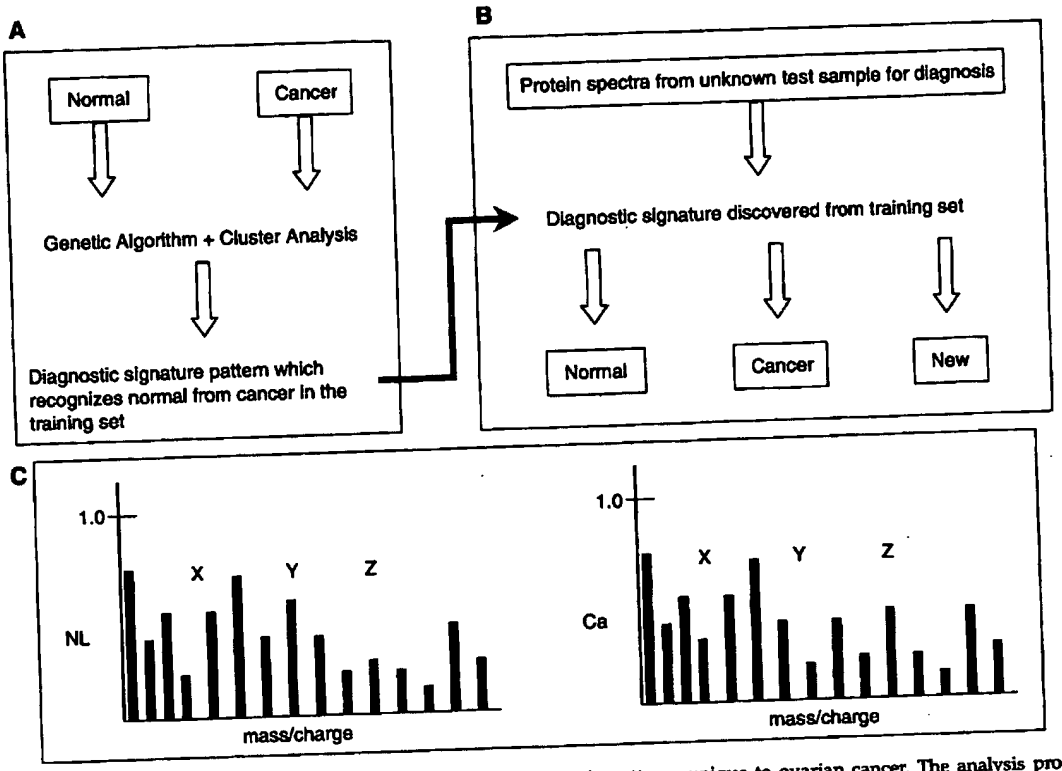

Fig. 2. Discovery algorithm for optimal discriminatory signature proteomic patterns unique to ovarian cancer. The analysis procedure is composed of two phases, the training set (A) and sample for diagnosis set (B). The training set contains samples from patients who are known to be normal (unaffected) or have cancer (affected with ovarian cancer in various stages). The bioinformatic program searches the serum mass spectroscopy spectra patterns between these two groups to find the smallest subset of five to 20 unique key features that discriminate fully between normal and cancer. This is defined as the ovarian cancer signature pattern. This signature pattern is then used in the second phase to identify unknown patient samples. The samples for diagnosis are placed in unaffected, affected, or new categories based on where their values for the key feature subset cluster in N(5) space. The third category is recognized as being neither normal nor cancer. (C) Presentation of a three mass/charge key feature subset example which distinguishes normal from cancer. Ca, cancer; NL, normal.

prospective and blinded studies are necessary to determine the robustness of these early findings and to form the basis for its application in prospective screening trials.

Proteomics for prognostication and treatment selection

Although most women are diagnosed with advanced ovarian cancer, and of that group over 80% ultimately die of their disease, we know also that there is a subset of women with early-stage disease who succumb to their cancer[4]. One explanation is that these women are incompletely or improperly staged. Another is that they have a fortuitously early-stage presentation of an aggressive cancer. Last, cancers may have or develop drug resistance under different selection criteria. We currently do not have reliable means of answering these questions or, more importantly, to identify those women at risk early enough to intervene. An important parallel application of the biomarker proteomic signature diagnostics and the data mining technology will be to identify the early-stage patients for whom our current interventions do not provide long-term disease remission or cure. This should be done in the context of a large prospective clinical trial of early-stage patients, homogeneously treated, for whom blood samples are ascertained prior to chemotherapeutic intervention. Long-term follow up will allow stratification of the training sets for cured patients and those who relapse. The identified signatures can be validated in subsequent prospective patient trials. This approach has been proposed as a pilot in advanced stage disease. The observation that the signature patterns identified to date by our group are not stage specific and consistently recognize all early-stage patients suggests that this approach may be successful.

Table 1. Preliminary results of weak cation exchange selection chip signature pattern test ($n = 250$ blinded samples)

	Correct/total	Percentage
Blinded unaffected test cohort	66/67	99
Unaffected	70/71	99
Benign gynecologic and nongynecologic inflammatory		99
Specificity		
Blinded ovarian cancer cohort	75/76	99
Stages II, III, and IV	36/36	100
Stage I		99
Sensitivity		

Data ascertained from ABI qTOF LC-MS-MS mass spectroscopy unit[19].

Therapeutic markers discovered through molecular and proteomic microarrays

The advances in technology have been applied to cell lines and patient samples both to advance early diagnostic biomarker discovery and to learn more about the phenotype of the ovarian cancer to optimize treatment decisions. This approach can take several directions, including transcriptomic assessment followed by proteomic confirmation or direct proteomic studies. Gene and protein expression and activation may be modified during chemotherapeutic drug treatment. These changes may be causative or in response to injury, resulting in drug resistance or signaling pathway changes.

Application of cDNA microarray analysis to ovarian cancer and other cancer cell lines and patient samples obtained before and after treatment have been performed by several groups[22–24]. The goal is to identify markers of resistance. This high throughput approach allows investigation of multiple putative markers at one time and placement of the markers into analytical perspective. One example is the study of camptothecin (CPT), a topoisomerase I inhibitor, the derivatives of which are used clinically to treat ovarian cancer and colorectal carcinomas[25,26]. The sensitivity of CPT in cancer patients is due to molecular responses to the DNA damage it causes[27,28]. cDNA microarrays of 1694 cancer-related genes were used to monitor the gene expression consequences of CPT treatment *in vitro* to S-phase synchronized HCT116 colon cancer cells[29]. Qualitative differences in cluster analysis patterns of gene expression were produced between low- and high-CPT exposure concentrations. Gene expression array analysis yielded gene function clusters that were differentially expressed with treatment.

Further proteomic technology advances allow signal pathway profiling of a variety of signaling pathways active in tumor and stroma. Laser capture microdissection of tumor epithelium and stroma provides template of select tumor subpopulations of the local tumor microenvironment that may be responsible for the tumor growth and death responses to treatment[30]. This small number of cells does not provide enough material, either RNA or protein, for detailed assessment using traditional assay templates. We have developed a microimmunoblot technique[31] that when coupled with microdissection of tumor samples provides high quality and reproducible results. Further, we have applied that to the development of reverse-phase protein or tissue lysate protein arrays[19,32]. We are now using tissue lysate arrays of tumor epithelium and stroma microdissected samples to profile the signaling pathways activated and regulated in ovarian cancer patients enrolled in our trials of the oral tyrosine kinase small molecular inhibitors imatinib mesylate (Gleevec) and ZD1839 (Iressa) for advanced and relapsed ovarian cancer patients. We hypothesize that application of these techniques will allow us to individualize our therapy to treat the cancer of the individual patient rather than the category of cancer in the population (Fig. 3). Identification of the specific signal events active in a particular cancer and targeting intervention to those specific molecular events may improve treatment while reducing toxicity and may allow us to understand better how ovarian cancer behaves and why in different patients.

Conclusion

Preliminary and promising results of ovarian cancer proteomic signature patterns have been documented by our group[18–20] and others[11,21,33]. Importantly, not all groups are using the same bioinformatic approach, thus validating the power of the information in the mass spectroscopy datastreams if mined appropriately. Further technologic advances have been made so that the features comprising the diagnostic patterns can be isolated and identified from the small blood volumes obtained. We are now applying advanced LC-MS-MS mass spectroscopy to the isolation of key features of the diagnostic patterns. While the pattern may reflect the organ-confined disease itself, or the host response to it, the cause of the pattern is irrelevant to the potential

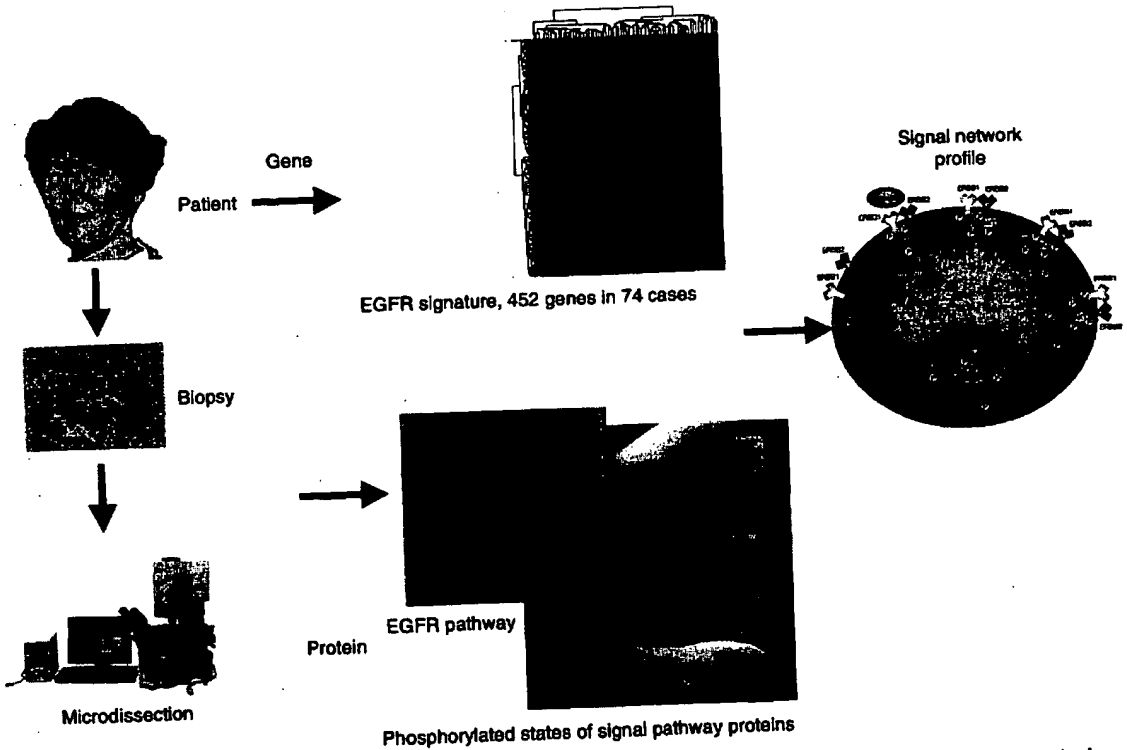

Fig. 3. Genomic and proteomic microarrays. Combining proteomic and transcriptomic microarrays to dissect the signaling events in the cell can yield insight into the status of molecular pathways active in the individual patient's cancer. Patient biopsy tissues are subjected to laser capture microdissection from which protein and RNA resources are obtained. cDNA arrays give insight into the gene expression levels, whereas the tissue lysate microarrays yield protein quantity and activation information. Complex bioinformatic tools analyze the arrays and are capable of finding pathways activated or deactivated in response to drug therapy. It is proposed that these technologies may be applied to individual patient analysis in the future to drive therapeutic decision making for each patient in the paradigm of individualized molecular medicine[18].

effectiveness of the pattern as a diagnostic biomarker. However, these differences pose new challenges to the isolation and characterization of key feature peptides and if not kept in perspective, may cloud our understanding and appreciation of potential value of the pattern concept. Proteomics is a promising direction for clinical and scientific advancement in our understanding and diagnosis of ovarian and other gynecologic cancers.

References

1 Jemal A, Murray T, Samuels A, Ghafoor A, Ward E, Thun MJ. Cancer statistics, 2003. *CA Cancer J Clin* 2003;53:5–26.
2 National Cancer Institute. Cancer Net PDQ cancer information summaries. Monographs on "Screening for breast cancer" (available at http://www.cancer.gov/cancer_information/pdq/).
3 Piver MS, Baker TR, Driscoll DL. Lack of substantial five year disease-free survival by primary aggressive surgery and cisplatin-based chemotherapy or by salvage intraperitoneal cisplatin-based chemotherapy. *Eur J Gynaecol Oncol* 1990;11:243–50.
4 Ozols RF, Rubin SC, Thomas GM, Robboy SJ. Epithelial ovarian cancer. In: Hoskins WJ, Perez CA, Young RC, eds. *Principle and Practice of Gynecologic Oncology*. Philadelphia: Lippincott Williams & Wilkins; 2000:981–1058.
5 Bast RC Jr, Klug TL, St John E *et al*. A radioimmunoassay using a monoclonal antibody to monitor the course of epithelial ovarian cancer. *N Engl J Med* 1983;309:883–7.
6 Menon U, Jacobs I. Tumor markers. In: Hoskins WJ, Parker CA, Young RC, eds. *Principles and Practice of Gynecologic Oncology*. Philadelphia: Lippincott Williams & Wilkins; 2000:165–82.
7 Menon U, Jacobs IJ. Recent developments in ovarian cancer screening. *Curr Opin Obstet Gynecol* 2000;12:39–42.
8 Jacobs IJ, Skates SJ, MacDonald N *et al*. Screening for ovarian cancer: a pilot randomised controlled trial. *Lancet* 1999;353:1207–10.
9 Piver MS, Wong C. Role of prophylactic surgery for women with genetic predisposition to cancer. *Clin Obstet Gynecol* 1998;41:215–24.
10 Cohen LS, Escobar PF, Scharm C, Glimco B, Fishman DA. Three-dimensional power Doppler ultrasound improves the diagnostic accuracy for ovarian cancer prediction. *Gynecol Oncol* 2001;82:40–8.

11 Menon U, Jacobs I. Screening for ovarian cancer. *Best Pract Res Clin Obstet Gynaecol* 2002;16:469–82.
12 Jacobs I, Bast RC Jr. The CA 125 tumour-associated antigen: a review of the literature. *Hum Reprod* 1989;4:1–12.
13 Skates SJ, Xu FJ, Yu YH *et al.* Toward an optimal algorithm for ovarian cancer screening with longitudinal tumor markers. *Cancer* 1995;76:2004–10.
14 Skates SJ. Screening for ovarian cancer-risk, education, worry: path to appropriate use? *Gynecol Oncol* 2002;85: 1–2.
15 Norum LF, Erikstein B, Nustad K. Elevated CA125 in breast cancer – A sign of advanced disease. *Tumour Biol* 2001;22:223–8.
16 Sjovall K, Nilsson B, Einhorn N. The significance of serum CA 125 elevation in malignant and nonmalignant diseases. *Gynecol Oncol* 2002;85:175–8.
17 Petricoin EF, Ardekani AM, Hitt BA *et al.* Use of proteomic patterns in serum to identify ovarian cancer. *Lancet* 2002; 359:572–7.
18 Liotta LA, Kohn EC, Petricoin EF. Clinical proteomics: personalized molecular medicine. *JAMA* 2001;286: 2211–4.
19 Petricoin EF, Zoon KC, Kohn EC, Barrett JC, Liotta LA. Clinical proteomics: translating benchside promise into bedside reality. *Nat Rev Drug Discov* 2002;1:683–95.
20 Liotta LA, Petricoin EF III, Ardekani AM *et al.* General keynote: proteomic patterns in sera serve as biomarkers of ovarian cancer. *Gynecol Oncol* 2003;88:S25–8 (discussion S37–42).
21 Daly MB, Ozols RF. The search for predictive patterns in ovarian cancer: proteomics meets bioinformatics. *Cancer Cell* 2002;1:111–2.
22 Schena M, Shalon D, Davis RW, Brown PO. Quantitative monitoring of gene expression patterns with a complementary DNA microarray. *Science* 1995;270:467–70.
23 Schena M, Shalon D, Heller R, Chai A, Brown PO, Davis RW. Parallel human genome analysis: microarray-based expression monitoring of 1000 genes. *Proc Natl Acad Sci USA* 1996;93:10614–9.
24 DeRisi J, Penland L, Brown PO *et al.* Use of a cDNA microarray to analyse gene expression patterns in human cancer. *Nat Genet* 1996;14:457–60.
25 Scherf U, Ross DT, Waltham M *et al.* A gene expression database for the molecular pharmacology of cancer. *Nat Genet* 2000;24:236–44.
26 Ross DT, Scherf U, Eisen MB *et al.* Systematic variation in gene expression patterns in human cancer cell lines. *Nat Genet* 2000;24:227–35.
27 Murren JR, Beidler DR, Cheng YC. Camptothecin resistance related to drug-induced down-regulation of topoisomerase I and to steps occurring after the formation of protein-linked DNA breaks. *Ann N Y Acad Sci* 1996;803:74–92.
28 Goldwasser F, Bae I, Valenti M, Torres K, Pommier Y. Topoisomerase I-related parameters and camptothecin activity in the colon carcinoma cell lines from the National Cancer Institute anticancer screen. *Cancer Res* 1995;55:2116–21.
29 Zhou Y, Gwadry FG, Reinhold WC *et al.* Transcriptional regulation of mitotic genes by camptothecin-induced DNA damage: microarray analysis of dose- and time-dependent effects. *Cancer Res* 2002;62:1688–95.
30 Liotta LA, Kohn EC. The microenvironment of the tumour–host interface. *Nature* 2001;411:375–9.
31 Jenkins RE, Hawley SR, Promwikorn W, Brown J, Hamlett J, Pennington SR. Regulation of growth factor induced gene expression by calcium signalling: integrated mRNA and protein expression analysis. *Proteomics* 2001;1:1092–104.
32 Paweletz CP, Charboneau L, Bichsel VE *et al.* Reverse phase protein microarrays which capture disease progression show activation of pro-survival pathways at the cancer invasion front. *Oncogene* 2001;20:1981–9.
33 Urban N. Specific keynote: ovarian cancer risk assessment and the potential for early detection. *Gynecol Oncol* 2003;88:S75–9 (discussion S80–3).
34 Petricoin EF III, Ornstein DK, Paweletz CP *et al.* Serum proteomic patterns for detection of prostate cancer. *J Natl Cancer Inst* 2002;94:1576–8.

Accepted for publication June 1, 2003.

EXHIBIT L

translational medicine

A Novel Approach Toward Development of a Rapid Blood Test for Breast Cancer

Antonia Vlahou,[1,4] Christine Laronga,[2] Lori Wilson,[2] Betsy Gregory,[1] Keith Fournier,[2] Dean McGaughey,[3] Roger R. Perry,[2] George L. Wright, Jr.,[1,4] O. John Semmes[1,4]

Abstract

Mammography remains the diagnostic test of choice for breast cancer, but 20% of cancers still go undetected. Many serum biomarkers have been reported for breast cancer but none have proven to represent effective diagnostic strategies. ProteinChip® mass spectrometry is an innovative technology that searches the proteome for differentially expressed proteins, allowing for the creation of a panel or profile of biomarkers. The objective of this study was to construct unique cancer-associated serum profiles that, combined with a classification algorithm, would enhance the detection of breast cancer. Pretreatment serum samples from 134 female patients (45 with cancer, 42 with benign disease, 47 normal) were procured prospectively following institutional review board–approved protocols. Proteins were denatured, applied onto ProteinChip® affinity surfaces, and subjected to surface enhanced laser desorption/ionization (SELDI) time-of-flight mass spectrometry. The SELDI output was analyzed using Biomarker Pattern Software to develop a classification tree based on group-specific protein profiles. The cross-validation analysis of cancer versus normal revealed sensitivity and specificity rates of 80% and 79%, and for cancer versus benign disease, 78% and 83%, respectively. When 2 different chip surfaces were combined the sensitivity and specificity increased to 90% and 93%, respectively. The sensitivity and specificity of this technique are comparable to those of mammography and, if confirmed in a larger study, this technique could provide the means toward development of a simple blood test to aid in the early detection of breast cancer. The combination of SELDI ProteinChip® mass spectrometry and a classification- and regression-tree algorithm has the potential to use serum protein expression profiles for detection and diagnosis of breast cancer.

Clinical Breast Cancer, Vol. 4, No. 3, 203-209, 2003

Key words: Algorithm, Mass spectrometry, Protein profiling, Proteomics, SELDI, Serum

Introduction

Breast cancer remains the most common cancer affecting women today. However, although there are > 200,000 new cases diagnosed per year, there is still no blood test currently available for detection. Mammography is the best available screening test for this disease, with a sensitivity of 75%–90%, and remains the gold standard against which all new modalities must be compared.[1] However, 20% of breast cancers will go undetected by conventional imaging. The shortcomings of mammographic detection are particularly evident when examining young women who are more likely to have dense breasts and/or are carriers of a genetic predisposition such as *BRCA 1* or *BRCA 2*, for the development of breast cancer at an early age (50% of the carriers of a gene mutation will develop breast cancer by age 50, compared with 2% of the general population). Genetic testing of women at high risk is becoming more widespread and will result in increased identification of younger women underserved by routine imaging. An alternative method of diagnosis must be devised not only for those who are genetically predisposed but also for improved detection in the general population.

Attempts to identify a single serum biomarker for diagnosis of breast cancer have been unsuccessful. Biomarkers (or proteins) that have been identified are of limited utility for 3 reasons. First, they are found in only approximately 30% of early breast cancers and therefore are not useful for

[1]Departments of Microbiology and Molecular Cell Biology
[2]Department of Surgery
[3]Department of Internal Medicine
[4]Virginia Prostate Center
Eastern Virginia Medical School and the Sentara Cancer Institute, Norfolk

Submitted: June 23, 2003; Revised: Jul 28, 2003; Accepted: Jul 30, 2003

Address for correspondence: Christine Laronga, MD, Department of Surgery, Eastern Virginia Medical School, 825 Fairfax Ave, Suite 610, Norfolk, VA 23507
Fax: 757-446-8961; e-mail: laronge@evms.edu

Table 1 Demographics of the Cancer and Control Groups

Characteristic	Normal (n = 47)	Benign (n = 42)	Cancer (n = 45)
Median Age (Years)	46.5	47.2	59.3
Range (Years)	21-78	30-69	31-91
Race			
White	40 (85%)	33 (79%)	20 (44%)
Black	3 (6%)	6 (14%)	24 (53%)
Other	4 (9%)	3 (7%)	1 (2%)
Tumor Stage			
1	-	-	14 (31%)
2	-	-	14 (31%)
3	-	-	6 (13%)
4	-	-	3 (7%)
Ductal Carcinoma In Situ	-	-	8 (18%)

screening purposes.[3] Second, they may have prognostic value only, such as the case with HER2. Third, they may be useful only for monitoring stability of disease and recurrence, such as the case with Ca 27.29.[2,3] To be clinically useful for detection, a biomarker must be present in the majority of breast cancers and be identifiable when the cancer is in its earliest, most curable stage. Because of the molecular heterogeneity of tumorigenesis, a single biomarker may not provide the answer. The identification and simultaneous analysis of a panel of biomarkers, reflecting various biologic characteristics of the cancer and host response, would appear to have a greater potential for overcoming the current limitations and improve early detection of breast cancer.

For many years, 2-dimensional gel electrophoresis has been the principal tool for this purpose because it is able to resolve thousands of proteins in 1 experiment;[4] however, it has limitations in detection range, is labor intensive, requires large quantities of starting material, lacks interlaboratory reproducibility, and is not practical for clinical application. The innovative surface enhanced laser desorption/ionization (SELDI) time-of-flight mass spectrometry ProteinChip® technology is fast, has high throughput capability, requires orders of magnitude lower amounts of the protein sample, can effectively resolve low-mass proteins (2-20 kd), and is directly applicable for clinical assay development.[4-10] This technology uses patented ProteinChip® arrays coated with a chemical to affinity-capture protein molecules from complex mixtures. Various types of ProteinChip® arrays with different affinity matrices such as hydrophobic, ionic, and metal-binding, are available in order to optimize protein-binding affinities. In addition, application of preactivated surfaces allows covalent immobilization of antibodies, receptors, DNA, glycoproteins, and other markers for specific affinity capture.[6,8] Retained proteins are subsequently analyzed by time-of-flight mass spectrometry. With the aid of SELDI software, a retentate map is generated depicting the mass/charge, which corresponds to the molecular weight. Different spectra can then be combined or compared to elucidate protein profile changes between samples.

Our laboratory and others have previously demonstrated efficacy of the SELDI technology for biomarker discovery, and, when coupled with an artificial intelligence algorithm, for differentiating cancer from noncancerous tissue with high accuracy.[6,7,11-17] Based on these very positive results, the present study was designed to evaluate the SELDI-based protein profiling and classification system for differentiating breast cancer from noncancerous tissue.

Methods

Serum Samples

Female patients with abnormal mammogram or clinical breast examination results who required an operative surgical biopsy were eligible to participate in this study for breast cancer detection. They were enrolled through after signing an institutional review board-approved informed consent form.

Pretreatment serum samples were obtained at the same time as preoperative laboratory studies and therefore were separated in time by ≥ 1 week from any clinical breast examination, diagnostic imaging, or diagnostic biopsy (fine needle aspiration or core). The samples were then retrospectively categorized as benign or cancerous upon pathologic confirmation. Normal serum samples were randomly collected from healthy volunteers during the same time period (December 2001 to May 2002) as the benign and cancer specimens were obtained and were not drawn in concert with any clinical breast evaluation or diagnostic imaging. All serum samples (from normal volunteers and patients with benign disease or cancer) were directly separated into aliquots and stored at -80°C. All clinical information, including age, race, menopausal status, personal breast history, histologic diagnosis, and, in cases of cancer, clinical and surgical stage, tumor type, tumor grade, and receptor status were recorded in the breast study database. No attempts were made to separate the samples based on comorbid conditions, medications taken, or timing of blood drawing with respect to menstrual cycle.

The demographics of the patients and the stage distribution of the breast cancers are presented in Table 1. Benign conditions included low-risk conditions (fibroadenomas, cysts, epithelial-related calcifications) as well as disease with increased risk for breast cancer (atypical lobular or ductal hyperplasia, and fibrocystic disease with severe hyperplasia).

SELDI Processing of Serum Samples

Serum samples were applied to the strong anion exchange (SAX) and immobilized copper chip surfaces. In brief, 21 µL of serum was mixed with 30 µL of 8 mol/L urea/1% 3-[(3-cholamidopropyl)dimethylaminol-1-propanesulphonate

(CHAPS)–phosphate-buffered saline (PBS; pH 7.4) buffer for 10 minutes at 4°C, followed by the addition of 100 µL of 1 mol/L urea/0.125% CHAPS-PBS buffer and 600 µL of binding buffer compatible with the type of surface used (PBS for immobilized copper and 20 mmol/L HEPES/0.1% Triton for SAX). Diluted samples of 50 µL were then applied to the chips using a bioprocessor. After a 30-minute incubation, nonspecifically bound molecules were removed by 3 brief washes in binding buffer followed by 3 washes with high-pressure liquid chromatography–gradient water. Sinapinic acid (2 × 1 µL of 50% sinapinic acid in 50% 0.1% trifluoroacetic acid) was applied to the chip array surface and mass spectrometry performed using a Protein Biology System II SELDI mass spectrometer. Mass/intensity data were collected by averaging a total of 192 laser shots. Mass calibration was performed using the all-in-one peptide standard that contains vasopressin, hirudin, human insulin, somatostatin, and bovine insulin (β-chain recombinant). All samples were processed in duplicate.

Processing of SELDI Data

With use of the SELDI software, protein peaks were labeled and their intensities normalized for total ion current (mass range, 1.5-200 kd) to account for variation in ionization efficiencies. Peak clustering was performed using the Biomarker Wizard software with the following settings: signal/noise ratio (first pass), 3; minimum peak threshold, 10%; cluster mass window, 0.3%; signal/noise ratio (second pass), 1.5. Peak mass and intensity were exported to a spreadsheet, and the peak intensities from each duplicate spectrum were averaged. Pattern recognition and sample classification were performed using the Biomarker Pattern Software (BPS). The decision trees described in the result section were generated using the Gini method nonlinear combinations. A 10-fold cross-validation analysis was performed as an initial evaluation of the test error of the algorithm. Briefly, this process involves splitting the data set into 10 random segments and using 9 of them for training and the tenth as a test set for the algorithm. For these 9 segments, the sample is labeled "unblinded" as cancer, normal, or benign to allow the computer to learn what protein features can be used to differentiate among the cohorts compared. The computer is first trained in an unblinded fashion to recognize what is normal and what is cancer in order to learn to discriminate between the 2 conditions. Multiple trees were initially generated with all the peaks included as variables by varying the splitting factor by increments of 0.1. These trees were evaluated by cross-validation analysis (the remaining tenth random segment is subjected to the decision tree chosen in a blinded fashion). The peaks that formed the main splitters of the tree with the highest prediction rates were then selected. The tree was then rebuilt based on these peaks alone and reevaluated by cross-validation analysis, such that all samples would be reevaluated using the chosen decision tree to determine if the results are the same.

Figure 1 Decision-Tree Algorithm Using Strong Anion Exchange Chip Surface

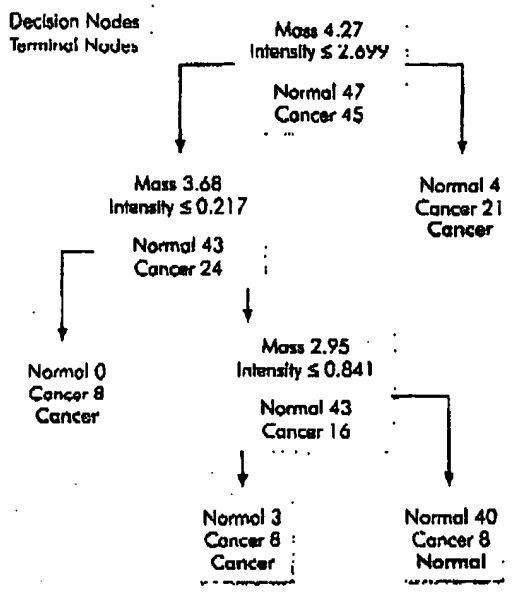

Decision tree classifying the cancer and normal groups utilizing a single chip surface. The mass and intensity levels of the peak forming the splitting rules are shown. For example, the question forming the first splitting rule is the following: are the intensity levels of the peak at 6.11 kd lower or equal to those at 2.68 kd? Samples that follow the rule go the left daughter node and samples that do not follow the rule go to the right daughter node. The numbers of cancer and normal samples in each node are shown. The classification of each terminal node is shown and is determined by the samples in majority. Mass of main splitter shown in kd.

Results

Differentiation of Cancer and Control Groups with the Decision-Tree Algorithm

A combined total of 134 serum samples from patients with breast cancer (n = 45), patients with benign breast diseases (n = 42), and women with no evidence of breast disease (n = 47) were analyzed by SELDI mass spectrometry using the immobilized copper ProteinChip® surface. The protein profiles of the cancer and control groups were analyzed by a decision-tree classification algorithm (BPS). In brief, this algorithm splits the data set into 2 bins at each branch based on decision rules (Figures 1 and 2). The rules are formed by the peak intensities being either greater or less than a specific value for each selected mass. Samples that follow the rule (ie, peak intensity is ≤ the cutoff intensity value) go to the left daughter node. When splitting can no longer be performed, terminal nodes are generated and classified according to the samples in the majority; in this case, the terminal node is classified as either cancer or benign/normal specimen (Figures 1 and 2).

The BPS algorithm is not very efficient in comparing 3 groups simultaneously, and therefore 2-group comparisons (cancer vs. normal and cancer vs. benign) were performed. Figures 1 and 2 illustrate the decision trees that yielded the highest precision in differentiating the 2 groups. From a total of 67

Figure 2 Decision-Tree Algorithm Using Immobilized Copper Chip Surface

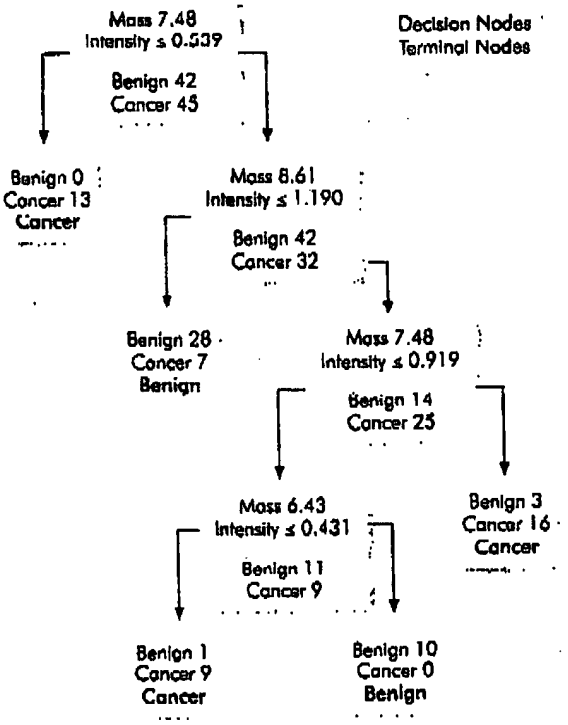

The number of samples in each node and the classification of terminal nodes are shown. Mass of main splitter shown in kd.

peaks, ranging from 2.5 kd to 30 kd, 3 peaks were selected by the BPS algorithm to discriminate cancer from the normal group (Figure 1). Peaks at 2.95 kd, 3.68 kd, and 4.27 kd form the main splitters of the decision tree (Figure 1). These peaks were different from those selected by the algorithm to discriminate cancer from benign disease. From 52 protein clusters analyzed, 3 masses of 6.43 kd, 7.48 kd, and 8.61 kd were selected as main splitters for separating cancer from benign samples. A 10-fold cross-validation analysis was performed as an initial evaluation of the accuracy of the algorithm in classifying breast cancer. Sensitivities of 78%-80% with specificities of 79%-83% were obtained (Table 2). Attempts to combine the normal and benign groups for comparison with the cancer group yielded poor decision trees. One explanation is that different proteins were selected by the algorithm to classify normal versus cancer and benign versus cancer samples. Use of a different type of bioinformatics algorithm will be necessary to analyze the combined normal/benign cohorts.

Table 2 Prediction of Breast Cancer Using Strong Anion Exchange Chip Surface

	Sensitivity	Specificity
Cancer Versus Normal		
Learning Set	82.2% (37/45)	85.1% (40/47)
Cross-Validation	80.0% (36/45)	78.7% (37/47)
Cancer Versus Benign		
Learning Set	84.4% (38/45)	90.4% (38/42)
Cross-Validation	77.7% (35/45)	83.0% (35/42)

Numbers in parentheses denote the number of correctly classified among total number of samples in the group.

Combination of Chip Chemistries Increases Diagnostic Accuracy

In an effort to increase the volume of the proteome examined and to enhance the chance of detecting protein biomarkers, a subset of samples randomly chosen (30 cancers and 30 normal donors) was applied to both the immobilized copper and SAX chip arrays. Both surfaces effectively resolved low-mass (< 20 kd) protein peaks, whereas the SAX surface was superior in resolving larger (> 20 kd) protein masses. Figure 3 shows representative protein spectra from 1 cancer serum sample processed on SAX and immobilized copper chips.

From a total of 134 protein clusters (53 detected on immobilized copper ranging from 2.5 kd to 30 kd; 81 detected on SAX ranging from 0.5 kd to 40 kd), 4 protein peaks were selected by the BPS algorithm to differentiate breast cancer from normal samples (Figure 4). Three peaks (2.95 kd, 3.94 kd, and 3.97 kd) were detected on the immobilized copper chip, and 1 peak (4.03 kd) was detected on the SAX surface. The mass spectra and gray-scale views as well as the intensity distribution for these 4 masses throughout the samples are shown in Figure 5. A 10-fold cross-validation analysis was performed as an initial evaluation of the accuracy of the algorithm in predicting breast cancer. A specificity of 93.3% and a sensitivity of 90% were obtained (Table 3).

Discussion

Despite advances in diagnostic imaging, mammography remains the gold standard screening modality for detecting breast cancer. Advantages of mammography are that it is readily accessible, noninvasive, and relatively inexpensive. Although its sensitivity is approximately 75%-90%, the positive predictive value is quite low (25%).[18] Furthermore, limitations in mammography are seen in women who are young, have dense breasts, are undergoing hormone-replacement therapy, or have a germ-line predisposing mutation (BRCA 1 or BRCA 2).[19] Clearly, an adjunct to mammography is needed. This new modality must possess the same advantages as mammography, such as being readily accessible and reproducible, posing minimal risk to patients, and being relatively inexpensive. A simple blood test would fulfill all these criteria, and the concept is not only appealing, it is feasible.

Unfortunately, years of research have failed to produce a serum marker in women. The vast majority of biomarkers (proteins) identified are not present in most breast cancers.[2,3] Knowing that breast cancer is a heterogeneous dis-

Figure 3 Protein Spectra Processed on Immobilized Copper and Strong Anion Exchange Chips

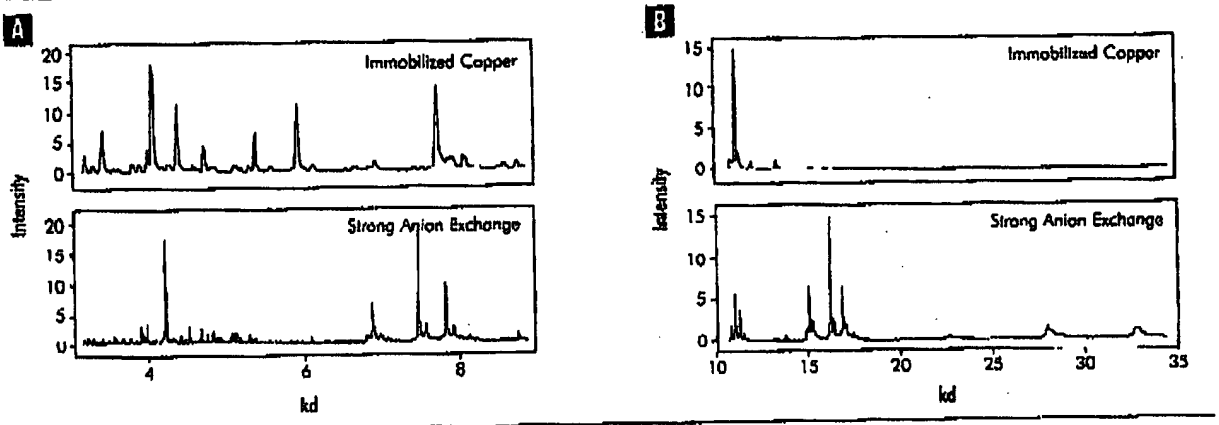

Protein spectra of one representative cancer serum sample processed on a surface with affinity for metal-binding proteins and a positively charged surface. The 3-9 and 10-35 kd mass ranges are shown. Different protein profiles are captured by the 2 surfaces.

ease, perhaps the answer lies in a panel or profile of biomarkers (proteins). This profile would reflect not only the tumor itself but the host response as well. Because such profiles could represent phenotypic events commonly altered during neoplastic transformation and progression, a subset of the multiple biomarkers (proteins) would be present in the majority of tumors.

SELDI is a highly sensitive, specific, and high-throughput technology that can analyze complex biologic samples without the need for difficult preseparation steps inherent to other proteomic approaches. In addition, proteins of low molecular weight and extreme isoelectric focus are easily resolved and analyzed based on relative concentration and mass. The resulting protein profile of a given sample can then be analyzed by advanced bioinformatic tools and compared for similarities and differences with other samples. Directed learning algorithms are applied to case and control to generate a decision path using distinguishing profiles. Once the optimum discriminatory decision process is created, blinded samples can then be subjected to analysis to confirm the utility of the algorithm.

Our initial investigations with the SELDI technology began with prostate cancer. Using serum, prostate-specific antigen, prostate-specific membrane antigen, and prostatic acid phosphatase were detected at the predicted molecular mass with a variability of < 1%.[9] When sera from a total of approximately 400 individuals including patients with prostate cancer, men with benign prostate hyperplasia and normal individuals were processed by SELDI and analyzed by a decision tree classification algorithm, sensitivities and specificities of 95% were obtained.[12,15] Other reports from our laboratory and other investigators further support the potential of SELDI in discriminating cancer from noncancer controls based on differences in protein patterns observed in sera, urine, cell lysates, and other body fluids.[5,7,10,11,13,14,16,17] Li and colleagues demonstrated that analysis of the SELDI data with a combination of bioinformatic tools provided sensitivity and specificity rates for breast cancer of 93% and 91%, respectively.[17] In our study, we employed simpler statistical approaches than those used by Li and colleagues and explored the idea of chip chemistry combination as a means of biomarker discovery.

We analyzed our cohort of patients with breast cancer using the same serum protocol and chip surface as was established in our earlier studies.[9,11] The algorithm employed for the analysis of the breast cancer data set differs from the decision tree used in our earlier prostate studies; the BPS used in the present study is a simple commercial package bundled with the Protein Biology System II instrument and

Figure 4 Decision-Tree Algorithm Using Immobilized Copper and Strong Anion Exchange Chip Surfaces

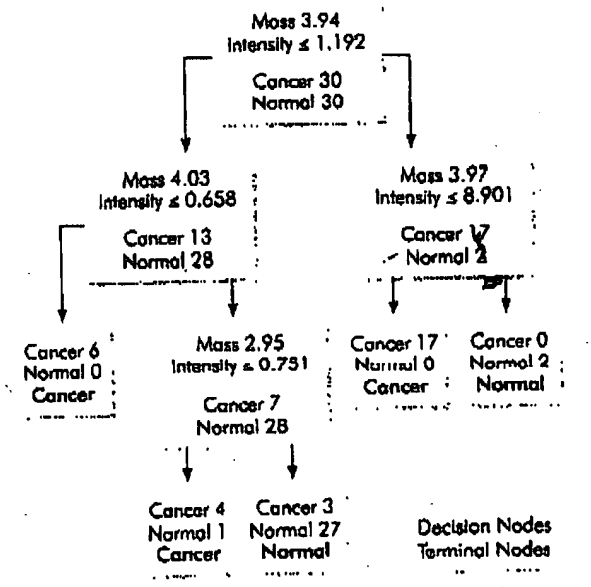

The number of samples in each node and the classification of terminal nodes are shown. Mass of main splitter shown in kd.

Figure 5 Mass Spectra and Gray-Scale Views of 4 Masses Detected in Cancer and Normal Samples

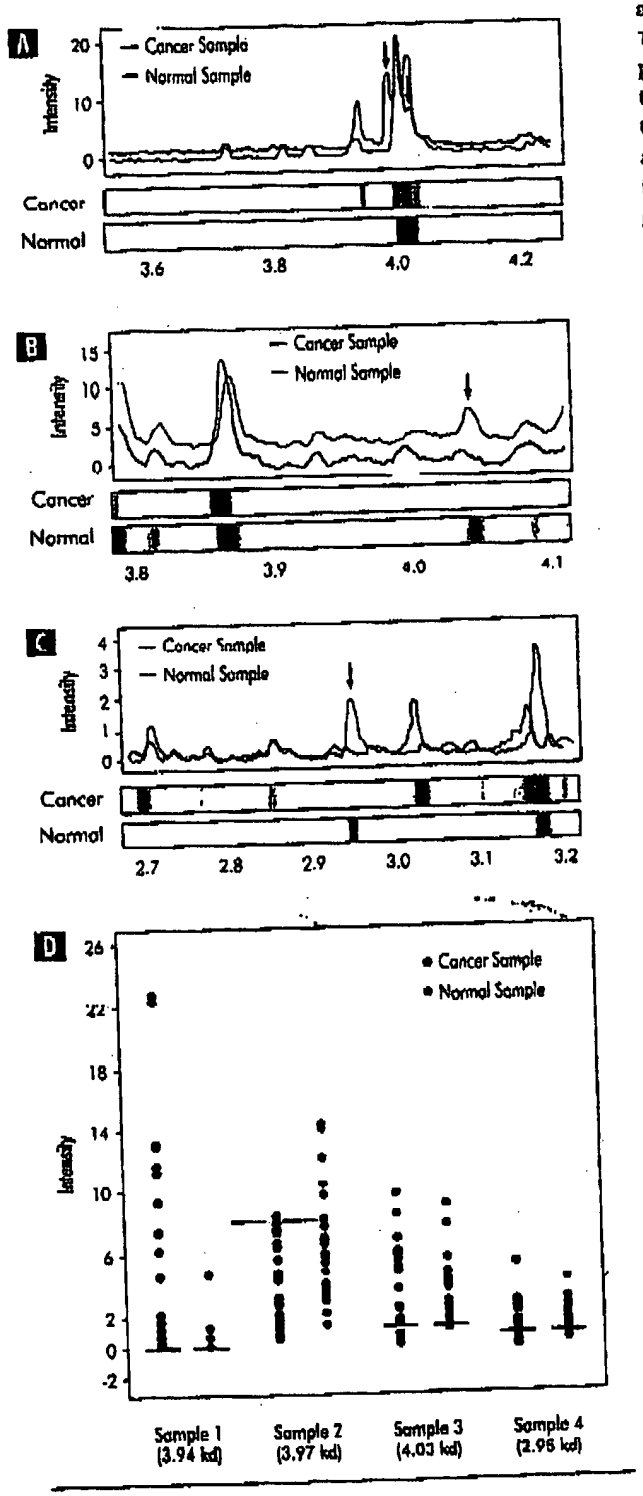

Spectra (top) and gray-scale or gel (bottom) views of the peaks (arrows) forming the splitting rules (A-C). Intensity distribution of these peaks throughout the samples (D). The horizontal lines correspond to the intensity cutoff levels that form the splitting rule in the decision tree. The mass of the peaks is shown in kd.

therefore readily available software for the analysis of SELDI data. Our cross validation analysis of cancer versus normal samples revealed a sensitivity and specificity of 80% and 79%, respectively, and of cancer versus benign disease, 78% and 83%, respectively. These results are in the range reported for mammography, but are lower than the rates obtained in our study of prostate cancer. The explanation for this may be a reflection of the heterogeneity of breast cancer as demonstrated by the lack of a single biomarker present in the majority of tumors, as opposed to prostate-specific antigen in prostate cancer. Alternatively, the assumption that the ideal chip surface and protocol for breast cancer is the same as that for prostate cancer may be incorrect.

In an attempt to improve the classification accuracy, a randomly selected subset of cancer and normal samples were subjected to 2 different chip chemistries, immobilized copper and SAX, and the combined SELDI data analyses by the classification and regression trees algorithm. As expected, several differences in the mass spectra were observed between the 2 surfaces. By combining the data from both chip chemistries, the cross validation analysis revealed sensitivity and specificity of 90%-93%. Using a similar combinatorial approach also provided higher detection rates for ovarian cancer in serum compared with the use of a single surface alone.[11]

Evaluation of the classifiers by cross-validation analysis offers some degree of statistical confidence of the potential of this approach as a breast cancer detection tool. However, the sample size in this study decreases the validity of generalized conclusions. It should therefore be emphasized that complete evaluation of these classifiers will require testing its prediction rates for larger blinded and independent serum sets. Peak selection and analysis with the DTS algorithm are currently operator-dependent processes. More specifically, large numbers of decision trees have to be evaluated based on cross-validation or test-set prediction rates by the operator. Besides the subjective factor involved, this process has the drawback of potentially overfitting the classifier to the specific study set. Preselection of the most significant peaks by statistical approaches and automation of the algorithm are avenues for improvement that should be addressed in future studies. Indeed, improvement of the peak labeling process and optimization of the learning algorithm is a major shortcoming for all computational strategies currently used for protein-profiling approaches and essential for the development of robust classifiers.

Furthermore, based on our experience with the application of protein profiling to the early detection of cancer, we believe that comparative analysis of different types of algorithms will be of paramount importance to assess the bioinformatic features required for development of a robust classification system. The type of bioinformatics analysis employed in the current study is limited by its ability to compare and contrast only 2 separate cohorts simultaneously. Therefore, additional algorithms capable of distinguishing normal versus benign versus cancerous samples are being evaluated. This will also eventually allow the comparison of

Table 3 Prediction of Breast Cancer Using Strong Anion Exchange and Immobilized Copper Chip Surfaces

	Sensitivity	Specificity
Learning Set	90% (27/30)	96.7% (29/30)
Cross-Validation	90% (27/30)	93.3% (28/30)

Performance of the decision tree in predicting breast cancer using 2 chip surfaces. Numbers in parentheses denote the number of correctly classified samples among the total number of samples in the group.

samples from women with other types of epithelial cancers and benign conditions from other organ sites.

Conclusion

SELDI time-of-flight analysis of serum samples is a novel, rapid, and reproducible technology. Identification of multiple differentially expressed proteins in combination with bioinformatic software can generate classifiers separating normal from benign or cancerous disease states with high sensitivity and specificity. However, the current study was a pilot study and was designed to determine the feasibility of generating differentiating protein profiles for breast cancer detection. A second study using larger sample sizes for each cohort is currently under analysis. Future studies will include separation of specimens based on age and menstrual cycle; defining impact of comorbid conditions on protein profiles; distinction of profiles between breast cancer and other cancers; and finally, stratification of samples based on stage of disease. Only after these important issues have been addressed and enough samples in each category have been accrued can we then move to validation studies involving multiple institutions.

With advancement of this technology, many possibilities exist, such as discovery of novel biomarkers, earlier detection of breast cancer (some of the samples analyzed in this study were from ductal carcinoma in situ), refinement of the current staging system, better prognostication, tailored and individualized therapy, monitoring of disease response, and earlier detection of recurrence. However, the more immediate goal is to offer a simple blood test to be used as an adjunct to mammography, not a replacement, for the earlier detection of breast cancer.

Acknowledgements

This study was supported by grants from the National Cancer Institute Early Detection Research Network (CA86067) and the Virginia Prostate Center.

References

1. Donegan WL. Evaluation of a palpable breast mass. *N Engl J Med* 1992; 327:937-942.
2. Bast RC Jr, Ravdin P, Hayes DF, et al. 2000 update of recommendations for the use of tumor markers in breast and colorectal cancer: clinical practice guidelines of the American Society of Clinical Oncology. *J Clin Oncol* 2001; 19:1865-1878.
3. Hayes DF, Trock B, Harris AL. Assessing the clinical impact of prognostic factors: when is "statistically significant" clinically useful? *Breast Cancer Res Treat* 1998; 52:305-319.
4. Merchant M, Weinberger SR. Recent advancements in surface-enhanced laser desorption/ionization-time of flight-mass spectrometry. *Electrophoresis* 2000; 21:1164-1177.
5. Vlahou A, Schellhammer PF, Mendrinos S, et al. Development of a novel proteomic approach for the detection of transitional cell carcinoma of the bladder in urine. *Am J Pathol* 2001; 158:1491-1502.
6. Xiao Z, Jiang X, Beckett ML, et al. Generation of a baculovirus recombinant prostate-specific membrane antigen and its use in the development of a novel protein biochip quantitative immunoassay. *Protein Expr Purif* 2000; 19:12-21.
7. Adam BL, Davis JW, Ward MD, et al. Protein profiling of seminal plasma using Ciphergen's SELDI protein chip technology for early detection of prostate cancer. *Proc Am Assoc Cancer Res* 2001; 42:142 (Abstract #762).
8. Xiao Z, Adam BL, Cazares LH, et al. Quantitation of serum prostate-specific membrane antigen by a novel protein biochip immunoassay discriminates benign from malignant prostate disease. *Cancer Res* 2001; 61:6029-6033.
9. Wright GL, Jr., Cazares LH, Leung SM, et al. ProteinChip(R) surface enhanced laser desorption/ionization (SELDI) mass spectrometry: a novel protein biochip technology for detection of prostate cancer biomarkers in complex protein mixtures. *Prostate Cancer Prostatic Dis* 1999; 2:264-270.
10. Cazares LH, Adam BL, Ward MD, et al. Normal, benign, preneoplastic, and malignant prostate cells have distinct protein expression profiles resolved by surface enhanced laser desorption/ionization mass spectrometry. *Clin Cancer Res* 2002; 8:2541-2552.
11. Vlahou A, Schorge JO, Gregory BW, et al. Diagnosis of ovarian cancer using decision tree-classification of mass spectral data. *J Biomed Biotechnol*. In press.
12. Adam BL, Qu Y, Davis JW, et al. Serum protein fingerprinting coupled with a pattern-matching algorithm distinguishes prostate cancer from benign prostate hyperplasia and healthy men. *Cancer Res* 2002; 62:3609-3614.
13. Paweletz CP, Gillespie JW, Ornstein DK, et al. Rapid protein profiling of cancer progression directly from human tissue using a protein biochip. *Drug Dev Res* 2000; 49:34-42.
14. Paweletz CP, Trock B, Pennanen M, et al. Proteomic patterns of nipple aspirate fluids obtained by SELDI-TOF: Potential for new biomarkers to aid in the diagnosis of breast cancer. *Dis Markers* 2001; 17:301-307.
15. Qu Y, Adam BL, Yasui Y, et al. Boosted decision tree analysis of surface-enhanced laser desorption/ionization mass spectral serum profiles discriminates prostate cancer from noncancer patients. *Clin Chem* 2002; 48:1835-1843.
16. Petricoin EF, Ardekani AM, Hitt BA, et al. Use of proteomic patterns in serum to identify ovarian cancer. *Lancet* 2002; 359:572-577.
17. Li J, Zhang Z, Rosenzweig J, et al. Proteomics and bioinformatics approaches for identification of serum biomarkers to detect breast cancer. *Clin Chem* 2002; 48:1296-1304.
18. Elmore JG, Barton MB, Moceri VM, et al. Ten-year risk of false positive screening mammograms and clinical breast examinations. *N Engl J Med* 1998; 338:1089-1096.
19. Saarenmaa I, Salminen T, Geiger U, et al. The effect of age and density of the breast on the sensitivity of breast cancer diagnostic by mammography and ultasonography. *Breast Cancer Res Treat* 2001; 67:117-123.

EXHIBIT M

Clinical Chemistry 45:10
1695–1707 (1999)

Review

Kinetics of Serum Tumor Marker Concentrations and Usefulness in Clinical Monitoring

JEAN-MICHEL BIDART,[1] FRANÇOIS THUILLIER,[2*] CHRISTINE AUGEREAU,[3] JACQUELINE CHALAS,[4] ALAIN DAVER,[5] NELLY JACOB,[6] FRANÇOISE LABROUSSE,[7] and HÉLÈNE VOITOT[8]

Only a few markers have been instrumental in the diagnosis of cancer. In contrast, tumor markers play a critical role in the monitoring of patients. The patient's clinical status and response to treatment can be evaluated rapidly using the tumor marker half-life ($t_{1/2}$) and the tumor marker doubling time (DT). This report reviews the interest of determining these kinetic parameters for prostate-specific antigen, human chorionic gonadotropin, α-fetoprotein, carcinoembryonic antigen, cancer antigen (CA) 125, and CA 15-3. A rise in tumor markers (DT) is a yardstick with which benign diseases can be distinguished from metastatic disease, and the DT can be used to assess the efficacy of treatments. A decline in the tumor marker concentration ($t_{1/2}$) is a predictor of possible residual disease if the timing of blood sampling is soon after therapy. The discrepancies in results obtained by different groups may be attributable to the multiplicity of immunoassays, the intrinsic characteristics of each marker (e.g., antigen specificity, molecular heterogeneity, and associated forms), individual factors (e.g., nonspecific increases and renal and hepatic diseases) and methods used to calculate kinetics (e.g., exponential models and timing of blood sampling). This kinetic approach could be of interest to optimize patient management.

Only a few markers have been instrumental in the diagnosis of cancer; they include α-fetoprotein (AFP),[9] human chorionic gonadotropin (hCG), and calcitonin. Although the concentration of an isolated tumor marker before any treatment may have a prognostic value, they are not widely used in comparison to conventional prognostic factors. In contrast, tumor markers play a critical role in the monitoring of patients. However, recourse to tumor markers as a yardstick of treatment or to signal the emergence of a recurrence or a metastasis has been based only on a succession of values with no regard for knowledge of the exponential nature of tumor growth, which is a theoretical and practical basis of cancer therapy. In an economy-conscious environment in which cost-effective medicine is an overriding concern, physicians treating cancer patients need convenient, efficient methods to rapidly evaluate response to therapy and to offer alternative treatment when appropriate *(1–4)*. A challenging approach to rapid evaluation of clinical response and monitoring is the determination of tumor marker half-life ($t_{1/2}$) and tumor marker doubling time (DT), kinetic parameters associated with changes in marker concentrations. The $t_{1/2}$ is calculated according to the formula $dt/\log(tm_1/tm_2)$, where tm_1 and tm_2 are the tumor marker values at times 1 and 2, respectively, and dt the interval between the two dates. The DT is determined according to the interval required to double the serum concentration. This report reviews the interest of determining kinetic parameters of the tumor markers that are the most relevant for the monitoring of patients. The main characteristics of prostate-specific antigen (PSA), hCG, AFP, carcinoembryonic antigen (CEA), cancer antigen (CA) 125, and CA 15-3, are presented in Table 1.

[1] Département de Biologie Clinique, Institut Gustave-Roussy, 94805 Villejuif, France.
[2] Laboratoire de Biochimie, Centre Hospitalier de Meaux, 6/8 Rue Saint Fiacre, 77100 Meaux, France.
[3] Laboratoire de Biochimie, Hôpital Boucicaut, 75015 Paris, France.
[4] Laboratoire de Biochimie, Hôpital Antoine-Béclère, 92141 Clamart, France.
[5] Laboratoire de Radioimmunologie, Centre Paul-Papin, 49033 Angers, France.
[6] Laboratoire de Biochimie, Centre Hospitalier Pitié-Salpétrière, 75013 Paris, France.
[7] Laboratoire de Biochimie, Hôpital Laennec, 75007 Paris, France.
[8] Laboratoire de Biochimie, Hôpital Beaujon, 92110 Clichy, France.
The authors are members of the "Groupe d'Evaluation et de Recherche des Biologistes de l'Assistance Publique-Hôpitaux de Paris" (GERBAP-CANCER; Coordinator, F. Thuillier).
This review is dedicated to Prof. A. Lemonnier, founder of the GERBAP.
*Author for correspondence. Fax 33-164353706; e-mail fthuillier@fc.horus-medical.fr.
Received April 27, 1999; accepted July 12, 1999.

[9] Nonstandard abbreviations: AFP, α-fetoprotein; hCG, human chorionic gonadotropin; $t_{1/2}$, half-life; DT, doubling time; PSA, prostate-specific antigen; CEA, carcinoembryonic antigen; CA, cancer antigen; BPH, benign prostatic hyperplasia; hCGβ, hCG β subunit; and NSGCTT, nonseminomatous germ-cell testicular tumor.

Dynamic Aspects of Tumor Markers

PSA

Serum PSA concentrations increase with age at a rate of 0.04 μg/L per year in healthy adult males *(5)*. The rate at which PSA increases annually is between 0.07 and 0.27 μg/L in patients with benign prostatic hyperplasia (BPH), between 0.47 and 3.08 μg/L for patients with localized cancers, and between 1.02 and 26.49 μg/L for patients with metastatic disease *(6)*. The serum PSA concentration is generally proportional to intra- and extracapsular growth of prostate carcinoma *(7)*. A linear relationship has been reported between serum PSA and the size of prostate cancer *(6, 8, 9)*. BPH provokes a rise of 0.3 μg/L per gram of hyperplastic tissue, whereas a rise of 3.5 μg/L per gram is observed for tumor tissue *(8)*. This relationship between tumor size and PSA production is not unanimously accepted. Brawer et al. *(10)* reported that the PSA_{index}, defined as the ratio between the serum PSA value and the tumor mass, is linked to the extent of the cancer but not correlated with the PSA concentration. The PSA concentration is a biological yardstick distinguishing patients with BPH from patients with localized, loco-regional, or advanced metastatic adenocarcinomas *(5, 11, 12)*.

There is a clear relationship between the DT and the International Union against Cancer tumor-node-metastasis classification before any treatment *(8)*. The DT apparently exceeds 48 months in stages T_1, T_2, and is less than 24 months for stages T_3 and T_4 *(8)*. This slow progression makes it possible to monitor therapy over 3- to 6-month periods. DT values vary from 73.9 to 98.9 years in controls and from 12.4 to 16.9 years in BPH patients *(6)*. In patients with prostate cancer, the pattern is biphasic. The first phase is linear, with an identical DT for localized and metastatic disease (13.6–18.6 years), and the second phase is exponential, with a DT of 2.4 years for localized cancers and 1.8 years for metastasis. DT values must be determined before starting therapy because prostate tumors grow very slowly, particularly when the initial concentration is low. The initial PSA concentration and DT should not be considered as isolated prognostic factors because their values are correlated with the tumor volume and grade *(13)*. Carter and Pearson *(14)* focused their study on trends in PSA with age, gland volume (measurement of PSA density), and time (measurement of PSA velocity). These tools are used for the screening of adenomas and localized cancers and to assess tumor extension in conjunction with other variables (e.g., biopsy and Gleason score).

Prostatectomy is appropriate for a tumor recurrence when the DT is <9 months. When the DT is >1 year, antiandrogenic treatment is more appropriate *(15)*. Zagars and Pollack *(12)* used a percentage of decrease relative to pretreatment concentrations to decide whether additional therapy was required or not. Patients with stages B_1, B_2, and C prostate cancer whose DT is <3.8 months require prompt surgery. Patients with a DT exceeding 3.8 months can be treated less aggressively (e.g., antiandrogens) *(16)*. A DT attaining 12 months or less should be considered eligible for multimodal therapy, and a slow DT (5 years) eligible for watchful waiting without therapy *(17)*. According to Pollack et al. *(18)*, although a correlation exists between the PSA concentration, the DT, and the time to relapse, it is not considered judicious to select a particular course of treatment on the basis of the DT value given the large number of variables involved.

Radical prostatectomy is indicated for a clinically localized tumor, and the efficiency of the treatment is assessed by long-term monitoring. PSA is undetectable within 21 days after prostatectomy *(19–21)*, at which point, any PSA concentration above the lower limit of detection signifies the presence of residual tumor. This argues in favor of using ultrasensitive assays. The PSA $t_{1/2}$, calculated with t_0 measured 2 days after prostatectomy, is close to 2.5 days and similar in several studies *(21)*. In contrast, when the t_0 value is measured 5 min postoperatively, the $t_{1/2}$ value is equal to 1.5 days *(21, 22)*. Calculating $t_{1/2}$ values helps distinguish patients in complete remission from those likely to develop a recurrence ($t_{1/2}$, 2.98 ± 1.33 days), although they have undetectable concentrations, and from patients in whom PSA will never return to the baseline value. van Straalen et al. *(23)* found a biphasic pattern for the disappearance of PSA after prostatectomy, with a first phase presenting a $t_{1/2}$ of 1.6 days and a second phase with a $t_{1/2}$ of 4.6 days. The PSA concentration should therefore be measured at least 30 days postoperatively. Even with a $t_{1/2}$ value of 1.6 days, patients may be considered cured if PSA remains undetectable over 24 months postoperatively *(24)*. The elimination of free PSA also exhibits a biphasic kinetic profile *(25, 26)*. The $t_{1/2}$ of free PSA [0.5–0.8 h in fast phase (first phase), 7–14 h in slow phase (second phase)] is shorter than that of total PSA, and the ratio between free and total PSA can be a useful tool *(25)*. The elimination of PSA complexed to α_1-antichymotrypsin is nonexponential, and free PSA released during surgery does not form complexes with α_1-antichymotrypsin. Elimination of total PSA is a combination of these mechanisms *(26)*. PSA concentrations are undetectable in patients 3 days after surgery for BPH (open surgery; $t_{1/2}$, 0.55 ± 0.39 days), 28 days after radical prostatectomy ($t_{1/2}$, 2.5 ± 1.33 days for one compartment and 0.94 ± 0.8 days and 7.62 ± 6.35 days for two compartments), and 21 days after radical cystectomy ($t_{1/2}$, 1.92 ± 1.2 d for one compartment). For others, the PSA $t_{1/2}$ in BPH patients (1.4 days for free PSA; 2.4 days for total PSA) is shorter than the PSA $t_{1/2}$ in cancer patients (2.1 days for free PSA; 3.4 days total PSA) *(27)*. Cystoprostatectomy is a good model for a pharmacokinetic study of PSA *(28)*. Calculations of $t_{1/2}$ must take in account blood loss during surgery *(29)*. Adjuvant radiotherapy increases the percentage of patients with undetectable PSA concentrations after prostatectomy *(30, 31)*. All patients with documented clinical recurrences had previously displayed renewed PSA secretion during monitoring. It is therefore of interest to monitor slight variations in PSA. The PSA kinetic profile is a key to

Table 1. Main characteristics of tumor markers.

	PSA	hCG	AFP
First description	1971 by Hara et al. *(140)*	1927 by Ascheim and Zondek *(141)*	1956 by Bergstrand and Czar *(142)*
Structure	Glycoproteins *(143)*; Monomer, 34 kDa; carbohydrates 7%; five isomers *(146)*, pI 6.8 to 7.2 *(143)* Chymotryptic activity Antichymotrypsin and α-macroglobulin linked forms	Glycoproteins *(144)*; Heterodimer 45 kDa; carbohydrates, 30% (four N-glycan and four O-glycan chains); seven isomers, pI 3.8–4.7	Mucin-like glycoprotein *(145)*; 67–69 kDa (4–5% glycans); mono, bi, or trimer; two isomers (ph 4.85 and 5.2)
Gene	One gene on 19q3; 6 kb; four introns, five exons Homology with gene for kallicrein-1hGK1 at 12 kb from PSA gene *(146)*	α subunit: one gene on 6q21, 1-23; four exons β subunit: six genes on 19q13,3 (52 kb); three exons *(147)*	Chromosome 4 (long arm)
Site of production	Prostatic acini, breast, parotide	Trophoblastic cells of the placenta, pituitary	Liver, vitellus (fetal synthesis)
Half-life	1.5–3.2 days after radical prostatectomy	24–36 h ($t_{1/2}$ = 3.6, 18.0, 53.0 h) *(148)* β: 3–4 h ($t_{1/2}$ = 1.0, 23.4, 194 h) α: 2 h ($t_{1/2}$ = 0.6, 6.2, 21.9 h)	5–6 days *(149)*
Standard/calibrator	Yang or Hybritech	hCG: 75/537 (hCG CR119; 9286 kIU/g) hCGβ: 75/569 prepared from hCG CR119 hCGα:[a] 75/751 prepared from hCG CR119	
Reference values	4 μg/L *(150)* Increased production in men with age	hCG <10 IU/L; hCGβ <0.1 μg/L; hCGα <0.5 μg/L *(151)*	8.5–20 μg/L Increased at birth, 150 μg/L
Clinical interest in oncology	Monitoring of prostate cancer	hCG and free hCGβ: diagnosis and monitoring of patients with trophoblastic tumors and testicular cancers free hCGβ: monitoring of patients with nontrophoblastic cancers, particularly bladder cancer *(152)*	Diagnosis and monitoring of hepatocarcinomas, testicular cancer, teratocarcinomas, and germinal ovarian cancers *(153)*
	CEA	**CA 125**	**CA 15-3**
First description	1955 by Gold and Freedmann *(154)*	1981 by Bast et al. *(155)*	1984 by Kufe et al. *(156)*; 1984 by Hilkens et al. *(157)*
Structure	Glycoproteins; 180–200 kDa *(158)*; monomer; carbohydrates, 50–60% *(159)*	Mucin-like glycoprotein; 200–250 kDa	Glycoproteins
Gene	Chromosome 19 (long arm)	Chromosome 17 (long arm)	One locus (*DF3*), multiple alleles *(160)*
Site of production	Fetal gut, healthy colonic mucosa (differentiated surface epithelial cells)	Epithelial ovarian cells	Breast
Half-life	3–11 days *(161)*	5–10 days	Not determined
Standard/calibrator	WHO international reference preparation CEA (73/601)		
Antibodies	Very few specific epitopes *(162)*	Monoclonal antibody OC 125 *(163)*	Two monoclonal antibodies (mAb115-D8 and mAb DF3) *(164)*
Reference values	<5 μg/L	<35 kilounits/L	<30 kilounits/L
Clinical interest in oncology	Monitoring of early recurrence in colorectal adenocarcinoma	Prognostic value and monitoring in ovarian carcinomas	Monitoring of breast cancer

[a] hCGα, α subunit of hCG.

differentiation between local and metastatic recurrences (i.e., biological recurrences) several months before clinical signs.

In patients treated with radiotherapy alone, the use of PSA kinetics is controversial *(32)*. The tumor marker $t_{1/2}$ varies widely (11–275 days) among subjects *(33)* and is related to the activity of residual surviving cancer cells and to PSA-secreting cancer cells located outside the radiotherapy target volume. Fifty percent of biopsies performed 1 year after irradiation are PSA positive. Stage, grade, and pretreatment PSA concentrations are apparently not linked to PSA kinetics *(34, 35)*. These observations have been challenged by other authors *(12, 14, 18, 32, 36)*. Remission has been associated with normalization of PSA between 6 months and 3 years and recurrence in the absence of normalization *(37)*. A DT of <8 months may predict distant metastasis *(32)*.

In patients treated with hormonal therapy, the regulation of PSA synthesis is dependent on androgen activity. Hormonal therapy thus can modify PSA secretion. The androgen suppression syndrome, corresponding to increased PSA induced by nonsteroid antiandrogens is infrequent; consequently, monitoring of PSA is widely used in hormone therapy. After a treatment failure, the DT may be used for individual patients requiring androgen therapy *(17)*. A decrease in PSA, measured at 3 and 6 months, is a prognostic indicator correlated with survival. After 6 months of treatment, it is possible to separate subjects who are not responders from those who are *(38, 39)*. However, ~10% of nonresponders do not display an increase in PSA. Furthermore, the absence of a biological response revealed by the PSA concentration preceded clinical unresponsiveness by 6–12 months, over a mean evolution of 20 months.

hCG AND AFP

In gestational trophoblastic diseases, measurement of both the hCG concentration and the rate at which it decreases after surgery and/or chemotherapy have been demonstrated as essential for the management of patients. After evacuation of a molar pregnancy, the hCG concentration should be monitored every week until normalization and then every month during the first year. The disappearance of hCG is usually achieved within 8 weeks in ~40% of patients, within 9 to 22 weeks in ~55% of cases, and in >22 weeks in 5% of patients. In some cases, hCG concentrations remain stable or increase, suggesting the presence of persistent evolutive trophoblastic disease (molar retention, invasive mole, or choriocarcinoma). hCG regression curves have been used in several studies for early recognition of persistent disease in patients. Several reports propose normal regression corridors that allow the detection of 85–90% of patients with persistent disease within 4–6 weeks *(40, 41)*. Similarly, patients are identified within 8 weeks based on regression curves established from data including those of patients with a temporary hCG plateau. Yedema et al. *(42)* attempted to identify patients with persistent trophoblastic disease, based on a normal hCG regression curve constructed by fitting data from 130 patients with a hydatidiform mole with uneventful hCG regression. A biexponential regression model indicates two median hCG $t_{1/2}$ of 1.8 and 12.8 days. Using the 95th percentile limit, Yedema et al. *(42)* identified >90% of the 77 patients with persistent disease within 14 weeks and >50% within 6 weeks. Special attention must be paid to the 5% of disease-free patients who continue to have increased hCG concentrations 22–25 weeks after evacuation and to those who have persistent trophoblastic disease after initially spontaneous hCG regression to the reference value.

Patients who develop high-risk metastatic trophoblastic disease require intensive chemotherapy. These patients present one or several of the following factors: a pretreatment serum hCG concentration >40 000 IU/L, a diagnosis of choriocarcinoma, a history of a nonmolar pregnancy, metastases, and resistance to chemotherapy *(43)*. The ratio of free hCG β subunit (hCGβ) to total hCGβ (free hCGβ + hCG) is often higher in these patients than in patients with a hydatidiform mole or low-risk disease. During the first week of chemotherapy, marker values generally increase initially because of the destruction of tumor cells. Remission is achieved when marker concentrations are undetectable. Both hCG and hCGβ detection tests are among the most sensitive assays because they are capable of detecting 10^4 cancer cells. However, a recurrent tumor may arise from this small number of cells. Treatment must, therefore, be continued after the normalization of both hCG and hCGβ. Prolonged decay of either hCG or free hCGβ identifies patients who are unlikely to achieve a complete remission or long-term survival and indicates that additional chemotherapy or a switch to a different chemotherapy regimen is required *(44)*.

hCG, free hCGβ, and AFP are also the most useful markers for the diagnosis, prognosis, and monitoring of patients with testicular germ-cell tumors such as choriocarcinoma, embryonal carcinoma, and teratocarcinoma. Tumors may be located within the gonads or, on rare occasions, extragonadal. In nonseminomatous germ-cell testicular tumor (NSGCTT), increased concentrations of hCG and free hCGβ were found in ~60% and in 40–70% of cases, respectively *(45)*. Combining the three markers makes it possible to detect ~90% of patients with NSGCTT. hCG is of less interest as a marker in seminoma because it is increased in only ~16% of patients; serum values are generally <200 IU/L. Values exceeding 5000 IU/L indicate the presence of NSGCTT. Interestingly, 20–50% and 9–17% of patients with seminoma have increased free hCGβ and hCG α subunit, respectively. The prognostic value of both the hCG concentration before chemotherapy and its $t_{1/2}$ has been widely investigated, with the aim of identifying the 20–30% of patients with NSGCTT who fail to respond to therapy *(46–48)*. Several reports have indicated that the kinetics of both hCG and AFP are good indicators of patients likely to be refractory to treatment *(49, 50)*, whereas others conclude that the

analysis of tumor marker values cannot be used to predict who is at a higher risk or to tailor treatment accordingly *(48, 51)*. In fact, the tumor marker concentration before therapy appears to be a stronger predictor of treatment failure than marker $t_{1/2}$ *(52)*. Furthermore, after orchidectomy, patients with increased AFP relapse more frequently than patients with increased hCG *(53)*.

Currently, no firm conclusions can be drawn about the usefulness of markers for identifying poor risk patients. A major explanation for the discrepancies between the conclusions of the different studies is the methodology used. For example, unpredictable transient rises in hCG/hCGβ concentrations after chemotherapy may occur as a result of tumor lysis with a subsequent release of a given marker; consequently, comparisons of $t_{1/2}$ calculated from marker values before treatment and after the second cycle of chemotherapy are often unreliable. In a retrospective study, Toner et al. *(54)* showed that a prolonged marker $t_{1/2}$ (>7 days for AFP; >3 days for hCG) is a reliable indicator of residual tumor and a significant predictor of survival. In contrast to other studies, Toner et al. *(54)* determined the $t_{1/2}$ of each marker from the first two values measured within 3 months after the start of the treatment. Although markers were not measured systematically during initial treatment, this study provides a more reliable method for the use of serial measurements of markers in the management of patients with germ-cell tumors. Studies on AFP also confirm that the analytic strategy is crucial in attempts to improve the sensitivity of tests based on marker $t_{1/2}$. This critical point will be discussed later.

AFP is also used as a marker for both the diagnosis and monitoring of patients suffering from hepatocellular carcinoma *(55)*. Measurement of AFP is used to assess the completeness of surgical resection and response to therapy or recurrences. Hepatocellular carcinoma frequently recurs after surgery; with serial determination of serum AFP, such recurrences could be detected at least 3 and up to 18 months before the onset of symptoms. The interval between surgery and recurrence correlates with the AFP DT. A decrease in serum AFP indicates clinical response to chemotherapy; if DT does not decrease, serial measurement obviates prolonged ineffective therapy. However, a negative value does not exclude the presence of subclinical disease *(56)*. An increase in serum AFP signifies that chemotherapy should be changed *(57)*. Finally, measuring the $t_{1/2}$ of serum AFP has been useful for the management of patients with malignant germ-cell tumors of the ovary *(58)* and children presenting with teratoma, endodermal sinus tumor, or hepatoblastoma *(59, 60)*.

CEA

CEA is the only useful marker for monitoring colorectal cancer *(61)*. For >25 years now, sequential CEA measurements have been used to monitor the response of colorectal cancer to surgery *(62–64)*. Serial measurements of serum CEA, instead of a single determination, are recommended for the detection of recurrences in colon cancer *(65, 66)*. The NIH Consensus Conference in 1981 emphasized that serial CEA determination, not a single determination, should be mandatory in clinical decision-making *(67)*. In Dukes stage A disease, which rarely recurs, CEA monitoring is not justified for monitoring purposes. Follow-up of CEA is recommended, however, for patients with Dukes B and C adenocarcinoma *(68)*. Recurrent disease occurs within 30 months and at a median time of 17 months in most patients. It rarely occurs after 5 years *(69)*. The postoperative CEA concentration is a significant prognostic factor for survival. When tumor resection is complete, the postoperative CEA value decreases to 2.5 μg/L or less within the first month *(65)*. When the postoperative CEA concentration falls to <5 μg/L, only 18% of patients will relapse. In contrast, recurrent disease occurs in 63% of the patients when the CEA concentration remains above 10 μg/L *(70)*. The median lead time from increase in marker concentration to clinical recurrence is from 3 to 8 months *(71)*. The sensitivity of postoperative CEA measurements varies according to the site of recurrence. The CEA test is inappropriate for the early diagnosis of localized recurrence *(72)*. CEA kinetics permit differentiation between local and metastatic liver recurrences, with mean slope values attaining, respectively, 0.17 and 2.2 μg/L in 10 days *(66)*. Calculating the CEA ascending slope in a computerized surveillance program has been shown to differentiate types of recurrent tumor *(66)*. Slope analysis has been used to predict the site of recurrence and to plan second-look surgery. Different decision rules have been proposed on the basis of the evolution of the CEA concentration *(73, 74)*. When Denstman et al. *(75)* compared various rules, they concluded that steadily rising concentrations (>12% per month) clearly indicated tumor recurrence. A linear relationship between log CEA and time exists during the logarithmic growth phase of recurrent tumors. This relationship is expressed by the DT, which varies according to the site of the metastatic lesions. The DT can be used to assess the efficacy of various treatments *(76, 77)* and is particularly correlated with the duration of survival *(78)*. Monthly CEA measurements during the first 3 years and then at 3-month intervals for 2 years are, therefore, recommended for postoperative monitoring *(69)*.

The calculated $t_{1/2}$ should be an earlier predictor than analysis of the CEA ascending slope. After complete surgical resection and in the absence of recurrent disease, CEA concentrations decrease exponentially to reference values, with a $t_{1/2}$ of ~5 days. In patients with a recurrence, a dissociation from the theoretical line of the $t_{1/2}$ is observed before the CEA concentration decreases to the reference interval *(79)*.

Postoperative chemotherapy and particularly combination fluorouracil-levamisole may be effective for metastatic tumors *(80)*. CEA appears to be a practical index and a criterion for evaluating the efficacy of treatment. A 20% decrease in the CEA concentration is considered a positive response to treatment, conferring a substantial

improvement of survival *(81, 82)*. The efficacy of regional chemotherapy has been assessed in patients with nonresectable liver metastasis from colorectal cancer: because CEA concentrations may vary considerably between patients, an individual reference value is first established as the arithmetical mean of serial CEA values during the first three courses of chemotherapy. The efficacy of the chemotherapy regimen is indicated by a decrease in the CEA curve to below the individual reference value *(83)*. In recurrent or nonresectable colorectal cancer, different indices, devised with serum CEA fluctuations over time, are helpful in assessing and comparing the effects of various treatments, especially the CEA DT ratio when the CEA DT is modified *(84)*. For the management of patients with hepatic metastases from colorectal cancer, measurement of CEA is mandatory before and after surgery to appreciate whether the resection was curative. Furthermore, postoperative CEA concentrations are among the criteria used to stratify patients for adjuvant treatment *(85)*.

Serial measurements of CEA provide a practical tool for patients undergoing chemotherapy for advanced colorectal cancer. However, scanning techniques are required to confirm the response suggested by any change in marker expression *(86)*.

CA 125

CA 125 is a useful marker for epithelial ovarian tumors *(87, 88)*. The preoperative serum CA 125 concentration is correlated with the tumor burden and stage, but its prognostic significance is controversial *(89, 90)*. The postoperative concentration is highly correlated with the residual tumor mass *(89)* and has a significant value that is predictive for survival *(91)*. It must be determined at least 3 weeks after surgery because CA 125 is released when the abdominal cavity is opened *(92, 93)*. Disease progression occurs in 61% of patients presenting with increased CA 125 concentrations before chemotherapy and in only 33% patients with values <35 kilounits/L *(94)*. After the first course of chemotherapy, the predictive value of the CA 125 concentration for disease-free survival is highly significant *(95)*.

During chemotherapy, changes in CA 125 concentrations correlate with the evolution of the disease. The median time to normalization is 1.5 months in patients having attained a complete remission and 4 months in patients having achieved partial remission *(96)*. Increased CA 125 concentrations precede clinical detection of disease and are always associated with tumor progression, as substantiated by second-look surgery. However, in patients with normalized CA 125 concentrations, second-look surgery is still necessary because a CA 125 concentration within the reference interval does not exclude tumor. More than 40% of the patients with a serum CA 125 concentration within the reference interval still have microscopic or macroscopic tumor at second-look surgery *(87)*.

The prognostic value of the $t_{1/2}$ of CA 125 has been analyzed during induction therapy to identify high-risk patients. In patients with stage I and stage II disease whose tumor had been completely resected, the marker $t_{1/2}$ varied from 5.1 to 12 days in different studies *(96–101)*. The greatest difference in progression rate was found at a $t_{1/2}$ of 20 days. The median times to progression were 43–50 months and 11–23 months in stage I and stage II disease, respectively *(94)*. Patients with a marker $t_{1/2}$ <20 days have a good prognosis, those with a marker $t_{1/2}$ from 20 to 40 days have an intermediate prognosis, and those with a marker $t_{1/2}$ >40 days have a poor prognosis, with actuarial survival at 2 years attaining 76%, 48%, and 0%, respectively *(102, 103)*. The CA 125 $t_{1/2}$ is the most valuable prognostic factor for survival and for the probability of achieving a complete remission in stage III or IV ovarian cancer responding to initial chemotherapy *(104)*. The $t_{1/2}$ of CA 125 during early chemotherapy is an independent prognostic factor for achieving a complete response and for survival *(91)*. Evaluating the time required for normalization of CA 125 has also been proposed. A final model including the tumor size, performance status, and the time to normalization of CA 125 permits an accurate prediction of the prognosis *(105)*.

Additional monitoring of declining CA 125 concentrations is based on the exponential regression curve proposed by Buller et al. *(99)*, calculated as serum CA 125 = $e^{[i - s(\text{days after surgery})]}$, where i is the y-axis intercept and reflects the initial tumor burden, and s the slope of the regression curve, with s being dependent on the extent of cytoreductive surgery and on response to chemotherapy. In patients whose tumors had been completely removed, the marker $t_{1/2}$ was 10.4 days *(99)*. Comparing patients results with those obtained by this model permits an evaluation of treatment efficacy. Divergence from the ideal regression curve can be determined within 30 to 60 days of initial surgery and always leads to treatment failure. Therapy can, therefore, be modified without waiting for second-look findings. Comparison with the model also predicts the presence of residual disease, the risk of recurrence, and overall survival *(106, 107)*. After comparing these two exponential regression models, Yedema et al. *(100)* showed that survival correlates better with the $t_{1/2}$ calculated according to Buller et al. *(99)* than according to van der Burg et al. *(94)*. The CA 125 exponential regression curve was the most important prognostic factor for actuarial survival when analyzed with age, disease stage, grade, the intensity of chemotherapy, and residual disease in the Cox model. With the proportional hazard model, the disease stage was the most predictive variable for survival, and the CA 125 $t_{1/2}$ calculated according to Buller et al. *(99)* was the only additional prognostic factor for survival in stage III-IV patients early during the course of therapy *(100)*. During salvage treatment with Taxol, the regression rate did not correlate with the progression-free interval or survival *(108)*.

Rustin et al. *(109)* selected a specific percentage of decrease in the CA 125 concentration during chemotherapy as evidence for response to treatment. In a large

retrospective trial, two response rates were defined according to a reduction of either 50% or 75% in the serum CA 125 concentration from baseline. Three or four CA 125 measurements were required at the end of each cycle of chemotherapy to determine the response rates, the last sample being at least 28 days after the previous sample. The definitions proposed were based on 117 patients in a first trial and further tested on several hundred patients. The results showed better correlation with reduction of lesions in the patients than WHO, Eastern Cooperative Oncology Group, or Gynecologic Oncology Group criteria and were proposed for use in addition to or as replacements for these criteria. A few studies have been devoted to the CA 125 DT at relapse of ovarian cancer. There is no relationship between the $t_{1/2}$, DT, and survival, but the log cell kill, estimated by combining the marker $t_{1/2}$ and DT, was correlated with individual survival *(96)*. Riedinger et al. *(110)* studied the prognostic significance of the initial $t_{1/2}$ of CA 125 measured during first-line chemotherapy in 62 patients with epithelial stages III and IV ovarian cancer. The results showed a strong correlation between the $t_{1/2}$ and the DT, the slope representing initial CA 125 regression and disease-free survival as well as overall survival. The initial $t_{1/2}$, measured during the first cycles of first-line chemotherapy, appeared to be a critical predictor of response to therapy.

CA 15-3

When breast cancer patients are monitored by serum CA 15-3 concentration, the serum antigen profile in each patient is the criterion during follow-up most indicative of recurrent disease and of response to various treatments. And yet, a third of breast cancer patients with metastasis have CA 15-3 concentrations within the reference interval *(111)*. The use of CA 15-3 kinetic parameters was proposed in patients at high risk of relapse: an increase in the tumor marker should be considered an early indicator of relapse. After radical resection of tumor, CA 15-3 exhibits substantial variation at abnormal concentrations *(112)*. CA 15-3 does not have a negative predictive value. The evolution during follow-up is based on the ratio of two serial CA 15-3 measurements over 1 month *(113)*. CA 15-3 is informative and biologically significant in a few cases if the variation between the preoperative determination and the determination 30 days after surgery is higher than threefold the analytical variation of the assay, even if values fall short of the cutoff. Both cutoff-based and dynamic criteria are used during the monitoring of breast cancer patients to detect early metastasis and even to assess the cure of relapses *(114)*. However, a clinical benefit has not been established, although an increasing CA 15-3 concentration can be considered synonymous with recurrence after primary treatment *(61)*.

DISCUSSION

Measuring tumor marker kinetics may be a useful way of improving the efficacy of cancer treatment, but at present there is no consensus as to the usefulness of determining marker dynamics during the monitoring of patients. Indeed, as illustrated by this review devoted to the main tumor markers used, the conclusions of distinct studies addressing the interest of measuring kinetics of a particular marker in a given cancer are frequently at variance. The discrepancies in comparisons of the dynamic results obtained by different groups may be attributable to several factors, including (*a*) the methodological approaches used to measure markers, which are often dependent on the nature and structure of tumor markers; (*b*) individual factors such as the pathophysiological state of the patient or the treatment regimen; and (*c*) the methods used to calculate kinetics and the interpretation of data.

Nature and Structure of Tumor Markers

During the last decade, invaluable efforts have been used to enhance the sensitivity and specificity of detection with tumor markers. Markers are now measured by immunochemical methods, most often based on the classic "two-site" sandwich immunoassay procedure. Its characteristics, particularly the affinity and the specificity of the monoclonal or polyclonal antibodies used, play a critical role in the design of the assay. Antibodies are usually selected for their high affinity to ensure better sensitivity in the immunoassay. Specificity is contingent on more selective recognition of the antigen structure by the antibody on the tumor marker molecule. Indeed, antigen proteins have several distinct antigenic determinants or epitopes protruding from their surface. The number of epitopes is roughly related to the molecular size of the protein. Extensive immunochemical analysis of protein antigens is a mammoth task, and only a few immunochemical maps of tumor markers have in fact been raised. These observations partly explain why two separate kits measuring the same molecule can yield different results. This is particularly true for the detection of hCG and PSA, for which ~40 commercial tests are currently available. Furthermore, the heterogeneous "faces" of tumor markers complicates the interpretation of data. Indeed, these molecules can exist in biological fluids as several entities, including subunits (hCG), associated forms (PSA), and degradation products (Table 1). There may also be variations in both their peptidic and carbohydrate structures that are attributable to either physiological or tumor processes. This has been particularly investigated for hCG-related molecules *(45)*. The structure of hCG is close to that of lutropin, which is detectable in healthy individuals. Not only must detection of hCG be specific in regard to potential cross-reactivity with lutropin (i.e., epitopic specificity), but tumors are capable of secreting various hCG-related molecules [free hCGβ, free hCG α subunit, and β-core fragment; for a review, see Ref. *(45)*], the clinical significance of which differs according to the tumor histologic type (i.e., structural specificity). In testicular and placental tumors, for example, should we analyze the rate at which either hCG or hCGβ declines or

both? PSA circulates in both a protein-linked form and as free PSA. The kinetics of PSA analyzed by methods measuring total PSA may differ from those measured by free-PSA assays. This question must be addressed because specific measurement of free PSA is now available *(115)*. Furthermore, part of the PSA is totally masked on the complex and is not accessible to the detection capacity of the kits currently available *(116)*. Changes in the only carbohydrate chain of AFP have also been described in patients with cancer, compared with that present on normal fetal AFP *(117)*. Some immunoassays bind differently to the two AFP molecules *(118)*. Pitfalls in the interpretation of the kinetics of CA markers are probably more related to their structural heterogeneity than to epitope specificity. Indeed, these markers are defined on the basis of their recognition by specific antibodies and their structure, i.e., the structure of the molecule bearing the "CA" determinant, which still remains unknown. These determinants are often large heterogeneous mucin-like molecules that vary in size according to the pathophysiological state of the individual. Thus, although immunoassays are comparable in terms of epitope specificity, the determination of kinetic parameters may be affected by changes in the structure of the CA-bearing molecule during the course of treatment. Improving the comparability of immunoassays, particularly those used to measure tumor markers, remains a challenge for the future. Through undaunted efforts, international societies have given concrete expression to better characterization of antibodies *(119, 120)*.

Individual Factors

Individual factors such as the pathophysiological state of the patient or the treatment regimen may also affect the measurement and interpretation of marker kinetics. During the monitoring of neoplastic disease, nonspecific increases in tumor marker concentrations can be caused by a variety of benign pathologies *(121–124)*. Inflammatory diseases are frequently the cause of nonspecific increases in the so-called CA markers. Tumor markers often increase after surgery because of a serous response. In contrast, a false decrease in tumor markers may be attributable to procedures leading to hemodilution (e.g., parenteral nutrition and blood transfusion). An increase in serum AFP may occur in cases of hepatic regeneration *(56)*. Kinetics may also be transiently affected by renal and hepatic diseases, because these tissues are involved in the metabolism of markers *(125, 126)*, and by the aging process *(127)*. Furthermore, tumor recurrences and metastasis may exhibit patterns of marker secretion that are different from that of primary tumors. This factor should be taken into account when interpreting the DT. Aggressive chemotherapy and radiotherapy may provoke massive destruction of cancer cells, leading to a transient increase in serum markers that should not be interpreted as the tumor escaping eradication via chemoresistance. Some therapies stimulate synthesis *(128)*. Increased CEA synthesis has been observed during interferon treatment *(129)*. PSA is controlled by androgens and gonadotropin-releasing hormone *(130)*. The potential effects on tumor marker concentrations of conventional drug therapy used to treat benign diseases in cancer patients remain to be established. Taxol is suspected of modifying CA 125 synthesis in ovarian cancer *(131)*. Finally, anti-species human immunoglobulins, particularly anti-mouse antibodies, are encountered in some patients *(132, 133)*. Human anti-mouse antibodies are sometimes observed in patients who have been submitted to immunoscintigraphy for the detection of recurrences. Human anti-mouse antibodies, autoantibodies, anti-idiotypic antibodies, and rheumatoid factor may generate false-positive results and, thus, interfere with marker dynamics.

Surgical intervention itself may amplify the shedding of markers into the circulation and therefore generate false-positive results. After abdominal surgery, CA 125 increases through tumor handling and peritoneal damage. During surgical intervention, the rupture of natural barriers facilitates the transfer of CA 125 into blood. Increases have been observed in postoperative CA 125 concentrations in malignant and benign diseases of the ovary as well as in diseases of the gastrointestinal tract. Consequently, caution should be exercised when interpreting CA 125 concentrations after abdominal surgery, and especially in patients whose pretreatment CA 125 concentrations were within the reference interval or moderately increased *(93)*.

Marker Determination Methods and the Analysis of Kinetics

The $t_{1/2}$ or DT of a marker can be calculated after repeated measurements only if the tumor marker is determined with the same method to avoid analytical variations attributable to different kits. Discrepancies between the conclusions of clinical studies may also be related to the methods used to evaluate kinetic parameters. Although tumor growth is exponential, most graphic representations are rarely based on logarithmic units. Logarithmic representation eliminates nonspecific variations. Furthermore, kinetics can be represented as a unique parameter, with the slope depicting either the $t_{1/2}$ or the DT. This parameter is a characteristic of the behavior of tumor growth. It could be included in a Kaplan-Meier model or any other suitable model to evaluate the efficacy of therapy during the monitoring of patients. Studies comparing two models, based on either linear or exponential regression, showed that the exponential model correlates better with clinical factors *(99, 107)*. However, for many authors *(111, 134, 135)*, there is no difference in the mathematical methods used to determine kinetic parameters.

In fact, the number of sequential measurements, the timing, and the interval between the measurements are probably the main source of variation in the establishment of kinetic factors. For example, a comparison of kinetics that were calculated after chemotherapy using either the

presurgery or prechemotherapy concentrations as the baseline value and either the first normalized concentration as the second value or all of the data available indicated that the exponential regression model including the presurgery and all other values correlated better with overall survival *(100)*. The timing of blood sampling is also critical, and it should be scrupulously respected. The marker concentration before treatment may have a prognostic significance, but this value should not be considered as the baseline value, i.e., the origin of the slope of the regression curve. Indeed, several factors contribute to the fluctuation of tumor marker concentrations between diagnosis and the beginning of treatment. As noted previously, chemotherapy as well as surgery induces either cytolysis and transient marker secretion or a reduction in the tumor volume. Thus, the kinetics of markers in patients treated with the same protocol may be particularly difficult to interpret *(92, 136)*. For example, kinetics during the monitoring of breast cancer show three distinct patterns: tumor regression, tumor progression followed by tumor regression, and tumor regression followed by resistance to therapy with major tumor progression. Kinetics evaluated immediately after treatment should not be used *(137)*. The first sample, which could be considered a legitimate value for the origin of the slope of the elimination curve, should be obtained after surgical excision or after induction chemotherapy. Other sequential samples can be collected following a sequence that will depend on the $t_{1/2}$ of the marker. As described previously for the measurement of PSA after radical prostatectomy *(21)*, if the t_0 value is measured 5 min after surgery, the PSA concentration will be higher and the $t_{1/2}$ shorter than if the t_0 is measured 2 days after surgery. Many authors do not agree with sampling 5 min after surgery *(138)*.

In conclusion, several questions and issues need to be addressed when applying dynamic evaluation of markers to the monitoring of patients, particularly the method used to calculate the kinetics and the choice of the data to be included in the mathematical model. However, using tumor kinetics appears to be a more rational way of using tumor markers than the common cutoff point. Indeed, the determination of the $t_{1/2}$ and DT often provides the most relevant predictive factors for the estimation of disease-free and overall survival, treatment efficacy, and for the decision regarding optimal treatment and cost-effectiveness in terms of toxicity and patient benefit. This approach could be a way to optimize patient management by limiting ineffective treatment and, consequently, the clinical costs of what may be pointless therapies once these dynamic data have clarified the clinical picture *(139)*.

We thank Lorna Saint-Ange for editing the manuscript and Véronique Letourneur for expert technical assistance.

References

1. Gion M, Mione R, Barioli P, Dittadi R. Dynamic use of tumor markers, rationale-clinical applications and pitfalls. Anticancer Res 1996;16:2279–84.
2. Wu J, Nakamura R. Human circulating tumor markers, current concepts and clinical applications. Chicago, IL: American Society of Clinical Pathologists, 1997:263pp.
3. Hayes DF, Bast RC, Desch CE, Fritsche H, Kemeny NE, Jessup M, et al. Tumor marker utility system: a framework to evaluate clinical utility of tumor markers. J Natl Cancer Inst 1996;88: 1456–66.
4. Pamies RJ, Crawford DR. Tumor markers: an update. Med Clin N Am 1996;80:185–99.
5. Carter HB, Pearson JD, Metter EJ, Brant LJ, Chan DW, Andres R, et al. Longitudinal evaluation of prostate-specific antigen levels in men with and without prostate disease. JAMA 1992;267: 2215–20.
6. Carter HB, Morrell CH, Pearson JD, Brant LJ, Plato CC, Metter EJ, et al. Estimation of prostatic growth using serial prostate-specific antigen measurements in men with and without prostate disease. Cancer Res 1992;52:3323–8.
7. Stamey TA, Dietrick DD, Issa MM. Large, organ confined, impalpable transition zone prostate cancer: association with metastatic levels of prostate specific antigen. J Urol 1993;149: 510–5.
8. Schmid HP, McNeal JE, Stamey TA. Observations on the doubling time of prostate cancer. The use of serial prostate-specific antigen in patients with untreated disease as a measure of increasing cancer volume. Cancer 1993;71:2031–40.
9. Weber JP, Oesterling JE, Peters CA, Partin AW, Chan DW, Walsh PC. The influence of reversible androgen deprivation on serum prostate-specific antigen levels in men with benign prostatic hyperplasia. J Urol 1989;141:987–92.
10. Brawer MK, Aramburu EA, Chen GL, Preston SD, Ellis WJ. The inability of prostate specific antigen index to enhance the predictive value of prostate specific antigen in the diagnosis of prostatic carcinoma. J Urol 1993;150:369–73.
11. Stamey TA, Kabalin JN. Prostate specific antigen in the diagnosis and treatment of adenocarcinoma of the prostate. I. Untreated patients. J Urol 1989;141:1070–5.
12. Zagars GK, Pollack A. The fall and rise of prostate-specific antigen. Kinetics of serum prostate-specific antigen levels after radiation therapy for prostate cancer. Cancer 1993;72:832–42.
13. Cadeddu JA, Pearson JD, Partin AW, Epstein JI, Carter HB. Relationship between changes in prostate-specific antigen and prognosis of prostate cancer. Urology 1993;42:383–9.
14. Carter HB, Pearson JD. PSA velocity for the diagnosis of early prostate cancer. A new concept. Urol Clin N Am 1993;20:665–70.
15. Hanks GE, D'Amico A, Epstein BE, Schultheiss TE. Prostatic-specific antigen doubling times in patients with prostate cancer: a potentially useful reflection of tumor doubling time. Int J Radiat Oncol Biol Phys 1993;27:125–7.
16. D'Amico AV, Hanks GE. Linear regressive analysis using prostate-specific antigen doubling time for predicting tumor biology and clinical outcome in prostate cancer. Cancer 1993;72:2638–43.
17. Hanks GE, Hanlon AL, Lee WR, Slivjak A, Schultheiss TE. Pretreatment prostate-specific antigen doubling times: clinical utility of this predictor of prostate cancer behavior. Int J Radiat Oncol Biol Phys 1996;34:549–53.
18. Pollack A, Zagars GK, Kavadi VS. Prostate specific antigen doubling time and disease relapse after radiotherapy for prostate cancer. Cancer 1994;74:670–8.
19. Oesterling JE, Chan DW, Epstein JI, Kimball AW Jr, Bruzek DJ, Rock RC, et al. Prostate specific antigen in the preoperative and

postoperative evaluation of localized prostatic cancer treated with radical prostatectomy. J Urol 1988;139:766–72.
20. Stamey TA, Graves HC, Wehner N, Ferrari M, Freiha FS. Early detection of residual prostate cancer after radical prostatectomy by an ultrasensitive assay for prostate specific antigen. J Urol 1993;149:787–92.
21. Semjonow A, Hamm M, Rathert P. Half-life of prostate-specific antigen after radical prostatectomy: the decisive predictor of curative treatment? Eur Urol 1992;21:200–5.
22. Semjonow A, Hamm M, Rathert P. Prediction of tumor recurrence after radical prostatectomy using elimination kinetics of prostate-specific antigen. World J Urol 1993;11:218–20.
23. van Straalen JP, Bossens MM, de Reijke TM, Sanders GT. Biological half-life of prostate-specific antigen after radical prostatectomy. Eur J Clin Chem Clin Biochem 1994;32:53–5.
24. Semjonow A, Hamm M, Rathert P. Elimination kinetics of prostate-specific antigen in serum and urine. Int J Biol Markers 1994;9:15–20.
25. Lein M, Brux B, Jung K, Henke W, Koenig F, Stephan C, et al. Elimination of serum total and free prostate-specific antigen after radical retropubic prostatectomy. Eur J Clin Chem Clin Biochem 1997;35:591–5.
26. Bjork T, Ljungberg B, Pironen T, Abrahamsson PA, Pettersson K, Cockett AT, et al. Rapid elimination of free prostate-specific antigen contrasts the slow, capacity-limited elimination of PSA complexed to α_1-antichymotrypsin in serum. Urology 1998;51: 57–62.
27. Ravery V, Meulemans A, Boccon-Gibod L. Clearance of free and total PSA after prostatic surgery. Eur Urol 1998;33:251–4.
28. Haab F, Meulemans A, Boccon-Gibod L, Dauge MC, Delmas V, Boccon-Gibod L. Clearance of serum PSA after open surgery for benign prostatic hypertrophy, radical cystectomy, and radical prostatectomy. Prostate 1995;26:334–8.
29. Brandle E, Gottfried HW, Maier S, Flohr P, Steinbach G, Hautmann RE. [Is radical prostatectomy a suitable model for determination of PSA half-life?]. Urologe A 1995;34:419–23.
30. Morgan WR, Zincke H, Rainwater LM, Myers RP, Klee GG. Prostate specific antigen values after radical retropubic prostatectomy for adenocarcinoma of the prostate: impact of adjuvant treatment (hormonal and radiation). J Urol 1991;145:319–23.
31. Oesterling JE. Andrews PE, Suman VJ, Zincke H, Myers RP. Preoperative androgen deprivation therapy: artificial lowering of serum prostate specific antigen without downstaging the tumor. J Urol 1993;149:779–82.
32. Zagars GK, Pollack A. Kinetics of serum prostate-specific antigen after external beam radiation for clinically localized prostate cancer. Radiother Oncol 1997;44:213–21.
33. Vijayakumar S, Quadri SF, Karrison TG, Trinidad CO, Chan SK, Halpern HJ, et al. Localized prostate cancer: use of serial prostate-specific antigen measurements during radiation therapy. Radiology 1992;184:271–4.
34. Zagars GK, von Eschenbach AC. Prostate-specific antigen. An important marker for prostate cancer treated by external beam radiation therapy. Cancer 1993;72:538–48.
35. Ritter MA, Messing EM, Shanahan TG, Potts S, Chappell RJ, Kinsella TJ. Prostate-specific antigen as a predictor of radiotherapy response and patterns of failure in localized prostate cancer. J Clin Oncol 1992;10:1208–17.
36. Kaplan ID, Cox RS, Bagshaw MA. Prostate specific antigen after external beam radiotherapy for prostatic cancer: follow-up. J Urol 1993;149:519–22.
37. Fijuth J, Chauvet B, Vincent P, Felix-Faure C, Reboul F. Serum prostate-specific antigen in monitoring the response of carcinoma of the prostate to radiation therapy. Radiother Oncol 1992;23:236–40.
38. Stamey TA, Kabalin JN, Ferrari M, Yang N. Prostate specific antigen in the diagnosis and treatment of adenocarcinoma of the prostate. IV. Anti-androgen treated patients. J Urol 1989;141: 1088–90.
39. Stamey TA, Ferrari MK, Schmid HP. The value of serial prostate specific antigen determinations 5 years after radiotherapy: steeply increasing values characterize 80% of patients. J Urol 1993;150:1856–9.
40. Morrow CP, Kletzy OA, Disaia PJ, Towsend DE, Mishell DR, Nakamura RM. Clinical and laboratory correlates of molar pregnancy and trophoblastic disease. Am J Obstet Gynecol 1977; 128:424–30.
41. Schlaerth JB, Morrox CP, Kletzy OA, Nalick RH, D'Ablaing GA. Prognostic characteristics of serum chorionic gonadotropin titer regression following molar pregnancy. Obstet Gynecol 1981;58: 478–82.
42. Yedema KA, Verheijen RH, Kenemans P, Schijf CP, Borm GF, Segers MF, et al. Identification of patients with persistent trophoblastic disease by means of a normal human chorionic gonadotropin regression curve. Am J Obstet Gynecol 1993;168: 787–92.
43. Mortakis AE, Braga CA. "Poor prognosis" metastatic gestational trophoblastic disease: the prognostic significance of the scoring system in predicting chemotherapy failure. Obstet Gynecol 1990;76:272–7.
44. International Germ Cell Cancer Collaborative Group. International Germ Cell Consensus Classification: a prognostic factor-based staging system for metastatic germ cell cancers. J Clin Oncol 1997;15:594–603.
45. Bidart JM, Bellet D. Human chorionic gonadotropin: molecular forms, detection and clinical implications. Trends Endocrinol Metab 1993;4:285–91.
46. Thompson DK, Haddow JE. Serial monitoring of serum α-fetoprotein and chorionic gonadotropin in males with germ cell tumors. Cancer 1979;43:1820–9.
47. Picozzi VJ, Freiha FS, Hannigan JF, Torti FM. Prognostic significance of a decline in serum chorionic gonadotropin levels after chemotherapy for advanced germ-cell carcinoma. Ann Intern Med 1984;100:183–6.
48. Culine S, Kramar A, Biron P, Droz JP. Chemotherapy in adult germ cell tumors. Crit Rev Oncol Hematol 1996;22:229–63.
49. Germa-Lluch JR, Begent RH, Bagshawe KD. Tumour marker levels and prognosis in malignant teratoma of the testis. Br J Cancer 1980;42:850–5.
50. Gerl L, Lamerz R, Mann K, Clemm C, Wilmanns W. Is serum tumor marker half-life a guide to prognosis in metastatic nonseminomatous germ cell tumors? Anticancer Res 1997;17: 3047–9.
51. Stevens MJ, Norman AR, Dearnaley DP, Horwich A. Prognostic significance of early tumor marker half-life in metastatic testicular teratoma. J Clin Oncol 1995;13:87–92.
52. de Wit R, Sylvester R, Tsitsa C, de Mulder PH, Sleyfer DT, ten Bokkel Huinink WW, et al. Tumour marker concentration at the start of chemotherapy is a stronger predictor of treatment failure than marker half-life: a study in patients with disseminated non-seminomatous testicular cancer. Br J Cancer 1997;75: 432–5.
53. Saxman SB, Nichols CR, Foster RS, Messemer JE, Donohue JP, Einhorn LH. The management of patients with clinical stage I nonseminomatous testicular tumors and persistently elevated serologic markers. J Urol 1996;155:587–9.
54. Toner GC, Geller NL, Tan C, Nisselbaum J, Bosl GJ. Serum tumor marker half-life during chemotherapy allows early prediction of complete response and survival in nonseminomatous germ cell tumors. Cancer Res 1990;50:5904–10.

55. Shirabe K, Takenaka K, Gion T, Shimada M, Fujiwara Y, Sugimachi K. Significance of α-fetoprotein levels for detection of early recurrence of hepatocellular carcinoma after hepatic resection. J Surg Oncol 1997;64:143–6.
56. Johnson PJ, Williams R. Serum α-fetoprotein estimations on doubling time in hepatocellular carcinoma: influence of therapy and possible value in early detection. J Natl Cancer Inst 1980; 64:1329–32.
57. Buamah PK, James OFN, Skillen AW, Harris AL. The value of tumor marker kinetics in the management of patients with primary hepatocellular carcinoma. J Surg Oncol 1988;37:161–4.
58. Kawai M, Furuhashi Y, Kano T, Misawa T, Nakashima N, Hattori S, et al. α-Fetoprotein in malignant germ cell tumors of the ovary. Gynecol Oncol 1990;39:160–6.
59. Walhof CM, Van Sonderen L, Voute PA, Delemarre JF, Half-life of α-fetoprotein in patients with a teratoma, endodermal sinus tumor, or hepatoblastoma. Pediatr Hematol Oncol 1988;5:217–27.
60. Han SJ, Yoo S, Choi SH, Hwang EH. Actual half-life of alpha-fetoprotein as a prognostic tool in pediatric malignant tumors. Pediatr Surg Int 1997;12:599–602.
61. American Society of Clinical Oncology. Clinical practice guidelines for the use of tumor markers in breast and colorectal cancer. J Clin Oncol 1996;14:2843–77.
62. Sorokin JJ, Sugarbaker PH, Zamcheck N, Pisick M, Kupchik HZ, Moore FD. Serial carcinoembryonic antigen assays. Use in detection of cancer recurrence. JAMA 1974;228:49–53.
63. Mackay AM, Patel S, Carter S, Stevens U, Laurence DJR, Cooper EH, et al. Role of serial plasma CEA assays in detection of recurrent and metastatic colorectal carcinomas. Br Med J 1974; 4:382–5.
64. Sikorska H, Schuster J, Gold P. Clinical applications of carcinoembryonic antigen. Cancer Detect Prev 1988;12:321–55.
65. Minton JP, Martin EW Jr. The use of serial CEA determinations to predict recurrence of colon cancer and when to do a second-look operation. Cancer 1978;42:1422–7.
66. Staab HJ, Anderer FA, Stumpf E, Fischer R. Slope analysis of the postoperative CEA time course and its possible application as an aid in diagnosis of disease progression in gastrointestinal cancer. Am J Surg 1978;136:322–7.
67. National Institutes of Health. Carcinoembryonic antigen: its role as a marker in the management of cancer. A National Institutes of Health Consensus Development Conference. Ann Intern Med 1981;94:407–9.
68. Minton JP, Hoehn JL, Gerber DM, Horsley JS, Connolly DP, Salwan F, et al. Results of a 400-patient carcinoembryonic antigen second-look colorectal cancer study. Cancer 1985;55: 1284–90.
69. Sugarbaker PH, Gianola FJ, Dwyer A, Neuman NR. A simplified plan for follow-up of patients with colon and rectal cancer supported by prospective studies of laboratory and radiologic test results. Surgery 1987;102:79–87.
70. Chu DZJ, Erickson CA, Russell P, Thompson C, Lang NP, Broadwater RJ, et al. Prognostic significance of carcinoembryonic antigen in colorectal carcinoma. Arch Surg 1991;126:314–6.
71. Staab HJ, Anderer FFA, Stumpf E, Hornung A, Fischer R, Kienginger G. Eighty-four potential second-look operations based on sequential carcinoembryonic antigen determinations and clinical investigations in patients with recurrent gastrointestinal cancer. Am J Surg 1985;149:198–204.
72. Moertel CG, Shutt AJ, Go VLW. Carcinoembryonic antigen test for recurrent colorectal carcinoma. Inadequacy for early detection. JAMA 1978;239:1065–6.
73. Steele G Jr, Ellenberg S, Ramming K, O'Connell M, Moertel C, Lessner H, et al. CEA monitoring among patients in multi-institutional adjuvant GI therapy protocols. Ann Surg 1982;196: 162–9.
74. Boey J, Cheung HC, Lai CK, Wong J. A prospective evaluation of serum carcinoembryonic antigen (CEA) levels in the management of colorectal carcinoma. World J Surg 1984;8:279–86.
75. Denstman F, Rosen L, Khuchandani IT, Sheets J, Stasik JJ, Riether R. Comparing predictive decision rules in postoperative CEA monitoring. Cancer 1986;58:2089–95.
76. Staab HJ, Anderer FA, Hornung A, Stumpf E, Fisher R. Doubling time of circulating CEA and its relation to survival of patients with recurrent colorectal cancer. Br J Cancer 1982;46:773–81.
77. Umehara Y, Kimura T, Yoshida M, Oba N, Harada Y. Comparison of doubling times of serum carcinoembryonic antigen produced by various metastatic lesions in recurrent gastric and colorectal carcinomas. Cancer 1993;71:4055–9.
78. Korenaga D, Saeki H, Mawatari K, Orita H, Maekawa S, Ikeda T, et al. Serum carcinoembryonic antigen concentration doubling time correlates with tumor biology and life expectancy in patients with recurrent gastrointestinal carcinoma. Arch Surg 1997;132: 188–94.
79. Takahashi Y, Mai M. Usefulness of sequential post-surgical tumor markers monitoring: prediction of remaining cancers by calculating dissociation from a half life period line. Ann Cancer Res Ther 1993;2:87–9.
80. Moertel CG, Fleming TR, MacDonald JS, Haller DG, Laurie JA, Goodman PJ, et al. Levamisole and fluorouracil for adjuvant therapy of resected colon carcinoma. N Engl J Med 1990;322: 352–8.
81. Hine KR, Dykes PW. Prospective randomised trial of early cytotoxic therapy for recurrent colorectal carcinoma detected by serum CEA. Gut 1984;25:682–8.
82. Allen-Mersh TG, Kemeny N, Niedzwiecki D, Shurgot B, Daly JM. Significance of a fall in serum CEA concentration in patients treated with cytotoxic chemotherapy for disseminated colorectal disease. Gut 1987;28:1625–6.
83. Quentmeier A, Schlag P, Hohenberger P, Schwarz V, Abel U. Assessment of serial carcinoembryonic antigen: determinations to monitor the therapeutic progress and prognosis of metastatic liver disease treated by regional chemotherapy. J Surg Oncol 1989;40:112–8.
84. Iwama T, Mishima Y, Sato H. A proposal of indices to describe the carcinoembryonic antigen time course in order to assess the effects of treating recurrent colorectal carcinoma. Jpn J Surg 1990;20:123–6.
85. Hohenberger P, Schlag PM, Gernerth T, Herfath C. Pre- and postoperative carcinoembryonic antigen determinations in hepatic resection for colorectal metastases. Predictive value and implications for adjuvant treatment based on multivariate analysis. Ann Surg 1994;219:135–41.
86. Ward U, Primrose JN, Finan PJ, Perren TJ, Selby P, Purves DA, et al. The use of tumor markers CEA, CA-195 and CA-242 in evaluating the response to chemotherapy in patients with advanced colorectal cancer. Br J Cancer 1993;67:1132–5.
87. van der Burg MEL, Lammes FB, Verweij J. CA 125 in ovarian cancer. Neth J Med 1992;40:36–51.
88. Kenemans P, Yedema CA, Bon GG, Von Mensdorff Pouilly S. CA 125 in gynecological pathology: a review. Eur J Obstet Gynecol Reprod Biol 1993;49:115–24.
89. Makar AP, Kristensen GB, Kaern J, Bormer OP, Abeler VM, Trope CG, et al. Prognostic value of pre- and postoperative serum CA 125 levels in ovarian cancer: new aspects and multivariate analysis. Obstet Gynecol 1992;6:1002–10.
90. Nagele F, Petru E, Medl M, Kainz C, Graf AH, Sevelda P. Preoperative CA 125. an independent prognostic factor in pa-

tients with stage I epithelial ovarian cancer. Obstet Gynecol 1995;86:259–64.

91. Gadducci A, Zola P, Landoni F, Maggino T, Sartori E, Bergamino T, Cristofani R. Serum half life of CA 125 during early chemotherapy as an independent prognostic variable for patients with advanced epithelial ovarian cancer: results of a multicentric Italian study. Gynecol Oncol 1995;58:42–7.
92. Mogensen O, Brock A, Nyland MH. CA 125 measurements in ovarian cancer patients during their first postoperative week. Int J Gynecol Cancer 1993;3:54–6.
93. Yedema CA, Kenemans P, Thomas CM, Massuger LF, Wobbes T, Verstraeten R, et al. CA 125 serum levels in the early post operative period do not reflect tumour reduction obtained by cytoreductive surgery. Eur J Cancer 1993;29:966–71.
94. van der Burg MEL, Lammes FB, Van Putten WLJ, Stoter G. Ovarian cancer: the prognostic value of the serum half-life of CA 125 during induction chemotherapy. Gynecol Oncol 1988;30: 307–12.
95. Fisken J, Leonard RCF, Stewart M, Beattie GJ, Sturgeon C, Aspinall L, et al. The prognostic value of early CA 125 serum assay in epithelial ovarian carcinoma. Br J Cancer 1993;68: 140–5.
96. Willemse HB, Aalders JG, de Bruyn HWA, Mulder NH, Sleijfer DT, de Vries EGE. CA 125 in ovarian cancer: relation between half-life, doubling time and survival. Eur J Cancer 1991;8:993–5.
97. Markowska J, Kopczynski Z, Szewierski Z, Manys G. CA 125 in monitoring chemotherapy of patients with ovarian cancer. Eur J Gynecol Oncol 1990;3:209–14.
98. Markowska J, Manys G, Szewierski Z. CA 125 in monitoring clinical course in ovarian cancer patients. A prospective clinical study. Eur J Gynecol Oncol 1992;2:201–4.
99. Buller RE, Berman ML, Bloss JD, Manetta A, Disaia PJ. CA 125 regression: a model for epithelial ovarian cancer response. Am J Obstet Gynecol 1991;165:360–7.
100. Yedema CA, Kenemans P, Voorhorst F, Bon G, Schijf C, Beex L, et al. CA 125 half-life in ovarian cancer: a multivariate survival analysis. Br J Cancer 1993;67:1361–7.
101. Cruickshank DJ, Terry PB Fullerton WT. The potential value of CA 125 as a tumour marker in small volume, non-evaluable epithelial ovarian cancer. Int J Biol Markers 1991;4:247–52.
102. Hawkins RE, Roberts K, Wiltshaw E, Mundy J, Fryatt IJ, McCready VR. The prognostic significance of the half-life of serum CA 125 in patients responding to chemotherapy for epithelial ovarian cancer. Br J Obstet Gynaecol 1989;96:1395–9.
103. Hunter VJ, Daly L, Helms M, Soper JT, Berchuck A, Clarke-Pearson DL, et al. The prognostic significance of CA 125 half-life in patients with ovarian cancer who have received primary chemotherapy after surgical cytoreduction. Am J Obstet Gynecol 1990;163:1164–7.
104. Meier W, Stieber P, Fateh-Moghadam A, Eiermann W, Hepp H. [Prognostic significance of the CA 125 half-life for the further outcome of ovarian cancer]. Geburtsh Frauenheilkd 1992;52: 528–32.
105. Frasci G, Conforti S, Zullo F, Mastrantonio P, Comella G, Comella P, et al. A risk model for ovarian carcinoma patients using CA 125. Cancer 1996;77:1122–30.
106. Buller RE, Berman ML, Bloss JD, Manetta A, DiSaia PJ. Serum CA 125 regression in epithelial ovarian cancer: correlation with reassessment findings and survival. Gynecol Oncol 1992;47: 87–92.
107. Buller RE, Vasilev S, Disaia PJ. CA 125 kinetics. A cost effective clinical tool to evaluate clinical trial outcomes in the 1990s. Am J Obstet Gynecol 1996;174:1241–54.
108. Pearl ML, Yashar CM, Johnston CM, Reynolds RK, Roberts JA. Exponential regression of CA 125 during salvage treatment of ovarian cancer with taxol. Gynecol Oncol 1994;53:339–43.
109. Rustin GJS, Nelstrop AE, McClean P, Brady MF, McGuire WP, Hoskins WJ, et al. Defining response of ovarian carcinoma to initial chemotherapy according to serum CA 125. J Clin Oncol 1996;14:1545–51.
110. Riedinger JM, Barillot I, Coudert B, Fargeot P, Berrioolo-Riedinger A, Guerrin J. Valeur pronostique de la demi-vie initiale du CA 125 mesurée au cours de la chimiothérapie d'induction chez 62 patientes porteuses de tumeur épithéliale ovarienne stade III et IV. Bull Cancer 1996;83:654–63.
111. Schmidt-Rhode P, Schultz KD, Sturm G, Raab-Frick A, Prinz H. CA 15.3 as a tumor marker in breast cancer. Int J Biol Markers 1987;3:33–8.
112. Gion M, Fila G, Biasoli R, Vignati G, Mione R, Saracchini S, et al. Kinetic use of tumor markers in the follow-up of patients operated for primary breast cancer. J Nuclear Med Allied Sci 1990;34:1–7.
113. Dnistrian AM, Schwartz MK, Greenberg EJ, Smith CA, Schwartz DC. CA 15.3 and carcinoembryonic antigen in the clinical evaluation of breast cancer. Clin Chim Acta 1991;200:81–94.
114. Gion M, Ruggeri G, Mione R, Marconato R, Casell A, Nosadini A, et al. A new approach to tumor marker assessment by perioperative determination in breast and colorectal cancer. Int J Biol Markers 1993;1:8–13.
115. Jung K, Stephan C, Lein M, Henke W, Schnorr D, Brux B, et al. Analytical performance and clinical validity of two free prostate-specific antigen assays compared. Clin Chem 1996;42:1026–33.
116. McCormack RT, Rittenhouse HG, Finlay JA, Sokoloff RL, Wang TJ, Wolfert RL, et al. Molecular forms of prostate-specific antigen and the human kallikrein gene family: a new era. Urology 1995;45:729–44.
117. Aoyagi Y, Saitoh A, Susuki Y, Igarashi K, Oguro M, Yokota T, et al. Fucosylation index of alphafoetoprotein, a possible aid in the early recognition of hepatocellular carcinoma, a possible patients with cirrhosis. Hepatology 1993;17:50–2.
118. Bellet DH, Wands JR, Isselbacher KJ, Bohuon C. Serum α-fetoprotein levels in human disease: perspective from a highly specific monoclonal radioimmunoassay. Proc Natl Acad Sci U S A 1984;81:3869–73.
119. Nap M, Vitali A, Nustad K, Bast RC Jr, O'Brien TJ, Nilsson O, et al. Immunohistochemical characterization of 22 monoclonal antibodies against the CA125 antigen: 2nd report from the ISOBM TD-1 Workshop. Tumour Biol 1996;17:325–31.
120. Sokoloff RL, Wolfert RL, Rittenhouse HG. Standardization of PSA immunoassays: proposals and practical limitations. J Clin Ligand Assay 1995;1886–92.
121. Ferrero JM, Largillier R, Ramaioli A, Heudier P, Teissier E, Namer M. Valeur pronostique de la normalisation précoce du CA 125 au cours de la chimiothérapie des tumeurs de l'ovaire stades III et IV. Bull Cancer 1997;84:722–8.
122. Daoud E, Bodor G, Weaver C, Ladenson JH, Scott MG. CA 125 concentrations in malignant and non malignant disease. Clin Chem 1991;37:1968–74.
123. Ruibal Morell A. CEA serum levels in non-neoplastic diseases. Int J Biol Markers 1992;7:160–6.
124. Liaw YF, Tai DI, Chen JJ, Chu CM, Huang MJ. α-Fetoprotein changes in the course of chronic hepatitis: relation to bridging hepatic necrosis and hepatocellular carcinoma. Liver 1986;6: 133–7.
125. Oberbauer R, Banyai S, Schmidt A, Kornek G, Scheithauer W, Mayer G. Serum tumor markers after renal transplantation. Transplantation 1996;62:1506–9.
126. Lye WC, Tambyah P, Leong SO, Lee EJ. Serum tumor markers in

patients on dialysis and kidney transplantation. Adv Perit Dial 1994;10:109–11.

127. Lopez LA, Del Villar V, Ulla M, Fernandez F, Fernandez LA, Santos I, et al. Prevalence of abnormal levels of serum tumour markers in elderly people. Age Ageing 1996;25:45–50.

128. Wadler S, Schwartz EL, Golman M, Lyver A, Rader M, Zimmerman M, et al. Fluorouracil and recombinant α-2a-interferon; an active regimen against advanced colorectal carcinoma. J Clin Oncol 1989;7:1769–75.

129. Greiner JW, Guadagni F, Goldstein D, Borden EC, Ritts RE Jr, Witt P, et al. Evidence of serum carcinoembryonic antigen and tumor associated glycoprotein-72 in patients administered interferons. Cancer Res 1991;51:4155–63.

130. Ruckle HC, Oesterling JE. Prostate-specific antigen and androgen deprivation therapy. World J Urol 1993;11:227–32.

131. van der Burg MEL, Myles JD, Hoskins PJ, Ten Bokkel Huinink WW, Eisenhauer E. CA125 is an unreliable marker for monitoring response to Taxol therapy in patients with relapsed ovarian cancer [Abstract]. Eur J Cancer 1993;29A:133.

132. Boerman OC, Segers MF, Poels LG, Kenemans P, Thomas CMJMB. Heterophilic antibodies in human sera causing falsely increased results in the CA 125 immunofluorometric assay. Clin Chem 1990;36:888–91.

133. Reinsberg J. Interference by human antibodies with tumor marker assays. Hybridoma 1995;4:205–8.

134. Cruickshank DJ, Paul J, Lewis CR, McAllister EJ, Kaye SB. An independent evaluation of the potential clinical usefulness of proposed CA-125 indices previously shown to be of prognostic significance in epithelial ovarian cancer. Br J Cancer 1992;65: 597–600.

135. Rustin GJ, Nelstrop AE, McClean P, Brady MF, McGuire WP, Hoskins WJ, et al. Defining response of ovarian carcinoma to initial chemotherapy according to serum CA 125. J Clin Oncol 1996;14:1545–51.

136. van der Zee AG, Duk JM, Aalders JG, Boontje AH, ten Hoor KA, de Bruijn HW. The effect of abdominal surgery on the serum concentration of the tumour-associated antigen CA 125. Br J Obstet Gynaecol 1990;97:934–41.

137. Kiang DT, Greenberg LJ, Kennedy BJ. Tumor marker kinetics in the monitoring of breast cancer. Cancer 1990;65:193–9.

138. Stamey TA. Lower limits of detection, biological detection limits, functional sensitivity, or residual cancer detection limit ? Sensitivity reports on prostate specific antigen assays mislead clinicians. Clin Chem 1996;42:849–52.

139. Leaning MS, Gallivan S, Newlands ES, Dent J, Brampton M, Smith DB, Bagshawe KD. Computer system for assisting with clinical interpretation of tumour marker data. Br Med J 1992; 305:804–7.

140. Hara M, Koyamagi Y, Inoue T, Fukuyama T. Some physicochemical characteristics of γ-seminoprotein; an antigenic component specific for human seminal plasma. Jpn J Legal Med 1971;25: 322–4.

141. Ascheim S, Zondek B. Das Hormon Der Hypophysenvorderlapens: Testobjeckt zum Nachweis des Hormons. Klin Wochenschr 1927;6:248–52.

142. Bergstrand CG, Czar B. Demonstration of a new protein fraction in serum from the human fetus. Scand J Clin Lab Investig 1956;8:1070–7.

143. Armbruster DA. Prostate-specific antigen: biochemistry, analytical methods and clinical application. Clin Chem 1993;39:181–95.

144. Pierce JG, Parsons TF. Glycoprotein hormones: structure and function. Annu Rev Biochem 1981;50:465–95.

145. Deutsch HF. Chemistry and biology of a fetoprotein. Adv Cancer Res 1991;56:253–311.

146. Chu TM, Kawinski E, Hibi N, Crogham G, Wiley J, Killian CS, et al. Prostate-specific antigen domain of human prostate-specific antigen identified with monoclonal antibodies. J Urol 1989;141: 151–5.

147. Jameson JL, Hollenberg AN. Regulation of chorionic gonadotropin gene expression. Endocr Rev 1993;14:203–21.

148. Korhonen J, Alfthan H, Ylostalo P, Veldhuis J, Stenman UH. Disappearance of human chorionic gonadotropin and its α- and β-subunits after term pregnancy. Clin Chem 1997;43:2155–63.

149. Keller RH, Lyman S. α-Fetoprotein: biological and clinical potential. In: Rhodes BA, ed. Tumor imaging. New York: Masson Publishing, 1982:41–52.

150. Oesterling JE. Prostate-specific antigen: a critical assessment of the most useful tumor marker for adenocarcinoma of the prostate. J Urol 1991;145:907–23.

151. Stenman UH, Bidart JM, Birken S, Mann K, Nisula B, O'Connor J. Standardization of protein immunoprocedures. Choriogonadotropin (CG). Scand J Clin Lab Investig Suppl 1993;216:42–78.

152. Alfthan H, Stenman UH. Pathophysiological importance of various molecular forms of human choriogonadotropin. Mol Cell Endocrinol 1996;125:107–20.

153. Lamerz R. AFP isoforms and their clinical significance. Anticancer Res 1997;17:2927–30.

154. Gold P, Freedman SO. Demonstration of tumor-specific antigens in human colonic carcinoma by immunological tolerance and adsorption techniques. J Exp Med 1965;21:439–62.

155. Bast RC, Freeney M, Lazarus H, Nadler LM, Colvin RB, Knapp RC. Reactivity of a monoclonal antibody with human ovarian carcinoma. J Clin Investig 1981;68:1331–7.

156. Kufe D, Imghirami G, Miyako A. Differential reactivity of a novel monoclonal antibody (DF3) with human malignant versus benign breast tumors. Hybridoma 1984;3:223–32.

157. Hilkens J, Hilgers J, Buijs F. Monoclonal antibodies against human milk fat globule membranes detecting differentiation antigens of mammary gland and its tumors. Int J Cancer 1984; 34:197–206.

158. Thomas P, Toth CA, Saini KS, Jessup JM. Steele G Jr. The structure, metabolism and function of the carcinoembryonic antigen gene family. Biochim Biophys Acta 1990;1032:177–89.

159. Yamashita K, Totami K, Kuroki M, Ueda I, Kobata A. Structural studies of the carbohydrate moieties of carcinoembryonic antigens. Cancer Res 1987;47:3451–9.

160. Siddiqui J, Abe M, Hayes DF, Shani E, Yunis E, Kufe DW.Isolation and sequencing on and cDNA coding for human DF3 breast carcinoma associated antigen. Proc Natl Acad Sci U S A 1988; 85:2320–3.

161. Verheist J, Van den Broecke E, Van Meerbeeck J, De Backer W, Blockx P, Vermeire P. Calculation of half-life of carcinoembryonic antigen after lung tumor resection: a case report. Eur Respir J 1991;4:374–6.

162. Hammarstrom S, Shively JE, Paxton RJ, Beatty BG, Larsson A, Ghosh R, et al. Antigenic sites in carcinoembryonic antigen. Cancer Res 1989;49:4852–8.

163. O'Brien T, Raymond LR, Bannon GA, Ford DH, Hardadottir H, Miller FC, et al. New monoclonal antibodies identify the glycoprotein carrying the CA 125 epitope. Am J Obstet Gynecol 1991;165:1857–64.

164. Tobias R, Rothwel C, Wagner J, Green A, Liu YSV. Development and evaluation of radioimmunoassay for the detection of a monoclonal antibody defined breast cancer associated antigen 115D8/DF3 [Abstract]. Proceeding of the Symposium of the American Association for Analytical Clinical Chemistry, 24 July 1985, Atlanta, GA:73–4.

EXHIBIT N

?.J.; Bohlen, P. Heparin-
nd MK, Members of a
ıtally Regulated Proteins.
2), 850–854.
.; Hada, H.; Tsuji, T.;
kibara, S.; Muramatsu, T.
ıe, and its Application to
ng Mouse Brain and Sera
omas. J. Biochem. (Tokyo)

:. Serum Hyaluronan as a
241–253.
Vinci, R.; Calatroni, A.
cid Glycosaminoglycans in
sential Thrombocythaemia.

ans as Glycosaminoglycans
ıe Dot Blot Analysis. Anal.

J. IMMUNOASSAY & IMMUNOCHEMISTRY, 23(1), 49–68 (2002)

TWO-STEP SANDWICH ENZYME IMMUNOASSAY USING MONOCLONAL ANTIBODIES FOR DETECTION OF SOLUBLE AND MEMBRANE-ASSOCIATED HUMAN MEMBRANE TYPE 1-MATRIX METALLOPROTEINASE

Takanori Aoki,[1,*] Kayoko Yonezawa,[1] Eiko Ohuchi,[1] Noboru Fujimoto,[1] Kazushi Iwata,[1] Taketoshi Shimada,[2] Takayuki Shiomi,[3] Yasunori Okada,[3] and Motoharu Seiki[4]

[1]Biopharmaceutical Department, Fuji Chemical Industries, Ltd., 530 Chokeiji, Takaoka, Toyama 933-8511, Japan
[2]Department of Otolaryngology, School of Medicine, Kyoto Prefectural University of Medicine, Kyoto, Japan
[3]Department of Pathology, School of Medicine, Keio University, Japan
[4]Department of Cancer Cell Research, Institute of Medical Science, The University of Tokyo, Tokyo, Japan

*Corresponding author. E-mail: t-aoki@fuji-chemi.co.jp

www.dekker.com

ABSTRACT

A two-step sandwich enzyme immunoassay (EIA) system for the detection of human membrane Type 1-matrix metalloproteinase (MT1-MMP) was established by using two monoclonal antibodies against recombinant MT1-MMP. MT1-MMP in which samples were reacted with solid-phase antibody and then detected with peroxidase-labeled second antibody. At least 1.25 ng/mL was detected by the EIA system, and linearity was obtained between 1.25 and 160 ng/mL. This EIA system is specific for MT1-MMP and did not show cross-reactivity against several other MMP's examined. Shedding of soluble MT1-MMP into the medium by some cancer cell lines was also detected by this system. However, soluble MT1-MMP in serum from normal and cancer patients was under the detection limit. Membrane-associated MT1-MMP of cancer cell lines was also detected after solubilization of the membranes with extraction buffer containing detergent. Additionally, MT1-MMP in clinical samples was examined. Elevated levels of MT1-MMP were detected in homogenate of cancer tissue compared with the levels for normal tissue and the level of MT1-MMP in tumors correlated with the rate of metastasis to the regional lymph nodes. Thus, we demonstrated that this EIA system is the first to measure MT1-MMP in clinical specimens, thus suggesting its useful for diagnosis of cancer or prediction of malignancy.

INTRODUCTION

Matrix metalloproteinases (MMPs) are zinc-dependent endopeptidases that degrade the extracellular matrix (ECM) and contribute to both physiological and pathological connective tissue remodeling.(1) In the MMP family, some members are soluble enzymes secreted into tissue cavities, but others are anchored to the plasma membrane by having either a transmembrane domain or a signal for glycosylphosphatidylinositol (GPI) anchoring at their C-terminus.(8) To date, six MMP members are known as membrane-type MMPs (MT-MMPs).(2–7) Most of the soluble MMPs are secreted as a latent form (proMMPs) and activated through proteolytic processing by serine proteinases including trypsin, plasmin, plasma kallikrein, and neutrophil elastase.(9) However, proMMP-2 (pro-gelatinase A), which has been implicated in the through invasion of the basement

y (EIA) system
Type 1-matrix
ished by using
mbinant MT1-
acted with solid-
roxidase-labeled
detected by the
:tween 1.25 and
MT1-MMP and
ıl other MMP's
nto the medium
by this system.
om normal and
nit. Membrane-
as also detected
extraction buffer
MMP in clinical
MT1-MMP were
mpared with the
-MMP in tumors
: regional lymph
system is the first
, thus suggesting
n of malignancy.

c-dependent endopepti-
and contribute to both
ıodeling.(1) In the MMP
l into tissue cavities, but
ving either a transmem-
nositol (GPI) anchoring
ers are known as mem-
the soluble MMPs are
ted through proteolytic
plasmin, plasma kallik-
MP-2 (pro-gelatinase A),
asion of the basement

membrane by malignant tumors, cannot be activated by these serine proteinases, but is activated by the MT1-MMP that is frequently expressed in cancer cells.(9–11) It is known that expression levels of MT1-MMP correlate with the activation of proMMP-2 in cancer tissue.(12) In addition, since MT1-MMP has the ability to digest ECM components such as collagen, fibronectin, vitronectin, and cartilage proteoglycan, it is presumed to play a key role in tumor invasion.(13–15)

MT1-MMP localizes on the surface of invasive tumor cells, especially on invadopodia as an integral membrane protein.(16) However, some fraction of MT1-MMP may be released from the cell surface, as demonstrated with a human breast carcinoma cell line, MDA-MB-231, which sheds MT1-MMP into the culture medium upon treatment with concanavalin A (Con A).(17,18) If MT1-MMP, localized on the cancer cell surface, is processed and shed into the circulation, it would be a marker for malignancy of tumors. MT1-MMP shed from tumor cells may be a target for enzyme immunoassay (EIA), like other soluble MMPs.(19–26) In addition, measurement of MT1-MMP levels in tumor tissue may also help to establish a prognosis. However, a quantitative and sensitive method to measure soluble and membrane-bound MT1-MMP has not been available.

In the present study, we developed monoclonal antibodies against MT1-MMP and used them to establish a two-step sandwich EIA system for detection of spontaneously solubilized MT1-MMP and extracted MT1-MMP from cells and tissues. The system was applied for determination of MT1-MMP in culture media, cells in culture, sera, and tumor tissue homogenates in order to evaluate the correlation between MT1-MMP production and metastatic ability of cancers.

EXPERIMENTAL

Materials

The following materials were obtained commercially: bovine serum albumin (BSA, Fraction V) from Sigma Chem. Co. (St. Louis, MO, USA); horseradish peroxidase (HRP, grade I) from Roche Diagnostics, GmbH (Mannheim, Germany); MonoAb-ID EIA kit from Zymed Lab., Inc. (San Francisco, CA, USA); PD-10, chelating Sepharose FF, CNBr-activated Sepharose 4B, and Sephacryl S-300HR from Amersham Pharmacia Biotech UK Ltd. (Buckinghamshire, UK); Ultrogel AcA 44 from LKB (Villeneuve-la-Garenne, France); protein A-Cellulofine from Seikagaku Corp. (Tokyo, Japan); UK-10 membrane filters from Advantec (Tokyo, Japan); nitrocellulose filters (Trans-Blot transfer medium, 0.45 m)

and prestained sodium dodecyl sulfate-polyacrylamide gel electrophoresis (SDS-PAGE) standards (low range) from Bio-Rad Lab. (Richmond, CA, USA); 1 × 8-wells Micro Well Module in frame from Nunc (Roskilde, Denmark); fetal bovine serum (FBS) from JRH Bioscience, (Lenexa, KS, USA); Dulbecco's modified Eagle medium (DMEM) from Nissui Pharmaceutical Co., Ltd. (Tokyo, Japan); skim milk from Difco Laboratories (Detroit, MI, USA); *N*-(6-maleimidocaproyloxy) succinimide (EMCS) and 3,3′-diaminobenzidine (DAB) from Dojindo Laboratories (Kumamoto, Japan); S-acetylmercaptosuccinic anhydride from Aldrich Chem. Co. (Milwaukee, WI, USA); 2-mercaptoethanol, SDS, and Tween 20 from Nacalai Tesque, Inc. (Kyoto, Japan); 3,3′,5,5′-tetramethylbenzidine (TMB) solution from Calbiochem (La Jolla, CA, USA); dotMatric protein assay kit from Geno Technology, Inc. (St. Louis, MO, USA); BCA protein assay kit from Pierce (Rockford, IL, USA); pTrcHis from Invitrogen (Carlsbad, CA, USA); Con A, isopropyl-D-thiogalacto-pyranoside (IPTG), and other chemicals from Wako Pure Chem. Ind., Ltd. (Osaka, Japan).

MMP-1, -2, -3, -7, -8, -9, -13, -19 and -20 were purified as described in detail elsewhere.(19–26)

The following human cell lines were also purchased: MDA-MB-231 from the American Type Culture Collection (Rockville, MD, USA) and HT1080, SCC-25, and HeLa from Dainippon Pharmaceutical Co., Ltd. (Osaka, Japan).

The expression vector pSGΔMT1-MMP for a deletion mutant of MT1-MMP(ΔMT1-MMP) lacking the transmembrane domain and cytoplasmic tail was prepared as described previously.(27)

Serum from normal subjects and cancer patients were used for the assay. All serum samples were stored at −40°C and usually assayed within 3 months.

Preparation of Recombinant MT1-MMP in *E. coli*

Expression vector for *E. coli* (pUCΔMT1-MMP) was constructed with pUC19 and ΔMT1-MMP by digestion with Sma I and Hind III of pSGΔMT1-MMP.(27) JM109 cells transformed with the plasmid were grown at 37°C to log-phase, and protein expression was induced by adding 0.5 mM IPTG. Growth of the cells was continued for 4 h, and then the cells were harvested. The pellet from a 400 mL culture was suspended in 20 mL of 50 mM *tris*-HCl buffer, pH 8.0, and incubated with 20 mg of egg-white lysozyme. After storage on ice for 20 min, the cells were disrupted by sonication; and then insoluble recombinant protein, in the form of inclusion bodies, was collected by centrifugation.

de gel electrophoresis
Lab. (Richmond, CA,
om Nunc (Roskilde,
Bioscience, (Lenexa,
DMEM) from Nissui
from Difco Labora-
) succinimide (EMCS)
oratories (Kumamoto,
Aldrich Chem. Co.
and Tween 20 from
ethylbenzidine (TMB)
latric protein assay kit
BCA protein assay kit
itrogen (Carlsbad, CA,
(IPTG), and other
, Japan).
purified as described in

hased: MDA-MB-231
ville, MD, USA) and
rmaceutical Co., Ltd.

a deletion mutant of
ane domain and cyto-
7)
ents were used for the
and usually assayed

P in *E. coli*

MMP) was constructed
Sma I and Hind III of
with the plasmid were
ssion was induced by
continued for 4 h, and
00 mL culture was sus-
.0, and incubated with
e for 20 min, the cells
recombinant protein, in
rifugation.

The pellet was washed twice with 50 mM *tris*-HCl buffer, pH 7.0, then solubilized with 2 mL of 50 mM *tris*-HCl buffer, pH 7.0, containing 8 M urea, 1% SDS, and 1% 2-mercaptoethanol, and thereafter incubated for 30 min at room temperature. The solubilized inclusion bodies were subjected to SDS-PAGE. The gels were sliced and recombinant MT1-MMP was recovered by electroelution done with a homemade apparatus. Buffer for the protein was exchanged for 50 mM sodium phosphate buffer, pH 7.0, containing 0.1 M NaCl and 10 mM ethylenediaminetetraacetic acid (EDTA) by using a PD-10 column; and the recombinant protein was used for immunization or as the EIA standard protein. The protein concentration of the recombinant MT1-MMP in the SDS buffer was determined by means of the dotMetric protein assay kit used according to the instructions of Geno Technology, Inc.

Inclusion bodies expressed in *E. coli* bearing pTrcHisMT1-MMP were dissolved in 50 mM phosphate buffer, pH 7.0, containing 8 M urea, 0.5 M NaCl, and 10 mM imidazole (binding buffer) and applied to a nickel-chelating Sepharose FF gel column. The recombinant protein (HisMT1-MMP) was eluted with the binding buffer containing 0.5 M imidazole. Refolding of the recombinant protein was done in 50 mM *tris*-HCl buffer, pH 8.6, containing 0.15 M NaCl. Soluble fraction was concentrated by UK-10, and applied to a Sephacryl S-300HR gel column, which was equilibrated with 50 mM *tris*-HCl buffer, pH 7.0, containing 0.15 M NaCl. Refolded HisMT1-MMP was digested with 0.1 μg/mL trypsin for 1 h at 37°C and then used for epitope mapping.

Preparation of Monoclonal Antibodies Against MT1-MMP

Two 6-week-old female BALB/c mice were immunized intraperitoneally with 58 μg of purified recombinant MT1-MMP emulsified with an equal volume of Freund's complete adjuvant. Subsequent booster injections of 66 μg of immunogen in saline were administered intraperitoneally after 20 and 35 days and then intravenously after 70 days. Three days after the intravenous injection, the spleens were removed, and the splenocytes were isolated for fusion with mouse myeloma cells (SP-2/0-Ag14). The hybridization, as well as subsequent culturing and cloning of the hybrids, was carried out as described by Oi and Herzenberg.(28) Antibodies (IgG1) were purified from ascitic fluids by 40% saturated ammonium sulfate fractionation, followed by protein A-Cellulofine column chromatography. Clones 222-1D8 and 222-2D12 obtained were of the IgG1/κ family, and used in this study.

Preparation of Fab'-HRP Conjugate

$F(ab')_2$ was prepared from the purified monoclonal antibody (clone 222-1D8) by digestion with pepsin. The $F(ab')_2$ obtained was then reduced with 2-aminoethanethiol, and the resulting Fab' was conjugated with HRP by using EMCS.(29)

Two-Step Sandwich EIA System for MT1-MMP

Twenty-five microliters of specimen containing MT1-MMP was diluted with 100 μL of 30 mM sodium phosphate buffer, pH 7.0, containing 1% BSA, 3% horse serum, 0.1 M NaCl, 10 mM EDTA, 0.42% SDS, and 0.4% 2-mercaptoethanol (dilution buffer). Aliquots of the diluted samples (100 μL) were transferred to microplate wells previously coated with anti-MT1-MMP IgG, clone 222-2D12, and the plate was then incubated overnight at 4°C without shaking. The plate was next washed three times with 10 mM sodium phosphate buffer, pH 7.0, containing 0.1 M NaCl and 0.1% (w/v) Tween 20 (washing buffer). One hundred microliters of 0.2 μg/mL anti-MT1-MMP Fab' (clone 222-1D8)-HRP conjugate in 30 mM sodium phosphate buffer, pH 7.0, containing 1% BSA, 0.1 M NaCl and 10 mM EDTA was added to each well. The plate was then incubated for 1 h at room temperature and thereafter washed three times with the washing buffer. TMB solution (100 μL) was dispensed into each well, and incubation continued for 20 min at room temperature. The reaction was stopped by adding 100 μL of 1 M sulfuric acid, and the absorbance at 450 nm was measured with a microplate reader (Tosoh model MPR-A4, Tokyo).

Preparation of Samples Containing MT1-MMP from Culture Media and Cell Extracts

HT1080, MDA-MB-231, SCC-25, and HeLa cells were cultured in 7 mL of DMEM, supplemented with 10% FBS in an atmosphere of humidified 5% CO_2 in air at 37°C in 10 cm tissue culture dishes (2×10^6 cells/dish). The confluent cells were rinsed twice with 5 mL of phosphate-buffered saline (PBS) and then cultured with 7 mL of serum-free medium containing 200 μg/mL of Con A. The conditioned media were harvested 3 days later and used for the EIA. The cells were scraped off into 1 mL of PBS containing 10 mM EDTA and washed in the same buffer. After centrifugation, the cells were resuspended in 0.4 mL of 50 mM *tris*-HCl buffer, pH 7.0, containing 0.15 M NaCl, 10 mM $CaCl_2$, and 0.05% Brij35

ugate

ıoclonal antibody (clone
ɔtained was then reduced
'as conjugated with HRP

MT1-MMP

ıg MT1-MMP was diluted
, pH 7.0, containing 1%
A, 0.42% SDS, and 0.4%
ıe diluted samples (100 μL)
ated with anti-MT1-MMP
cubated overnight at 4°C
three times with 10 mM
M NaCl and 0.1% (w/v)
:rs of 0.2 μg/mL anti-MT1-
30 mM sodium phosphate
:l and 10 mM EDTA was
'or 1 h at room temperature
hing buffer. TMB solution
lion continued for 20 min at
ıdding 100 μL of 1 M sulfu-
:ed with a microplate reader

ſT1-MMP from
ctracts

HeLa cells were cultured
FBS in an atmosphere of
)cm tissue culture dishes
ed twice with 5 mL of phos-
ł with 7 mL of serum-free
:onditioned media were har-
: cells were scraped off into
hed in the same buffer. After
0.4 mL of 50 mM *tris*-HCl
M $CaCl_2$, and 0.05% Brij35

(TNCB), and homogenized with a homogenizer or weakly sonicated. The homogenates/sonicates were clarified by centrifugation, and the supernatants were recovered as cell extracts.

Electrophoresis and Immunoblotting

Samples were subjected to SDS-PAGE (12% total acrylamide) and transferred onto nitrocellulose membranes. Monoclonal antibodies of clones 222-1D8, 222-2D12, 113-15E7, and 114-1F2 were conjugated with HRP by using *S*-acetylmercaptosuccinic anhydride.(29) The membranes reacted with 1 μg/mL of each IgG-HRP overnight at room temperature in 30 mM sodium phosphate buffer, pH 7.0, containing 0.1 M NaCl and 3% skim milk. After having been washed with 30 mM sodium phosphate buffer, pH 7.0, containing 0.1 M NaCl, the membranes were stained by the hydrogen peroxide system with 0.5 mg/mL DAB. Anti-MT1-MMP monoclonal antibodies, clones 113-15E7 and 114-1F2, were used for detection of the hemopexin-like domain and catalytic domain of MT1-MMP, respectively.(2)

Affinity Concentration of MT1-MMP from Human Serum

Monoclonal antibody against MT1-MMP (clone 222-2D12, 5 mg) in sodium borate buffer, pH 8.0, containing 0.5 M NaCl was reacted with 0.5 g CNBr-activated Sepharose 4B and gently shaken for 2 h at room temperature and then overnight at 4°C. The unreacted sites were blocked with 0.2 M glycine-NaOH buffer, pH 8.0.

5 mL of the serum from a patient with metastatic carcinoma was diluted with 20 mL of the dilution buffer. This sample was applied to a column of IgG (clone 222-2D12) coupled to 1 mL Sepharose 4B gel. The column was washed with PBS, and then the protein was eluted with 0.1 M glycine-HCl buffer, pH 2.0. The eluate was neutralized and concentrated to 100 μL. An aliquot of the concentrated sample was subjected to the EIA system.

Preparation of Tissue Homogenates for the EIA System

Frozen tissues of head and neck, and lung cancers stored at −40°C were minced and homogenized in 0.4 mL of TNCB with a spindle-type homogenizer. The homogenates were clarified by centrifugation, and the

supernatants were recovered as tissue extracts and subjected to the EIA. Protein concentrations of the tissue and cell extracts were determined with the Micro BCA protein assay kit, according to the instructions of Pierce. MT1-MMP levels in the samples were calculated and reported as ng/mg protein.

RESULTS

Purification of Recombinant MT1-MMP for Use as Immunogen and EIA Standard Protein

A recombinant soluble MT1-MMP (△MT1-MMP) lacking its transmembrane domain and cytoplasmic tail was expressed in *E. coli* by using a bacterial expression plasmid (pUC△MT1-MMP). The recombinant protein was expressed as insoluble inclusion bodies, which were solubilized with 62.5 mM *tris*-HCl buffer, pH 6.8, containing 8 M urea, 1% SDS and 1% 2-mercaptoethanol. Then, △MT1-MMP was purified by preparative SDS-PAGE to a grade showing a single band on SDS-PAGE at the position of about 60 kDa, as shown in Figure 1A. The yield of △MT1-MMP was 2.6 mg from 400 mL of culture medium.

Specificity of the Monoclonal Antibodies

Using the purified protein as an antigen, we prepared hybridoma cell lines. The cell lines were selected by the ELISA method and immunoblotting using the recombinant protein. Five clones (222-1D8, 222-2D12, 222-3E12, 222-4G5, and 222-9A3) secreting monoclonal antibodies against MT1-MMP were obtained. According to the results of isotype assay for each monoclonal antibody conducted with the MonoAb-ID kit, all of the light chains were the κ type, but the heavy chains were $\gamma 1$ for four clones and $\gamma 3$ for one. Various combinations of two monoclonal antibodies were examined to develop sandwich EIA for MT1-MMP, and we chose the combination of clone 222-2D12 for the solid phase and 222-1D8 for the conjugate coupled with HRP.

Immunoblot analysis was performed to confirm the specificity of the monoclonal antibodies. △MT1-MMP (0.8 μg) was subjected to SDS-PAGE and transferred onto a nitrocellulose membrane. The membrane was reacted with 1 μg/mL IgG-HRP (clones 222-1D8 and 222-12D2) overnight at room temperature and was then stained by the hydrogen peroxide system with

d subjected to the EIA.
:ts were determined with
ıe instructions of Pierce.
and reported as ng/mg

IP for Use as
Protein

MT1-MMP) lacking its
; expressed in *E. coli* by
MMP). The recombinant
n bodies, which were
.8, containing 8 M urea,
MT1-MMP was purified
a single band on SDS-
ı in Figure 1A. The yield
ure medium.

ıtibodies

prepared hybridoma cell
thod and immunoblotting
D8, 222-2D12, 222-3E12,
ıntibodies against MT1-
)f isotype assay for each
\b-1D kit, all of the light
γ1 for four clones and γ3
antibodies were examined
chose the combination of
for the conjugate coupled

firm the specificity of the
s subjected to SDS-PAGE
he membrane was reacted
-12D2) overnight at room
gen peroxide system with

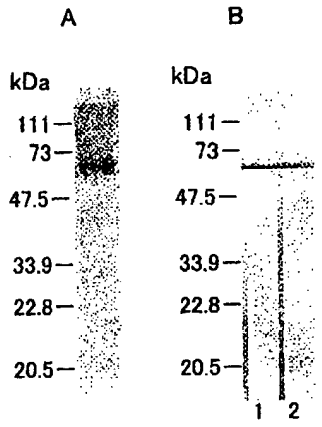

Figure 1. SDS-PAGE and immunoblotting of ΔMT1-MMP. A, Purified MT1-MMP (8 μg) was subjected to SDS-PAGE (12% total acrylamide) under reducing conditions. The gel was stained with CBB. B, Purified ΔMT1-MMP (0.8 μg) was subjected to SDS-PAGE (12% total acrylamide) under reducing conditions and then transferred onto a nitrocellulose membrane. The membrane was reacted with 1 μg/mL IgG-HRP (lane 1, clone 222-1D8; and lane 2, 222-12D2) overnight at room temperature in 30 mM sodium phosphate buffer, pH 7.0, containing 0.1 M NaCl, and 3% skim milk and was stained by the hydrogen peroxide system with 0.5 mg/mL DAB.

DAB. As shown in Figure 1B, both clones 222-1D8 and 222-12D2 reacted with ΔMT1-MMP 57 kDa.

In order to determine the epitope for these monoclonal antibodies, epitope mapping was performed by immunoblot analysis using trypsin-treated ΔMT1-MMP fragments tagged with His 6. The blotted membrane was reacted with the antibodies prepared in the present study (clones 222-1D8 and 222-12D2), anti-hemopexin-like domain (clone 113-15E7), and anti-catalytic domain (clone 114-1F2) of MT1-MMP, and the antibodies were visualized as stated in Experimental. As shown in Figure 2, both clones 222-1D8 and 222-12D2 reacted strongly with the hemopexin-like domain of MT1-MMP (31 and 33 kDa-bands), similarly as clone 113-15E7.(2)

Cross-reactivity of these antibodies with MT2-, MT3-, MT4-, and MT5-MMPs was also tested. Clone 222-1D8 slightly reacted with MT5-MMP, but not with MT2-, MT3-, or MT4-MMP. On the other hand, clone 222-2D12 did not react with any of the MT-MMPs examined by immunoblotting (data not shown).

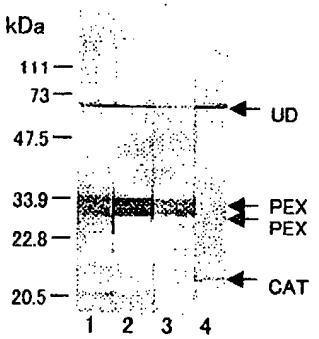

Figure 2. Epitope mapping of the anti-ΔMT1-MMP monoclonal antibodies. Refolded ΔMT1-MMP was digested with trypsin (1 μg/lane) for 1 h at 37°C and subjected to SDS-PAGE (12% total acrylamide) under reducing conditions and reacted with anti-MT1-MMP antibodies. The membrane was then stained with 1 μg/mL IgG-HRP (lane 1, clone 222-1D8; lane 2, 222-12D2; lane 3, 113-15E7; lane 4, 114-1F2). The arrows in the figure indicate undigested HisΔMT1-MMP (UD), hemopexin-like domain (PEX) and catalytic domain (CAT) of MT1-MMP, respectively.

Standard Assay Curve for MT1-MMP by Sandwich EIA System

Figure 3 shows standard curve obtained with the sandwich EIA for MT1-MMP using the combination of clone 222-2D12 for the solid phase and 222-1D8 for the conjugate coupled with HRP. The sensitivity was 1.25 ng/mL (0.025 ng/well, two SDs above the zero point), and linearity was obtained between 1.25 and 160 ng/mL (0.025–3.2 ng/well). The intra-assay CVs ($n=8$) at 8 different concentrations of MT1-MMP was 3.9–9.3%.

Precision and Accuracy

The intra- and inter-assay reproducibility and recoveries of MT1-MMP were examined in serum. When different amounts of MT1-MMP (71.2, 35.6, and 17.8 ng/mL) were added to serum as a standard, recoveries of 89.0–102.5% were obtained. The intra-assay CVs and inter-assay CVs were 2.5–3.4% ($n=8$) and 3.1–5.0 % ($n=8$), respectively.

Recovery of MT1-MMP from culture medium or extracts of MDA-MB-231 cells was also examined. Recovery rates of ΔMT1-MMP (40, 20, and 10 ng/mL) added to the culture medium or cell extract as a standard

UD

PEX
PEX

CAT

-MMP monoclonal antibodies.
(1 μg/lane) for 1 h at 37°C and
under reducing conditions and
mbrane was then stained with
2, 222-12D2; lane 3, 113-15E7;
te undigested His△MT1-MMP
domain (CAT) of MT1-MMP,

y Sandwich EIA System

ied with the sandwich EIA
one 222-2D12 for the solid
bled with HRP. The sensi-
s above the zero point), and
g/mL (0.025–3.2 ng/well). The
trations of MT1-MMP was

acy

ity and recoveries of MT1-
ent amounts of MT1-MMP
um as a standard, recoveries
ay CVs and inter-assay CVs
respectively.
iedium or extracts of MDA-
tes of △MT1-MMP (40, 20,
or cell extract as a standard

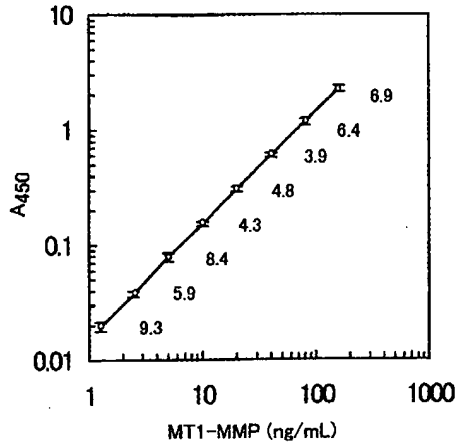

Figure 3. Standard curve determined for MT1-MMP by the sandwich EIA system. Purified △MT1-MMP was analyzed by the sandwich EIA as described in Experimental. Vertical bars show mean value ± SD of 8 independent measurements ($n = 8$) at different concentrations. Numbers in the figure indicate the intra-assay CVs (%).

Table 1. Precision and Accuracy of the EIA System for MT1-MMP

Specimen	Recovery (%)	Intra-Assay CV (%)	Inter-Assay CV (%)
Normal serum	89.0–102.5	2.5 ($n=8$)	3.1 ($n=8$)
Cultured medium*	92.8–105.8	6.9 ($n=6$)	7.1 ($n=6$)
Cell homogenate*	90.0–101.7	9.5 ($n=6$)	10.2 ($n=6$)

*Prepared from Con A-stimulated MDA-MB-231 cells as described in Experimental Section.

were 92.8–105.8 or 90.0–101.7%, respectively. Results of intra- and inter-assay in culture medium and cell extract are shown in Table 1.

Characterization of the EIA System for MT1-MMP

The cross-reactivity of the EIA for MT1-MMP toward various MMPs was examined by using MMP-1, 2, 3, 7, 8, 9, 13, 19, and 20; but no signal was obtained from these MMPs, as documented in Table 2.

Table 2. Cross-Reactivity of the EIA System for MT1-MMP toward Other MMP's

MMPs	Concentration (μg/mL)	A_{450}
MMP-1	1	0.025
MMP-2	1	0.024
MMP-3	1	0.027
MMP-7	1	0.026
MMP-8	1	0.028
MMP-9	1	0.039
MMP-13	1	0.026
MMP-19	1	0.027
MMP-20	1	0.071
MT1-MMP	0.16	2.206
Blank	–	0.027

Determination of MT1-MMP in Human Cell Lines by the EIA

To measure MT1-MMP expression levels in human cancer cell lines, we lysed HT1080, MDA-MB-231, SCC-25, and HeLa cells and subjected the lysates to the EIA. MT1-MMP was detected in HT1080, MDA-MB-231, and SCC-25 cells, but not in HeLa cells (Table 3). At the same time, MT1-MMP released from the cells was measured. A substantial amount of MT1-MMP was detected in the medium conditioned by HT1080, MDA-MB-231, and SCC-25 cells, and it increased following Con A treatment of the cells (Table 4). As expected, MT1-MMP was not detected in the cell extract of HeLa cells. In a comparison of Tables 3 and 4, the production levels (ng/mg) by these cell lines corresponded well to the levels of MT1-MMP secreted into the medium (ng/mL) by each cell line.

MT1-MMP in Human Serum

The EIA system was applied to serum samples from 2 normal and 121 various cancer patients, including those having metastasis (Table 5). However, MT1-MMP levels in all the serum samples were under the lower detection limit (1.25 ng/mL) of the assay system. The serum from a patient with metastatic carcinoma was concentrated 50-fold by using anti-MT1-MMP monoclonal antibody (clone 222-2D12) coupled with

: EIA
Other

A_{450}
0.025
0.024
0.027
0.026
0.028
0.039
0.026
0.027
0.071
2.206
0.027

l Lines by the EIA

uman cancer cell lines, we
a cells and subjected the
HT1080, MDA-MB-231,
: 3). At the same time,
A substantial amount of
l by HT1080, MDA-MB-
ın A treatment of the cells
:ted in the cell extract of
)roduction levels (ng/mg)
MT1-MMP secreted into

ım

:s from 2 normal and 121
g metastasis (Table 5).
)les were under the lower
stem. The serum from
ıtrated 50-fold by using
!22-2D12) coupled with

Table 3. Measurement by the EIA of MT1-MMP Extracted from Human Cell Lysates

Cell Line	MT-MMP* (ng/mg)
HT1080	36.1
MDA-MB-231	26.7
SCC-25	14.7
HeLa	UD

*Detected as MT1-MMP (ng) per protein (mg) in each cell homogenate.

Table 4. Measurement by the EIA of MT1-MMP in Culture Media of Human Cell Lines

	Concentration of MT1-MMP (ng/mL)	
Cell Line	Without Con A	With Con A
HT1080	10.1	80.3
MDA-MB-231	7.6	48.8
SCC-25	2.8	43.1
HeLa	UD	UD

UD: under the lower detection limit (< 1.25 ng/mL).

Table 5. List of Human Serum Samples Examined by the EIA

Serum	*n*
Cancer patient	
Colon	31
Breast	26
Stomach	25
Prostate (bone metastasis)	17
Liver (metastasis)	4
Others	18
Normal	2
Total	123

Sepharose 4B gel, and MT1-MMP in the eluate was determined by the EIA. MT1-MMP level in the serum sample was estimated to be less than 25 pg/mL, because it was undetectable even in the 50-fold concentrated eluate.

Determination of MT1-MMP in Human Carcinoma Tissue Samples

Tissue homogenates of cancer patients were then examined by using the EIA system. Head and neck cancers (laryngeal, pharyngeal, oral, and salivary gland) and normal tissues adjacent to the cancers were isolated and subjected to the EIA after lysis. The MT1-MMP levels in normal ($n = 26$) and tumor tissues ($n = 80$) were 0.8 ± 1.1 and 5.0 ± 4.3 ng/mg (mean $\pm$ SD), respectively (Figure 4). The MT1-MMP levels were significantly 6.3-fold higher in tumors than in normal tissues ($P < 0.001$ by Student's t test).

Specimens were also isolated from lung cancer patients ($n = 51$) at different stages (TNM classification) and analyzed similarly.(35) Again, MT1-MMP levels were higher in tumors than in normal tissues (Figure 5A). Furthermore, tumor specimens with regional lymph node metastasis (N1–N3) showed higher levels of MT1-MMP than those designated N0 ($P < 0.05$ by Student's t test), as shown in Figure 5B.

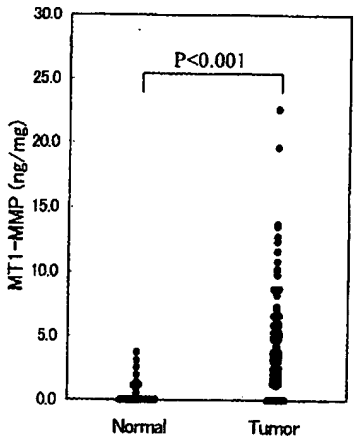

Figure 4. MT1-MMP levels in head and neck cancer tissue homogenates. MT1-MMP levels in homogenates from head and neck cancers ($n = 80$) and from normal tissue adjacent to such cancers ($n = 26$) were determined by the sandwich EIA as described in Experimental. $p < 0.001$ by Student's t test.

s determined by the EIA.
l to be less than 25 pg/mL,
ıcentrated eluate.

P in
mples

: then examined by using
:al, pharyngeal, oral, and
cancers were isolated and
' levels in normal ($n = 26$)
$\pm$ 4.3 ng/mg (mean $\pm$ SD),
were significantly 6.3-fold
)1 by Student's t test).
cancer patients ($n = 51$)
yzed similarly.(35) Again,
ıormal tissues (Figure 5A).
ıph node metastasis (N1–
ie designated N0 ($P < 0.05$

er tissue homogenates. MT1-
ıcers ($n = 80$) and from normal
ıined by the sandwich EIA as
est.

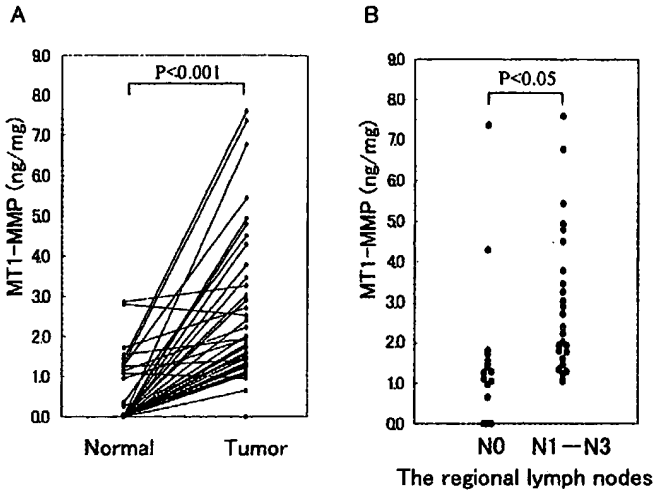

Figure 5. MT1-MMP levels in lung cancer tissue homogenates. MT1-MMP levels in homogenates from lung tissue were determined by the sandwich EIA as described in Experimental. Significance of the difference was evaluated by Student's t test ($p < 0.05$). A: MT1-MMP levels in homogenates from cancer and adjacent normal tissues are shown. B: MT1-MMP levels in the tissue homogenates are separately indicated according to the degree of regional lymph node metastasis.

DISCUSSION

We established a two-step sandwich EIA system to measure both soluble and membrane-associated MT1-MMP. Monoclonal antibodies used for the EIA were generated against recombinant MT1-MMP that was lacking its transmembrane domain and cytoplasmic tail. The recombinant MT1-MMP expressed in *E. coli* as inclusion bodies was solubilized with *tris*-HCl buffer, pH 7.0, containing urea, SDS and 2-mercaptoethanol, and then purified by preparative SDS-PAGE. The purified MT1-MMP did not show any enzymatic activities, and it was stable after 24 h incubation at 37°C without the presence of EDTA or phenylmethylsulfonyl fluoride. The stable recombinant protein was suitable for use as the standard protein for the EIA.

Five monoclonal antibodies were obtained, and we chose a particular combination of two of them for the two-step sandwich EIA system. The established EIA system was quantitative and specific for MT1-MMP, showing no cross-reactivity against the other MMP's examined. By epitope analysis, we proved that these two antibodies recognized the hemopexin-like domain of MT1-MMP. Therefore, these antibodies cannot distinguish

between pro form and active form of MT1-MMP. Theoretically, this EIA system, using this pair of antibodies against the hemopexin-like domain, could detect all three types of MT1-MMP molecules, i.e., membrane-associated form, shed form, and the 43 kDa form described previously.(2,17,30) This EIA system likely reflects the expression levels of MT1-MMP.

This system was applied to detect MT1-MMP in human cancer cell lines and in clinical samples. A human breast carcinoma cell line MDA-MB-231 is reported to express MT1-MMP and to shed it into culture medium upon treatment with ConA.(17,18) Consistent with these previous reports, shed MT1-MMP was detected in the culture medium by this EIA method. Shed MT1-MMP was also detected in the conditioned medium of HT1080 and SCC-25 cells after ConA treatment (Table 3). Other cancer cell lines (SW837, MG-63, and CaSki) also produced shed MT1-MMP, but it was not detectable in the culture medium of HeLa, MCF7, Burkitt's lymphoma (Raji, Daudi), and leukaemia (K-562, HL-60) cell lines (data not shown). These results agree with the expression of MT1-MMP assessed by Northern blot analysis of the cell lines.(31) MT1-MMP detected in conditioned medium paralleled expression levels of MT1-MMP in the cells and may reflect metastatic ability of the cells.

On the other hand, MT1-MMP levels in sera from two normal adults and from 121 patients with cancer including 21 with metastasis, were below the lower detection limit of this assay system (1.25 ng/mL). It seems that the EIA cannot detect MT1-MMP from serum specimens, because the amount of shed MT1-MMP is very limited. MT1-MMP level in the serum was estimated to be less than 25 pg/mL.

MT1-MMP is usually anchored to the cell surface through its hydrophobic transmembrane domain at the C-terminus and contributes to activation of proMMP-2 and degradation of ECM under physiological or pathological conditions. Thus, it is also important to determine quantity of MT1-MMP in tumors. In order to extract MT1-MMP from the cell surface, we disrupted the cells with a lysis buffer containing SDS and 2-mercaptoethanol, and then subjected the lysates to the EIA. The EIA system effectively detected solubilized MT1-MMP from cancer cell lines as well as the shed MT1-MMP (Tables 3 and 4). These results suggested that the EIA could detect membrane-bound MT1-MMP from tumor tissue after the solubilization step using denaturants.

Then, we applied the method to detect MT1-MMP in clinical specimens. Head and neck cancer tissue and adjacent normal tissue were surgically dissected and subjected to the analysis. MT1-MMP was detected in both normal and cancer tissues, but the levels in tumors (5.0 ng/mL, $n = 80$) were significantly higher than those in the normal tissues (0.8 ng/mL, $n = 26$;

MP. Theoretically, this EIA
he hemopexin-like domain,
molecules, i.e., membrane-
43 kDa form described
ects the expression levels of

MMP in human cancer cell
rcinoma cell line MDA-MB-
shed it into culture medium
with these previous reports,
ıedium by this EIA method.
ditioned medium of HT1080
le 3). Other cancer cell lines
d MT1-MMP, but it was not
MCF7, Burkitt's lymphoma
cell lines (data not shown).
-MMP assessed by Northern
MP detected in conditioned
-MMP in the cells and may

sera from two normal adults
l with metastasis, were below
1.25 ng/mL). It seems that the
ecimens, because the amount
MMP level in the serum was

cell surface through its hydro-
ninus and contributes to acti-
ECM under physiological or
portant to determine quantity
act MT1-MMP from the cell
s buffer containing SDS and
lysates to the EIA. The EIA
MMP from cancer cell lines as
). These results suggested that
-MMP from tumor tissue after

t MT1-MMP in clinical speci-
ıcent normal tissue were surgi-
s. MT1-MMP was detected in
ls in tumors (5.0 ng/mL, $n = 80$)
rmal tissues (0.8 ng/mL, $n = 26$;

Figure 4). The same tendency was observed with lung cancer (Figure 5A). Lung tumor specimens with regional lymph node metastasis (N1–N3) showed higher levels of MT1-MMP than those with no metastasis (N0; Figure 5B). As this EIA system requires denaturation of specimens, it could not distinguish MT1-MMP/TIMP complexes from free MT1-MMP. Consequently, this EIA could not demonstrate the biological behavior of MT1-MMP/TIMP complexes or free MT1-MMP in metastasis. This may be reason why there was no clear correlation between the MT1-MMP level and the stage of the primary tumor (data not shown).

The expression of MT1-MMP has been detected by immunostaining or Northern blot analysis in a variety of tumor tissues, including head and neck, lung, breast, gastric, colon, and so on (2,12,31,32). Furthermore, a positive correlation between expression levels MT1-MMP and metastasis of breast carcinoma, thyroid carcinoma, and colorectal cancer have reported (12,33,34). Since MT1-MMP expressed in tumors is a marker for invasive and metastatic potential, we believe our EIA system, which reflects the expression level of MT1-MMP, is useful for the prognosis of cancer patients.

REFERENCES

1. Nagase, H.; Woessner, J.F. Matrix Metalloproteinases. J. Biol. Chem. **1999**, *274* (31), 21491–21494.
2. Sato, H.; Takino, T.; Okada, Y.; Cao, J.; Shinagawa, A.; Yamamoto, E.; Seiki, M. A Matrix Metalloproteinase Expressed on the Surface of Invasive Tumour Cells. Nature **1994**, *370* (6484), 61–65.
3. Will, H.; Hinzmann, B. cDNA Sequence and mRNA Tissue Distribution of a Novel Human Matrix Metalloproteinase With a Potential Transmembrane Segment. Eur. J. Biochem. **1995**, *231* (3), 602–608.
4. Takino, T.; Sato, H.; Shinagawa, A.; Seiki, M. Identification of the Second Membrane-Type Matrix Metalloproteinase (MT-MMP-2) Gene From a Human Placenta cDNA Library. MT-MMPs Form a Unique Membrane-Type Subclass in the MMP Family. J. Biol. Chem. **1995**, *270* (39), 23013–23020.
5. Puente, X.S.; Pendas, A.M.; Llano, E.; Velasco, G.; López-Otín, C. Molecular Cloning of a Novel Membrane-Type Matrix Metalloproteinase From a Human Breast Carcinoma. Cancer Res. **1996**, *56* (5), 944–949.
6. Llano, E.; Pendas, A.M.; Freije, J.P.; Nakano, A.; Knäuper, V.; Murphy, G.; López-Otín, C. Related Articles, Protein, Nucleotide Identification and Characterization of Human MT5-MMP, a New

27. Cao, J.; Sato, H.; Takino, T.; Seiki, M. The C-Terminal Region of Membrane Type Matrix Metalloproteinase is a Functional Transmembrane Domain Required for Pro-Gelatinase A Activation. J. Biol. Chem. **1995**, *270* (2), 801–805.
28. Oi, V.T.; Herzenberg, L.A. Immunoglobulin-Producing Hybrid Cell Lines. In *Selected Methods in Cellular Immunology;* Mishell, B.B., Shiigi, S.M., Eds.; W. H. Freeman and Company: San Francisco, 1980; 351–372.
29. Ishikawa, E.; Imagawa, M.; Hashida, S.; Yoshitake, S.; Hamaguchi, Y.; Ueno, T. Enzyme-Labeling of Antibodies and Their Fragments for Enzyme Immunoassay and Immunohistochemical Staining. J. Immunoassay **1983**, *4* (3), 209–327.
30. Lehti, K.; Lohi, J.; Valtanen, H.; Keski-Oja, J. Proteolytic Processing of Membrane-Type-1 Matrix Metalloproteinase is Associated With Gelatinase A Activation at the Cell Surface. Biochem. J. **1998**, *334* (pt 2), 345–353.
31. Okada, A.; Bellocq, J.P.; Rouyer, N.; Chenard, M.P.; Rio, M.C.; Chambon, P.; Basset, P. Membrane-Type Matrix Metalloproteinase (MT-MMP) Gene is Expressed in Stromal Cells of Human Colon, Breast, and Head and Neck Carcinomas. Proc. Natl. Acad. Sci. USA **1995**, *92* (7), 2730–2734.
32. Polette, M.; Nawrocki, B.; Gilles, C.; Sato, H.; Seiki, M.; Tournier, J.M.; Birembaut, P. MT-MMP Expression and Localisation in Human Lung and Breast Cancers. Virchows Arch. **1996**, *428* (1), 29–35.
33. Nakamura, H.; Ueno, H.; Yamashita, K.; Shimada, T.; Yamamoto, E.; Noguchi, M.; Fujimoto, N.; Sato, H.; Seiki, M.; Okada, Y. Enhanced Production and Activation of Progelatinase A Mediated by Membrane-Type 1 Matrix Metalloproteinase in Human Papillary Thyroid Carcinomas. Cancer Res. **1999**, *59* (2), 467–473.
34. Sardinha, T.C.; Nogueras, J.J.; Xiong, H.; Weiss, E.G.; Wexner, S.D.; Abramson, S. Membrane-Type 1 Matrix Metalloproteinase mRNA Expression in Colorectal Cancer. Dis. Colon. Rectum. **2000**, *43* (3), 389–395.
35. Sobin, L.H.; Wittekind, C. *TNM Classification of Malignant Tumours*; 5th Ed.; John Wiley & Sons, Inc.: New York, 1997.

Received June 22, 2001
Accepted July 9, 2001
Manuscript 3045

Membrane-Bound Activator of Progelatinase A Overexpressed in Brain Tumors. Cancer Res. **1999**, *59* (11), 2570–2576.

7. Pei, D. Leukolysin/MMP25/MT6-MMP: A Novel Matrix Metalloproteinase Specifically Expressed in the Leukocyte Lineage. Cell Res. **1999**, *9* (4), 291–303.
8. Itoh, Y.; Kajita, M.; Kinoh, H.; Mori, H.; Okada, A.; Seiki, M. Membrane Type 4 Matrix Metalloproteinase (MT4-MMP, MMP-17) is a Glycosyl-Phosphatidylinositol-Anchored Proteinase. J. Biol. Chem. **1999**, *274* (48), 34260–34266.
9. Stetler-Stevenson, W.G.; Aznavoorian, S.; Liotta, L.A. Tumor Cell Interactions With the Extracellular Matrix During Invasion and Metastasis. Ann. Rev. Cell Biol. **1993**, *9*, 541–573.
10. Nomura, H.; Sato, H.; Seiki, M.; Mai, M.; Okada, Y. Expression of Membrane-Type Matrix Metalloproteinase in Human Gastric Carcinomas. Cancer Res. **1995**, *55* (15), 3263–3266.
11. Okada, Y.; Morodomi, T.; Enghild, J.J.; Suzuki, K.; Yasui, A.; Nakanishi, I.; Salvesen, G.; Nagase, H. Matrix Metalloproteinase 2 From Human Rheumatoid Synovial Fibroblasts. Purification and Activation of the Precursor and Enzymic Properties. Eur. J. Biochem. **1990**, *194* (3), 721–730.
12. Ueno, H.; Nakamura, H.; Inoue, M.; Imai, K.; Noguchi, M.; Sato, H.; Seiki, M.; Okada, Y. Expression and Tissue Localization of Membrane-Types 1, 2, and 3 Matrix Metalloproteinases in Human Invasive Breast Carcinomas. Cancer Res. **1997**, *57* (10), 2055–2060.
13. Ohuchi, E.; Imai, K.; Fujii, Y.; Sato, H.; Seiki, M.; Okada, Y. Membrane Type 1 Matrix Metalloproteinase Digests Interstitial Collagens and Other Extracellular Matrix Macromolecules. J. Biol. Chem. **1997**, *272* (4), 2446–2451.
14. d'Ortho, M.P.; Will, H.; Atkinson, S.; Butler, G.; Messent, A.; Gavrilovic, J.; Smith, B.; Timpl, R.; Zardi, L.; Murphy, G. Membrane-Type Matrix Metalloproteinases 1 and 2 Exhibit Broad-Spectrum Proteolytic Capacities Comparable to Many Matrix Metalloproteinases. Eur. J. Biochem. **1997**, *250* (3), 751–757.
15. Pei, D.; Weiss, S.J. Transmembrane-Deletion Mutants of the Membrane-Type Matrix Metalloproteinase-1 Process Progelatinase A and Express Intrinsic Matrix-Degrading Activity. J. Biol. Chem. **1996**, *271* (15), 9135–9140.
16. Nakahara, H.; Howard, L.; Thompson, E.W.; Sato, H.; Seiki, M.; Yeh, Y.; Chen, W.T. Transmembrane/Cytoplasmic Domain-Mediated Membrane Type 1-Matrix Metalloprotease Docking to Invadopodia is Required for Cell Invasion. Proc. Natl. Acad. Sci. USA **1997**, *94* (15), 7959–7964.

atinase A Overexpressed in
), 2570–2576.
': A Novel Matrix Metallo-
Leukocyte Lineage. Cell Res.

i, H.; Okada, A.; Seiki, M.
nase (MT4-MMP, MMP-17)
red Proteinase. J. Biol. Chem.

S.; Liotta, L.A. Tumor Cell
latrix During Invasion and
541–573.
, M.; Okada, Y. Expression
oteinase in Human Gastric
3263–3266.
J.; Suzuki, K.; Yasui, A.;
Matrix Metalloproteinase 2
ibroblasts. Purification and
Properties. Eur. J. Biochem.

mai, K.; Noguchi, M.; Sato,
and Tissue Localization of
letalloproteinases in Human
. **1997**, *57* (10), 2055–2060.
H.; Seiki, M.; Okada, Y.
oteinase Digests Interstitial
ix Macromolecules. J. Biol.

.; Butler, G.; Messent, A.;
; Zardi, L.; Murphy, G.
ises 1 and 2 Exhibit Broad-
parable to Many Matrix
7, *250* (3), 751–757.
-Deletion Mutants of the
se-1 Process Progelatinase A
Activity. J. Biol. Chem. **1996**,

E.W.; Sato, H.; Seiki, M.;
toplasmic Domain-Mediated
e Docking to Invadopodia is
cad. Sci. USA **1997**, *94* (15),

17. Imai, K.; Ohuchi, E.; Aoki, T.; Nomura, H.; Fujii, Y.; Sato, H.; Seiki, M.; Okada, Y. Membrane-Type Matrix Metalloproteinase 1 is a Gelatinolytic Enzyme and is Secreted in a Complex With Tissue Inhibitor of Metalloproteinases 2. Cancer Res. **1996**, *56* (12), 2707–2710.
18. Harayama, T.; Ohuchi, E.; Aoki, T.; Sato, H.; Seiki, M.; Okada, Y. Shedding of Membrane Type 1 Matrix Metalloproteinase in a Human Breast Carcinoma Cell Line. Jpn. J. Cancer Res. **1999**, *90* (9), 942–950.
19. Zhang, J.; Fujimoto, N.; Iwata, K.; Sakai, T.; Okada, Y.; Hayakawa, T. A One-Step Sandwich Enzyme Immunoassay for Human Matrix Metalloproteinase-1 (Interstitial Collagenase) Using Monoclonal Antibodies. Clin. Chim. Acta **1993**, *219* (1–2), 1–14.
20. Fujimoto, N.; Mouri, N.; Iwata, K.; Ohuchi, E.; Okada, Y.; Hayakawa, T. A One-Step Sandwich Enzyme Immunoassay for Human Matrix Metalloproteinase 2 (72-kDa Gelatinase Type IV Collagenase) Using Monoclonal Antibodies. Clin. Chim. Acta **1993**, *221* (1–2), 91–103.
21. Obata, K.; Iwata, K.; Okada, Y.; Kohrin, Y.; Ohuchi, E.; Yoshida, S.; Shinmei, M.; Hayakawa, T. A One-Step Sandwich Enzyme Immunoassay for Human Matrix Metalloproteinase-3 (Stromelysin-1) Using Monoclonal Antibodies. Clin. Chim. Acta **1992**, *211* (1–2), 59–72.
22. Ohuchi, E.; Azumano, I.; Yoshida, S.; Iwata, K.; Okada, Y. A One-Step Sandwich Enzyme Immunoassay for Human Matrix Metalloproteinase 7 (Matrilysin) Using Monoclonal Antibodies. Clin. Chim. Acta **1996**, *244* (2), 181–198.
23. Matsuki, H.; Fujimoto, N.; Iwata, K.; Knäuper, V.; Okada, Y.; Hayakawa, T. A One-Step Sandwich Enzyme Immunoassay for Human Matrix Metalloproteinase 8 (Neutrophil Collagenase) Using Monoclonal Antibodies. Clin. Chim. Acta **1996**, *244* (2), 129–143.
24. Okada, Y.; Gonoji, Y.; Naka, K.; Tomita, K.; Nakanishi, I.; Iwata, K.; Yamashita, K.; Hayakawa, T. Matrix Metalloproteinase 9 (92kDa Gelatinase/Type IV Collagenase) From HT 1080 Human Fibrosarcoma Cells. J. Biol. Chem. **1992**, *267* (30), 21712–21719.
25. Tamei, H.; Azumano, I.; Iwata, K.; Yoshihara, Y.; López-Otín, C.; Vizoso, F.; Knäuper, V.; Murphy, G. One-Step Sandwich Enzyme Immunoassays for Human Matrix Metalloproteinase 13 (Collagenase-3) Using Monoclonal Antibodies. Connective Tissue **1998**, *30*, 15–21.
26. Wang, T.; Aoki, T.; Iwata, K.; Takata, T.; Uchida, T.; Knäuper, V.; Llano, E.; Okada, Y.; Bartlett, J.D. One-Step Sandwich Enzyme Immunoassay Using Monoclonal Antibodies for Detection of Human Enamelysin (MMP-20). Eur. J. Oral Sci. **2000**, *108* (6), 530–537.

27. Cao, J.; Sato, H.; Takino, T.; Seiki, M. The C-Terminal Region of Membrane Type Matrix Metalloproteinase is a Functional Transmembrane Domain Required for Pro-Gelatinase A Activation. J. Biol. Chem. **1995**, *270* (2), 801–805.
28. Oi, V.T.; Herzenberg, L.A. Immunoglobulin-Producing Hybrid Cell Lines. In *Selected Methods in Cellular Immunology;* Mishell, B.B., Shiigi, S.M., Eds.; W. H. Freeman and Company: San Francisco, 1980; 351–372.
29. Ishikawa, E.; Imagawa, M.; Hashida, S.; Yoshitake, S.; Hamaguchi, Y.; Ueno, T. Enzyme-Labeling of Antibodies and Their Fragments for Enzyme Immunoassay and Immunohistochemical Staining. J. Immunoassay **1983**, *4* (3), 209–327.
30. Lehti, K.; Lohi, J.; Valtanen, H.; Keski-Oja, J. Proteolytic Processing of Membrane-Type-1 Matrix Metalloproteinase is Associated With Gelatinase A Activation at the Cell Surface. Biochem. J. **1998**, *334* (pt 2), 345–353.
31. Okada, A.; Bellocq, J.P.; Rouyer, N.; Chenard, M.P.; Rio, M.C.; Chambon, P.; Basset, P. Membrane-Type Matrix Metalloproteinase (MT-MMP) Gene is Expressed in Stromal Cells of Human Colon, Breast, and Head and Neck Carcinomas. Proc. Natl. Acad. Sci. USA **1995**, *92* (7), 2730–2734.
32. Polette, M.; Nawrocki, B.; Gilles, C.; Sato, H.; Seiki, M.; Tournier, J.M.; Birembaut, P. MT-MMP Expression and Localisation in Human Lung and Breast Cancers. Virchows Arch. **1996**, *428* (1), 29–35.
33. Nakamura, H.; Ueno, H.; Yamashita, K.; Shimada, T.; Yamamoto, E.; Noguchi, M.; Fujimoto, N.; Sato, H.; Seiki, M.; Okada, Y. Enhanced Production and Activation of Progelatinase A Mediated by Membrane-Type 1 Matrix Metalloproteinase in Human Papillary Thyroid Carcinomas. Cancer Res. **1999**, *59* (2), 467–473.
34. Sardinha, T.C.; Nogueras, J.J.; Xiong, H.; Weiss, E.G.; Wexner, S.D.; Abramson, S. Membrane-Type 1 Matrix Metalloproteinase mRNA Expression in Colorectal Cancer. Dis. Colon. Rectum. **2000**, *43* (3), 389–395.
35. Sobin, L.H.; Wittekind, C. *TNM Classification of Malignant Tumours*; 5th Ed.; John Wiley & Sons, Inc.: New York, 1997.

Received June 22, 2001
Accepted July 9, 2001
Manuscript 3045

EXHIBIT O

Expression and Shedding of CD44 Variant Isoforms in Patients With Gynecologic Malignancies

Douglas D. Taylor, PhD, Cicek Gercel-Taylor, PhD, and Stanley A. Gall, MD

OBJECTIVES: *The presence of CD44 isoforms was evaluated in ascitic fluid and serum samples of patients with gynecologic malignancies. Previously, the shedding of tumor-associated cell surface antigens has been demonstrated in the blood and malignant effusions of gynecologic cancer patients. Thus, the shedding of CD44 was also studied in ascitic fluids and sera of these patients, to address variant isoform expression as a biomarker of gynecologic cancer.*

METHODS: *The expression of CD44 isoforms by ovarian tumor cells was examined by flow cytometry using variant-specific monoclonal antibodies. The release of these isoforms into the peripheral circulation and ascites was assayed by Western immunoblot analysis.*

RESULTS: *Flow cytometric analysis of ovarian tumor cell lines revealed a strong expression of CD44 with significant levels of v4/5 and v6 isoforms. The presence of circulating CD44 isoforms was detectable in the sera of six of eight cancer patients, as well as in 12 of 16 ascitic fluids. Of the CD44-positive specimens, all six positive sera expressed detectable levels of variant CD44. The CD44v6 was present in all of the positive sera samples tested. In the ascites, the "shed" CD44 appeared to be associated predominantly with shed particles (vesicles) of plasma membranes (membrane fragments). Of ten CD44-positive ascites samples, all expressed significant levels of variant CD44.*

CONCLUSIONS: *In addition to mediating metastasis, the differential expression and shedding of CD44 isoforms into the circulation may represent important determinants in the escape of tumors from immune surveillance, and their detection may be a diagnostic or prognostic marker.* (J Soc Gynecol Invest 1996;3:289–94)

KEY WORDS: CD44, metastasis, ovarian cancer, shedding.

Most clinical and experimental data suggest that metastasis is a nonrandom, organ-specific process.[1] The interactions between tumor cells and the extracellular matrices observed during metastasis are mediated by the repertoire of adhesion molecules expressed on the tumor cell surface and the unique composition of organ-specific matrices.[2] These tumor-surface adhesion molecules are involved in all the intermediate steps described in the metastatic cascade. Modulation of two adhesion molecules, E-cadherin (decreased) and CD44 (increased) have been correlated clearly with the acquisition of invasive capacity of primary tumor cells.[1]

The cell-surface glycoprotein CD44 represents a polymorphic family of integral membrane proteins, found on a wide variety of cells. CD44 is encoded by 20 exons, at least ten of which are expressed variably because of alternative splicing of nuclear RNA. Although the exact function of CD44 has yet to be defined conclusively, it has been implicated in lymphocyte homing, lymphohemopoiesis, and T cell activation.[3–7] Alternative splicing, differential N- and O-linked glycosylation, chondroitin sulfation, and phosphorylation may be responsible for the diversity in the size of CD44 molecules, with apparent molecular weights ranging from 85 to 260 kDa.[8–10] Numerous combinations of the variant exons have been detected, resulting in more than 30 different isoforms being reported for various tissue types. The CD44s (standard) isoform lacks the variant exons (v1–v10) and appears to be expressed almost ubiquitously. The CD44s is broadly distributed in hematopoietic cells, fibroblasts, and numerous tumors of mesenchymal and neuroectodermal origin, whereas expression of CD44 isoforms containing the variant exons appears to have a restricted distribution.

In addition to differences in their polypeptide sequences and posttranslational modifications, the two isoforms may exhibit different functions. CD44s displays a high affinity for hyaluronate and also binds collagen, laminin, and fibronectin, whereas CD44 variant isoforms mediates attachment to surface-bound hyaluronate.[11] Because CD44s is a primary cell surface receptor for hyaluronate, it appears to play a critical role in cell-cell and cell-substrate adhesion.[12] The cytoplasmic tail of CD44 associates with cytoskeletal proteins and mediates cell motility.

From the Departments of Obstetrics and Gynecology, University of Louisville School of Medicine, Louisville, Kentucky.

Address correspondence and reprint requests to: Dr. Douglas D. Taylor, Division of Gynecologic Oncology, Department of Obstetrics & Gynecology, Medical-Dental Research Building, Rm. 438, 511 South Floyd Street, Louisville, KY 40202.

1071-5576/96/$15.00
PII S1071-5576(96)00022-6

Table 1. Clinical Characteristics of Patients on the Gynecologic Oncology Service From Whom Serum and/or Ascitic Fluids Were Obtained

Patient designation	Age (y)	Stage	Tumor site
Patient 1	76	IV	Endometrium
Patient 2	69	IV	Endometrium
Patient 3	61	Recurrent	Ovary
Patient 4	64	IIIc	Ovary
Patient 5	64	III	Ovary
Patient 6	43	IB	Cervix
Patient 7	71	IIIA	Cervix
Patient 8	69	IV	Ovary
Patient 9	47	IIIC	Ovary
Patient 10	71	IV	Endometrium
Patient 11	77	III	Ovary
Patient 12	57	Recurrent	Fallopian tube
Patient 13	59	III	Ovary
Patient 14	47	III	Peritoneal
Patient 15	76	IV	Endometrium
Patient 16	73	IV	Endometrium

Although the precise function of the variant isoforms is unclear, the expressions of variant exons, in particular the v6 and v8–v10, are correlated with metastatic potential in several human tumor types.

Recent investigations have suggested that CD44 expression on target cells represents one of several cellular adhesion molecules that regulate lymphocyte cytotoxicity.[13] This dichotomy between the role of increased CD44 expression necessary for metastasis and the need to diminish surface CD44 expression to circumvent immunologic killing has yet to be addressed. Our previous studies[14,15] addressed immunosuppressive materials released (shed) by various tumors. These studies focused on particles (vesicles) of plasma membranes from viable tumor cells (termed membrane fragments [MF]). We demonstrated that these MFs can suppress lymphocyte and monocyte activation.[15,16] We have proposed that the variable isoform expression and shedding of CD44 may provide a means for tumors to escape surveillance by activated lymphoid cells. In this report, we demonstrate the differential expression and shedding of CD44 isoforms by patients with gynecologic tumors.

MATERIALS AND METHODS

Patients and Clinical Materials

Malignant effusions and serum samples were obtained from patients of the Division of Gynecologic Oncology, within the Department of Obstetrics and Gynecology of the University of Louisville School of Medicine. The diagnoses included in this study are shown in Table 1. The acquisition and encoding of patient material was approved by the University Human Studies Committee.

Cells and Culture Conditions

The SKOV-3 cell line was obtained from the American Type Culture Collection (Rockville, MD). Ovarian tumor lines have been established in our laboratory from patients 4 and 8 (Table 1), and were described previously.[17] The above cells were grown in Dulbecco's modified Eagle's medium, supplemented with 10% fetal bovine serum, 1 mmol/L sodium pyruvate, 0.1 mmol/L nonessential amino acids, 200 mmol/L L-glutamine, 100 mg/mL streptomycin, and 100 IU/mL penicillin, in a humidified 5% CO_2 atmosphere.

Flow Cytometry

The cell surface expression of CD44 was assessed by flow cytometry. Cell cultures were treated with ethylenediaminetetra-acetic acid (EDTA) and removed from the culture flask by scraping. The cells were centrifuged, and the cell pellet was resuspended in ice-cold phosphate-buffered saline (PBS). The cell suspensions (10^6) were stained for CD44, in general, or for specific variants by incubating with a murine monoclonal pan-anti-CD44 antibody (T Cell Sciences, Cambridge, MA) or anti-CD44v4/5 and CD44v6 (R&D Systems, Minneapolis, MN) for 45 minutes at 4C. The cells were washed three times with ice-cold PBS, and the cells were further incubated with fluorescein isothiocyanate (FITC)-conjugated rabbit anti-mouse immunoglobulins (Ig) (Dako Corporation, Carpinteria, CA) for 45 minutes at 4C. The cells were washed three times with ice-cold PBS and fixed with 1% paraformaldehyde in Ca^{++}-Mg^{++}-free PBS for 30 minutes at 4C. The percent of cells labeled by this procedure was determined using a Coulter Epics fluorescene-activated cell sorter gated for tumor cells, with nonviable cells being (Hialeah, FL) removed by gating. Positive cells were determined as the percentage of cells fluorescent greater than cells incubated with only the FITC second antibody (negative control).

Sodium Dodecyl Sulfate Electrophoresis and Western Blotting

For electrophoretic separation of cell-associated CD44, cell cultures, in log-phase growth, were treated with EDTA and removed from the culture flask. The cells were centrifuged, and the cell pellet was resuspended with an iso-osmotic lysing buffer that contained 0.5% Triton X-100. This suspension was centrifuged at 10,000 revolutions per minute for 10 minutes, and the supernatant was mixed with 2× Laemmli sample buffer. For electrophoretic separation of serum- or ascitic-derived CD44, sera and ascitic were subjected to immunoprecipitation. Serum or ascitic samples (1 mL) were incubated overnight at 4C with pan-anti-CD44 antibody and agarose-conjugated anti-mouse Ig. The precipitate was washed three times with PBS containing 1% Triton X-100, 0.5% sodium deoxycholate, and 0.1% sodium dodecyl sulfate (SDS). The

Table 2. Expression of CD44 Isoforms by a Commercially Obtained Ovarian Tumor Cell Line and Two Recently Derived Ovarian Tumor Lines, as Determined by Flow Cytometry

Cells derived from patient	% pan-CD44 positive	% CD44 v6 positive	% CD44 v4/5 positive
SKOV-3	97.9	6.0	5.1
Patient 4	99.8	24.9	13.3
Patient 8	98.8	17.7	11.9

Percent positive cells were those cells exhibiting fluorescence above background (stained with an irrelevant primary antibody and fluorescein-conjugated secondary antibody. The primary antibodies were variant specific murine monoclonal antibodies.

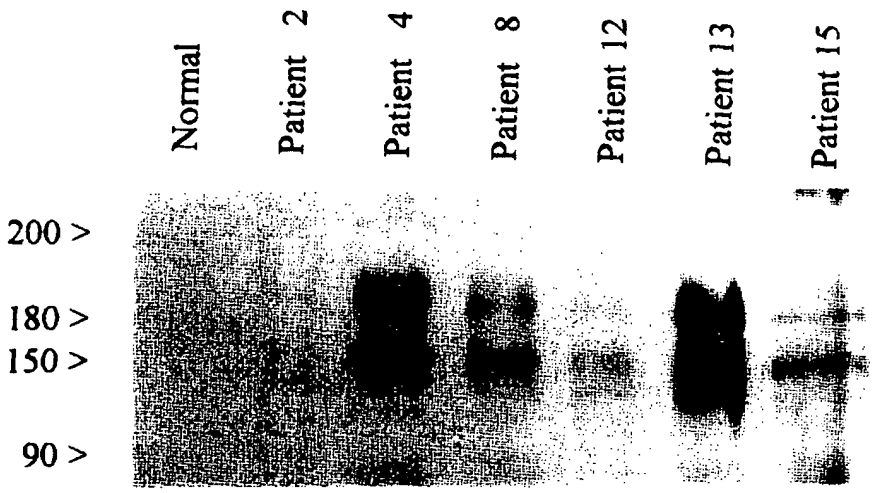

Figure 1. Western blot analysis of presence of CD44 isoforms and levels in serum samples obtained from gynecologic oncology patients. Serum samples (1 mL) were immunoprecipitated with pan-anti-CD44, and the pellets were resuspended in sample buffer and applied to sodium dodecyl sulfate–polyacrylamide gel electrophoresis. After electrophoresis, immunoblot analysis was performed with monoclonal anti-CD44s (recognizing all isoforms). CD44-reactive bands were visualized by enhanced chemiluminence. Molecular-weight estimates were based on simultaneously run, prestained standards.

immunoprecipitate was then resuspended in electrophoresis sample buffer, containing 2-mercapto-ethanol, 4% SDS, and 6% urea.

The proteins were separated by SDS-polyacrylamide gel elecrophoresis (PAGE) using the method of Laemmli.[20] Electrophoresis was performed using a 3% acrylamide focusing gel and a 7.5% acrylamide separating gel. Molecular-weight estimates were based on simultaneous electrophoresis of prestained molecular-weight standards (Bio-Rad, Richmond, CA). Following the electrophoretic separation, the proteins were electrophoretically transferred to nitrocellulose paper, and the nitrocellulose paper was blocked using 5% nonfat dry milk. The presence of CD44 was detected using a primary mouse monoclonal pan-anti-CD44 (T Cell Sciences) or anti-CD44v6 (R&D Systems) incubated at room temperature for 45 minutes. This primary antibody incubation was followed by three washes with 0.2% Tween-20 in PBS and a 45-minute incubation with a secondary peroxidase-labeled $F(ab)_2$ of rabbit antimouse Igs. The blots were visualized by staining for peroxidase with enhanced chemiluminence (ECL) (Amersham Life Sciences, Arlington Heights, IL).

Membrane Fragment Isolation

Membrane fragments were isolated from ascitic fluids by the ultracentrifugal procedure of Taylor et al.[18] In brief, the samples were initially centrifuged at 400 × *g*, and the supernatant was further centrifuged at 27,000 × *g* for 15 minutes to remove any cell debris. The supernatant was then centrifuged at 100,000 × *g* for 1 hour, and the resulting pellet was washed and resuspended in PBS at 3× the original concentration. Previous assessments of this material from electron microscopy and enzymatic markers had indicated that these were plasma membrane-derived vesicles ranging from 10 to 100 nm in diameter.[18]

Slot-Blot Analysis

The presence and distribution of CD44 in ascitic samples was evaluated by slot-immunoblot analysis. Initially, these samples (0.2 mL) were applied to nitrocellulose paper using a slot-blot manifold (Bio-Rad). The nitrocellulose paper was then blocked using 5% nonfat dry milk for 45 minutes at room temperature. After three washes, the presence of CD44 was detected using a primary mouse monoclonal antiCD44 (T Cell Sciences, Cambridge, MA), incubated on the rotating shaker at room temperature for 45 minutes. This primary antibody incubation was followed by three washes with 0.2% Tween-20 in PBS and a 45-minute incubation with a secondary peroxidase-labeled $F(ab)_2$ of rabbit antimouse Ig (Dako Corporation, Carpinteria, CA). The blots were visualized by staining for peroxidase with ECL (Amersham Life Sciences). Five of these

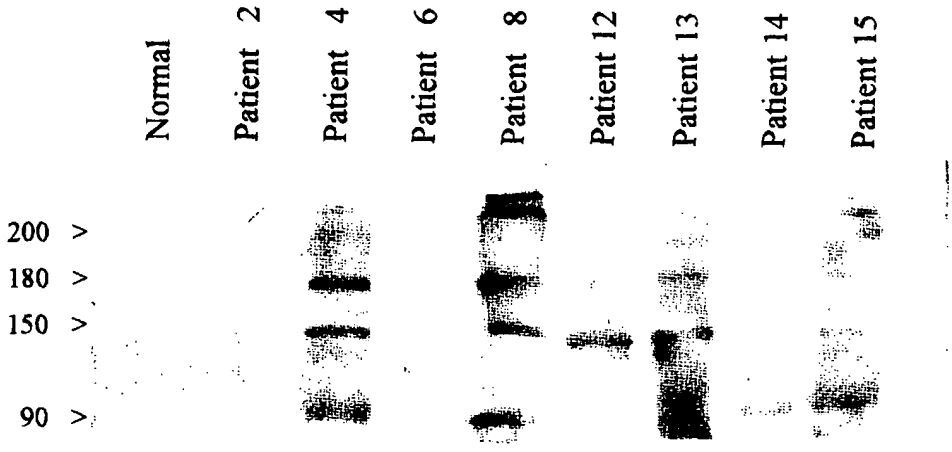

Figure 2. Western blot analysis of presence of CD44 isoforms and levels in serum samples obtained from gynecologic oncology patients. Serum samples (1 mL) were immunoprecipitated with pan-anti-CD44, and the pellets were resuspended in sample buffer and applied to sodium dodecyl sulfate–polyacrylamide electrophoresis. After electrophoresis, immunoblot analysis was performed with monoclonal anti-CD44v6. CD44-reactive bands were visualized by enhanced chemiluminence. Molecular-weight estimates were based on simultaneously run, prestained standards.

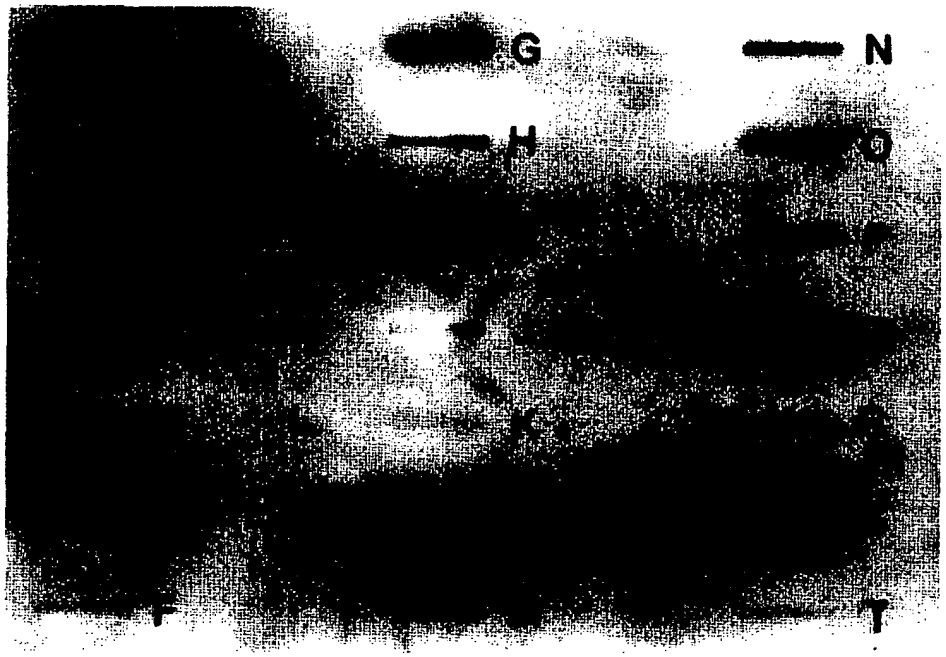

Figure 3. Slot-immunoblot for CD44 in ascitic fluids of gynecologic oncology patients and CD44-positive controls. Slot A presents CD44S, B shows bovine serum albumin as a negative control, C = CD44E, D = patient 1, E = patient 2, F = patient 3, G = patient 4, H = patient 5, I = patient 6, J = patient 7, K = patient 8, L = patient 9, M = patient 10, N = patient 11, O = patient 12, P = patient 13, Q = patient 14, R = patient 15, S = patient 16, T = negative control.

ascitic fluids were separated into their MF fraction and the MF-free supernatant (see above). Before blotting, the level of protein was determined by the method of Lowry et al.[19] and all samples were adjusted to identical protein concentrations. Utilizing the slot-immunoblot approach, these fractions were then assessed for the presence of CD44.

RESULTS

Expression of CD44 by Ovarian Tumor Cells

Because CD44 has been implicated in a number of cellular functions, including cell motility and metastasis formation, the cell surface expression of CD44 isoforms on ovarian tumor cells was examined by flow cytometry (Table 2). Tumor cells derived from patients 4 and 8 expressed high levels of surface CD44, similar to SKOV-3 cells. To determine which isoforms of CD44 were expressed by these ovarian tumor cells, flow cytometric analysis was performed using variant-specific monoclonal antibodies. This investigation revealed that a portion of the cells from patients 4 and 8 expressed both CD44v4/5 and CD44v6. The levels of variant CD44 isoforms expressed on our recently established lines were greater than on SKOV-3.

Presence of Circulating CD44

Our previous work demonstrated the shedding of cell surface antigens from tumor cells and their subsequent appearance in the peripheral circulation and malignant effusions. The presence of circulating CD44 was assayed by combining immunoprecipitation and Western immunoblotting of sera samples from gynecologic cancer patients (Figure 1). CD44 was detectable in six of the eight (75%) sera samples we analyzed. Circulating variant CD44 isoforms were detectable in all six of the CD44+ sera samples tested. Serum from normal control individuals failed to exhibit detectable levels of CD44. The Western immunoblot analysis was repeated using CD44v6-specific monoclonal antibody (Figure 2). The CD44-positive specimens tested were all reactive with the anti-CD44v6 antibody, with only bands at 150 and 180 kD being recognized by this variant-specific antibody.

Presence of Shed CD44 in Ascitic Fluids

The presence of CD44 in the ascitic fluids from cancer patients was assayed by slot-immunoblotting (Figure 3). CD44 was

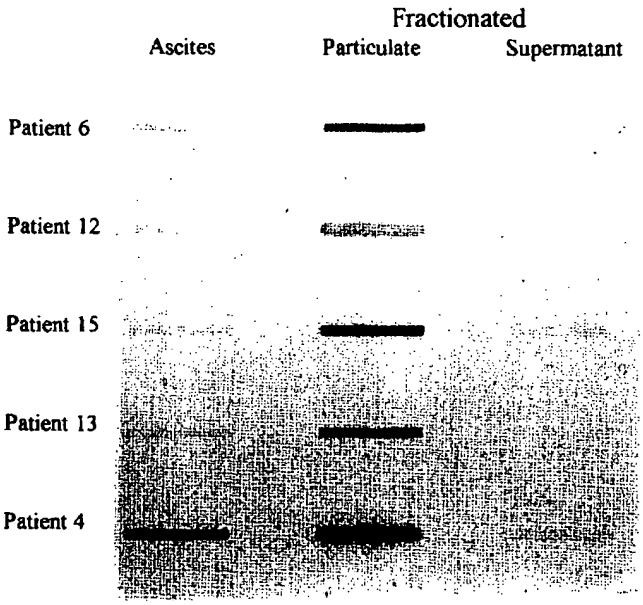

Figure 4. Slot immunoblot for CD44 in ascitic fluid samples obtained from gynecologic oncology patients. Ascitic fluids were either unfractionated or fractionated into membrane fragment-containing pellet (particulate) and the membrane fragment-free supernatant (supernatant).

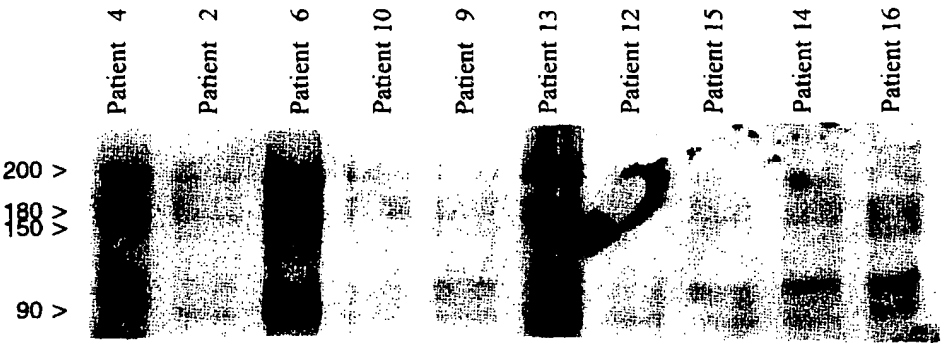

Figure 5. Western blot analysis of presence of CD44 isoforms and levels associated with ascites-derived membrane fragments obtained from gynecologic oncology patients. Ascites-derived membrane fragments (50 μg) were suspended in 2× sample buffer and applied to sodium dodecyl sulfate–polyacrylamide gel electrophoresis. Following electrophoresis, immunoblot analysis was performed with monoclonal antiCD44S (recognizing all isoforms). CD44-reactive bands were visualized by enhanced chemiluminence. Molecular-weight estimates were based on simultaneously run, prestained standards.

detectable in 12 (patients 2, 4–6, and 9–16) of the 16 (75%) ascitic fluids analyzed. Five of these ascitic fluids were separated into the plasma MF (or particulate) fractions and the MF-free supernatants. As a result of the protein concentration adjustment, the MFs were concentrated 2.5-fold. We observed CD44 to be shed primarily as particulate MFs in these patients, with little detectable MF-free CD44 (Figure 4).

To assess the isoform distribution in the ascites-derived MFs, we assayed shed MF-associated CD44 by combining immunoprecipitation and Western immunoblotting of solubilized MFs from ascitic samples of gynecologic cancer patients (Figure 5). CD44 was detectable in all ten of the ascitic fluid specimens tested (100%). Variant CD44 isoforms were also detectable in all ten of these ascites-derived MF preparations (100%).

DISCUSSION

Numerous investigations have correlated the expression of CD44 with the metastatic potential of various tumors.[1,13,21,22] More recently, studies have evaluated the expression of CD44 splice variants to understand the role of CD44 isoforms in metastasis formation.[7,23] Although the standard isoform (CD44s) has been implicated in cellular motility via its role as a hyaluronate receptor, the function of the variant CD44 isoforms has not been delineated.

In the present report, the expression of CD44 by tumor cells isolated from patients with gynecologic malignancies was described (Table 2), together with its shedding and ultimate appearance in the ascitic and peripheral circulation. Recently established ovarian tumor lines were demonstrated to be highly positive for CD44, with these lines expressing both CD44v4/5 and CD44v6. Patients 4 and 8, from whom these cell lines were derived, possessed widely metastatic disease, including brain metastases (in patient 4). The degree of metastatic spread in the patient from whom SKOV-3 was derived was unclear.

We further demonstrated that CD44 can be detected in the serum (Figure 1) and ascitic fluids (Figures 3 and 5) of most gynecologic oncology patients (Table 3 presents a composite of all patients). The ability to measure CD44 variant isoforms in the ascites or peripheral circulation may serve as a diagnostic and/or prognostic marker for gynecologic tumors; however, analysis of materials from various stages of disease must be evaluated before this conclusion can be firmly established. Previously, we demonstrated that tumor plasma membrane-derived components can appear in sera and ascites in two forms: either as individual soluble components or as actively shed fragments of the tumor cell plasma membrane (primarily as vesicles). The CD44 shed into the ascitic fluids of these gynecologic cancer patients, appeared to be associated primarily with tumor-derived plasma membrane fragments (Figure 4).

Because previous studies have failed to identify a common function between the major isoforms of CD44, the role of tumor-derived variant CD44 isoforms may be due to their availability in a shed form. Because we demonstrated that shed

Table 3. Composite of panCD44 and Variant CD44 Isoform Expression in Serum and Ascitic Samples of the 16 Gynecologic Cancer Patients Included in the Present Study

Patient designation	Serum expression (panCD44/ variant CD44)	Ascitic expression (panCD44/ variant CD44)
Patient 1	ND	–
Patient 2	–	+/+
Patient 3	ND	–
Patient 4	+/+	+/+
Patient 5	ND	+/ND
Patient 6	–	+/+
Patient 7	ND	–
Patient 8	+/+	–
Patient 9	ND	+/+
Patient 10	ND	+/+
Patient 11	ND	+/ND
Patient 12	+/+	+/+
Patient 13	+/+	+/+
Patient 14	+/+	+/+
Patient 15	+/+	+/+
Patient 16	ND	+/+
Normal	–	–

ND = not determined.
Determined by Western immunoblot analysis, utilizing a panCD44 monoclonal antibody.

tumor-derived MFs can modulate the host's immune system (primarily suppressing it)[15,16] and significant levels of variant CD44 isoforms, produced by these tumor cells, appeared to be shed, the consequences of variant CD44 isoforms are being investigated in the regulation of lymphoid activation and tumoricidal activity.

REFERENCES

1. Honn KV, Tang DG. Adhesion molecules and tumor cell interaction with endothelium and subendothelial matrix. Cancer Metastasis Rev 1992;11:353–75.
2. Hamilton MS, Ball J, Bromidge E, Franklin IM. Surface antigen expression of human neoplastic plasma cells includes molecules associated with lymphocyte recirculation and adhesion. Brit J Haematol 1991;78:60–5.
3. Shimizu Y, VanSeventer GA, Siraganian R, Wahl L, Shaw S. Dual role of the CD44 molecule in T cell adhesion and activation. J Immunol 1989;143:2457–63.
4. Zhou DFH, Ding JF, Picker LJ, Bargatze RF, Butcher EC, Goeddel DV. Molecular cloning and expression of Pgp-I. The mouse homology of the human H-CAM (Hermes) lymhocyte homing receptor. J Immunol 1989;143:3390–5.
5. Denning SM, Le PT, Singer KH, Haynes BF. Antibodies against the CD44 p80, lymphocyte homing receptor molecule augment human peripheral blood T cell activation. J Immunol 1990;144: 7–15.
6. Miyake K, Medina KL, Hayashi S, Ono S, Hamaoka T, Kincade PW. Monoclonal antibodies to Pgp-I/CD44 block lymphohemapoiesis in long-term bone marrow cultures. J Exp Med 1990; 171:477–88.
7. Arch R, Wirth K, Hofmann M, et al. Participation in normal immune responses of a metastasis-inducing splice variant of CD44. Science 1992;257:682–5.
8. Brown TA, Bouchard T, St John T, Wayner E, Carter WG. Human keratinocytes express a new CD44 core protein (CD44E) as a heparan-sulfate intrinsic membrane proteoglycan with additional exons. J Cell Biol 1991;113:207–21.
9. Stamenkovic I, Aruffo A, Amiot M, Seed B. The hematopoietic and epithelial forms of CD44 are distinct polypeptides with different adhesion potentials for hyaluronate bearing cells. EMBO J 1991;10:343–8.
10. Screaton GR, Bell MV, Jackson DG, Cornelis FB, Gerth U, Bell JI. Genomic structure of DNA encoding the lymphocyte homing receptor CD44 reveals at least 12 alternatively spliced exons. Proc Natl Acad Sci U S A 1992;89:12160–4.
11. Peach RJ, Hollenbaugh D, Stamenkovic I, Aruffo A. Identification of hyaluronic acid binding sites in the extracellular domain of CD44. J Cell Biol 1993;122:257–64.
12. Thomas L, Byers HR, Vink J, Stamenkovic I. CD44H regulates tumor cell migration on hyaluronate-coated substrate. J Cell Biol 1992;118:971–7.
13. Pandolfi F, Trentin L, Boyle LA, et al. Expression of cell adhesion molecules in human melanoma cell lines and their role in cytotoxicity mediated by tumor-infiltrating lymphocytes. Cancer 1992;69:1165–73.
14. Taylor DD, Homesley HD, Doellgast GJ. Identification of antigenic components recognized by "membrane bound" antibodies from ovarian cancer patients. Am J Reprod Immunol 1984;6: 179–84.
15. Taylor DD, Black PH. Inhibition of macrophage Ia antigen expression by shed plasma membrane vesicles from metastatic murine melanoma lines. J Natl Cancer Inst 1985;74:859–67.
16. Taylor DD, Levy EM, Black PH. Shed membrane vesicles: a mechanism for tumor-induced immunosuppression. In: Immunity to Cancer. Mitchell MS, Reif AE, eds. New York: Academic Press, 1985:369–73.
17. Owens K, Gercel-Taylor C, Taylor DD, Day TG, Doering DL. Isolation and characterization of an ovarian carcinoma cell line as a model for drug resistance. Proc Am Assoc Cancer Res 1993; 34:26.
18. Taylor DD, Chou IN, Black PH. Isolation of plasma membrane fragments from cultured murine melanoma cells. Biochem Biophys Res Comm 1983;113:470–6.
19. Lowry OH, Rosenbrough NJ, Farr AL, Randall RJ. Protein measurement with the Folin phenol reagent. J Biol Chem 1951; 193:265–75.
20. Laemmli UK. Cleavage of structural proteins during the assembly of the head of the bacteriophage T4. Nature 1970;227:680–5.
21. Birch M, Mitchell S, Hart IR. Isolation of human melanoma cell variants expressing high and low levels of CD44. Cancer Res 1991;51:6660–7.
22. Sy MS, Guo YJ, Stamenkovic I. Distinct effects of two CD44 isoforms on tumor growth in vivo. J Exp Med 1991;174:859–66.
23. Hofmann M, Rudy W, Zoller M, et al. CD44 splice variants confer metastatic behavior in rats: homologous sequences are expressed in human tumor cell lines. Cancer Res 1991;51: 5292–7.

Clin. exp. Immunol. (1991) 85, 3-8

EXHIBIT P

Detection of circulating intercellular adhesion molecule-1 antigen in malignant diseases

M. TSUJISAKI, K. IMAI, H. HIRATA, Y. HANZAWA*, J. MASUYA, T. NAKANO, T. SUGIYAMA, M. MATSUI†, Y. HINODA & A. YACHI *Department of Internal Medicine, Sapporo Medical College, Sapporo, * Life Sciences Laboratories, Ajinomoto, Yokohama, and † Suntory Institute, Osaka, Japan*

(Accepted for publication 4 March 1991)

SUMMARY

A new monoclonal antibody (MoAb) HA58 (IgG1) was prepared, which recognizes the binding site on the intercellular adhesion molecule-1 (ICAM-1) antigen to the lymphocyte function-associated antigen-1 (LFA-1). The double-determinant immunoassay (DDIA) was established with use of MoAb HA58 and another anti-ICAM-1, MoAb CL207, to detect the soluble, shedding ICAM-1 antigen. Human recombinant interferon-gamma (IFN-γ) induced not only the expression of cell surface ICAM-1, but also the shedding ICAM-1 antigen in an IFN-γ concentration-dependent and incubation-time-dependent manner. DDIA was applied to detect the shedding ICAM-1 antigen in the sera of patients with malignant or benign diseases. The incidence of positivity for ICAM-1 antigen in malignant diseases was higher than that in benign diseases or in healthy controls. Furthermore, the sera of cancer patients with liver metastasis showed higher levels of the shedding ICAM-1 antigen. These findings suggest that serum ICAM-1 antigen may be a useful marker to monitor tumor burden in cancer patients.

Keywords ICAM-1 circulating ICAM-1 in sera malignant disease

INTRODUCTION

Intercellular adhesion molecule-1 (ICAM-1), a 80-110-kD glycoprotein, has been found to be a ligand for the lymphocyte function-associated antigen-1 (LFA-1) molecule (Rothlein *et al.*, 1986; Marlin & Springer, 1987; Makgova *et al.*, 1988). ICAM-1 plays an important role in inflammatory diseases (Barton *et al.*, 1989) and in malignant diseases (Johnson *et al.*, 1989). It has been suggested that the binding of T lymphocytes to vascular endothelial cells occurs between the ICAM-1 and LFA-1 molecules (Haskard *et al.*, 1986). The release of cytokines (interferon, IL-1, tumour necrosis factor, etc.) at sites of inflammation and immune response causes cell activation and results in augumented expression of adhesion molecules including ICAM-1 on the host's cell surface (Rothlein *et al.*, 1988).

Furthermore, the ICAM-1 antigen has recently been reported to be a member of the immunoglobulin supergene family with five-domain structures (Staunton *et al.*, 1988) and also to function as a receptor for rhinovirus (Greve *et al.*, 1989; Staunton *et al.*, 1989). These findings suggest the possibility that ICAM-1 antigen acts as a functional receptor molecule, as well as the ligand for LFA-1.

We describe here the estblishment of a new monoclonal antibody (MoAb) HA58 to ICAM-1, and the measurement of the levels of circulating ICAM-1 antigen in patient sera. The latter would provide a novel view of ICAM-1 in respect to the diseases.

Correspondence: K. Imai, MD, Department of Internal Medicine, Sapporo Medical College, S-1, W-16, Chuo-ku, Sapporo 060 Japan.

MATERIALS AND METHODS

Cell lines

Human colonic carcinoma BM314 and WiDr, gastric carcinoma MKN45 and KATOIII, pancreatic carcinoma Panc-1 and PK-1, hepatocellular carcinoma o-Hc-4 and c-Hc-20, and lung adenocarcinoma HLC-1 cell lines were grown in RPMI 1640 medium supplemented with 10% fetal calf serum (FCS), 2 mM L-glutamine and gentamycin sulphate (25 μg/ml). These lines were obtained from the Japanese Cancer Research Resources Bank, Tokyo, Japan.

Monoclonal antibodies

MoAb HA58 (IgG1) was secreted by a hybridoma constructed with X63-Ag8.653 myeloma cells and splenocytes from a BALB/c mouse that was immunized with a weekly intraperitoneal injection of 1×10^7 colonic carcinoma BM314 cells treated with interferon-gamma (IFN-γ) (200 U/ml for 24 h). Subcloning and growing of hybridomas were done according to standard procedures (Imai *et al.*, 1984). MoAbs secreted from the resulting hybridomas were purified from ascitic fluid either by affinity chromatography on protein A-Sepharose (Ey, Prowes

& Jenkin, 1978), by ion exchange chromatography on DEAE or by caprylic acid precipitation (Russo *et al.*, 1983). MoAbs were biotinylated according to a published procedure (Guesdon, Ternynck & Avrameas, 1979). MoAb CL207 (IgG1) to ICAM-1 was developed as described elsewhere (Maio *et al.*, 1989).

MoAb AI206 (IgG1) is an anti-idiotypic MoAb to MoAb YH206 (IgM) which reacts with adenocarcinoma-associated antigen (Sugiyama *et al.*, 1991).

Binding assay

Flow cytometry using EPICS (Coulter Electronics, Hialeah, FL) was performed to assess the reactivity of MoAbs to IFN-γ-treated or non-treated cells as described by Kitagawa *et al.* (1986). Briefly, 100 μl of MoAb (20 μg/ml) were added to the washed cells (1×10^6) and incubated for 1 h at 4°C. Following washings, 50 μl of FITC-labelled rabbit anti-mouse immunoglobulin (Zymed, San Francisco, CA) was added and incubated for 1 h at 4°C. After being washed, FITC-labelled cells were analysed on an EPICS.

Competition assay

In order to test whether the epitopes recognized with MoAb HA58 and CL207 were different, competition assay was performed. IFN-γ-treated cultured colonic carcinoma BM314 cells were pre-incubated with an excess of unlabelled MoAb for 1 h at 4°C. After washing, ^{125}I-labelled MoAb (1×10^5 ct/min per well) was added to test for the ability to bind. After incubation for 1 h, bound radioactivity was counted. Results were calculated as percentage of blocking, compared with negative control.

Immunochemical analysis of antigen recognized with MoAbs

Western blot analysis was performed as described elsewhere (Ban, Imai & Yachi, 1989). Cultured BM314 cells treated with IFN-γ were solubilized with NP40 detergent. The resulting extract was analysed by SDS-PAGE and then transferred to nitrocellulose membrane. After blocking with 3% BSA, vertically sliced nitrocellulose membranes were incubated with purified MoAb at room temperature for 2 h. Strips were washed three times for 10 min each in PBS containing 1/300 dilution of peroxidase-conjugated rabbit anti-mouse IgG (Dako, Tokyo, Japan). After being washed with PBS, the strips were incubated in a freshly prepared solution. The immobilized horseradish peroxidase was visualized with 120 ml of 0·005% 4-chloro-1-naphthol (w/v) in 20 mM Tris–HCl buffer (pH 7·5), 17% methanol (v/v) and 60 μl of H_2O_2 (final concentration 0·05% (v/v)). After a 15-min incubation at room temperature, the strips were removed into water. Antigen–antibody binding was identified by the presence of a black stain.

The immunodepletion experiment was done as follows: the antigen in the extract from IFN-γ-treated colonic carcinoma BM314 cells was completely depleted by CNBr-activated Sepharose 4B coated with 10 mg of MoAb HA58. The remaining extract was analysed by Western blotting with MoAb CL207.

Spent media of cultured cells and serum specimens

Spent media were collected from the flasks in which 3×10^5/ml of cells had been incubated for 3 days to test for shedding ICAM-1 antigen from cells. Serum specimens of healthy controls (aged 35–78 years) were obtained from volunteers among our departmental staff. Samples of cancers and benign diseases were

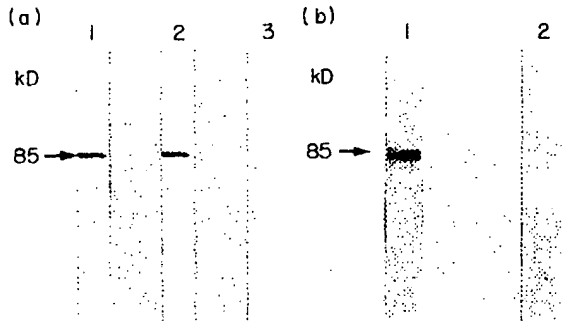

Fig. 1. Western blot analysis of the corresponding antigen detected by MoAb HA58 or CL207. (a) The extract from IFN-γ-treated colonic cancer BM314 cells was used as an antigen under reducing conditions. Reactivity of the antigen with MoAb HA58 (lane 1), MoAb CL207 (lane 2) and MoAb AI206 (lane 3) was assessed by Western blot (7·5% gel); (b) immunodepletion experiment. The extract from IFN-γ-treated colonic cancer BM314 cells had been immunodepleted by either MoAb AI206 (IgG 1) (lane 1) or MoAb HA58 (IgG 1) (lane 2) before the remaining extract was analysed by Western blotting under reducing conditions using MoAb CL207 to the ICAM-1 molecule (7·5% gel).

obtained from patients at our college hospital: gastric cancer ($n = 51$), colonic cancer ($n = 29$), gall bladder cancer ($n = 14$), pancreatic cancer ($n = 15$), oesophageal cancer ($n = 6$), pancreatitis ($n = 8$) and cholecystitis ($n = 13$). Miscellaneous diseases included collagen disease ($n = 16$), infection ($n = 15$), cardiovascular diseases ($n = 6$) and diseases of metabolism ($n = 7$). Liver metastasis of the carcinoma was diagnosed by use of CT and echogram.

Double-determinant immunoassay (DDIA)

DDIA using the FAST system (Becton Dickinson, Mountain View, CA) was employed to obtain a quantitative analysis of the antigen. Microtitre plates (96-well) were first incubated with purified MoAb CL207 or HA58 (20 μg/ml) and then blocked by 3% BSA. The spent media of cultured cells or aliquots of serum samples diluted 1/200 in PBS were then incubated with the beads. After being washed with PBS containing 0·05% Tween 20, the beads were incubated with biotinylated MoAb HA58 or CL207. Avidin-conjugated peroxidase (Vector, Burlingame, CA) was diluted 1/1000 in 0·05 M PBS with 0·5 M NaCl, pH 8·0, and incubated with the beads. The degree of substrate reaction was determined with OPD at 492 nm in a Micro-ELISA Autoreader MR 580 (Dynatech, Cambridge, MA). Results were expressed as units (1 U corresponds to 2 μg of purified antigen) calculated from the titration curve of ICAM-1 antigen.

RESULTS

Characterization of corresponding epitope recognized with MoAb HA58

The mol. wt of the antigen recognized with MoAb HA58 was approximately 85 kD, which was the same mol. wt as that recognized with MoAb CL207 in SDS-PAGE (Fig. 1a). In order to determine whether MoAbs HA58 and CL207 recognize the same molecule, sequential immunodepletion experiments were performed. The result is shown in Fig. 1b. The extract from IFN-γ-treated colonic carcinoma BM314 cells had been immunodepleted by Sepharose 4B coated with either irrelevant MoAb AI206 (IgG1) as negative control or MoAb HA58 (IgG1) before

Table 1. Epitopes recognized with anti-ICAM-1 monoclonal antibodies HA58 and CL207

Pre-incubated with unlabelled MoAb	^{125}I-labelled MoAb		
	HA58	CL207	MA208
HA58	4251 ± 562	23 210 ± 1856	21 503 ± 1951
CL207	33 135 ± 2433	3612 ± 462	22 419 ± 1888
MA208*	31 281 ± 2142	22 341 ± 1947	2816 ± 304
HU-20*	34 654 ± 1946	24 516 ± 2051	20 987 ± 2103
Medium	32 561 ± 2650	26 184 ± 2149	23 344 ± 1917

IFN-γ-treated BM314 cells were pre-incubated with an excess of unlabelled MoAbs, and then tested for their ability to bind ^{125}I-labelled MoAbs. Results are expressed as bound mean ct/min ± s.d. of triplicate values.

*Anti-CEA MoAb MA208 and anti-HLA class II MoAb HU-20 were used as negative controls.

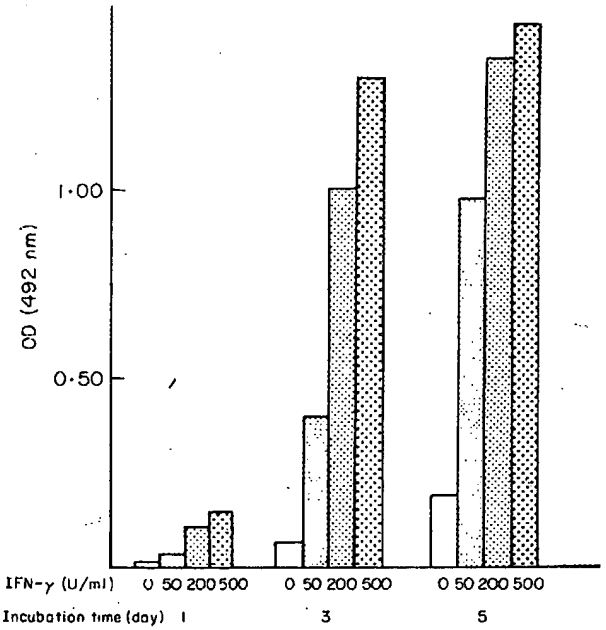

Fig. 2. Detection of the shedding ICAM-1 antigen in spent media of cancer cells with ELISA. Effect of the concentration and incubation time of IFN-γ upon the accumulation of ICAM-1 was compared. The spent media of gastric cancer MKN45 cells were used as an antigen.

the remaining extract was analysed by Western blotting under reducing condition, using MoAb CL207. MoAb CL207 failed to immunoprecipitate 85-kD molecules after depletion by MoAb HA58 (lane 2), whereas MoAb CL207 reacted with the molecules after depletion by irrelevant MoAb A1206 (lane 1). This result suggests that these two MoAbs react with the same antigenic molecule, ICAM-1.

A further competition assay was done to examine whether the epitopes recognized with MoAb CL207 and MoAb HA58 were different. Binding activity of ^{125}I-labelled MoAb HA58 to ICAM-1$^+$ cells (IFN-γ-treated BM314 cells) was inhibited only

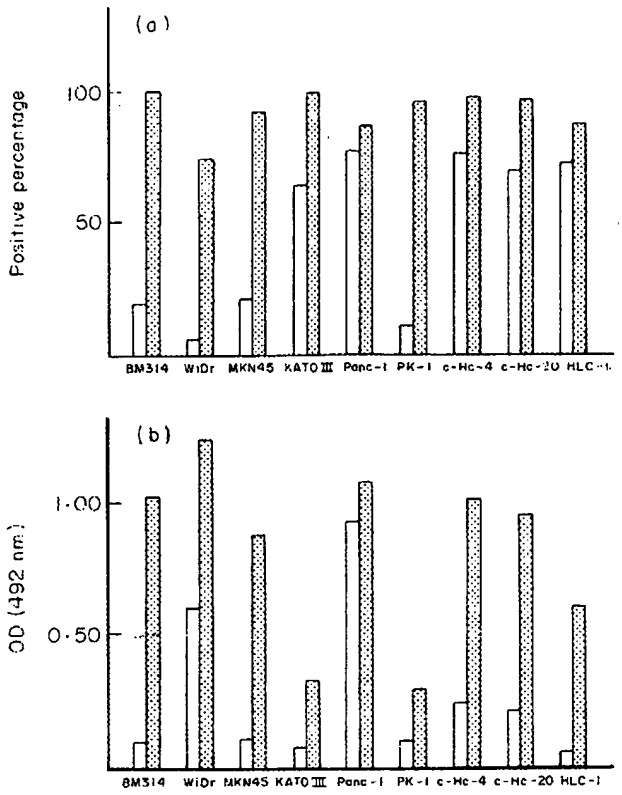

Fig. 3. (a) ICAM-1 expression on cultured cell surface treated (▨) or untreated (□) IFN-γ. Positive percentages of ICAM-1-bearing cells were measured by MoAb HA58, using flow cytometry; (b) shedding ICAM-1 antigen in the spent media of cultured cells. Detection of the shedding ICAM-1 antigen was done, using spent media of cultured cells which were incubated for 3 days with (▨) and without (□) IFN-γ (200 U/ml).

with MoAb HA58, but not with MoAb CL207 nor with irrelevant MoAbs. In contrast, ^{125}I-labelled MoAb CL207 competed with MoAb CL207, but not with MoAb HA58 nor with the others (Table 1).

These results from Western blot analysis, immunodepletion and competition experiments strongly suggest that MoAb HA58 and CL207 recognize distinct epitopes on ICAM-1.

DDIA to detect soluble ICAM-1 antigen

In order to determine the most sensitive combination of a catcher (coating MoAb) and a tracer (labelled MoAb) to detect soluble ICAM-1 antigen, DDIA was performed by four combinations (MoAbs HA58–HA58, CL207–CL207, HA58–CL207 and CL207–HA58). The combination of coating MoAb CL207 as a catcher and biotinylated MoAb HA58 as a tracer is the most sensitive means for ELISA to detect the soluble ICAM-1 molecule, whereas the other combinations (including a combination of the same MoAb) are not sensitive enough for measurement (data not shown). Shedding ICAM-1 antigen in the spent media of cultured cells was then measured, using coated MoAb CL207 and biotinylated MoAb HA58. This assay was first applied to examine the effect of IFN-γ concentration and incubation time upon the accumulation of the shedding ICAM-1 antigen from cultured gastric carcinoma MKN45 cells. As shown in Fig. 2, the amounts of shedding ICAM-1 antigen increased in an IFN-γ concentration- and time-dependent manner.

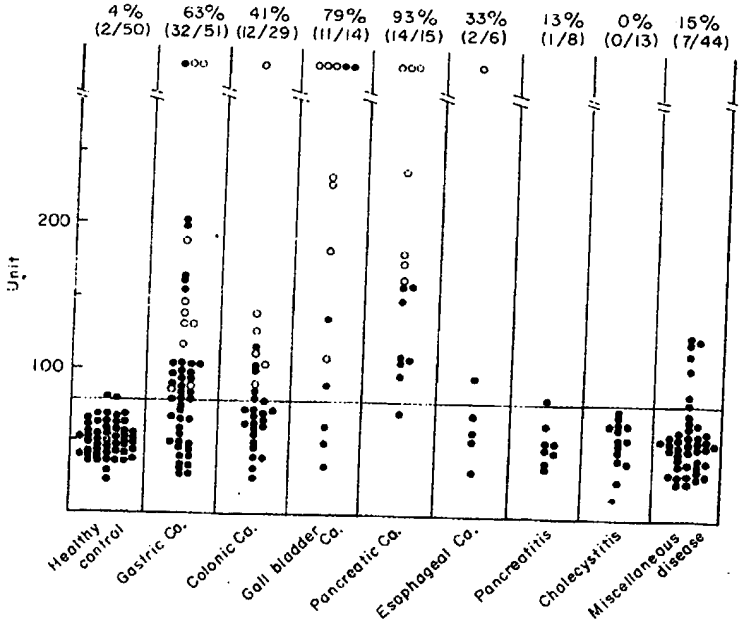

Fig. 4. Measurement of circulating ICAM-1 antigen in the sera of patients with malignant and non-malignant diseases (cut-off value, 75 U). Patients' sera with metastasis (○) and without metastasis (●).

Table 2. The average ICAM-1 levels in the sera of cancer patients with and without liver metastasis

	Average levels of circulating ICAM-1		
	With metastasis	Without metastasis	P^*
Gastric cancer	138·4±79·9 (n=14)	76·7±43·4 (n=40)	<0·005
Colonic cancer	150·7±104·0 (n=7)	62·1±21·9 (n=20)	<0·005
Gall bladder cancer	228·3±87·7 (n=5)	100·6±87·1 (n=7)	<0·025
Pancreatic cancer	251·9±90·3 (n=7)	101·4±35·2 (n=9)	<0·005
Oesophageal cancer	364·3 (n=1)	61·5±23·8 (n=5)	
Total	184·2±97·7 (n=34)	78·0±44·9 (n=81)	<0·005

Results are expressed as ICAM-1 units (mean±s.d.).

*Significance of different ICAM-1 levels between cancers with and without metastasis, calculated with Student's t-test.

The expression and shedding of ICAM-1 antigen in cultured cells

In order to examine the relationship between the expression of ICAM-1 antigen on the cell surface and the soluble ICAM-1 antigen in the spent media, before and after treatment of cultured cells with IFN-γ, flow cytometry and DDIA were performed. As shown in Fig. 3a, the flow cytometry data indicated that IFN-γ-treated cells expressed more ICAM-1 antigen on cell surfaces than did the non-treated cells. Next, soluble ICAM-1 antigen shed in the spent media from IFN-γ-treated cultured cells were measured by DDIA. The levels of ICAM-1 antigen in the spent media of IFN-γ-treated cells were much higher than those of non-treated cells (Fig. 3b).

These results indicate that both expression and shedding of ICAM-1 antigen increased when cultured carcinoma cells of the stomach, the colon, the pancreas, the liver and the lung were treated with IFN-γ.

Measurement of circulating ICAM-1 antigens in the sera of patients with malignant and non-malignant diseases

Next, the circulating ICAM-1 antigen was measured in the sera of patients with malignant and non-malignant diseases. The cut-off value (mean value ±2 s.d.) was set as 75 U, based on the data of 50 healthy control sera. Patients with malignant disease tended to have higher mean levels of circulating ICAM-1 antigen than those with benign disease or healthy controls. The incidences of positivity for ICAM-1 antigen in pancreatic cancer, gall bladder cancer, gastric cancer and other cancer were 93%, 79%, 63% and approximately 50%, respectively (Fig. 4). However, those in benign diseases and healthy controls were, respectively, 12% and 4%. According to these results, the incidence of positivity in malignant diseases was significantly (P<0·01) higher than that in benign disease. Furthermore, it is noteworthy that the sera of cancer patients with liver metastases

showed higher levels of ICAM-1 antigens than those of patients without metastases ($P < 0.005$, Table 2).

DISCUSSION

MoAb HA58 (IgG1) was established using IFN-γ-treated colonic cancer BM314 cells as an immunogen. This new MoAb recognized ICAM-1, which was induced with IFN-γ (Dustin *et al.*, 1986), and crossreacted with MoAb CL207 in immunodepletion experiments.

There have been several reports describing other MoAbs to ICAM-1 (Staunton *et al.*, 1990). We do not know, however, whether MoAb HA58 recognizes the same epitope as other MoAbs. Nevertheless, our preliminary experiments (data not shown) suggest that MoAb HA58 appears to recognize the binding site (or close to it) of the ICAM-1 molecule to LFA-1, since NK activity against K562 cells was strongly reduced when the target cells were treated with MoAb HA58, and the aggregation of ICAM-1- and LFA-1-bearing cells was blocked when the cells were treated with MoAb HA58. In contrast, MoAb CL207 was reported to recognize a distinct epitope which was not the binding site for LFA-1, since MoAb CL207 had no influence on NK activity or on aggregation of cells (Maio *et al.*, 1989).

Because these two MoAbs recognize different epitopes, the DDIA was established to detect the circulating ICAM-1 antigen in patients' sera. To our knowledge, this is the first description of circulating ICAM-1 in the sera of patients. The incidence of positivity for the ICAM-1 antigens was higher in patients with malignancy (93% in pancreatic cancer, 79% in gall bladder cancer, 63% in gastric cancer) than in patients with benign diseases (13% in pancreatitis, 0% in cholecystitis). Furthermore, the sera of cancer patients with liver metastasis showed particularly high levels (Fig. 4, Table 2). In addition, our preliminary results showed that the molecular weight of the ICAM-1 in the serum was similar to that in the extract from IFN-γ-treated cancer cells.

Immunostaining of cancerous tissue with MoAb HA58 showed that the ICAM-1 antigen was expressed not only on malignant cells but also on stromal cells (mainly fibroblasts) near cancer nests, and the stromal cells immediately adjacent to cancer nests, in comparison to those cells farther away from the nests, have a higher ICAM-1 expression (manuscript in preparation). These results suggest that the expression of ICAM-1 antigen was augumented on the fibroblasts surrounding cancer cells. We speculate that tumour cells activate T cells to produce cytokines (e.g. IFN-γ), resulting in strong expression of the ICAM-1 on surrounding fibroblasts, as well as on tumour cells.

We suggest, therefore, that the higher levels of circulating ICAM-1 antigen in malignant diseases reflect the host's immune response to malignant cells and surrounding cells. The incidence of positivity and the levels of the antigen were not so high in benign diseases, including inflammatory diseases, suggesting that ICAM-1 is generated not only from inflammatory cells but also from tumour cells and immunoreactive cells to the tumour. Shedding ICAM-1 antigen may also block the attachment of cytotoxic T cells and/or NK cells to cancer cells, since LFA-1 could be blocked with soluble ICAM-1. This could be one of the escape mechanisms of cancer cells from the immunosurveillance system of the host.

ACKNOWLEDGMENTS

We acknowledge the technical help of Ms M. Takeda and the secretarial assistance of Ms H. Yamashita. This work was financed by Grant-in-Aid for Scientific Research on Priority Areas (K.I.) and by Grants-in-Aid for Cancer Research (M.T., K.I., A.Y.) from the Ministry of Health and Welfare, Japan.

REFERENCES

BAN, T., IMAI, K. & YACHI, A. (1989) Immunohistological and immunochemical characterization of a novel pancreas cancer-associated antigen MUSE11. *Cancer Res.* **49**, 7141.

BARTON, R.W., ROTHLEIN, R., KSIAZEK, J. & KENNEDY, C. (1989) The effect of anti-intercellular adhesion molecule-1 on phorbol-ester-induced rabbit lung inflammation. *J. Immunol.* **143**, 1278.

DUSTIN, M.L., ROTHLEIN, R., BHAN, A.K., DINARELLO, C.A. & SPRINGER, T.A. (1986) Induction by IL-1 and interferon, tissue distribution, biochemistry, and function of a natural adherence molecule (ICAM-1). *J. Immunol.* **137**, 245.

EY, P.L., PROWES, S.J. & JENKIN, C.R. (1978) Isolation of pure IgG1, IgG2a and IgG2b immunoglobulins from mouse serum using protein A-Sepharose. *Immunochemistry*, **15**, 429.

GREVE, J.M., DAVIS, G., MEYER, A.M., FORTE, C.P., YOST, S.C., MARLOR, C.W., KAMARCK, M.E. & MCCELLAND, A. (1989) The major human rhinovirus receptor is ICAM-1. *Cell*, **56**, 839.

GUESDON, J.L., TERNYNCK, T. & AVRAMEAS, S. (1979) The use of avidinbiotin interaction in immunoenzymatic techniques. *Histochem. Cytochem.* **27**, 1131.

HASKARD, D., CAVENDER, D., BEATTY, P., SPRINGER, T. & ZIFF, M. (1986) T lymphocyte adhesion to endothelial cells: mechanisms demonstrated by anti-LFA-1 monoclonal antibodies. *J. Immunol.* **137**, 2901.

IMAI, K., MORIYA, Y., FUJITA, H., TSUJISAKI, M., KAWAHARADA, M. & YACHI, A. (1984) Immunologic characterization and molecular profile of carcinoembryonic antigen detected by monoclonal antibodies. *J. Immunol.* **132**, 2992.

JOHNSON, J.P., STADE, B.G., HOLZMANN, B., SCHWABLE, W. & RIETHMULLER, G. (1989) De novo expression of intercellular-adhesion molecule 1 in melanoma correlates with increased risk of metastasis. *Proc. natl Acad. Sci. USA*, **86**, 641.

KITAGAWA, H., OHKOUCHI, E., FUKUDA, A., IMAI, K. & YACHI, A. (1986) Characterization of carcinoembryonic antigen-specific monoclonal antibodies and specific carcinoembryonic antigen assay in sera of patients. *Jpn. J. Cancer Res.* **77**, 922.

MAIO, M., TESSITONI, G., PINTO, A., TEMPONI, M., COLOMBATTI, A. & FERRONE, S. (1989) Differential role of distinct determinants of intercellular adhesion molecule-1 in immunologic phenomena. *J. Immunol.* **143**, 181.

MAKGOVA, M.W., SANDERS, M.E., LUCE, G.E.G., DUSTIN, M.L., SPRINGER, T.A., CLARK, E.A., MANHONI, P. & SHAW, S. (1988) ICAM-1 a ligand for LFA-1 dependent adhesion of B, T and myeloid cells. *Nature*, **331**, 86.

MARLIN, S.D. & SPRINGER, T.A. (1987) Purified intercellular adhesion molecule-1 (ICAM-1) is a ligand for lymphocyte function-associated antigen 1 (LFA-1). *Cell*, **51**, 813.

ROTHLEIN, R., DUSTIN, M.L., MARLIN, S.D. & SPRINGER, T.A. (1986) A human intercellular adhesion molecule (ICAM-1) distinct from LFA-1. *J. Immunol.* **137**, 1270.

ROTHLEIN, R., CZAJKOWSKI, M., O'NEILL, M.M., MARLIN, S.D., MAINOLFI, E. & MERLUZZI, V.J. (1988) Induction of intercellular adhesion molecule 1 on primary and continuous cell lines by pro-inflammatory cytokines: regulation by pharmacologic agents and neutralizing antibodies. *J. Immunol.* **141**, 1665.

RUSSO, C., CALLEGARO, L., LANZA, E. & FERRONE, S. (1983) Purification of IgG monoclonal antibody by caprylic acid precipitation. *J. immunol. Methods*, **65**, 269.

STAUNTON, D.E., MARLIN, S.D., STRATOWA, C., DUSTIN, M.L. & SPRINGER, T.A. (1988) Primary Structure of ICAM-1 demonstrates interaction between members of the immunoglobulin and integrin supergene families. *Cell*, **52**, 925.

STAUNTON, D.E., MERLUZZI, V.J., ROTHLEIN, R., BARTON, R., MARLIN, S.D. & SPRINGER, T.A. (1989) A cell adhesion molecule, ICAM-1, is the major surface receptor for rhinoviruses. *Cell*, **56**, 849.

STAUNTON, D.E., DUSTIN, M.L., ERICKSON, H.P. & SPRINGER, T.A. (1990) The arrangement of the immunoglobulin-like domains of ICAM-1 and the binding sites for LFA-1 and rhinovirus. *Cell*, **61**, 243.

SUGIYAMA, T., IMAI, K., ONO, A., TAKAYAMA, Y., TSUJISAKI, M., TAKI, T., HINODA, Y. & YACHI, A. (1991) Conformational structure of a monoclonal anti-idiotypic antibody to the monoclonal anti-adenocarcinoma associated carbohydrate antibody YH206. *J. Immunol.* (In press).

EXHIBIT Q

[CANCER RESEARCH 51, 2879-2884, June 1, 1991]

Immunochemical Detection of a Small Cell Lung Cancer-associated Ganglioside ($FucG_{M1}$) Antigen in Serum[1]

A. J. Vangsted,[2] H. Clausen, T. B. Kjeldsen, T. White, B. Sweeney, S. Hakomori, L. Drivsholm, and J. Zeuthen

Department of Tumor Cell Biology, The Fibiger Institute, Danish Cancer Society [A. J. V., J. Z.], and Department of Oral Diagnosis, The Royal Dental College [H. C.], Copenhagen, Denmark; The Biomembrane Institute, Seattle, Washington 98119 [H. C., T. B. K., T. W., B. S., S. H.]; and Department of Oncology, Bispebjerg Hospital, Copenhagen, Denmark [L. D.]

ABSTRACT

Recently, the ganglioside $FucG_{M1}$ (Fucα1-2Galβ1-3GalNAcβ1-4[NeuAcα2-3]-Galβ1-4Glcβ1-1Cer) was identified as a small cell lung cancer (SCLC) marker both in chemical and histochemical studies. In order to further determine whether the $FucG_{M1}$ ganglioside is shed from the tumor site and consequently is present in the serum of SCLC patients, we produced a series of new monoclonal antibodies raised against $FucG_{M1}$ and related glycolipids. Shedding of the $FucG_{M1}$ ganglioside was studied both *in vitro* and *in vivo* using SCLC cell lines and nude mice xenografts of SCLC cells as model systems, and finally immunochemical analyses were performed on serum samples from patients with SCLC. High-performance thin-layer chromatography immunostaining demonstrated the presence of $FucG_{M1}$ in conditioned culture media obtained from $FucG_{M1}$-positive SCLC cell lines. Furthermore, tumor extracts of SCLC cell line xenografts in nude mice were positive for the $FucG_{M1}$ marker, and more importantly the marker was also present in serum samples from these mice. Twenty serum samples were obtained from patients with histologically verified SCLC. Eight patients had localized disease, and the remaining patients had disseminated cancer involving metastases to other organ sites. Sera from 4 of these patients were clearly positive, and 2 additional cases were found to be weakly positive. The positive patient sera were all from patients with extensive disease. Sera from 12 patients with non-SCLC and 20 healthy individuals were all found to be negative. These results clearly establish the $FucG_{M1}$ glycolipid as a potential serum marker of SCLC for which a sensitive immunoassay should be developed and tested using a larger series of serum samples.

INTRODUCTION

SCLC[3] comprises 20 to 25% of all lung cancer cases (1), and with a 5-year survival rate of 2 to 5% it is the histological subtype of lung cancer with the poorest prognosis (2). SCLC is surgically incurable due to the rapid proliferation and metastatic spread by the time of diagnosis (3), but SCLC tumors are generally sensitive to chemo- and radiation therapy, which emphasize the importance of accurate and early detection of SCLC for effective therapy.

SCLC has been characterized as a neuroendocrine tumor because of the presence of neuroendocrine differentiation markers and the presence of neurosecretory granules. Several serum markers have been suggested for SCLC, including neuron-specific enolase and the creatine kinase-BB isoenzyme. None of these markers has shown an absolute specificity for SCLC (4, 5).

Nilsson *et al.* (6) originally identified the glycolipid $FucG_{M1}$ (Fucα1-2Galβ1-3GalNAcβ1-4[NeuAcα2-3]-Galβ1-4Glcβ1-1Cer) as a selective tumor-associated marker of SCLC cells. $FucG_{M1}$ and related structures are illustrated in Fig. 1. Using specific monoclonal antibodies they analyzed glycolipid extracts of a variety of normal human tissues and tumor tissues by HPTLC immunostaining and found the $FucG_{M1}$ glycolipid to be strongly associated with SCLC although some normal tissues, excluding normal lung tissue, also contained the glycolipid (6–9). Recently, the SCLC-associated expression of $FucG_{M1}$ was further substantiated by immunohistology of frozen tissue sections, where the presence of $FucG_{M1}$ was demonstrated in 90% of the cases as compared to 12% positive cases observed in other lung cancers (10).

Gangliosides have been identified in serum samples from patients with malignant melanoma, presumably as a result of shedding from tumor cells, and the detection of these antigens in serum may provide an aid for diagnosis and follow-up (11–13). In this report, we present evidence that the $FucG_{M1}$ ganglioside is shed *in vitro* and *in vivo* from SCLC cells and that this antigen also may be detected in serum samples from SCLC patients.

MATERIALS AND METHODS

Cell Lines. NCI-H69, CALU-1, CALU-3, SK-MES, and SK-LU1 cells were obtained from the American Type Culture Collection (Rockville, MD). NCI-H345 and NCI-H510 cells were kindly provided by Dr. T. Schwartz (Laboratory of Molecular Endocrinology, Copenhagen, Denmark). GLC-14, GLC-16, and TOO54A cells (14, 15) were kindly provided by Dr. K. Rygaard (State University Hospital, Copenhagen).

Monoclonal Antibodies. MAbs directed to the $FucG_{M1}$ and $FucG_{A1}$ antigens were produced according to standard procedures (16). Purified glycolipids (2 μg), adsorbed on acid-treated *Salmonella minnesota* (50 μg), were used as antigens for i.v. immunization of BALB/c mice (3-month-old) 3–5 times with 2–3-week intervals between immunizations. Fusion with SP/2-0 or NS-1 hypoxanthine phosphoribosyltransferase-negative myeloma cells was performed 3 days after the last i.v. immunization. The screening and further selection of hybridomas with specificity for $FucG_{M1}$ (TKH5 and 1D7) was based on reactivity with purified glycolipids using enzyme-linked immunosorbent assay as well as HPTLC immunostaining techniques (17, 18). Both MAbs (TKH5 and 1D7) were identified as being of the IgG3 isotype. An additional MAb, TKH4, specifically bound $FucG_{A1}$ but did not react with $FucG_{M1}$ or other glycolipid antigens. The MAb MH2 was prepared similarly using a biosynthetically produced AG_{M1} ganglioside.[4]

Purification of Antibodies. One-tenth volume of 1.0 M Tris (pH 8.0) was added to the MAb-containing culture supernatant, adsorbed on a protein A-Sepharose column (Pharmacia, Uppsala, Sweden), washed with 100 mM Tris (pH 8.0), eluted with 100 mM glycine buffer (pH 3.0), and collected into tubes containing 0.1 volume of 1 M Tris, pH 8.2. The IgG3 anti-$FucG_{M1}$ MAbs (TKH5 and 1D7) were immediately

Received 10/1/90; accepted 3/25/91.

The costs of publication of this article were defrayed in part by the payment of page charges. This article must therefore be hereby marked *advertisement* in accordance with 18 U.S.C. Section 1734 solely to indicate this fact.

[1] This study was supported in part by Project Grants 74-26/89 and 74-26/90 from the Danish Cancer Society and by the National Union against Lung Diseases, Denmark, the Biomembrane Institute, the NIH, the Lundbeck Foundation, Jenny Vissing, and the Danish Medical Research Council.

[2] To whom requests for reprints should be addressed, at Department of Tumor Cell Biology, The Fibiger Institute, Danish Cancer Society, Ndr. Frihavnsgade 70, DK-2100 Copenhagen, Denmark.

[3] The abbreviations used are: SCLC, small cell lung cancer; HPTLC, high-performance thin-layer chromatography; MAb, monoclonal antibody; FCS, fetal calf serum; FITC, fluorescein isothiocyanate; FACS, fluorescence-activated cell sorter; PBS, phosphate-buffered saline; $FucG_{M1}$, Fucα1-2Galβ1-3GalNAcβ1-4[NeuAcα2-3]-Galβ1-4Glcβ1-1Cer; $FucG_{A1}$, fucosyl-asialo-G_{M1}.

[4] T. White, S. B. Levery, M. Stroud, S. Hakomori, A. J. Vangsted, and H. Clausen, manuscript in preparation.

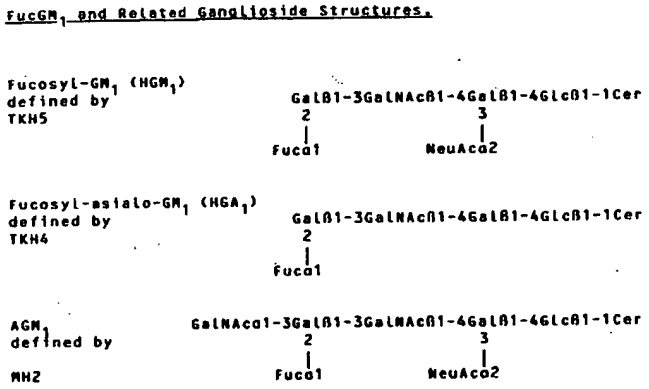

Fig. 1. Schematic representation of the gangliosides $FucG_{M1}$, Fuc-asialo-G_{M1}, and AG_{M1}. The MAbs TKH5, TKH4, and MH2 with specificity for $FucG_{M1}$, Fuc-asialo-G_{M1}, and AG_{M1}, respectively, are indicated. *Glc*, glucose; *Gal*, galactose, *GlcNAc*, *N*-acetylglucosamine; *GalNAc*, *N*-acetylgalactosamine; *Fuc*, fucose; *Cer*, ceramide; *NeuAc*, neuraminic acid.

collected and dialyzed (molecular weight cutoff, 12,000–14,000; Spectra/por, Los Angeles, CA) against PBS (pH 7.4).

Culture of Cell Lines. NCI-H69, NCI-H345, NCI-H510, GLC-14, and GLC-16 cells were grown in RPMI 1640 containing 10% FCS. CALU-1 cells were grown in McCoy's 5a medium containing 10% FCS, whereas CALU-1, SK-MES, T0054A, and SK-LU1 cells were grown in modified Eagle's medium containing 10% FCS supplemented with 7 nonessential amino acids and sodium pyruvate. All lung cancer cell cultures were supplemented with L-glutamine, penicillin, and streptomycin (100 units/ml, 0.5 mg/ml). Conditioned media in a total volume of 50 ml from GLC-14, GLC-16, and NCI-H69 cells were obtained from cell cultures in the exponential growth phase. The NCI-H69 cells were also propagated *in vivo* as xenografts in athymic nude BALB/c mice. Hybridoma cells were cultured in RPMI 1640 containing 15% FCS supplemented with L-glutamine and sodium pyruvate. All cell cultures were routinely screened for possible *Mycoplasma* contamination at monthly intervals and were negative throughout these experiments.

Nude Mouse Xenografts. Cells ($3–5 \times 10^7$) of the cell lines GLC-14, GLC-16, NCI-H69, and T0054A were inoculated s.c. into the flanks of athymic nude BALB/c mice. When the xenografted mice showed symptoms of dehydration and loss of weight, the tumors and organs such as liver, lung, spleen, and mesenteric lymph nodes were collected. Blood samples were collected in heparinized test tubes containing aprotinin (Trasylol; Bayer, Leverkusen, Germany) at a final concentration of 2000 Kallikrein inhibitor units/ml. Tumor, organs, and plasma samples were immediately frozen at −80°C.

Serum Samples. Serum samples (700–800 μl) were obtained from 20 patients with histologically verified SCLC as classified according to WHO II criteria. The sera were obtained at the time of diagnosis and before the patients received chemotherapy, and all patients participated in a follow-up study. Eight patients had localized disease, and 12 patients had disseminated cancer involving metastases to other organ sites. Clinical information on these patients (age, sex, blood type, state of disease, and organ site involvement) and results from analyses of serum samples are summarized in Table 1. Twelve serum samples from patients with non-SCLC cancer as well as 20 serum samples from normal individuals were used as control sera.

Immunofluorescence Staining Procedure. One million to 5 million cells were incubated with 100 μl protein A-purified TKH5 or 1D7 MAb (dilution, 1:100) in PBS for 1 h and washed 3 times, followed by incubation with 100 μl FITC-conjugated goat anti-mouse immunoglobulin (code F-261; Dako A/S, Glostrup, Denmark) at a final dilution of 1:80. All procedures were done at 4°C. An IgG3 monoclonal antibody of nonrelated specificity was used for control staining. Immunofluorescence staining was analyzed by fluorescence microscopy as well as by FACS analysis.

FACS Analysis. One hundred μl of cell suspension adjusted to 10^6 cells/ml were incubated with 100 μl of MAb TKH5 or 1D7 MAbs (dilution, 1:100 in PBS) for 1 h at 4°C and washed three times, followed by incubation at the same temperature for 1 h with FITC-conjugated anti-mouse antibodies. After three washings in PBS, the cells were resuspended in 200 μl sheath fluid (Becton Dickinson, Mountain View, CA) and analyzed in a FACScan flow cytometer (Becton Dickinson). Control samples were incubated with nonrelated IgG3 MAb and FITC-conjugated anti-mouse immunoglobulin only. Five thousand cells were analyzed for each sample and gated to include only intact viable cells.

Extraction of $FucG_{M1}$ from Conditioned Media and Sera. Serum samples (700–800 μl) and conditioned media (50 ml) were extracted using isopropyl alcohol:hexane:serum (55:20:20, v/v/v). Control samples consisted of complete media and 10% FCS only. Total lipid extracts were evaporated to dryness under N_2, resuspended in PBS containing 0.1 M KCl, and bound on a Bond-Elute C18 disposable cartridge column (Analytichem International, Harbor City, CA). Columns were washed with PBS and distilled H_2O and eluted with chloroform:methanol (2:1, v/v). The eluate was dried under N_2, dissolved in 30 μl chloroform:methanol (2:1, v/v), and analyzed by HPTLC in a volume of 5 μl.

Extraction from Tumors, Organs, and Cell Lines. Tissues and cell lines were homogenized in and extracted twice with isopropyl alcohol:hexane:water (55:25:20, v/v/v). The extraction and purification were performed as described above.

Table 1 *Summary of clinical data and presence or absence of $FucG_{M1}$ in serum samples for patients with histologically verified SCLC*

Patient	Age	Sex	Blood group (ABO, rhesus)	State of disease	Organ site involvement	$FucG_{M1}$ in serum HPTLC[a]
1	66	M	O; Rh+	Disseminated	Liver, bone marrow	+
2	60	F	O; Rh+	Localized		−
3	65	M	A; Rh+	Localized		−
4	57	M	A; Rh−	Disseminated	Liver, bone marrow	(+)
5	65	M	B; Rh+	Disseminated	Pancreas, liver	−
6	64	M	A; Rh+	Localized		(+)
7	44	M	O; Rh+	Disseminated	Liver, bone marrow	−
8	65	M	A; Rh−	Disseminated	Liver	−
9	54	F	A; Rh+	Localized		−
10	57	F	O; Rh+	Disseminated	Liver, bone marrow	+
11	44	M	A; Rh+	Disseminated	Bone marrow	−
12	57	F	O; Rh−	Disseminated	Liver, bone marrow	−
13	63	M	A; Rh+	Disseminated	Liver, skin-metastases	+
14	33	F	A; Rh+	Localized		−
15	62	F	B; Rh+	Disseminated	Liver	−
16	65	M	B; Rh−	Localized		−
17	52	M	O; Rh+	Disseminated	Bone marrow	−
18	67	M	A; Rh+	Disseminated	Liver, bone marrow	+
19	67	M	B; Rh+	Localized		−
20	57	M	A; Rh+	Localized		−

[a] Data shown in Fig. 4.

Preparation of Glycolipids. $FucG_{M1}$ was purified from bovine thyroids as previously described (19, 20), and fucosyl-asialo-G_{M1} ($FucG_{A1}$) was prepared from purified $FucG_{M1}$ by acid hydrolysis at 100°C. AG_{M1} and AG_{A1} were prepared biosynthetically from $FucG_{M1}$ and $FucAG_{A1}$ using purified blood group A transferase.[4] G_{M1} ganglioside was isolated from bovine brain, and asialo-G_{M1} was prepared by acid hydrolysis of G_{M1} ganglioside. Other α1-2-fucosyl-containing glycolipids were prepared as previously described (21).

HPTLC Immunostaining of Glycolipids. The total ganglioside fraction isolated from tissues and sera (5 μl/30 μl ganglioside extract obtained from 700–800 μl serum samples) were separated on HPTLC plates (Merck, Darmstadt, Germany) using a chloroform:methanol:H_2O (50:40:10, v/v/v) solvent system. HPTLC plates were briefly air dried and immersed in 0.5% 5-poly(isobutylmethacrylate) beads (Polysciences, Inc., Warrington, PA) in ether for 2 min and blocked at room temperature with 5% bovine serum albumin in PBS for 30 min followed by overnight incubation at 4°C with the MAb TKH5. Rabbit anti-mouse IgG:IgM (Code Z-109; Dako A/S) were exposed at room temperature for 1.5 h at a final concentration of 1:1000, and finally the plates were labeled with ^{125}I-protein A (specific activity, 30 mCi/mg total protein A) (Amersham International, Amersham, United Kingdom). X-OMAT AR films (Kodak H 165-1496) were exposed overnight with dried plates.

RESULTS

Characterization of Monoclonal Antibodies. Two hybridomas (TKH5 and 1D7) producing monoclonal antibodies that bound $FucG_{M1}$ but not $FucG_{A1}$ or any of a panel of additional standard glycolipids were isolated from two independent fusions. Both of these MAbs were of the IgG3 isotype and were found to be specific for the $FucG_{M1}$ relevant structures as shown in Fig. 2. Further attempts to produce MAbs of other isotypes (IgG or IgM) against the $FucG_{M1}$ antigen were unsuccessful. One additional hybridoma (TKH4) that produced an IgM isotype MAb that bound $FucG_{A1}$ but not $FucG_{M1}$ or other standard glycolipids was also generated. The MAb TKH5 specifically labeled 7 of 10 different SCLC cell lines tested but none of 38 other carcinomas of various origins.

Immunofluorescence Staining of Cell Lines. Six different SCLC cell lines were selected for further study. Immunofluorescence staining of these cell lines showed that 3 of the 6 selected SCLC cell lines were positive when stained with either of the 2 different MAbs (TKH5 or 1D7). No difference in staining intensity was detected when unfixed cells were compared to cells fixed in 4% formaldehyde or 96% ethanol. Fixation in acetone, however, partially abolished the staining. Neuraminidase pretreatment of the cells did not affect binding. Neuraminidase treatment of purified $FucG_{M1}$ glycolipid, even in the presence of detergent (sodium taurocholate), did not result in desialylation to any significant degree, presumably because the sialic acid residue in $FucG_{M1}$ is positioned at the internal galactose.[5] Indirect immunofluorescence staining resulted in a homogeneous ring-shaped membrane-associated fluorescence staining pattern. The percentage of immunofluorescence-positive cells varied among different SCLC cell lines as demonstrated by immunofluorescence and the FACS analysis shown in Fig. 3. Ten % of the cells from the GLC-16 and NCI-H69 cell lines were positive for the $FucG_{M1}$ antigen. This percentage was much higher in GLC-14 cells, where as many as 80% of the cells were positive. The cell lines NCI-H345, NCI-H510, and T0054A were all negative in immunofluorescence, as were all four non-SCLC cell lines included in this study.

[5] H. Clausen and S. Hakomori, unpublished observations.

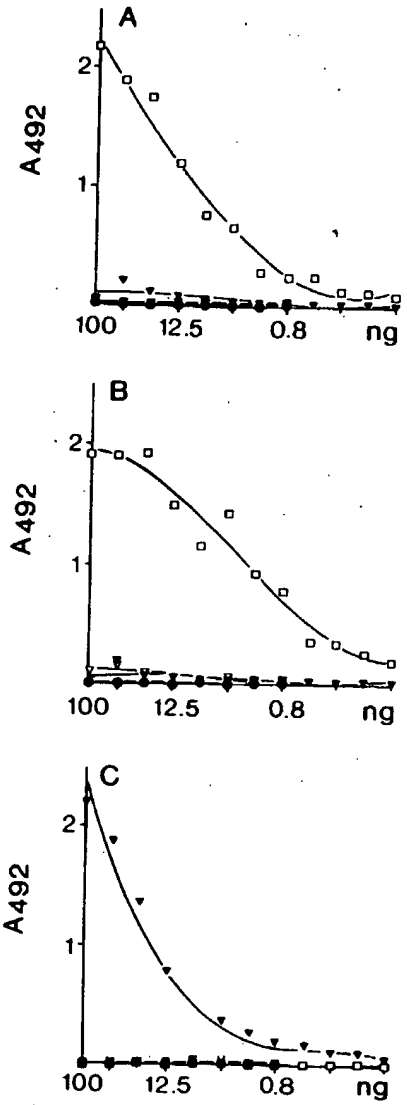

Fig. 2. Titers of gangliosides tested in enzyme-linked immunosorbent assay with three different antibodies. Binding specificity of the monoclonal antibodies TKH5, 1D7, and TKH4 to purified glycolipids. *Abscissa*, concentrations of gangliosides $FucG_{M1}$, $FucG_{A1}$, and asialo-G_{M1} starting at 100 ng followed by 2-fold dilutions. Antibodies were used as undiluted culture supernatants from hybridoma cells.

Immunohistochemical Detection of $FucG_{M1}$ from SCLC Cell Lines, Tumors, and Serum Samples from SCLC Xenografted Nude Mice. The results from HPTLC immunostaining of cells, supernatants, nude mouse xenograft tumors, and mouse sera are summarized in Table 2. The cell extracts obtained from the immunofluorescence-positive cells cultured *in vitro* and *in vivo* were found to be positive for the ganglioside $FucG_{M1}$. The ganglioside $FucG_{M1}$ was also detected in the conditioned media from 2 of 3 positive cell lines. In addition, in athymic nude mice xenografted with these cell lines, mouse sera were positive in 2 of the 3 cases. The cell line GLC-14 showed similar results in both model systems. This was in contrast to the cell lines GLC-16 and NCI-H69 which were only positive for the antigen in either one of the two model systems. In the case of GLC-16 $FucG_{M1}$ was identified in conditioned media but not in xenograft serum. NCI-H69 cells showed the opposite pattern. The reason for this controversy is unknown, but the two cell lines,

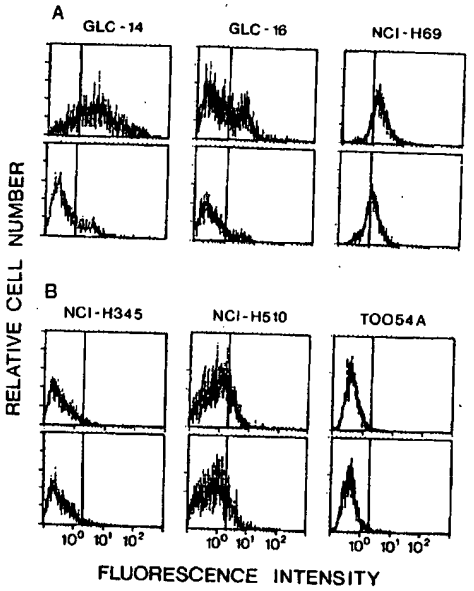

Fig. 3. FACS evaluation of SCLC cells stained for $FucG_{M1}$. *A*, the 3 different $FucG_{M1}$-positive SCLC cell lines (GLC-14, GLC-16, and NCI-H69). *First row*, increase in fluorescence intensity due to staining with the MAb TKH5; *second row*, background staining with the secondary antibody (FITC-conjugated goat anti-mouse immunoglobulin) of cells. An 80% increase after specific staining was noted in GLC-14 cells as compared to a 10% increase observed in GLC-16 as well as with NCI-H69 cells. *B*, corresponding immunofluorescence staining profiles of the 3 different $FucG_{M1}$-negative SCLC cell lines (NCI-H345, NCI-H510, and T0054A).

Table 2 *Summary of immunochemical detection of* $FucG_{M1}$

Cell line	Immunofluorescence positive cells (%)	HPTLC immunostaining of cell extracts	HPTLC immunostaining of conditioned media	HPTLC immunostaining of xenograft tumor extracts	HPTLC immunostaining of sera xenografted nude mice
GLC-14	80	++	+	+	+
GLC-16	10	+	+	+	Negative
NCI-H69	10	++	Negative	+	+
NCI-H34	0	Negative	ND[a]	ND	ND
NCI-H51	0	Negative	ND	ND	ND
T0054A	0	Negative	ND	Negative	Negative

[a] ND, not determined.

GLC-16 and NCI-H69, showed only a small fraction (10%) of positive cells in culture, whereas GLC-14 was more homogeneously positive (80%) (Table 2). The immunoreactive $FucG_{M1}$ antigen from different sources defined by the MAb TKH5 migrated slightly differently in HPTLC. The mobility of immunoreactive $FucG_{M1}$ from the established cell lines (in cell extracts or from nude mouse xenograft tumors) migrated as a double band in contrast to a slower-migrating single $FucG_{M1}$ immunoreactive band, when media or sera were analyzed, presumably due to differences in the ceramide composition (22). The $FucG_{M1}$ antigen was also detectable by HPTLC immunostaining in total extracts from livers of mice xenografted with the 80% $FucG_{M1}$-positive GLC-14 cell line suggesting the presence of SCLC metastases in the liver. In contrast to this, tissues from lung, spleen, and mesenteric lymph nodes were found to be consistently negative, similar to the organs from nude mice used as controls.

Detection of $FucG_{M1}$ in Serum Samples from SCLC Patients. The results of HPTLC immunostaining of 18 of a total of 20 patient serum samples are illustrated in Fig. 4. Fig. 4*A* illustrates the staining of the $FucG_{M1}$ ganglioside by the MAb TKH5. Sera from patients 1, 10, 13, and 18 stained positively, and only trace amounts were detected in serum samples from patients 4 and 6. The $FucG_{M1}$-positive samples were found only for patients with extended disease. Sera from patients with localized disease or other histological types of lung cancer or from 20 healthy individuals were negative for $FucG_{M1}$. Fig. 4*A* (*Lanes 2* and *3*) illustrates the HPTLC immunostaining pattern of the MAbs TKH4 and MH2[4] raised against $FucG_{A1}$ and AG_{M1}, respectively (for structures see Fig. 1). None of the $FucG_{M1}$-negative sera were positive for these alternative glycosylation variants of the ganglioside core structure. At least one patient serum from an individual with blood group A (patient 18) was strongly positive for the $FucG_{M1}$ ganglioside but not for the AG_{M1} glycolipid (MH2) (Fig. 4).

DISCUSSION

Shedding of tumor-associated antigens resulting from aberrant glycosylation may have important diagnostic applications (23, 24). In cultures of melanoma cells, monosialo- and disialogangliosides were found to be shed in conditioned media (25–27), and disialogangliosides have been identified in serum samples from patients with malignant melanoma (11–13).

In this study, we have demonstrated that the ganglioside antigen $FucG_{M1}$ is present in the conditioned media from $FucG_{M1}$-positive SCLC cell cultures, as well as in tumors and serum samples from nude mice xenografted with the same $FucG_{M1}$-positive SCLC cells. The ganglioside $FucG_{M1}$ was also

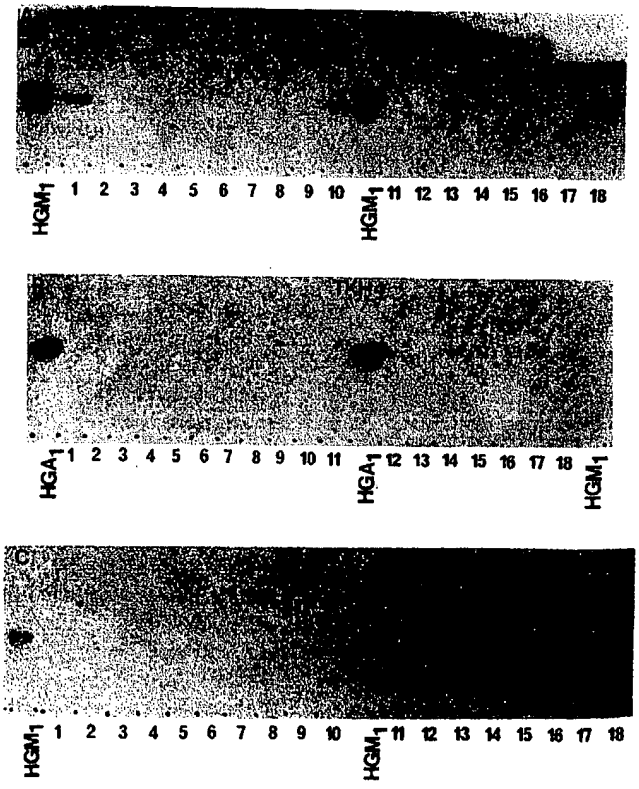

Fig. 4. HPTLC immunostaining of 18 SCLC patient sera of a total of 20 analyzed, by the use of MAbs TKH5, TKH4, and MH2. Sera (700–800 μl) were extracted as described in "Materials and Methods," and the extract was dissolved in 30 μl chloroform:methanol (2:1, v/v). A 5-μl sample was applied per lane. The solvent system for HPTLC was chloroform:methanol:H_2O (50:40:10, v/v/v). *A*, MAb TKH5 specific for $FucG_{M1}$; *B*, MAb TKH4 specific for Fuc-asialo-G_{M1}; *C*, MH2 specific for AG_{M1}. *HG_{M1}*, $FucG_{M1}$; *HG_{A1}*, Fuc-asialo-G_{M1} (standards).

detected in total extracts of liver tissues from tumor-bearing mice but not from other organs analyzed. Since no histologically verified metastases could be detected in liver sections from tumor-bearing mice, it is, however, uncertain whether this positive reaction was due to the presence of micrometastases. Interestingly, only the serum samples from mice xenografted with the SCLC cell line expressing high levels of $Fuc G_{M1}$ (GLC-14 cells) or the *in vivo* propagated cell line (NCI-H69) shed detectable levels of the ganglioside antigen. Although this could be interpreted as if only a few SCLC cells actually shed antigen to serum, the combined findings of antigen shedding *in vitro* and *in vivo* suggest that the results obtained more likely are due to limited sensitivity of the HPTLC immunostaining method used for the detection of the $Fuc G_{M1}$ antigen. Using similar analytical techniques, but including extraction of the glycolipid antigen from small amounts of patient serum, 4 serum samples of a total of 20 analyzed were found to be positive for $Fuc G_{M1}$. All $Fuc G_{M1}$-positive serum samples were from patients with large tumor load and extensive disease, and the frequency of positive samples corresponds to a detection rate of 25% in all SCLC patients analyzed with disseminated disease.

Total lipid extracts from SCLC patient sera were also analyzed for alternative glycosylation products which theoretically could be present as a result of different ABO blood group status (28). The blood group A− variant of gangliosides was not detected, although at least one of the patients belonging to blood group A strongly expressed $Fuc G_{M1}$ (patient 18). The MAb MH2 with specificity for the AG_{M1} glycolipid, however, had less affinity than the anti-$Fuc G_{M1}$ MAbs. Additional factors such as A_1A_2 histo-blood group subgrouping could influence these results (28). Interestingly, the asialo derivative of $Fuc G_{M1}$, $Fuc G_{A1}$, was not detected in any serum samples either. This result could be due to the relative sialidase resistance of the internal sialic acid in the $Fuc G_{M1}$ ganglioside.

The currently most accepted serum markers for SCLC are neuron-specific enolase and the creatine kinase-BB isoenzyme. At the time of diagnosis, elevated concentrations of neuron-specific enolase and the creatine kinase-BB isoenzyme have been detected in 70% of plasma samples from SCLC patients with disseminated disease followed by subsequent changes in plasma levels as a result of chemotherapeutic responses (29–32). However, both of these serum markers have also been detected in patients with non-SCLC (4, 5). No false-positive reactions for the ganglioside $Fuc G_{M1}$ have been found in our present limited analysis of patients with non-SCLC cancers or in the normal controls using HPTLC immunostaining. In the present study, the lipids were extracted from small volumes and prepared for analysis by HPTLC immunostaining, which implies that a high concentration of antigen was required for detection. This method was chosen here because we explicitly wanted to combine immunological detection with a more direct chemical method to visualize and confirm the nature of the serum glycolipid antigen. The $Fuc G_{M1}$ carbohydrate structure is generally considered not to occur in glycoproteins (28). It is possible that the development of more sensitive immunoassays for $Fuc G_{M1}$, which will require smaller amounts of antigen, will further increase the frequency of $Fuc G_{M1}$-positive sera from patients with SCLC. Attempts to achieve this have thus far been hampered by the poor stability of the present $Fuc G_{M1}$-specific MAbs after further purification.

In this paper we have demonstrated that the SCLC-associated antigen glycolipid $Fuc G_{M1}$ may be detected in sera of patients with SCLC. This finding could have further implications for the classification of lung cancer and the diagnosis of SCLC.

ACKNOWLEDGMENTS

We thank J. Schmidt for her excellent technical assistance.

REFERENCES

1. Hardy, J. D., Ewing, H. P., Neely, W. A., Straus, H. K., and Vance, R. B. Lung carcinoma: survey of 2286 cases with emphasis on small cell type. Ann. Surg., *193:* 539–548, 1981.
2. Miller, A. B., Fox, W., and Tall, R. Five-year follow-up of the Medical Research Council comparative trial of surgery and radiotherapy for the treatment of small cell or oat cell carcinoma of the bronchus. Lancet, *2:* 501–505, 1969.
3. Minna, J. D., Higgins, G. A., and Glatstein, E. J. Cancer of the lung. *In:* V. T. De Vita, S. Helmanns, and S. A. Rosenberg (eds.), Principles and Practice of Oncology, pp. 396–474. Philadelphia: J. B. Lippincott Co., 1981.
4. Gomm, S. A., Keevil, B. G., Thatcher, N., Hasleton, P. S., and Swindell, R. S. The value of tumour markers in lung cancer. Br. J. Cancer, *58:* 797–804, 1988.
5. Jaques, G., Bepler, G., Holle, R., Wolf, M., Hannich, T., Gropp, C., and Havemann, K. Prognostic value of pretreatment carcinoembryonic antigen, neuron-specific enolase, and creatine kinase-BB levels in sera of patients with small cell lung cancer. Cancer (Phila.), *62:* 125–134, 1988.
6. Nilsson, O., Månsson, J-E., Brezicka, T., Holmgren, J., Lindholm, L., Sörenson, S., Yngvason, F., and Svennerholm, L. Fucosyl-GM1-A ganglioside associated with small cell lung carcinomas. Glycoconjugate J., *1:* 43–49, 1984.
7. Fredman, P., Brezicka, T., Holmgren, J., Lindholm, L., Nilsson, O., and Svennerholm, L. Binding specificity of monoclonal antibodies to ganglioside, Fuc-GM1. Biochim. Biophys. Acta, *875:* 316–323, 1986.
8. Nilsson, O., Brezicka, F. T., Holmgren, J., Sörenson, S., Svennerholm, L., Yngvason, F., and Lindholm, L. Detection of a ganglioside antigen associated with small cell lung carcinomas using monoclonal antibodies directed against fucosyl-GM1. Cancer Res., *46:* 1403–1407, 1986.
9. Fuchs, B. B., Avrova, N. F., Starosvetskaya, N. A., Boltovskaya, M. N., Zaraisky, E. I., Karpova, O. B., Reznikova, E. V., Soldatova, L. N., and Stepanow, A. A. Biochemical and immunochemical analysis of gangliosides of human small cell lung carcinoma: production of monoclonal antibodies against a unique marker of small cell lung carcinoma, ganglioside Fuc-GM1. Biotechnol. Appl. Biochem., *10:* 273–286, 1988.
10. Brezicka, F. T., Olling, S., Nilsson, O., Bergh, J., Holmgren, J., Sörenson, S., Yngvason, F., and Lindholm, L. Immunohistological detection of fucosyl-G_{M1} ganglioside in human lung cancer and normal tissues with monoclonal antibodies. Cancer Res., *49:* 1300–1305, 1989.
11. Ladisch, S., and Wu, Z-L. Detection of a tumour-associated ganglioside in plasma of patients with neuroblastoma. Lancet, *1:* 136–138, 1985.
12. Schulz, G., Cheresh, D. A., Varki, N. M., Yu, A., Staffileno, L. K., and Reisfeld, R. A. Detection of ganglioside G_{D2} in tumour tissues and sera of neuroblastoma patients. Cancer Res., *44:* 5914–5920, 1984.
13. Sela, B-A., Iliopoulos, D., Guerry D., Herlyn, D., and Koprowski, H. Levels of disialogangliosides in sera of melanoma patients monitored by sensitive thin-layer chromatography and immunostaining. J. Natl. Cancer Inst., *81:* 1489–1492, 1989.
14. Berendsen, H. H., de Leij, L., de Vries, E. G. E., Mesander, G., Mulder, N-H., de Jong, B., Buys, C. H. C. M., Postmus, P. E., Poppema, S., Sluiter, H. J., and The, H. T. Characterization of three small cell lung cancer cell lines established from one patient during longitudinal follow-up. Cancer Res., *48:* 6891–6899, 1988.
15. Engelholm, S. A., Vindeløv, L., Spang-Thomsen, M., Brünner, N., Tommerup, N., Nielsen, M. H., and Hansen, H. H. Genetic instability of cell lines derived from a single human small cell carcinoma of a lung. Eur. J. Cancer Clin. Oncol., *21:* 815–824, 1985.
16. Köhler, G., and Milstein, C. Continuous cultures of fused cells secreting antibody of predefined specificity. Nature (Lond.), *256:* 495–497, 1975.
17. Kannagi, R., Stroup, R., Cochran, N. A., Urdal, D. L., Young, W. W., Jr., and Hakomori, S. Factors affecting expression of glycolipid tumor antigens: influence of ceramide composition and coexisting glycolipid on the antigenicity of gangliotriaosylceramide in murine lymphoma cells. Cancer Res., *43:* 4997–5005, 1983.
18. Kannagi, R., Nudelman, E., Levery, S. B., and Hakomori, S. A series of human erythrocyte glycosphingolipids reacting to the monoclonal antibody directed to a developmentally regulated antigen SSEA-1. J. Biol. Chem., *257:* 4865–4874, 1982.
19. Macher, B. A., Pacuszka, T., Mullin, B. R., Sweeley, C. C., Brady, R. O., and Fishman, P. H. Isolation and identification of a fucose-containing ganglioside from bovine thyroid gland. Biochim. Biophys. Acta, *588:* 35–43, 1979.
20. Van Dessel, G. A. F., Lagrou, A. R., Hilderson, H. J. J., Dierick, W. S. H., and Laüwers, W. F. J. Structure of the major gangliosides from bovine thyroid. J. Biol. Chem., *254:* 9305–9310, 1979.

21. Clausen, H., Levery, S. B., Kannagi, R., and Hakomori, S. Novel blood group H glycolipid antigens exclusively expressed in blood group A and AB erythrocytes (type 3 chain H). I. Isolation and chemical characterization. J. Biol. Chem., *261:* 1380–1387, 1986.
22. Spitalnik, S. L., Spitalnik, P. F., Dubois, C., Mulshine, J., Magnani, J. L., Cuttitta, F., Civin, C. I., Minna, J. D., and Ginsburg, V. Glycolipid antigen expression in human lung cancer. Cancer Res., *46:* 4751–4755, 1986.
23. Hakomori, S-I. Aberrant glycosylation in cancer cell membranes as focused on glycolipids: overview and perspectives. Cancer Res., *45:* 2405–2414, 1985.
24. Hakomori, S-I. Tumor associated glycolipid markers: possible targets for drug and immunotoxin delivery. *In:* Gregoriadis, G., Senior, J., and Poste, G. (eds.), Targeting of Drugs with Synthetic Systems, pp. 25–40. New York: Plenum Publishing Corporation, 1986.
25. Bernhard, H., Zum Büschenfelde, K-H. M., and Dippold, W. G. Ganglioside GD_3 shedding by human malignant melanoma cells. Int. J. Cancer, *44:* 155–160, 1989.
26. Tai, T., Paulson, J. C., Cahan, L. D., and Irie, R. F. Ganglioside GM2 as a human tumor antigen (OFA-I-1). Proc. Natl. Acad. Sci. USA, *80:* 5392–5396, 1983.
27. Hirabayashi, Y., Hamaoka, A., Matsumoto, M., Matsubara, T., Tagawa, M., Wakabayashi, S., and Taniguchi, M. Syngeneic monoclonal antibody against melanoma antigen with interspecies cross-reactivity recognizes G_{M3}, a prominent ganglioside of B16 melanoma. J. Biol. Chem., *260:* 13328–13333, 1985.
28. Clausen, H., and Hakomori, S. ABH and related histo-blood group antigens; immunochemical differences in carrier isotypes and their distribution. Vox Sang., *56:* 1–20, 1989.
29. Bork, E., Hansen, M., Urdal, P., Paus, E., Holst, J. J., Schifter, S., Fenger, M., and Engbaek, F. Early detection of response in small cell bronchogenic carcinoma by changes in serum concentrations of creatine kinase, neuron specific enolase, calcitonin, ACTH, serotonin and gastrin releasing peptide. Eur. J. Cancer Clin. Oncol., *24:* 1033–1038, 1988.
30. Esscher, T., Bergh, J., Steinholtz, L., Nõu, E., Nilsson K., and Påhlman, S. Neuron-specific enolase in small-cell carcinoma of the lung: the value of combined immunocytochemistry and serum determination. Anticancer Res., *9:* 1717–1720, 1989.
31. Burghuber, O. C., Worofka, B., Schernthaner, G., Vetter, N., Neumann, M., Dudczak, R., and Kuzmits, R. Serum neuron-specific enolase is a useful tumor marker for small cell lung cancer. Cancer (Phila.), *65:* 1386–1390, 1990.
32. Jørgensen, L. G., Østerlind, K., Hansen, H. H., and Cooper, E. H. The prognostic influence of serum neuron specific enolase in small cell lung cancer. Br. J. Cancer, *58:* 805–857, 1988.

This Page is Inserted by IFW Indexing and Scanning Operations and is not part of the Official Record

BEST AVAILABLE IMAGES

Defective images within this document are accurate representations of the original documents submitted by the applicant.

Defects in the images include but are not limited to the items checked:

- ☒ BLACK BORDERS
- ☐ IMAGE CUT OFF AT TOP, BOTTOM OR SIDES
- ☐ FADED TEXT OR DRAWING
- ☐ BLURRED OR ILLEGIBLE TEXT OR DRAWING
- ☐ SKEWED/SLANTED IMAGES
- ☐ COLOR OR BLACK AND WHITE PHOTOGRAPHS
- ☐ GRAY SCALE DOCUMENTS
- ☐ LINES OR MARKS ON ORIGINAL DOCUMENT
- ☒ REFERENCE(S) OR EXHIBIT(S) SUBMITTED ARE POOR QUALITY
- ☐ OTHER: _____

IMAGES ARE BEST AVAILABLE COPY.
As rescanning these documents will not correct the image problems checked, please do not report these problems to the IFW Image Problem Mailbox.